Radiation Oncology Physics:
A Handbook for Teachers and Students

E.B. Podgorsak
Technical Editor
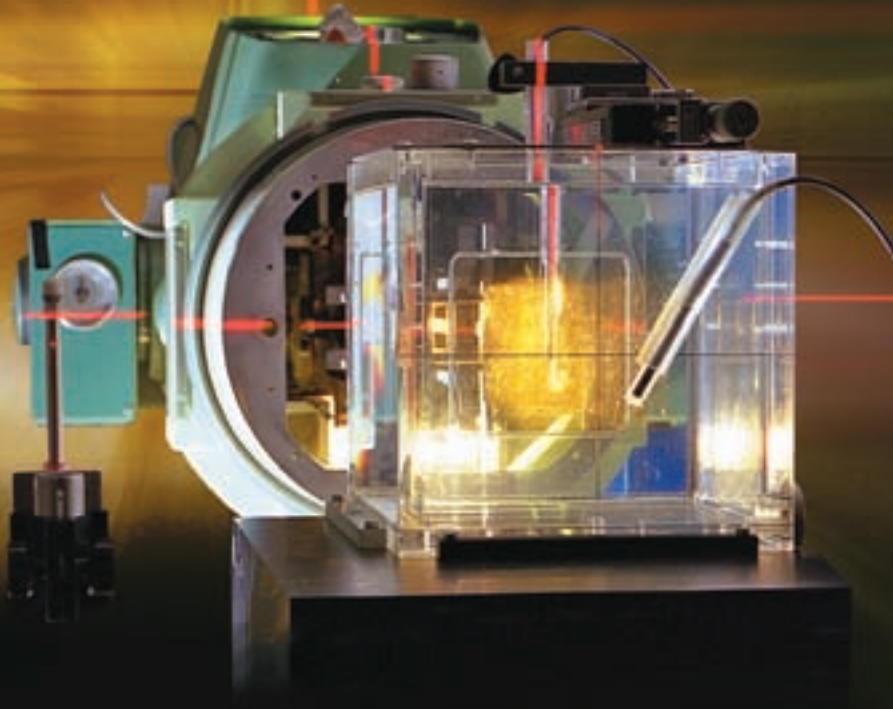
IAEA

COMP/CCPM

EFOMP

ESTRO

IOMP

WHO

RADIATION ONCOLOGY PHYSICS:
A HANDBOOK FOR TEACHERS AND STUDENTS

The following States are Members of the International Atomic Energy Agency:

AFGHANISTAN	GREECE	PAKISTAN
ALBANIA	GUATEMALA	PANAMA
ALGERIA	HAITI	PARAGUAY
ANGOLA	HOLY SEE	PERU
ARGENTINA	HONDURAS	PHILIPPINES
ARMENIA	HUNGARY	POLAND
AUSTRALIA	ICELAND	PORTUGAL
AUSTRIA	INDIA	QATAR
AZERBAIJAN	INDONESIA	REPUBLIC OF MOLDOVA
BANGLADESH	IRAN, ISLAMIC REPUBLIC OF	ROMANIA
BELARUS	IRAQ	RUSSIAN FEDERATION
BELGIUM	IRELAND	SAUDI ARABIA
BENIN	ISRAEL	SENEGAL
BOLIVIA	ITALY	SERBIA AND MONTENEGRO
BOSNIA AND HERZEGOVINA	JAMAICA	SEYCHELLES
BOTSWANA	JAPAN	SIERRA LEONE
BRAZIL	JORDAN	SINGAPORE
BULGARIA	KAZAKHSTAN	SLOVAKIA
BURKINA FASO	KENYA	SLOVENIA
CAMEROON	KOREA, REPUBLIC OF	SOUTH AFRICA
CANADA	KUWAIT	SPAIN
CENTRAL AFRICAN	KYRGYZSTAN	SRI LANKA
REPUBLIC	LATVIA	SUDAN
CHILE	LEBANON	SWEDEN
CHINA	LIBERIA	SWITZERLAND
COLOMBIA	LIBYAN ARAB JAMAHIRIYA	SYRIAN ARAB REPUBLIC
COSTA RICA	LIECHTENSTEIN	TAJIKISTAN
CÔTE D'IVOIRE	LITHUANIA	THAILAND
CROATIA	LUXEMBOURG	THE FORMER YUGOSLAV
CUBA	MADAGASCAR	REPUBLIC OF MACEDONIA
CYPRUS	MALAYSIA	TUNISIA
CZECH REPUBLIC	MALI	TURKEY
DEMOCRATIC REPUBLIC	MALTA	UGANDA
OF THE CONGO	MARSHALL ISLANDS	UKRAINE
DENMARK	MAURITANIA	UNITED ARAB EMIRATES
DOMINICAN REPUBLIC	MAURITIUS	UNITED KINGDOM OF
ECUADOR	MEXICO	GREAT BRITAIN AND
EGYPT	MONACO	NORTHERN IRELAND
EL SALVADOR	MONGOLIA	UNITED REPUBLIC
ERITREA	MOROCCO	OF TANZANIA
ESTONIA	MYANMAR	UNITED STATES OF AMERICA
ETHIOPIA	NAMIBIA	URUGUAY
FINLAND	NETHERLANDS	UZBEKISTAN
FRANCE	NEW ZEALAND	VENEZUELA
GABON	NICARAGUA	VIETNAM
GEORGIA	NIGER	YEMEN
GERMANY	NIGERIA	ZAMBIA
GHANA	NORWAY	ZIMBABWE

The Agency's Statute was approved on 23 October 1956 by the Conference on the Statute of the IAEA held at United Nations Headquarters, New York; it entered into force on 29 July 1957. The Headquarters of the Agency are situated in Vienna. Its principal objective is "to accelerate and enlarge the contribution of atomic energy to peace, health and prosperity throughout the world".

RADIATION ONCOLOGY PHYSICS: A HANDBOOK FOR TEACHERS AND STUDENTS

COPYRIGHT NOTICE

FOREWORD

In the late 1990s the IAEA initiated for its Member States a systematic and comprehensive plan to support the development of teaching programmes in medical radiation physics. Multiple projects were initiated at various levels that, together with the well known short term training courses and specialization fellowships funded by the IAEA Technical Cooperation programme, aimed at supporting countries to develop their own university based master of science programmes in medical radiation physics.

One of the early activities of the IAEA in this period was the development of a syllabus in radiotherapy physics, which had the goal of harmonizing the various levels of training that the IAEA provided. This was carried out during 1997–1998, and the result of this work was released as a report used for designing IAEA training courses. In 1999–2000 a more detailed teachers' guide was developed, in which the various topics in the syllabus were expanded to form a detailed 'bullet list' containing the basic guidelines of the material to be included in each topic so that lectures to students could be prepared accordingly. During the period 2001–2002 E.B. Podgorsak (Canada) was appointed editor of the project and redesigned the contents so that the book became a comprehensive handbook for teachers and students, with coverage deeper than a simple teachers' guide. The initial list of topics was expanded considerably by engaging an enhanced list of international contributors. The handbook was published as working material in 2003 and placed on the Internet in order to seek comments, corrections and feedback.

This handbook aims at providing the basis for the education of medical physicists initiating their university studies in the field. It includes the recent advances in radiotherapy techniques; however, it is not designed to replace the large number of textbooks available on radiotherapy physics, which will still be necessary to deepen knowledge in the specific topics reviewed here. It is expected that this handbook will successfully fill a gap in the teaching material for medical radiation physics, providing in a single manageable volume the largest possible coverage available today. Its wide dissemination by the IAEA will contribute to the harmonization of education in the field and will be of value to newcomers as well as to those preparing for their certification as medical physicists, radiation oncologists, medical dosimetrists and radiotherapy technologists.

Endorsement of this handbook has been granted by the following international organizations and professional bodies: the International Organization for Medical Physics (IOMP), the European Society for Therapeutic Radiology and Oncology (ESTRO), the European Federation of Organisations for Medical Physics (EFOMP), the World Health Organization

PREFACE

Radiotherapy, also referred to as radiation therapy, radiation oncology or therapeutic radiology, is one of the three principal modalities used in the treatment of malignant disease (cancer), the other two being surgery and chemotherapy. In contrast to other medical specialties that rely mainly on the clinical knowledge and experience of medical specialists, radiotherapy, with its use of ionizing radiation in the treatment of cancer, relies heavily on modern technology and the collaborative efforts of several professionals whose coordinated team approach greatly influences the outcome of the treatment.

The radiotherapy team consists of radiation oncologists, medical physicists, dosimetrists and radiation therapy technologists: all professionals characterized by widely differing educational backgrounds and one common link — the need to understand the basic elements of radiation physics, and the interaction of ionizing radiation with human tissue in particular. This specialized area of physics is referred to as radiation oncology physics, and proficiency in this branch of physics is an absolute necessity for anyone who aspires to achieve excellence in any of the four professions constituting the radiotherapy team. Current advances in radiation oncology are driven mainly by technological development of equipment for radiotherapy procedures and imaging; however, as in the past, these advances rely heavily on the underlying physics.

This book is dedicated to students and teachers involved in programmes that train professionals for work in radiation oncology. It provides a compilation of facts on the physics as applied to radiation oncology and as such will be useful to graduate students and residents in medical physics programmes, to residents in radiation oncology, and to students in dosimetry and radiotherapy technology programmes. The level of understanding of the material covered will, of course, be different for the various student groups; however, the basic language and knowledge for all student groups will be the same. The text will also be of use to candidates preparing for professional certification examinations, whether in radiation oncology, medical physics, dosimetry or radiotherapy technology.

The intent of the text is to serve as a factual supplement to the various textbooks on medical physics and to provide basic radiation oncology physics knowledge in the form of a syllabus covering all modern aspects of radiation oncology physics. While the text is mainly aimed at radiation oncology professionals, certain parts of it may also be of interest in other branches of medicine that use ionizing radiation not for the treatment of disease but for the diagnosis of disease (diagnostic radiology and nuclear medicine). The contents

may also be useful for physicists who are involved in studies of radiation hazards and radiation protection (health physics).

This book represents a collaborative effort by professionals from many different countries who share a common goal of disseminating their radiation oncology physics knowledge and experience to a broad international audience of teachers and students. Special thanks are due to J. Denton-MacLennan for critically reading and editing the text and improving its syntax.

E.B. Podgorsak

CONTRIBUTORS

Andreo, P.	University of Stockholm, Karolinska Institute, Sweden
Evans, M.D.C.	McGill University Health Centre, Canada
Hendry, J.H.	International Atomic Energy Agency
Horton, J.L.	University of Texas MD Anderson Cancer Center, United States of America
Izewska, J.	International Atomic Energy Agency
Mijnheer, B.J.	Netherlands Cancer Institute, Netherlands
Mills, J.A.	Walsgrave Hospital, United Kingdom
Olivares, M.	McGill University Health Centre, Canada
Ortiz López, P.	International Atomic Energy Agency
Parker, W.	McGill University Health Centre, Canada
Patrocinio, H.	McGill University Health Centre, Canada
Podgorsak, E.B.	McGill University Health Centre, Canada
Podgorsak, M.B.	Roswell Park Cancer Institute, United States of America
Rajan, G.	Bhabha Atomic Research Centre, India
Seuntjens, J.P.	McGill University Health Centre, Canada
Shortt, K.R.	International Atomic Energy Agency
Strydom, W.	Medical University of Southern Africa, South Africa
Suntharalingam, N.	Thomas Jefferson University Hospital, United States of America
Thwaites, D.I.	University of Edinburgh, United Kingdom
Tolli, H.	International Atomic Energy Agency

CONTENTS

Chapter 1

BASIC RADIATION PHYSICS

E.B. PODGORSAK
Department of Medical Physics,
McGill University Health Centre,
Montreal, Quebec, Canada

1.1. INTRODUCTION

1.1.1. Fundamental physical constants (rounded off to four significant figures)

- Avogadro's number: $N_A = 6.022 \times 10^{23}$ atoms/g-atom.
- Avogadro's number: $N_A = 6.022 \times 10^{23}$ molecules/g-mole.
- Speed of light in vacuum: $c = 299\ 792\ 458$ m/s ($\approx 3 \times 10^8$ m/s).
- Electron charge: $e = 1.602 \times 10^{-19}$ C.
- Electron rest mass: $m_{e^-} = 0.5110$ MeV/c^2.
- Positron rest mass: $m_{e^+} = 0.5110$ MeV/c^2.
- Proton rest mass: $m_p = 938.3$ MeV/c^2.
- Neutron rest mass: $m_n = 939.6$ MeV/c^2.
- Atomic mass unit: u = 931.5 MeV/c^2.
- Planck's constant: $h = 6.626 \times 10^{-34}$ J·s.
- Permittivity of vacuum: $\varepsilon_0 = 8.854 \times 10^{-12}$ C/(V·m).
- Permeability of vacuum: $\mu_0 = 4\pi \times 10^{-7}$ (V·s)/(A·m).
- Newtonian gravitation constant: $G = 6.672 \times 10^{-11}$ m^3·kg^{-1}·s^{-2}.
- Proton mass/electron mass: $m_p/m_e = 1836.0$.
- Specific charge of electron: $e/m_e = 1.758 \times 10^{11}$ C/kg.

1.1.2. Important derived physical constants and relationships

- Speed of light in a vacuum:

$$c = \frac{1}{\sqrt{\varepsilon_0 \mu_0}} \approx 3 \times 10^8 \text{ m/s} \tag{1.1}$$

● Reduced Planck's constant × speed of light in a vacuum:

$$\hbar c = \frac{h}{2\pi} c = 197.3 \text{ MeV} \cdot \text{fm} \approx 200 \text{ MeV} \cdot \text{fm} \tag{1.2}$$

● Fine structure constant:

$$\alpha = \frac{e^2}{4\pi\varepsilon_0} \frac{1}{\hbar c} = \frac{1}{137} \tag{1.3}$$

● Bohr radius:

$$a_0 = \frac{\hbar c}{\alpha m_e c^2} = \frac{4\pi\varepsilon_0}{e^2} \frac{(\hbar c)^2}{m_e c^2} = 0.5292 \text{ Å} \tag{1.4}$$

● Rydberg energy:

$$E_R = \frac{1}{2} m_e c^2 \alpha^2 = \frac{1}{2}\left(\frac{e^2}{4\pi\varepsilon_0}\right)^2 \frac{m_e c^2}{(\hbar c)^2} = 13.61 \text{ eV} \tag{1.5}$$

● Rydberg constant:

$$R_\infty = \frac{E_R}{2\pi\hbar c} = \frac{m_e c^2 \alpha^2}{4\pi\hbar c} = \frac{1}{4\pi}\left(\frac{e^2}{4\pi\varepsilon_0}\right)^2 \frac{m_e c^2}{(\hbar c)^3} = 109\ 737 \text{ cm}^{-1} \tag{1.6}$$

● Classical electron radius:

$$r_e = \frac{e^2}{4\pi\varepsilon_0 m_e c^2} = 2.818 \text{ fm} \tag{1.7}$$

● Compton wavelength of the electron:

$$\lambda_C = \frac{h}{m_e c} = 0.0243 \text{ Å} \tag{1.8}$$

1.1.3. Physical quantities and units

- Physical quantities are characterized by their numerical value (magnitude) and associated unit.
- Symbols for physical quantities are set in italic type, while symbols for units are set in roman type (e.g. m = 21 kg; E = 15 MeV).
- The numerical value and the unit of a physical quantity must be separated by a space (e.g. 21 kg and not 21kg; 15 MeV and not 15MeV).
- The currently used metric system of units is known as the Système international d'unités (International System of Units), with the international abbreviation SI. The system is founded on base units for seven basic physical quantities:

Length l: metre (m).
Mass m: kilogram (kg).
Time t: second (s).
Electric current I: ampere (A).
Temperature T: kelvin (K).
Amount of substance: mole (mol).
Luminous intensity: candela (cd).

All other quantities and units are derived from the seven base quantities and units (see Table 1.1).

TABLE 1.1. THE BASIC AND SEVERAL DERIVED PHYSICAL QUANTITIES AND THEIR UNITS IN THE INTERNATIONAL SYSTEM OF UNITS AND IN RADIATION PHYSICS

Physical quantity	Symbol	Unit in SI	Units used in radiation physics	Conversion
Length	l	m	nm, Å, fm	1 m = 10^9 nm = 10^{10} Å = 10^{15} fm
Mass	m	kg	MeV/c^2	1 MeV/c^2 = 1.78×10^{-30} kg
Time	t	s	ms, μs, ns, ps	1 s = 10^3 ms = 10^6 μs = 10^9 ns = 10^{12} ps
Current	I	A	mA, μA, nA, pA	1 A = 10^3 mA = 10^6 μA = 10^9 nA
Charge	Q	C	e	1 e = 1.602×10^{-19} C
Force	F	N		1 N = 1 kg·m·s^{-2}
Momentum	p	N·s		1 N·s = 1 kg·m·s^{-1}
Energy	E	J	eV, keV, MeV	1 eV = 1.602×10^{-19} J = 10^{-3} keV

1.1.4. Classification of forces in nature

There are four distinct forces observed in the interaction between various types of particle (see Table 1.2). These forces, listed in decreasing order of strength, are the strong force, electromagnetic (EM) force, weak force and gravitational force, with relative strengths of 1, 1/137, 10^{-6} and 10^{-39}, respectively.

- The ranges of the EM and gravitational forces are infinite ($1/r^2$ dependence, where r is the separation between two interacting particles);
- The ranges of the strong and weak forces are extremely short (of the order of a few femtometres).

Each force results from a particular intrinsic property of the particles, such as:

— Strong charge for the strong force transmitted by massless particles called gluons;
— Electric charge for the EM force transmitted by photons;
— Weak charge for the weak force transmitted by particles called W and Z^0;
— Energy for the gravitational force transmitted by hypothetical particles called gravitons.

1.1.5. Classification of fundamental particles

Two classes of fundamental particle are known: quarks and leptons.

- Quarks are particles that exhibit strong interactions. They are constituents of hadrons (protons and neutrons) with a fractional electric charge (2/3 or –1/3) and are characterized by one of three types of strong charge called colour: red, blue and green. There are six known quarks: up, down, strange, charm, top and bottom.

TABLE 1.2. THE FOUR FUNDAMENTAL FORCES IN NATURE

Force	Source	Transmitted particle	Relative strength
Strong	Strong charge	Gluon	1
EM	Electric charge	Photon	1/137
Weak	Weak charge	W and Z^0	10^{-6}
Gravitational	Energy	Graviton	10^{-39}

● Leptons are particles that do not interact strongly. Electrons (e), muons (μ), taus (τ) and their corresponding neutrinos (ν_e, ν_μ, ν_τ) are in this category.

1.1.6. Classification of radiation

As shown in Fig. 1.1, radiation is classified into two main categories, non-ionizing and ionizing, depending on its ability to ionize matter. The ionization potential of atoms (i.e. the minimum energy required to ionize an atom) ranges from a few electronvolts for alkali elements to 24.5 eV for helium (noble gas).

● Non-ionizing radiation (cannot ionize matter).
● Ionizing radiation (can ionize matter either directly or indirectly):
  —Directly ionizing radiation (charged particles): electrons, protons, α particles and heavy ions.
  —Indirectly ionizing radiation (neutral particles): photons (X rays and γ rays), neutrons.

Directly ionizing radiation deposits energy in the medium through direct Coulomb interactions between the directly ionizing charged particle and orbital electrons of atoms in the medium.

Indirectly ionizing radiation (photons or neutrons) deposits energy in the medium through a two step process:

● In the first step a charged particle is released in the medium (photons release electrons or positrons, neutrons release protons or heavier ions);
● In the second step the released charged particles deposit energy to the medium through direct Coulomb interactions with orbital electrons of the atoms in the medium.
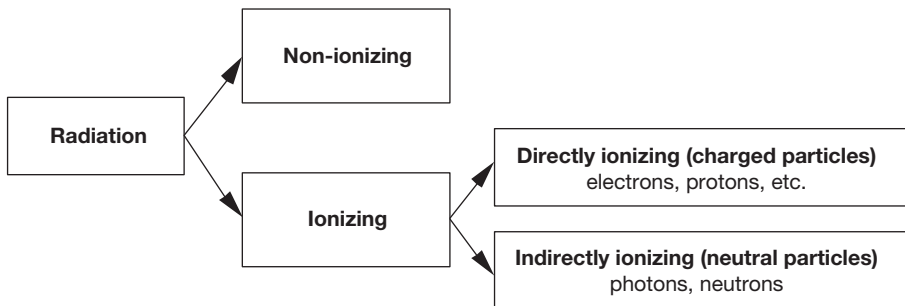
FIG. 1.1. Classification of radiation.

Both directly and indirectly ionizing radiations are used in the treatment of disease, mainly but not exclusively for malignant disease. The branch of medicine that uses radiation in the treatment of disease is called radiotherapy, therapeutic radiology or radiation oncology. Diagnostic radiology and nuclear medicine are branches of medicine that use ionizing radiation in the diagnosis of disease.

1.1.7. Classification of ionizing photon radiation

- Characteristic X rays: resulting from electron transitions between atomic shells.
- Bremsstrahlung: resulting from electron–nucleus Coulomb interactions.
- γ rays: resulting from nuclear transitions.
- Annihilation quanta: resulting from positron–electron annihilation.

1.1.8. Einstein's relativistic mass, energy and momentum relationships

$$m(v) = \frac{m_0}{\sqrt{1-\left(\dfrac{v}{c}\right)^2}} = \frac{m_0}{\sqrt{1-\beta^2}} = \gamma m_0 \tag{1.9}$$

$$E = m(v)c^2 \tag{1.10}$$

$$E_0 = m_0 c^2 \tag{1.11}$$

$$E_K = E - E_0 = (\gamma - 1)E_0 \tag{1.12}$$

$$E^2 = E_0^2 + p^2 c^2 \tag{1.13}$$

where

v	is the particle velocity;
c	is the speed of light in a vacuum;
β	is the normalized particle velocity (i.e. $\beta = v/c$);
$m(v)$	is the particle mass at velocity v;
m_0	is the particle rest mass (at velocity $v = 0$);
E	is the total energy of the particle;
E_0	is the rest energy of the particle;
E_K	is the kinetic energy of the particle;
p	is the momentum of the particle.

● For photons, $E = h\nu$ and $E_0 = 0$; thus using Eq. (1.13) we obtain $p = h\nu/c = h/\lambda$, where ν and λ are the photon frequency and wavelength, respectively.

1.1.9. Radiation quantities and units

The most important radiation quantities and their units are listed in Table 1.3. Also listed are the definitions of the various quantities and the relationships between the old and the SI units for these quantities.

1.2. ATOMIC AND NUCLEAR STRUCTURE

1.2.1. Basic definitions for atomic structure

The constituent particles forming an atom are protons, neutrons and electrons. Protons and neutrons are known as nucleons and form the nucleus of the atom.

● Atomic number Z: number of protons and number of electrons in an atom.
● Atomic mass number A: number of nucleons in an atom (i.e. number of protons Z plus number of neutrons N in an atom: $A = Z + N$).
● There is no basic relation between A and Z, but the empirical relationship

$$Z = \frac{A}{1.98 + 0.0155 A^{2/3}} \tag{1.14}$$

furnishes a good approximation for stable nuclei.
● Atomic mass M: expressed in atomic mass units u, where 1 u is equal to 1/12 of the mass of the ^{12}C atom or 931.5 MeV/c^2. The atomic mass M is smaller than the sum of the individual masses of constituent particles because of the intrinsic energy associated with binding the particles (nucleons) within the nucleus.
● Atomic g-atom (gram-atom): number of grams that correspond to N_A atoms of an element, where $N_A = 6.022 \times 10^{23}$ atoms/g-atom (Avogadro's number). The atomic mass numbers of all elements are defined such that A grams of every element contain exactly N_A atoms. For example: 1 g-atom of ^{60}Co is 60 g of ^{60}Co. In 60 g of ^{60}Co (1 g-atom) there is Avogadro's number of ^{60}Co atoms.

TABLE 1.3. RADIATION QUANTITIES, UNITS AND CONVERSION BETWEEN OLD AND SI UNITS

Quantity	Definition	SI unit	Old unit	Conversion
Exposure (X)	$X = \dfrac{\Delta Q}{\Delta m_{air}}$	$2.58 \times \dfrac{10^{-4}\,C}{kg\ air}$	$R = \dfrac{1\ esu}{cm^3\ air_{STP}}$	$1\ R = 2.58 \times \dfrac{10^{-4}\,C}{kg\ air}$
Dose (D)	$D = \dfrac{\Delta E_{ab}}{\Delta m}$	$1\ Gy = 1\dfrac{J}{kg}$	$1\ rad = 100\dfrac{erg}{g}$	$1\ Gy = 100\ rad$
Equivalent dose (H)	$H = Dw_R$	$1\ Sv$	$1\ rem$	$1\ Sv = 100\ rem$
Activity $(\mathcal{A})$	$\mathcal{A} = \lambda N$	$1\ Bq = 1\ s^{-1}$	$1\ Ci = 3.7 \times 10^{10}\ s^{-1}$	$1\ Bq = \dfrac{1\ Ci}{3.7 \times 10^{10}}$

ΔQ is the charge of either sign collected;
Δm_{air} is the mass of air;
ΔE_{ab} is the absorbed energy;
Δm is the mass of medium;
w_R is the radiation weighing factor;
λ is the decay constant;
N is the number of radioactive atoms;
R   stands for roentgen;
Gy   stands for gray;
Sv   stands for sievert;
Bq   stands for becquerel;
Ci   stands for curie;
STP   stands for standard temperature (273.2 K) and standard pressure (101.3 kPa).

● Number of atoms N_a per mass of an element:

$$\frac{N_a}{m} = \frac{N_A}{A}$$

● Number of electrons per volume of an element:

$$Z\ \frac{N_a}{V} = \rho Z \frac{N_a}{m} = \rho Z \frac{N_A}{A}$$

● Number of electrons per mass of an element:

$$Z \frac{N_a}{m} = \frac{Z}{A} N_A$$

Note that $(Z/A) \approx 0.5$ for all elements, with the one notable exception of hydrogen, for which $(Z/A) = 1$. Actually, (Z/A) slowly decreases from 0.5 for low Z elements to 0.4 for high Z elements.
● In nuclear physics the convention is to designate a nucleus X as $^A_Z X$, where A is the atomic mass number and Z is the atomic number; for example, the ^{60}Co nucleus is identified as $^{60}_{27}$Co, the ^{226}Ra nucleus as $^{226}_{88}$Ra.
● In ion physics the convention is to designate ions with + or – superscripts. For example, $^4_2 He^+$ stands for a singly ionized ^{4}He atom and $^4_2 He^{2+}$ stands for a doubly ionized ^{4}He atom, which is the α particle.
● If we assume that the mass of a molecule is equal to the sum of the masses of the atoms that make up the molecule, then for any molecular compound there are N_A molecules per g-mole of the compound, where the g-mole (gram-mole or mole) in grams is defined as the sum of the atomic mass numbers of the atoms making up the molecule; for example, a g-mole of water is 18 g of water and a g-mole of CO_2 is 44 g of CO_2. Thus 18 g of water or 44 g of carbon dioxide contain exactly N_A molecules (or $3N_A$ atoms, since each molecule of water and carbon dioxide contains three atoms).

1.2.2. Rutherford's model of the atom

The model is based on the results of an experiment carried out by Geiger and Marsden in 1909 with α particles scattered on thin gold foils. The experiment tested the validity of the Thomson atomic model, which postulated that the positive charges and negative electrons were uniformly distributed over the spherical atomic volume, the radius of which was of the order of a few ångström. Theoretical calculations predict that the probability for an α particle to be scattered on such an atom with a scattering angle exceeding 90° is of the order of 10^{-3500}, while the Geiger–Marsden experiment showed that approximately 1 in 10^4 α particles was scattered with a scattering angle $\theta > 90°$ (probability 10^{-4}).

From the findings of the Geiger–Marsden experiment, Rutherford in 1911 concluded that the positive charge and most of the mass of the atom are concentrated in the atomic nucleus (diameter a few femtometres) and negative electrons are smeared over on the periphery of the atom (diameter a few ångströms).

In α particle scattering the positively charged α particle has a repulsive Coulomb interaction with the more massive and positively charged nucleus.

The interaction produces a hyperbolic trajectory of the α particle, and the scattering angle θ is a function of the impact parameter b. The limiting case is a direct hit with $b = 0$ and $\theta = \pi$ (backscattering) that, assuming conservation of energy, determines the distance of closest approach $D_{\alpha\text{–N}}$ in the backscattering interaction:

$$E_K(\alpha) = \frac{z_\alpha Z_N e^2}{4\pi\varepsilon_0 D_{\alpha\text{–N}}} \quad \Rightarrow \quad D_{\alpha\text{–N}} = \frac{z_\alpha Z_N e^2}{4\pi\varepsilon_0 E_K(\alpha)} \tag{1.15}$$

where

z_α is the atomic number of the α particle;
Z_N is the atomic number of the scattering material;
$E_K(\alpha)$ is the initial kinetic energy of the α particle.

The repulsive Coulomb force between the α particle (charge $+2e$) and the nucleus (charge $+Ze$) is governed by $1/r^2$ as follows:

$$F_{Coul} = \frac{2Ze^2}{4\pi\varepsilon_0 r^2} \tag{1.16}$$

resulting in the following b versus θ relationship:

$$b = \frac{1}{2} D_{\alpha\text{–N}} \cot\frac{\theta}{2} \tag{1.17}$$

The differential Rutherford scattering cross-section is then expressed as follows:

$$\left(\frac{d\sigma}{d\Omega}\right)_R = \left(\frac{D_{\alpha\text{–N}}}{4}\right)^2 \frac{1}{\sin^4(\theta/2)} \tag{1.18}$$

1.2.3. Bohr's model of the hydrogen atom

Bohr expanded Rutherford's atomic model in 1913 and based it on four postulates that combine classical, non-relativistic mechanics with the concept of angular momentum quantization. Bohr's model successfully deals with one-electron entities such as the hydrogen atom, singly ionized helium atom, doubly ionized lithium atom, etc.

The four Bohr postulates are as follows:

- Postulate 1: Electrons revolve about the Rutherford nucleus in well defined, allowed orbits (shells). The Coulomb force of attraction $F_{Coul} = Ze^2/(4\pi\varepsilon_0 r^2)$ between the negative electrons and the positively charged nucleus is balanced by the centrifugal force $F_{cent} = m_e v^2/r$, where Z is the number of protons in the nucleus (atomic number), r is the radius of the orbit, m_e is the electron mass and v is the velocity of the electron in the orbit.
- Postulate 2: While in orbit, the electron does not lose any energy despite being constantly accelerated (this postulate is in contravention of the basic law of nature, which is that an accelerated charged particle will lose part of its energy in the form of radiation).
- Postulate 3: The angular momentum $L = m_e vr$ of the electron in an allowed orbit is quantized and given as $L=n\hbar$, where n is an integer referred to as the principal quantum number and $\hbar = h/(2\pi)$, where h is Planck's constant. The simple quantization of angular momentum stipulates that the angular momentum can have only integral multiples of a basic value ($\hbar$).
- Postulate 4: An atom or ion emits radiation when an electron makes a transition from an initial orbit with quantum number n_i to a final orbit with quantum number n_f for $n_i > n_f$.

The radius r_n of a one-electron Bohr atom is given by:

$$r_n = a_0 \left(\frac{n^2}{Z} \right) = 0.529 \text{ Å} \left(\frac{n^2}{Z} \right) \tag{1.19}$$

where a_0 is the Bohr radius ($a_0 = 0.529$ Å).

The velocity v_n of the electron in a one-electron Bohr atom is:

$$v_n = \alpha c \left(\frac{Z}{n} \right) = \frac{c}{137} \left(\frac{Z}{n} \right) \tag{1.20}$$

where α is the fine structure constant ($\alpha = 1/137$).

The energy levels for orbital electron shells in monoelectronic atoms (e.g. hydrogen, singly ionized helium and doubly ionized lithium) are given by:

$$E_n = -E_R \left(\frac{Z}{n} \right)^2 = -13.6 \text{ eV} \left(\frac{Z}{n} \right)^2 \tag{1.21}$$

where

E_R is the Rydberg energy (13.61 eV);
n is the principal quantum number ($n = 1$, ground state; $n > 1$, excited state);
Z is the atomic number ($Z = 1$ for a hydrogen atom, $Z = 2$ for singly ionized helium, $Z = 3$ for doubly ionized lithium, etc.).

The wave number k of the emitted photon is given by:

$$k = \frac{1}{\lambda} = R_\infty Z^2 \left(\frac{1}{n_f^2} - \frac{1}{n_i^2} \right) = 109\ 737\ \text{cm}^{-1} Z^2 \left(\frac{1}{n_f^2} - \frac{1}{n_i^2} \right) \tag{1.22}$$

where R_∞ is the Rydberg constant.

Bohr's model results in the energy level diagram for the hydrogen atom shown in Fig. 1.2.

1.2.4. Multielectron atoms

For multielectron atoms the fundamental concepts of the Bohr atomic theory provide qualitative data for orbital electron binding energies and electron transitions resulting in emission of photons. Electrons occupy allowed shells, but the number of electrons per shell is limited to $2n^2$, where n is the shell number (the principal quantum number).

- The K shell binding energies $E_B(K)$ for atoms with $Z > 20$ may be estimated with the following relationship:

$$E_B(K) = E_R Z_{eff}^2 = E_R (Z - s)^2 = E_R (Z - 2)^2 \tag{1.23}$$

where Z_{eff}, the effective atomic number, is given by $Z_{eff} = Z - s$, where s is the screening constant equal to 2 for K shell electrons.
- Excitation of an atom occurs when an electron is moved from a given shell to a higher n shell that is either empty or does not contain a full complement of electrons.
- Ionization of an atom occurs when an electron is removed from the atom (i.e. the electron is supplied with enough energy to overcome its binding energy in a shell).
- Excitation and ionization processes occur in an atom through various possible interactions in which orbital electrons are supplied with a given amount of energy. Some of these interactions are: (i) Coulomb
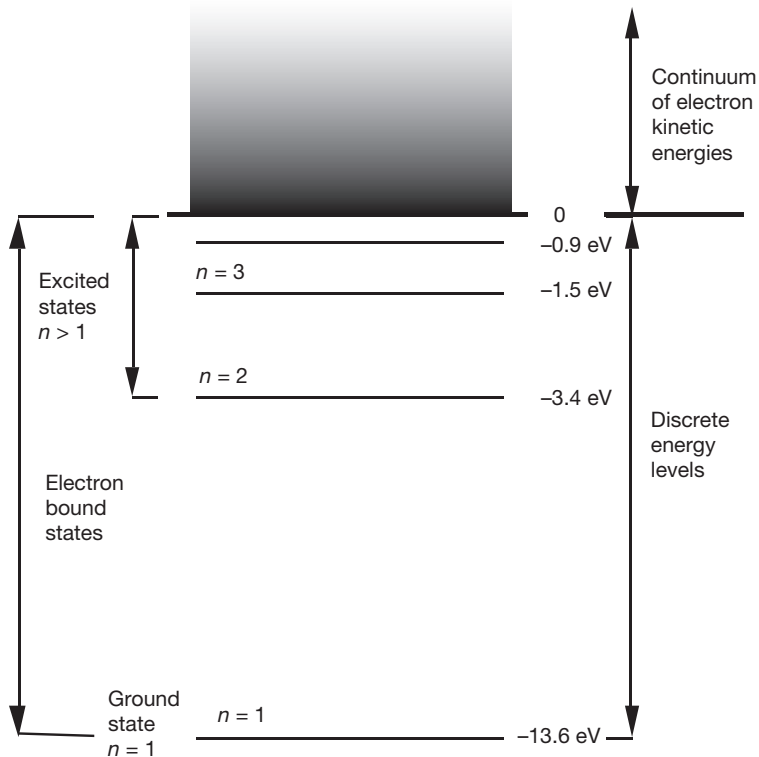
FIG. 1.2. Energy level diagram for a hydrogen atom (ground state: n = 1, excited states: n > 1).

interaction with a charged particle; (ii) the photoelectric effect; (iii) the Compton effect; (iv) triplet production; (v) internal conversion; (vi) electron capture; (vii) the Auger effect; and (viii) positron annihilation.

- An orbital electron from a higher n shell will fill an electron vacancy in a lower n atomic shell. The energy difference between the two shells will be either emitted in the form of a characteristic photon or it will be transferred to a higher n shell electron, which will be ejected from the atom as an Auger electron.
- Energy level diagrams of multielectron atoms resemble those of one-electron structures, except that inner shell electrons are bound with much larger energies, as shown for a lead atom in Fig. 1.3.
- The number of characteristic photons (sometimes called fluorescent photons) emitted per orbital electron shell vacancy is referred to as fluorescent yield ω, while the number of Auger electrons emitted per orbital

electron vacancy is equal to $(1 - \omega)$. The fluorescent yield depends on the atomic number Z of the atom and on the principal quantum number of a shell. For atoms with $Z < 10$ the fluorescent yield $\omega_K = 0$; for $Z \approx 30$ the fluorescent yield $\omega_K \approx 0.5$; and for high atomic number atoms $\omega_K = 0.96$, where ω_K refers to the fluorescent yield for the K shell (see Fig. 1.9).

1.2.5. Nuclear structure

Most of the atomic mass is concentrated in the atomic nucleus consisting of Z protons and $(A - Z)$ neutrons, where Z is the atomic number and A is the atomic mass number of a given nucleus.
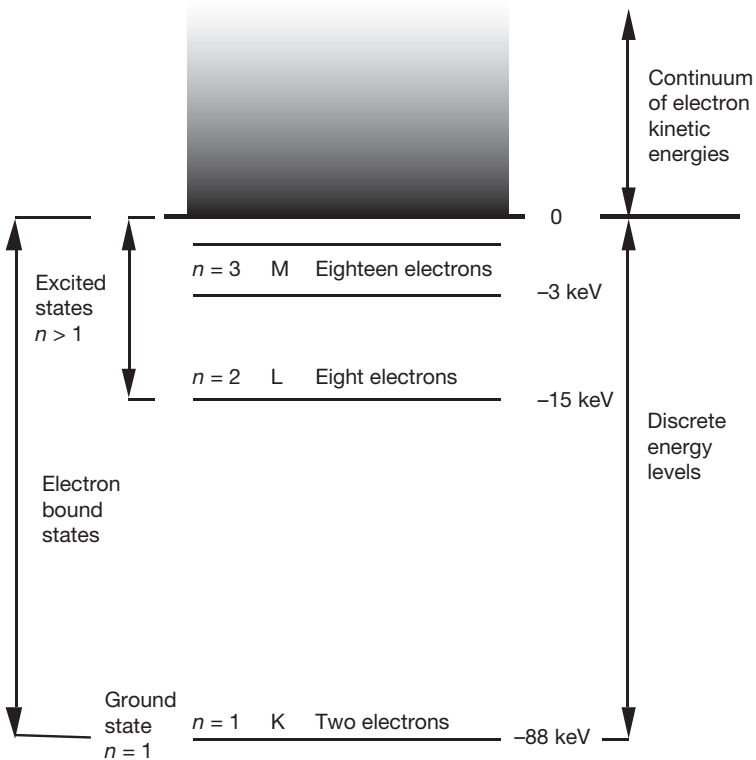
FIG. 1.3. Energy level diagram for a multielectron atom (lead). The n = 1, 2, 3, 4… shells are referred to as the K, L, M, O… shells, respectively. Electronic transitions that end in low n shells are referred to as X ray transitions because the resulting photons are in the X ray energy range. Electronic transitions that end in high n shells are referred to as optical transitions because they result in ultraviolet, visible or infrared photons.

- The radius r of the nucleus is estimated from:

$$r = r_0 \sqrt[3]{A} \tag{1.24}$$

where r_0 is a constant (~1.4 fm) assumed equal to ½ of r_e, the classical electron radius.

- Protons and neutrons are commonly referred to as nucleons and are bound in the nucleus with the strong force. In contrast to electrostatic and gravitational forces, which are inversely proportional to the square of the distance between two particles, the strong force between two nucleons is a very short range force, active only at distances of the order of a few femtometres. At these short distances the strong force is the predominant force, exceeding other forces by several orders of magnitude.

- The binding energy E_B per nucleon in a nucleus varies slowly with the number of nucleons A, is of the order of ~8 MeV/nucleon and exhibits a broad maximum of 8.7 MeV/nucleon at $A \approx 60$. For a given nucleus it may be calculated from the energy equivalent of mass deficit Δm as follows:

$$\frac{E_B}{\text{nucleon}} = \Delta m c^2 / A = [Z m_p c^2 + (A - Z) m_n c^2 - M c^2]/A \tag{1.25}$$

where

M is the nuclear mass in atomic mass units u (note that $uc^2 = 931.5$ MeV);

$m_p c^2$ is the proton rest energy;

$m_n c^2$ is the neutron rest energy.

1.2.6. Nuclear reactions

Much of the present knowledge of the structure of nuclei comes from experiments in which a particular nuclide A is bombarded with a projectile a. The projectile undergoes one of three possible interactions: (i) elastic scattering (no energy transfer occurs; however, the projectile changes trajectory); (ii) inelastic scattering (the projectile enters the nucleus and is re-emitted with less energy and in a different direction); or (iii) nuclear reaction (the projectile a enters the nucleus A, which is transformed into nucleus B and a different particle b is emitted).

- Nuclear reactions are designated as follows:

$$a + A \rightarrow B + b \quad \text{or} \quad A(a, b)B \tag{1.26}$$

- A number of physical quantities are rigorously conserved in all nuclear reactions. The most important of these quantities are charge, mass number, linear momentum and mass–energy.
- The threshold energy for a nuclear reaction is defined as the smallest value of a projectile's kinetic energy at which a nuclear reaction can take place. The threshold kinetic energy $E_K^{thr}(a)$ of projectile a is derived from relativistic conservation of energy and momentum as:

$$E_K^{thr}(a) = \frac{(m_B c^2 + m_b c^2)^2 - (m_A c^2 + m_a c^2)^2}{2 m_A c^2} \tag{1.27}$$

where m_A, m_a, m_B and m_b are the rest masses of the target A, projectile a and products B and b, respectively.

1.2.7. Radioactivity

Radioactivity is characterized by a transformation of an unstable nucleus into a more stable entity that may be unstable and will decay further through a chain of decays until a stable nuclear configuration is reached. The exponential laws that govern the decay and growth of radioactive substances were first formulated by Rutherford and Soddy in 1902 and then refined by Bateman in 1910.

- The activity $\mathcal{A}(t)$ of a radioactive substance at time t is defined as the product of the decay constant λ and the number of radioactive nuclei $N(t)$:

$$\mathcal{A}(t) = \lambda N(t) \tag{1.28}$$

- The simplest radioactive decay is characterized by a radioactive parent nucleus P decaying with a decay constant λ_P into a stable daughter nucleus D:

$$P \xrightarrow{\lambda_P} D \tag{1.29}$$

— The number of radioactive parent nuclei $N_P(t)$ as a function of time t is governed by the following relationship:

$$N_P(t) = N_P(0)e^{-\lambda_P t} \tag{1.30}$$

where $N_P(0)$ is the initial number of parent nuclei at time $t = 0$.

— Similarly, the activity of parent nuclei $\mathcal{A}_P(t)$ at time t is given as:

$$\mathcal{A}_P(t) = \mathcal{A}_P(0)e^{-\lambda_P t} \tag{1.31}$$

where $\mathcal{A}_P(0)$ is the initial activity of parent nuclei at time $t = 0$.

● The half-life $t_{1/2}$ of a radioactive substance is the time during which the number of radioactive nuclei decays to half of the initial value $N_P(0)$ present at time $t = 0$:

$$N_P(t = t_{1/2}) = (1/2)N_P(0) = N_P(0)e^{-\lambda_P t_{1/2}} \tag{1.32}$$

● The decay constant λ_P and half-life $(t_{1/2})_P$ for the parent are thus related as follows:

$$\lambda_P = \frac{\ln 2}{t_{1/2}} \tag{1.33}$$

● The specific activity a is defined as the parent's activity per unit mass:

$$a = \frac{\mathcal{A}_P}{m} = \frac{\lambda_P N}{m} = \lambda_P \frac{N_A}{A_P} = \frac{N_A \ln 2}{A_P \ (t_{1/2})_P} \tag{1.34}$$

where N_A is Avogadro's number and A_P is the parent's atomic mass number.

● The average (mean) life τ_P of a radioactive substance represents the average life expectancy of all parent radioactive atoms in the substance at time $t = 0$:

$$\mathcal{A}_P(0)\tau_P = \int_0^\infty \mathcal{A}_P(0)e^{-\lambda_P t} dt = \frac{\mathcal{A}_P(0)}{\lambda_P} \tag{1.35}$$

● The decay constant λ_P and average life τ_P are thus related as follows:

$$\lambda_P = 1/\tau_P \tag{1.36}$$

resulting in the following relationship between $(t_{1/2})_P$ and τ_P:

$$(t_{1/2})_P = \tau_P \ln 2 \tag{1.37}$$

● A more complicated radioactive decay occurs when a radioactive parent nucleus P decays with a decay constant λ_P into a daughter nucleus D which in turn is radioactive and decays with a decay constant λ_D into a stable granddaughter G:

$$P \overset{\lambda_P}{\rightarrow} D \overset{\lambda_D}{\rightarrow} G \tag{1.38}$$

— The activity of the daughter $\mathcal{A}_D(t)$ may then be expressed as:

$$\mathcal{A}_D(t) = \frac{\lambda_D}{\lambda_D - \lambda_P} \mathcal{A}_P(0)(e^{-\lambda_P t} - e^{-\lambda_D t}) \tag{1.39}$$

where $\mathcal{A}_P(0)$ is the initial activity of the parent nuclei present at time $t = 0$ (i.e. $\mathcal{A}_P(0) = \lambda_P N_P(0)$, where $N_P(0)$ is the number of parent nuclei at $t = 0$).

— The maximum activity of daughter nuclei occurs at time t_{max} given by:

$$t_{max} = \frac{\ln(\lambda_D/\lambda_P)}{\lambda_D - \lambda_P} \tag{1.40}$$

under the condition that $N_D = 0$ at time $t = 0$.

● Special considerations in parent → daughter → granddaughter relationships:

— For $\lambda_D < \lambda_P$ or $(t_{1/2})_D > (t_{1/2})_P$ we obtain the following general relationship:

$$\frac{\mathcal{A}_D}{\mathcal{A}_P} = \frac{\lambda_D}{\lambda_D - \lambda_P}[1 - e^{-(\lambda_D - \lambda_P)t}] \tag{1.41}$$

— For $\lambda_D > \lambda_P$ or $(t_{1/2})_D < (t_{1/2})_P$ we obtain transient equilibrium with:

$$\frac{\mathcal{A}_D}{\mathcal{A}_P} = \frac{\lambda_D}{\lambda_D - \lambda_P} \quad \text{for} \quad t \gg t_{max} \tag{1.42}$$

— For $\lambda_D \gg \lambda_P$ or $(t_{1/2})_D \ll (t_{1/2})_P$ we obtain secular equilibrium and

$$\mathcal{A}_D/\mathcal{A}_P \approx 1 \tag{1.43}$$

1.2.8.   Activation of nuclides

Activation of nuclides occurs when a stable parent isotope P is bombarded with neutrons in a nuclear reactor and transforms into a radioactive daughter D that decays into a granddaughter G:

$$P \quad \overset{\sigma\phi}{\rightarrow} \quad D \quad \overset{\lambda_D}{\rightarrow} \quad G \tag{1.44}$$

The probability for activation is determined by the cross-section σ for the nuclear reaction, usually expressed in barns per atom, where 1 barn = 10^{-24} cm^2.

- Activity of the daughter $\mathcal{A}_D(t)$ is expressed as:

$$\mathcal{A}_D(t) = \frac{\sigma\phi\lambda_D}{\lambda_D - \sigma\phi} N_P(0)(e^{-\sigma\phi t} - e^{-\lambda_D t}) \tag{1.45}$$

  where $N_P(0)$ is the initial number of parent nuclei.
- This result is similar to the $P \rightarrow D \rightarrow G$ relationship above (Eq. (1.39)) in which an unstable parent P decays into an unstable daughter D that in turn decays into granddaughter G. However, the decay constant λ_P in the $P \rightarrow D \rightarrow G$ decay relationship is replaced by $\sigma\phi$, where σ is the cross-section for activation of the parent nuclei (cm^2/atom) and ϕ is the fluence rate of neutrons in the reactor (cm$^{-2}\cdot$s^{-1}).
- The time t_{max} at which the maximum activity $\mathcal{A}_D$ occurs in the activation process is then, similarly to Eq. (1.40), given by:

$$t_{max} = \frac{\ln\dfrac{\lambda_D}{\sigma\phi}}{\lambda_D - \sigma\phi} \tag{1.46}$$

- In situations where $\sigma\phi \ll \lambda_D$, the daughter activity relationship of Eq. (1.45) transforms into a simple exponential growth relationship:

$$\mathcal{A}_D(t) = \sigma\phi N_P(0)(1 - e^{-\lambda_D t}) \tag{1.47}$$

- An important example of nuclear activation is the production of the ^{60}Co isotope by bombarding ^{59}Co with thermal neutrons in a nuclear reactor:

$$^{59}_{27}\text{Co} + \text{n} \quad \rightarrow \quad ^{60}_{27}\text{Co} + \gamma \tag{1.48}$$

or in shorthand notation $^{59}_{27}\text{Co}(n, \gamma)^{60}_{27}\text{Co}$, with an activation cross-section σ of 37×10^{-24} cm^2/atom (37 barn/atom with 1 barn = 10^{-24} cm^2) and typical reactor neutron fluence rates ϕ of the order of 10^{13} cm$^{-2} \cdot$s^{-1}.

1.2.9. Modes of radioactive decay

A radioactive parent X with atomic number Z and atomic mass number A decays into a daughter Y through the following possible modes of decay: α, β^-, β^+, electron capture γ and internal conversion.

α decay:

$$^A_Z\text{X} \rightarrow {}^{A-4}_{Z-2}\text{Y} + {}^4_2\text{He}(\alpha) \tag{1.49}$$

where $^4_2\text{He}(\alpha)$ is a ^{4}He nucleus referred to as an α particle. An example of α decay is the decay of ^{226}Ra into ^{222}Rn with a half-life of 1600 years:

$$^{226}_{88}\text{Ra} \rightarrow {}^{222}_{86}\text{Rn} + {}^4_2\text{He} \tag{1.50}$$

β^- decay:

$$^A_Z\text{X} \rightarrow {}^A_{Z+1}\text{Y} + \beta^- + \bar{\nu}_e \tag{1.51}$$

A neutron transforms into a proton, and an electron β^- and antineutrino $\bar{\nu}_e$, sharing the available energy, are ejected from the nucleus. An example of β^- decay is the decay of ^{60}Co nuclei into excited ^{60}Ni nuclei with a half-life of 5.26 years:

$$^{60}_{27}\text{Co} \rightarrow {}^{60}_{28}\text{Ni}^* + \beta^- + \bar{\nu}_e \tag{1.52}$$

β^+ decay:

$$^A_Z\text{X} \rightarrow {}^A_{Z-1}\text{Y} + \beta^+ + \nu_e \tag{1.53}$$

A proton transforms into a neutron, and a positron β^+ and neutrino ν_e, sharing the available energy, are ejected from the nucleus. An example of β^+ decay is the decay of ^{13}N into ^{13}C:

$$^{13}_7\text{N} \rightarrow {}^{13}_6\text{C} + \beta^+ + \nu_e \tag{1.54}$$

Electron capture:

$$_Z^A X + e_K^- \rightarrow _{Z-1}^A Y + \nu_e \qquad (1.55)$$

The nucleus captures one of its own K shell orbital electrons, a proton transforms into a neutron and a neutrino ν_e is ejected. An example of electron capture is the decay of ^{125}I into ^{125}Te in an excited state, which decays to the ^{125}Te ground state through γ decay and internal conversion:

$$_{53}^{125} I + e_K^- \rightarrow _{52}^{125} Te^* + \nu_e \qquad (1.56)$$

The resulting K shell vacancy is filled with a higher level orbital electron and the transition energy is emitted from the atom in the form of characteristic photons or Auger electrons.

γ decay:

$$_Z^A X^* \rightarrow _Z^A X + \gamma \qquad (1.57)$$

An excited nucleus $_Z^A X^*$, generally produced through β^- or β^+ decay, attains its ground state $_Z^A X$ through emission of one or several γ photons. An example of γ decay is the transition of the excited $_{28}^{60} Ni^*$, resulting from the β^- decay of ^{60}Co, into stable $_{28}^{60}$Ni through an emission of two γ rays with energies of 1.17 and 1.33 MeV.

Internal conversion:

$$_Z^A X^* \rightarrow _Z^A X + e_K^- \qquad (1.58)$$

Rather than being emitted as a γ photon, the nuclear excitation energy may be transferred to a K shell orbital electron that is ejected with a kinetic energy equal to the excitation energy less the orbital electron binding energy. The resulting K shell vacancy is filled with a higher level orbital electron and the transition energy is emitted in the form of characteristic photons or Auger electrons. An example of internal conversion is the decay of excited ^{125}Te, which results from an electron capture decay of ^{125}I, into stable ^{125}Te through emission of 35 keV γ rays (7%) and internal conversion electrons (93%).

1.3. ELECTRON INTERACTIONS

As an energetic electron traverses matter, it interacts with matter through Coulomb interactions with atomic orbital electrons and atomic nuclei. Through these collisions the electrons may lose their kinetic energy (collision and radiative losses) or change their direction of travel (scattering). Energy losses are described by stopping power; scattering is described by scattering power.

The collisions between the incident electron and an orbital electron or nucleus of an atom may be elastic or inelastic. In an elastic collision the electron is deflected from its original path but no energy loss occurs, while in an inelastic collision the electron is deflected from its original path and some of its energy is transferred to an orbital electron or emitted in the form of bremsstrahlung. Energetic electrons experience thousands of collisions as they traverse an absorber, hence their behaviour is described by a statistical theory of multiple scattering embracing the individual elastic and inelastic collisions with orbital electrons and nuclei.

The type of interaction that the electron undergoes with a particular atom of radius a depends on the impact parameter b of the interaction, defined as the perpendicular distance between the electron direction before the interaction and the atomic nucleus (see Fig. 1.4).
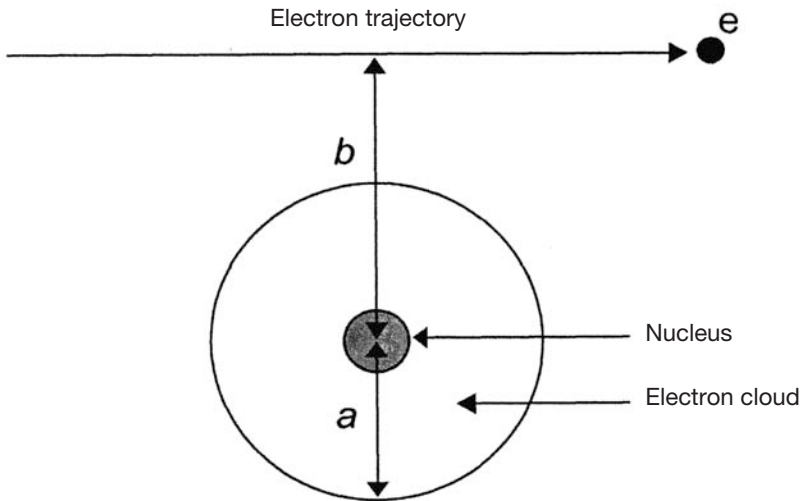
FIG. 1.4. Interaction of an electron with an atom, where a is the atomic radius and b is the impact parameter.

- For $b \gg a$ the electron will undergo a soft collision with the whole atom and only a small amount of energy will be transferred from the incident electron to orbital electrons.
- For $b \approx a$ the electron will undergo a hard collision with an orbital electron and an appreciable fraction of the electron's kinetic energy will be transferred to the orbital electron.
- For $b \ll a$ the incident electron undergoes a radiative interaction (collision) with the atomic nucleus. The electron will emit a photon (bremsstrahlung) with energy between zero and the incident electron kinetic energy. The energy of the emitted bremsstrahlung photon depends on the magnitude of the impact parameter b; the smaller the impact parameter, the higher the energy of the bremsstrahlung photon.

1.3.1. Electron–orbital electron interactions

- Coulomb interactions between the incident electron and orbital electrons of an absorber result in ionizations and excitations of absorber atoms:
  - Ionization: ejection of an orbital electron from the absorber atom;
  - Excitation: transfer of an orbital electron of the absorber atom from an allowed orbit to a higher allowed orbit (shell).
- Atomic excitations and ionizations result in collisional energy losses and are characterized by collision (ionization) stopping powers.

1.3.2. Electron–nucleus interactions

- Coulomb interactions between the incident electron and nuclei of the absorber atom result in electron scattering and energy loss of the electron through production of X ray photons (bremsstrahlung). These types of energy loss are characterized by radiative stopping powers.
- Bremsstrahlung production is governed by the Larmor relationship, which states that the power P emitted in the form of photons from an accelerated charged particle is proportional to the square of the particle acceleration a and the square of the particle charge q, or:

$$P = \frac{q^2 a^2}{6\pi\varepsilon_0 c^3} \tag{1.59}$$

- The angular distribution of the emitted photons (bremsstrahlung) is proportional to $\sin^2\theta/(1 - \beta\cos\theta)^5$, where θ is the angle between the acceleration of the charged particle and a unit vector connecting the charge with the point of observation and β is the standard relativistic v/c.

- At small velocities υ of the charged particle ($\beta \rightarrow 0$) the angular distribution goes as $\sin^2 \theta$ and exhibits a maximum at $\theta = 90°$. However, as the velocity of the charged particle increases from 0 towards c, the angular distribution of the emitted photons becomes increasingly more forward peaked.
- The angle at which the photon emission intensity is maximum can be calculated from the following relationship:

$$\theta_{max} = \arccos\left[\frac{1}{3\beta}(\sqrt{1+15\beta^2} - 1)\right] \tag{1.60}$$

that for $\beta \rightarrow 0$ gives $\theta_{max} = \pi/2$ and for $\beta \rightarrow 1$ gives $\theta_{max} = 0$, indicating that in the diagnostic radiology energy range (orthovoltage beams) most X ray photons are emitted at $90°$ to the electron path, while in the megavoltage range (linac beams) most photons are emitted in the direction of the electron beam striking the target.
- The energy loss by radiation and the radiative yield g increase directly with the absorber atomic number Z and the kinetic energy of electrons. The radiation yield for X ray targets in the diagnostic radiology energy range (~100 keV) is of the order of 1%, while in the megavoltage energy range it amounts to 10–20%.

1.3.3. Stopping power

The inelastic energy losses by an electron moving through a medium with density ρ are described by the total mass–energy stopping power $(S/\rho)_{tot}$, which represents the kinetic energy E_K loss by the electron per unit path length x, or:

$$(S/\rho)_{tot} = \frac{1}{\rho}\frac{dE_K}{dx} \quad (\text{MeV·cm}^2/\text{g}) \tag{1.61}$$

$(S/\rho)_{tot}$ consists of two components: the mass collision stopping power $(S/\rho)_{col}$, resulting from electron–orbital electron interactions (atomic excitations and ionizations), and the mass radiative stopping power $(S/\rho)_{rad}$, resulting from electron–nucleus interactions (bremsstrahlung production):

$$(S/\rho)_{tot} = (S/\rho)_{col} + (S/\rho)_{rad} \tag{1.62}$$

- $(S/\rho)_{col}$ has an important role in radiation dosimetry, since the dose D in the medium may be expressed as:

$$D = \phi(S/\rho)_{\text{col}} \qquad (1.63)$$

where ϕ is the fluence of electrons.

- $(S/\rho)_{\text{tot}}$ is used in the calculation of electron range R as follows:

$$R = \int_0^{E_{\text{Ki}}} \left(\frac{S}{\rho}(E_{\text{K}}) \right)_{\text{tot}}^{-1} dE_{\text{K}} \qquad (1.64)$$

where E_{ki} is the initial kinetic energy of the electron.

- Both $(S/\rho)_{\text{rad}}$ and $(S/\rho)_{\text{tot}}$ are used in the determination of radiation yield (also referred to as bremsstrahlung efficiency) Y as:

$$Y = \frac{1}{E_{\text{Ki}}} \int_0^{E_{\text{Ki}}} \frac{(S/\rho)_{\text{rad}}}{(S/\rho)_{\text{tot}}} \, dE_{\text{K}} \qquad (1.65)$$

- The stopping power focuses on the energy loss by an electron moving through a medium. When attention is focused on the absorbing medium, one is interested in the linear rate of energy absorption by the absorbing medium as the electron traverses the medium. The rate of energy absorption, called the linear energy transfer (LET), is defined as the average energy locally imparted to the absorbing medium by an electron of specified energy in traversing a given distance in the medium.

- In radiation dosimetry the concept of restricted stopping power (S_Δ/ρ) is introduced, which accounts for that fraction of the collisional stopping power $(S/\rho)_{\text{col}}$ that includes all the soft collisions plus those hard collisions that result in delta rays with energies less than a cut-off value Δ. In radiation dosimetry this cut-off energy is usually taken as 10 keV, an energy that allows an electron just to traverse an ionization chamber gap of 1 mm in air. Delta rays are defined as electrons that acquire sufficiently high kinetic energies through hard collisions so as to enable them to carry this energy a significant distance away from the track of the primary particle and produce their own ionizations of absorber atoms.

1.3.4. Mass scattering power

When a beam of electrons passes through an absorbing medium, the electrons undergo multiple scattering through Coulomb interactions between the incident electrons and nuclei of the absorber. The angular and spatial spread of a pencil electron beam can be approximated by a Gaussian distribution. The multiple scattering of electrons traversing a path length l through an absorbing medium is commonly described by the mean square angle of

scattering $\overline{\theta^2}$ that is proportional to the mass thickness ρl of the absorber. Analogously to the definition of stopping power, the International Commission on Radiation Units and Measurements (ICRU) defines the mass scattering power T/ρ as:

$$\frac{T}{\rho} = \frac{1}{\rho}\frac{\mathrm{d}\overline{\theta^2}}{\mathrm{d}l} \quad \text{or} \quad \frac{T}{\rho} = \frac{\overline{\theta^2}}{\rho l} \tag{1.66}$$

The scattering power varies approximately as the square of the absorber atomic number and inversely as the square of the electron kinetic energy.

1.4. PHOTON INTERACTIONS

1.4.1. Types of indirectly ionizing photon radiation

Depending on their origin, the indirectly ionizing photon radiations fall into one of the following four categories:

- Bremsstrahlung (continuous X rays), emitted through electron–nucleus interactions.
- Characteristic X rays (discrete), emitted in transitions of orbital electrons from one allowed orbit to a vacancy in another allowed orbit.
- γ rays (discrete), emitted through nuclear transitions in γ decay.
- Annihilation radiation (discrete, typically 0.511 MeV), emitted through positron–electron annihilation.

1.4.2. Photon beam attenuation

The intensity $I(x)$ of a narrow monoenergetic photon beam, attenuated by an attenuator of thickness x, is given as:

$$I(x) = I(0)e^{-\mu(h\nu, Z)x} \tag{1.67}$$

where

$I(0)$ is the original intensity of the unattenuated beam;
$\mu(h\nu, Z)$ is the linear attenuation coefficient, which depends on photon energy $h\nu$ and attenuator atomic number Z.

● The half-value layer (HVL or $x_{1/2}$) is defined as that thickness of the attenuator that attenuates the photon beam intensity to 50% of its original value:

$$x_{1/2} = \text{HVL} = (\ln 2)/\mu \qquad (1.68)$$

● Similarly, the tenth-value layer (TVL or $x_{1/10}$) is defined as that thickness of the attenuator that attenuates the photon beam intensity to 10% of its original value:

$$x_{1/10} = \text{TVL} = (\ln 10)/\mu \qquad (1.69)$$

● HVL and TVL are thus related as follows:

$$x_{1/10} = x_{1/2}\frac{\ln 10}{\ln 2} = 3.3x_{1/2} \qquad (1.70)$$

● The mass attenuation coefficient μ_m, atomic attenuation coefficient $_a\mu$ and electronic attenuation coefficient $_e\mu$ are proportional to the linear attenuation coefficient μ through the following relationships:

$$\mu = \rho\mu_m = \frac{\rho N_A}{A}\,_a\mu = \frac{\rho N_A Z}{A}\,_e\mu \qquad (1.71)$$

where ρ, Z and A are the density, atomic number and atomic mass number, respectively, of the attenuator.

● Typical units for the linear, mass, atomic and electronic attenuation coefficients are: cm^{-1}, cm^2/g, cm^2/atom and $\text{cm}^2/\text{electron}$, respectively, implying that thickness x in the exponent $(-\mu x)$ must be given in cm, g/cm^2, atoms/cm^2 and electrons/cm^2, respectively.

● For use in radiation dosimetry two additional attenuation coefficients are defined: the energy transfer coefficient μ_{tr} and the energy absorption coefficient μ_{ab} (often designated as μ_{en}). The two coefficients are related to μ as follows:

$$\mu_{tr} = \mu\frac{\bar{E}_{tr}}{h\nu} \qquad (1.72)$$

and

$$\mu_{ab} = \mu \frac{\bar{E}_{ab}}{h\nu} \tag{1.73}$$

where

$\bar{E}_{tr}$ is the average energy transferred to charged particles (electrons and positrons) in the attenuator;

$\bar{E}_{ab}$ is the average energy deposited by charged particles in the attenuator.

● The energy transfer coefficient μ_{tr} and the energy absorption coefficient μ_{ab} are related through the radiative fraction g as follows:

$$\mu_{ab} = \mu_{tr}(1 - g) \tag{1.74}$$

1.4.3. Types of photon interaction

Photons may undergo various possible interactions with the atoms of an attenuator; the probability or cross-section for each interaction depends on the energy $h\nu$ of the photon and on the atomic number Z of the attenuator.

● The photon interactions may be with a tightly bound electron (i.e. with an atom as a whole (photoelectric effect, coherent scattering)), with the field of the nucleus (pair production) or with an essentially free orbital electron (Compton effect, triplet production).
● In the context of photon interactions, a tightly bound electron is an orbital electron with a binding energy of the order of, or slightly larger than, the photon energy, while a free electron is an electron with a binding energy that is much smaller than the photon energy.
● During the interaction the photon may completely disappear (photo-electric effect, pair production, triplet production) or it may be scattered coherently (coherent scattering) or incoherently (Compton effect).

1.4.4. Photoelectric effect

In the photoelectric effect (sometimes referred to as the photoeffect) the photon interacts with a tightly bound orbital electron of an attenuator and disappears, while the orbital electron is ejected from the atom as a photo-electron with a kinetic energy E_K given as:

$$E_K = h\nu - E_B \tag{1.75}$$

where $h\nu$ is the incident photon energy and E_B is the binding energy of the electron.

- The atomic attenuation coefficient for the photoelectric effect $_a\tau$ is proportional to $Z^4/(h\nu)^3$, while the mass attenuation coefficient for the photoelectric effect τ_m is proportional to $(Z/h\nu)^3$, where Z is the atomic number of the attenuator and $h\nu$ is the photon energy.
- In addition to a steady decrease in τ_m with an increasing $h\nu$, the plot of τ_m versus $h\nu$ also shows sharp discontinuities in τ_m when $h\nu$ equals the binding energy for a particular electronic shell of the attenuator. These discontinuities, called absorption edges, reflect the fact that for $h\nu$ less than the binding energy photons cannot undergo the photoelectric effect with electrons in that particular shell, while for $h\nu$ greater than or equal to the binding energy they can.
- The average energy transferred from the photon with energy $h\nu > E_B(K)$ to electrons $(\bar{E}_K)_{tr}^{PE}$ in the photoelectric effect is given as follows:

$$(\bar{E}_K)_{tr}^{PE} = h\nu - P_K\,\omega_K E_B(K) \tag{1.76}$$

where $E_B(K)$ is the binding energy of the K shell orbital electron (photoelectron), P_K is the fraction of all photoelectric effect interactions that occur in the K shell and ω_K is the fluorescent yield for the K shell. The range of P_K is from 1.0 at low atomic numbers Z to 0.8 at high atomic numbers (see Fig. 1.9).

1.4.5. Coherent (Rayleigh) scattering

In coherent (Rayleigh) scattering the photon interacts with a bound orbital electron (i.e. with the combined action of the whole atom). The event is elastic in the sense that the photon loses essentially none of its energy and is scattered through only a small angle. Since no energy transfer occurs from the photon to charged particles, Rayleigh scattering plays no role in the energy transfer coefficient; however, it contributes to the attenuation coefficient.

- The atomic cross-section for Rayleigh scattering $_a\sigma_R$ is proportional to $(Z/h\nu)^2$ and the mass attenuation coefficient σ_R/ρ is proportional to $Z/(h\nu)^2$.
- In tissue and tissue equivalent materials the relative importance of Rayleigh scattering in comparison with other photon interactions is small, as it contributes only a few per cent or less to the total attenuation coefficient.

1.4.6. Compton effect (incoherent scattering)

The Compton effect (incoherent scattering) represents a photon interaction with an essentially 'free and stationary' orbital electron. The incident photon energy $h\nu$ is much larger than the binding energy of the orbital electron. The photon loses part of its energy to the recoil (Compton) electron and is scattered as photon $h\nu'$ through a scattering angle θ, as shown schematically in Fig. 1.5. Angle ϕ represents the angle between the incident photon direction and the direction of the recoil electron.

- The change in photon wavelength $\Delta\lambda$ is given by the well known Compton relationship:

$$\Delta\lambda = \lambda_C(1 - \cos\theta) \tag{1.77}$$

where λ_C is the Compton wavelength of the electron, expressed as:

$$\lambda_C = \frac{h}{m_e c} = 0.024 \text{ Å} \tag{1.78}$$

- The relationship for $\Delta\lambda$ is calculated from equations representing conservation of energy and momentum in the Compton process:

$$h\nu + m_e c^2 = h\nu' + m_e c^2 + E_K \tag{1.79}$$

$$\frac{h\nu}{c} = \frac{h\nu'}{c}\cos\theta + \frac{m_e\upsilon}{\sqrt{1-\left(\dfrac{\upsilon}{c}\right)^2}}\cos\phi \tag{1.80}$$

and

$$0 = \frac{h\nu'}{c}\sin\theta - \frac{m_e\upsilon}{\sqrt{1-\left(\dfrac{\upsilon}{c}\right)^2}}\sin\phi \tag{1.81}$$

where ε is the normalized incident photon energy:

$$\varepsilon = \frac{h\nu}{m_e c^2}$$
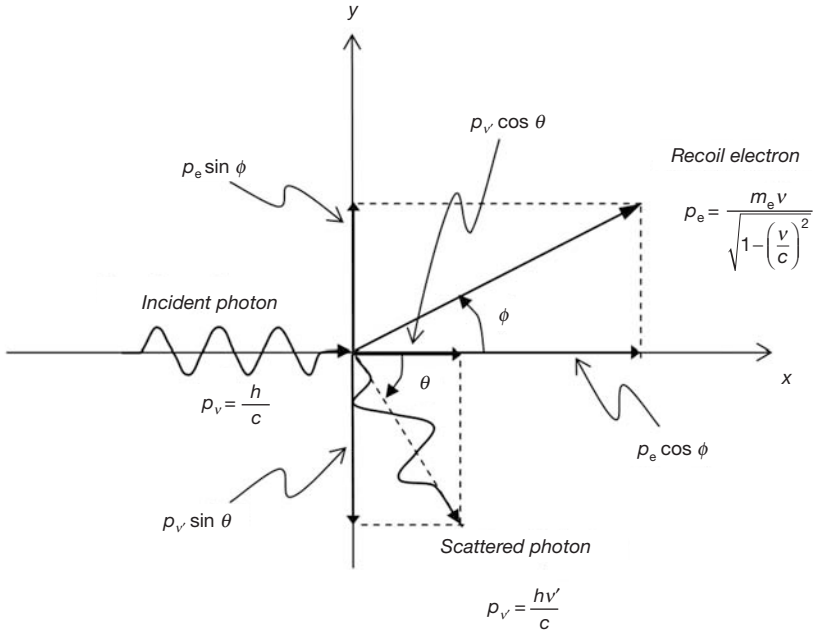
FIG. 1.5. Schematic diagram of Compton scattering. An incident photon with energy hv interacts with a loosely bound (essentially free) atomic electron. The electron is ejected from the atom as a recoil (Compton) electron with kinetic energy E_K and a scattered photon with energy hv' = hv − E_K is produced (see Eq. (1.79)).

and E_K is the kinetic energy of the recoil electron. Equation (1.79) represents conservation of energy; Eqs (1.80) and (1.81) represent conservation of momentum along the x axis and y axis, respectively, of Fig. 1.5.

● The scattering angle θ and the recoil electron angle ϕ are related through the following relationship:

$$\cot \phi = (1 + \varepsilon) \tan(\theta/2) \tag{1.82}$$

From Eq. (1.82) it is evident that the range of angle ϕ is between 0 for $\theta = \pi$ (photon backscattering) and $\pi/2$ for $\theta = 0$ (photon forward scattering) for any arbitrary photon energy. For a given θ, the higher the incident photon energy, the smaller is the recoil electron angle ϕ.

● The Compton interaction represents a photon interaction with an essentially free and stationary electron ($hv \gg E_B$). Consequently, the atomic Compton attenuation coefficient $_a\sigma_C$ depends linearly on the atomic

number Z of the attenuator, while $_e\sigma_C$ and σ_C/ρ, the electronic and mass Compton attenuation coefficients, respectively, are independent of Z.

- The electronic Compton attenuation coefficient $_e\sigma_C$ steadily decreases with $h\nu$ from a value of 0.665×10^{-24} cm^2/electron at low photon energies to 0.21×10^{-24} cm^2/electron at $h\nu = 1$ MeV; 0.051×10^{-24} cm^2/electron at $h\nu = 10$ MeV; and 0.008×10^{-24} cm^2/electron at $h\nu = 100$ MeV.

- The scattered photon energy $h\nu$ and the kinetic energy of the Compton electron E_K are given as follows:

$$h\nu' = h\nu \frac{1}{1+\varepsilon(1-\cos\theta)} \quad \text{and} \quad E_K = h\nu \frac{\varepsilon(1-\cos\theta)}{1+\varepsilon(1-\cos\theta)} \qquad (1.83)$$

- The energy of photons scattered at 90º and 180º is thus given as:

$$h\nu'(\theta=90°) = \frac{h\nu}{1+\varepsilon} \quad \text{and} \quad h\nu'(\theta=180°) = \frac{h\nu}{1+2\varepsilon} \qquad (1.84)$$

which for large incident photon energies ($\varepsilon = h\nu/(m_ec^2) \to \infty$ results in m_ec^2 and $0.5\,m_ec^2$ for $\theta = 90°$ and $\theta = 180°$, respectively.

- The maximum (for $\theta = 180°$ (i.e. photon backscattering)) and mean fractions of the incident photon energy transferred to the Compton recoil electron are given in Fig. 1.6. The mean fraction is used in the determination of the Compton effect contribution to the energy transfer coefficient.

- For example, from Fig. 1.6 we determine that a 1 MeV photon undergoing a Compton backscattering event would result in a recoil electron with a kinetic energy of 800 keV and a backscattered photon with an energy of 200 keV.

- On average, a 1 MeV photon undergoing Compton scattering will produce a 440 keV recoil electron and a 560 keV scattered photon; a 100 keV photon will produce a 15 keV recoil electron and a 85 keV scattered photon; a 10 MeV photon will produce a 6.9 MeV recoil electron and a 3.1 MeV scattered photon; and a 100 MeV photon will produce an 80 MeV recoil electron and a 20 MeV scattered photon.

1.4.7. Pair production

In pair production the photon disappears and an electron–positron pair with a combined kinetic energy equal to $h\nu - 2m_ec^2$ is produced in the nuclear Coulomb field.
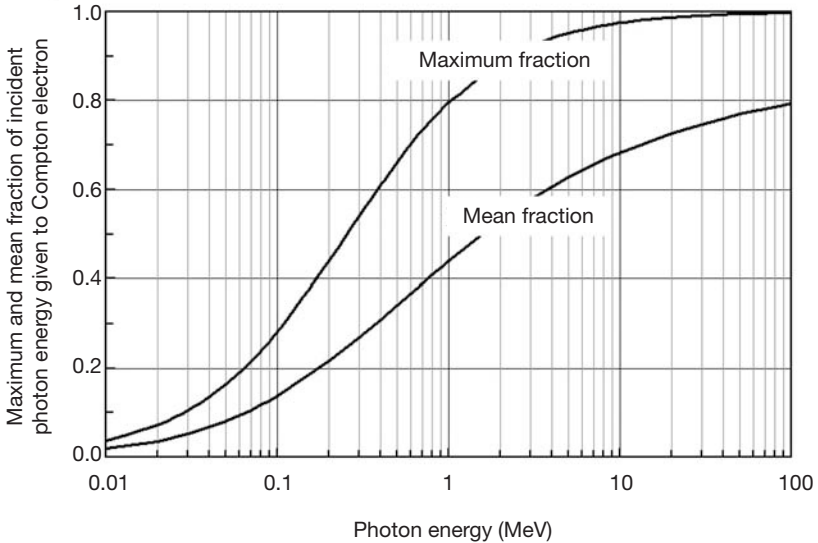
FIG. 1.6. Maximum and mean fractions of incident photon energy transferred to a Compton recoil electron in the photon energy range from 10 keV to 100 MeV. Data are obtained from the National Institute of Science and Technology (NIST) in Washington, DC (www.nist.gov).

- Since mass is produced out of photon energy in the form of an electron–positron pair, pair production has an energy threshold (minimum photon energy required for the effect to happen) of $2m_ec^2 = 1.02$ MeV.
- When pair production occurs in the field of an orbital electron, the effect is referred to as triplet production, and three particles (an electron–positron pair and the orbital electron) share the available energy. The threshold for this effect is $4m_ec^2$.
- The probability for pair production is zero for photon energies below the threshold energy and increases rapidly with photon energy above the threshold.
- The atomic attenuation coefficient for pair production $_a\kappa$ and the mass attenuation coefficient for pair production κ/ρ vary approximately as Z^2 and Z, respectively, where Z is the atomic number of the attenuator.

1.4.8. Photonuclear reactions

Photonuclear reactions (also referred to as photodisintegration reactions) occur when a high energy photon is absorbed by the nucleus of an atom, resulting in an emission of a neutron ((x, n) reaction) or proton ((x, p) reaction) and a transformation of the nucleus into a radioactive reaction product.

- The threshold for a particular photonuclear reaction depends on the reaction and the nucleus and is of the order of 10 MeV or higher for most nuclei (with the exception of the deuteron and ^{9}Be nuclei, for which the threshold is of the order of 2 MeV).
- The probability for photonuclear reactions is much smaller than that for other photon interactions, and their contribution to the total attenuation coefficient amounts to only a few per cent at photon energies above the reaction threshold.
- While photonuclear reactions do not play an active role in photon attenuation considerations, they are of concern in high energy radiotherapy treatment rooms because of the neutron production through the (x, n) reactions and because of the radioactivity that is induced in the treatment room air and in machine components through the (x, n) reaction. Both the neutrons and the radioactivity pose a health hazard to personnel and must be dealt with in the treatment room and treatment machine design. The neutron problem is dealt with special treatment room doors incorporating borated hydrogenous materials to thermalize and absorb the neutrons, the radioactivity with adequate room ventilation (six to eight air changes per hour) and use of machine components with a low reaction cross-section and short half-life of the reaction product.

1.4.9. Contributions to attenuation coefficients

For a given photon energy $h\nu$ and attenuator Z, the attenuation coefficient μ, energy transfer coefficient μ_{tr} and energy absorption coefficient μ_{ab} are given as a sum of coefficients for individual photon interactions (the energy absorption coefficient is often designated as μ_{en}):

$$\mu = \tau + \sigma_R + \sigma_C + \kappa \tag{1.85}$$

$$\mu_{tr} = \tau_{tr} + (\sigma_C)_{tr} + \kappa_{tr} = \tau \frac{(\bar{E}_K)^{PE}_{tr}}{h\nu} + \sigma_C \frac{(\bar{E}_K)^{CE}_{tr}}{h\nu} + \kappa \frac{(\bar{E}_K)^{PP}_{tr}}{h\nu} \tag{1.86}$$

$$\mu_{ab} = \mu_{en} = \mu_{tr}(1-g) \tag{1.87}$$

where g is the radiative fraction, and the average energies transferred to charged particles (electrons and positrons) for the photoelectric effect, the Compton effect and pair production are designated as $(\bar{E}_K)^{PE}_{tr}$, $(\bar{E}_K)^{CE}_{tr}$ and $(\bar{E}_K)^{PP}_{tr}$, respectively.

- $(\bar{E}_K)^{PE}_{tr}$ may be approximated by $h\nu - P_K\omega_K E_B(K)$, where $E_B(K)$ is the binding energy of the K shell electron, P_K is the fraction of all photo-electric effect interactions that occur in the K shell and ω_K is the fluorescent yield for the K shell.
- $(\bar{E}_K)^{CE}_{tr}$ is obtained from tabulated values or from the graph shown in Fig. 1.6.
- $(\bar{E}_K)^{PP}_{tr} = h\nu - 2m_e c^2$.
- Note that in Rayleigh scattering no energy transfer occurs and therefore Rayleigh scattering contributes neither to the energy transfer coefficient nor to the energy absorption coefficient.

The individual components of the attenuation coefficients, when summed, result in the total mass attenuation, mass–energy transfer and mass–energy absorption coefficients as follows:

$$\frac{\mu}{\rho} = \frac{\tau}{\rho} + \frac{\sigma_R}{\rho} + \frac{\sigma_C}{\rho} + \frac{\kappa}{\rho} \tag{1.88}$$

$$\frac{\mu_{tr}}{\rho} = \frac{\tau_{tr}}{\rho} + \frac{(\sigma_C)_{tr}}{\rho} + \frac{\kappa_{tr}}{\rho}$$

$$= \frac{1}{\rho}\left(\tau \frac{h\nu - P_K\omega_K E_B(K)}{h\nu} + \sigma_C \frac{(\bar{E}_K)^{CE}_{tr}}{h\nu} + \kappa \frac{h\nu - 2m_e c^2}{h\nu}\right) \tag{1.89}$$

$$\frac{\mu_{ab}}{\rho} = \frac{\mu_{tr}}{\rho}(1-g) \tag{1.90}$$

Figure 1.7 shows the mass attenuation coefficient μ/ρ in (a) and the mass–energy transfer coefficient (μ_{tr}/ρ) and mass–energy absorption coefficient (μ_{ab}/ρ) in (b) for lead in the photon energy range from 10 keV to 100 MeV.
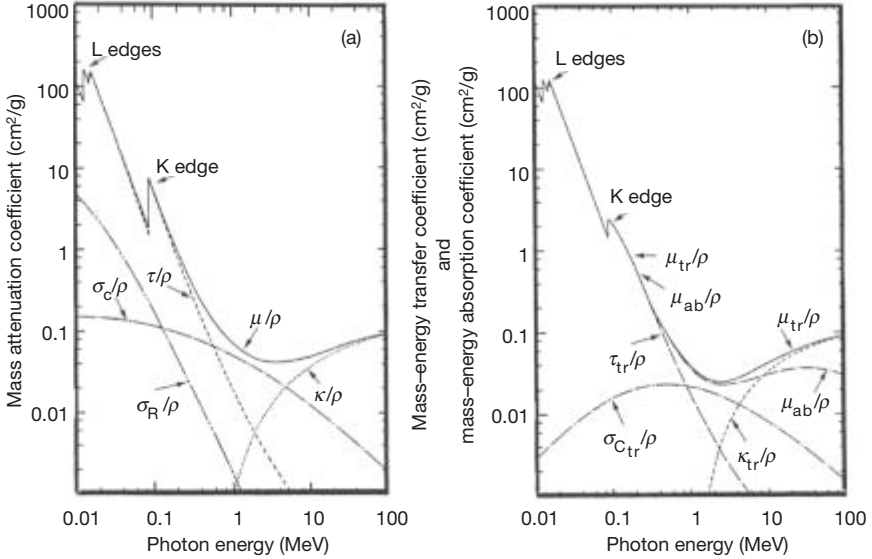
FIG. 1.7. Mass attenuation coefficient μ/ρ (a); mass–energy transfer coefficient μ_{tr}/ρ and mass–energy absorption coefficient μ_{ab}/ρ (b) for lead in the photon energy range between 10 keV and 100 MeV. The dotted–dashed curves represent contributions of individual effects, while the solid curves represent the sum of the contributions of the individual effects as given by Eq. (1.88) for μ/ρ, Eq. (1.89) for μ_{tr}/ρ and Eq. (1.90) for μ_{ab}/ρ. For photon energies below 2 MeV, $\mu_{tr}/\rho \approx \mu_{ab}/\rho$, because the radiative fraction g in this energy region is negligible. Above 2 MeV, g increases with photon energy, causing the divergence between the mass–energy transfer and mass–energy absorption coefficients.

1.4.10. Relative predominance of individual effects

The probability for a photon to undergo any one of the various interaction phenomena with an attenuator depends on the energy $h\nu$ of the photon and on the atomic number Z of the attenuating material. In general, the photoelectric effect predominates at low photon energies, the Compton effect at intermediate energies and pair production at high photon energies.

Figure 1.8 shows the regions of relative predominance of the three most important individual effects with $h\nu$ and Z as parameters. The two curves display the points in the $(h\nu, Z)$ diagram for which $_a\sigma_C = {_a\tau}$ or $_a\sigma_C = {_a\kappa}$ and thus delineate the regions of photoelectric effect predominance at low photon energies, Compton effect predominance at intermediate energies and pair
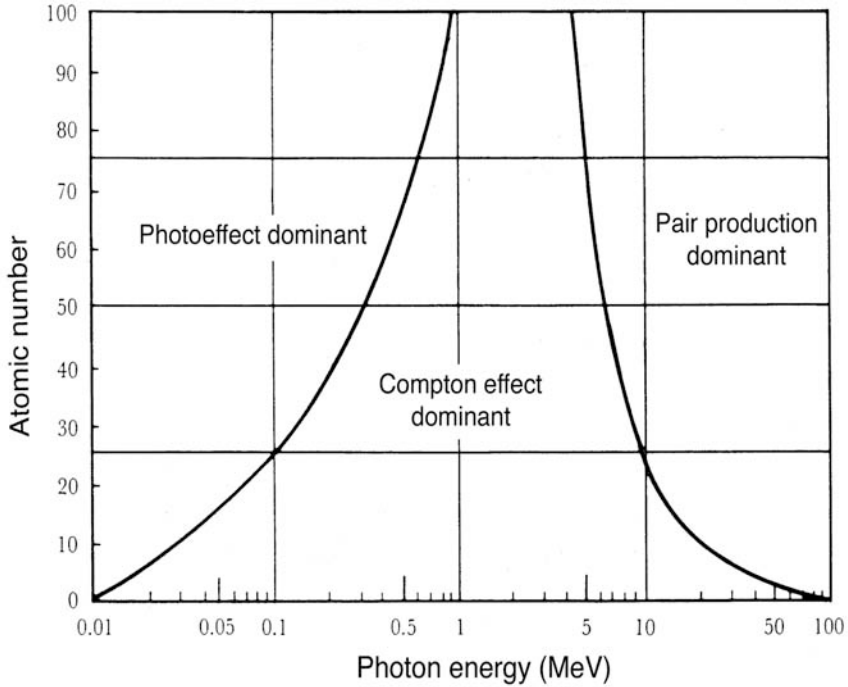
FIG. 1.8. Regions of relative predominance of the three main forms of photon interaction with matter. The left curve represents the region where the atomic coefficients for the photoelectric effect and Compton effect are equal ($_a\tau = {_a\sigma_C}$), the right curve is for the region where the atomic Compton coefficient equals the atomic pair production coefficient ($_a\sigma_C = {_a\kappa}$).

production predominance at high photon energies. For example, a 100 keV photon will interact with lead ($Z = 82$) predominantly through the photoelectric effect and with soft tissue ($Z_{eff} = 7.5$) predominantly through the Compton effect. A 10 MeV photon, on the other hand, will interact with lead predominantly through pair production and with tissue predominantly through the Compton effect.

1.4.11. Effects following photon interactions

In the photoelectric effect, the Compton effect and triplet production, vacancies are produced in atomic shells through the ejection of orbital electrons. For the orthovoltage and megavoltage photons used in the diagnosis

and treatment of disease with radiation, the shell vacancies occur mainly in inner atomic shells and are followed by characteristic X rays or Auger electrons, the probability for the former given by the fluorescent yield ω (see Fig. 1.9), while the probability for the Auger effect is $1 - \omega$.

Pair production and triplet production are followed by the annihilation of the positron with a 'free' and stationary electron, producing two annihilation quanta, most commonly with energies of 0.511 MeV each and emitted at 180° from each other to satisfy the conservation of charge, momentum and energy. An annihilation of a positron before it has expended all of its kinetic energy is referred to as annihilation in flight and produces photons with energies exceeding 0.511 MeV.

1.4.12. Summary of photon interactions

Table 1.4 summarizes the main characteristics of the photoeffect, Rayleigh scattering, the Compton effect and pair production.
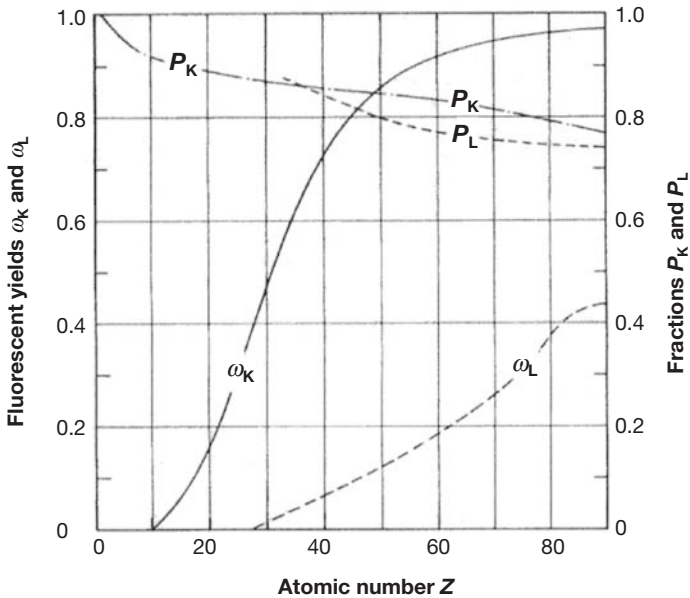
FIG. 1.9. Fluorescent yields ω_K for $h\nu > (E_B)_K$ and ω_L for $(E_B)_L < h\nu < (E_B)_K$ as well as fractions P_K for $h\nu > (E_B)_K$ and P_L for $(E_B)_L < h\nu < (E_B)_K$ against the atomic number Z. Data were obtained from F.H. Attix, Introduction to Radiological Physics and Radiation Dosimetry, Wiley, New York (1986).

TABLE 1.4. MAIN CHARACTERISTICS OF THE PHOTOELECTRIC EFFECT, RAYLEIGH SCATTERING, THE COMPTON EFFECT AND PAIR PRODUCTION

	Photoelectric effect	Rayleigh scattering	Compton effect	Pair production
Photon interaction	With whole atom (bound electron)	With bound electrons	With free electrons	With nuclear Coulomb field
Mode of photon interaction	Photon disappears	Photon scattered	Photon scattered	Photon disappears
Energy dependence	$\dfrac{1}{(h\nu)^3}$	$\dfrac{1}{(h\nu)^2}$	Decreases with energy	Increases with energy
Threshold	No	No	No	$2m_ec^2$
Linear attenuation coefficient	τ	σ_R	σ_C	κ
Particles released	Photoelectron	None	Compton (recoil) electron	Electron–positron pair
Atomic coefficient dependence on Z	$_a\tau \propto Z^4$	$_a\sigma_R \propto Z^2$	$_a\sigma_C \propto Z$	$_a\kappa \propto Z^2$
Mass coefficient dependence on Z	$\dfrac{\tau}{\rho} \propto Z^3$	$\dfrac{\sigma_R}{\rho} \propto Z$	Independent	$\dfrac{\kappa}{\rho} \propto Z$
Average energy transferred	$h\nu - P_K\omega_K E_B(K)$	0	$(\bar{E}_K)^{CE}_{tr}$ (see Fig. 1.6)	$h\nu - 2m_ec^2$
Subsequent effect	Characteristic X ray, Auger effect	None	Characteristic X ray, Auger effect	Annihilation radiation
Significant energy region for water	<20 keV	<20 keV	20 keV– 10 MeV	>10 MeV

1.4.13. Example of photon attenuation

For 2 MeV photons in lead ($Z = 82$; $A = 207.2$ g/g-atom; $\rho = 11.36$ g/cm^3) the photoelectric effect, coherent scattering, the Compton effect and pair production linear attenuation coefficients are: $\tau = 0.055$ cm^{-1}, $\sigma_R = 0.008$ cm^{-1}, $\sigma_C = 0.395$ cm^{-1} and $\kappa = 0.056$ cm^{-1}. The average energy transferred to charged particles $(\bar{E}_K)_{tr} = 1.13$ MeV and the average energy absorbed in lead is $(\bar{E}_K)_{ab} = 1.04$ MeV.

Calculate the linear attenuation coefficient μ; mass attenuation coefficient μ_m; atomic attenuation coefficient $_a\mu$; mass–energy transfer coefficient μ_{tr}/ρ; mass–energy absorption coefficient μ_{ab}/ρ; and radiative fraction g:

$$\mu = \tau + \sigma_R + \sigma_C + \kappa = (0.055 + 0.008 + 0.395 + 0.056) \text{ cm}^{-1} = 0.514 \text{ cm}^{-1}$$

$$(1.91)$$

$$\mu_m = \frac{\mu}{\rho} = \frac{0.514 \text{ cm}^{-1}}{11.36 \text{ g/cm}^3} = 0.0453 \text{ cm}^2/\text{g} \tag{1.92}$$

$$_a\mu = \left(\frac{\rho N_A}{A}\right)^{-1}\mu = \frac{207.2 \text{ g/g-atom} \times 0.514 \text{ cm}^{-1}}{11.36 \text{ g/cm}^3 \times 6.022 \times 10^{23} \text{ atom/g-atom}}$$

$$= 1.56 \times 10^{-23} \text{ cm}^2/\text{atom} \tag{1.93}$$

$$\frac{\mu_{tr}}{\rho} = \frac{(\bar{E}_K)_{tr}}{h\nu}\frac{\mu}{\rho} = \frac{1.13 \text{ MeV} \times 0.0453 \text{ cm}^2/\text{g}}{2 \text{ MeV}} = 0.0256 \text{ cm}^2/\text{g} \tag{1.94}$$

$$\frac{\mu_{ab}}{\rho} = \frac{\mu_{en}}{\rho} = \frac{(\bar{E}_K)_{ab}}{h\nu}\frac{\mu}{\rho} = \frac{1.04 \text{ MeV} \times 0.0453 \text{ cm}^2/\text{g}}{2 \text{ MeV}} = 0.0236 \text{ cm}^2/\text{g}$$

$$(1.95)$$

$$g = \frac{(\bar{E}_K)_{tr} - (\bar{E}_K)_{ab}}{(\bar{E}_K)_{tr}} = 1 - \frac{(\bar{E}_K)_{ab}}{(\bar{E}_K)_{tr}} = 1 - \frac{1.04 \text{ MeV}}{1.13 \text{ MeV}} = 0.08 \tag{1.96}$$

or

$$g = 1 - \frac{\mu_{ab}/\rho}{\mu_{tr}/\rho} = 1 - \frac{0.0236 \text{ cm}^2/\text{g}}{0.0256 \text{ cm}^2/\text{g}} = 0.08 \tag{1.97}$$

The mass–energy transfer coefficient μ_{tr}/ρ can also be determined using Eq. (1.89) with:

$$h\nu - P_K \omega_K E_B = 2 \text{ MeV} - 0.8 \times 0.96 \times 0.088 \text{ MeV} = 1.93 \text{ MeV}$$
(from Fig. 1.9) $\tag{1.98}$

$$(\bar{E}_K)_{tr}^{CE} = 0.53 \times 2 \text{ MeV} = 1.06 \text{ MeV (from Fig. 1.6)} \tag{1.99}$$

$$h\nu - 2m_e c^2 = 2 \text{ MeV} - 1.02 \text{ MeV} = 0.98 \text{ MeV} \tag{1.100}$$

to obtain

$$\frac{\mu_{tr}}{\rho} = \frac{1}{11.36}\left(\frac{1.93}{2} \times 0.055 + \frac{1.06}{2} \times 0.395 + \frac{0.98}{2} \times 0.056\right) \frac{\text{cm}^2}{\text{g}} = 0.0254 \frac{\text{cm}^2}{\text{g}}$$

$$\tag{1.101}$$

in good agreement with the result obtained in Eq. (1.94).

Thus, as shown schematically in Fig. 1.10, a 2 MeV photon in lead will on average:

- Transfer 1.13 MeV to charged particles (electrons and positrons); and
- 0.87 MeV will be scattered through Rayleigh and Compton scattering.

Of the 1.13 MeV of energy transferred:

- 1.04 MeV will be absorbed in lead; and
- 0.09 MeV will be re-emitted through bremsstrahlung radiative loss.

The radiative fraction g for 2 MeV photons in lead is 0.08.

1.4.14. Production of vacancies in atomic shells

There are eight main means of producing vacancies in atomic shells and transforming the atom from a neutral state into an excited positive ion:
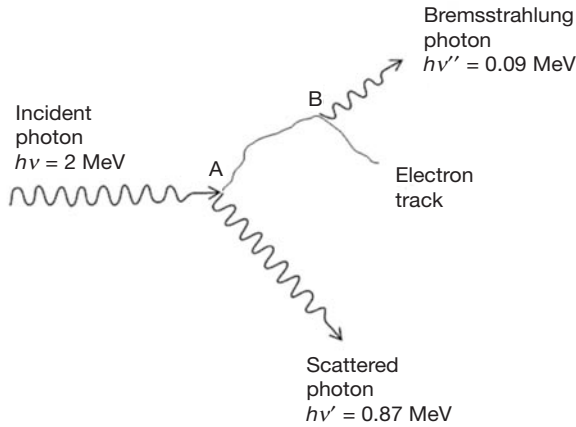
FIG. 1.10. Schematic diagram of general photon interactions with an atom. In this example a 2 MeV photon hv interacts with a lead atom. An individual 2 MeV photon, as it encounters a lead atom at point A, may interact with the atom through the photoelectric effect, Rayleigh scattering, the Compton effect or pair production, or it may not interact at all. However, for a large number of 2 MeV photons striking lead, we may state that on average: 1.13 MeV will be transferred at point A to charged particles (mainly to fast energetic electrons, but possibly also to positrons if the interaction is pair production); 0.87 MeV will be scattered through Rayleigh and Compton scattering (hv'). Of the 1.13 MeV transferred to charged particles: 1.04 MeV will be absorbed in lead over the fast charged particle tracks, and 0.09 MeV will be emitted in the form of bremsstrahlung photons (hv'').

- Coulomb interaction (1) of an energetic charged particle with an orbital electron.
- Photon interactions:
  —Photoelectric effect (2);
  —Compton effect (3);
  —Triplet production (4).
- Nuclear decay:
  —Electron capture (5);
  —Internal conversion (6).
- Positron annihilation (7).
- Auger effect (8).

Note that pair production does not produce shell vacancies. Vacancies in inner atomic shells are not stable; they are followed by emission of characteristic photons or Auger electrons and cascade to the outer shell of the ion. The ion eventually attracts an electron from its surroundings and reverts to a neutral atom.

BIBLIOGRAPHY

ATTIX, F.H., Introduction to Radiological Physics and Radiation Dosimetry, Wiley, New York (1986).

ATTIX, F.H., ROESCH, W.C., TOCHILIN, E., Radiation Dosimetry, Academic Press, New York (1968).

EVANS, R.D., The Atomic Nucleus, McGraw-Hill, New York (1955).

HALE, J., The Fundamentals of Radiological Science, Thomas, Springfield, IL (1974).

JOHNS, H.E., CUNNINGHAM, J.R., The Physics of Radiology, Thomas, Springfield, IL (1984).

KASE, K.R., BJARNGARD, B.E., ATTIX, F.H. (Eds), The Dosimetry of Ionizing Radiation, Academic Press, San Diego, CA (1985).

KHAN, F., The Physics of Radiation Therapy, 3rd edn, Lippincott, Williams and Wilkins, Baltimore, MD (2003).

ROHLF, J.W., Modern Physics from α to Z^0, Wiley, New York (1994).

JAYARAMAN, S., LANZL, L.H., Clinical Radiotherapy Physics, CRC Press, Boca Raton, FL (1996).

Chapter 2

DOSIMETRIC PRINCIPLES, QUANTITIES AND UNITS

J.P. SEUNTJENS
Department of Medical Physics,
McGill University Health Centre,
Montreal, Quebec, Canada

W. STRYDOM
Department of Medical Physics,
Medical University of Southern Africa,
Pretoria, South Africa

K.R. SHORTT
Division of Human Health,
International Atomic Energy Agency,
Vienna

2.1. INTRODUCTION

Radiation measurements and investigations of radiation effects require various specifications of the radiation field at the point of interest. Radiation dosimetry deals with methods for a quantitative determination of energy deposited in a given medium by directly or indirectly ionizing radiations. A number of quantities and units have been defined for describing the radiation beam, and the most commonly used dosimetric quantities and their units are defined below. A simplified discussion of cavity theory, the theory that deals with calculating the response of a dosimeter in a medium, is also given.

2.2. PHOTON FLUENCE AND ENERGY FLUENCE

The following quantities are used to describe a monoenergetic ionizing radiation beam: particle fluence, energy fluence, particle fluence rate and energy fluence rate. These quantities are usually used to describe photon beams and may also be used in describing charged particle beams.

- The particle fluence Φ is the quotient dN by dA, where dN is the number of particles incident on a sphere of cross-sectional area dA:

$$\Phi = \frac{dN}{dA} \tag{2.1}$$

The unit of particle fluence is m^{-2}. The use of a sphere of cross-sectional area dA expresses in the simplest manner the fact that one considers an area dA perpendicular to the direction of each particle and hence that particle fluence is independent of the incident angle of the radiation.
- Planar particle fluence is the number of particles crossing a plane per unit area and hence depends on the angle of incidence of the particle beam.
- The energy fluence Ψ is the quotient of dE by dA, where dE is the radiant energy incident on a sphere of cross-sectional area dA:

$$\Psi = \frac{dE}{dA} \tag{2.2}$$

The unit of energy fluence is J/m^2. Energy fluence can be calculated from particle fluence by using the following relation:

$$\Psi = \frac{dN}{dA} E = \Phi E \tag{2.3}$$

where E is the energy of the particle and dN represents the number of particles with energy E.

Almost all realistic photon or particle beams are polyenergetic, and the above defined concepts need to be applied to such beams. The concepts of particle fluence spectrum and energy fluence spectrum replace the particle fluence and energy fluence, respectively. They are defined respectively as:

$$\Phi_E(E) \equiv \frac{d\Phi}{dE}(E) \tag{2.4}$$

and

$$\Psi_E(E) \equiv \frac{d\Psi}{dE}(E) = \frac{d\Phi}{dE}(E)E \tag{2.5}$$

where $\Phi_E(E)$ and $\Psi_E(E)$ are shorthand notations for the particle fluence spectrum and the energy fluence spectrum differential in energy E, respectively.

Figure 2.1 shows a photon fluence and an energy fluence spectrum generated by an orthovoltage X ray unit with a kVp value of 250 kV and an
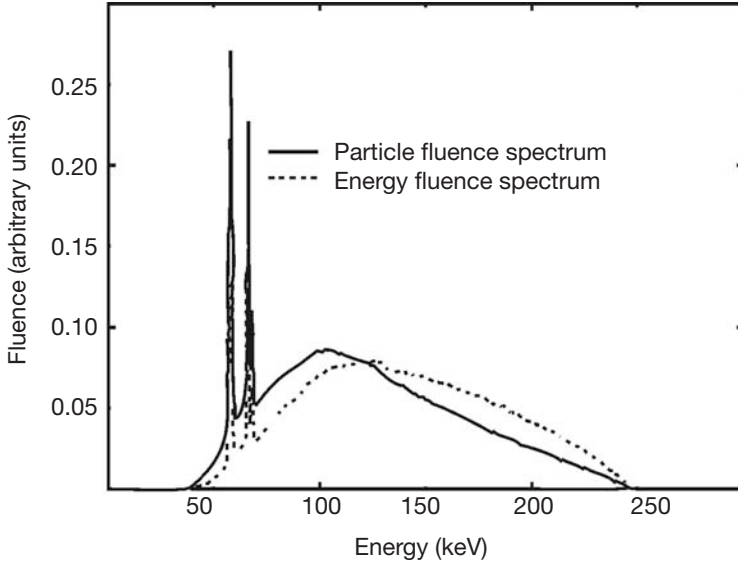
FIG. 2.1. Photon fluence and energy fluence spectra at 1 m from the target of an X ray machine with a tube potential of 250 kV and added filtration of 1 mm Al and 1.8 mm Cu (target material: W; inherent filtration: 2 mm Be).

added filtration of 1 mm Al and 1.8 mm Cu (target material: W; inherent filtration: 2 mm Be). The two spikes superimposed on the continuous bremsstrahlung spectrum represent the K_α and the K_β characteristic X ray lines produced in the tungsten target.

The particle fluence rate $\dot\Phi$ is the quotient of $d\Phi$ by dt, where $d\Phi$ is the increment of the fluence in time interval dt:

$$\dot\Phi = \frac{d\Phi}{dt} \tag{2.6}$$

with units of $m^{-2} \cdot s^{-1}$.

The energy fluence rate (also referred to as intensity) is the quotient of $d\Psi$ by dt, where $d\Psi$ is the increment of the energy fluence in the time interval dt:

$$\dot\Psi = \frac{d\Psi}{dt} \tag{2.7}$$

The unit of energy fluence rate is W/m^2 or $J \cdot m^{-2} \cdot s^{-1}$.

2.3. KERMA

Kerma is an acronym for kinetic energy released per unit mass. It is a non-stochastic quantity applicable to indirectly ionizing radiations such as photons and neutrons. It quantifies the average amount of energy transferred from indirectly ionizing radiation to directly ionizing radiation without concern as to what happens after this transfer. In the discussion that follows we will limit ourselves to photons.

The energy of photons is imparted to matter in a two stage process. In the first stage, the photon radiation transfers energy to the secondary charged particles (electrons) through various photon interactions (the photoelectric effect, the Compton effect, pair production, etc.). In the second stage, the charged particle transfers energy to the medium through atomic excitations and ionizations.

In this context, the kerma is defined as the mean energy transferred from the indirectly ionizing radiation to charged particles (electrons) in the medium $d\bar{E}_{tr}$ per unit mass dm:

$$K = \frac{d\bar{E}_{tr}}{dm}$$
(2.8)

The unit of kerma is joule per kilogram (J/kg). The name for the unit of kerma is the gray (Gy), where 1 Gy = 1 J/kg.

2.4. CEMA

Cema is the acronym for converted energy per unit mass. It is a non-stochastic quantity applicable to directly ionizing radiations such as electrons and protons. The cema C is the quotient of dE_c by dm, where dE_c is the energy lost by charged particles, except secondary electrons, in collisions in a mass dm of a material:

$$C = \frac{dE_c}{dm}$$
(2.9)

The unit of cema is joule per kilogram (J/kg). The name for the unit of cema is the gray (Gy).

2.5. ABSORBED DOSE

Absorbed dose is a non-stochastic quantity applicable to both indirectly and directly ionizing radiations. For indirectly ionizing radiations, energy is imparted to matter in a two step process. In the first step (resulting in kerma), the indirectly ionizing radiation transfers energy as kinetic energy to secondary charged particles. In the second step, these charged particles transfer some of their kinetic energy to the medium (resulting in absorbed dose) and lose some of their energy in the form of radiative losses (bremsstrahlung, annihilation in flight).

The absorbed dose is related to the stochastic quantity energy imparted. The absorbed dose is defined as the mean energy $\bar{\varepsilon}$ imparted by ionizing radiation to matter of mass m in a finite volume V by:

$$D = \frac{d\bar{\varepsilon}}{dm} \tag{2.10}$$

The energy imparted $\bar{\varepsilon}$ is the sum of all the energy entering the volume of interest minus all the energy leaving the volume, taking into account any mass–energy conversion within the volume. Pair production, for example, decreases the energy by 1.022 MeV, while electron–positron annihilation increases the energy by the same amount.

Note that because electrons travel in the medium and deposit energy along their tracks, this absorption of energy does not take place at the same location as the transfer of energy described by kerma. The unit of absorbed dose is joule per kilogram (J/kg). The name for the unit of absorbed dose is the gray (Gy).

2.6. STOPPING POWER

Stopping powers are widely used in radiation dosimetry, but they are rarely measured and must be calculated from theory. For electrons and positrons the Bethe theory is used to calculate stopping powers.

The linear stopping power is defined as the expectation value of the rate of energy loss per unit path length (dE/dx) of the charged particle. The mass stopping power is defined as the linear stopping power divided by the density of the absorbing medium. Division by the density of the absorbing medium almost eliminates the dependence of the mass stopping power on mass density, except for the density effect discussed further below. Typical units for the linear and mass stopping powers are MeV/cm and MeV·cm^2/g, respectively.

Two types of stopping power are known: collision (ionization), resulting from interactions of charged particles with atomic orbital electrons; and radiative, resulting from interactions of charged particles with atomic nuclei.

The unrestricted mass collision stopping power expresses the average rate of energy loss by a charged particle in all hard and soft collisions.

- A soft collision occurs when a charged particle passes an atom at a considerable distance (i.e. $b \gg a$, where b is the impact parameter and a the atomic radius). The net effect of the collision is that a very small amount of energy is transferred to an atom of the absorbing medium in a single collision.
- In a hard collision where $b \approx a$, a secondary electron (often referred to as a delta electron or historically as a delta ray) with considerable energy is ejected and forms a separate track.
- In the unrestricted mass collision stopping power the maximum energy transfer to an orbital electron allowed due to a hard collision is half of the kinetic energy of the electron (collision of indistinguishable particles) or the full kinetic energy of a positron (collision of distinguishable particles).

The theory of the mass collision stopping power for heavy charged particles, electrons and positrons as a result of soft and hard collisions combines the Bethe theory for soft collisions with the stopping power as a result of energy transfers due to hard collisions. The result of this, for a heavy charged particle with mass M and velocity υ, where the energy transfer due to hard collisions is limited to $2m_e c^2 \beta^2/(1 - \beta^2)$, where $\beta = \upsilon/c$, is:

$$\frac{S_{col}}{\rho} = \frac{4\pi N_A Z}{A} \frac{r_e^2 m_e c^2}{\beta^2} z^2 \left[\ln\left(\frac{2m_e \upsilon^2}{I}\right) - \ln(1 - \beta^2) - \beta^2 - \frac{C}{Z} \right] \qquad (2.11)$$

where

r_e is the classical electron radius (2.82 fm);
z is the projectile charge in units of electron charge;
I is the mean excitation potential of the medium;
C/Z is the shell correction.

The mean excitation potential I is a geometric mean value of all ionization and excitation potentials of an atom of the absorbing material. Since binding effects influence the exact value of I, calculation models are often inadequate to estimate its value accurately. Hence, I values are usually derived

from measurements of stopping powers in heavy charged particle beams, for which the effects of scattering in these measurements is minimal.

For elemental materials I varies approximately linearly with Z, with, on average, $I = 11.5Z$. For compounds, I is calculated assuming additivity of the collision stopping power, taking into account the fraction by weight of each atom constituent in the compound.

The shell correction C/Z accounts for the decrease in mass stopping power when the passing particle's velocity has ceased to be much greater than that of the atomic electrons in the stopping medium, an effect that leads to a violation of the Born approximation, which underlies the derivation of the mass collision stopping power. The electrons in the K shell are the first affected by this, followed by the L shell electrons, etc. C/Z is a function of the medium and of the velocity of the fast charged particle.

The following observations can be made about Eq. (2.11):

- The mass stopping power does not depend on the projectile mass and is proportional to the inverse square of the projectile velocity. Note that the term $2m_e v^2$ under the logarithm has no relation to the kinetic energy of any of the particles involved in the collision process.
- The mass stopping power gradually flattens to a broad minimum for kinetic energies $E_K \approx 3m_e c^2$.
- The leading factor Z/A is responsible for a decrease of about 20% in stopping power from carbon to lead. The term $-\ln I$ causes a further decrease in stopping power with Z.
- In a given medium, the square dependence on the projectile charge (z^2) causes heavy charged particles with double the charge to experience four times the stopping power.

For electrons and positrons, energy transfers due to soft collisions are combined with those due to hard collisions using the Møller (for electrons) and Bhabba (for positrons) cross-sections for free electrons. The complete mass collisional stopping power for electrons and positrons, according to ICRU Report No. 37, is:

$$\frac{S_{col}}{\rho} = \frac{N_A Z}{A} \frac{\pi r_0^2 2 m_e c^2}{\beta^2} [\ln(E_K/I)^2 + \ln(1+\tau/2) + F^{\pm}(\tau) - \delta] \qquad (2.12)$$

with F^- given for electrons as:

$$F^-(\tau) = (1 - \beta^2)[1 + \tau^2/8 - (2\tau + 1) \ln 2]$$

and F^+ given for positrons as:

$$F^+(\tau) = 2\ln 2 - (\beta^2/12)[23 + 14/(\tau + 2) + 10/(\tau + 2)^2 + 4/(\tau + 2)^3]$$

In this equation, $\tau = E_K/m_e c^2$ and $\beta = v/c$.

The density effect correction δ accounts for the fact that the effective Coulomb force exerted on a fast charged particle by atoms that are distant from the particle track is reduced as a result of the polarization of the medium caused by the charged particle. The density effect affects the soft collision component of the stopping power. It plays a significant role in the values of ratios of the stopping power of a dense material to that of a non-dense material (such as, for example, water to air), and various models for it have been developed.

The mass radiative stopping power is the rate of energy loss by electrons or positrons that results in the production of bremsstrahlung. The Bethe–Heitler theory leads to the following formula for the mass radiative stopping power:

$$\frac{S_{rad}}{\rho} = \sigma_0 \frac{N_A Z^2}{A}(E_K + m_e c^2)\bar{B}_r \tag{2.13}$$

where $\sigma = \alpha(e^2/(4\pi\varepsilon_0 m_e c^2))^2 = 5.80 \times 10^{-28}$ cm^2/atom, where α is the fine structure constant and $\bar{B}_r$ is a function of Z and E_K, varying between 5.33 and 15 for energies in the range from less than 0.5 MeV to 100 MeV.

This factor, together with the increase of the radiative stopping power proportional with E_K, is responsible for the increase in total stopping power at energies above 2 MeV as depicted in Fig. 2.2. Note that the Z^2 dependence of the mass radiative stopping power in contrast to the Z dependence of the mass collision stopping power makes this mode of energy loss more prominent in high Z materials.

The concept of restricted mass collision stopping power is introduced to calculate the energy transferred to a localized region of interest. By limiting the energy transfer to secondary charged (delta) particles to a threshold (often denoted as Δ), highly energetic secondary particles are allowed to escape the region of interest.

The restricted stopping power is lower than the unrestricted stopping power. The choice of the energy threshold depends on the problem at hand. For problems involving ionization chambers a frequently used threshold value is 10 keV (the range of a 10 keV electron in air is of the order of 2 mm). For microdosimetric quantities one usually takes 100 eV as a reasonable threshold value.
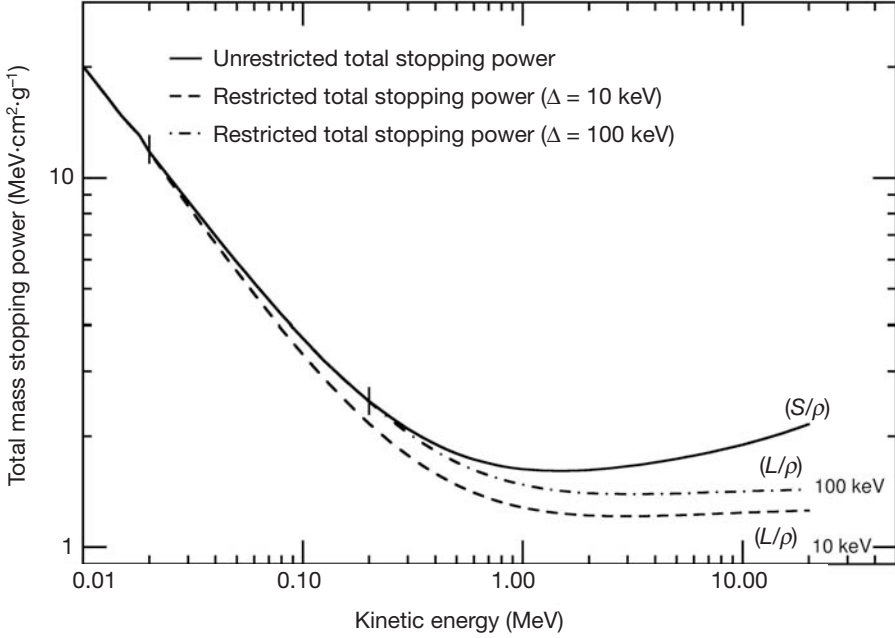
FIG. 2.2.   Unrestricted S/ρ and restricted ((L/ρ)_Δ with Δ = 10 and 100 keV) total mass stopping powers for carbon (ρ = 1.70 g/cm³), based on data published in ICRU Report No. 37. Vertical lines indicate the points at which restricted and unrestricted mass stopping powers begin to diverge as the kinetic energy increases.

The restricted linear collision stopping power (also referred to as linear energy transfer (LET)) L_Δ of a material, for charged particles, is the quotient of dE_Δ by dl, where dE_Δ is the energy lost by a charged particle due to soft and hard collisions in traversing a distance dl minus the total kinetic energy of the charged particles released with kinetic energies in excess of Δ:

$$L_\Delta = dE_\Delta/dl \tag{2.14}$$

The restricted mass collision stopping power is the restricted linear collision stopping power divided by the density of the material.

As the threshold for maximum energy transfer in the restricted stopping power increases, the restricted mass stopping power tends to the unrestricted mass stopping power for $\Delta \rightarrow E_K/2$. Note also that since energy transfers to secondary electrons are limited to $E_K/2$, unrestricted and restricted electron mass stopping powers are identical for kinetic energies lower than or equal to 2Δ. This is indicated in Fig. 2.2 by vertical lines at 20 keV and 200 keV.

The total mass stopping power is the sum of the collision mass stopping power and the radiative mass stopping power. Figure 2.2 shows the total unrestricted and restricted (Δ = 10 keV, 100 keV) electron mass stopping powers for carbon, based on data in ICRU Report No. 37.

2.7. RELATIONSHIPS BETWEEN VARIOUS DOSIMETRIC QUANTITIES

2.7.1. Energy fluence and kerma (photons)

The energy transferred to electrons by photons can be expended in two distinct ways:

- Through collision interactions (soft collisions and hard collisions);
- Through radiative interactions (bremsstrahlung and electron–positron annihilation).

The total kerma is therefore usually divided into two components: the collision kerma K_{col} and the radiative kerma K_{rad}.

- The collision kerma K_{col} is that part of kerma that leads to the production of electrons that dissipate their energy as ionization in or near the electron tracks in the medium, and is the result of Coulomb force interactions with atomic electrons. Thus the collision kerma is the expectation value of the net energy transferred to charged particles per unit mass at the point of interest, excluding both the radiative energy loss and energy passed from one charged particle to another.
- The radiative kerma K_{rad} is that part of kerma that leads to the production of radiative photons as the secondary charged particles slow down and interact in the medium. These interactions most prominently are bremsstrahlung as a result of Coulomb field interactions between the charged particle and the atomic nuclei, but can also result from annihilation in flight.

The total kerma K is thus given by the following:

$$K = K_{col} + K_{rad} \tag{2.15}$$

The average fraction of the energy transferred to electrons that is lost through radiative processes is represented by a factor referred to as the radiative fraction $\bar{g}$. Hence the fraction lost through collisions is $(1 - \bar{g})$.

A frequently used relation between collision kerma K_{col} and total kerma K may be written as follows:

$$K_{col} = K(1 - \bar{g}) \tag{2.16}$$

For monoenergetic photons the collision kerma K_{col} at a point in a medium is related to the energy fluence Ψ at that point in the medium by the following:

$$K_{col} = \Psi \left(\frac{\mu_{en}}{\rho} \right) \tag{2.17}$$

where (μ_{en}/ρ) is the mass–energy absorption coefficient for the monoenergetic photons in the medium.

For polyenergetic beams a formally similar relation exists, but use is made of spectrum averaged quantities. If a photon energy fluence spectrum $\Psi_E(E)$ is present at the point of interest, the collision kerma at that point is obtained as follows:

$$K_{col} = \int_0^{E_{max}} \Psi_E(E) \left(\frac{\mu_{en}}{\rho} \right) dE = \Psi \left(\frac{\bar{\mu}_{en}}{\rho} \right) \tag{2.18}$$

In Eq. (2.18):

$$\Psi = \int_0^{E_{max}} \Psi_E(E) dE$$

stands for the total (integrated) energy fluence, and:

$$\left(\frac{\bar{\mu}_{en}}{\rho} \right) = \frac{1}{\Psi} \int_0^{E_{max}} \Psi_E(E) \frac{\mu_{en}}{\rho}(E) dE$$

is a shorthand notation for the mass–energy absorption coefficient for the medium averaged over the energy fluence spectrum.

For monoenergetic photons the total kerma K at a point in a medium is related to the energy fluence Ψ in the medium by the following:

$$K = \Psi \left(\frac{\mu_{tr}}{\rho} \right) \tag{2.19}$$

where (μ_{tr}/ρ) is the mass–energy transfer coefficient of the medium for the given monoenergetic photon beam. For polyenergetic beams, similarly as above, spectrum averaged mass–energy transfer coefficients can be used in conjunction with total energy fluence to obtain the total kerma.

Note that, using Eq. (2.17), one can obtain the frequently used relation between collision kerma in two different materials, material 1 and material 2, as follows:

$$\frac{K_{col,2}}{K_{col,1}} = \frac{\Psi_2 \left(\dfrac{\bar{\mu}_{en}}{\rho} \right)_2}{\Psi_1 \left(\dfrac{\bar{\mu}_{en}}{\rho} \right)_1} \equiv (\Psi)_{2,1} \left(\frac{\bar{\mu}_{en}}{\rho} \right)_{2,1} \tag{2.20}$$

This equation is often used in circumstances in which the fluence ratio $(\Psi)_{2,1}$ can be assumed to be unity through a proper scaling of dimensions (the scaling theorem), for very similar materials or for situations in which the mass of material 2 is sufficient to provide buildup but at the same time small enough so as not to disturb the photon fluence in material 1 (e.g. dose to a small mass of tissue in air).

2.7.2. Fluence and dose (electrons)

Under the conditions that (a) radiative photons escape the volume of interest and (b) secondary electrons are absorbed on the spot (or there is a charged particle equilibrium (CPE) of secondary electrons), the absorbed dose to medium D_{med} is related to the electron fluence Φ_{med} in the medium as follows:

$$D_{med} = \Phi_{med} \left(\frac{S_{col}}{\rho} \right)_{med} \tag{2.21}$$

where $(S_{col}/\rho)_{med}$ is the unrestricted mass collision stopping power of the medium at the energy of the electron.

Owing to electron slowdown in a medium, even for a monoenergetic starting electron kinetic energy E_K, there is always present a primary fluence spectrum that ranges in energy from E_K down to zero and is commonly denoted by $\Phi_{med,E}$.

In this case, the absorbed dose to the medium can be obtained by an integration of Eq. (2.20):

$$D_{med} = \int_0^{E_{max}} \Phi_{med,E}(E)\left(\frac{S_{col}}{\rho}\right)_{med}(E)\,dE = \Phi_{med}\left(\frac{\bar{S}_{col}}{\rho}\right)_{med} \qquad (2.22)$$

The right hand side of Eq. (2.21) shows that absorbed dose can be calculated using a formally similar equation as Eq. (2.20) by making use of spectrum averaged collision stopping power and total fluence.

Based on Eq. (2.22) and under the same assumptions, for two media, med_1 and med_2, the ratio of absorbed doses can be calculated as:

$$\frac{D_{med_2}}{D_{med_1}} = (\Phi)_{med_2,med_1}\left(\frac{\bar{S}_{col}}{\rho}\right)_{med_2,med_1} \qquad (2.23)$$

where the shorthand notations:

$$(\Phi)_{med_2,med_1} \quad \text{and} \quad \left(\frac{\bar{S}_{col}}{\rho}\right)_{med_2,med_1}$$

are being used for the ratio of the electron fluences (often referred to as the electron fluence ratio) and the collision stopping powers in the media med_2 and med_1, respectively.

The full, realistic electron fluence spectrum consists of primary charged particles that, for example, are the result of a polyenergetic photon beam interacting in the medium. These primary charged particles are slowed down and result in secondary particle fluence. This fluence thus contains charged particles that result from slowing down through soft collisions as well as hard, knock-on collisions. Electrons created as a result of the latter process are designated delta electrons.

2.7.3.   Kerma and dose (charged particle equilibrium)

Generally, the transfer of energy (kerma) from the photon beam to charged particles at a particular location does not lead to the absorption of energy by the medium (absorbed dose) at the same location. This is due to the non-zero (finite) range of the secondary electrons released through photon interactions.

Since radiative photons mostly escape from the volume of interest, one relates absorbed dose usually to collision kerma. In general, however, the ratio of dose and collision kerma is often denoted as:

$$\beta = D/K_{col} \tag{2.24}$$

If radiative photons escape the volume of interest, an assumption is made that $\beta \approx 1$.

Figure 2.3 illustrates the relation between collision kerma and absorbed dose under buildup conditions; under conditions of CPE in part (a) and under conditions of transient charged particle equilibrium (TCPE) in part (b).

As a high energy photon beam penetrates the medium, collision kerma is maximal at the surface of the irradiated material because photon fluence is greatest at the surface. Initially, the charged particle fluence, and hence the absorbed dose, increases as a function of depth until the depth of dose maximum z_{max} is attained.

If there were no photon attenuation or scattering in the medium, but yet production of electrons, a hypothetical situation, as illustrated in Fig. 2.3(a), would occur: the buildup region (with $\beta < 1$) is followed by a region of complete CPE where $D = K_{col}$ (i.e. $\beta = 1$). g

In the more realistic situation, however, due to photon attenuation and scattering in the medium, a region of TCPE occurs (Fig. 2.3(b)) where there exists an essentially constant relation between collision kerma and absorbed dose. This relation is practically constant since, in high energy photon beams, the average energy of the generated electrons and hence their range does not change appreciably with depth in the medium.

In the special case in which true CPE exists (at the depth of maximum dose in the medium), the relation between absorbed dose D and total kerma K is given by:

$$D = K_{col} = K(1 - \bar{g}) \tag{2.25}$$

where $\bar{g}$ is the radiative fraction, depending on the electron kinetic energy; the higher the energy, the larger is $\bar{g}$. The radiative fraction also depends on the material considered, with higher values of $\bar{g}$ for higher Z materials. For electrons produced by ^{60}Co rays in air the radiative fraction equals 0.0032.

The buildup of absorbed dose is responsible for the skin sparing effect in the case of high energy photon beams. However, in practice the surface dose is small but does not equal zero because of the electron contamination in the beam due to photon interactions in the media upstream from the phantom or
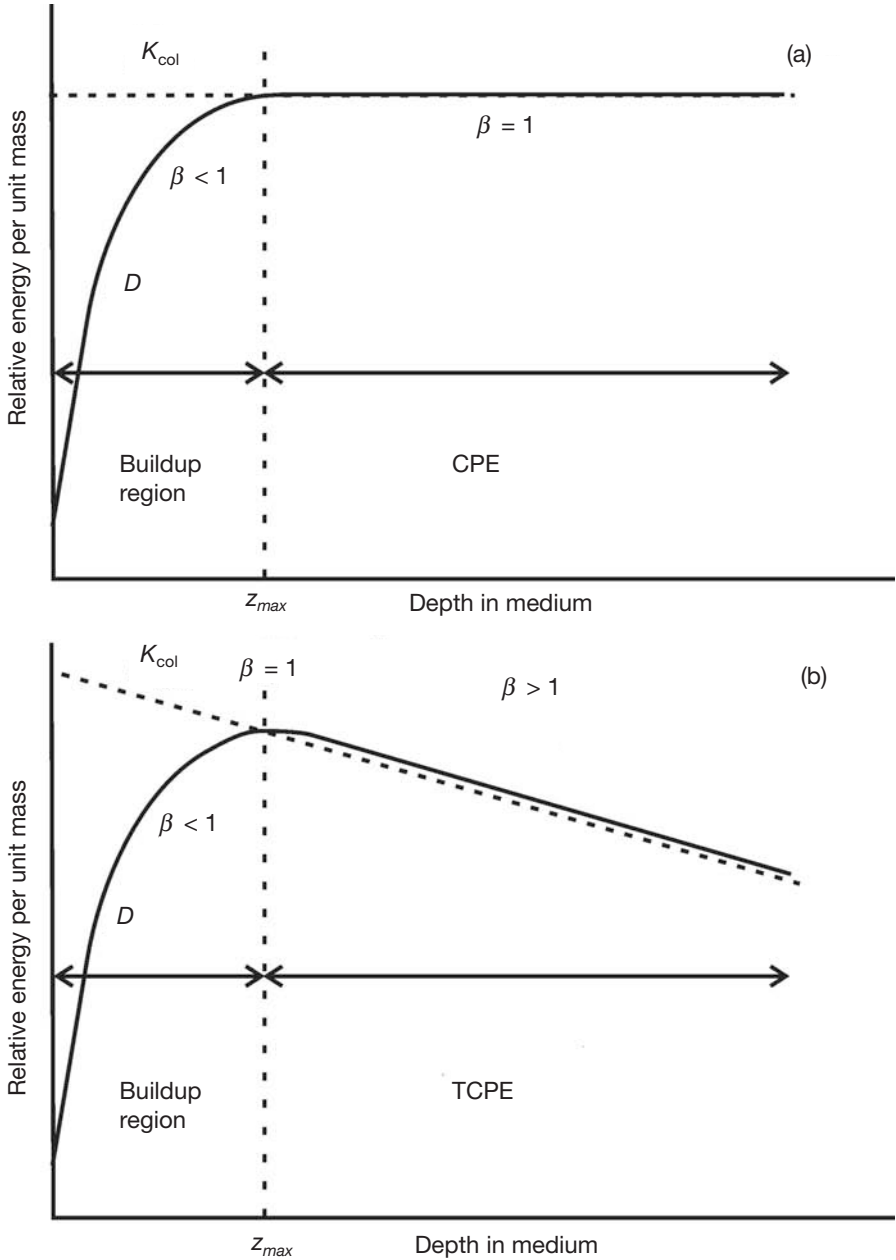
FIG. 2.3. Collision kerma and absorbed dose as a function of depth in a medium irradiated by a high energy photon beam for (a) the hypothetical case of no photon attenuation or scattering and for (b) the realistic case.

due to charged particles generated in the accelerator head and beam modifying devices.

2.7.4. Collision kerma and exposure

Exposure X is the quotient of dQ by dm, where dQ is the absolute value of the total charge of the ions of one sign produced in air when all the electrons and positrons liberated or created by photons in mass dm of air are completely stopped in air:

$$X = \frac{dQ}{dm} \qquad (2.26)$$

The unit of exposure is coulomb per kilogram (C/kg). The unit used for exposure is the roentgen R, where 1 R = 2.58×10^{-4} C/kg. In the SI system of units, roentgen is no longer used and the unit of exposure is simply 2.58×10^{-4} C/kg of air.

The average energy expended in air per ion pair formed W_{air} is the quotient of E_K by N, where N is the mean number of ion pairs formed when the initial kinetic energy E_K of a charged particle is completely dissipated in air:

$$W_{air} = \frac{E}{N} \qquad (2.27)$$

The current best estimate for the average value of W_{air} is 33.97 eV/ion pair or $33.97 \times 1.602 \times 10^{19}$ J/ion pair:

$$\frac{W_{air}}{e} = \frac{33.97 \ (\text{eV/ion pair}) \times 1.602 \times 10^{-19}(\text{J/eV})}{1.602 \times 10^{-19}(\text{C/ion pair})} = 33.97 \ \text{J/C} \qquad (2.28)$$

Multiplying the collision kerma by (e/W_{air}), the number of coulombs of charge created per joule of energy deposited, gives the charge created per unit mass of air or exposure:

$$X = (K_{col})_{air} \left(\frac{e}{W_{air}} \right) \qquad (2.29)$$

The relation between total kerma and exposure is obtained by combining Eqs (2.25) and (2.29):

$$K_{air} = X \left(\frac{W_{air}}{e} \right) \frac{1}{1 - \bar{g}} \qquad (2.30)$$

2.8. CAVITY THEORY

In order to measure the absorbed dose in a medium, it is necessary to introduce a radiation sensitive device (dosimeter) into the medium. Generally, the sensitive medium of the dosimeter will not be of the same material as the medium in which it is embedded. Cavity theory relates the absorbed dose in the dosimeter's sensitive medium (cavity) to the absorbed dose in the surrounding medium containing the cavity. Cavity sizes are referred to as small, intermediate or large in comparison with the ranges of secondary charged particles produced by photons in the cavity medium. If, for example, the range of charged particles (electrons) is much larger than the cavity dimensions, the cavity is regarded as small. Various cavity theories for photon beams have been developed, which depend on the size of the cavity; for example, the Bragg–Gray and Spencer–Attix theories for small cavities and the Burlin theory for cavities of intermediate sizes.

2.8.1. Bragg–Gray cavity theory

The Bragg–Gray cavity theory was the first cavity theory developed to provide a relation between the absorbed dose in a dosimeter and the absorbed dose in the medium containing the dosimeter.

The conditions for application of the Bragg–Gray cavity theory are:

(a) The cavity must be small when compared with the range of charged particles incident on it, so that its presence does not perturb the fluence of charged particles in the medium;
(b) The absorbed dose in the cavity is deposited solely by charged particles crossing it (i.e. photon interactions in the cavity are assumed negligible and thus ignored).

The result of condition (a) is that the electron fluences in Eq. (2.22) are the same and equal to the equilibrium fluence established in the surrounding medium. This condition can only be valid in regions of CPE or TCPE. In addition, the presence of a cavity always causes some degree of fluence perturbation that requires the introduction of a fluence perturbation correction factor.

Condition (b) implies that all electrons depositing the dose inside the cavity are produced outside the cavity and completely cross the cavity. No secondary electrons are therefore produced inside the cavity and no electrons stop within the cavity.

Under these two conditions, according to the Bragg–Gray cavity theory, the dose to the medium D_{med} is related to the dose in the cavity D_{cav} as follows:

$$D_{med} = D_{cav}\left(\frac{\bar{S}}{\rho}\right)_{med,cav} \tag{2.31}$$

where $(\bar{S}/\rho)_{med,cav}$ is the ratio of the average unrestricted mass collision stopping powers of the medium and the cavity. The use of unrestricted stopping powers rules out the production of secondary charged particles (or delta electrons) in the cavity and the medium.

Although the cavity size is not explicitly taken into account in the Bragg–Gray cavity theory, the fulfilment of the two Bragg–Gray conditions will depend on the cavity size, which is based on the range of the electrons in the cavity medium, the cavity medium and the electron energy. A cavity that qualifies as a Bragg–Gray cavity for high energy photon beams, for example, may not behave as a Bragg–Gray cavity in a medium energy or low energy X ray beam.

2.8.2. Spencer–Attix cavity theory

The Bragg–Gray cavity theory does not take into account the creation of secondary (delta) electrons generated as a result of hard collisions in the slowing down of the primary electrons in the sensitive volume of the dosimeter. The Spencer–Attix cavity theory is a more general formulation that accounts for the creation of these electrons that have sufficient energy to produce further ionization on their own account. Some of these electrons released in the gas cavity would have sufficient energy to escape from the cavity, carrying some of their energy with them. This reduces the energy absorbed in the cavity and requires modification of the stopping power of the gas. The Spencer–Attix theory operates under the two Bragg–Gray conditions; however, these conditions now even apply to the secondary particle fluence in addition to the primary particle fluence.

The secondary electron fluence in the Spencer–Attix theory is divided into two components based on a user defined energy threshold Δ. Secondary electrons with kinetic energies E_K less than Δ are considered slow electrons that deposit their energy locally; secondary electrons with energies larger than or equal to Δ are considered fast (slowing down) electrons and are part of the electron spectrum. Consequently, this spectrum has a low energy threshold of Δ and a high energy threshold of E_{K0}, where E_{K0} represents the initial electron kinetic energy. Since the lowest energy in the spectrum is Δ, the maximum energy loss of a fast electron with kinetic energy E_K larger than or equal to 2Δ

cannot be larger than Δ, and the maximum energy loss of a fast electron with kinetic energy less than 2Δ cannot be larger than $E_K/2$ (where $\Delta \leq E_K < 2\Delta$).

The energy deposition must be calculated as the product of $L_\Delta(E_K)/\rho$, the restricted collision stopping power with threshold Δ, and $\Phi_{\text{med},E_K}^{\text{e-e}}$, the fast electron fluence ranging in energy from Δ to E_{K0} (e-e stands for the contribution of delta electrons in the slowing down spectrum).

Owing to the Bragg–Gray condition, which stipulates that there must not be electron production in the cavity, the electrons with energy Δ must be capable of crossing the cavity. The threshold value Δ is hence related to the cavity size and is defined as the energy of the electron with a range equal to the mean chord length across the cavity.

The Spencer–Attix relation between the dose to the medium and the dose in the cavity is thus written as:

$$D_{\text{med}}/D_{\text{cav}} = s_{\text{med,cav}} \tag{2.32}$$

where $s_{\text{med,cav}}$ is the ratio of the mean restricted mass collision stopping powers of the medium to that of the cavity.

Using the medium electron fluence spectrum $\Phi_{\text{med},E_K}^{\text{e-e}}(E_K)$, the full expression is:

$$s_{\text{med,cav}} = \frac{\int_\Delta^{E_{K0}} \Phi_{\text{med},E_K}^{\text{e-e}}(E_K)(L_{\Delta,\text{med}}/\rho)\mathrm{d}(E_K) + \text{TE}_{\text{med}}}{\int_\Delta^{E_{K0}} \Phi_{\text{med},E_K}^{\text{e-e}}(E_K)(L_{\Delta,\text{cav}}/\rho)\mathrm{d}(E_K) + \text{TE}_{\text{cav}}} \tag{2.33}$$

The terms TE_{med} and TE_{cav} are called the track end terms and account for a part of the energy deposited by electrons with initial kinetic energies between Δ and 2Δ. These electrons can have an energy loss that brings their kinetic energy to lower than Δ. Their residual energy after such events should be deposited on the spot, and these electrons are removed from the spectrum. The track end terms are approximated by Nahum as:

$$\text{TE}_{\text{med}} = \Phi_{\text{med},E_K}^{\text{e-e}}(\Delta)\frac{S_{\text{med}}(\Delta)}{\rho}\Delta \tag{2.34}$$

and

$$\text{TE}_{\text{cav}} = \Phi_{\text{med},E_K}^{\text{e-e}}(\Delta)\frac{S_{\text{cav}}(\Delta)}{\rho}\Delta \tag{2.35}$$

Note that the unrestricted collision stopping powers can be used here because the maximum energy transfer for an electron with energy less than 2Δ is less than Δ.

Monte Carlo calculations have shown that the difference between the Spencer–Attix and Bragg–Gray cavity theories is non-negligible yet generally not very significant. Since collision stopping powers for different media show similar trends as a function of particle energy, their ratio for the two media is a very slowly varying function with energy.

The value of the stopping power water to air ratio for ionization chambers is only weakly dependent on the choice of the cut-off energy. For Farmer type chambers and for parallel-plate chambers used in radiotherapy physics a nominal value of 10 keV is often used.

For a typical ionization chamber used in water, the energy dependence of the stopping power water to air ratio arises mainly from the difference in the density effect correction between the two materials.

2.8.3. Considerations in the application of cavity theory to ionization chamber calibration and dosimetry protocols

A dosimeter can be defined generally as any device that is capable of providing a reading that is a measure of the average absorbed dose deposited in its (the dosimeter's) sensitive volume by ionizing radiation. A dosimeter can generally be considered as consisting of a sensitive volume filled with a given medium, surrounded by a wall of another medium.

In the context of cavity theories, the sensitive volume of the dosimeter can be identified as the 'cavity', which may contain a gaseous, liquid or solid medium. Gas is often used as the sensitive medium, since it allows a relatively simple electrical means for collection of charges released in the sensitive medium by radiation.

The medium surrounding the cavity of an ionization chamber depends on the situation in which the device is used. In an older approach, the wall (often supplemented with a buildup cap) serves as the buildup medium and the Bragg–Gray theory provides a relation between the dose in the gas and the dose in the wall. This is referred to as a thick walled ionization chamber and forms the basis of cavity chamber based air kerma in-air standards and of the C_λ based dosimetry protocols of the 1970s. If, however, the chamber is used in a phantom without a buildup material, since typical wall thicknesses are much thinner than the range of the secondary electrons, the proportion of the cavity dose due to electrons generated in the phantom greatly exceeds the dose contribution from the wall, and hence the phantom medium serves as the medium and the wall is treated as a perturbation to this concept.

In the case of a thick walled ionization chamber in a high energy photon beam, the wall thickness must be greater than the range of secondary electrons in the wall material to ensure that the electrons that cross the cavity arise in the wall and not in the medium. The Bragg–Gray cavity equation then relates the dose in the cavity to the dose in the wall of the chamber. The dose in the medium is related to the dose in the wall by means of a ratio of the mass–energy absorption coefficients of the medium and the wall $(\bar{\mu}_{en}/\rho)_{med,wall}$ by assuming that:

(a)   The absorbed dose is the same as the collision kerma;
(b)   The photon fluence is not perturbed by the presence of the chamber.

The dose to the cavity gas is related to the ionization produced in the cavity as follows:

$$D_{gas} = \frac{Q}{m}\left(\frac{\overline{W}_{gas}}{e}\right) \qquad (2.36)$$

where Q is the charge (of either sign) produced in the cavity and m is the mass of the gas in the cavity.

Spencer–Attix cavity theory can be used to calculate the dose in the medium as:

$$D_{med} = D_{wall}\left(\frac{\bar{\mu}_{en}}{\rho}\right)_{med,wall} = D_{gas}s_{wall,gas}\left(\frac{\bar{\mu}_{en}}{\rho}\right)_{med,wall}$$

$$= \frac{Q}{m}\left(\frac{\overline{W}_{gas}}{e}\right)s_{wall,gas}\left(\frac{\bar{\mu}_{en}}{\rho}\right)_{med,wall} \qquad (2.37)$$

where $s_{wall,gas}$ is the ratio of restricted mass collision stopping powers for a cavity wall and gas with threshold Δ. In practice, there are additional correction factors associated with Eq. (2.37) to satisfy assumptions (a) and (b) made above.

A similar equation to Eq. (2.37) is used for air kerma in-air calibrations; however, here the quantity of interest is not the dose to the medium, but the air kerma in air. In this case, a substantial wall correction is introduced to ensure the presence of complete CPE in the wall to satisfy assumption (a) above.

In the case of a thin walled ionization chamber in a high energy photon or electron beam, the wall, cavity and central electrode are treated as a

perturbation to the medium fluence, and the equation now involves the ratio of restricted collision stopping powers of the medium to that of the gas $s_{\text{med,gas}}$ as:

$$D_{\text{med}} = \frac{Q}{m} \left(\frac{\overline{W}_{\text{gas}}}{e} \right) s_{\text{med,gas}} p_{\text{fl}} \, p_{\text{dis}} \, p_{\text{wall}} \, p_{\text{cel}} \tag{2.38}$$

where

p_{fl} is the electron fluence perturbation correction factor;
p_{dis} is the correction factor for displacement of the effective measurement point;
p_{wall} is the wall correction factor;
p_{cel} is the correction factor for the central electrode.

Values for these multiplicative correction factors are summarized for photon and electron beams in typical dosimetry protocols (see Section 9.7 for details).

2.8.4. Large cavities in photon beams

A large cavity is a cavity with dimensions such that the dose contribution made by electrons inside the cavity originating from photon interactions outside the cavity can be ignored when compared with the contribution of electrons created by photon interactions within the cavity.

For a large cavity the ratio of dose cavity to medium is calculated as the ratio of the collision kerma in the cavity to the medium and is therefore equal to the ratio of the average mass–energy absorption coefficients of the cavity gas to that of the medium $(\bar{\mu}/\rho)_{\text{gas,med}}$:

$$\frac{D_{\text{gas}}}{D_{\text{med}}} = \left(\frac{\bar{\mu}_{\text{en}}}{\rho} \right)_{\text{gas,med}} \tag{2.39}$$

where the mass–energy absorption coefficients have been averaged over the photon fluence spectra in the cavity gas (numerator) and in the medium (denominator).

2.8.5. Burlin cavity theory for photon beams

Burlin extended the Bragg–Gray and Spencer–Attix cavity theories to cavities of intermediate dimensions by introducing, on a purely phenomeno-logical basis, a large cavity limit to the Spencer–Attix equation using a

weighting technique. He provided a formalism to calculate the value of the weighting parameter.

The Burlin cavity theory can be written in its simplest form as follows:

$$\frac{D_{\text{gas}}}{D_{\text{med}}} = d s_{\text{gas,med}} + (1-d)\left(\frac{\bar{\mu}_{\text{en}}}{\rho}\right)_{\text{gas,med}} \tag{2.40}$$

where

d	is a parameter related to cavity size, approaching unity for small cavities and zero for large cavities;
$s_{\text{gas,med}}$	is the mean ratio of the restricted mass stopping powers of the cavity and the medium;
D_{gas}	is the absorbed dose in the cavity;
$(\bar{\mu}_{\text{en}}/\rho)_{\text{gas,med}}$	is the mean ratio of the mass–energy absorption coefficients for the cavity and the medium.

The Burlin theory effectively requires that:

- The surrounding medium and the cavity medium be homogeneous;
- A homogeneous photon field exist everywhere throughout the medium and the cavity;
- CPE exist at all points in the medium and the cavity that are further than the maximum electron range from the cavity boundary;
- The equilibrium spectra of secondary electrons generated in the medium and the cavity be the same.

Burlin provided a method for estimating the weighting parameter d in his theory. It is expressed as the average value of the electron fluence reduction in the medium. Consistent with experiments with β sources he proposed that the electron fluence in the medium $\Phi_{\text{med}}^{\text{e-e}}$ decays, on average, exponentially. The value of the weighting parameter d in conjunction with the stopping power ratio can be calculated as:

$$d = \frac{\displaystyle\int_0^L \Phi_{\text{med}}^{\text{e-e}} e^{-\beta l}\,\mathrm{d}l}{\displaystyle\int_0^L \Phi_{\text{med}}^{\text{e-e}}\,\mathrm{d}l} = \frac{1-e^{-\beta L}}{\beta L} \tag{2.41}$$

where β is an effective electron fluence attenuation coefficient that quantifies the reduction in particle fluence from its initial medium fluence value through a cavity of average length L. For convex cavities and isotropic electron fluence distributions, L can be calculated as $4V/S$, where V is the cavity volume and S its surface area. Burlin described the buildup of the electron fluence $\Phi_{gas}^{e\text{-}e}$ inside the cavity using a similar, complementary equation:

$$1 - d = \frac{\int_0^L \Phi_{gas}^{e\text{-}e}(1 - e^{-\beta l})\,\mathrm{d}l}{\int_0^L \Phi_{gas}^{e\text{-}e}\,\mathrm{d}l} = \frac{\beta L - 1 + e^{-\beta L}}{\beta L} \tag{2.42}$$

Burlin's theory is consistent with the fundamental constraint of cavity theory: that the weighting factors of both terms add up to unity (i.e. d and $1 - d$). It had relative success in calculating ratios of absorbed dose for some types of intermediate cavities. More generally, however, Monte Carlo calculations show that, when studying ratios of directly calculated absorbed doses in the cavity to absorbed dose in the medium as a function of cavity size, the weighting method is too simplistic and additional terms are necessary to calculate dose ratios for intermediate cavity sizes. For these and other reasons, the Burlin cavity theory is no longer used in practice.

2.8.6. Stopping power ratios

Although cavity theory was designed to calculate ratios of absorbed doses, the practical application of the Spencer–Attix cavity theory has always required additional correction factors. Since the central component of the Spencer–Attix cavity theory results in averaging stopping powers, Spencer–Attix dose ratios are often referred to as 'stopping power ratios'.

In photon beams, except at or near the surface, average restricted stopping power ratios of water to air do not vary significantly as a function of depth. Stopping power ratios (with $\Delta = 10$ keV) under full buildup conditions are shown in Table 2.1.

Stopping power ratios not only play a role in the absolute measurement of absorbed dose, they are also relevant in performing accurate relative measurements of absorbed dose in regimes in which the energy of the secondary electrons changes significantly from one point in a phantom to another. An important example of this is apparent from Fig. 2.4, which shows restricted stopping power ratios ($\Delta = 10$ keV) of water to air for electron beams as a function of depth in water. Note that these curves are for monoenergetic

TABLE 2.1.   AVERAGE RESTRICTED STOPPING POWER RATIO OF WATER TO AIR, $s_{\text{water,air}}$, FOR DIFFERENT PHOTON SPECTRA IN THE RANGE FROM ^{60}Co γ RAYS TO 35 MV X RAYS

Photon spectrum	$s_{\text{water,air}}$
^{60}Co	1.134
4 MV	1.131
6 MV	1.127
8 MV	1.121
10 MV	1.117
15 MV	1.106
20 MV	1.096
25 MV	1.093
35 MV	1.084
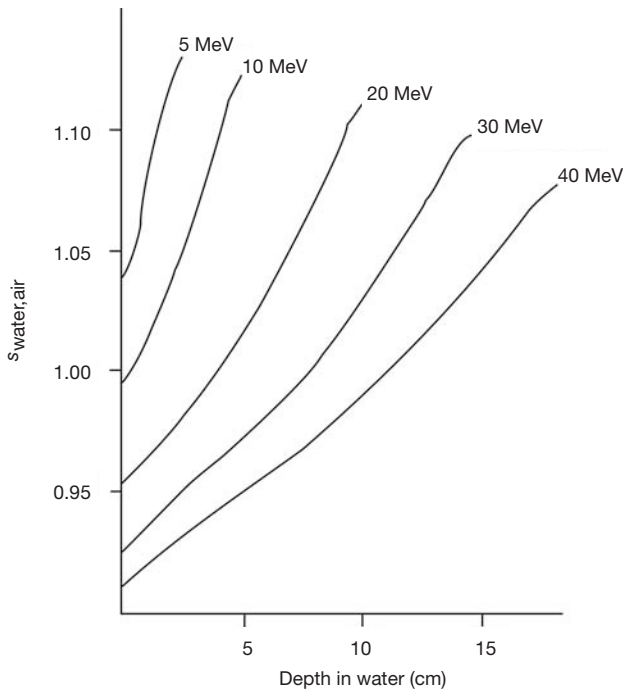
FIG. 2.4. *Restricted collision stopping power water to air ratio ($\Delta = 10$ keV) as a function of depth for different monoenergetic electron energies.*

electrons; protocols or codes of practice for electron dosimetry provide fits of stopping power ratios for realistic accelerator beams. However, Fig. 2.4 shows clearly that the accurate measurement of electron beam depth dose curves requires depth dependent correction factors.

More detailed information on stopping power ratios is given in Section 9.5.

BIBLIOGRAPHY

ATTIX, F.H., Introduction to Radiological Physics and Radiation Dosimetry, Wiley, New York (1986).

GREENING, J.R., Fundamentals of Radiation Dosimetry, Adam Hilger, Bristol (1981).

INTERNATIONAL COMMISSION ON RADIATION UNITS AND MEASUREMENTS, Stopping Powers for Electrons and Positrons, Rep. 37, ICRU, Bethesda, MD (1984).

— Fundamental Quantities and Units for Ionizing Radiation, Rep. 60, ICRU, Bethesda, MD (1998).

JOHNS, H.E., CUNNINGHAM, J.R., The Physics of Radiology, Thomas, Springfield, IL (1985).

KHAN, F.M., The Physics of Radiation Therapy, Lippincott, Williams and Wilkins, Baltimore, MD (2003).

Chapter 3

RADIATION DOSIMETERS

J. IZEWSKA
Division of Human Health,
International Atomic Energy Agency,
Vienna

G. RAJAN
Medical Physics and Safety Section,
Bhabha Atomic Research Centre,
Mumbai, Maharashtra, India

3.1. INTRODUCTION

A radiation dosimeter is a device, instrument or system that measures or evaluates, either directly or indirectly, the quantities exposure, kerma, absorbed dose or equivalent dose, or their time derivatives (rates), or related quantities of ionizing radiation. A dosimeter along with its reader is referred to as a dosimetry system.

Measurement of a dosimetric quantity is the process of finding the value of the quantity experimentally using dosimetry systems. The result of a measurement is the value of a dosimetric quantity expressed as the product of a numerical value and an appropriate unit.

To function as a radiation dosimeter, the dosimeter must possess at least one physical property that is a function of the measured dosimetric quantity and that can be used for radiation dosimetry with proper calibration. In order to be useful, radiation dosimeters must exhibit several desirable characteristics. For example, in radiotherapy exact knowledge of both the absorbed dose to water at a specified point and its spatial distribution are of importance, as well as the possibility of deriving the dose to an organ of interest in the patient. In this context, the desirable dosimeter properties will be characterized by accuracy and precision, linearity, dose or dose rate dependence, energy response, directional dependence and spatial resolution.

Obviously, not all dosimeters can satisfy all characteristics. The choice of a radiation dosimeter and its reader must therefore be made judiciously, taking into account the requirements of the measurement situation; for example, in radiotherapy ionization chambers are recommended for beam calibrations

(reference dosimetry: see Chapter 9) and other dosimeters, such as those discussed below, are suitable for the evaluation of the dose distribution (relative dosimetry) or dose verification.

3.2. PROPERTIES OF DOSIMETERS

3.2.1. Accuracy and precision

In radiotherapy dosimetry the uncertainty associated with the measurement is often expressed in terms of accuracy and precision. The precision of dosimetry measurements specifies the reproducibility of the measurements under similar conditions and can be estimated from the data obtained in repeated measurements. High precision is associated with a small standard deviation of the distribution of the measurement results. The accuracy of dosimetry measurements is the proximity of their expectation value to the 'true value' of the measured quantity. Results of measurements cannot be absolutely accurate and the inaccuracy of a measurement result is characterized as 'uncertainty'.

The uncertainty is a parameter that describes the dispersion of the measured values of a quantity; it is evaluated by statistical methods (type A) or by other methods (type B), has no known sign and is usually assumed to be symmetrical.

The error of measurement is the difference between the measured value of a quantity and the true value of that quantity.

- An error has both a numerical value and a sign.
- Typically, the measurement errors are not known exactly, but they are estimated in the best possible way, and, where possible, compensating corrections are introduced.
- After application of all known corrections, the expectation value for errors should be zero and the only quantities of concern are the uncertainties.

3.2.1.1. Type A standard uncertainties

If a measurement of a dosimetric quantity x is repeated N times, then the best estimate for x is $\bar{x}$, the arithmetic mean value of all measurements x_i:

$$\bar{x} = \frac{1}{N}\sum_{i=1}^{N} x_i \tag{3.1}$$

The standard deviation σ_x characterizes the average uncertainty for an individual result x_i and is given by:

$$\sigma_x = \sqrt{\frac{1}{N-1}\sum_{i=1}^{N}(x_i - \bar{x})^2} \tag{3.2}$$

The standard deviation of the mean value is given by:

$$\sigma_{\bar{x}} = \frac{1}{\sqrt{N}}\sigma_x = \sqrt{\frac{1}{N(N-1)}\sum_{i=1}^{N}(x_i - \bar{x})^2} \tag{3.3}$$

- The standard uncertainty of type A, denoted u_A, is defined as the standard deviation of the mean value, $u_A = \sigma_{\bar{x}}$.
- The standard uncertainty of type A is obtained by a statistical analysis of repeated measurements and, in principle, can be reduced by increasing the number of measurements.

3.2.1.2. Type B standard uncertainties

Type B standard uncertainties u_B cannot be estimated by repeated measurements; rather, they are intelligent guesses or scientific judgements of non-statistical uncertainties associated with the measurement. They include influences on the measuring process, application of correction factors or physical data taken from the literature.

It is often assumed that type B standard uncertainties have a probability distribution, such as a normal (Gaussian) or a rectangular distribution (equal probability anywhere within the given limits). Type B standard uncertainties can be derived by estimating the limit beyond which the value of the factor is not going to lie, and a fraction of this limit is taken as u_B. The fraction is chosen according to the distribution assumed.

3.2.1.3. Combined and expanded uncertainties

The equation that determines a dosimetric quantity Q at a point P is of the type:

$$Q_P = M \prod_{i=1}^{N} F_i \qquad (3.4)$$

where M is the reading provided by the dosimetry system and F_i is the correction or conversion coefficient.

- The combined standard uncertainty u_C associated with the quantity Q is a quadratic summation of type A (u_A) and type B (u_B) uncertainties:

$$u_C = \sqrt{u_A^2 + u_B^2} \qquad (3.5)$$

- The combined uncertainty is assumed to exhibit a normal distribution and is multiplied by a coverage factor, denoted by k, to obtain the expanded uncertainty $U = k u_C$. The result of the measurement of the quantity Q is then expressed by $Q_P \pm U$.
- The expanded uncertainty U with the coverage factor $k = 2$, corresponding to the 95% confidence level, is often used to represent the overall uncertainty, which relates to the accuracy of the measurement of the quantity Q.

3.2.2. Linearity

Ideally, the dosimeter reading M should be linearly proportional to the dosimetric quantity Q. However, beyond a certain dose range a non-linearity sets in. The linearity range and the non-linearity behaviour depend on the type of dosimeter and its physical characteristics.

Two typical examples of response characteristics of dosimetry systems are shown in Fig. 3.1. Curve A first exhibits linearity with dose, then a supralinear behaviour, and finally saturation. Curve B first exhibits linearity and then saturation at high doses.

In general, a non-linear behaviour should be corrected for. A dosimeter and its reader may both exhibit non-linear characteristics, but their combined effect could produce linearity over a wider range.

3.2.3. Dose rate dependence

Integrating systems measure the integrated response of a dosimetry system. For such systems the measured dosimetric quantity should be independent of the rate of that quantity.
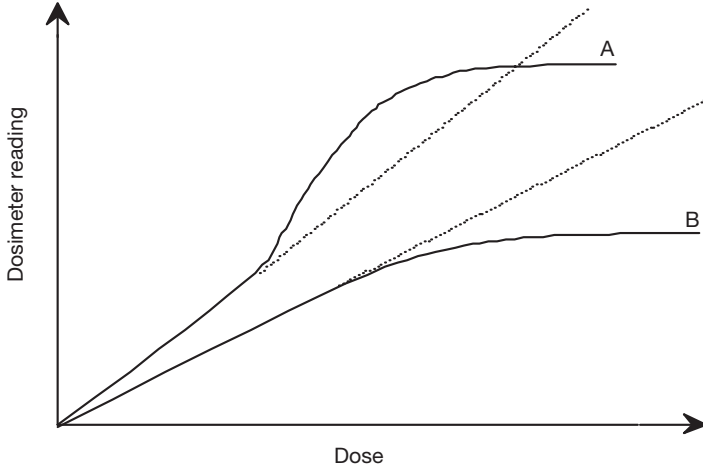
FIG. 3.1. Response characteristics of two dosimetry systems. Curve A first exhibits linearity with dose, then supralinear behaviour and finally saturation. Curve B first exhibits linearity and then saturation at high doses.

Ideally, the response of a dosimetry system M/Q at two different dose rates $((dQ/dt)_1$ and $(dQ/dt)_2)$ should remain constant. In reality, the dose rate may influence the dosimeter readings and appropriate corrections are necessary, for example recombination corrections for ionization chambers in pulsed beams.

3.2.4. Energy dependence

The response of a dosimetry system M/Q is generally a function of radiation beam quality (energy). Since the dosimetry systems are calibrated at a specified radiation beam quality (or qualities) and used over a much wider energy range, the variation of the response of a dosimetry system with radiation quality (called energy dependence) requires correction.

Ideally, the energy response should be flat (i.e. the system calibration should be independent of energy over a certain range of radiation qualities). In reality, the energy correction has to be included in the determination of the quantity Q for most measurement situations. In radiotherapy, the quantity of interest is the dose to water (or to tissue). As no dosimeter is water or tissue equivalent for all radiation beam qualities, the energy dependence is an important characteristic of a dosimetry system.

3.2.5. Directional dependence

The variation in response of a dosimeter with the angle of incidence of radiation is known as the directional, or angular, dependence of the dosimeter. Dosimeters usually exhibit directional dependence, due to their constructional details, physical size and the energy of the incident radiation. Directional dependence is important in certain applications, for example in in vivo dosimetry while using semiconductor dosimeters. Therapy dosimeters are generally used in the same geometry as that in which they are calibrated.

3.2.6. Spatial resolution and physical size

Since the dose is a point quantity, the dosimeter should allow the determination of the dose from a very small volume (i.e. one needs a 'point dosimeter' to characterize the dose at a point). The position of the point where the dose is determined (i.e. its spatial location) should be well defined in a reference coordinate system.

Thermoluminescent dosimeters (TLDs) come in very small dimensions and their use, to a great extent, approximates a point measurement. Film dosimeters have excellent 2-D and gels 3-D resolution, where the point measurement is limited only by the resolution of the evaluation system. Ionization chamber type dosimeters, however, are of finite size to give the required sensitivity, although the new type of pinpoint microchambers partially overcomes the problem.

3.2.7. Readout convenience

Direct reading dosimeters (e.g. ionization chambers) are generally more convenient than passive dosimeters (i.e. those that are read after due processing following the exposure, for example TLDs and films). While some dosimeters are inherently of the integrating type (e.g. TLDs and gels), others can measure in both integral and differential modes (ionization chambers).

3.2.8. Convenience of use

Ionization chambers are reusable, with no or little change in sensitivity within their lifespan. Semiconductor dosimeters are reusable, but with a gradual loss of sensitivity within their lifespan; however, some dosimeters are not reusable (e.g. films, gels and alanine). Some dosimeters measure dose distribution in a single exposure (e.g. films and gels) and some dosimeters are

quite rugged (i.e. handling will not influence sensitivity, for example ionization chambers), while others are sensitive to handling (e.g. TLDs).

3.3. IONIZATION CHAMBER DOSIMETRY SYSTEMS

3.3.1. Chambers and electrometers

Ionization chambers are used in radiotherapy and in diagnostic radiology for the determination of radiation dose. The dose determination in reference irradiation conditions is also called beam calibration (see Chapter 9 for details). Ionization chambers come in various shapes and sizes, depending upon the specific requirements, but generally they all have the following properties:

- An ionization chamber is basically a gas filled cavity surrounded by a conductive outer wall and having a central collecting electrode (see Fig. 3.2). The wall and the collecting electrode are separated with a high quality insulator to reduce the leakage current when a polarizing voltage is applied to the chamber.
- A guard electrode is usually provided in the chamber to further reduce chamber leakage. The guard electrode intercepts the leakage current and allows it to flow to ground, bypassing the collecting electrode. It also ensures improved field uniformity in the active or sensitive volume of the chamber, with resulting advantages in charge collection.
- Measurements with open air ionization chambers require temperature and pressure correction to account for the change in the mass of air in the chamber volume, which changes with the ambient temperature and pressure.
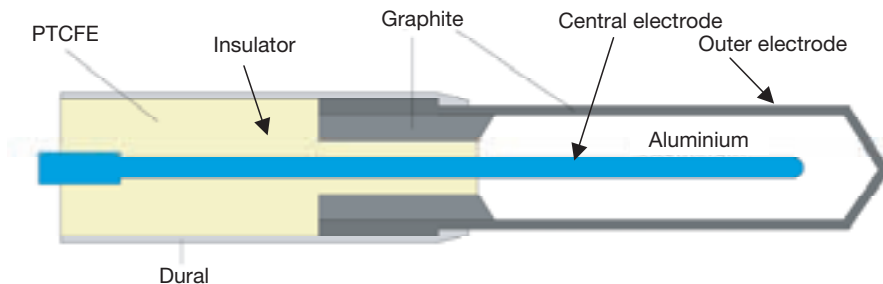
FIG. 3.2. Basic design of a cylindrical Farmer type ionization chamber.

Electrometers are devices for measuring small currents, of the order of 10^{-9} A or less. An electrometer used in conjunction with an ionization chamber is a high gain, negative feedback, operational amplifier with a standard resistor or a standard capacitor in the feedback path to measure the chamber current or charge collected over a fixed time interval, as shown schematically in Fig. 3.3.

3.3.2. Cylindrical (thimble type) ionization chambers

The most popular cylindrical ionization chamber is the 0.6 cm^3 chamber designed by Farmer and originally manufactured by Baldwin, but now available from several vendors, for beam calibration in radiotherapy dosimetry. Its chamber sensitive volume resembles a thimble, and hence the Farmer type chamber is also known as a thimble chamber. A schematic diagram of a Farmer type thimble ionization chamber is shown in Fig. 3.2; ionization chamber based dosimetry systems are discussed in Section 9.2.

Cylindrical chambers are produced by various manufacturers, with active volumes between 0.1 and 1 cm^3. They typically have an internal length no greater than 25 mm and an internal diameter no greater than 7 mm. The wall material is of low atomic number Z (i.e. tissue or air equivalent), with the thickness less than 0.1 g/cm^2. A chamber is equipped with a buildup cap with a thickness of about 0.5 g/cm^2 for calibration free in air using ^{60}Co radiation.

The chamber construction should be as homogeneous as possible, although an aluminium central electrode of about 1 mm in diameter is typically

C_f

R_f

-

+

I

$V = I_1 R_f$ (rate mode)

$V = (I_1 \times t)/C_f$ (integrated mode)

R_f = feedback resistor
(variable to vary sensitivity)

C_f = feedback capacitor
(variable to vary sensitivity)
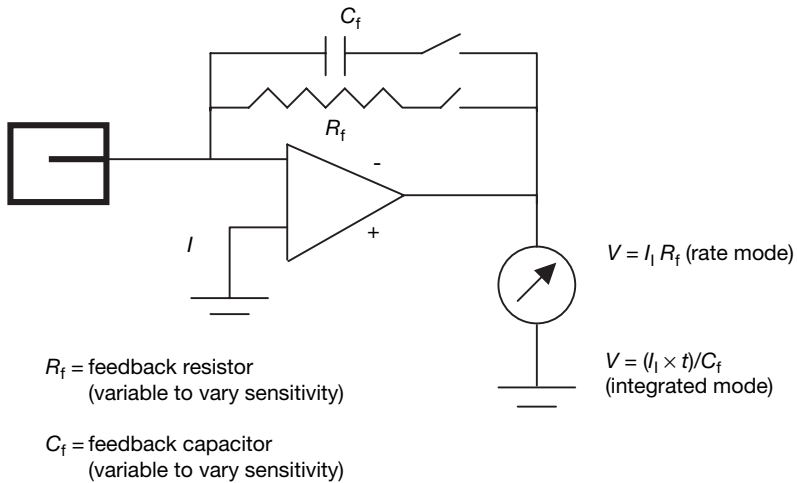
FIG. 3.3. Electrometer in feedback mode of operation.

used to ensure flat energy dependence. Construction details of various commercially available cylindrical chambers are given in the IAEA Technical Reports Series (TRS) 277 and TRS 398 codes of practice. The use of the cylindrical chamber in electron and photon beam dosimetry is discussed in Chapter 9.

3.3.3. Parallel-plate (plane-parallel) ionization chambers

A parallel-plate ionization chamber consists of two plane walls, one serving as an entry window and polarizing electrode and the other as the back wall and collecting electrode, as well as a guard ring system. The back wall is usually a block of conducting plastic or a non-conducting material (usually Perspex or polystyrene) with a thin conducting layer of graphite forming the collecting electrode and the guard ring system on top. A schematic diagram of a parallel-plate ionization chamber is shown in Fig. 3.4.

The parallel-plate chamber is recommended for dosimetry of electron beams with energies below 10 MeV. It is also used for surface dose and depth dose measurements in the buildup region of megavoltage photon beams. Dose measurements in the buildup region of photon beams are discussed in Section 6.13. The characteristics of commercially available parallel-plate chambers and the use of these chambers in electron beam dosimetry are explained in detail in the TRS 381 and TRS 398 codes of practice. Some parallel-plate chambers require significant fluence perturbation correction because they are provided with an inadequate guard width.

3.3.4. Brachytherapy chambers

Sources used in brachytherapy are low air kerma rate sources that require chambers of sufficient volume (about 250 cm^3 or more) for adequate sensitivity. Well type chambers or re-entrant chambers are ideally suited for calibration and standardization of brachytherapy sources. Figure 3.5 shows a schematic diagram of a well type chamber.

Well type chambers should be designed to accommodate sources of the typical sizes and shapes that are in clinical use in brachytherapy and are usually calibrated in terms of the reference air kerma rate.

3.3.5. Extrapolation chambers

Extrapolation chambers are parallel-plate chambers with a variable sensitive volume. They are used in the measurement of surface doses in ortho-

Schnitt A–B
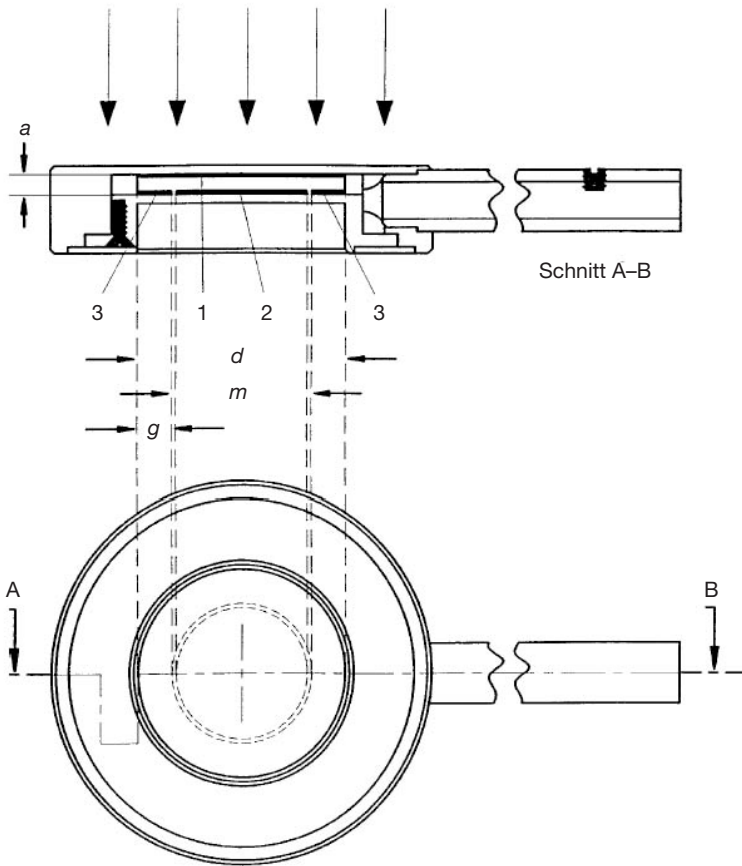
FIG. 3.4. Parallel-plate ionization chamber. 1: the polarizing electrode. 2: the measuring electrode. 3: the guard ring. a: the height (electrode separation) of the air cavity. d: the diameter of the polarizing electrode. m: the diameter of the collecting electrode. g: the width of the guard ring.

voltage and megavoltage X ray beams and in the dosimetry of β rays, and low energy X rays. They can also be used in absolute radiation dosimetry when directly embedded into a tissue equivalent phantom. The cavity perturbation for electrons can be eliminated by making measurements as a function of the cavity thickness and then extrapolating to zero thickness. Using this chamber, the cavity perturbation for parallel-plate chambers of finite thickness can be estimated.
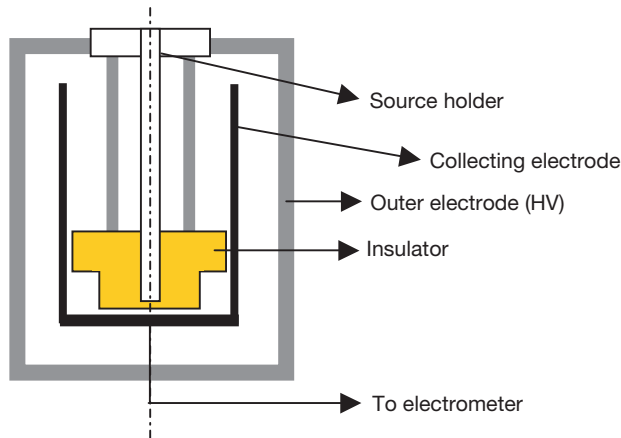
FIG. 3.5. Basic design of a brachytherapy well type chamber.

3.4. FILM DOSIMETRY

3.4.1. Radiographic film

Radiographic X ray film performs several important functions in diagnostic radiology, radiotherapy and radiation protection. It can serve as a radiation detector, a relative dosimeter, a display device and an archival medium.

Unexposed X ray film consists of a base of thin plastic with a radiation sensitive emulsion (silver bromide (AgBr) grains suspended in gelatin) coated uniformly on one or both sides of the base.

- Ionization of AgBr grains, as a result of radiation interaction, forms a latent image in the film. This image only becomes visible (film blackening) and permanent subsequently to processing.
- Light transmission is a function of the film opacity and can be measured in terms of optical density (OD) with devices called densitometers.
- The OD is defined as $OD = \log_{10} (I_0/I)$ and is a function of dose. I_0 is the initial light intensity and I is the intensity transmitted through the film.
- Film gives excellent 2-D spatial resolution and, in a single exposure, provides information about the spatial distribution of radiation in the area of interest or the attenuation of radiation by intervening objects.

- The useful dose range of film is limited and the energy dependence is pronounced for lower energy photons. The response of the film depends on several parameters, which are difficult to control. Consistent processing of the film is a particular challenge in this regard.
- Typically, film is used for qualitative dosimetry, but with proper calibration, careful use and analysis film can also be used for dose evaluation.
- Various types of film are available for radiotherapy work (e.g. direct exposure non-screen films for field size verification, phosphor screen films used with simulators and metallic screen films used in portal imaging).
- Unexposed film would exhibit a background OD called the fog density (OD_f). The density due to radiation exposure, called the net OD, can be obtained from the measured density by subtracting the fog density.
- OD readers include film densitometers, laser densitometers and automatic film scanners. The principle of operation of a simple film densitometer is shown in Fig. 3.6.

Ideally, the relationship between the dose and OD should be linear, but this is not always the case. Some emulsions are linear, some are linear over a limited dose range and others are non-linear. The dose versus OD curve, known as the sensitometric curve (also known as the characteristic or H&D curve, in honour of Hurter and Driffield, who first investigated the relationship) must therefore be established for each film before using it for dosimetry work.

A typical H&D curve for a radiographic film is shown in Fig. 3.7. It has four regions: (1) fog, at low or zero exposures; (2) toe; (3) a linear portion at
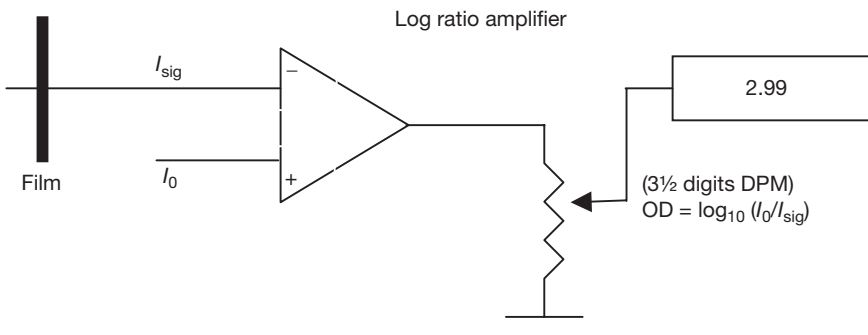
FIG. 3.6. Basic film densitometer.

intermediate exposures; and (4) shoulder and saturation at high exposures. The linear portion is referred to as optimum measurement conditions, the toe is the region of underexposure and the shoulder is the region of overexposure.

Important parameters of film response to radiation are gamma, latitude and speed:

- The slope of the straight line portion of the H&D curve is called the gamma of the film.
- The exposure should be chosen to make all parts of the radiograph lie on the linear portion of the H&D curve, to ensure the same contrast for all ODs.
- The latitude is defined as the range of exposures over which the ODs will lie in the linear region.
- The speed of a film is determined by giving the exposure required to produce an OD of 1.0 greater than the OD of fog.

Typical applications of a radiographic film in radiotherapy are qualitative and quantitative measurements, including electron beam dosimetry, quality control of radiotherapy machines (e.g. congruence of light and radiation fields and the determination of the position of a collimator axis, the so called star
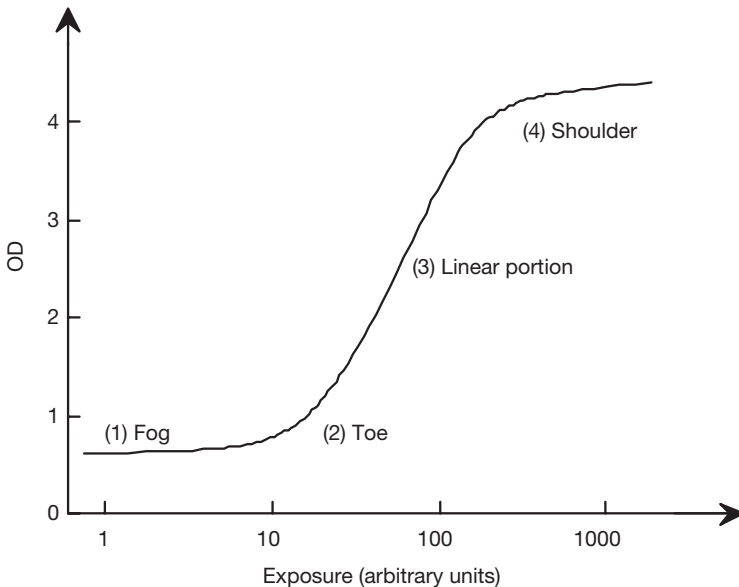
FIG. 3.7. Typical sensitometric (characteristic H&D) curve for a radiographic film.

test), verification of treatment techniques in various phantoms and portal imaging.

3.4.2. Radiochromic film

Radiochromic film is a new type of film in radiotherapy dosimetry. The most commonly used is a GafChromic film. It is a colourless film with a nearly tissue equivalent composition (9.0% hydrogen, 60.6% carbon, 11.2% nitrogen and 19.2% oxygen) that develops a blue colour upon radiation exposure.

Radiochromic film contains a special dye that is polymerized upon exposure to radiation. The polymer absorbs light, and the transmission of light through the film can be measured with a suitable densitometer. Radiochromic film is self-developing, requiring neither developer nor fixer. Since radiochromic film is grainless, it has a very high resolution and can be used in high dose gradient regions for dosimetry (e.g. measurements of dose distributions in stereotactic fields and in the vicinity of brachytherapy sources).

Dosimetry with radiochromic films has a few advantages over radiographic films, such as ease of use; elimination of the need for darkroom facilities, film cassettes or film processing; dose rate independence; better energy characteristics (except for low energy X rays of 25 kV or less); and insensitivity to ambient conditions (although excessive humidity should be avoided). Radiochromic films are generally less sensitive than radiographic films and are useful at higher doses, although the dose response non-linearity should be corrected for in the upper dose region.

- Radiochromic film is a relative dosimeter. If proper care is taken with calibration and the environmental conditions, a precision better than 3% is achievable.
- Data on the various characteristics of radiochromic films (e.g. sensitivity, linearity, uniformity, reproducibility and post-irradiation stability) are available in the literature.

3.5. LUMINESCENCE DOSIMETRY

Some materials, upon absorption of radiation, retain part of the absorbed energy in metastable states. When this energy is subsequently released in the form of ultraviolet, visible or infrared light, the phenomenon is called luminescence. Two types of luminescence, fluorescence and phosphorescence, are known, which depend on the time delay between stimulation and the emission of light. Fluorescence occurs with a time delay of between 10^{-10} and 10^{-8} s;

phosphorescence occurs with a time delay exceeding 10^{-8} s. The process of phosphorescence can be accelerated with a suitable excitation in the form of heat or light.

- If the exciting agent is heat, the phenomenon is known as thermoluminescence and the material is called a thermoluminescent material, or a TLD when used for purposes of dosimetry.
- If the exciting agent is light, the phenomenon is referred to as optically stimulated luminescence (OSL).

As discussed in Section 1.4, the highly energetic secondary charged particles, usually electrons, that are produced in the primary interactions of photons with matter are mainly responsible for the photon energy deposition in matter. In a crystalline solid these secondary charged particles release numerous low energy free electrons and holes through ionizations of atoms and ions. The free electrons and holes thus produced will either recombine or become trapped in an electron or hole trap, respectively, somewhere in the crystal.

The traps can be intrinsic or can be introduced in the crystal in the form of lattice imperfections consisting of vacancies or impurities. Two types of trap are known in general: storage traps and recombination centres.

- A storage trap merely traps free charge carriers and releases them during the subsequent (a) heating, resulting in the thermoluminescence process, or (b) irradiation with light, resulting in the OSL process.
- A charge carrier released from a storage trap may recombine with a trapped charge carrier of opposite sign in a recombination centre (luminescence centre). The recombination energy is at least partially emitted in the form of ultraviolet, visible or infrared light that can be measured with photodiodes or photomultiplier tubes (PMTs).

3.5.1. Thermoluminescence

Thermoluminescence is thermally activated phosphorescence; it is the most spectacular and widely known of a number of different ionizing radiation induced thermally activated phenomena. Its practical applications range from archaeological pottery dating to radiation dosimetry. In 1968 Cameron, Suntharalingam and Kenney published a book on the thermoluminescence process that is still considered an excellent treatise on the practical aspects of the thermoluminescence phenomenon. A useful phenomenological model of the thermoluminescence mechanism is provided in terms of the band model for

solids. The storage traps and recombination centres, each type characterized with an activation energy (trap depth) that depends on the crystalline solid and the nature of the trap, are located in the energy gap between the valence band and the conduction band. The states just below the conduction band represent electron traps, the states just above the valence band are hole traps. The trapping levels are empty before irradiation (i.e. the hole traps contain electrons and the electron traps do not).

During irradiation the secondary charged particles lift electrons into the conduction band either from the valence band (leaving a free hole in the valence band) or from an empty hole trap (filling the hole trap).

The system may approach thermal equilibrium through several means:

- Free charge carriers recombine with the recombination energy converted into heat;
- A free charge carrier recombines with a charge carrier of opposite sign trapped at a luminescence centre, the recombination energy being emitted as optical fluorescence;
- The free charge carrier becomes trapped at a storage trap, and this event is then responsible for phosphorescence or the thermoluminescence and OSL processes.

3.5.2. Thermoluminescent dosimeter systems

The TLDs most commonly used in medical applications are LiF:Mg,Ti, LiF:Mg,Cu,P and $Li_2B_4O_7$:Mn, because of their tissue equivalence. Other TLDs, used because of their high sensitivity, are $CaSO_4$:Dy, Al_2O_3:C and CaF_2:Mn.

- TLDs are available in various forms (e.g. powder, chips, rods and ribbons).
- Before they are used, TLDs need to be annealed to erase the residual signal. Well established and reproducible annealing cycles, including the heating and cooling rates, should be used.

A basic TLD reader system consists of a planchet for placing and heating the TLD, a PMT to detect the thermoluminescence light emission and convert it into an electrical signal linearly proportional to the detected photon fluence and an electrometer for recording the PMT signal as a charge or current. A basic schematic diagram of a TLD reader is shown in Fig. 3.8.
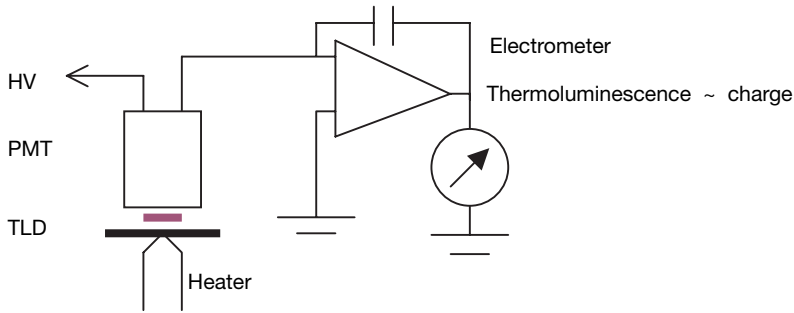
FIG. 3.8. TLD reader.

- The thermoluminescence intensity emission is a function of the TLD temperature T. Keeping the heating rate constant makes the temperature T proportional to time t, and so the thermoluminescence intensity can be plotted as a function of t if a recorder output is available with the TLD measuring system. The resulting curve is called the TLD glow curve. In general, if the emitted light is plotted against the crystal temperature one obtains a thermoluminescence thermogram (Fig. 3.9).
- The peaks in the glow curve may be correlated with trap depths responsible for thermoluminescence emission.
- The main dosimetric peak of the LiF:Mg,Ti glow curve between 180ºC and 260ºC is used for dosimetry. The peak temperature is high enough so as not to be affected by room temperature and still low enough so as not to interfere with black body emission from the heating planchet.
- The total thermoluminescence signal emitted (i.e. the area under the appropriate portion of the glow curve) can be correlated to dose through proper calibration.
- Good reproducibility of heating cycles during the readout is important for accurate dosimetry.
- The thermoluminescence signal decreases in time after the irradiation due to spontaneous emission of light at room temperature. This process is called fading. Typically, for LiF:Mg,Ti, the fading of the dosimetric peak does not exceed a few per cent in the months after irradiation.
- The thermoluminescence dose response is linear over a wide range of doses used in radiotherapy, although it increases in the higher dose region, exhibiting supralinear behaviour before it saturates at even higher doses.
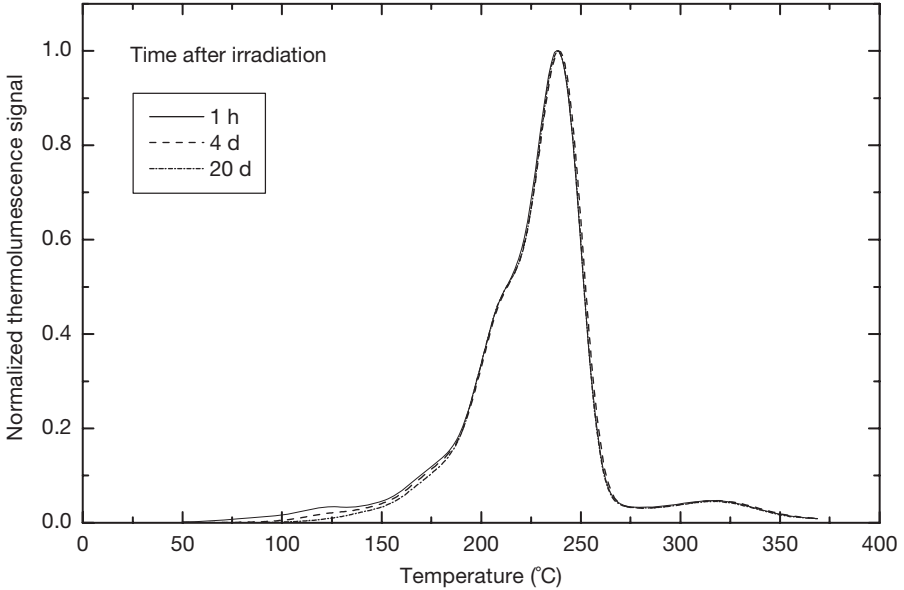
FIG. 3.9. A typical thermogram (glow curve) of LiF:Mg,Ti measured with a TLD reader at a low heating rate.

- TLDs need to be calibrated before they are used (thus they serve as relative dosimeters). To derive the absorbed dose from the thermoluminescence reading a few correction factors have to be applied, such as those for energy, fading and dose response non-linearity.
- Typical applications of TLDs in radiotherapy are: in vivo dosimetry on patients (either as a routine quality assurance procedure or for dose monitoring in special cases, for example complicated geometries, dose to critical organs, total body irradiation (TBI), brachytherapy); verification of treatment techniques in various phantoms (e.g. anthropomorphic phantoms); dosimetry audits (such as the IAEA–World Health Organization (WHO) TLD postal dose audit programme); and comparisons among hospitals.

3.5.3. Optically stimulated luminescence systems

OSL is based on a principle similar to that of thermoluminescence dosimetry. Instead of heat, light (from a laser) is used to release the trapped energy in the form of luminescence. OSL is a novel technique offering a

potential for in vivo dosimetry in radiotherapy. The integrated dose measured during irradiation can be evaluated using OSL directly afterwards.

The optical fibre optically stimulated thermoluminescent dosimeter consists of a small (~1 mm^3) chip of carbon doped aluminium oxide (Al$_2$O$_3$:C) coupled with a long optical fibre, a laser, a beam splitter and a collimator, a PMT, electronics and software. To produce OSL, the chip is excited with laser light through an optical fibre, and the resulting luminescence (blue light) is carried back in the same fibre, reflected through 90º by the beam splitter and measured in a PMT.

The optical fibre dosimeter exhibits high sensitivity over the wide range of dose rates and doses used in radiotherapy. The OSL response is generally linear and independent of energy as well as the dose rate, although the angular response requires correction.

Various experimental set-ups exist, such as pulsed OSL or OSL used in conjunction with radioluminescence. Radioluminescence is emitted promptly at the time of dosimeter irradiation and provides information on the dose rate during irradiation, while OSL provides the integrated dose thereafter. This technique, although not yet used routinely in radiotherapy, may prove to be a valuable tool for in vivo dosimetry in the future.

3.6. SEMICONDUCTOR DOSIMETRY

3.6.1. Silicon diode dosimetry systems

A silicon diode dosimeter is a p–n junction diode. The diodes are produced by taking n type or p type silicon and counter-doping the surface to produce the opposite type material. These diodes are referred to as n–Si or p–Si dosimeters, depending upon the base material. Both types of diode are commercially available, but only the p–Si type is suitable for radiotherapy dosimetry, since it is less affected by radiation damage and has a much smaller dark current.

Radiation produces electron–hole (e–h) pairs in the body of the dosimeter, including the depletion layer. The charges (minority charge carriers) produced in the body of the dosimeter, within the diffusion length, diffuse into the depleted region. They are swept across the depletion region under the action of the electric field due to the intrinsic potential. In this way a current is generated in the reverse direction in the diode.

- Diodes are used in the short circuit mode, since this mode exhibits a linear relationship between the measured charge and dose. They are usually operated without an external bias to reduce leakage current.
- Diodes are more sensitive and smaller in size than typical ionization chambers. They are relative dosimeters and should not be used for beam calibration, since their sensitivity changes with repeated use due to radiation damage.
- Diodes are particularly useful for measurement in phantoms, for example of small fields used in stereotactic radiosurgery or high dose gradient areas such as the penumbra region. They are also often used for measurements of depth doses in electron beams. For use with beam scanning devices in water phantoms, they are packaged in a waterproof encapsulation. When used in electron beam depth dose measurements, diodes measure directly the dose distribution (in contrast to the ionization measured by ionization chambers).
- Diodes are widely used in routine in vivo dosimetry on patients or for bladder or rectum dose measurements. Diodes for in vivo dosimetry are provided with buildup encapsulation and hence must be appropriately chosen, depending on the type and quality of the clinical beams. The encapsulation also protects the fragile diode from physical damage.
- Diodes need to be calibrated when they are used for in vivo dosimetry, and several correction factors have to be applied for dose calculation. The sensitivity of diodes depends on their radiation history, and hence the calibration has to be repeated periodically.
- Diodes show a variation in dose response with temperature (this is particularly important for long radiotherapy treatments), dependence of signal on the dose rate (care should be taken for different source to skin distances), angular (directional) dependence and energy dependence even for small variations in the spectral composition of radiation beams (important for the measurement of entrance and exit doses).

3.6.2. MOSFET dosimetry systems

A metal-oxide semiconductor field effect transistor (MOSFET), a miniature silicon transistor, possesses excellent spatial resolution and offers very little attenuation of the beam due to its small size, which is particularly useful for in vivo dosimetry. MOSFET dosimeters are based on the measurement of the threshold voltage, which is a linear function of absorbed dose. Ionizing radiation penetrating the oxide generates charge that is permanently trapped, thus causing a change in threshold voltage. The integrated dose may be measured during or after irradiation. MOSFETs

require a connection to a bias voltage during irradiation. They have a limited lifespan.

- A single MOSFET dosimeter can cover the full energy range of photons and electrons, although the energy response should be examined, since it varies with radiation quality. For megavoltage beams, however, MOSFETs do not require energy correction, and a single calibration factor can be used.
- MOSFETs exhibit small axial anisotropy (±2% for 360º) and do not require dose rate corrections.
- Similarly to diodes, single MOSFETs exhibit a temperature dependence, but this effect has been overcome by specially designed double detector MOSFET systems. In general, they show non-linearity of response with the total absorbed dose; however, during their specified lifespan, MOSFETs retain adequate linearity. MOSFETs are also sensitive to changes in the bias voltage during irradiation (it must be stable), and their response drifts slightly after the irradiation (the reading must be taken in a specified time after exposure).
- MOSFETs have been in use for the past few years in a variety of radiotherapy applications for in vivo and phantom dose measurements, including routine patient dose verification, brachytherapy, TBI, intensity modulated radiotherapy (IMRT), intraoperative radiotherapy and radiosurgery. They are used with or without additional buildup, depending on the application.

3.7. OTHER DOSIMETRY SYSTEMS

3.7.1. Alanine/electron paramagnetic resonance dosimetry system

Alanine, one of the amino acids, pressed in the form of rods or pellets with an inert binding material, is typically used for high dose dosimetry. The dosimeter can be used at a level of about 10 Gy or more with sufficient precision for radiotherapy dosimetry. The radiation interaction results in the formation of alanine radicals, the concentration of which can be measured using an electron paramagnetic resonance (known also as electron spin resonance) spectrometer. The intensity is measured as the peak to peak height of the central line in the spectrum. The readout is non-destructive.

- Alanine is tissue equivalent and requires no energy correction within the quality range of typical therapeutic beams. It exhibits very little fading for

many months after irradiation. The response depends on environmental conditions during irradiation (temperature) and storage (humidity).

● At present, alanine's potential application for radiotherapy is in dosimetry comparisons among hospitals.

3.7.2. Plastic scintillator dosimetry system

Plastic scintillators are a relatively new development in radiotherapy dosimetry. The light generated in the scintillator during its irradiation is carried away by an optical fibre to a PMT located outside the irradiation room. A typical set-up requires two sets of optical fibres, which are coupled to two different PMTs, allowing subtraction of the background Cerenkov radiation from the measured signal. The response of the scintillation dosimeter is linear in the dose range of therapeutic interest.

Plastic scintillators are almost water equivalent in terms of electron density and atomic composition. Typically, they match the water mass stopping power and mass energy absorption coefficient to within ±2% for the range of beam energies in clinical use, including the kilovoltage region. Scintillators are nearly energy independent and can thus be used directly for relative dose measurements.

● Plastic scintillation dosimeters can be made very small (about 1 mm^3 or less) and yet give adequate sensitivity for clinical dosimetry. Hence they can be used in cases where high spatial resolution is required (e.g. high dose gradient regions, buildup regions, interface regions, small field dosimetry and doses very close to brachytherapy sources). Due to flat energy dependence and small size, plastic scintillators are ideal dosimeters for brachytherapy applications.

● Dosimetry based on plastic scintillators is characterized by good repro-ducibility and long term stability. Scintillators suffer no significant radiation damage (up to about 10 kGy), although the light yield should be monitored when used clinically.

● Plastic scintillators are independent of dose rate and can be used from 10 μGy/min (ophthalmic plaque dosimetry) to about 10 Gy/min (external beam dosimetry). They have no significant directional dependence and need no ambient temperature or pressure corrections.

3.7.3. Diamond dosimeters

Diamonds change their resistance upon radiation exposure. When applying a bias voltage, the resulting current is proportional to the dose rate of

radiation. Commercially available diamond dosimeters are designed to measure relative dose distributions in high energy photon and electron beams. The dosimeter is based on a natural diamond crystal sealed in a polystyrene housing with a bias applied through thin golden contacts.

- Diamonds have a small sensitive volume, of the order of a few cubic millimetres, which allows the measurement of dose distributions with an excellent spatial resolution.
- Diamond dosimeters are tissue equivalent and require nearly no energy correction. Owing to their flat energy response, small physical size and negligible directional dependence, diamonds are well suited for use in high dose gradient regions, for example for stereotactic radiosurgery.
- In order to stabilize their dose response, diamonds should be irradiated prior to each use to reduce the polarization effect. They exhibit some dependence of the signal on the dose rate, which has to be corrected for when measuring a given physical quality (e.g. depth dose). Also, they have an insignificant temperature dependence, of the order of 0.1%/ºC or less.
- High sensitivity and resistance to radiation damage are other important features of diamond dosimeters. They are waterproof and can be used for measurements in a water phantom.

3.7.4. Gel dosimetry systems

Gel dosimetry systems are the only true 3-D dosimeters suitable for relative dose measurements. The dosimeter is at the same time a phantom that can measure absorbed dose distribution in a full 3-D geometry. Gels are nearly tissue equivalent and can be moulded to any desired shape or form.

Gel dosimetry can be divided into two types:

- Fricke gels based on the well established Fricke dosimetry;
- Polymer gels.

In Fricke gels, Fe^{2+} ions in ferrous sulphate solutions are dispersed throughout gelatin, agarose or PVA matrix. Radiation induced changes are either due to direct absorption of radiation or via intermediate water free radicals. Upon radiation exposure, ferrous ions Fe^{2+} are converted into ferric ions Fe^{3+} with a corresponding change in paramagnetic properties that may be measured using nuclear magnetic resonance (NMR) relaxation rates or optical techniques. A 3-D image of the dose distribution is created. A major limitation of Fricke gel systems is the continual post-irradiation diffusion of ions, resulting in a blurred dose distribution.

In polymer gel, monomers such as acrylamid are dispersed in a gelatin or agarose matrix. Upon radiation exposure, monomers undergo a polymerization reaction, resulting in a 3-D polymer gel matrix that is a function of absorbed dose that can be evaluated using NMR, X ray computed tomography (CT), optical tomography, vibrational spectroscopy or ultrasound.

- A number of polymer gel formulations are available, including polyacrylamide gels, generally referred to as PAG gels (e.g. BANG gel), and the new normoxic gels (e.g. MAGIC gel); the latter are not sensitive to the presence of atmospheric oxygen.
- There is a semilinear relationship between the NMR relaxation rate and the absorbed dose at a point in the gel dosimeter. Hence, by mapping the relaxation rates using an NMR scanner, the dose map can be derived by computation and by proper calibration.
- Due to the large proportion of water, polymer gels are nearly water equivalent and no energy corrections are required for photon and electron beams used in radiotherapy.
- No significant dose rate effects in polymer gels have been observed using NMR evaluation, although dose response depends on the temperature at which the dosimeter is evaluated. The strength of the magnetic field during evaluation may also influence the dose response. Care should be taken of post-irradiation effects such as continual polymerization, gelation and strengthening of the gel matrix, which may lead to image distortion.
- Gel dosimetry is a highly promising relative dosimetry technique that may prove particularly useful for dose verification in complex clinical situations (e.g. IMRT), in anatomically shaped phantoms, and for evaluation of doses in brachytherapy, including cardiovascular brachytherapy.

3.8. PRIMARY STANDARDS

Primary standards are instruments of the highest metrological quality that permit determination of the unit of a quantity from its definition, the accuracy of which has been verified by comparison with standards of other institutions of the same level. Primary standards are realized by the primary standards dosimetry laboratories (PSDLs) in about 20 countries worldwide. Regular international comparisons between the PSDLs, and with the Bureau international des poids et mesures (BIPM), ensure international consistency of the dosimetry standards.

Ionization chambers used in hospitals for calibration of radiotherapy beams must have a calibration traceable (directly or indirectly) to a primary standard. Primary standards are not used for routine calibrations, since they represent the unit for the quantity at all times. Instead, the PSDLs calibrate secondary standard dosimeters for secondary standards dosimetry laboratories (SSDLs) that in turn are used for calibrating the reference instruments of users, such as therapy level ionization chambers used in hospitals.

3.8.1. Primary standard for air kerma in air

Free-air ionization chambers are the primary standard for air kerma in air for superficial and orthovoltage X rays (up to 300 kV); they cannot function as a primary standard for ^{60}Co beams, since the air column surrounding the sensitive volume (for establishing the electronic equilibrium condition in air) would become very long. This would make the chamber very bulky and the various required corrections and their uncertainties would become problematic.

- At ^{60}Co energy, graphite cavity ionization chambers with an accurately known chamber volume are used as the primary standard.
- The use of the graphite cavity chamber is based on the Bragg–Gray cavity theory.

3.8.2. Primary standards for absorbed dose to water

The standards for absorbed dose to water enable therapy level ionization chambers to be calibrated directly in terms of absorbed dose to water instead of air kerma in air. This simplifies the dose determination procedure at the hospital level and improves the accuracy compared with the air kerma based formalism. Standards for absorbed dose to water calibration are now available for ^{60}Co beams in several PSDLs, some of which have extended their calibration services to high energy photon and electron beams from accelerators.

Ideally, the primary standard for absorbed dose to water should be a water calorimeter that would be an integral part of a water phantom and would measure the dose under reference conditions. However, difficulties in the establishment of this standard have led to the development of a primary standard of absorbed dose in various different ways.

At present there are three basic methods used for the determination of absorbed dose to water at the primary standard level: (1) the ionometric method; (2) the total absorption method based on chemical dosimetry; and

(3) calorimetry. The three methods are discussed below and in more detail in Chapter 9.

3.8.3. Ionometric standard for absorbed dose to water

A graphite cavity ionization chamber with an accurately known active volume, constructed as a close approximation to a Bragg–Gray cavity, is used in a water phantom at a reference depth. Absorbed dose to water at the reference point is derived from the cavity theory using the mean specific energy imparted to the air in the cavity and the restricted stopping power ratio of the wall material to the cavity gas. The BIPM maintains an ionometric standard of absorbed dose to water.

3.8.4. Chemical dosimetry standard for absorbed dose to water

In chemical dosimetry systems the dose is determined by measuring the chemical change produced in the medium (the sensitive volume of the dosimeter) using a suitable measuring system.

- The most widely used chemical dosimetry standard is the Fricke dosimeter.
- The Fricke solution has the following composition: 1mM $FeSO_4$ or $Fe(NH_4)_2(SO_4)_2$ + 0.8N H_2SO_4 air saturated + 1mM NaCl.
- Irradiation of a Fricke solution oxidizes ferrous ions Fe^{2+} into ferric ions Fe^{3+}; the latter exhibit a strong absorption peak at λ = 304 nm, whereas ferrous ions do not show any absorption at this wavelength.
- Radiation induced ferric ion concentration can be determined using spectrophotometry, which measures the absorbance (in OD units) of the solution.
- The Fricke dosimeter response is expressed in terms of its sensitivity, known as the radiation chemical yield, G value, and defined as the number of moles of ferric ions produced per joule of the energy absorbed in the solution.
- The chemical dosimetry standard is realized by the calibration of a transfer dosimeter in a total absorption experiment and the subsequent application of the transfer dosimeter in a water phantom, in reference conditions.
- The response of the Fricke solution is determined first using the total absorption of an electron beam. An accurate determination of the energy response of the transfer instrument is necessary (i.e. knowing the electron energy, the beam current and the absorbing mass accurately, the total absorbed energy can be determined and related to the change in

absorbance of the Fricke solution). Next, the absorbed dose to water at the reference point in a water phantom is obtained using the Fricke dosimeter as the transfer dosimeter.

3.8.5. Calorimetric standard for absorbed dose to water

Calorimetry is the most fundamental method of realizing the primary standard for absorbed dose, since temperature rise is the most direct consequence of energy absorption in a medium. Graphite is in general an ideal material for calorimetry, since it is of low atomic number Z and all the absorbed energy reappears as heat, without any loss of heat in other mechanisms (such as the heat defect). The graphite calorimeter is used by several PSDLs to determine the absorbed dose to graphite in a graphite phantom. The conversion to absorbed dose to water at the reference point in a water phantom may be performed by an application of the photon fluence scaling theorem or by measurements based on cavity ionization theory.

- Graphite calorimeters are electrically calibrated by depositing a known amount of electrical energy into the core.
- Water calorimeters offer a more direct determination of the absorbed dose to water at the reference point in a water phantom. The absorbed dose to water is derived from the measured temperature rise at a point in water, relying on an accurate knowledge of the specific heat capacity. No scaling laws are required, as in the case of graphite calorimetry; however, there are corrections that need to be introduced to compensate for technical complications related to a heat defect due to water radiolysis and heat transport.
- Water calorimeters are calibrated through the calibration of their thermistors in terms of the absolute temperature difference rather than through energy deposition, as is the case for graphite calorimeters.

3.9. SUMMARY OF SOME COMMONLY USED DOSIMETRIC SYSTEMS

Radiation dosimeters and dosimetry systems come in many shapes and forms, and they rely on numerous physical effects for storage and readout of the dosimetric signal. The four most commonly used radiation dosimeters are:

- Ionization chambers;
- Radiographic films;

- TLDs;
- Diodes.

The strengths and weaknesses of these four dosimeters are summarized in Table 3.1.

TABLE 3.1. MAIN ADVANTAGES AND DISADVANTAGES OF THE FOUR COMMONLY USED DOSIMETRIC SYSTEMS

	Advantage	Disadvantage
Ionization chamber	Accurate and precise Recommended for beam calibration Necessary corrections well understood Instant readout	Connecting cables required High voltage supply required Many corrections required for high energy beam dosimetry
Film	2-D spatial resolution Very thin: does not perturb the beam	Darkroom and processing facilities required Processing difficult to control Variation between films and batches Needs proper calibration against ionization chamber measurements Energy dependence problems Cannot be used for beam calibration
TLD	Small in size: point dose measurements possible Many TLDs can be exposed in a single exposure Available in various forms Some are reasonably tissue equivalent Not expensive	Signal erased during readout Easy to lose reading No instant readout Accurate results require care Readout and calibration time consuming Not recommended for beam calibration
Diode	Small size High sensitivity Instant readout No external bias voltage Simple instrumentation	Requires connecting cables Variability of calibration with temperature Change in sensitivity with accumulated dose Special care needed to ensure constancy of response Cannot be used for beam calibration

BIBLIOGRAPHY

ATTIX, F.H., Introduction to Radiological Physics and Radiation Dosimetry, Wiley, New York (1986).

CAMERON, J.R., SUNTHARALINGAM, N., KENNEY, G.K., Thermoluminescent Dosimetry, University of Wisconsin Press, Madison, WI (1968).

HORTON, J., Handbook of Radiation Therapy Physics, Prentice Hall, New York (1987).

INTERNATIONAL ATOMIC ENERGY AGENCY, Absorbed Dose Determination in Photon and Electron Beams, Technical Reports Series No. 277, IAEA, Vienna (1987).

— Calibration of Dosimeters Used in Radiotherapy, Technical Reports Series No. 374, IAEA, Vienna (1994).

— The Use of Plane Parallel Ionization Chambers in High Energy Electron and Photon Beams, Technical Reports Series No. 381, IAEA, Vienna (1997).

— Absorbed Dose Determination in External Beam Radiotherapy, Technical Reports Series No. 398, IAEA, Vienna (2000).

INTERNATIONAL ORGANIZATION FOR STANDARDIZATION, Guide to Expression of Uncertainty in Measurement, ISO, Geneva (1992).

KHAN, F.M., The Physics of Radiation Therapy, Lippincott, Williams and Wilkins, Baltimore, MD (2003).

KLEVENHAGEN, S.C., Physics and Dosimetry of Therapy Electron Beams, Medical Physics Publishing, Madison, WI (1993).

VAN DYK, J. (Ed.), Modern Technology of Radiation Oncology: A Compendium for Medical Physicists and Radiation Oncologists, Medical Physics Publishing, Madison, WI (1999).

Chapter 4

RADIATION MONITORING INSTRUMENTS

G. RAJAN
Medical Physics and Safety Section,
Bhabha Atomic Research Centre,
Mumbai, Maharashtra, India

J. IZEWSKA
Division of Human Health,
International Atomic Energy Agency,
Vienna

4.1. INTRODUCTION

Radiation exposure to humans can be broadly classified as internal and external exposure. Sealed sources, which are unlikely to cause internal exposure, are used almost exclusively in radiotherapy. This chapter deals with the monitoring of external exposures.

- External exposure monitoring refers to measuring:
  — Radiation levels in and around work areas;
  — Radiation levels around radiotherapy equipment or source containers;
  — Equivalent doses received by individuals working with radiation.
- Radiation monitoring is carried out:
  — To assess workplace conditions and individual exposures;
  — To ensure acceptably safe and satisfactory radiological conditions in the workplace;
  — To keep records of monitoring, over a long period of time, for the purposes of regulation or good practice.
- Radiation monitoring instruments are used both for area monitoring and for individual monitoring. The instruments used for measuring radiation levels are referred to as area survey meters (or area monitors) and the instruments used for recording the equivalent doses received by individuals working with radiation are referred to as personal dosimeters (or individual dosimeters). All instruments must be calibrated in terms of the appropriate quantities used in radiation protection.

4.2. OPERATIONAL QUANTITIES FOR RADIATION MONITORING

Recommendations regarding dosimetric quantities and units in radiation protection dosimetry are set forth by the International Commission on Radiation Units and Measurements (ICRU). The recommendations on the practical application of these quantities in radiation protection are established by the International Commission on Radiological Protection (ICRP).

The operational quantities are defined for practical measurements both for area and individual monitoring. In radiation protection radiation is characterized as either weakly or strongly penetrating, depending on which dose equivalent is closer to its limiting value. In practice, the term 'weakly penetrating' radiation usually applies to photons below 15 keV and to β radiation.

For the purpose of area monitoring, the ambient dose equivalent $H^*(d)$ and directional dose equivalent $H'(d,\Omega)$ are defined. They link the external radiation field to the effective dose equivalent in the ICRU sphere phantom (see Chapter 16), at depth d, on a radius in a specified direction Ω.

- For strongly penetrating radiation the depth d = 10 mm is used; the ambient dose equivalent is denoted as $H^*(10)$ and the directional dose equivalent as $H'(10,\Omega)$.
- For weakly penetrating radiation the ambient and directional dose equivalents in the skin at d = 0.07 mm, $H^*(0.07)$ and $H'(0.07,\Omega)$, are relevant, and in the lens of the eye at d = 3 mm, $H^*(3)$ and $H'(3,\Omega)$, are relevant.

For individual monitoring the personal dose equivalent $H_p(d)$ is defined, which is the dose equivalent in soft tissue below a specified point on the body at depth d (see also Chapter 16).

- For strongly penetrating radiation the depth d = 10 mm is used and the personal dose equivalent is denoted as $H_p(10)$.
- For weakly penetrating radiation the personal dose equivalent in the skin at d = 0.07 mm, $H_p(0.07)$, and in the lens of the eye at d = 3 mm, $H_p(3)$, are used.
- $H_p(d)$ can be measured with a dosimeter that is worn at the surface of the body and covered with an appropriate layer of tissue equivalent material.

4.3. AREA SURVEY METERS

Radiation instruments used as survey monitors are either gas filled detectors or solid state detectors (e.g. scintillator or semiconductor detectors). A gas filled detector is usually cylindrical in shape, with an outer wall and a central electrode well insulated from each other. The wall is usually made of tissue equivalent material for ionization chamber detectors and of brass or copper for other types of detector.

Depending upon the design of the gas filled detector and the voltage applied between the two electrodes, the detector can operate in one of three regions, shown in Fig. 4.1 (i.e. the ionization region B, proportional region C or Geiger–Müller (GM) region E). Regions of recombination and of limited proportionality in the 'signal versus applied voltage' plot (regions A and D, respectively, in Fig. 4.1) are not used for survey meters.
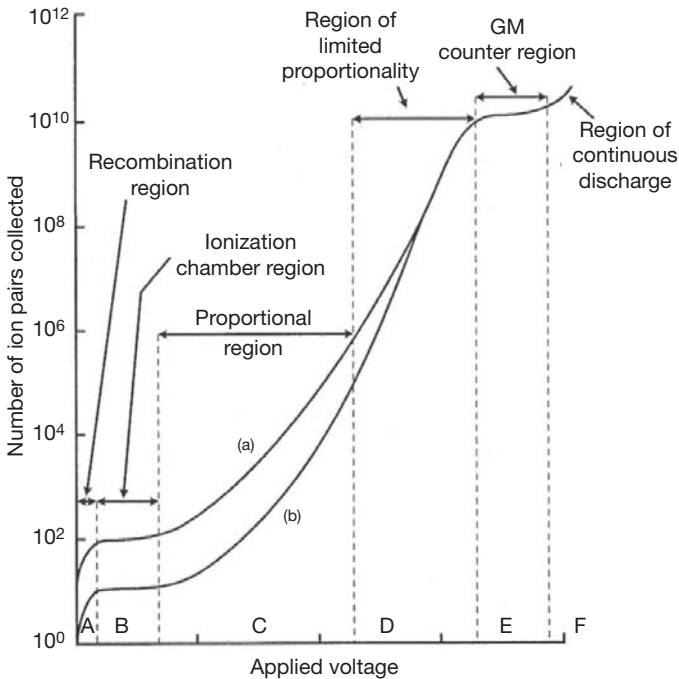
FIG. 4.1. *Various regions of operation of a gas filled detector. Region A represents the recombination region, region B the ionization region, region C the proportionality region, region D the region of limited proportionality and region E the GM region. Curve (a) is for 1 MeV β particles, curve (b) for 100 keV β particles.*

FIG. 4.2. Area survey meters commonly used for radiation protection level measurements: ionization chambers, a proportional counter and GM counters.

- Survey meters come in different shapes and sizes, depending upon the specific application (see Fig. 4.2).
- The gas is usually a non-electronegative gas in order to avoid negative ion formation by electron attachment, which would increase the collection time in the detector, thus limiting the dose rate that can be monitored. The increase in charge collection time results from the relatively slow mobility of ions, which is about three orders of magnitude smaller than that of electrons. Noble gases are generally used in these detectors.
- β–γ survey meters have a thin end window to register weakly penetrating radiation. The γ efficiency of these detectors is only a few per cent (as determined by the wall absorption), while the β response is near 100% for β particles entering the detector.
- Owing to their high sensitivity, the tubes of GM based γ monitors are smaller in size than ionization chamber type detectors.

- Depending upon the electronics used, detectors can operate in a 'pulse' mode or in the 'mean level' or current mode. Proportional and GM counters are normally operated in the pulse mode.
- Owing to the finite resolving time (the time required by the detector to regain its normal state after registering a pulse), these detectors will saturate at high intensity radiation fields. Ionization chambers operating in the current mode are more suitable for higher dose rate measurements.

4.3.1. Ionization chambers

In the ionization region the number of primary ions of either sign collected is proportional to the energy deposited by the charged particle tracks in the detector volume. Owing to the linear energy transfer (LET) differences, the particle discrimination function can be used (see Fig. 4.1). Buildup caps are required to improve detection efficiency when measuring high energy photon radiation, but they should be removed when measuring lower energy photons (10–100 keV) and β particles.

4.3.2. Proportional counters

In the proportional region there is an amplification of the primary ion signal due to ionization by collision between ions and gas molecules (charge multiplication). This occurs when, between successive collisions, the primary ions gain sufficient energy in the neighbourhood of the thin central electrode to cause further ionization in the detector. The amplification is about 10^3–10^4-fold.

Proportional counters are more sensitive than ionization chambers and are suitable for measurements in low intensity radiation fields. The amount of charge collected from each interaction is proportional to the amount of energy deposited in the gas of the counter by the interaction.

4.3.3. Neutron area survey meters

Neutron area survey meters operate in the proportional region so that the photon background can be easily discriminated against.

- Thermal neutron detectors usually have a coating of a boron compound on the inside of the wall, or the counter is filled with BF_3 gas.
- A thermal neutron interacts with a ^{10}B nucleus causing an (n, α) reaction, and the α particles can easily be detected by their ionizing interactions.
- To detect fast neutrons the same counter is surrounded by a moderator made of hydrogenous material (Fig. 4.3); the whole assembly is then a fast

FIG. 4.3. Neutron dose equivalent rate meter with a thermalizing polyethylene sphere with a diameter of 20 cm.

neutron counter. The fast neutrons interacting with the moderator are thermalized and are subsequently detected by a BF_3 counter placed inside the moderator.

- Filter compensation is applied to reduce thermal range over-response so that the response follows the ICRP radiation weighting factors w_R (see Chapter 16). The output is approximately proportional to the dose equivalent in soft tissue over a wide range (10 decades) of neutron energy spectra.
- Other neutron detectors (e.g. those based on ^{3}He) also function on the same principles.

4.3.4. Geiger–Müller counters

The discharge spreads in the GM region throughout the volume of the detector and the pulse height becomes independent of the primary ionization or the energy of the interacting particles. In a GM counter detector the gas

multiplication spreads along the entire length of the anode. Gas filled detectors cannot be operated at voltages beyond the GM region because they continuously discharge.

Owing to the large charge amplification (nine to ten orders of magnitude), GM survey meters are widely used at very low radiation levels (e.g. in areas of public occupancy around radiotherapy treatment rooms). They are particularly applicable for leak testing and detection of radioactive contamination.

GM counters exhibit strong energy dependence at low photon energies and are not suitable for use in pulsed radiation fields. They are considered indicators of radiation, whereas ionization chambers are used for more precise measurements.

GM detectors suffer from very long dead times, ranging from tens to hundreds of milliseconds. For this reason, GM counters are not used when accurate measurements are required of count rates of more than a few hundred counts per second. A portable GM survey meter may become paralysed in a very high radiation field and yield a zero reading. Ionization chambers should therefore be used in areas where radiation rates are high.

4.3.5. Scintillator detectors

Detectors based on scintillation (light emission) are known as scintillation detectors and belong to the class of solid state detectors. Certain organic and inorganic crystals contain activator atoms, emit scintillations upon absorption of radiation and are referred to as phosphors. High atomic number phosphors are mostly used for the measurement of γ rays, while plastic scintillators are mostly used with β particles.

- Scintillating phosphors include solid organic materials such as anthracene, stilbene and plastic scintillators as well as thallium activated inorganic phosphors such as NaI(Tl) or CsI(Tl).
- A photomultiplier tube (PMT) is optically coupled to the scintillator to convert the light pulse into an electric pulse. Some survey meters use photodiodes in place of PMTs.

4.3.6. Semiconductor detectors

Bulk conductivity detectors are formed from intrinsic semiconductors of very high bulk resistivity (e.g. CdS or CdSe). They act like solid state ionization chambers on exposure to radiation and, like scintillation detectors, belong to the class of solid state detectors.

Extrinsic (i.e. doped with trace quantities of impurities such as phosphorus or lithium) semiconductors such as silicon or germanium are used to form junction detectors. They too act as solid state ionization chambers on application of a reverse bias to the detectors and on exposure to radiation.

The sensitivity of solid state detectors is about 10^4 times higher than that of gas filled detectors, owing to the lower average energy required to produce an ion pair in solid detector materials compared with air (typically one order of magnitude lower) and the higher density of the solid detector materials compared with air (typically three orders of magnitude higher). These properties facilitate the miniaturization of solid state radiation monitoring instruments.

4.3.7. Commonly available features of area survey meters

The commonly available features of area survey meters are:

- A 'low battery' visual indication;
- Automatic zeroing, automatic ranging and automatic back-illumination facilities;
- A variable response time and memory to store the data;
- The option of both 'rate' and 'integrate' modes of operation;
- An analog or digital display, marked in conventional (exposure/air kerma) or 'ambient dose equivalent' or 'personal dose equivalent' units;
- An audio indication of radiation levels (through the 'chirp' rate);
- A resettable/non-resettable alarm facility with adjustable alarm levels;
- A visual indication of radiation with flashing LEDs;
- Remote operation and display of readings.

4.3.8. Calibration of survey meters

Protection level area survey meters must be calibrated against a reference instrument that is traceable (directly or indirectly) to a national standards laboratory.

A reference instrument for γ radiation is generally an ionization chamber (Fig. 4.4) with a measuring assembly. Reference instruments do not indicate directly the dose equivalent H required for calibration of radiation protection monitoring instruments. Rather, they measure basic radiation quantities such as the air kerma in air for photon radiation, and the dose equivalent H is then determined by using appropriate conversion coefficients h:

$$H = hN_R M_R \tag{4.1}$$
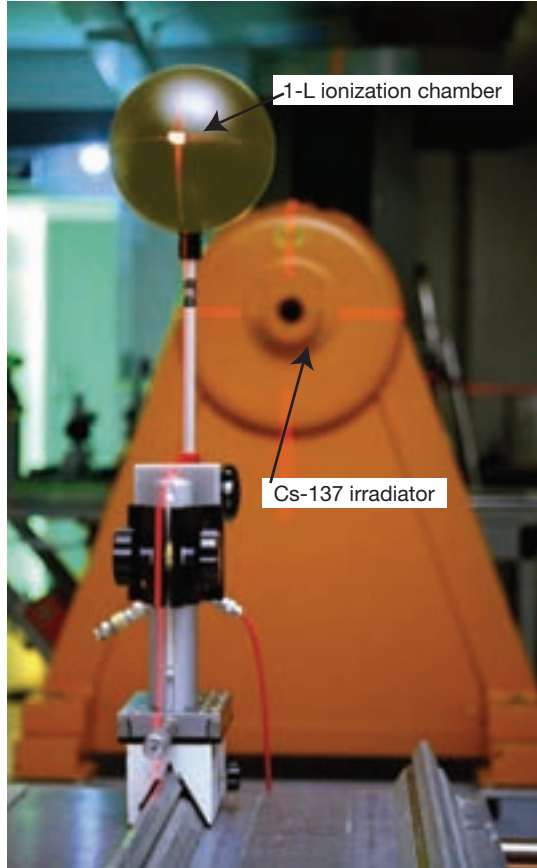
FIG. 4.4. Reference ionization chamber used for the calibration of area survey meters in a ^{137}Cs γ beam.

where

N_R is the calibration factor (e.g. in terms of air kerma in air or air kerma rate in air) of the reference chamber under reference conditions;

M_R is the reading of the reference instrument corrected for influence quantities.

A reference instrument is calibrated free in air for the range of reference radiation qualities (defined by the International Organization for Standardization (ISO)). The same reference qualities should be used for the calibration of radiation protection monitoring instruments.

CHAPTER 4

Typically, calibration of survey meters in terms of the ambient dose equivalent $H^*(10)$ involves three steps:

- The air kerma in air is measured in a reference field, using a reference standard.
- The values of the conversion coefficient:

$$h_{H^*} = [H^*(10)/(K_{air})_{air}]$$

are theoretically available. Using these data for the calibration beam quality, a reference instrument reading can be converted to $H^*(10)$.
- The survey monitor being calibrated is then placed at the calibration point and its reading M is determined. The calibration factor in terms of the ambient dose equivalent N_{H^*} for the survey monitor is determined from the equation $N_{H^*} = H^*(10)/M$.

4.3.9. Properties of survey meters

4.3.9.1. Sensitivity

The sensitivity S is defined as the inverse of the calibration coefficient N. Using decade resistances, larger detector volumes or detector gases under higher pressures, a wide range of equivalent dose rates can be covered with ionization chamber based survey meters (e.g. 1 μSv/h–1 Sv/h).

Owing to finite resolving time, GM based systems would saturate beyond a few thousand counts per second. Low dead time counters or dead time correction circuits enable these detectors to operate at higher intensity radiation fields.

Scintillation based systems are more sensitive than GM counters because of higher γ conversion efficiency and dynode amplification. Scintillation based systems are generally used for surveys at very low radiation levels (e.g. contamination monitoring and lost source detection surveys). However, they can also be used at higher radiation levels, since their resolving time is quite low (a few microseconds or lower) compared with GM counters.

4.3.9.2. Energy dependence

Survey meters are calibrated at one or more beam qualities, but are often used in situations in which the radiation field is complex or unknown. These survey meters should hence have a low energy dependence over a wide energy range.

In the past, survey meters were designed to exhibit a flat energy response that follows exposure or air kerma in air.

For measuring the equivalent dose:

$$N_{H^*} = [H^*(10)/M] = [H^*(10)/(K_{air})_{air}]/[(K_{air})_{air}/M]$$

a meter's response with energy should vary as the quantity:

$$[H^*(10)/(K_{air})_{air}]$$

GM counters exhibit strong energy dependence for low energy photons (<80 keV).

4.3.9.3. Directional dependence

By rotating the survey monitor about its vertical axis, the directional response of the instrument can be studied. A survey monitor usually exhibits isotropic response, as required for measuring ambient dose equivalent, within ±60º to ±80º with respect to the reference direction of calibration, and typically has a much better response for higher photon energies (>80 keV).

4.3.9.4. Dose equivalent range

Survey meters may cover a range from nSv/h to Sv/h, but the typical range in use is μSv/h to mSv/h.

4.3.9.5. Response time

The response time of the survey monitor is defined as the *RC* time constant of the measuring circuit, where *R* is the decade resistor used and *C* the capacitance of the circuit.

Low dose equivalent ranges would have high *R* and hence high *RC* values, and so the indicator movement would be sluggish. It takes at least three to five time constants for the monitor reading to stabilize.

4.3.9.6. Overload characteristics

Survey meters must be subjected to dose rates of about ten times the maximum scale range to ensure that they read full scale rather than near zero on saturation.

Some survey meters, especially the older models, may read zero on overload (i.e. when the equivalent dose rate exceeds the scale range). Such survey meters should not be used for monitoring, since the worker may wrongly assume that there is no radiation in an area where the radiation field is actually very high.

GM survey meters are not suitable for use in pulsed fields, due to the possible overload effect, and ionization chamber based survey meters should be used instead.

4.3.9.7. Long term stability

Survey meters must be calibrated in a standards dosimetry laboratory with the frequency prescribed by the regulatory requirements of the country, typically once every three years; they also need calibration immediately after repair or immediately upon detection of any sudden change in response.

The long term stability of survey meters must be checked at regular intervals using a long half-life source in a reproducible geometry.

4.3.9.8. Discrimination between different types of radiation

End window GM counters have a removable buildup cap to discriminate β from γ rays. For β measurements the end cap must be removed to allow β particles to enter the sensitive volume.

4.3.9.9. Uncertainties in area survey measurements

The standards laboratory provides, along with the survey monitor calibration, the uncertainty associated with the calibration factor. Subsequent measurements at the user department provide a type A uncertainty. The uncertainties due to energy dependence and angular dependence of the detector, and the variation in the user field conditions compared with calibration conditions, contribute to type B uncertainties. These two types of uncertainty are added in quadrature to obtain the combined uncertainty associated with the survey meter measurements.

The combined uncertainty is multiplied by the coverage factor $k = 2$ or $k = 3$ to correspond to the confidence limits of 95% or 99%, respectively. The uncertainty of measurements with area monitors is typically within ±30% under standard laboratory conditions.

4.4. INDIVIDUAL MONITORING

Individual monitoring is the measurement of the radiation doses received by individuals working with radiation. Individuals who regularly work in controlled areas or those who work full time in supervised areas (see Chapter 16 for the definitions) should wear personal dosimeters to have their doses monitored on a regular basis. Individual monitoring is also used to verify the effectiveness of radiation control practices in the workplace. It is useful for detecting changes in radiation levels in the workplace and to provide information in the event of accidental exposures.

- The most widely used individual monitoring systems are based on thermoluminescence or film dosimetry, although other techniques, such as radiophotoluminescence (RPL) and optically stimulated luminescence (OSL), are in use in some countries. Albedo dosimeters and nuclear track emulsions are used for monitoring fast neutron doses.
- Self-reading pocket dosimeters and electronic personal dosimeters (EPDs) are direct reading dosimeters and show both the instantaneous dose rate and the accumulated dose at any point in time.

As explained in Section 4.2, the operational quantity for the individual monitoring of external exposure is the personal dose equivalent $H_p(d)$ with the recommended depth $d = 10$ mm for strongly penetrating radiation and $d = 0.07$ mm for weakly penetrating radiation. Personal dosimeters are calibrated in these quantities.

4.4.1. Film badge

A special emulsion photographic film in a light-tight wrapper enclosed in a case or holder with windows, with appropriate filters, is known as a film badge (Fig. 4.5). The badge holder creates a distinctive pattern on the film indicating the type and energy of the radiation received. While one filter is adequate for photons of energy above 100 keV, the use of a multiple filter system is necessary for lower energy photons.

Since the film is non-tissue equivalent, a filter system must be used to flatten the energy response, especially at lower photon beam qualities, to approximate the response of a tissue equivalent material.
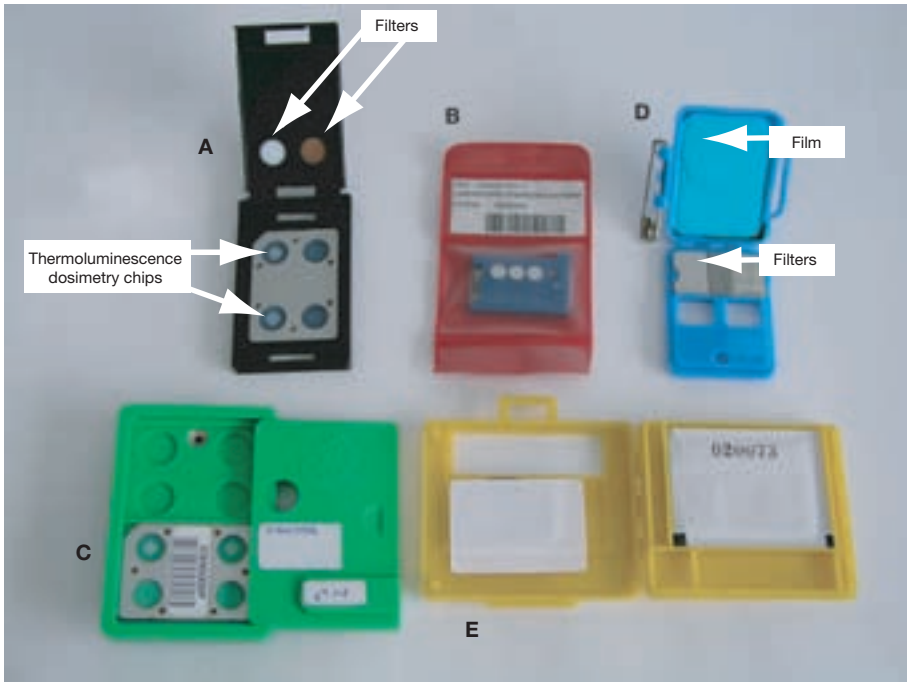
FIG. 4.5. Personal dosimeters: examples of thermoluminescence dosimetry badges (A, B, C) and film badges (D, E).

- Cumulative doses from β, X, γ and thermal neutron radiation are evaluated by measuring the film optical densities (ODs) under different filters and then comparing the results with calibration films that have been exposed to known doses of well defined radiation of different types.
- Film can also serve as a monitor for thermal neutrons. The cadmium window absorbs thermal neutrons and the resulting γ radiation blackens the film below this window as an indication of the neutron dose.
- Nuclear track emulsions are used for monitoring of fast neutrons. The neutrons interact with hydrogen nuclei in the emulsion and surrounding material, producing recoil protons by elastic collisions. These particles create a latent image, which leads to darkening of the film along their tracks after processing.
- Films are adversely affected by many external agents, such as heat, liquids and excessive humidity. The latent image on undeveloped film fades with time, limiting possible wearing periods to three months in ideal conditions.
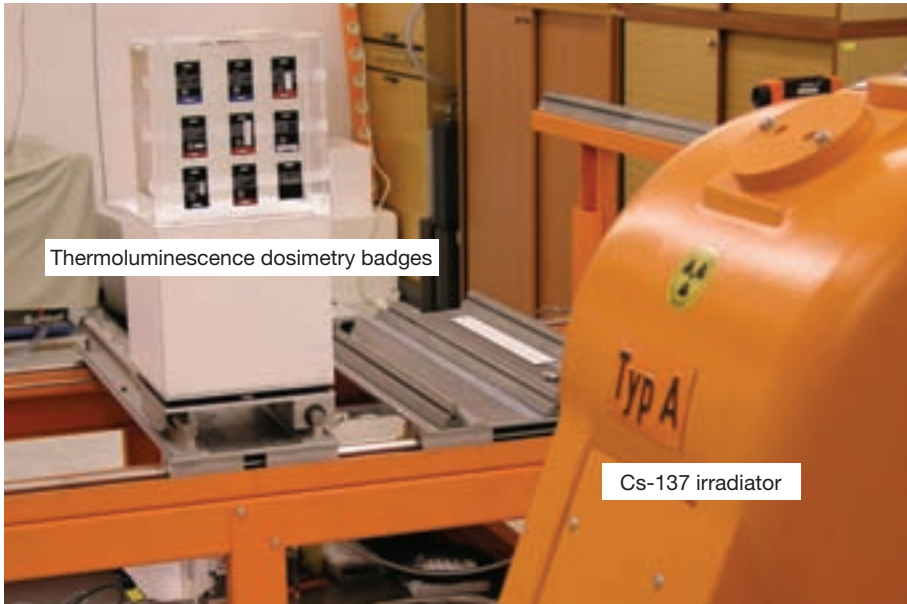
FIG. 4.6. Calibration of personal dosimeters on a PMMA slab phantom using a standard ^{137}Cs γ beam.

4.4.2.   Thermoluminescence dosimetry badge

A thermoluminescence dosimetry badge (see Fig. 4.5) consists of a set of thermoluminescent dosimeter (TLD) chips enclosed in a plastic holder with filters. The most frequently used thermoluminescence dosimetry materials (also referred to as phosphors) are LiF:Ti,Mg, $CaSO_4$:Dy and CaF_2:Mn. Different badge designs (thermoluminescence dosimetry materials and filters) are in use in different countries.

The doses of β, X and γ radiation registered by the dosimeter are evaluated by measuring the output under different filters and then comparing the results with calibration curves established for the calibration badge, which has been exposed to known doses under well defined conditions.

- Badges that use high atomic number Z thermoluminescence dosimetry materials are not tissue equivalent and, like film, also require filters to match their energy response to that of tissue. Badges using low Z phosphors do not require such complex filter systems.

- The thermoluminescence signal exhibits fading, but the problem is less significant than for films.
- The badges currently used for β monitoring have a relatively high threshold for β particles (about 50 keV) because of the thickness of the detector and its cover.
- TLDs are convenient for monitoring doses to parts of the body (e.g. eyes, arm or wrist, or fingers) using special types of dosimeter, including extremity dosimeters.
- Various techniques have been used for neutron monitoring, such as using the body as a moderator to thermalize neutrons (similarly to albedo dosimeters) or using LiF enriched with ^{6}Li for enhanced thermal neutron sensitivity due to the (n, α) reaction of thermal neutrons in ^{6}Li.

4.4.3. Radiophotoluminescent glass dosimetry systems

Radiophotoluminescent glass dosimeters are accumulation type solid state dosimeters that use the phenomenon of RPL to measure the radiation dose. The material used is silver activated phosphate glass. The dosimeters come in the shape of small glass rods.

- When silver activated phosphate glass is exposed to radiation, stable luminescence centres are created in silver ions Ag^+ and Ag^{++}. The readout technique uses pulsed ultraviolet laser excitation. A PMT registers the orange fluorescence emitted by the glass.
- The RPL signal is not erased during the readout, thus the dosimeter can be reanalysed several times and the measured data reproduced. Accumulation of the dose is also possible, and may be used for registration of the lifetime dose.
- Commercially available radiophotoluminescent dosimeters typically cover the dose range of 30 μSv to 10 Sv. They have a flat energy response within 12 keV to 8 MeV for $H_p(10)$.
- The RPL signal exhibits very low fading and is not sensitive to the environmental temperature, making it convenient for individual monitoring.

4.4.4. Optically stimulated luminescence systems

OSL is now commercially available for measuring personal doses. Optically stimulated luminescent dosimeters contain a thin layer of aluminium oxide (Al_2O_3:C). During analysis the aluminium oxide is stimulated with

selected frequencies of laser light producing luminescence proportional to the radiation exposure.

- Commercially available badges are integrated, self-contained packets that come preloaded, incorporating an aluminium oxyde (Al_2O_3) strip sandwiched within a filter pack that is heat sealed. Special filter patterns provide qualitative information about conditions during exposure.
- Optically stimulated luminescent dosimeters are highly sensitive; for example, the Luxel system can be used down to 10 μSv with a precision of ±10 μSv. This high sensitivity is particularly suitable for individual monitoring in low radiation environments. The dosimeters can be used in a wide dose range of up to 10 Sv in photon beams from 5 keV to 40 MeV.
- The dosimeters can be reanalysed several times without losing sensitivity and may be used for up to one year.

4.4.5. Direct reading personal monitors

In addition to passive dosimetry badges, direct reading personal dosimeters are widely used:

- To provide a direct readout of the dose at any time;
- For tracking the doses received in day to day activities;
- In special operations (e.g. source loading surveys and handling of radiation incidents or emergencies).

Direct reading personal dosimeters fall into two categories: (1) self-reading pocket dosimeters and (2) electronic personal dosimeters (EPDs).

Self-reading pocket dosimeters resemble a pen and consist of an ionization chamber that acts as a capacitor. The capacitor is fully charged and reads zero before use. On exposure to radiation for a period of time, the ionization produced in the chamber discharges the capacitor; the exposure (or air kerma) is proportional to the discharge, which can be directly read against light through a built-in eyepiece. However, the use of pocket dosimeters has declined in recent years because of their poor useful range, charge leakage problems and poor sensitivity compared with EPDs.

EPDs based on miniature GM counters or silicon detectors are available with a measurement range of down to 30 keV photon energy.

— Modern EPDs are calibrated in the personal equivalent dose (i.e. in terms of $H_p(10)$ or $H_p(0.07)$ for both photons and β radiation). EPDs provide an instantaneous display of accumulated equivalent dose at any time.

— EPDs have automatic ranging facilities and give a visual and an audio indication (flashing or a chirping frequency proportional to the dose equivalent rate), so that changes in the radiation field can be recognized immediately.

— EPDs are very useful in emergency situations for immediate readout of the equivalent doses received.

4.4.6. Calibration of personal dosimeters

Personal dosimeters should be calibrated in terms of operational quantities for individual monitoring of external exposure (i.e. the personal dose equivalent $H_p(d)$ with the recommended depth $d = 10$ mm for strongly penetrating radiation and $d = 0.07$ mm for weakly penetrating radiation (see Section 4.2)).

For calibration, dosimeters should be irradiated on standardized phantoms that provide an approximation of the backscatter conditions of the human body. Three types of phantom are recommended that cover the needs of calibration of whole body dosimeters, wrist or ankle dosimeters and finger dosimeters: a slab phantom to represent a human torso, a pillar phantom for wrist or ankle dosimeters and a rod phantom for finger dosimeters. The standard phantoms are composed of ICRU tissue. The ISO recommends special water phantoms (referred to as ISO slab phantoms), although in practice PMMA phantoms are used with the appropriate corrections.

Calibration of personal dosimeters in terms of $H_p(d)$ involves three steps:

- Air kerma in air $(K_{air})_{air}$ is measured in a reference field, using a reference ionization chamber calibrated by a standards laboratory.
- $[H_p(d)/(K_{air})_{air}]_{slab} = h_{kHp}$ values are theoretically available. Using these data for the calibration beam quality, a reference instrument reading can be converted to $[H_p(d)]_{slab}$.
- The dosimeter badge being calibrated is then placed at the calibration point on a phantom and its reading M is determined. $N_{Hp} = H_p(d)/M$ gives the calibration factor in terms of the personal dose equivalent for the dosimeter badge.

4.4.7. Properties of personal monitors

4.4.7.1. Sensitivity

Film and thermoluminescence dosimetry badges can measure equivalent doses as low as 0.1 mSv and up to 10 Sv; optically stimulated luminescent and

radiophotoluminescent dosimeters are more sensitive, with a lower detection limit of 10–30 μSv. Personal dosimeters are generally linear in the dose range of interest in radiation protection.

4.4.7.2. Energy dependence

Film exhibits a strong energy dependence and film badges are empirically designed to reduce their energy response to within ±20%. A LiF TLD is nearly tissue equivalent and exhibits acceptable energy dependence characteristics. $CaSO_4$:Dy shows significant energy dependence and its energy response is reduced by empirical adjustments in the badge design.

Commercially available radiophotoluminescent dosimeters (e.g. Asahi, PTW and Toshiba) have a flat energy response from 12 keV to 8 MeV, while commercially available optically stimulated luminescent dosimeters (e.g. Landauer) have a flat energy response from 5 keV to 40 MeV.

For direct reading pocket dosimeters the energy dependence is within ±20% over the range from 40 keV to 2 MeV. For EPDs containing energy compensated detectors the energy dependence is within ±20% over the energy range from 30 keV to 1.3 MeV.

The energy response values quoted above can vary in energy range and in the degree of flatness, depending on the individual monitor material and construction details.

4.4.7.3. Uncertainties in personal monitoring measurements

The ICRP has stated that, in practice, it is usually possible to achieve an uncertainty of about 10% at the 95% confidence level ($k = 2$) for measurements of radiation fields in laboratory conditions. However, in the workplace, where the energy spectrum and orientation of the radiation field are generally not well known, the uncertainties in a measurement made with an individual dosimeter will be significantly greater, and may be a factor of one for photons and still greater for neutrons and electrons.

The uncertainty in measurements with EPDs is about 10% for low dose rates (2 mSv/h) and increases to 20% for higher dose rates (<100 mSv/h) in laboratory conditions.

4.4.7.4. Equivalent dose range

Personal monitors must have as wide a dose range as possible so that they can cover both radiation protection and accidental situations (typically from 10 μSv to about 10 Sv). The dose range normally covered by film and TLDs is

from about 100 μSv to 10 Sv and that by optically stimulated luminescent and radiophotoluminescent dosimeters is 10 μSv to 10 Sv.

Self-reading pocket dosimeters can measure down to about 50 μSv; the upper dose limit of the available pocket dosimeters is around 200 mSv. EPDs measure in the range from 0.1 μSv to 10 Sv.

4.4.7.5. *Directional dependence*

According to the ICRU, an individual dosimeter must be iso-directional, (i.e. its angular response relative to normal incidence must vary as the ICRU directional dose equivalent quantity $H'(10, \Omega)$) (see Section 4.2). The directional dependence must be evaluated and the appropriate corrections derived.

4.4.7.6. *Discrimination between different types of radiation*

Film dosimeters can identify and estimate doses of X rays, γ rays, β particles and thermal neutrons. TLDs and optically stimulated luminescent and radiophotoluminescent dosimeters generally identify and estimate doses of X rays and γ and β radiation.

BIBLIOGRAPHY

ATTIX, F.H., Introduction to Radiological Physics and Radiation Dosimetry, Wiley, New York (1986).

CLARK, M.J., et al., Dose quantities for protection against external radiations: Guidance on the 1990 recommendations of ICRP, Doc. NRPB **4** 3 (1993).

FOOD AND AGRICULTURE ORGANIZATION OF THE UNITED NATIONS, INTERNATIONAL ATOMIC ENERGY AGENCY, INTERNATIONAL LABOUR ORGANISATION, OECD NUCLEAR ENERGY AGENCY, PAN AMERICAN HEALTH ORGANIZATION, WORLD HEALTH ORGANIZATION, International Basic Safety Standards for Protection against Ionizing Radiation and for the Safety of Radiation Sources, Safety Series No. 115, IAEA, Vienna (1996).

INTERNATIONAL ATOMIC ENERGY AGENCY, Calibration of Radiation Protection Monitoring Instruments, Safety Reports Series No. 16, IAEA, Vienna (2000).

INTERNATIONAL COMMISSION ON RADIATION UNITS AND MEASUREMENTS, Determination of Dose Equivalents Resulting from External Radiation Sources, Rep. 43, ICRU, Bethesda, MD (1988).

— Measurement of Dose Equivalents from External Photon and Electron Radiations, Rep. 47, ICRU, Bethesda, MD (1992).

— Quantities and Units in Radiation Protection Dosimetry, Rep. 51, ICRU, Bethesda, MD (1993).

INTERNATIONAL COMMISSION ON RADIOLOGICAL PROTECTION, Conversion Coefficients for Use in Radiological Protection Against External Radiation, Publication 74, Pergamon Press, Oxford and New York (1997).

INTERNATIONAL ORGANIZATION FOR STANDARDIZATION, X and Gamma Reference Radiations for Calibrating Dosemeters and Dose Ratemeters and for Determining their Response as a Function of Energy, ISO 4037. See also High Rate Series of Filtered X-radiations, ISO 4037-1979/Addendum 1(1983); and Low Rate Series of Filtered X-radiations, ISO 4037-1979/Amendment 1-1983 (E), ISO, Geneva (1979).

— Reference Beta Radiations for Calibrating Dosimeters and Dose Rate Meters and for Determining their Response as a Function of Beta Radiation Energy, ISO 6980, ISO, Geneva (1984).

— Dosimetry of the Reference Radiation Fields Used for Determining the Response of Protection Level Dosimeters and Dose-rate Meters at Photon Energies Between 4 and 9 MeV, ISO/DP 9991, ISO, Geneva (1988).

— Dosimetry of X and Gamma Reference Radiations for Radiation Protection over the Energy Range from 9 keV to 1.3 MeV, ISO/DIS 8963, ISO, Geneva (1988).

KNOLL, G.F., Radiation Detection and Measurement, Wiley, New York (1979).

NATIONAL RADIOLOGICAL PROTECTION BOARD, New Radiation Quantities Recommended by ICRU for Practical Use in Radiation Protection: Their Implementation in the United Kingdom, NRPB, Didcot, UK (1986).

Chapter 5

TREATMENT MACHINES FOR EXTERNAL BEAM RADIOTHERAPY

E.B. PODGORSAK
Department of Medical Physics,
McGill University Health Centre,
Montreal, Quebec, Canada

5.1. INTRODUCTION

Since the inception of radiotherapy soon after the discovery of X rays by Roentgen in 1895, the technology of X ray production has first been aimed towards ever higher photon and electron beam energies and intensities, and more recently towards computerization and intensity modulated beam delivery. During the first 50 years of radiotherapy the technological progress was relatively slow and mainly based on X ray tubes, van de Graaff generators and betatrons.

The invention of the ^{60}Co teletherapy unit by H.E. Johns in Canada in the early 1950s provided a tremendous boost in the quest for higher photon energies and placed the cobalt unit at the forefront of radiotherapy for a number of years. The concurrently developed medical linacs, however, soon eclipsed cobalt units, moved through five increasingly sophisticated generations and became the most widely used radiation source in modern radiotherapy. With its compact and efficient design, the linac offers excellent versatility for use in radiotherapy through isocentric mounting and provides either electron or megavoltage X ray therapy with a wide range of energies.

In addition to linacs, electron and X ray radiotherapy is also carried out with other types of accelerator, such as betatrons and microtrons. More exotic particles, such as protons, neutrons, heavy ions and negative π mesons, all produced by special accelerators, are also sometimes used for radiotherapy; however, most contemporary radiotherapy is carried out with linacs or teletherapy cobalt units.

5.2. X RAY BEAMS AND X RAY UNITS

Clinical X ray beams typically range in energy between 10 kVp and 50 MV and are produced when electrons with kinetic energies between 10 keV and 50 MeV are decelerated in special metallic targets.

Most of the electron's kinetic energy is transformed in the target into heat, and a small fraction of the energy is emitted in the form of X ray photons, which are divided into two groups: characteristic X rays and bremsstrahlung X rays.

5.2.1. Characteristic X rays

Characteristic X rays result from Coulomb interactions between the incident electrons and atomic orbital electrons of the target material (collision loss).

In a given Coulomb interaction between the incident electron and an orbital electron, the orbital electron is ejected from its shell and an electron from a higher level shell fills the resulting orbital vacancy. The energy difference between the two shells may either be emitted from the atom in the form of a characteristic photon (characteristic X ray) or transferred to an orbital electron that is ejected from the atom as an Auger electron.

- The fluorescent yield ω gives the number of fluorescent (characteristic) photons emitted per vacancy in a shell ($0 \leq \omega \leq 1$) and ranges from zero for low Z atoms through 0.5 for copper ($Z = 29$) to 0.96 for high Z atoms for K shell vacancies, which are the most prominent sources of characteristic X rays.
- The photons emitted through electronic shell transitions have discrete energies that are characteristic of the particular target atom in which the transitions have occurred; hence the term characteristic radiation.

5.2.2. Bremsstrahlung (continuous) X rays

Bremsstrahlung X rays result from Coulomb interactions between the incident electron and the nuclei of the target material. During the Coulomb interaction between the incident electron and the nucleus, the incident electron is decelerated and loses part of its kinetic energy in the form of bremsstrahlung photons (radiative loss).

- Photons with energies ranging from zero to the kinetic energy of the incident electron may be produced, resulting in a continuous bremsstrahlung spectrum;
- The bremsstrahlung spectrum produced in a given X ray target depends on the kinetic energy of the incident electron as well as on the thickness and atomic number Z of the target.

5.2.3. X ray targets

According to the range R of electrons of a given kinetic energy E_K in the target material, targets are divided into two main groups: thin and thick.

A thin target has a thickness much smaller than R, while the thickness of a thick target is of the order of R. For thin target radiation, the energy radiated is proportional to the product $E_K Z$, where Z is the atomic number of the target. The intensity versus photon energy (photon spectrum) is constant from zero to the kinetic energy E_K of the incident electron, and zero for all energies above E_K.

A thick target may be considered as consisting of a large number of superimposed thin targets. The intensity $I(h\nu)$ of a thick target spectrum is expressed as:

$$I(h\nu) = CZ(E_K - h\nu) \tag{5.1}$$

where

C is a proportionality constant;
$h\nu$ is the photon energy.

X rays are used in diagnostic radiology for diagnosis of disease and in radiation oncology (radiotherapy) for treatment of disease. X rays produced by electrons with kinetic energies between 10 keV and 100 keV are called superficial X rays, those with electron kinetic energies between 100 keV and 500 keV are called orthovoltage X rays, while those with electron kinetic energies above 1 MeV are called megavoltage X rays.

Superficial and orthovoltage X rays are produced with X ray tubes (machines), while megavoltage X rays are most commonly produced with linacs and sometimes with betatrons and microtrons.

Typical thin and thick target bremsstrahlung spectra originating from 100 keV electrons striking a thin and thick target, respectively, are shown in Fig. 5.1.

5.2.4. Clinical X ray beams

A typical spectrum of a clinical X ray beam consists of line spectra that are characteristic of the target material and that are superimposed on to the continuous bremsstrahlung spectrum. The bremsstrahlung spectrum originates in the X ray target, while the characteristic line spectra originate in the target and in any attenuators placed into the beam.

- The relative proportion of the number of characteristic photons to bremsstrahlung photons in an X ray beam spectrum varies with the electron beam kinetic energy and atomic number of the target. For example, X ray beams produced in a tungsten target by 100 keV electrons contain about 20% characteristic photons and 80% bremsstrahlung photons, while in the megavoltage range the contribution of characteristic photons to the total spectrum is negligible.
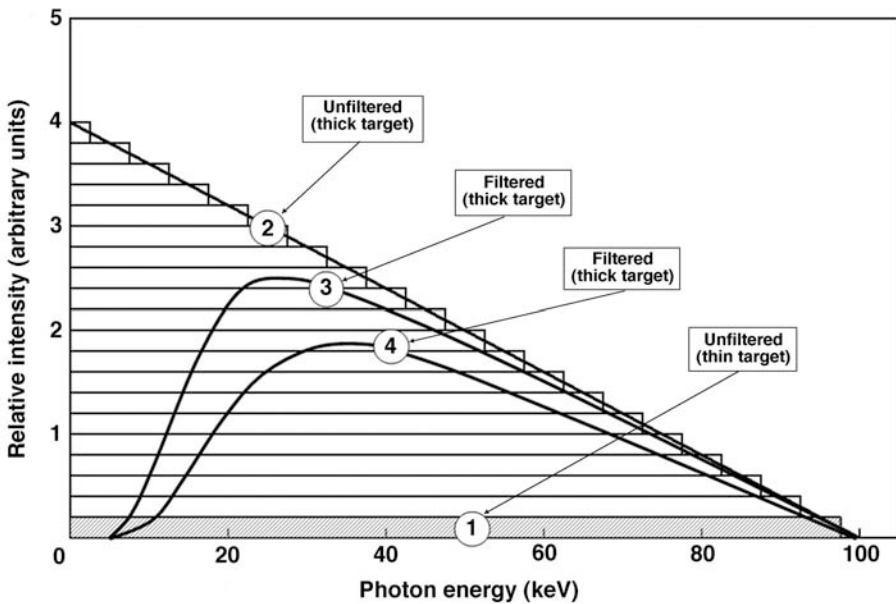
FIG. 5.1. Typical thin target (curve 1) and thick target (curves 2, 3 and 4) spectra for an X ray tube in which 100 keV electrons strike the target. Curve (1) is for a thin target producing a constant intensity for photon energies from zero to the kinetic energy of electrons striking the target (100 keV). Curve (2) represents an unfiltered spectrum (inside the X ray tube) for a thick target and a superposition of numerous thin target spectra; the spectrum of curve (3) is for a beam filtered by an X ray tube window (low energy photons are filtered out); the spectrum of curve (4) is for a beam filtered by the X ray tube window and additional filtration.

● In the diagnostic energy range (10–150 kV) most photons are produced at 90° from the direction of electron acceleration, while in the megavoltage energy range (1–50 MV) most photons are produced in the direction of electron acceleration (forward direction: 0°).

5.2.5. X ray beam quality specifiers

Various parameters, such as photon spectrum, half-value layer (HVL), nominal accelerating potential (NAP) and beam penetration into tissue equivalent media, are used as X ray beam quality indices (see Sections 9.8.1 and 9.8.2 for details):

● A complete X ray spectrum is very difficult to measure; however, it gives the most rigorous description of beam quality.
● The HVL is practical for beam quality description in the superficial (HVL in aluminium) and orthovoltage (HVL in copper) X ray energy range, but not practical in the megavoltage energy range because in this energy range the attenuation coefficient is only a slowly varying function of beam energy.
● The effective energy of a heterogeneous X ray beam is defined as that energy of a monoenergetic photon beam that yields the same HVL as does the heterogeneous beam.
● The NAP is sometimes used for describing the megavoltage beam quality. The NAP is determined by measuring the ionization ratio in a water phantom at depths of 10 and 20 cm for a 10×10 cm^2 field at the nominal source to axis distance (SAD) of 100 cm.
● Recent dosimetry protocols recommend the use of tissue–phantom ratios or percentage depth doses (PDDs) at a depth of 10 cm in a water phantom as an indicator of megavoltage beam effective energy (beam quality index).

5.2.6. X ray machines for radiotherapy

Superficial and orthovoltage X rays used in radiotherapy are produced with X ray machines. The main components of a radiotherapeutic X ray machine are: an X ray tube; a ceiling or floor mount for the X ray tube; a target cooling system; a control console; and an X ray power generator. A schematic diagram of a typical therapy X ray tube is shown in Fig. 5.2.

● The electrons producing the X ray beams in the X ray tube (Coolidge tube) originate in the heated filament (cathode) and are accelerated in a

vacuum towards the target (anode) by an essentially constant potential electrostatic field supplied by the X ray generator.

- The efficiency for X ray production in the superficial and orthovoltage energy range is of the order of 1% or less. Most of the electron kinetic energy deposited in the X ray target (~99%) is transformed into heat and must be dissipated through an efficient target cooling system.
- To maximize the X ray yield in the superficial and orthovoltage energy range the target material should have a high atomic number Z and a high melting point.
- With X ray tubes, the patient dose is delivered using a timer and the treatment time must incorporate the shutter correction time (see Section 6.16), which accounts for the time required for the power supply components to attain the steady state operating conditions.
- The X ray tube current is controlled by a hot filament emission of electrons, which, in turn, is controlled by the filament temperature (thermionic emission). For a given filament temperature the X ray tube current increases with the tube (anode) voltage, first rising linearly with voltage in the space charge limited region and saturating at higher voltages when all electrons emitted from the cathode are pulled to the anode.
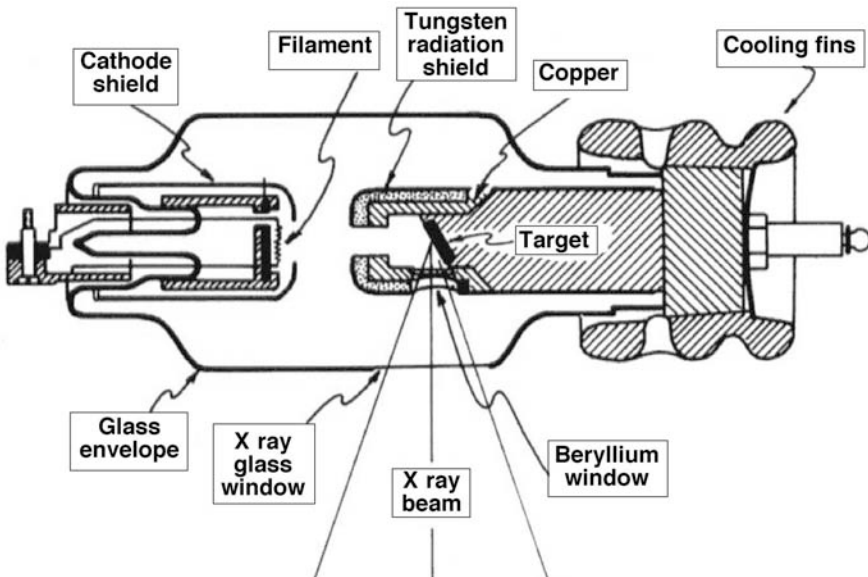
FIG. 5.2. Typical therapy X ray tube (reprinted from Johns, H.E., and Cunningham, J.R., with permission).

● Research is currently being carried out on cold field emission cathodes produced with carbon nanotubes (CNTs). The CNT based cold cathode X ray technology may lead to more durable as well as miniature and portable X ray sources for industrial and medical applications.

5.3. GAMMA RAY BEAMS AND GAMMA RAY UNITS

5.3.1. Basic properties of gamma rays

For use in external beam radiotherapy, γ rays are obtained from specially designed and built sources that contain a suitable, artificially produced radioactive material.

● The parent source material undergoes a β decay, resulting in excited daughter nuclei that attain ground state through emission of γ rays (γ decay).
● The important characteristics of radioisotopes in external beam radiotherapy are:
  — High γ ray energy;
  — High specific activity;
  — Relatively long half-life;
  — Large specific air kerma rate constant Γ_{AKR}.
● The specific activity a (activity $\mathcal{A}$ per mass m of radioactive nuclide) is inversely proportional to the half-life $t_{1/2}$:

$$a = \frac{\mathcal{A}}{m} = \frac{N_A \ln 2}{t_{1/2} A} \qquad (5.2)$$

where

N_A is Avogadro's number (6.022×10^{23} atoms/g-atom);
A is the atomic mass number.

● The air kerma rate in air $(\dot{K}_{air})_{air}$ is given by the following relation:

$$(\dot{K}_{air})_{air} = \frac{\mathcal{A}\Gamma_{AKR}}{d^2} \qquad (5.3)$$

where

$\mathcal{A}$ is the source activity;
d is the distance between the point of interest and the point source.

- The basic physical properties of the two γ emitters (^{60}Co and ^{137}Cs) currently used for external beam teletherapy and a potential source for teletherapy units (^{152}Eu) are listed in Table 5.1. Of the three radioisotopes, ^{60}Co is the most widely used, since it offers the most practical approach to external beam radiotherapy, considering the energy of emitted photons, half-life, specific activity and means of production.

5.3.2.   Teletherapy machines

Treatment machines incorporating γ ray sources for use in external beam radiotherapy are called teletherapy machines. They are most often mounted isocentrically, allowing the beam to rotate about the patient at a fixed SAD. Modern teletherapy machines have SADs of 80 or 100 cm.

The main components of a teletherapy machine are: a radioactive source; a source housing, including beam collimator and source movement mechanism; a gantry and stand in isocentric machines or a housing support assembly in stand-alone machines; a patient support assembly; and a machine console.

5.3.3.   Teletherapy sources

The most widely used teletherapy source uses ^{60}Co radionuclides contained inside a cylindrical stainless steel capsule and sealed by welding. A double welded seal is used to prevent any leakage of the radioactive material.

- To facilitate interchange of sources from one teletherapy machine to another and from one isotope production facility to another, standard source capsules have been developed.
- The typical diameter of the cylindrical teletherapy source is between 1 and 2 cm; the height of the cylinder is about 2.5 cm. The smaller the source diameter, the smaller is its physical penumbra and the more expensive is the source. Often a diameter of 1.5 cm is chosen as a compromise between the cost and penumbra.
- Typical source activities are of the order of 5000–10 000 Ci (185–370 TBq) and provide a typical dose rate at 80 cm from the teletherapy source of the order of 100–200 cGy/min. Often the output of a teletherapy machine

TABLE 5.1. PHYSICAL PROPERTIES OF RADIONUCLIDES USED IN EXTERNAL BEAM RADIOTHERAPY

	Co-60	Cs-137	Eu-152
Half-life (a)	5.3	30	13.4
Specific activity (Ci/g)	1100[a] (~250[b])	80	180[a] (~150[b])
Photon energy (MeV)	1.17 and 1.33	0.662	0.6–1.4
Specific γ rate constant Γ [Rm^2/(Ci·h)]	1.31	0.33	1.06
Specific air kerma rate constant Γ_{AKR} [μGy·m^2/(GBq·h)]	309	78	250
HVL (cm Pb)	1.1	0.5	1.1
Means of production	^{59}Co + n in reactor	Fission by-product	^{151}Eu + n in reactor

[a] Theoretical specific activity: $a = (N_A \ln 2)/(t_{1/2}A)$.
[b] The practical specific activity is smaller than the theoretical specific activity because the source is not carrier free (i.e. the source contains stable isotopes in addition to radioactive isotopes (e.g. ^{59}Co mixed with ^{60}Co)).

  is stated in Rmm (roentgens per minute at 1 m) as a rough guide for the source strength.
- Teletherapy sources are usually replaced within one half-life after they are installed; however, financial considerations often result in longer source usage.
- The ^{60}Co radionuclides in a teletherapy source decay with a half-life of 5.26 years into ^{60}Ni with the emission of electrons (β particles) with a maximum energy of 320 keV and two γ rays with energies of 1.17 MeV and 1.33 MeV. The emitted γ rays constitute the therapy beam; the electrons are absorbed in the cobalt source or the source capsule, where they produce relatively low energy and essentially negligible bremsstrahlung X rays and characteristic X rays.

5.3.4. Teletherapy source housing

The housing for the teletherapy source is called the source head, and consists of a steel shell with lead for shielding purposes and a mechanism for bringing the source in front of the collimator opening to produce the clinical γ ray beam.

● Currently two methods are in use for moving the teletherapy source from the beam off into the beam on position and back: (i) a source on a sliding drawer and (ii) a source on a rotating cylinder. Both methods incorporate a safety feature in which the beam is terminated automatically in the event of a power failure or emergency.

● When the source is in the beam off position, a light source appears in the beam on position above the collimator opening, allowing an optical visualization of the radiation field, as defined by the machine collimators and any special shielding blocks.

● Some radiation will escape from the unit even when the source is in the beam off position. The head leakage typically amounts to less than 1 mR/h (0.01 mSv/h) at 1 m from the source. International regulations require that the average leakage of a teletherapy machine head be less than 2 mR/h (0.02 mSv/h) at 1 m from the source.

5.3.5.   Dose delivery with teletherapy machines

The prescribed target dose is delivered with the help of two treatment timers: primary and secondary. The primary timer actually controls the treatment time, the secondary timer serves as a backup timer in case of the primary timer's failure.

The set treatment time must incorporate the shutter error, which accounts for the travel time of the source from the beam off position towards the beam on position at the start of irradiation and for the reverse travel at the end of irradiation.

5.3.6.   Collimator and penumbra

Collimators of teletherapy machines provide square and rectangular radiation fields typically ranging from 5×5 to 35×35 cm^2 at 80 cm from the source. The geometric penumbra, which results from a finite source diameter, may be minimized by using small diameter sources and by using penumbra trimmers as close as possible to the patient's skin (see Section 6.9 for further discussion of the penumbra).

5.4.   PARTICLE ACCELERATORS

Numerous types of accelerator have been built for basic research in nuclear and high energy physics, and most of them have been modified for at

least some limited use in radiotherapy. Irrespective of the accelerator type, two basic conditions must be met for particle acceleration:

- The particle to be accelerated must be charged;
- An electric field must be provided in the direction of particle acceleration.

The various types of accelerator differ in the way they produce the accelerating electric field and in how the field acts on the particles to be accelerated. As far as the accelerating electric field is concerned there are two main classes of accelerator: electrostatic and cyclic.

— In electrostatic accelerators the particles are accelerated by applying an electrostatic electric field through a voltage difference, constant in time, whose value fixes the value of the final kinetic energy of the particle. Since the electrostatic fields are conservative, the kinetic energy that the particle can gain depends only on the point of departure and point of arrival and hence cannot be larger than the potential energy corresponding to the maximum voltage drop existing in the machine. The energy that an electrostatic accelerator can reach is limited by the discharges that occur between the high voltage terminal and the walls of the accelerator chamber when the voltage drop exceeds a certain critical value (typically 1 MV).

— The electric fields used in cyclic accelerators are variable and nonconservative, associated with a variable magnetic field and resulting in some close paths along which the kinetic energy gained by the particle differs from zero. If the particle is made to follow such a closed path many times over, one obtains a process of gradual acceleration that is not limited to the maximum voltage drop existing in the accelerator. Thus the final kinetic energy of the particle is obtained by submitting the charged particle to the same, relatively small, potential difference a large number of times, each cycle adding a small amount of energy to the kinetic energy of the particle.

Examples of electrostatic accelerators used in medicine are superficial and orthovoltage X ray tubes and neutron generators. The best known example of a cyclic accelerator is the linac; other examples are microtrons, betatrons and cyclotrons.

5.4.1. Betatron

The betatron was developed in 1940 by D.W. Kerst as a cyclic electron accelerator for basic physics research; however, its potential for use in radiotherapy was realized soon after.

- The machine consists of a magnet fed by an alternating current of frequency between 50 and 200 Hz. The electrons are made to circulate in a toroidal (doughnut shaped) vacuum chamber that is placed into the gap between two magnet poles. A schematic diagram of a betatron is given in Fig. 5.3(a).
- Conceptually, the betatron may be considered an analogue of a transformer: the primary current is the alternating current exciting the magnet and the secondary current is the electron current circulating in the vacuum chamber (doughnut).
- The electrons are accelerated by the electric field induced in the doughnut shape by the changing magnetic flux in the magnet; they are kept in a circular orbit by the magnetic field present.
- In the 1950s betatrons played an important role in megavoltage radiotherapy. However, the development of linacs pushed them into oblivion because of the numerous advantages offered by linacs over betatrons, such as: much higher beam output (up to 10 Gy/min for linacs versus 1 Gy/min for betatrons); larger field size; full isocentric mounting; more compact design; and quieter operation.

5.4.2. Cyclotron

The cyclotron was developed in 1930 by E.O. Lawrence for acceleration of ions to a kinetic energy of a few megaelectronvolts. Initially, the cyclotron was used for basic nuclear physics research, but later on found important medical uses in the production of radioisotopes for nuclear medicine as well as in the production of proton and neutron beams for radiotherapy. The recent introduction of positron emission tomography (PET)/computed tomography (CT) machines for use in radiotherapy (see Section 15.10) has dramatically increased the importance of cyclotrons in medicine. PET/CT machines rely on glucose labelled with positron emitting ^{18}F produced by proton cyclotrons.

- In a cyclotron the particles are accelerated along a spiral trajectory guided inside two evacuated half-cylindrical electrodes (referred to as dees because of their D shaped form) by a uniform magnetic field (1 T)

that is produced between the pole pieces of a large magnet. Figure 5.3(b) is a diagram of a cyclotron.

● A radiofrequency (RF) voltage with a constant frequency between 10 and 30 MHz is applied between the two electrodes and the charged particle is accelerated while crossing the gap between the two electrodes.

● Inside the electrodes there is no electric field and the particle drifts under the influence of the magnetic field in a semicircular orbit with a constant speed until it crosses the gap again. If, in the meantime, the electric field has reversed its direction, the particle will again be accelerated across the gap, gain a small amount of energy and drift in the other electrode along a semicircle of a larger radius than the former one, resulting in a spiral orbit and a gradual increase in kinetic energy after a large number of gap crossings.

5.4.3. Microtron

The microtron is an electron accelerator that combines the features of a linac with a cyclotron. The concept of the microtron was developed by
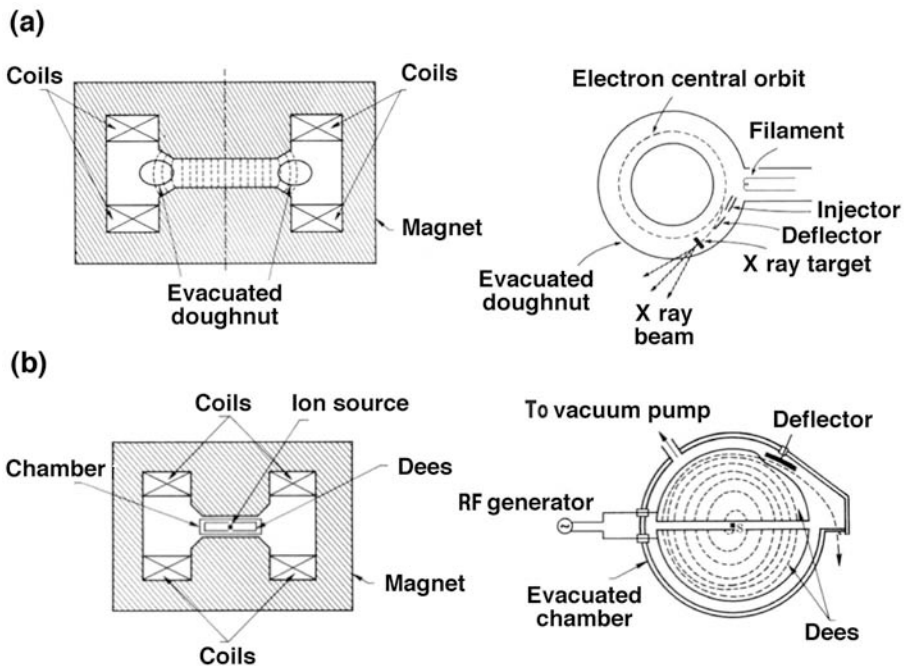
FIG. 5.3. Two cyclic accelerators: (a) a betatron and (b) a cyclotron.

135

V.I. Veksler in 1944, and the machine is used in modern radiotherapy, albeit to a much smaller extent than linacs.

Two types of microtron have been developed: circular and racetrack.

- In the circular microtron the electron gains energy from a microwave resonant cavity and describes circular orbits of increasing radius in a uniform magnetic field. To keep the particle in phase with the microwave power, the cavity voltage, frequency and magnetic field are adjusted in such a way that after each passage through the cavity the electrons gain an energy increment, resulting in an increase in the transit time in the magnetic field equal to an integral number of microwave cycles.
- In the racetrack microtron the magnet is split into two D shaped pole pieces that are separated to provide greater flexibility in achieving efficient electron injection and higher energy gain per orbit through the use of multicavity accelerating structures similar to those used in linacs. The electron orbits consist of two semicircular and two straight sections.

5.5. LINACS

Medical linacs are cyclic accelerators that accelerate electrons to kinetic energies from 4 to 25 MeV using non-conservative microwave RF fields in the frequency range from 10^3 MHz (L band) to 10^4 MHz (X band), with the vast majority running at 2856 MHz (S band).

In a linac the electrons are accelerated following straight trajectories in special evacuated structures called accelerating waveguides. Electrons follow a linear path through the same, relatively low, potential difference several times; hence linacs also fall into the class of cyclic accelerators, just like the other cyclic machines that provide curved paths for the accelerated particles (e.g. betatrons).

The high power RF fields used for electron acceleration in the accelerating waveguides are produced through the process of decelerating electrons in retarding potentials in special evacuated devices called magnetrons and klystrons.

Various types of linac are available for clinical use. Some provide X rays only in the low megavoltage range (4 or 6 MV), while others provide both X rays and electrons at various megavoltage energies. A typical modern high energy linac will provide two photon energies (6 and 18 MV) and several electron energies (e.g. 6, 9, 12, 16 and 22 MeV).

5.5.1. Linac generations

During the past 40 years medical linacs have gone through five distinct generations, making the contemporary machines extremely sophisticated in comparison with the machines of the 1960s. The five generations introduced the following new features:

- Low energy photons (4–8 MV): straight-through beam; fixed flattening filter; external wedges; symmetric jaws; single transmission ionization chamber; isocentric mounting.
- Medium energy photons (10–15 MV) and electrons: bent beam; movable target and flattening filter; scattering foils; dual transmission ionization chamber; electron cones.
- High energy photons (18–25 MV) and electrons: dual photon energy and multiple electron energies; achromatic bending magnet; dual scattering foils or scanned electron pencil beam; motorized wedge; asymmetric or independent collimator jaws.
- High energy photons and electrons: computer controlled operation; dynamic wedge; electronic portal imaging device (EPID); multileaf collimator (MLC).
- High energy photons and electrons: photon beam intensity modulation with MLC; full dynamic conformal dose delivery with intensity modulated beams produced with an MLC.

5.5.2. Safety of linac installations

The complexity of modern linacs raises concerns as to safety of operation from the point of view of patients and operators. The International Electrotechnical Commission (IEC) publishes international standards that express, as nearly as possible, an international consensus of opinion on relevant technical subjects; electron linacs are addressed in detail by the IEC. The IEC statement on the safety of linacs (IEC 60601-2-1, p. 13) is as follows:

"*The use of electron accelerators for radiotherapy purposes may expose patients to danger if the equipment fails to deliver the required dose to the patient, or if the equipment design does not satisfy standards of electrical and mechanical safety. The equipment may also cause danger to persons in the vicinity if the equipment fails to contain the radiation adequately and/or if there are inadequacies in the design of the treatment room.*"

The IEC document addresses three categories of safety issues — electrical, mechanical and radiation — and establishes specific requirements mainly for the manufacturers of linacs in the design and construction of linacs for use in radiotherapy. It also covers some radiation safety aspects of linac installation in customer's treatment rooms.

5.5.3. Components of modern linacs

Linacs are usually mounted isocentrically and the operational systems are distributed over five major and distinct sections of the machine, the:

- Gantry;
- Gantry stand or support;
- Modulator cabinet;
- Patient support assembly (i.e. treatment table);
- Control console.

A schematic diagram of a typical modern S band medical linac is shown in Fig. 5.4. Also shown are the connections and relationships among the various linac components listed above. The diagram provides a general layout of a linac's components; however, there are significant variations from one commercial machine to another, depending on the final electron beam kinetic energy as well as on the particular design used by the manufacturer.

— The length of the accelerating waveguide depends on the final electron kinetic energy, and ranges from ~30 cm at 4 MeV to ~150 cm at 25 MeV.
— The main beam forming components of a modern medical linac are usually grouped into six classes:
  (i) Injection system;
  (ii) RF power generation system;
  (iii) Accelerating waveguide;
  (iv) Auxiliary system;
  (v) Beam transport system;
  (vi) Beam collimation and beam monitoring system.

5.5.4. Configuration of modern linacs

At megavoltage electron energies the bremsstrahlung photons produced in the X ray target are mainly forward peaked and the clinical photon beam is produced in the direction of the electron beam striking the target.

- In the simplest and most practical configuration, the electron gun and the X ray target form part of the accelerating waveguide and are aligned directly with the linac isocentre, obviating the need for a beam transport system. A straight-through photon beam is produced and the RF power source is mounted in the gantry.
- The simplest linacs are isocentrically mounted 4 or 6 MV machines, with the electron gun and target permanently built into the accelerating waveguide, thereby requiring no beam transport nor offering an electron therapy option.
- Accelerating waveguides for intermediate (8–15 MeV) and high (15–30 MeV) electron energies are too long for direct isocentric mounting and thus are located either in the gantry, parallel to the gantry axis of rotation, or in the gantry stand. A beam transport system is then used to transport the electron beam from the accelerating waveguide to the X ray target. The RF power source in the two configurations is commonly mounted in the gantry stand. Various design configurations for modern isocentric linacs are shown in Fig. 5.5.
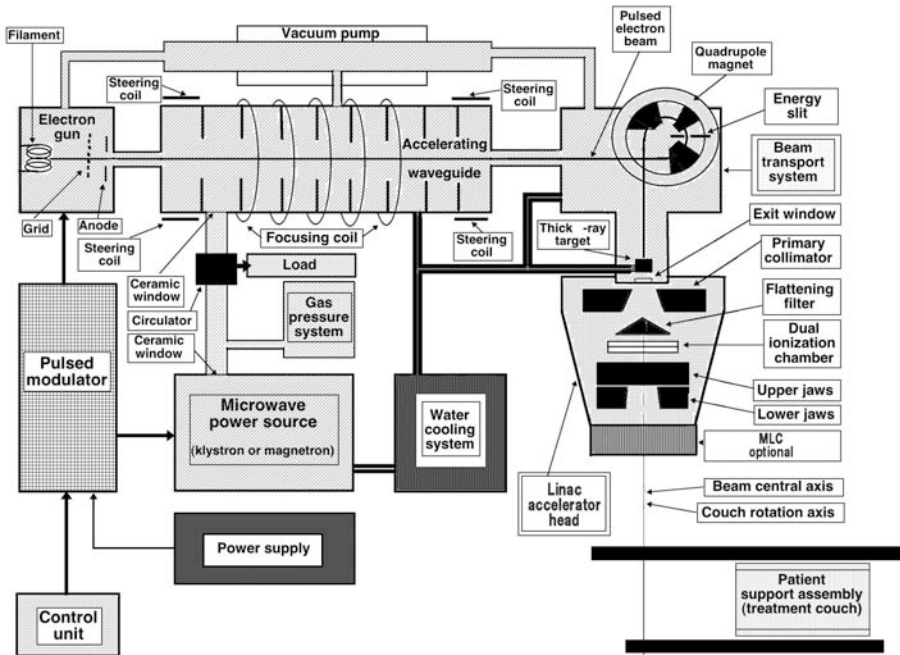
FIG. 5.4. Medical linac.

5.5.5. Injection system

The injection system is the source of electrons; it is essentially a simple electrostatic accelerator called an electron gun.

- Two types of electron gun are in use as sources of electrons in medical linacs:
  — Diode type;
  — Triode type.
- Both electron gun types contain a heated filament cathode and a perforated grounded anode; in addition, the triode electron gun also incorporates a grid.
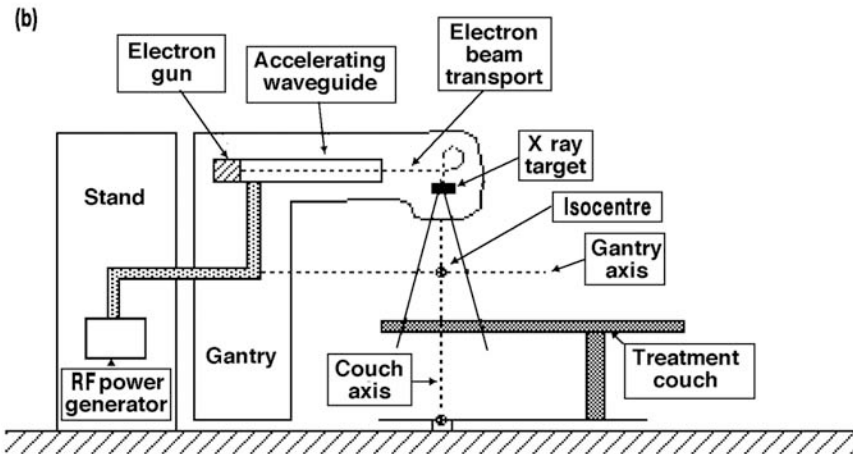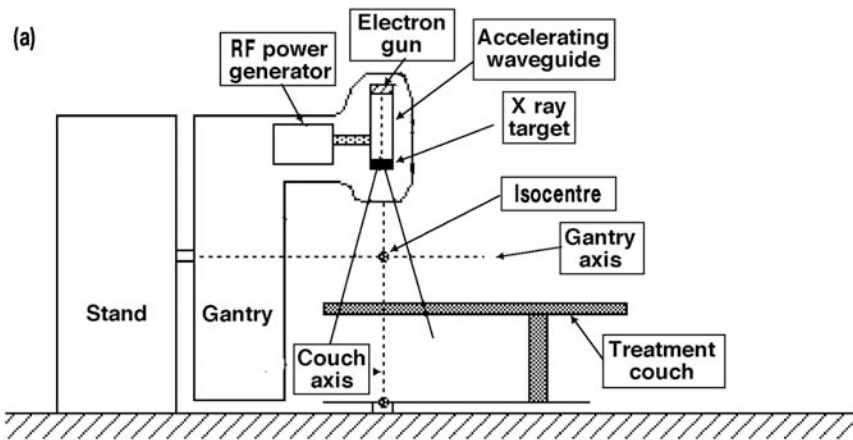
- Electrons are thermionically emitted from the heated cathode, focused into a pencil beam by a curved focusing electrode and accelerated towards the perforated anode through which they drift to enter the accelerating waveguide.
- The electrostatic fields used to accelerate the electrons in the diode gun are supplied directly from the pulsed modulator in the form of a negative pulse delivered to the cathode of the gun.
- In a triode gun, however, the cathode is held at a static negative potential (typically –20 kV). The grid of the triode gun is normally held sufficiently negative with respect to the cathode to cut off the current to the anode. The injection of electrons into the accelerating waveguide is then controlled by voltage pulses, which are applied to the grid and must be synchronized with the pulses applied to the microwave generator. A removable triode gun of a high energy linac is shown in Fig. 5.6(a).
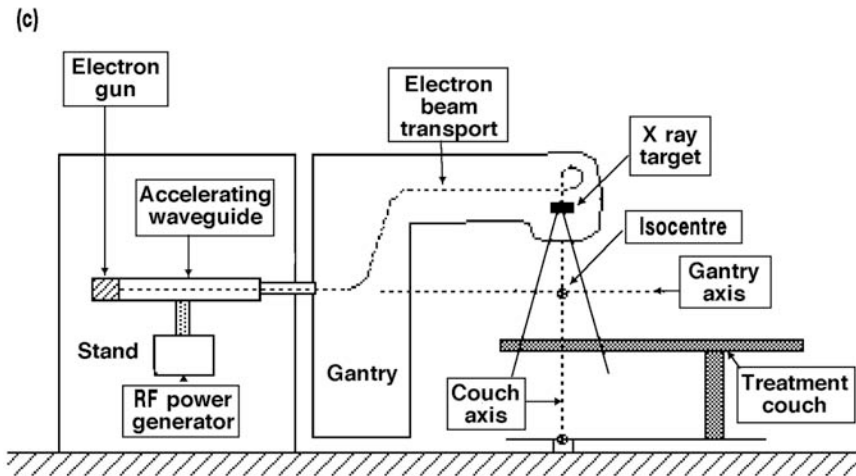
FIG. 5.5. Design configurations for isocentric medical linacs. (a) Straight-through beam design; the electron gun and target are permanently embedded into the accelerating waveguide; the machine produces only X rays with energies of 4–6 MV; the RF power generator is mounted in the gantry. (b) The accelerating waveguide is in the gantry parallel to the isocentre axis; electrons are brought to the movable target through a beam transport system; the RF power generator is located in the gantry stand; the machine can produce megavoltage X rays as well as electrons. (c) The accelerating waveguide and RF power generator are located in the gantry stand; electrons are brought to the movable target through a beam transport system; the machine can produce megavoltage X rays as well as electrons.
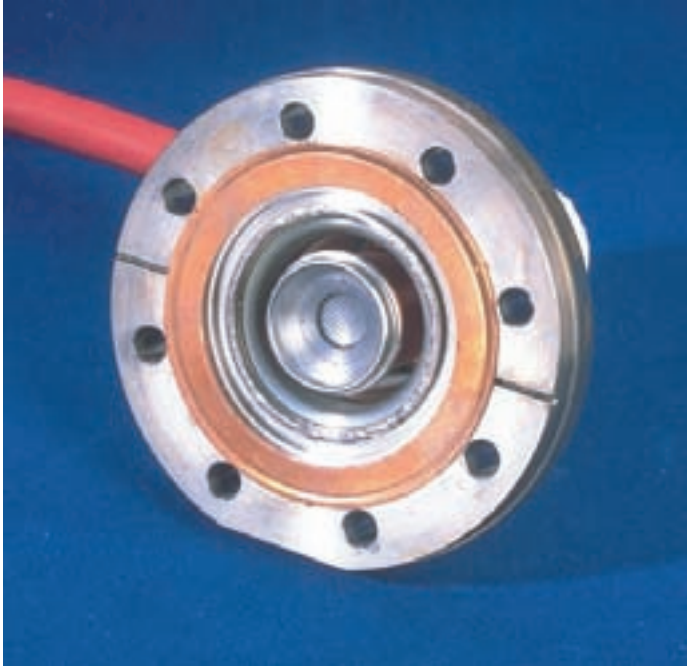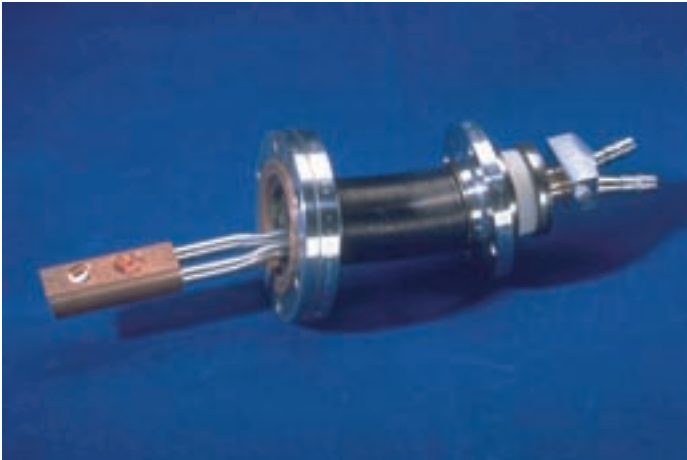
FIG. 5.6. Removable electron triode gun (a) and removable X ray target (b) for a typical high energy linac (Varian Clinac-18), allowing two photon modes and several electron modes. The target is water cooled and mounted with bellows to allow for movement into the pencil electron beam for X ray production and movement out of the pencil beam for electron beam production.

5.5.6. Radiofrequency power generation system

The microwave radiation used in the accelerating waveguide to accelerate electrons to the desired kinetic energy is produced by the RF power generation system, which consists of two major components:

- An RF power source;
- A pulsed modulator.

The RF power source is either a magnetron or a klystron. Both are devices that use electron acceleration and deceleration in a vacuum for the production of high power RF fields. Both types use a thermionic emission of electrons from a heated cathode and accelerate the electrons towards an anode in a pulsed electrostatic field; however, their design principles are completely different.

— The high voltage (~100 kV), high current (~100 A), short duration (~1 s) pulses required by the RF power source (magnetron or klystron) and the injection system (electron gun) are produced by a pulsed modulator. The circuitry of the pulsed modulator is housed in the modulator cabinet, which, depending on the particular linac installation design, is located in the treatment room, in a special mechanical room next to the treatment room or in the linac control room.

— A magnetron is a source of high power RF required for electron acceleration, while a klystron is an RF power amplifier that amplifies the low power RF generated by an RF oscillator commonly called the RF driver.

5.5.7. Accelerating waveguide

Waveguides are evacuated or gas filled metallic structures of rectangular or circular cross-section used in the transmission of microwaves. Two types of waveguide are used in linacs: RF power transmission waveguides and accelerating waveguides. The power transmission waveguides transmit the RF power from the power source to the accelerating waveguide in which the electrons are accelerated.

- The electrons are accelerated in the accelerating waveguide by means of an energy transfer from the high power RF fields, which are set up in the accelerating waveguide and are produced by the RF power generators.
- The simplest kind of accelerating waveguide is obtained from a cylindrical uniform waveguide by adding a series of discs (irises) with

circular holes at the centre, placed at equal distances along the tube. These discs divide the waveguide into a series of cylindrical cavities that form the basic structure of the accelerating waveguide in a linac.

The accelerating waveguide is evacuated to allow free propagation of electrons. The cavities of the accelerating waveguide serve two purposes:

— To couple and distribute microwave power between adjacent cavities;
— To provide a suitable electric field pattern for the acceleration of electrons.

Two types of accelerating waveguide have been developed for the acceleration of electrons:

 (i) Travelling wave structure;
(ii) Standing wave structure.

In the travelling wave structure the microwaves enter the accelerating waveguide on the gun side and propagate towards the high energy end of the waveguide, where they either are absorbed without any reflection or exit the waveguide to be absorbed in a resistive load or to be fed back to the input end of the accelerating waveguide. In this configuration only one in four cavities is at any given moment suitable for electron acceleration, providing an electric field in the direction of propagation.

In the standing wave structure each end of the accelerating waveguide is terminated with a conducting disc to reflect the microwave power, resulting in a buildup of standing waves in the waveguide. In this configuration, at all times, every second cavity carries no electric field and thus produces no energy gain for the electrons. These cavities therefore serve only as coupling cavities and can be moved out to the side of the waveguide structure, effectively shortening the accelerating waveguide by 50%. A cut-away view of a 6 MV standing wave accelerating waveguide is shown in Fig. 5.7.

5.5.8. Microwave power transmission

The microwave power produced by the RF generator is carried to the accelerating waveguide through rectangular uniform S band waveguides that are either evacuated or, more commonly, pressurized with a dielectric gas (Freon or sulphur hexafluoride, SF_6) to twice the atmospheric pressure.

An important component that must be inserted into the RF power transmission circuit between the RF generator and the accelerating waveguide is a
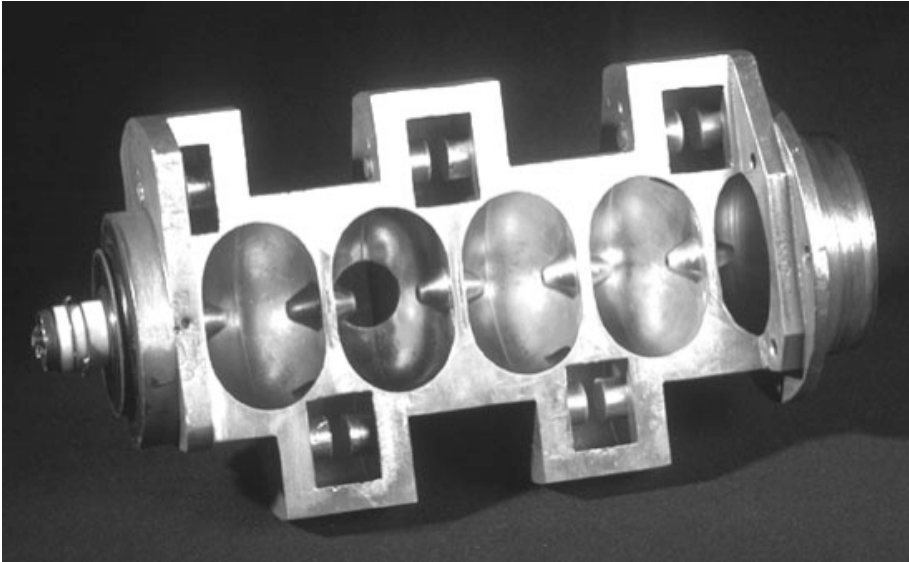
FIG. 5.7. Cutaway view of a standing wave accelerating waveguide for a 6 MV linac. The cavities are clearly visible: the accelerating cavities are on the central axis; the coupling cavities are off-side. The electron gun is on the left, the target on the right, both permanently embedded.

circulator (sometimes referred to as an isolator), which transmits the RF power from the RF generator to the accelerating waveguide but is impervious to reflected radiation moving in the opposite direction, thereby protecting the RF source from the reflected power.

5.5.9. Auxiliary system

The linac auxiliary system consists of several services that are not directly involved with electron acceleration, yet make the acceleration possible and the linac viable for clinical operation.

The linac auxiliary system comprises four systems:

- A vacuum pumping system producing a vacuum pressure of ~10^{-6} torr in the accelerating guide and the RF generator;
- A water cooling system used for cooling the accelerating guide, target, circulator and RF generator;
- An optional air pressure system for pneumatic movement of the target and other beam shaping components;
- Shielding against leakage radiation.

5.5.10. Electron beam transport

In low energy linacs the target is embedded in the accelerating waveguide and no beam transport between the accelerating waveguide and target is required.

Bending magnets are used in linacs operating at energies above 6 MeV, where the accelerating waveguides are too long for straight-through mounting. The accelerating waveguide is usually mounted parallel to the gantry rotation axis and the electron beam must be bent to make it strike the X ray target or be able to exit through the beam exit window. Three systems for electron bending have been developed:

- 90º bending;
- 270º bending (achromatic);
- 112.5º (slalom) bending.

In medium (10 MV) and high energy (above 15 MV) linacs an electron beam transport system is used for transporting the electron beam from the accelerating waveguide to the X ray target or to the linac exit window for electron beam therapy. The system consists of evacuated drift tubes and bending magnets. In addition, steering coils and focusing coils, used for steering and focusing of the accelerated electron beam, also form components of the beam transport system.

5.5.11. Linac treatment head

The linac head contains several components that influence the production, shaping, localizing and monitoring of the clinical photon and electron beams.

Electrons originating in the electron gun are accelerated in the accelerating waveguide to the desired kinetic energy and then brought, in the form of a pencil beam, through the beam transport system into the linac treatment head, where the clinical photon and electron beams are produced.

- The important components found in a typical head of a fourth or fifth generation linac include:
  — Several retractable X ray targets;
  — Flattening filters and electron scattering foils (also called scattering filters);
  — Primary and adjustable secondary collimators;
  — Dual transmission ionization chambers;

— A field defining light and a range finder;
— Optional retractable wedges;
— Optional MLC.

● Clinical photon beams are produced with a target–flattening filter combination.
● Clinical electron beams are produced by retracting the target and flattening filter from the electron pencil beam and:
— Either scattering the pencil beam with a single or dual scattering foil; or
— Deflecting and scanning the pencil beam magnetically to cover the field size required for electron treatment.

Special cones (applicators) are used to collimate the electron beams.

● Each clinical photon beam has its own target–flattening filter combination. The flattening filters and scattering foils (if used for electron beams) are mounted on a rotating carousel or sliding drawer for ease of mechanical positioning into the beam, as required.
● The primary collimator defines a maximum circular field, which is then further truncated with an adjustable rectangular collimator consisting of two upper and two lower independent jaws and producing rectangular and square fields with a maximum dimension of 40×40 cm^2 at the linac isocentre. The IEC recommends that the transmission of the primary X ray beam through the rectangular collimator should not exceed 2% of the open beam value.
● Dual transmission ionization chambers are used for monitoring the photon and electron radiation beam output as well as the radial and transverse beam flatness (see Section 5.5.14).
● The field defining light and the range finder provide convenient visual methods for correctly positioning the patient for treatment using reference marks. The field light illuminates an area that coincides with the radiation treatment field on the patient's skin, while the range finder is used to place the patient at the correct treatment distance by projecting a centimetre scale whose image on the patient's skin indicates the vertical distance from the linac isocentre.

5.5.12. Production of clinical photon beams in a linac

Clinical photon beams emanating from a medical linac are produced in an X ray target and flattened with a flattening filter. A high energy linac movable target is shown in Fig. 5.6(b).

At electron energies below 15 MeV (photon beam energies 15 MV) optimal targets have a high atomic number Z, while at electron energies above 15 MeV (photon beam energies above 15 MV) the optimal targets have a low

atomic number Z. Optimal flattening filters have a low Z irrespective of beam energy.

5.5.13. Beam collimation

In a typical modern medical linac, the photon beam collimation is achieved with two or three collimator devices:

- A primary collimator;
- Secondary movable beam defining collimators;
- An MLC (optional).

In addition to the primary and secondary collimators, clinical electron beams also rely on electron beam applicators (cones) for beam collimation.

— The primary collimator defines the largest available circular field size and is a conical opening machined into a tungsten shielding block, with the sides of the conical opening projecting on to edges of the target on one end of the block and on to the flattening filter on the other end. The thickness of the shielding block is usually designed to attenuate the average primary X ray beam intensity to less than 0.1% of the initial value (three tenth-value layers (TVLs)). According to IEC recommendations, the maximum leakage should not exceed 0.2% of the open beam value.

— The secondary beam defining collimators consist of four blocks, two forming the upper and two forming the lower jaws of the collimator. They can provide rectangular or square fields at the linac isocentre, with sides of the order of few millimetres up to 40 cm.

— Modern linacs incorporate independent (asymmetric) jaws that can provide asymmetric fields, most commonly one half or three quarter blocked fields in which one or two beam edges, respectively, are coincident with the beam central axis.

— MLCs are a relatively recent addition to linac dose delivery technology. In principle, the idea behind an MLC is simple; however, building a reliable MLC system presents a substantial technological challenge.

— The number of leaves in commercial MLCs is steadily increasing, and models with 120 leaves (60 pairs) covering fields up to 40×40 cm^2 and requiring 120 individually computer controlled motors and control circuits are currently available.

— MLCs are becoming invaluable in supplying intensity modulated fields in conformal radiotherapy, either in the step and shoot mode or in a continuous dynamic mode.

— Miniature versions of MLCs (micro MLCs) projecting 1.5–6 mm leaf widths and up to 10×10 cm^2 fields at the linac isocentre are currently commercially available. They may be used in radiosurgery as well as for head and neck treatments.

5.5.14. Production of clinical electron beams in a linac

The majority of higher energy linacs, in addition to providing single or dual photon energies, also provide electron beams with several nominal electron beam energies in the range from 6 to 30 MeV.

- To activate an electron beam mode, both the target and the flattening filter of the X ray beam mode are removed from the electron beam.
- The electron beam currents producing clinical electron beams are two to three orders of magnitude lower than the electron currents producing the clinical photon beams in the linac X ray target.
- The electron pencil beam exits the evacuated beam transport system through a thin window usually made of beryllium, which, with its low atomic number Z, minimizes the pencil beam scattering and bremsstrahlung production.
- Two techniques are available for producing clinical electron beams from electron pencil beams:
  — Pencil beam scattering. The scattering of the electron pencil beam over the relatively large area used in radiotherapy (up to 25×25 cm^2) is achieved by placing thin foils of high Z material (copper or lead) into the pencil beam at the level of the flattening filter in the X ray mode.
  — Pencil beam scanning. Electron pencil beam scanning is an alternative, albeit infrequently used, technique for producing clinical electron beams. The technique is usually implemented with two computer controlled magnets, which deflect the pencil beam in two orthogonal planes, thereby scanning the pencil beam across the clinical treatment field.

5.5.15. Dose monitoring system

IEC 60601-2-1 specifies in detail the standards for radiation monitors installed in clinical electron linacs. It deals with standards for the type of radiation detectors, display of monitor units (MUs), termination of radiation and monitoring of beam flatness and dose rate.

- Most common dose monitors in linacs are transmission ionization chambers permanently imbedded in the linac clinical photon and electron beams to monitor the beam output continuously during patient treatment.
- Most linacs use sealed ionization chambers to make their response independent of ambient temperature and pressure.
- The customary position of the dose monitor chambers is between the flattening filter or scattering foil and the photon beam secondary collimator.
- For patient safety, the linac dosimetry system usually consists of two separately sealed ionization chambers with completely independent biasing power supplies and readout electrometers. If the primary chamber fails during patient treatment, the secondary chamber will terminate the irradiation, usually after an additional dose of only a few per cent above the prescribed dose has been delivered.
- In the event of a simultaneous failure of both the primary and secondary ionization chambers, the linac timer will shut the machine down with a minimal overdose to the patient.
- The main requirements for the ionization chamber monitors are as follows:
  —Chambers must have a minimal effect on clinical photon and electron radiation beams;
  —Chamber response should be independent of ambient temperature and pressure (most linacs use sealed ionization chambers to satisfy this condition);
  —Chambers should be operated under saturation conditions.
- The primary ionization chamber measures MUs. Typically, the sensitivity of the chamber electrometer circuitry is adjusted in such a way that 1 MU corresponds to a dose of 1 cGy delivered in a water phantom at the depth of dose maximum on the central beam axis when irradiated with a $10 \times 10 \text{ cm}^2$ field at a source to surface distance (SSD) of 100 cm.
- Once the operator preset number of MUs has been reached, the primary ionization chamber circuitry shuts the linac down and terminates the dose delivery to the patient. Before a new irradiation can be initiated, it is necessary to reset the MU displays to zero. Furthermore, irradiation is not possible until a new selection of MUs has been made.
- In addition to monitoring the primary dose in MUs, the dose monitoring system also monitors other operating parameters such as the beam energy, flatness and symmetry. Measurement of all these additional parameters requires that the ionization chamber electrodes of the primary and secondary chambers be divided into several sectors, with the

resulting signals used in automatic feedback circuits to steer the electron beam through the accelerating waveguide, beam transport system and on to the target or scattering foil, thereby ensuring beam flatness and symmetry. The particular design of the ionization chamber electrodes and sectors varies from one manufacturer to another.

● Linacs must be equipped with a monitoring system that continuously displays the machine isocentre dose rate and terminates the beam when the measured dose rate exceeds twice the maximum specified by the technical machine description.

● When the linac is capable of producing more than one beam energy or more than one beam mode (X rays or electrons), after termination of irradiation further irradiation is prevented until the selection of energy and beam mode has been made afresh and entered into the control console.

● Similarly, for linacs capable of stationary as well as moving beam radio-therapy, after termination of irradiation further irradiation is prevented until stationary radiotherapy or moving beam radiotherapy has been selected afresh and entered into the control console.

5.6. RADIOTHERAPY WITH PROTONS, NEUTRONS AND HEAVY IONS

External beam radiotherapy is carried out mainly with machines that produce either X rays or electrons. In a few specialized centres around the world, external beam radiotherapy is also carried out with heavier particles, such as:

● Neutrons produced by neutron generators and cyclotrons;
● Protons produced by cyclotrons and synchrotrons;
● Heavy ions (helium, carbon, nitrogen, argon, neon) produced by synchro-cyclotrons and synchrotrons.

These particles offer some distinct advantages over the standard X ray and electron modalities, such as:

— Considerably lower oxygen enhancement ratio (OER) for neutrons (see Section 14.10);
— Improved dose–volume histograms (DVHs) for protons and heavy ions (see Section 7.6).

However, equipment for production of protons, neutrons and heavy ions is considerably more expensive than standard radiotherapy equipment, both in capital costs and in maintenance and servicing costs, thus precluding a widespread use in standard radiotherapy departments. The decreasing costs of proton cyclotrons are likely to result in a wider use of proton beam therapy in the future.

5.7. SHIELDING CONSIDERATIONS

External beam radiotherapy is carried out mainly with three types of equipment that produces either X rays or electrons:

- X ray machines (superficial and orthovoltage);
- Teletherapy (^{60}Co) machines;
- Linacs.

All radiotherapy equipment must be housed in specially shielded treatment rooms in order to protect personnel and the general public in areas adjacent to the treatment rooms. The treatment rooms must comply not only with structural building codes but also with national and international regulations that deal with shielding requirements to render an installation safe from the radiation protection point of view. During the planning stage for a radiotherapy machine installation, a qualified medical physicist determines the required thickness of primary and secondary barriers and provides the information to the architect and structural engineer for incorporation into the architectural drawing for the treatment room.

Superficial and orthovoltage X ray therapy rooms are shielded either with ordinary concrete (2.35 g/cm^3) or lead. In this energy range the photoelectric effect is the predominant mode of photon interaction with matter, making the use of lead very efficient for shielding purposes.

Megavoltage treatment rooms (often referred to as bunkers or vaults because of the large barrier thickness required for shielding) are most commonly shielded with ordinary concrete so as to minimize construction costs. The Compton effect is the predominant mode of photon interaction with shielding material in this energy range. To conserve space, other higher density materials may be used, with the required wall thickness inversely proportional to the density of the shielding material. Thus the use of high density concrete (5 g/cm^3) will cut the required thickness of an ordinary concrete barrier by approximately one half; however, it will also increase the construction material cost by a factor of 30.

Shielding issues related to linac bunkers are discussed in more detail in Section 16.17.

5.8. COBALT-60 TELETHERAPY UNITS VERSUS LINACS

After the inception of radiotherapy soon after the discovery of X rays by Roentgen in 1895, the technology of radiation production was first aimed towards ever higher photon energies and intensities and more recently towards computerization and intensity modulated beam delivery. During the first 50 years of radiotherapy, technological progress was relatively slow and mainly based on X ray tubes, van de Graaff generators and betatrons.

The first truly practical megavoltage therapy machine was the ^{60}Co teletherapy machine developed in Canada in the 1950s. The invention of ^{60}Co teletherapy provided a tremendous boost in the quest for higher photon energies and placed the ^{60}Co unit in the forefront of radiotherapy for a number of years, mainly because it incorporated a radioactive source that is characterized by features extremely useful for radiotherapy.

The important features of ^{60}Co teletherapy machines can be summarized as follows:

- Relatively high energy γ ray emission;
- Relatively long half-life;
- Relatively high specific activity;
- Relatively simple means of production.

Figure 5.8(a) shows a ^{60}Co teletherapy machine; Fig. 5.8(b) shows a stamp issued by Canada Post commemorating Canada's role in the development of the ^{60}Co machine.

Linacs were developed concurrently by two groups: W.W. Hansen's group at Stanford University in the USA and D.D. Fry's group at the Telecommunications Research Establishment in the UK. Both groups were interested in linacs for research purposes and profited heavily from the microwave radar technology developed during World War II, using 3000 MHz as the design frequency.

The potential for the use of linacs in radiotherapy became apparent in the 1950s, and the first clinical linac was installed in the 1950s at the Hammersmith Hospital in London. During subsequent years, the linac eclipsed the cobalt unit and became the most widely used radiation source in modern radiotherapy, with several thousand units in clinical practice around the world today. In

(a)

(b)

FIG. 5.8. Cobalt-60 teletherapy machine. (a) Theratron Equinox, a megavoltage external beam therapy system using cobalt technology, manufactured by MDS Nordion, Ottawa, Canada (published with permission from MDS Nordion). (b) Schematic diagram of a cobalt unit depicted on a postage stamp issued by Canada Post in 1988 in honour of H.E. Johns, who invented the ^{60}Co unit in the 1950s (© Canada Post Corporation, 1988; reproduced with permission).

contrast to a ^{60}Co unit, which provides essentially only one γ energy of 1.25 MeV, a linac can provide either megavoltage electron or X ray therapy with a wide range of energies. Figure 5.9 shows a modern dual energy linac.

In comparison with ^{60}Co machines, linacs have become very complex in design:

(a)

(b)

FIG. 5.9. Modern dual photon energy linac manufactured by Varian; the gantry and the patient support assembly are clearly shown. (a) The portal imager is retracted; (b) the portal imager is activated. (Photographs courtesy of Varian Oncology Systems.)

— In part because of the multimodality capabilities that have evolved and are available on most modern machines;
— In part because of an increased use of computer logic and microprocessors in the control systems of these machines;
— In part because of added features, such as high dose rate modes, multileaf collimation, electron arc therapy and the dynamic treatment option, which is characterized by a controlled motion on the collimators (dynamic wedge), MLC leaves (IMRT), gantry or table while the beam is turned on.

Despite the clear technological and practical advantages of linacs over ^{60}Co machines, the latter still occupy an important place in the radiotherapy armamentarium, mainly because of the considerably lower capital, installation and maintenance costs of ^{60}Co machines compared with linacs. In the developing world, ^{60}Co machines, because of their relatively lower costs, simplicity of design and ease of operation, are likely to play an important role in cancer therapy for the foreseeable future.

Many modern features of linacs, such as MLCs, dynamic wedges and dynamic operation, could be installed on modern ^{60}Co machines to allow, at a lower cost, a similar sophistication in treatment as linacs. It is unfortunate that manufacturers of ^{60}Co units are very slow in reacting to new technological developments in radiotherapy, conceding pre-eminence to linac manufacturers even in areas where it would be much easier and more practical to run ^{60}Co machines than linacs.

5.9. SIMULATORS AND COMPUTED TOMOGRAPHY SIMULATORS

Simulators and CT simulators are important components of equipment used in radiotherapy. They cover several crucial steps in the radiotherapeutic process that are not related to the actual dose delivery but are nonetheless very important, as they deal with the determination of target location, treatment planning and spatial accuracy in dose delivery. The determination of the target volume that is related to the extent of the disease (see Section 7.2) and its position relative to adjacent critical normal tissues can be achieved with various methods. These range from a simple clinical examination through planar X ray imaging to the use of complex modern imaging equipment such as CT scanners in conjunction with magnetic resonance (MR) and PET scanners. Both simulators and CT simulators incorporate three major systems: the mechanical, X ray tube and imaging equipment.

The major steps in the target localization and field design are:

● Acquisition of the patient data set;
● Localization of target and adjacent structures;
● Definition and marking of the patient coordinate system;
● Design of treatment fields;
● Transfer of data to the treatment planning system (TPS);
● Production of an image for treatment verification.

The six steps above can be achieved either with a conventional simulator or with a CT simulator; however, the CT simulator provides for the more elegant, reliable and practical means to achieve the six steps, in addition to providing reliable external and internal contours and electron density information.

5.9.1. Radiotherapy simulator

A radiotherapy simulator consists of a diagnostic X ray tube mounted on a rotating gantry, simulating geometries identical to those found on megavoltage therapy machines that are either isocentric teletherapy ^{60}Co units or isocentric linacs. Thus the simulator enjoys the same degrees of freedom as a megavoltage machine, but rather than providing a megavoltage beam for treatment it provides a diagnostic quality X ray beam suitable for imaging, either in the radiographic mode (image recorded on radiographic film) or in the fluoroscopic mode (image recorded on a TV monitor using an image intensifier).

A modern simulator should mimic all the mechanical features and geometric field arrangements of various megavoltage machines, ranging from ^{60}Co machines with an SAD of 80 cm to high energy linacs with an SAD of 100 cm.

In megavoltage machines, radiation fields are defined with collimators (upper and lower jaws), while in simulators the rectangular and square fields are defined with delineator wires to enable visualization of the target as well as of healthy tissues adjacent to the target.

A modern simulator covers the following processes:

● Tumour and adjacent normal tissue localization;
● Treatment simulation;
● Treatment plan verification;
● Monitoring of treatment.

5.9.2. Computed tomography simulator

CT simulators are CT scanners equipped with special features that make them useful for certain stages in the radiotherapeutic process. The special features typically are:

- A flat table top surface to provide a patient position during simulation that will be identical to the position during treatment on a megavoltage machine.
- A laser marking system to transfer the coordinates of the tumour isocentre, derived from the contouring of the CT data set, to the surface of the patient. Two types of laser marking systems are used: a gantry mounted laser and a system consisting of a wall mounted moveable sagittal laser and two stationary lateral lasers.
- A virtual simulator consisting of software packages that allow the user to define and calculate a treatment isocentre and then simulate a treatment using digitally reconstructed radiographs (DRRs).

A CT simulator essentially obviates the need for conventional simulation by carrying out two distinct functions:

— Physical simulation, which covers the first three of the six target localization steps listed above;
— Virtual simulation, which covers the last three of the six target localization steps listed above.

In CT simulation the patient data set is collected and target localization is carried out using CT images with fluoroscopy and radiography replaced by DRRs. A laser alignment system is used for marking and a virtual simulator software package is used for field design and production of verification images. Transfer of all necessary information to the TPS is achieved electronically.

The planar simulation X ray film provides a beam's eye view (BEV) of the treatment portal but does not provide 3-D information about anatomical structures. CT, on the other hand, provides anatomical information and target definition but does not allow a direct correlation with the treatment portals.

A DRR is the digital equivalent of a planar simulation X ray film (see also Section 7.4.8). It is reconstructed from a CT data set using virtual simulation software available on a CT simulator or a TPS and represents a computed radiograph of a virtual patient generated from a CT data set representing the actual patient. Just like a conventional radiograph, the DRR accounts for the divergence of the beam.

The basic approach to producing a DRR involves several steps: choice of virtual source position; definition of image plane; ray tracing from virtual source to image plane; determination of the CT value for each volume element traversed by the ray line to generate an effective transmission value at each pixel on the image plane; summation of CT values along the ray line (line integration); and grey scale mapping.

An extension of the DRR approach is the digitally composited radiograph (DCR), which provides an enhanced visualization of bony landmarks and soft tissue structures. This is achieved by differentially weighting ranges of CT numbers that correspond to different tissues to be enhanced or suppressed in the resulting DCR images.

5.10. TRAINING REQUIREMENTS

The increased complexity of radiotherapy equipment demands that equipment be used only by highly trained and competent staff, in order to minimize the potential for accidents. A recent report by the IAEA summarized the lessons learned from accidental exposures in radiotherapy, and a report by the American Association of Physicists in Medicine (AAPM) specifically addressed medical accelerator safety considerations.

Of vital importance in the purchase, installation and clinical operation of radiotherapy equipment are the following:

(a)   Preparation of an equipment specification document;
(b)   Design of the treatment room and radiation safety;
(c)   Acceptance testing of equipment;
(d)   Commissioning of equipment;
(e)   A quality assurance programme.

Items (a), (c) and (d) are addressed in detail in Chapter 10, item (e) is addressed in Chapter 12 and item (b) is addressed in Chapter 16.

BIBLIOGRAPHY

AMERICAN ASSOCIATION OF PHYSICISTS IN MEDICINE, Medical accelerator safety considerations: Report of AAPM Radiation Therapy Committee Task Group No. 35, Med. Phys. **20** (1993) 1261–1275.

COIA, L., SHULTHEISS, T.E., HANKS, G.E., A Practical Guide to CT Simulation, Advanced Medical Publishing, Madison, WI (1995).

GREENE, D., WILLIAMS, P.C., Linear Accelerators for Radiation Therapy, Institute of Physics Publishing, Bristol (1997).

INTERNATIONAL ATOMIC ENERGY AGENCY, Lessons Learned from Accidental Exposures in Radiotherapy, Safety Reports Series No. 17, IAEA, Vienna (2000).

INTERNATIONAL ELECTROTECHNICAL COMMISSION, Medical Electrical Equipment: Particular Requirements for the Safety of Electron Accelerators in the Range 1 MeV to 50 MeV, Rep. 60601-2-1, IEC, Geneva (1998).

JOHNS, H.E., CUNNINGHAM, J.R., The Physics of Radiology, Thomas, Springfield, IL (1984).

KARZMARK, C.J., NUNAN, C.S., TANABE, E., Medical Electron Accelerators, McGraw-Hill, New York (1993).

KHAN, F., The Physics of Radiation Therapy, Lippincott, Williams and Wilkins, Baltimore, MD (2003).

PODGORSAK, E.B., METCALFE, P., VAN DYK, J., "Medical accelerators", The Modern Technology in Radiation Oncology: A Compendium for Medical Physicists and Radiation Oncologists (VAN DYK, J., Ed.), Medical Physics Publishing, Madison, WI (1999) 349–435.

Chapter 6

EXTERNAL PHOTON BEAMS: PHYSICAL ASPECTS

E.B. PODGORSAK
Department of Medical Physics,
McGill University Health Centre,
Montreal, Quebec, Canada

6.1. INTRODUCTION

Radiotherapy procedures fall into two main categories: external beam radiotherapy and brachytherapy. In external beam radiotherapy the radiation source is at a certain distance from the patient and the target within the patient is irradiated with an external radiation beam. In brachytherapy (see Chapter 13) radiation sources are placed directly into the target volume (intracavitary or interstitial brachytherapy) or on to a target (surface mould or intraoperative radiotherapy). Most external beam radiotherapy is carried out with photon beams, some with electron beams and a very small fraction with more exotic particles such as protons, heavier ions or neutrons.

This chapter deals with external photon beam radiotherapy. Photon external beams are all characterized by the same physical parameters, but fall into various categories depending on their origin, means of production and energy. There are two origins of photon beams: γ rays, which originate from radioactive nuclei, and X rays, which originate in a target bombarded with energetic electrons. The X rays from a target consist of bremsstrahlung photons and characteristic photons. X rays are produced either in an X ray tube (superficial or orthovoltage X rays) or in a linac (megavoltage X rays).

6.2. QUANTITIES USED IN DESCRIBING A PHOTON BEAM

Radiation dosimetry deals with two distinctly different entities: one describes the photon radiation beam itself in terms of the number and energies of photons constituting the photon beam and the other describes the amount of energy the photon beam may deposit in a given medium such as air, water or biological material.

6.2.1. Photon fluence and photon fluence rate

The photon fluence ϕ is defined as the quotient dN by dA, where dN is the number of photons that enter an imaginary sphere of cross-sectional area dA:

$$\phi = \frac{dN}{dA} \tag{6.1}$$

The unit of photon fluence ϕ is cm^{-2}.
The photon fluence rate is defined as the photon fluence per unit time:

$$\varphi = \frac{d\phi}{dt} \tag{6.2}$$

The unit of photon fluence rate is cm$^{-2} \cdot$s^{-1}.

6.2.2. Energy fluence and energy fluence rate

The energy fluence Ψ describes the energy flow in a photon beam and is defined as the amount of energy dE crossing a unit area dA:

$$\Psi = \frac{dE}{dA} \tag{6.3}$$

The unit of energy fluence Ψ is MeV/cm^2.
For a monoenergetic beam, dE is the number of photons dN times their energy $h\nu$, and the energy fluence Ψ in terms of photon fluence ϕ is:

$$\Psi = \phi h\nu \tag{6.4}$$

The energy fluence rate Ψ is defined as the energy fluence per unit time:

$$\Psi = \frac{d\psi}{dt} \tag{6.5}$$

The unit of energy fluence rate is MeV$\cdot$cm$^{-2} \cdot$s^{-1}.

6.2.3. Air kerma in air

For a monoenergetic photon beam in air the air kerma in air $(K_{air})_{air}$ at a given point away from the source is proportional to the energy fluence Ψ or photon fluence ϕ as follows:

$$(K_{air})_{air} = \Psi \left(\frac{\mu_{tr}}{\rho} \right)_{air} = \phi h\nu \left(\frac{\mu_{tr}}{\rho} \right)_{air} \tag{6.6}$$

where $(\mu_{tr}/\rho)_{air}$ is the mass–energy transfer coefficient for air at photon energy $h\nu$.

Kerma K consists of two components: the collision kerma K^{col} and the radiative kerma K^{rad}:

$$K = K^{col} + K^{rad} \tag{6.7}$$

For monoenergetic photons in air the collision kerma K^{col} is proportional to Ψ and ϕ through the following relationship:

$$K^{col} = \Psi \left(\frac{\mu_{ab}}{\rho} \right)_{air} = h\nu\phi \left(\frac{\mu_{ab}}{\rho} \right)_{air} \tag{6.8}$$

where $(\mu_{ab}/\rho)_{air}$ is the mass–energy absorption coefficient for air at photon energy $h\nu$. Often in the literature the energy absorption coefficient μ_{ab} is denoted as μ_{en}.

The mass–energy transfer coefficient (μ_{tr}/ρ) and mass–energy absorption coefficient (μ_{ab}/ρ) are related through the following relationship:

$$\frac{\mu_{ab}}{\rho} = \frac{\mu_{tr}}{\rho}(1 - \bar{g}) \tag{6.9}$$

where $\bar{g}$ is the radiative fraction (i.e. the fraction of the energy of secondary charged particles (electrons) that is lost to bremsstrahlung rather than being deposited in the medium). For low atomic number Z materials and photon energies below 1 MeV, the radiative fraction $\bar{g} \approx 0$, $(\mu_{tr}/\rho) \approx (\mu_{ab}/\rho)$ and $K \approx K^{col}$.

6.2.4. Exposure in air

The collision air kerma in air $(K_{air}^{col})_{air}$ is related to exposure in air X through the following relationship:

$$(K_{air}^{col})_{air} = X(W_{air}/e) \tag{6.10}$$

where (W_{air}/e), as discussed in Section 9.1.3, is the average energy required to produce an ion pair in dry air (33.97 eV/ion pair).

The special unit of exposure is the roentgen (R), while the SI unit is 2.58×10^{-4} C/kg with 1 R = 2.58×10^{-4} C/kg. Thus:

$$(K_{air}^{col})_{air} = \left(2.58 \times 10^{-4} \frac{C}{kg_{air}R} \ 33.97 \frac{J}{C}\right)X = \left(0.876 \frac{cGy}{R}\right)X \tag{6.11}$$

with the exposure X given in roentgens.

6.2.5. Dose to small mass of medium in air

The concept 'dose to small mass of medium in air', also known as 'dose in free space', was introduced by Johns and Cunningham to characterize the output of a radiation unit and to gain a reference dose for dosimetric calculations involving tissue–air ratios (TARs) and peak scatter factors (PSFs). The 'dose to small mass of medium in air' is designated as D'_{med} and is based on a measurement of the air kerma in air. The concept has gained widespread use in orthovoltage and ^{60}Co therapy, but is of limited use in megavoltage linac beam therapy.

The steps involved in determining the 'dose to small mass of medium in air' D'_{med} at point P in a radiation beam from a signal M_P measured with an ionization chamber centred at point P in air are:

$$M_P \ \overset{(1)}{\to} \ X_P \ \overset{(2)}{\to} \ (K_{air})_{air} \ \overset{(3)}{\to} \ (K_{\Delta m})_{air} \ \overset{(4)}{\to} \ (K_{med})_{air} \ \overset{(5)}{\to} \ D'_{med} \tag{6.12}$$

where M_P is the signal measured with an ionization chamber at point P and corrected for influence quantities such as air temperature, air pressure and recombination loss (see Section 9.3). The ionization chamber should have an

appropriate buildup cap and an exposure calibration coefficient in air N_X or an air kerma in air calibration coefficient N_K.

● Step 1: Determine X_P, the exposure at point P, through:

$$X_P = M_P N_X \tag{6.13}$$

● Step 2: Determine $(K_{air})_{air}$, the air kerma in air at point P, through:

$$(K_{air})_{air} = 0.876 \frac{cGy}{R} X_P \tag{6.14}$$

Alternatively, $(K_{air})_{air}$ may be determined from M_P directly, if N_K for the chamber is known, as follows:

$$(K_{air})_{air} = M_P N_K \tag{6.15}$$

● Step 3: Determine collision kerma to Δm, an infinitesimal mass of any other material (e.g. water), in air from:

$$(K_{\Delta m})_{air} = (K_{air})_{air} \left(\frac{\bar{\mu}_{ab}}{\rho} \right)_{air}^{\Delta m} \tag{6.16}$$

where $(\bar{\mu}_{ab}/\rho)_{air}^{\Delta m}$ is the ratio of spectrum averaged mass–energy absorption coefficients for Δm and air.

● Step 4: Determine collision kerma to a spherical mass of medium centred around P and having a radius r_{med} just large enough to provide charged particle equilibrium (CPE) at point P:

$$(K_{med})_{air} = (K_{\Delta m})_{air}(r_{med}) \tag{6.17}$$

where $k(r_{med})$ is a correction factor accounting for the photon beam attenuation in the spherical mass of medium and approximated as:

$$k(r_{med}) \approx e^{-\left(\frac{\mu_{ab}}{\rho} \right)_{med} \rho r_{med}} \tag{6.18}$$

$(\mu_{ab}/\rho)_{med}$ in Eq. (6.18) is the mass–energy absorption coefficient and ρ is the density of the medium. For water, which is usually chosen as the

medium, $k(r_{med}) \approx 0.985$ for ^{60}Co photons and approximately 1 for lower photon energies.

● Step 5: 'Dose to small mass of medium in free space' D'_{med} is obtained from the following relationship:

$$D'_{med} = \beta(K_{med})_{air} = \beta 0.876 \ \frac{cGy}{R} \left(\frac{\mu_{ab}}{\rho} \right)_{air}^{med} X_P k(r_{med}) \qquad (6.19)$$

where β is a proportionality constant equal to 1.003, 1.001 and 1.0 for ^{60}Co, ^{137}Cs and X rays below 350 kVp, respectively. Often β is assumed equal to 1, even for ^{60}Co γ rays.

The product:

$$0.876 \ \frac{cGy}{R} \ \left(\frac{\mu_{ab}}{\rho} \right)_{air}^{med}$$

is usually referred to as the roentgen to cGy conversion factor $f_{med,}$ and the 'dose to small mass of medium in air', assuming that $\beta \approx 1$, can then be written as:

$$D'_{med} = f_{med} \, X k(r_{med}) \qquad (6.20)$$

6.3. PHOTON BEAM SOURCES

Photon sources are either isotropic or non-isotropic and they emit either monoenergetic or heterogeneous photon beams. The most common photon sources used in radiation oncology are X ray machines, teletherapy radio-isotope sources and linacs.

● An isotropic photon source produces the same photon fluence rate in all directions, while the photon fluence rate from a non-isotropic source depends on the direction of measurement.
● A plot of number of photons per energy interval versus photon energy is referred to as a photon spectrum. Photon spectra for a monoenergetic and a heterogeneous photon beam are shown in Figs 6.1(a) and (b), respectively. The area under the curve in Fig. 6.1(b) represents the total number of photons in the beam:

$$\phi = \int \frac{d\phi(h\nu)}{dh\nu}\, dh\nu \qquad\qquad (6.21)$$

- All photons in a monoenergetic photon beam have the same energy $h\nu$ (Fig. 6.1(a)). Photons in a heterogeneous X ray beam form a distinct spectrum, with photons present in all energy intervals from 0 to a maximum value $h\nu_{max}$, which is equal to the kinetic energy of electrons striking the target (Fig. 6.1(b)).
- In Fig. 6.1(b) the two spikes in the spectrum represent characteristic photons, while the continuous spectrum from 0 to $h\nu_{max}$ represents bremsstrahlung photons.
- γ ray sources are usually isotropic and produce monoenergetic photon beams, while X ray targets are non-isotropic sources producing heterogeneous photon spectra.
- Narrow monoenergetic photon beams will have identical first and second half-value layers (HVLs). In narrow heterogeneous photon beams, on the other hand, the second HVL will be either larger or smaller than the first HVL: larger in the superficial and orthovoltage range because of beam hardening effects and smaller in the high megavoltage range because of beam softening effects.

6.4. INVERSE SQUARE LAW

In external beam radiotherapy, photon sources are often assumed to be point sources and the beams they produce are divergent beams, as shown schematically in Fig. 6.2. Let us assume that we have a photon point source S and a square field with side a (area $A = a^2$) at a distance f_a from the source. At
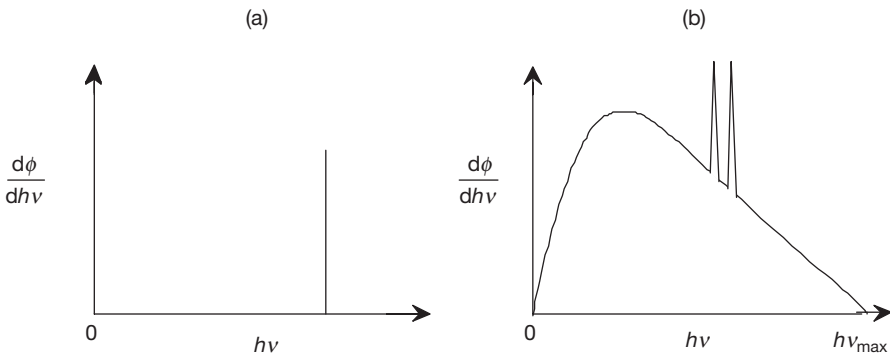
FIG. 6.1. Typical spectra for (a) monoenergetic and (b) heterogeneous photon beams.

a distance f_b we then have a square field with side b (area $B = b^2$), and the two fields are geometrically related as follows:

$$tg\beta = \frac{a/2}{f_a} = \frac{b/2}{f_b}$$

or

$$\frac{a}{b} = \frac{f_a}{f_b}$$

(6.22)

where β is the angle between the beam central axis and the geometric beam edge.

The photon source S emits photons and produces a photon fluence ϕ_A at distance f_a and a photon fluence ϕ_B at distance f_b. Since the total number of
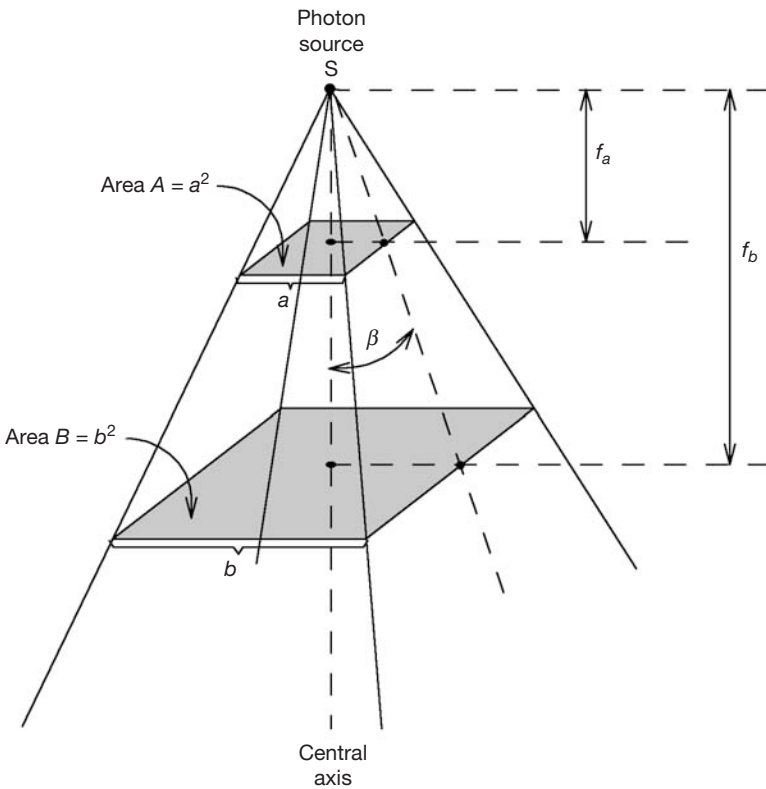
FIG. 6.2. Divergent photon beam originating in a photon point source. At distance f_a from the source S the field size is $A = a^2$, at distance f_b the field size is $B = b^2$.

168

photons N_{tot} crossing area A is equal to the total number of photons crossing area B (assuming no photon interactions take place in air between area A and area B), we can write:

$$N_{tot} = \phi_A A = \phi_B B$$

and

$$\frac{\phi_A}{\phi_B} = \frac{B}{A} = \frac{b^2}{a^2} = \frac{f_b^2}{f_a^2} \tag{6.23}$$

The photon fluence is thus inversely proportional to the square of the distance from the source. For example, if $f_b = 2f_a$ then the photon fluence at B will be exactly 1/4 of the photon fluence at A (i.e. $\phi_B = \phi_A/4$).

Since at a given point P in air the exposure in air X, air kerma in air $(K_{air})_{air}$ and 'dose to small mass of medium in air' D'_{med} are directly proportional to the photon fluence at point P, it is reasonable to conclude that the three quantities X, $(K_{air})_{air}$ and D'_{med} all follow this inverse square law behaviour:

$$\frac{X(f_a)}{X(f_b)} = \frac{(K_{air}(f_a))_{air}}{(K_{air}(f_b))_{air}} = \frac{D'_{med}(f_a)}{D'_{med}(f_b)} = \left(\frac{f_b}{f_a}\right)^2 \tag{6.24}$$

6.5. PENETRATION OF PHOTON BEAMS INTO A PHANTOM OR PATIENT

A photon beam propagating through air or a vacuum is governed by the inverse square law; a photon beam propagating through a phantom or patient, on the other hand, is affected not only by the inverse square law but also by the attenuation and scattering of the photon beam inside the phantom or patient. These three effects make the dose deposition in a phantom or patient a complicated process and its determination a complex task.

A direct measurement of the dose distribution inside the patient is essentially impossible, yet for a successful outcome of patient radiation treatment it is imperative that the dose distribution in the irradiated volume be known precisely and accurately. This is usually achieved through the use of several functions that link the dose at any arbitrary point inside the patient to the known dose at the beam calibration (or reference) point in a phantom.

The functions are usually measured with suitable radiation detectors in tissue equivalent phantoms, and the dose or dose rate at the reference point is determined for, or in, water phantoms for a specific set of reference conditions, such as depth, field size and source to surface distance (SSD), as discussed in detail in Section 9.1.

A typical dose distribution on the central axis of a megavoltage photon beam striking a patient is shown in Fig. 6.3. Several important points and regions may be identified. The beam enters the patient on the surface, where it delivers a certain surface dose D_s. Beneath the surface the dose first rises rapidly, reaches a maximum value at depth z_{max} and then decreases almost exponentially until it reaches a value D_{ex} at the patient's exit point. The techniques for relative dose measurements are discussed in detail in Section 6.13.
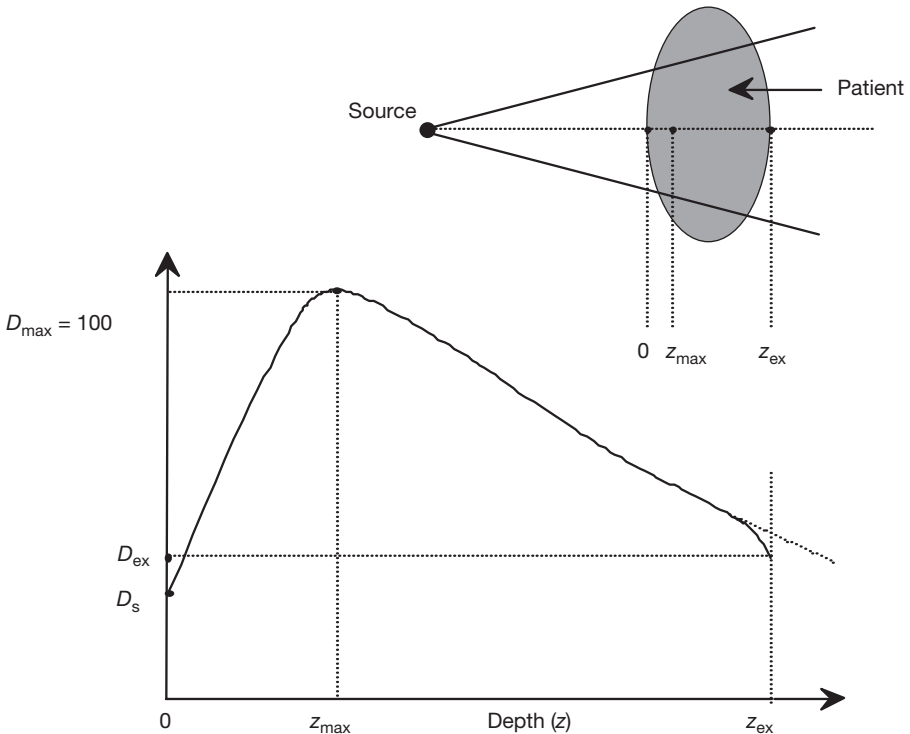
FIG. 6.3. Dose deposition from a megavoltage photon beam in a patient. D_s is the surface dose at the beam entrance side, D_{ex} is the surface dose at the beam exit side. D_{max} is the dose maximum often normalized to 100, resulting in a depth dose curve referred to as the percentage depth dose (PDD) distribution. The region between $z = 0$ and $z = z_{max}$ is referred to as the dose buildup region.

6.5.1. Surface dose

For megavoltage photon beams the surface dose is generally much lower than the maximum dose, which occurs at a depth z_{max} beneath the patient's surface. In megavoltage photon beams the surface dose depends on the beam energy and field size.

The larger the photon beam energy, the lower the surface dose, which for a 10×10 cm^2 field typically amounts to some 30% of the maximum dose for a cobalt beam, 15% for a 6 MV X ray beam and 10% for an 18 MV X ray beam. For a given beam energy the surface dose increases with the field size.

The low surface dose compared with the maximum dose is referred to as the skin sparing effect and represents an important advantage of megavoltage beams over orthovoltage and superficial beams in the treatment of deep seated tumours.

Orthovoltage and superficial beams do not exhibit the skin sparing effect, since their dose maximum occurs on the skin surface (i.e. the surface dose is equal to the maximum dose).

The surface dose is measured with thin window parallel-plate ionization chambers for both chamber polarities, with the average reading between the positive and negative polarities taken as the surface dose value (see Section 6.13).

The surface dose represents contributions to the dose from:

- Photons scattered from the collimators, flattening filter and air;
- Photons backscattered from the patient;
- High energy electrons produced by photon interactions in air and any shielding structures in the vicinity of the patient.

6.5.2. Buildup region

The dose region between the surface (depth $z = 0$) and depth $z = z_{max}$ in megavoltage photon beams is referred to as the dose buildup region and results from the relatively long range of energetic secondary charged particles (electrons and positrons) that first are released in the patient by photon interactions (photoelectric effect, Compton effect, pair production) and then deposit their kinetic energy in the patient (see Section 2.7.3).

- In the region immediately beneath the patient's surface, the condition of CPE does not exist and the absorbed dose is much smaller than the collision kerma. However, as the depth z increases, CPE is eventually reached at $z = z_{max}$, where z is approximately equal to the range of

secondary charged particles and the dose becomes comparable with the collision kerma.

● Beyond z_{max} both the dose and collision kerma decrease because of the photon attenuation in the patient, resulting in a transient rather than true CPE.

6.5.3.   Depth of dose maximum z_{max}

The depth of dose maximum z_{max} beneath the patient's surface depends on the beam energy and beam field size. The beam energy dependence is the main effect; the field size dependence is often ignored because it represents only a minor effect.

Nominal values for z_{max} range from zero for superficial and orthovoltage X ray beams, through 0.5 cm for ^{60}Co beams, to 5 cm for 25 MV beams, as shown in Table 6.1.

For a given beam energy, the largest z_{max} occurs for fields of ~5 × 5 cm^2. For fields larger than 5 × 5 cm^2, z_{max} decreases because of collimator scatter effects (for cobalt units) and collimator and flattening filter scatter effects (for linacs). For fields smaller than 5 × 5 cm^2, z_{max} decreases because of phantom scatter effects.

6.5.4.   Exit dose

The dose delivered to the patient at the beam exit point is referred to as the exit dose. As shown schematically in Fig. 6.3, close to the beam exit point the dose distribution curves slightly downwards from the extrapolated dose distribution curve. This relatively small effect is attributed to the missing scatter contribution at the exit point from points beyond the exit dose point. Similarly to the surface dose, the exit dose may be measured with a parallel-plate chamber, in this case with the chamber body orientated towards the source.

6.6.   RADIATION TREATMENT PARAMETERS

External beam radiotherapy with photon beams is carried out with three types of treatment machine: X ray units, isotope teletherapy units (mainly ^{60}Co units) and linacs. The main parameters in external beam dose delivery with photon beams are the: (a) depth of treatment; (b) field size; (c) SSD in SSD set-ups or source to axis distance (SAD) in SAD (isocentric) set-ups; and (d) photon beam energy.

TABLE 6.1.   TYPICAL DEPTHS OF DOSE MAXIMUM z_{max} FOR VARIOUS PHOTON BEAM ENERGIES AND A FIELD SIZE OF 5×5 cm^2

	Superficial	Orthovoltage	Co-60	4 MV	6 MV	10 MV	18 MV	25 MV
z_{max} (cm)	0	0	0.5	1	1.5	2.5	3.5	5

6.6.1.   Radiation beam field size

Beams used for radiotherapy have various shapes that usually represent a compromise between the actual target shape and the need for simplicity and efficiency in beam shaping. Four general groups of field shape are used in radiotherapy: square, rectangular, circular and irregular.

Square and rectangular fields are usually produced with collimators installed in radiotherapy machines, circular fields with special collimators attached to the treatment machine and irregular fields with custom made shielding blocks or with multileaf collimators (MLCs) attached to the treatment machine.

For any arbitrary radiation field an equivalent square or circular field may be found, meaning that the arbitrary field and the equivalent square or circular field will be characterized with similar beam parameters and functions that are of importance in radiation dosimetry.

An arbitrary rectangular field with sides a and b will be approximately equivalent to a square radiation field with sides a_{eq} when both fields have the same area/perimeter ratio (Day's rule):

$$\frac{ab}{2(a+b)} = \frac{a_{eq}^2}{4a_{eq}}$$

or

$$a_{eq} = \frac{2ab}{a+b} \tag{6.25}$$

An arbitrary square field with sides a_{eq} will be equivalent to a circular field with radius r_{eq} when both fields have the same area:

$$a_{eq}^2 = \pi r_{eq}^2$$

or

$$r_{eq} = \frac{a_{eq}}{\sqrt{\pi}} \tag{6.26}$$

6.6.2. Collimator factor

Exposure in air, air kerma in air and 'dose to small mass of medium in air' at a given point P in air contain contributions from two components: primary and scatter.

- The primary component is the major component; it comes directly from the source and does not depend on the field size.
- Scatter represents a minor yet non-negligible component; it consists of photons scattered into point P mainly from the collimator but also possibly from the air and the flattening filter of a linac. The scatter component depends on field size A (collimator setting): the larger the field size, the larger the collimator surface available for scattering and consequently the larger the scatter component.

Exposure in air X, air kerma in air $(K_{air})_{air}$ and 'dose to small mass of medium in air' D'_{med} depend on field size A and a parameter referred to as the collimator factor (CF) (or collimator scatter factor S_c in Khan's notation, or relative exposure factor (REF) in 1970s notation). The CF is defined as:

$$CF(A, hv) = S_c(A, hv) = REF(A, hv)$$

$$= \frac{X(A, hv)}{X(10, hv)} = \frac{(K_{air}(A, hv))_{air}}{(K_{air}(10, hv))_{air}} = \frac{D'(A, hv)}{D'(10, hv)} \qquad (6.27)$$

The geometry for the measurement of the CF is shown in Fig. 6.4; Fig. 6.4(a) shows the measurement of $D'(A, hv)$, while Fig. 6.4(b) shows the measurement of $D'(10, hv)$.

The CF is usually measured with an ionization chamber with a buildup cap of a size large enough to provide maximum dose buildup for the given energy beam. For small fields one may carry out the measurements at large distances from the source so that the buildup cap is fully covered; however, the data are usually corrected back to the nominal SSD of the machine by using the inverse square law.

The CF is normalized to 1 for the nominal field of 10×10 cm^2 at the nominal SSD for the treatment machine. It is larger than 1 for fields A exceeding 10×10 cm^2 and smaller than 1 for fields A smaller than 10×10 cm^2. It is usually measured at point P in air with a cylindrical ionization chamber equipped with an appropriate buildup cap and the chamber centre placed at (nominal SSD + z_{max}) from the source. SSD here stands for the nominal SSD

(typically 80 or 100 cm for cobalt units and 100 cm for linacs) and z_{max} for the depth of dose maximum in a phantom for the specific photon beam.

In some centres the CF is measured at the machine isocentre. The results are essentially identical to those obtained with measurements carried out at point P in air.

6.6.3. Peak scatter factor

The 'dose to small mass of medium' D'_P is measured with just enough material around the point of interest P to provide electronic equilibrium (ionization chamber with appropriate buildup cap). D'_P is related to D_P, the dose at z_{max} in a phantom at point P, through the PSF as follows:

$$\text{PSF}(A, h\nu) = \frac{D_P(z_{max}, A, f, h\nu)}{D'_P(A, h\nu)} \tag{6.28}$$

with the geometry shown in Fig. 6.5. Figure 6.5(a) shows measurement of D'_P and Fig. 6.5(b) shows measurement of D_P. The chamber in part (a) is placed at a distance of $f + z_{max}$ from the source.

At low photon energies $z_{max} = 0$, point P is on the surface, and the PSF is referred to as the backscatter factor. The PSF depends on field size A as well as on photon beam energy $h\nu$ and gives the factor by which the radiation dose at
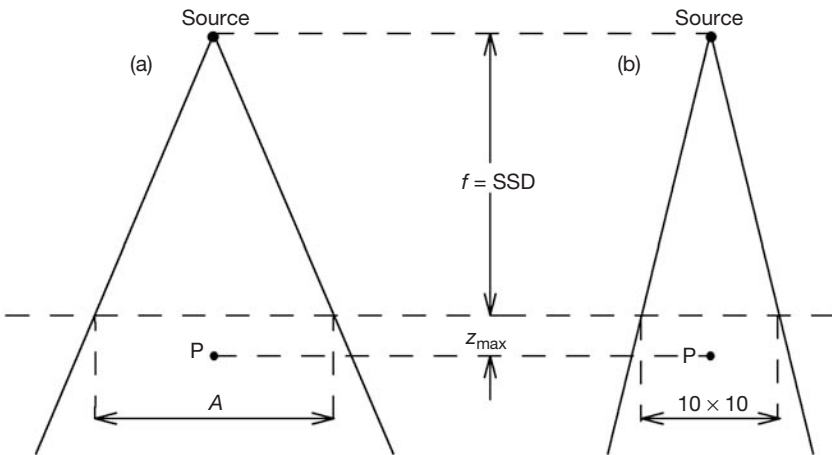
FIG. 6.4. Geometry for measurement of CF(A, hν). The 'dose to small mass of water' is measured at point P in air: in part (a) with field size A, in part (b) with field size 10 × 10 cm². Parameter f stands for the SSD.

point P in air is increased by radiation scattered to point P from the phantom or patient.

Typical values for the PSF range from ~1 for small fields of megavoltage beams, through 1.054 for a 10 × 10 cm² field in a cobalt beam to 1.10 for a 50 × 100 cm² field in a cobalt beam (used for total body irradiation (TBI)), to 1.50 for a 20 × 20 cm² field of orthovoltage X rays (HVL = 1 mm of Cu).

While backscattering is largest at very low photon energies (classical scattering), the energy of backscattered photons is small at low photon energies, causing a rapid absorption of the scattered photons in the medium. At intermediate and high photon energies the backscattering and side scattering decreases with energy; however, the scattered photons have a higher energy and larger penetrating power.

The interrelationship between the amount of backscattering and scattered photon penetration causes the PSF first to increase with beam energy, reaching a peak around HVL ~ 1 mm of Cu, and then to decrease with a further increase in beam energy. The beam quality at which maximum backscatter occurs depends on field size, shifting slightly towards harder radiation with an increase in field size.

For a given beam energy hv, the PSF increases with field size, as shown in Fig. 6.6 for a ^{60}Co beam.

The scatter factor (SF) (sometimes referred to as relative PSF) for field A is defined as the ratio:

$$SF(A, hv) = \frac{PSF(A, hv)}{PSF(10, hv)} \tag{6.29}$$
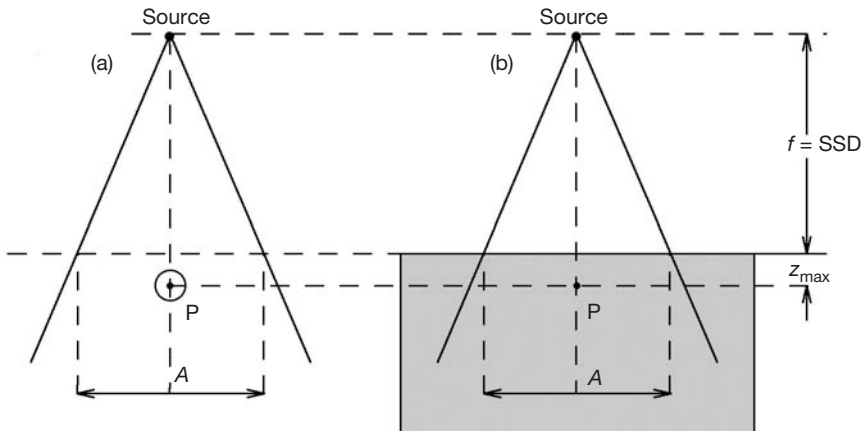
FIG. 6.5. *Geometry for measurement of the PSF at point P. (a) The measurement of D'_P; (b) the measurement of D_P. The field size A is the same in (a) and (b).*

and thus represents the PSF normalized to 1 for a 10×10 cm^2 field. In Khan's notation the scatter factor is referred to as the phantom scatter factor and is denoted as $S_p(A)$.

6.6.4. Relative dose factor

For a given photon beam at a given SSD, the dose rate at point P (at depth z_{max} in a phantom) depends on the field size A; the larger the field size, the larger the dose. The relative dose factor (RDF) (referred to as the total scatter factor ($S_{c,p}$) in Khan's notation, or sometimes the machine output factor) is defined as the ratio of $D_P(z_{max}, A, f, hv)$, the dose at P in a phantom for field A, to $D_P(z_{max}, 10, f, hv)$, the dose at P in a phantom for a 10×10 cm^2 field:

$$\mathrm{RDF}(A, hv) = S_{c,p}(A, hv) = \frac{D_P(z_{max}, A, f, hv)}{D_P(z_{max}, 10, f, hv)} \tag{6.30}$$

The geometry for measurement of the RDF(A, hv) is shown in Fig. 6.7(a) for the measurement of $D_P(z_{max}, A, f, hv)$ and in Fig. 6.7(b) for the measurement of $D_P(z_{max}, 10, f, hv)$.
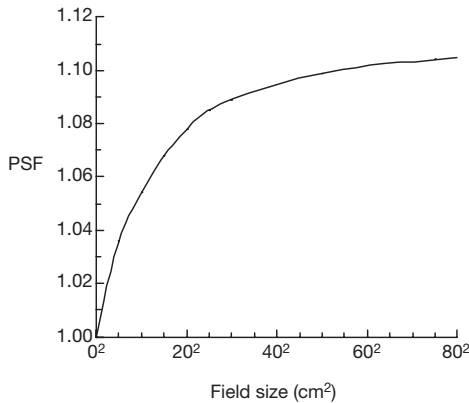
FIG. 6.6. PSF as a function of field size for a ^{60}Co γ ray beam.

From the basic definitions of the CF and the SF we can write RDF as the following product:

$$\mathrm{RDF}(10, hv) = \frac{D_{\mathrm{P}}(z_{\max}, A, f, hv)}{D_{\mathrm{P}}(z_{\max}, 10, f, hv)}$$

$$= \frac{D'_{\mathrm{P}}(A, hv)\mathrm{PSF}(A, hv)}{D'_{\mathrm{P}}(10, hv)\mathrm{PSF}(10, hv)} = \mathrm{CF}(A, hv)\,\mathrm{SF}(A, hv) \qquad (6.31)$$

or in Khan's notation:

$$S_{c,p}(A, hv) = S_c(A, hv)S_p(A, hv) \qquad (6.32)$$

indicating that the RDF(A) contains two components: scatter from the collimator and scatter from the phantom.

Figure 6.8 shows typical values for the RDF(A, hv), CF(A, hv) and SF(A, hv) against field size A for a ^{60}Co beam. All three functions are normalized to 1 for $A = 10 \times 10$ cm^2; they are larger than 1 for $A > 10 \times 10$ cm^2 and smaller than 1 for $A < 10 \times 10$ cm^2.

When extra shielding is used on an accessories tray or an MLC is used to shape the radiation field on a patient's surface into an irregular field B, then the
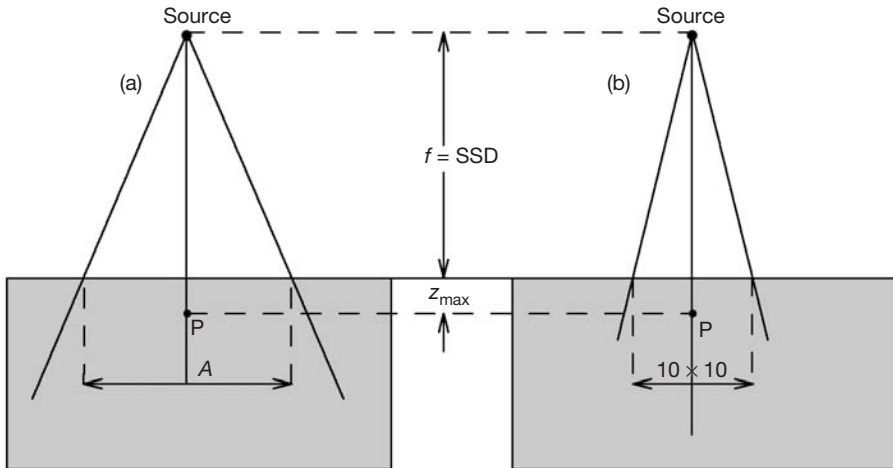
FIG. 6.7. Geometry for the measurement of the RDF(A). The dose at point P at z_{max} in a phantom is measured with field A in part (a) and with field 10×10 cm^2 in part (b).

RDF(B, hv) is in the first approximation given as:

$$\text{RDF}(B, hv) = \text{CF}(A, hv)\text{SF}(B, hv) \tag{6.33}$$

where field A represents the field set by the machine collimator and field B is the actual irregular field on the patient's surface.

We must note that the behaviour of an MLC as a block or a secondary collimator depends on the MLC design and on the manufacturer in the case of linacs, where the MLC replaces the upper or lower collimator jaws. In this case Eq. (6.33) must be used with caution and its validity should be verified before clinical use.

6.7. CENTRAL AXIS DEPTH DOSES IN WATER: SOURCE TO SURFACE DISTANCE SET-UP

6.7.1. Percentage depth dose

Central axis dose distributions inside the patient or phantom are usually normalized to $D_{max} = 100\%$ at the depth of dose maximum z_{max} and then
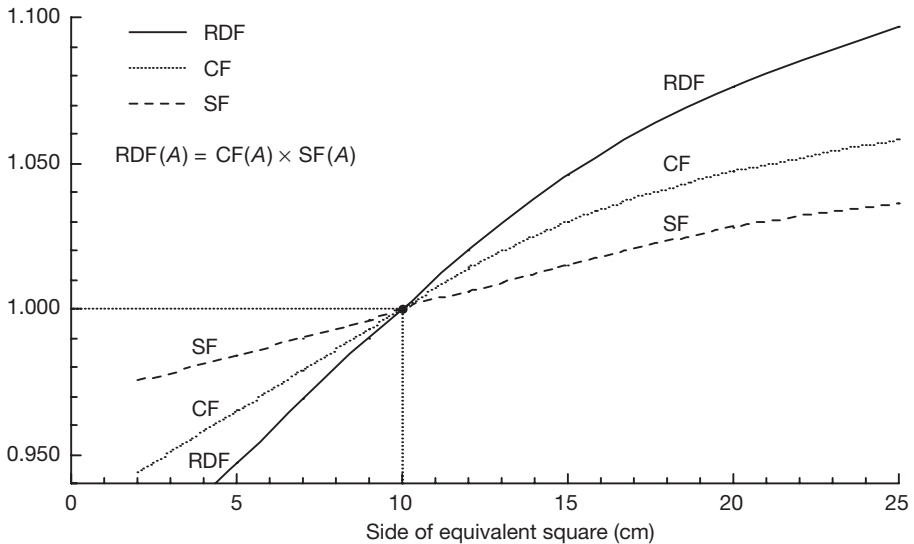
FIG. 6.8. Typical values for the RDF(A), CF(A) and SF(A) for a ^{60}Co γ ray beam as a function of square field size A. All three functions are normalized to 1 for a 10 × 10 cm^2 field.

referred to as the PDD distributions. The PDD is thus defined as follows:

$$PDD(z, A, f, h\nu) = 100 D_Q/D_P = 100 \dot{D}_Q/\dot{D}_P \tag{6.34}$$

where D_Q and $\dot{D}_Q$ are the dose and dose rate, respectively, at point Q at depth z on the central axis of the phantom and D_P and $\dot{D}_P$ are the dose and dose rate at point P at z_{max} on the central axis of the phantom.

The geometry for PDD definition is shown in Fig. 6.9. Point Q is an arbitrary point at depth z on the beam central axis; point P represents the specific dose reference point at $z = z_{max}$ on the beam central axis. The PDD depends on four parameters: depth in a phantom z, field size A, SSD (often designated with f) and photon beam energy $h\nu$. The PDD ranges in value from 0 at $z \to \infty$ to 100 at $z = z_{max}$.

The dose at point Q contains two components: primary and scatter.

● The primary component may be expressed as:

$$PDD^{pri} = 100 \; \frac{D_Q^{pri}}{D_P^{pri}} = 100 \left(\frac{f + z_{max}}{f + z} \right)^2 e^{-\mu_{eff}(z - z_{max})} \tag{6.35}$$
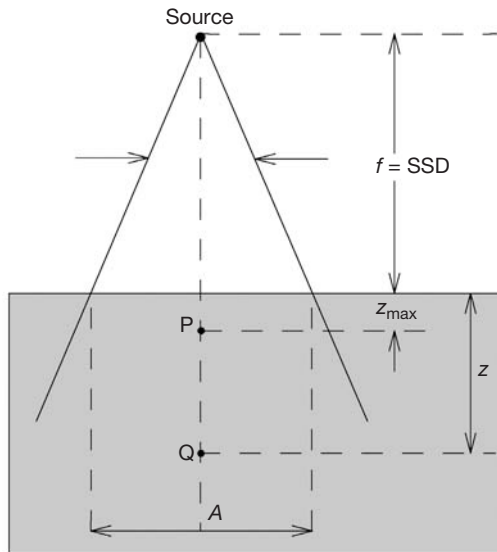
FIG. 6.9. Geometry for PDD measurement and definition. Point Q is an arbitrary point on the beam central axis at depth z, point P is the point at z_{max} on the beam central axis. The field size A is defined on the surface of the phantom.

where μ_{eff} is the effective linear attenuation coefficient for the primary beam in the phantom material (μ_{eff} for a ^{60}Co beam in water is 0.0657 cm^{-1}).

● The scatter component reflects the relative contribution of the scattered radiation to the dose at point Q.

As shown in Fig. 6.3, for constant A, f and $h\nu$ the PDD first increases from the surface to $z = z_{max}$ and then decreases with a further increase in z. The depth of dose maximum and the surface dose depend on the beam energy; the larger the beam energy, the larger the depth of dose maximum and the lower the surface dose.

— For constant z, f and $h\nu$ the PDD increases with increasing A because of increased scatter contribution to points on the central axis. An example for a ^{60}Co beam is given in Table 6.2.

— For constant z, A and $h\nu$ the PDD increases with increasing f because of a decreasing effect of z on the inverse square factor, which governs the primary component of the photon beam. An example for a ^{60}Co beam is given in Table 6.3.

— For constant z, A and f the PDD beyond z_{max} increases with beam energy because of a decrease in beam attenuation (i.e. because of an increase in beam penetrating power).

An example of PDD distributions for 10×10 cm^2 fields and various megavoltage photon beams is given in Fig. 6.10 and Table 6.4. The size of the buildup region increases with beam energy and the surface dose decreases with beam energy.

PDDs for radiotherapy beams are usually tabulated for square fields; however, the majority of fields used in radiotherapy are rectangular or irregularly shaped. The concept of equivalent squares is used to determine the square field that will be equivalent to the given rectangular or irregular field.

6.7.2. Scatter function

In radiation dose calculations it is often desirable to separate the scatter component from the total dose at Q:

Scatter component at Q = total dose at Q – primary dose at Q

$$= D'_P PSF(A, h\nu) PDD(z, A, f, h\nu)/100 - D'_P PSF(0, h\nu) PDD(z, 0, f, h\nu)/100$$

(6.36)

TABLE 6.2. PERCENTAGE DEPTH DOSES FOR A COBALT-60 BEAM IN WATER FOR VARIOUS FIELD SIZES AND AN SSD OF 100 cm

	A (cm^2)						
	0×0	5×5	10×10	15×15	20×20	25×25	50×50
PDD(5, A, 100, Co)	68.2[a]	76.7	80.4	82.0	83.0	83.4	85.2
PDD(10, A, 100, Co)	44.7[a]	53.3	58.7	61.6	63.3	64.4	67.3
PDD(15, A, 100, Co)	29.5[a]	36.5	41.6	44.9	47.1	48.6	49.7

[a]   Calculated using Eq. (6.35) with $\mu_{eff} = 0.0657$ cm^{-1}.

TABLE 6.3. PERCENTAGE DEPTH DOSES FOR A COBALT-60 BEAM IN WATER FOR VARIOUS SOURCE TO SURFACE DISTANCES, DEPTH z OF 5 cm IN A PHANTOM AND A FIELD OF $A = 10 \times 10$ cm^2

f = SSD (cm)	60	80	100	120	140
PDD(5, 10, f, Co)	76.2	78.8	80.0	81.3	82.3
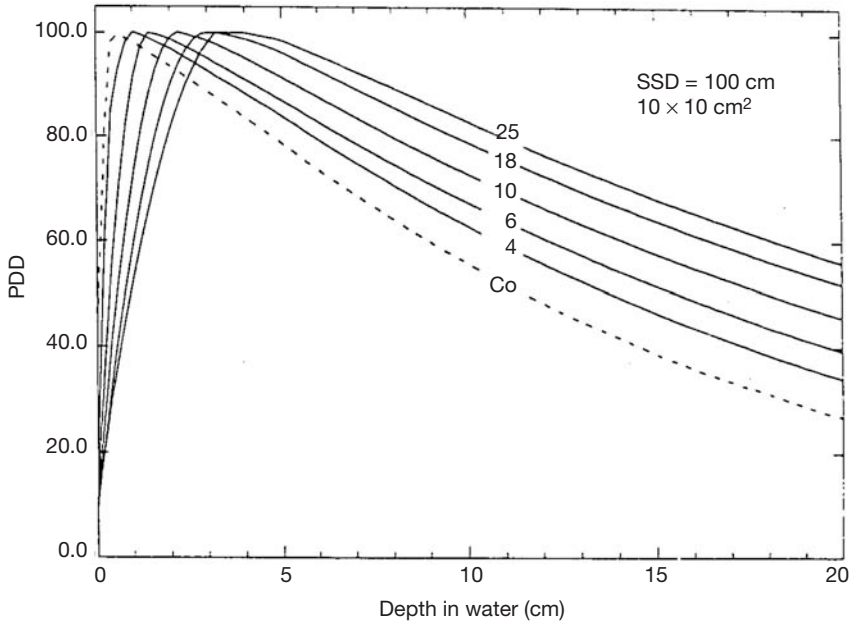
FIG. 6.10. PDD curves in water for a 10 × 10 cm^2 field at an SSD of 100 cm for various megavoltage photon beams ranging from ^{60}Co γ rays to 25 MV X rays.

TABLE 6.4. PERCENTAGE DEPTH DOSES FOR VARIOUS PHOTON BEAMS IN A WATER PHANTOM WITH A FIELD SIZE A OF 10×10 cm^2, AN SSD OF 100 cm AND TWO DEPTHS: 5 cm AND 10 cm

	Photon beam $h\nu$					
	Co-60	4 MV	6 MV	10 MV	18 MV	25 MV
Nominal z_{max} (cm)	0.5	1.0	1.5	2.5	3.5	5.0
PDD(5, 10, 100, $h\nu$)	80	84	86	92	97	98
PDD(10, 10, 100, $h\nu$)	59	65	67	74	80	82

The scatter function $S(z, A, f, h\nu)$ is then defined as:

$$S(z, A, f, h\nu) = \text{PSF}(A, h\nu)\text{PDD}(z, A, f, h\nu)$$
$$- \text{PSF}(0, h\nu)\text{PDD}(z, 0, f, h\nu) \tag{6.37}$$

giving the scatter dose at point Q per 100 cGy of primary dose at point P. Note: PSF(0) = 1 and PDD(z, 0, f, $h\nu$) is the primary PDD calculated with Eq. (6.35).

Similarly to the PDD, the scatter function S also depends on four parameters: depth z, field size A, SSD f and beam energy $h\nu$.

- For constant A, f and $h\nu$ the scatter function S first increases with z, reaches a peak and then slowly decreases, with a further increase in z.
- For constant z, f and $h\nu$, S increases with field size A.
- At $z = z_{max}$ the scatter function S is given by:

$$S(z_{max}, A, f, h\nu) = 100[\text{PSF}(A, h\nu) - 1] \tag{6.38}$$

6.8. CENTRAL AXIS DEPTH DOSES IN WATER: SOURCE TO AXIS DISTANCE SET-UP

When multiple fields are used for the treatment of a particular tumour inside the patient, isocentric (SAD) set-ups are often used because they are more practical in comparison with constant SSD set-ups. Most megavoltage units are mounted isocentrically with an SAD of 80 cm, or more commonly 100 cm, to allow this treatment option. In contrast to SSD set-ups, which rely on PDD distributions, SAD set-ups rely on other functions, such as TARs and tissue–phantom ratios (TPRs), for dosimetric calculations.

6.8.1. Tissue–air ratio

The $\text{TAR}(z, A_Q, hv)$ was originally introduced by Johns to simplify dose calculations in rotational radiotherapy, but its use was subsequently expanded to isocentric irradiations with multiple stationary fields. In rotational radiotherapy the radiation source moves in a circle around the axis of rotation, which is usually inside the tumour. During the rotation around the patient the SSD varies with the patient contour; however, the SAD remains constant.

$\text{TAR}(z, A_Q, hv)$ is defined as the ratio of the dose D_Q or dose rate $\dot{D}_Q$ at point Q on the central axis in the patient or phantom to the dose D'_Q or dose rate $\dot{D}_Q$, the 'dose (rate) to small mass of water in air', at the same point Q on the beam central axis:

$$\text{TAR}(z, A_Q, hv) = \frac{D_Q}{D'_Q} = \frac{\dot{D}_Q}{\dot{D}'_Q} \tag{6.39}$$

The geometry for TAR measurement is shown in Fig. 6.11(a) for measurement of D_Q in a phantom and in Fig. 6.11(b) for measurement of D'_Q in air. The field size A_Q is defined at point Q, which is normally placed in the isocentre of the treatment machine.

In contrast to $\text{PDD}(z, A, f, hv)$, which depends on four parameters, $\text{TAR}(z, A_Q, hv)$ depends only on three: depth z, field size A_Q at depth z and
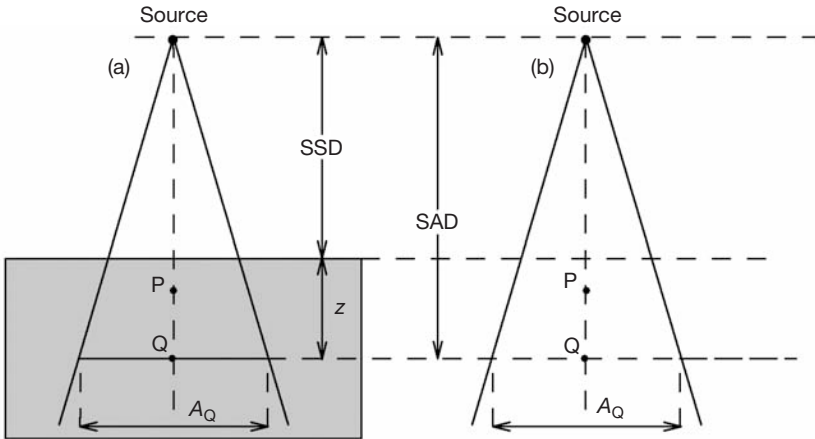
FIG. 6.11. Geometry for measurement and definition of TAR. (a) The dose is determined at point Q in a water phantom; (b) the 'dose to small mass of water' is determined at point Q. Point Q is at the machine isocentre at a distance SAD from the source. The beam field size A_Q is defined at depth z in the phantom.

beam energy $h\nu$; there is essentially no SSD or SAD dependence in the range of SSDs used clinically (50–150 cm). TARs for various ^{60}Co beams at depths of 5 and 10 cm in water are given in Table 6.5.

- For constant A_Q and $h\nu$, the TAR decreases with an increasing z beyond z_{max}.
- For constant z and $h\nu$, the TAR increases with increasing A_Q.
- For constant z and A_Q, the TAR increases with $h\nu$.
- For $z = z_{max}$, the TAR becomes identical to the PSF:

$$\text{TAR}(z = z_{max}, A_Q = A_P, h\nu) = \text{PSF}(A_P, \ h\nu) \tag{6.40}$$

- The zero area TAR (i.e. TAR$(z, 0, h\nu)$ may be calculated from

$$\text{TAR}(z, 0, h\nu) = e^{-\mu_{eff}(z - z_{max})} \tag{6.41}$$

where μ_{eff} is the effective attenuation coefficient for the photon beam $h\nu$. A 0×0 field is a hypothetical field in which the dose at depth in a phantom is entirely due to primary photons, since the volume that can scatter radiation is zero.

TARs are most reliably measured with ionization chambers; however, the measurements are much more cumbersome than those of PDDs. In the case of TARs the depth in water must be measured in such a way that the distance between the ionization chamber and the radiation source remains constant, which is difficult to achieve using automatic techniques. Moreover, the measurement of the 'dose to small mass of water' must be carried out with great care in order to ensure full buildup and readings free of radiation scattered into the chamber from the treatment room walls or floor.

Since the concept of 'dose to small mass of medium' is not recommended for use with megavoltage beams above ^{60}Co and 4 MV, the concept of TAR is not used in the dosimetry of medium and high energy photon beams. For these energies functions are used that are similar to the TAR but that do not suffer the limitations imposed on the measurement of the 'dose to small mass of medium'.

6.8.2. Relationship between TAR(d, A_Q, $h\nu$) and PDD(d, A, f, $h\nu$)

As shown in Fig. 6.12, a simple relationship may be derived between TAR(z, A_Q, $h\nu$) and the corresponding PDD(z, A, f, $h\nu$) from the basic

TABLE 6.5. TISSUE–AIR RATIOS FOR A COBALT-60 BEAM IN WATER FOR VARIOUS FIELD SIZES A_Q AND TWO DEPTHS IN A PHANTOM: 5 cm AND 10 cm

	A_Q (cm^2)					
	0×0	5×5	10×10	15×15	20×20	25×25
TAR(5, A_Q, Co)	0.744[a]	0.864	0.921	0.953	0.974	0.986
TAR(10, A_Q, Co)	0.536[a]	0.654	0.731	0.779	0.809	0.831
TAR(20, A_Q, Co)	0.278[a]	0.354	0.418	0.470	0.509	0.536

[a] Calculated using Eq. (6.41) with μ_{eff} = 0.0657 cm^{-1}.

definitions governing the two functions. The basic definitions for the two functions are:

$$\text{TAR}(z, A_Q, hv) = \frac{D_Q}{D'_Q} \tag{6.42}$$

$$\text{PDD}(z, A, f, hv) = 100 \frac{D_Q}{D_P} \tag{6.43}$$
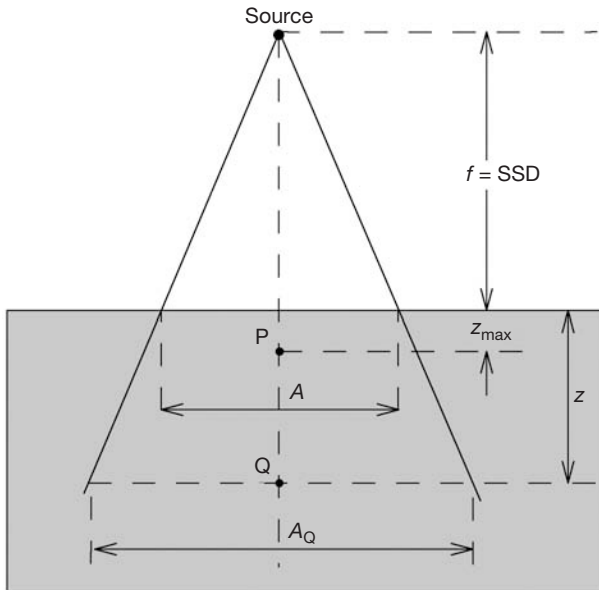
FIG. 6.12. *Geometry for the relationship between PDD(z, A, f, hv) and TAR(z, A_Q, hv).*

and solving Eqs (6.42) and (6.43) for D_Q we obtain:

$$D_Q = D_P \frac{\text{PDD}(z, A, f, hv)}{100} = D_Q' \text{TAR}(z, A_Q, hv) \tag{6.44}$$

D_P may now be written as:

$$D_P = D_P' \text{PSF}(A, hv) = D_Q' \left(\frac{f + z}{f + z_{\max}} \right)^2 \text{PSF}(A, hv) \tag{6.45}$$

and inserted into Eq. (6.44) to yield:

$$\begin{aligned} \text{TAR}(z, A_Q, hv) \\ = \text{PSF}(A, hv) \, \frac{\text{PDD}(z, A, f, hv)}{100} \left(\frac{f + z}{f + z_{\max}} \right)^2 \end{aligned} \tag{6.46}$$

For the special case of $z = z_{\max}$, where $\text{PDD}(z_{\max}, A, f, hv) = 100$, Eq. (6.46) shows that the $\text{PSF}(A, hv)$ is a special $\text{TAR}(z_{\max}, A, hv)$. The range of TARs is therefore from 0 at $z \to \infty$ to $\text{PSF}(A, hv)$ at $z = z_{\max}$.

Since the TAR does not depend on the SSD, a single TAR table for a given photon beam energy may be used to cover all possible SSDs used clinically.

Alternatively, PDDs for any arbitrary combination of z, A and $f = \text{SSD}$ may be calculated from a single TAR table.

Based on Eq. (6.46) we derive the following two relationships for PDDs at two different SSDs (f_1 and f_2).

● The first relationship assumes an identical field size A at the two SSDs, as shown in Fig. 6.13:

$$\frac{\text{PDD}(z, A, f_1, hv)}{\text{PDD}(z, A, f_2, hv)} = \left(\frac{\text{TAR}(z, A_{Q1}, hv)}{\text{TAR}(z, A_{Q2}, hv)} \right) \left(\frac{\dfrac{f_1 + z_{\max}}{f_1 + z}}{\dfrac{f_2 + z_{\max}}{f_2 + z}} \right)^2 \tag{6.47}$$

● The second relationship assumes the same field size A_Q at depth z at the two SSDs, as shown in Fig. 6.14:

$$\frac{\text{PDD}(z, A_1, f_1, h\nu)}{\text{PDD}(z, A_2, f_2, h\nu)} = \left(\frac{\text{PSF}(A_2, h\nu)}{\text{PSF}(A_1, h\nu)}\right) \left(\frac{\dfrac{f_1 + z_{\max}}{f_1 + z}}{\dfrac{f_2 + z_{\max}}{f_2 + z}}\right)^2 \qquad (6.48)$$

The relationships in Eqs (6.47) and (6.48) consist of two components each; the inverse square law correction component is the main component of the correction, and is referred to as the Mayneord factor. The second factor, represented by the ratio of TARs or PSFs, is often ignored, because its effect is much smaller than that produced by the Mayneord factor, and the Mayneord factor alone is used for correction of PDDs from one SSD to another.
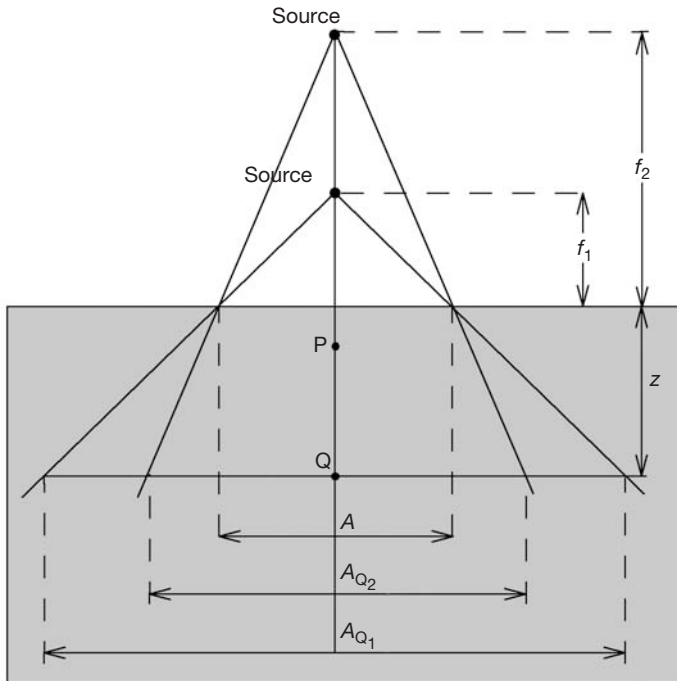
FIG. 6.13. Derivation of the PDD relationship for two SSDs, with field size A identical for both. Note that the field A on the phantom surface is the same for both SSDs; therefore the fields at depth z differ for the two SSDs but are related through simple geometrical relationships.

6.8.3.   Scatter–air ratio

Just as it was convenient in dealing with PDDs to separate the scattered component from the primary component to obtain the scatter function, it is sometimes useful to separate the primary component of the TAR from the total TAR to obtain the scatter contribution, which, in this case, is referred to as the scatter–air ratio (SAR), defined as:

$$\text{SAR}(z, A_Q, hv) = \text{TAR}(z, A_Q, hv) - \text{TAR}(z, 0, hv) \tag{6.49}$$

The SAR depends on the same three parameters as the TAR and gives the scatter contribution to the dose at point Q in a phantom per 1 cGy of dose to a small mass of water at point Q in air.
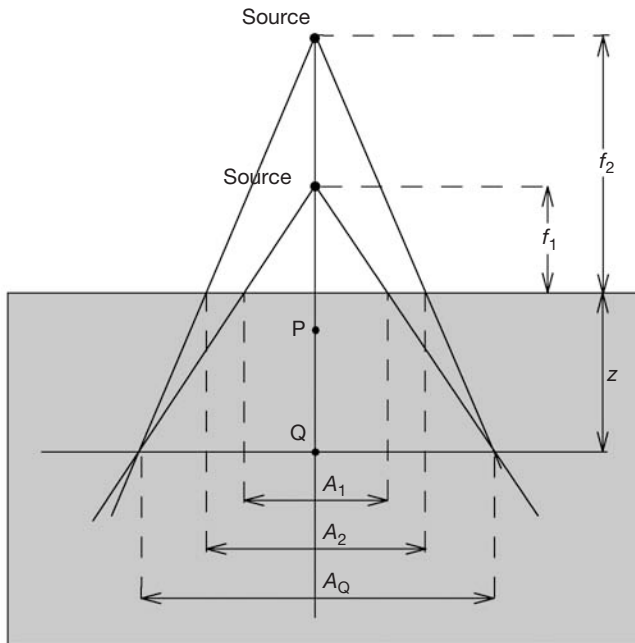
FIG. 6.14. Derivation of the PDD relationship for two SSDs with field size A_Q identical for both. Here the fields A_1 and A_2 on the phantom surface are related through simple geometrical relationships.

6.8.4. Relationship between SAR (*d*, *A*$_Q$, *hv*) and *S*(*z*, *A*, *f*, *hv*)

Similarly to the relationship between TAR(*z*, *A*$_Q$, *hv*) and PDD(*z*, *A*, *f*, *hv*), we can derive the relationship between SAR(*z*, *A*$_Q$, *hv*) and *S*(*z*, *A*, *f*, *hv*) to obtain:

$$\text{SAR}(z, A_Q, hv) = \frac{S(z, A, f, hv)}{100} \left(\frac{f + z}{f + z_{max}} \right)^2 \tag{6.50}$$

It is easy to see that:

$$S(z, A, f, hv) = 100\text{SAR}(z, A_Q, hv) \tag{6.51}$$

for any *z* when $f \rightarrow \infty$ and for any *f* when $z \rightarrow z_{max}$.

6.8.5. Tissue–phantom ratio and tissue–maximum ratio

The TAR concept works well in isocentric set-ups for photon energies of ^{60}Co and below. For megavoltage X rays produced by high energy linacs, however, the concept breaks down because of difficulties in measuring the 'dose to small mass of water in air' at those energies (the required size of the buildup cap for the ionization chamber becomes excessively large). To bypass this problem, the concept of tissue–phantom ratio (TPR) was introduced for use in megavoltage isocentric set-ups.

The TPR is defined as follows:

$$\text{TPR}(z, A_Q, hv) = \frac{D_Q}{D_{Qref}} = \frac{\dot{D}_Q}{\dot{D}_{Qref}} \tag{6.52}$$

where D_Q and $\dot{D}_Q$ are the dose and dose rate, respectively, in a phantom at arbitrary point Q on the beam central axis and D_{Qref} and $\dot{D}_{Qref}$ are the dose and dose rate, respectively, in a phantom at a reference depth z_{ref} (typically 5 or 10 cm) on the beam central axis.

The geometry for the measurement of doses D_Q and D_{Qref} is shown in Fig. 6.15.

A special TPR was defined for the reference depth z_{ref} equal to the depth of dose maximum z_{max}, which is referred to as the tissue–maximum ratio (TMR), defined as follows:
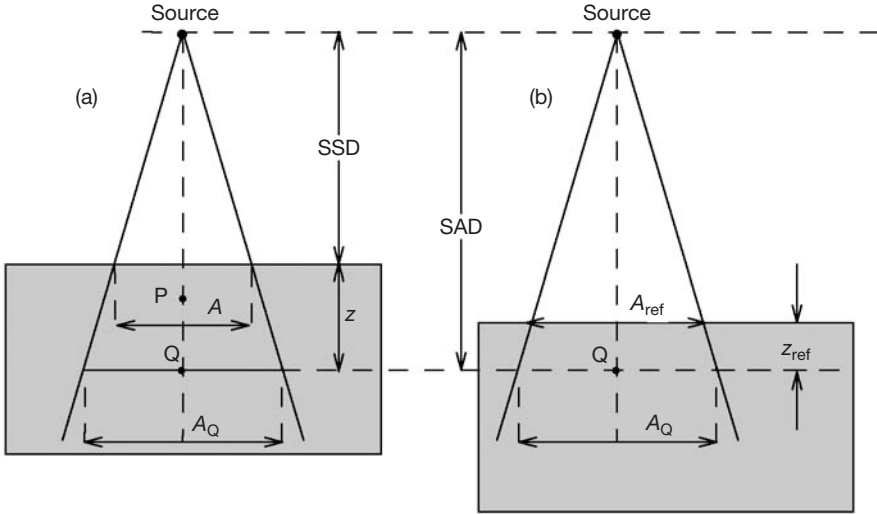
FIG. 6.15. Geometry for measurement of TPR(d, A_Q, hv). (a) The geometry for the measurement of D_Q at depth z in a phantom; (b) the geometry for the measurement of D_{Qref} at depth z_{ref} in a phantom. The distance between the source and the point of measurement, as well as the field size at the point of measurement, is the same for (a) and (b).

$$\text{TMR}(z, A_Q, hv) = \frac{D_Q}{D_{Qmax}} = \frac{\dot{D}_Q}{\dot{D}_{Qmax}} \tag{6.53}$$

where D_Q and $\dot{D}_Q$ are the dose and dose rate, respectively, at point Q at a depth z in a phantom and D_{Qmax} and $\dot{D}_{Qmax}$ are the dose and dose rate, respectively, at point Q at z_{max}.

The geometry for the definition of TMR is the same as in Fig. 6.15, except that z_{ref} is now z_{max}.

- Just like the TAR, the TPR and TMR depend on the three parameters z, A_Q, hv, but do not depend on the SAD or SSD.
- The range of TMR is from 0 for $z \rightarrow \infty$ to 1 for $z = z_{max}$ (i.e. $0 \leq \text{TMR}(z, A_Q, hv) \leq 1$.
- For constant A_Q and hv the TMR decreases with increasing z.
- For constant z and hv the TMR increases with increasing A_Q.
- For constant z and A_Q the TMR increases with increasing hv.

6.8.6. Relationship between TMR(z, A_Q, hv) and PDD(z, A, f, hv)

As shown in Fig. 6.16, a simple relationship may be derived between TMR(z, A_Q, hv) and the corresponding PDD(z, A, f, hv) from the basic definitions governing the two functions.

The basic definitions for the two functions are:

$$\text{TMR}(z, A_Q, hv) = \frac{D_Q}{D_{Qmax}} \tag{6.54}$$

$$\text{PDD}(z, A, f, hv) = 100 \frac{D_Q}{D_P} \tag{6.55}$$

Solving Eqs (6.54) and (6.55) for D_Q we obtain:

$$D_Q = D_P \frac{\text{PDD}(z, A, f, hv)}{100} = D_{Qmax} \text{TMR}(z, A_Q, hv) \tag{6.56}$$
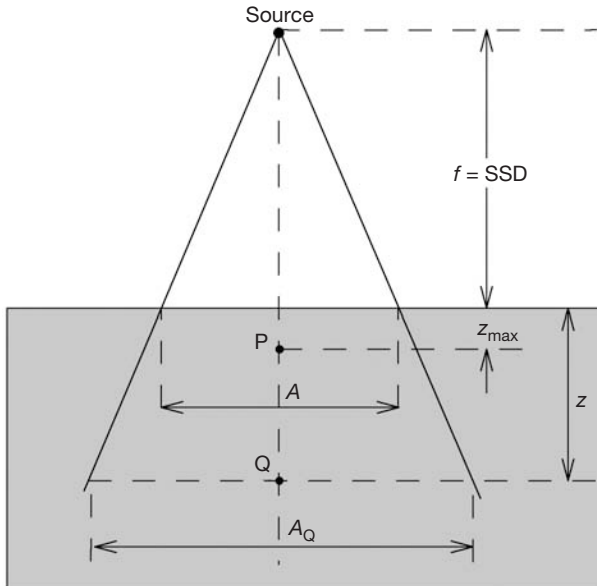
FIG. 6.16. *Geometry for derivation of the relationship between PDD(z, A, f, hv) and TMR(z, A_Q, hv).*

and expanding D_P and D_{Qmax} as follows:

$$D_P = D'_P \text{PSF}(A, h\nu) = D'_Q \left(\frac{f+z}{f+z_{max}} \right)^2 \text{PSF}(A, h\nu) \tag{6.57}$$

$$D_{Qmax} = D'_Q \, \text{PSF}(A_Q, h\nu) \tag{6.58}$$

we obtain:

$$\text{TMR}(z, A_Q, h\nu) = \frac{\text{PDD}(z, A, f, h\nu)}{100} \frac{\text{PSF}(A, h\nu)}{\text{PSF}(A_Q, h\nu)} \left(\frac{f+z}{f+z_{max}} \right)^2 \tag{6.59}$$

In the first approximation, ignoring the PSF ratio in Eq. (6.59), we have a very simple approximate relationship between $\text{TMR}(z, A_Q, h\nu)$ and $\text{PDD}(z, A, f, h\nu)$ as:

$$\text{TMR}(z, A_Q, h\nu) \approx \frac{\text{PDD}(z, A, f, h\nu)}{100} \left(\frac{f+z}{f+z_{max}} \right)^2 \tag{6.60}$$

The error in ignoring the ratio $\text{PSF}(A, h\nu)/\text{PSF}(A_Q, h\nu)$ is very small and can be estimated easily for a cobalt beam. For an extreme example, take the case with depth in a phantom $d = 20$ cm, field size $A = 20 \times 20$ cm^2 and SSD $f = 100$ cm to obtain $A_Q = 24 \times 24$ cm^2 and PSF(20, Co)/PSF(24, Co) = 1.078/1.083 = 0.995, or a 0.5% error. Errors for smaller fields and shorter SSDs are obviously smaller, making Eq. (6.60) a reasonable and very practical approximation for relating the TMR with the PDD.

6.8.7. Scatter–maximum ratio

Similarly to separating $\text{TAR}(z, A_Q, h\nu)$ into the primary component $\text{TAR}(z, 0, h\nu)$ and the scatter component $\text{SAR}(z, A_Q, h\nu)$, the $\text{TMR}(z, A_Q, h\nu)$ can be separated into the primary component $\text{TMR}(z, 0, h\nu)$ and the scatter component, referred to as the scatter–maximum ratio (SMR), defined as follows:

$$\text{SMR}(z, A_Q, h\nu) = \text{TMR}(z, A_Q, h\nu) \frac{\text{SF}(A_Q, h\nu)}{\text{SF}(0, h\nu)} - \text{TMR}(z, 0, h\nu) \tag{6.61}$$

where $SF(A_Q, h\nu)$ and $SF(0, h\nu)$ are the scatter factors for fields A_Q and 0, respectively, and photon energy $h\nu$, as defined in Eq. (6.29).

The ratio $SF(A_Q, h\nu)/SF(0, h\nu)$ is therefore:

$$\frac{SF(A_Q, h\nu)}{SF(0, h\nu)} = \frac{PSF(A_Q, h\nu)/PSF(10, h\nu)}{PSF(0, h\nu)/PSF(10, h\nu)} = PSF(A_Q, h\nu) \qquad (6.62)$$

since $PSF(0, h\nu) = 1$.

For ^{60}Co γ rays, SMRs are approximately the same as SARs. However, for megavoltage photon energies above ^{60}Co the SMRs should be calculated from the TMRs using Eq. (6.61) and:

$$TMR(z, 0, h\nu) = e^{-\mu_{eff}(z - z_{max})} \qquad (6.63)$$

where μ_{eff} is the effective attenuation coefficient for the photon beam $h\nu$.

6.9. OFF-AXIS RATIOS AND BEAM PROFILES

Dose distributions along the beam central axis give only part of the information required for an accurate dose description inside the patient. Dose distributions in 2-D and 3-D are determined with central axis data in conjunction with off-axis dose profiles.

In the simplest form, the off-axis data are given with beam profiles measured perpendicularly to the beam central axis at a given depth in a phantom. The depths of measurement are typically at z_{max} and 10 cm for verification of compliance with machine specifications, in addition to other depths required by the particular treatment planning system (TPS) used in the department. An example of typical dose profiles measured at various depths in water for two field sizes (10×10 and 30×30 cm^2) and a 10 MV X ray beam is shown in Fig. 6.17.

Combining a central axis dose distribution with off-axis data results in a volume dose matrix that provides 2-D and 3-D information on the dose distribution. The off-axis ratio (OAR) is usually defined as the ratio of dose at an off-axis point to the dose on the central beam axis at the same depth in a phantom.

Megavoltage X ray beam profiles consist of three distinct regions: central, penumbra and umbra.
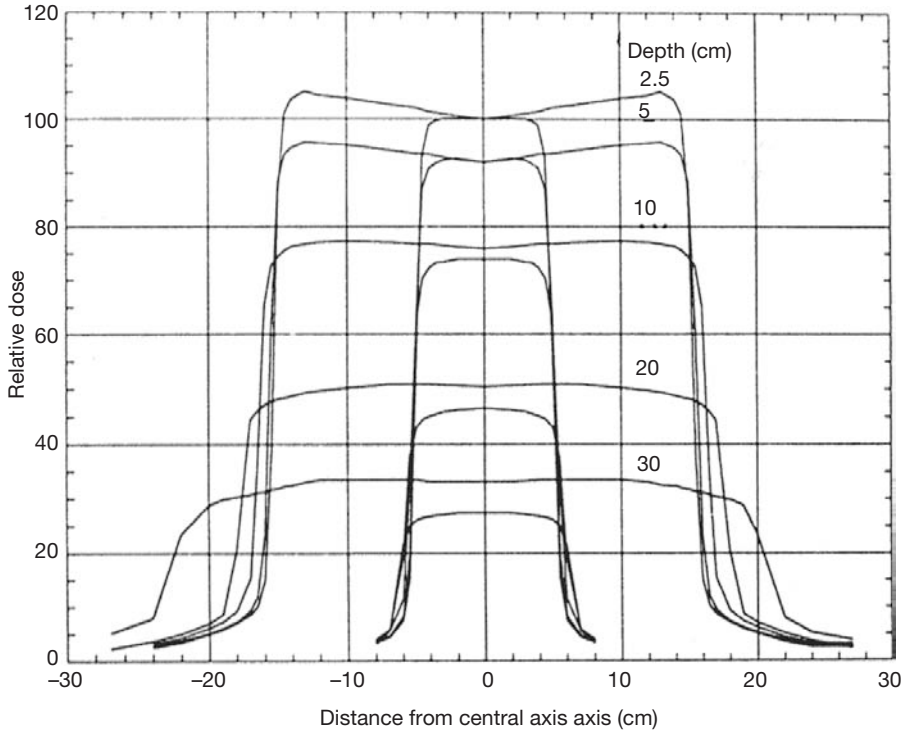
FIG. 6.17. An example of beam profiles for two field sizes (10 × 10 cm² and 30 × 30 cm²) and a 10 MV X ray beam at various depths in water. The central axis dose values are scaled by the appropriate PDD value for the two fields.

- The central region represents the central portion of the profile extending from the beam central axis to within 1–1.5 cm from the geometric field edges of the beam. The geometric field size, indicated by the optical light field, is usually defined as the separation between the 50% dose level points on the beam profile. In the central region, the beam profile for ^{60}Co beams is affected by the inverse square dose fall-off as well as by increased phantom thickness for off-axis points. For linacs, on the other hand, the central region of the beam profile is affected by the energy of electrons striking the thick target, by the target atomic number and by the flattening filter atomic number and geometric shape.
- In the penumbral region of the dose profile the dose changes rapidly and depends also on the field defining collimators, the finite size of the focal spot (source size) and the lateral electronic disequilibrium. The dose fall-off around the geometric beam edge is sigmoid in shape and extends

under the collimator jaws into the penumbral tail region, where there is a small component of dose due to the transmission through the collimator jaws (transmission penumbra), a component attributed to finite source size (geometric penumbra) and a significant component due to in-patient X ray scatter (scatter penumbra). The total penumbra is referred to as the physical penumbra and is the sum of the three individual penumbras: transmission, geometric and scatter. The physical penumbra depends on beam energy, source size, SSD, source to collimator distance and depth in a phantom.

- Umbra is the region outside the radiation field, far removed from the field edges. The dose in this region is generally low and results from radiation transmitted through the collimator and head shielding.

Dose profile uniformity is usually measured by a scan along the centre of both major beam axes for various depths in a water phantom. Two parameters that quantify field uniformity are then determined: field (beam) flatness and field (beam) symmetry.

6.9.1. Beam flatness

The beam flatness F is assessed by finding the maximum D_{max} and minimum D_{min} dose point values on the beam profile within the central 80% of the beam width and then using the relationship:

$$F = 100 \times \frac{D_{max} - D_{min}}{D_{max} + D_{min}} \tag{6.64}$$

Standard linac specifications generally require that F be less than 3% when measured in a water phantom at a depth of 10 cm and an SSD of 100 cm for the largest field size available (usually 40×40 cm^2).

Compliance with the flatness specifications at a depth of 10 cm in water results in 'over-flattening' at z_{max}, which manifests itself in the form of 'horns' in the profile, and in 'under-flattening', which progressively worsens as the depth z increases from 10 cm to larger depths beyond 10 cm, as evident from the profiles for the 30×30 cm^2 field in Fig. 6.17. The typical limitation on beam horns in the z_{max} profile is 5% for a 40×40 cm^2 field at SSD = 100 cm. The over-flattening and under-flattening of the beam profiles is caused by the lower beam effective energies in off-axis directions compared with those in the central axis direction.

6.9.2.   Beam symmetry

The beam symmetry S is usually determined at z_{max}, which represents the most sensitive depth for assessment of this beam uniformity parameter. A typical symmetry specification is that any two dose points on a beam profile, equidistant from the central axis point, are within 2% of each other. Alternately, areas under the z_{max} beam profile on each side (left and right) of the central axis extending to the 50% dose level (normalized to 100% at the central axis point) are determined and S is then calculated from:

$$S = 100 \times \frac{\text{area}_{\text{left}} - \text{area}_{\text{right}}}{\text{area}_{\text{left}} + \text{area}_{\text{right}}} \qquad (6.65)$$

The areas under the z_{max} profiles can often be determined using an automatic option on the water tank scanning device (3-D isodose plotter). Alternatively, using a planimeter or even counting squares on graph paper with a hard copy of the profile are practical options.

6.10. ISODOSE DISTRIBUTIONS IN WATER PHANTOMS

The physical characteristics of radiation beams are usually measured in phantoms under standard conditions that are as follows:

- A homogeneous, unit density phantom;
- A flat phantom surface;
- A perpendicular beam incidence on the phantom.

The central axis depth dose data in conjunction with dose profiles contain complete 2-D and 3-D information about a radiation beam. However, this information is difficult to visualize even for a single beam, let alone for a combination of several beams.

Planar and volumetric variations in depth doses are usually displayed by means of isodose curves or isodose surfaces, which connect points of equal dose in a volume of interest. The isodose curves and surfaces are usually drawn at regular intervals of absorbed dose and are expressed as a percentage of the dose at a specific reference point.

An isodose chart for a given single beam consists of a family of isodose curves usually drawn at regular increments of PDD. Two normalization conventions are in use:

— For SSD set-ups, all isodose values are normalized to 100 at point P on the central beam axis.
— For SAD set-ups, the isodose values are normalized to 100 at the isocentre.

The isodose charts for an SSD set-up are thus plots of PDD values, while isodose charts for an SAD set-up are plots of either TAR or TMR values.

For a ^{60}Co beam the dose at any depth is largest on the central beam axis and then decreases towards the beam edges. For megavoltage photon beams the off-axis dose at shallow depths is usually larger than the central axis dose at the same depth, as a consequence of flattening filter design. These filters provide flat beams at a depth of 10 cm in water, and to achieve this they must overcompensate at shallow depths. (Note that the effective beam energy in extreme off-axis directions is lower than the effective beam energy in the direction of the central beam axis.)

Figure 6.18 shows an example of isodose charts for a ^{60}Co beam in water: Fig. 6.18(a) shows an SSD set-up ($A = 10 \times 10$ cm^2; SSD = 80 cm); Fig. 6.18(b) shows an SAD set-up ($A_Q = 10 \times 10$ cm^2; SAD = 100 cm; depth of isocentre = 10 cm).
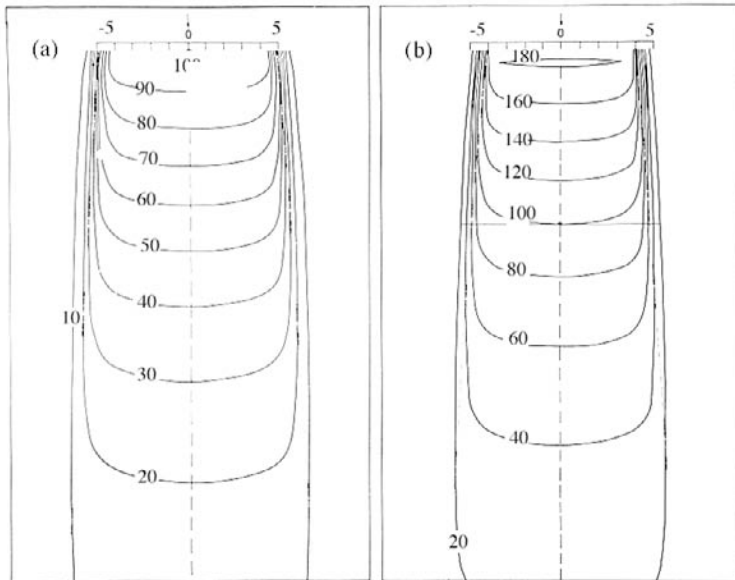
FIG. 6.18. Isodose curves for a ^{60}Co γ ray beam: (a) for an SSD set-up ($A = 10 \times 10$ cm^2; SSD = 80 cm) and (b) for an SAD set-up ($A_Q=10 \times 10$ cm^2, SAD = 100 cm; depth of isocentre = 10 cm).

Near the beam edges in the penumbra region the dose decreases rapidly with lateral distance from the beam central axis. This dose fall-off is caused not only by the geometric penumbra but also by the reduced side scatter.

Outside the geometric limits of the beam and the penumbra, the dose variation is the result of three components:

(i) Scatter from the radiation field;
(ii) Leakage through the collimator jaws and machine head housing;
(iii) Scatter from the collimation system.

Parameters that affect the single beam isodose distribution are beam quality, source size, beam collimation, field size, SSD and source to collimator distance.

Isodose charts are measured with ionization chambers, solid state detectors, standard radiographic film and radiochromic film.

In addition to direct measurements, isodose charts may also be generated by calculations using various algorithms for treatment planning, most commonly with commercially available TPSs.

Treatment by a single photon beam is seldom used except for superficial tumours. Deep seated tumours are usually treated with a combination of two or more beams so as to achieve an acceptable dose distribution within the tumour and the surrounding normal tissues (see Chapter 7). As a rule, the tumour dose is higher than the dose to the surrounding normal tissues, and the dose distribution within the tumour should be homogeneous to within +7% and –5% of the prescribed dose, if at all possible.

6.11. SINGLE FIELD ISODOSE DISTRIBUTIONS IN PATIENTS

In clinical situations the beam may be obliquely incident on the patient and the patient's surface may be curved or of irregular shape, requiring corrections for contour irregularities. In addition, some irradiated tissues, such as lung and bone, have densities that differ considerably from that of water, requiring corrections for tissue heterogeneities.

Isodose distributions in patients are determined by one of two radically different approaches:

● Correction based algorithms;
● Model based algorithms.

Correction based algorithms use depth dose data measured in water phantoms with a flat surface and normal incidence in conjunction with various methods to correct for irregular patient contours and oblique beam incidence, in contrast to the flat surface of a water phantom. They also correct for organ inhomogeneities to account for varying electron densities of organs, in contrast to the uniform electron density of a water phantom.

Model based algorithms obviate the correction problem by modelling the dose distributions from first principles and accounting for all geometrical and physical characteristics of the particular patient treatment.

Before clinical use both correction algorithms and model based algorithms must be verified experimentally, which often is a difficult task. The relative importance of individual corrections varies with the particular treatment geometry and the position of the target volume inside the patient. For conventional treatment techniques the correction based algorithms work reasonably well and produce reliable dose distributions; however, for the new sophisticated treatments such as 3-D conformal radiotherapy and intensity modulated radiotherapy (IMRT), they become problematic, because of the radical corrections that are required for these techniques. Model based algorithms hold great promise for the future; however, they are currently still under development.

6.11.1. Corrections for irregular contours and oblique beam incidence

A radiation beam striking an irregular or sloping patient surface produces an isodose distribution that differs from the standard distributions obtained on flat surfaces with a normal beam incidence. Two approaches are used to address this problem:

- The effect can be corrected through various calculation methods;
- The effect may be compensated for through the use of wedges, bolus materials or compensators.

Several methods have been developed to correct standard flat surface/ normal incidence isodose distributions for contour irregularities and oblique angles of beam incidence. The three most commonly used methods, applicable for angles of incidence up to 45º for megavoltage X ray beams and up to 30º for orthovoltage X ray beams, are:

— The effective SSD method;
— The TAR or TMR method;
— The isodose shift method.

The correction factors for these three methods can be understood with reference to Fig. 6.19, in which an irregular patient contour CC is treated with a beam with an SSD = f. The PDD at point S normalized to dose at point P on the beam central axis is referred to as PDD_{corr} and is calculated with one of the three methods listed above.

6.11.1.1. Effective source to surface distance method

In the effective SSD method, PDD_{corr} is determined from:

$$\text{PDD}_{\text{corr}} = \text{PDD}'(z, A, f, h\nu) \left(\frac{f + z_{\text{max}}}{f + h + z_{\text{max}}} \right)^2 \qquad (6.66)$$

where $\text{PDD}'(z, A, f, h\nu)$ is the PDD under standard conditions with the flat surface $C'C'$ and the second term represents an inverse square correction factor. The parameter h is the thickness of missing tissue, while the parameter $-h$ represents the thickness of excess tissue. An assumption is made that the PDD does not depend on the SSD for deviations from the nominal SSD of the
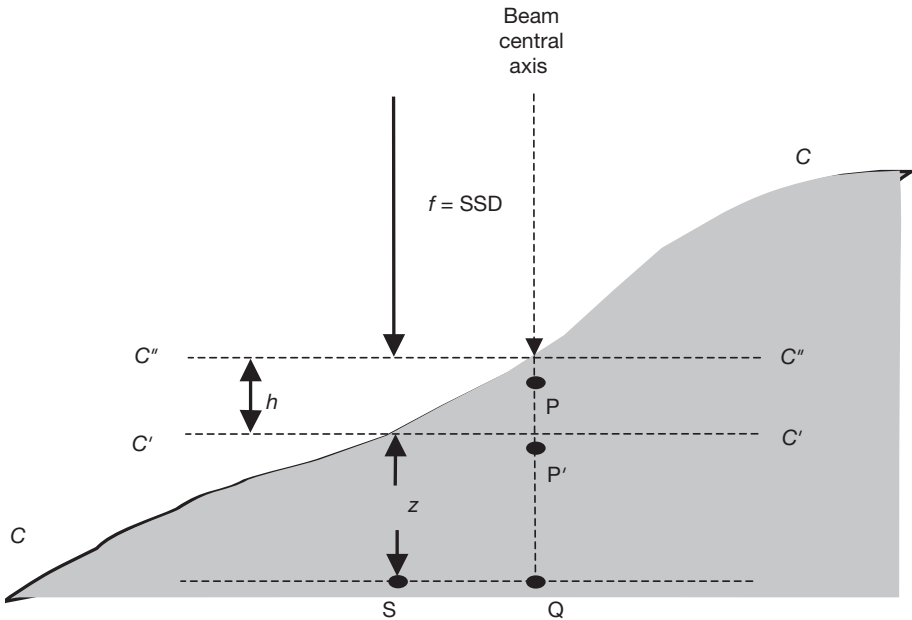
FIG. 6.19. Geometry used for dose determination at point S in a patient. CC represents the actual patient contour; C'C' and C"C" are flat phantom contours: C"C" at the nominal SSD and C'C' at SSD + h, where h represents the thickness of missing tissue directly above point S. Point P is the point of dose normalization at z_{max} on the central beam axis.

order of h (i.e. $h << f$). The resulting PDD is normalized to 100 at point P on the central beam axis.

Thus in the effective SSD method (see Fig. 6.19): (a) the isodose chart is shifted to the flat surface level at the $C'C'$ contour; (b) the PDD value for point S is read; and (c) the reading is corrected by an inverse square law factor.

6.11.1.2. Tissue–air ratio or tissue–maximum ratio method

In the TAR or TMR method, PDD_{corr} is given as:

$$PDD_{corr} = PDD''(z+h, A, f, hv) \ \frac{T(z, A_Q, hv)}{T(z+h, A_Q, hv)} \qquad (6.67)$$

where

A_Q is the field size at point S at a distance $(f + h + z)$ from the source.
T stands for either the TAR or the TMR, and an assumption is made that TARs and TMRs do not depend on the SSD.
PDD''   represents the PDD value at depth $(h + z)$ for a standard flat phantom with the surface at $C''C''$.
h is missing or excessive tissue. For missing tissue h is positive, for excess tissue h is negative.

6.11.1.3. Isodose shift method

In the isodose shift method, the value of the dose at S is shifted on a vertical ray line by $(h \times k)$, where h is the thickness of the missing or excess tissue and k is a factor depending on beam energy. The factor k is smaller than 1 and has a value of 0.7 for ^{60}Co beams to 5 MV beams, 0.6 for 5–15 MV beams and 0.5 for 15–30 MV beams. For missing tissue h is positive and the isodose is shifted away from the source, while for excess tissue h is negative and the isodose is shifted towards the source.

6.11.2. Missing tissue compensation

In addition to techniques to correct for contour irregularities and oblique beam incidence, as discussed in Section 6.11.1, many relatively simple techniques have been devised to compensate for missing tissue, most notably the use of wedges, bolus materials and compensators.

6.11.2.1. Wedge filters

Wedge filters may be used to even out the isodose surfaces for photon beams striking relatively flat patient surfaces under an oblique beam incidence.

Two types of wedge filter are in use: physical wedge filters and dynamic wedge filters.

- Physical wedges are made of lead, brass or steel. When placed in a radiation beam, they cause a progressive decrease in the intensity across the beam and a tilt of isodose curves under normal beam incidence.
- Dynamic wedges provide the wedge effect on isodose curves through a closing motion of a collimator block during irradiation.

The wedge angle is defined as the angle through which an isodose curve at a given depth in water (usually 10 cm) is tilted at the central beam axis under the condition of normal beam incidence.

Physical wedges are usually available with wedge angles of 15º, 30º, 45º and 60º; dynamic wedges are available with any arbitrary wedge angle in the range 0–60º.

The wedge (transmission) factor (WF) is defined as the ratio of doses at z_{max} in a water phantom on the beam central axis with and without the wedge.

Physical wedge filters may alter the X ray beam quality, causing beam hardening at energies of 6–10 MV and beam softening at energies above 15 MV. These effects will affect the central axis PDDs and should be accounted for in treatment planning isodose distribution calculations.

6.11.2.2. Bolus

Bolus is a tissue equivalent material placed directly on the skin surface to even out the irregular patient contour and thereby provide a flat surface for normal beam incidence. In principle, the use of bolus is straightforward and practical; however, it suffers a serious drawback: for megavoltage photon beams it results in the loss of the skin sparing effect in the skin under the bolus layer (i.e. skin sparing occurs in the bolus).

6.11.2.3. Compensators

Compensators are used to produce the same effect as the bolus yet preserve the skin sparing effect of megavoltage photon beams. They are custom-made devices that mimic the shape of the bolus but are placed in the radiation beam at some 15–20 cm from the skin surface so as not to disrupt the

skin sparing properties of the beam. Although compensators may be made of water equivalent materials, they are usually fabricated from lead or special low melting point alloys, such as Cerrobend (Lipowitz's metal).

Since compensators are placed at some distance from the skin surface so as not to affect the skin dose sparing, their shape must be adjusted for:

— Beam divergence;
— Linear attenuation coefficients of the compensator material relative to that of water;
— Reduction in scatter at various depths when the compensator is placed in the radiation beam away from the skin surface rather than in contact with the skin.

6.11.3. Corrections for tissue inhomogeneities

Standard isodose charts and depth dose tables are given for uniform density water phantoms. Radiation beams used in patient treatment, however, traverse various tissues that may differ from water in density and atomic number. These tissue inhomogeneities (also referred to as heterogeneities) affect the dose deposition in the patient and may result in isodose distributions that differ considerably from those obtained in water phantoms. The effects of inhomogeneities on radiation dose distributions depend on the amount, density and atomic number of the inhomogeneity, as well as on the quality of the photon beam, and may be separated into two distinct categories:

- Increase or decrease in the attenuation of the primary beam, which affects the distribution of the scattered radiation;
- Increase or decrease of the secondary electron fluence.

Three separate regions, in addition to inhomogeneity boundaries, are considered with regard to inhomogeneities: (1) the point of interest P located in front of the inhomogeneity; (2) P inside the inhomogeneity; and (3) P beyond the inhomogeneity.

In region (1), in front of the inhomogeneity, especially for megavoltage photon beams, the dose is not affected by the inhomogeneity, since the primary beam in this region is not affected and neither is the scatter component, except close to the boundary.

In region (2) the dose is mainly affected by changes in the secondary electron fluence and to a lesser extent by changes in the primary beam attenuation in the inhomogeneity. Under the conditions of electronic equilibrium and for a given photon energy fluence, the ratio of absorbed doses

in two different media is equal to the ratio of mass–energy absorption coefficients for the two media. Close to the soft tissue–lung interfaces there may be a partial loss of electronic equilibrium and an associated decrease in dose.

In region (3), beyond the inhomogeneity, the dose is mainly affected by changes in the primary beam attenuation and to a lesser extent by changes in scatter. Four empirical methods (see Section 7.5.6) are available for correcting the water phantom dose to estimate the dose at points in region (3):

— The TAR method;
— The power law TAR method;
— The equivalent TAR method;
— The isodose shift method.

Beyond healthy lung (density ~0.3 g/cm^3) the dose in soft tissues will increase, while beyond bone (density ~1.6 g/cm^3) it will decrease in comparison with dose measured in a uniform phantom.

Typical corrections for dose beyond healthy lung are: 4%, 3%, 2% and 1% per centimetre of lung for ^{60}Co γ beams and 4, 10 and 20 MV X rays, respectively.

The shielding effect of bone depends strongly on the beam energy; it is appreciable at low X ray energies because of a strong photoelectric effect presence and essentially negligible in the low megavoltage energy range (mainly Compton effect). At energies above 10 MeV the shielding effect of bone begins to increase with increasing energy because of the increase in the pair production cross-section.

6.11.4. Model based algorithms

Model based algorithms for computation of dose distributions in a patient currently fall into one of three categories:

● A relatively simple analytical calculation of first order Compton scatter and its addition to the primary dose at the point of interest. The method is fairly rudimentary as it assumes a parallel beam of monoenergetic photons and ignores heterogeneities and scattering higher than of the first order.
● The convolution–superposition method, which accounts for the indirect nature of dose deposition from photon interactions, separating the primary photon interactions from the transport of scattered photons and charged particles produced through the photoelectric effect (photoeffect), Compton scattering and pair production.

● The Monte Carlo method, which is the most promising of the model based dose computation methods, uses well established probability distributions governing the individual interactions of photons and electrons with the patient and their transport through the patient. Monte Carlo simulation is essential in all model based dose computations to characterize the clinical beam emanating from the radiation source, but can also be used directly to compute photon dose distributions for a given patient and treatment geometry. The current limitation of direct Monte Carlo calculations is the time required to calculate the large number of histories required to reduce stochastic or random uncertainties to acceptable levels. It is expected that advances in computer technology will, within a few years, reduce Monte Carlo calculation times to acceptable levels, and this will make Monte Carlo methods the standard approach to radiotherapy treatment planning. The electron densities for various tissues of individual patients are obtained with CT scanners or CT simulators and form an essential component of any Monte Carlo based dose distribution calculation.

6.12. CLARKSON SEGMENTAL INTEGRATION

Tables for the various dose functions, such as the PDD, TAR, PSF and TMR, etc., are usually given for a series of square fields. Values for these functions when fields are rectangular or circular may be obtained through determining the equivalent square for the rectangular field (Eq. (6.25)) or circular field (Eq. (6.26)) and then using the appropriate tabulated square field data for determining the value of a given dose function. Here, an assumption is made that there is a match between dose functions for rectangular fields and their equivalent square and circular fields. It has been shown experimentally that this assumption is valid for the range of field sizes and beam energies used in radiotherapy.

Radiation fields other than square, rectangular or circular are termed irregular fields. An irregular field will also have an equivalent square field and an equivalent circular field that will yield the same value of a given dose function as does the irregular field, but there are no simple means to determine the equivalent square or circle for a given irregular field. However, a technique, referred to as the Clarkson segmental integration, can be used to calculate the appropriate value of any given dose function for the given irregular field based on circular field data.

The Clarkson technique resolves the irregular field into sectors of circular beams originating at the point of interest Q in the phantom or patient. For

manual calculations, sectors with an angular width of 10º are usually used; for computer driven calculations the angular width is 5º or even smaller, in order to improve accuracy.

An assumption is made that a sector with a given field radius contributes $1/N$ of the total circular field value to the value of the given function F for the irregular field at point Q, where N is the number of sectors in a full circle of 360º.

The value of a given function F for an irregular field that in general depends on depth z of point Q, shape of the irregular field, SSD $= f$ and beam energy hv is then determined from the following segmental integration relationship:

$$F(z, \text{ irregular field}, f, hv) = \frac{1}{N} \sum_{i=1}^{N} F(z, r_i, f, hv)$$
(6.68)

where

N is the number of sectors in 360º (for manual calculations $N = 36$);

r_i is the radius from point Q to the edge of the field at the centre of sector i;

$F(z, r_i, f, hv)$ is the value of the dosimetric function F at depth z, SSD $= f$ and beam energy hv for the circular field with radius r_i.

An example of an irregular field is shown in Fig. 6.20 with two of 36 sectors highlighted: one is a simple sector with radius r_1 and the other is a composite sector with three radii: r_a, r_b and r_c.

● The contribution of the simple sector to the sum in Eq. (6.68) is simply equal to:

$(1/N)F(z, r_i, f, hv)$

● The composite sector consists of three components to yield the following contribution:

$(1/N)[F(z, r_a, f, hv) - F(z, r_b, f, hv) + F(z, r_c, f, hv)]$

to the sum given in Eq. (6.68), with two positive components that are contributed by portions of the radiation field and one negative
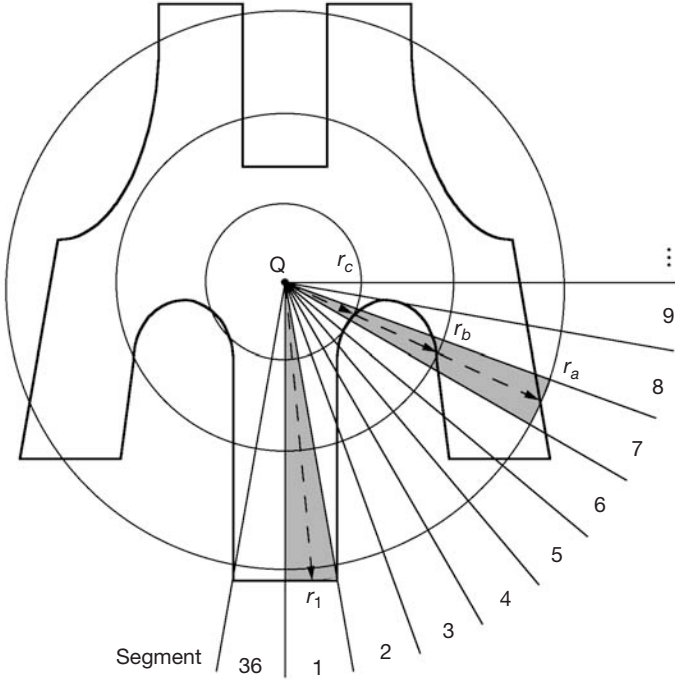
FIG. 6.20. An example of a mantle irregular field. Two segments out of 36 are highlighted. The first is simple with radius r_1, the seventh is composite with three radii: r_a, r_b and r_c.

component that accounts for the missing portion of the radiation field in the segment (sector).

Once the value of a dose function for a given irregular field is determined through the Clarkson integration technique, the equivalent square for the irregular field is also established by finding in tabulated square field data the square field that will give the same value for the dose function. The segmental integration technique was originally proposed by Clarkson in the 1940s and developed by Johns and Cunningham in the 1960s for determining the scatter component of the dose at an arbitrary point of interest in the patient, either inside or outside the direct radiation field.

For points inside the radiation field the scatter component is added to the primary beam component; for points outside the field the scatter component is added to the radiation transmitted through the shielding blocks, collimator or head shielding of the treatment machine.

The original implementation of the Clarkson technique was intended for use with orthovoltage and cobalt beams for which the primary dose rate was reasonably flat from the central axis to points near the edge of the field, where it began to decrease. In linac beams, however, the primary dose rate at shallow depths in the patient may actually increase at distances away from the central axis ('horns') as a result of flattening filter effects on the radiation beam. A flattening filter correction that depends on depth z in a phantom and radial distance r from the central axis is required to model, for the primary beam component, this increase in the dose rate away from the central beam axis.

6.13. RELATIVE DOSE MEASUREMENTS WITH IONIZATION CHAMBERS

Ionization chambers are used in clinical physics not only for photon and electron beam calibration at a reference point in a phantom but also for relative measurements of various parameters and dose functions, such as the CF, the RDF, dose profiles and PDDs, including the surface dose and doses in the buildup region. The dependence of various dose correction factors (such as ionization chamber polarity, ionic recombination, stopping power ratios and fluence correction) on beam energy (i.e. depth in a phantom) should be considered in relative dose measurements, although in many situations the dependence may be ignored.

Usually each task of dose determination is carried out with ionization chambers designed for the specific task at hand. For example:

- Doses and dose rates at reference points in a phantom for megavoltage photon beams and electron beams above 10 MeV are measured with relatively large volume (0.6 cm^3) cylindrical ionization chambers in order to obtain a reasonable signal and good signal to noise ratio.
- Relative dose distributions (e.g. central axis PDDs and beam profiles) for photon beams beyond z_{max} and for electron beams are usually measured with small volume (0.1 cm^3) ionization chambers in order to obtain good spatial resolution.
- Surface doses and doses in the buildup region for photon beams are measured with parallel-plate ionization chambers incorporating a thin polarizing electrode window (to be able to measure the surface dose) and a small electrode separation (typically 1 mm, for better spatial resolution).

- A typical megavoltage photon beam PDD curve, measured with positive and negative polarities with a parallel-plate ionization chamber in the dose buildup region and beyond, is shown in Fig. 6.21.
- In the buildup region the positive chamber polarity produces a larger signal than the negative polarity. The difference in signals is most pronounced on the phantom surface and then diminishes with depth until it disappears at depths of z_{max} and beyond. At z_{max} and beyond this curve is more conveniently measured with small volume cylindrical ionization chamber; the results will match those obtained with a parallel-plate chamber. In the buildup region, however, the cylindrical chamber will read an unrealistically high signal because of its excessive wall thickness.
- In the buildup region, signals for both positive and negative chamber polarities are measured with a parallel-plate ionization chamber, and the average reading between the two polarities is used as the true dose value. Signal averaging eliminates the chamber Compton current that results from photon interactions in the measuring electrode of the chamber. In the dose buildup region, these interactions cause a loss of electrons from the measuring electrode that is not fully compensated by the arrival of
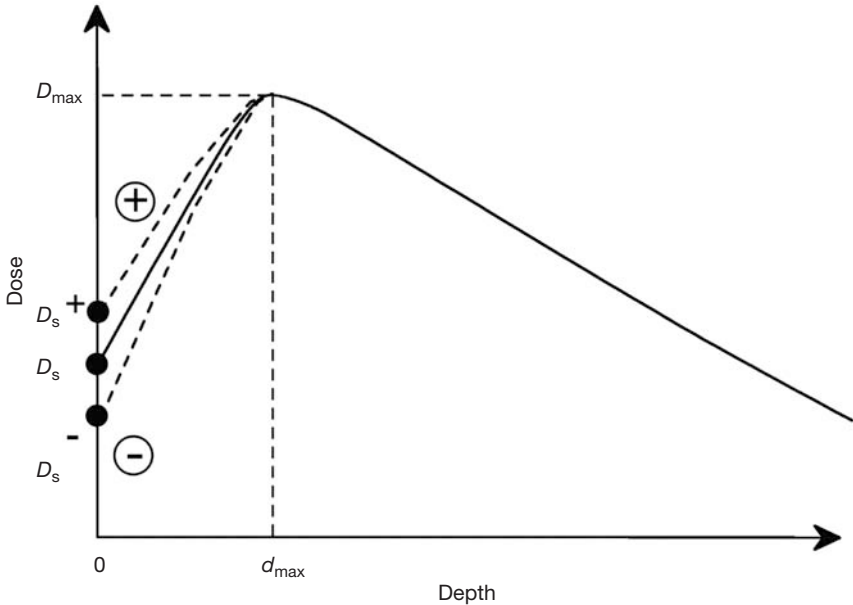
FIG. 6.21. Megavoltage photon beam depth doses measured with a parallel-plate ioniza-tion chamber. In the buildup region the positive polarity produces a higher reading than the negative polarity, beyond z_{max} both polarities give essentially identical signals.

electrons from the upper layers of the phantom. The electron difference results in a non-dosimetric current, which is referred to as the Compton current, and causes an increased reading for positive chamber polarity and a decreased reading for negative chamber polarity.

- For depths beyond z_{max}, both positive and negative chamber polarities yield the same reading, because electronic equilibrium exists on the measuring electrode (as many electrons land on the measuring electrode as are ejected by photon interactions from the measuring electrode).

- Ionic collection efficiency depends not only on the potential difference between the polarizing and measuring electrodes but also on the dose rate in the ionization chamber cavity. Therefore, in principle, when measuring depth doses, one should account for the change in ionic collection efficiency as a function of depth in a phantom. However, in practice, since ionic recombination loss in well behaved chambers is 2% or less, the changes in ionic recombination with depth are ignored when measuring relative depth doses.

- In general, stopping power ratios water to air and chamber correction factors are also depth dependent, and this dependence, according to the particular situation and accuracy required, might have to be accounted for when measuring depth doses with ionization chambers:

  — In photon beams, since the restricted stopping power ratio water to air is essentially independent of depth at depths larger than z_{max}, the signal corrected for the polarity effect can be treated as an indication of the relative dose to water. At depths shallower than z_{max}, the restricted stopping power ratio water to air varies by up to 2%, depending on field size and energy, a variation that is usually ignored.

  — In electron beams, the restricted stopping power ratio water to air varies significantly as a function of depth, requiring a correction to the measured ionization curve when relative dose is to be determined. For realistic beams as a function of depth z and energy (parametrized by R_{50}) the stopping power ratio water to air is given by the following fit (Burns et al.):

$$\left(\frac{\overline{L}}{\rho}\right)_{air}^{water}(z, R_{50})$$

$$= \frac{a + b(\ln R_{50}) + c(\ln R_{50})^2 + d(z/R_{50})}{1 + e(\ln R_{50}) + f(\ln R_{50})^2 + g(\ln R_{50})^3 + h(z/R_{50})} \qquad (6.69)$$

with the following values for the parameters: $a = 1.0752$; $b = -0.50867$; $c = 0.088670$; $d = -0.08402$; $e = -0.42806$; $f = 0.064627$; $g = 0.003085$; and $h = -0.12460$.

● Finally, in electron beams, for unguarded chambers (such as Farmer type thimble chambers), the fluence perturbation correction factor also varies as a function of energy at depth (by up to 5% in the range between z_{max} and the bremsstrahlung tail for a 20 MeV electron beam). Well guarded parallel-plate ionization chambers are therefore better suited for measurement of relative depth doses in electron beams than are thimble chambers.

6.14. DELIVERY OF DOSE WITH A SINGLE EXTERNAL BEAM

Outputs for X ray machines and isotope units are usually given in centigray per minute (cGy/min) at z_{max} in a phantom, while outputs for linacs are given in centigray per monitor unit (cGy/MU) at z_{max} in a phantom.

Transmission ionization chambers in linacs are usually adjusted such that the beam output corresponds to 1 cGy/MU at z_{max} for a 10×10 cm^2 field at SSD = 100 cm (i.e. $\dot{D}_P(z_{max}, 10, 100, h\nu) = 1$ cGy/MU (Fig. 6.9)).

$\dot{D}_P(z_{max}, A, 100, h\nu)$, the dose rate at point P for an arbitrary field size A, is then obtained from $\dot{D}_P(z_{max}, 10, 100, h\nu)$ as follows (see Eq. (6.30)):

$$\dot{D}_P(z_{max}, A, 100, h\nu) = \dot{D}_P(z_{max}, 10, 100, h\nu) \times \mathrm{RDF}(A, h\nu) \qquad (6.70)$$

The number of monitor units $\mathcal{MU}$ (in MUs) required to deliver a tumour dose TD at point Q (Fig. 6.9) using a single SSD field with field A is calculated from Eq. (6.34) recognizing that $\dot{D}_Q = \dot{\mathrm{TD}} = (\mathrm{TD})/(\mathcal{MU})$, where $\dot{\mathrm{TD}}$ is the tumour dose rate:

$$\mathcal{MU} = \frac{\mathrm{TD}}{\dot{D}_P(z_{max}, 10, 100, h\nu) \times \mathrm{RDF}(A, h\nu) \times \mathrm{PDD}(z, A, f, h\nu)} \qquad (6.71)$$

Similarly, for an SAD set-up (Fig. 6.15) the number of monitor units $\mathcal{MU}$ to deliver a tumour dose TD at point Q with a single isocentric beam with field size A_Q may be calculated using Eq. (6.52) recognizing that $\dot{D}_Q = \dot{\mathrm{TD}} = (\mathrm{TD})/(\mathcal{MU})$ and that $\dot{D}_{Qmax}(z_{max}, A_Q, \mathrm{SAD} = 100, h\nu)$ may be approximated as:

$$\dot{D}_{\mathrm{Qmax}}(z_{\mathrm{max}}, A_{\mathrm{Q}}, 100_{\mathrm{SAD}}, h\nu)$$

$$\approx \dot{D}_{\mathrm{P}}(z_{\mathrm{max}}, 10, 100_{\mathrm{SSD}}, h\nu) \times \mathrm{RDF}(A, h\nu) \times \left(\frac{f + z_{\mathrm{ref}}}{f}\right)^2 \qquad (6.72)$$

to obtain:

$$\mathcal{M}\mathcal{U} = \frac{\mathrm{TD}}{\dot{D}_{\mathrm{P}}(z_{\mathrm{max}}, 10, 100_{\mathrm{SSD}}, h\nu) \times \mathrm{RDF}(A, h\nu) \times \mathrm{TPR}(z, A_{\mathrm{Q}}, h\nu)}$$

$$\times \left(\frac{f}{f + z_{\mathrm{ref}}}\right)^2 \qquad (6.73)$$

6.15. EXAMPLE OF DOSE CALCULATION

Given $\dot{D}(15, 15, 80, \mathrm{Co})$ calculate $\dot{D}(10, 20, 140, \mathrm{Co})$, where $\dot{D}(15, 15, 80, \mathrm{Co}) = \dot{D}(z, A, f, \mathrm{Co})$ stands for the dose rate in cGy/min at point Q in a water phantom at a depth $z = 15$ cm on the central axis of a cobalt beam with a field size $A = 15 \times 15$ cm^2 and $SSD = f = 80$ cm.

The problem ties together the various basic functions and parameters that are routinely used in external beam radiotherapy and may be solved using either the SSD approach (with PDDs) or the SAD approach (with TARs). The two approaches, of course, should yield the same end result. The steps involved in going from $\dot{D}(15, 15, 80, \mathrm{Co})$ to $\dot{D}(10, 20, 140, \mathrm{Co})$ are given below for the SSD and the SAD approaches.

SSD approach (6.74)	SAD approach (6.75)
$\dot{D}(15,15,80,\mathrm{Co})$	$\dot{D}(15,15,80,\mathrm{Co})$
$\downarrow \quad \times \dfrac{100}{\mathrm{PDD}(15,15,80,\mathrm{Co})}$	$\downarrow \quad \times \dfrac{1}{\mathrm{TAR}(15,17.8,\mathrm{Co})}$
$\dot{D}(0.5,15,80,\mathrm{Co})$	$\dot{D}'_{95}(17.8,\mathrm{Co})$
$\downarrow \quad \times \dfrac{1}{\mathrm{PSF}(15,\mathrm{Co})}$	$\downarrow \quad \times \dfrac{95^2}{80.5^2}$

$$\dot{D}'_{80.5}(15_{80},\text{Co}) \qquad\qquad\qquad \dot{D}'_{80.5}(15_{80},\text{Co})$$

$$\downarrow\quad\times\frac{\text{CF}(11.4,\text{Co})}{\text{CF}(15,\text{Co})} \qquad\qquad \downarrow\quad\times\frac{\text{CF}(11.4,\text{Co})}{\text{CF}(15,\text{Co})}$$

$$\dot{D}'_{80.5}(11.4_{80},\text{Co}) \qquad\qquad\qquad \dot{D}'_{80.5}(11.4_{80},\text{Co})$$

$$\downarrow\quad\times\frac{80.5^2}{140.5^2} \qquad\qquad\qquad \downarrow\quad\times\frac{80.5^2}{150^2}$$

$$\dot{D}'_{140.5}(20_{140},\text{Co}) \qquad\qquad\qquad \dot{D}'_{150}(21.4_{150},\text{Co})$$

$$\downarrow\quad\times\text{PSF}(20,\text{Co}) \qquad\qquad \downarrow\quad\times\text{TAR}(10,21.4,\text{Co})$$

$$\dot{D}(0.5,20,140,\text{Co}) \qquad\qquad\qquad \dot{D}(10,20,140,\text{Co})$$

$$\downarrow\quad\times\text{PDD}(10,20,140,\text{Co})/100$$

$$\dot{D}(10,20,140,\text{Co})$$

where $\dot{D}'_{140.5}(20_{140},\text{Co})$ stands for the 'dose rate to small mass of water' at a distance of 140.5 cm from the source with the collimator set to give 20×20 cm^2 at 140 cm from the source, corresponding to 11.4×11.4 cm^2 at 80 cm from the source.

The general answer for the SSD approach is:

$$\frac{\dot{D}(10,20,140,\text{Co})}{\dot{D}(15,15,80,\text{Co})}$$

$$=\frac{\text{PDD}(10,20,140,\text{Co})}{\text{PDD}(15,15,80,\text{Co})}\times\frac{\text{PSF}(20,\text{Co})}{\text{PSF}(15,\text{Co})}\times\frac{\text{CF}(11.4,\text{Co})}{\text{CF}(15,\text{Co})}\times\frac{80.5^2}{140.5^2}$$

$$=\frac{\text{PDD}(10,20,140,\text{Co})}{\text{PDD}(15,15,80,\text{Co})}\times\frac{\text{RDF}(20,\text{Co})}{\text{RDF}(15,\text{Co})}\times\frac{\text{CF}(11.4,\text{Co})}{\text{CF}(20,\text{Co})}\times\frac{80.5^2}{140.5^2}$$

$$(6.76)$$

The general answer for the SAD approach is:

$$\frac{\dot{D}(10,20,140,\text{Co})}{\dot{D}(15,15,80,\text{Co})} = \frac{\text{TAR}(10,21.4,\text{Co})}{\text{TAR}(15,17.8,\text{Co})} \times \frac{\text{CF}(11.4,\text{Co})}{\text{CF}(15,\text{Co})} \times \frac{95^2}{150^2} \qquad (6.77)$$

Both answers with standard ^{60}Co machine data (see, for example, Br. J. Radiol. Suppl. 25) will yield for the ratio of the two dose rates 0.505 within ±1%.

In Eq. (6.74) we go to $\dot{D}'_{80.5}(11.4,\text{Co})$ from $\dot{D}(0.5,15,80,\text{Co})$ following a path that leads through $\dot{D}'_{80.5}(15_{80},\text{Co})$ as follows:

$$\dot{D}'_{80.5}(11.4,\text{Co}) = \dot{D}(0.5,15,80,\text{Co}) \times \frac{1}{\text{PSF}(15,\text{Co})} \times \frac{\text{CF}(11.4,\text{Co})}{\text{CF}(15,\text{Co})} \qquad (6.78)$$

We can also attain $\dot{D}'_{80.5}(11.4,\text{Co})$ by going in a phantom from $\dot{D}(0.5,15,80,\text{Co})$ to $\dot{D}(0.5,11.4,80,\text{Co})$ and then to $\dot{D}'_{80.5}(11.4_{80},\text{Co})$ as follows:

$$\dot{D}(0.5,15,80,\text{Co})$$
$$\downarrow \quad \times \frac{\text{RDF}(11.4,\text{Co})}{\text{RDF}(15,\text{Co})}$$
$$\dot{D}(0.5,11.4,80,\text{Co})$$
$$\downarrow \quad \times \frac{1}{\text{PSF}(11.4,\text{Co})}$$
$$\dot{D}'_{80.5}(11.4_{80},\text{Co}) \qquad (6.79)$$

Both paths, of course, will give identical end results, since, as can be shown using Eqs (6.29) and (6.31):

$$\frac{1}{\text{PSF}(15,\text{Co})} \times \frac{\text{CF}(11.4,\text{Co})}{\text{CF}(15,\text{Co})} = \frac{\text{RDF}(11.4,\text{Co})}{\text{RDF}(15,\text{Co})} \times \frac{1}{\text{PSF}(11.4,\text{Co})} \qquad (6.80)$$

6.16. SHUTTER CORRECTION TIME

In radiotherapy machines that use an electrical timer for measuring the dose delivery (radiotherapy X ray machines and teletherapy radioisotope machines), account must be taken of possible end effects (shutter correction

time) resulting from switching the beam on and off. In X ray machines the beam output builds up from zero to its full value as the generating voltage builds up in the first few seconds of the treatment. In isotope machines the source is moved into position at the start of the treatment and is returned to its safe position at the end of the treatment.

The shutter correction time τ_s is defined as the time that must be added to or subtracted from the calculated treatment time T_c to deliver accurately the prescribed dose to the patient. For a given therapy machine the shutter correction time is typically determined by measuring two doses (D_1 and D_n) at a given point P (e.g. at z_{max} in a phantom):

- D_1 is measured with a relatively long exposure time T (of the order of 5 min), contains one end effect and is given by $D_1 = \dot{D}(T + \tau_s)$ or $\dot{D} = D_1/(T + \tau_s)$.
- D_n is measured cumulatively with n dose segments, each having an exposure time T/n. The dose D_n thus contains n end effects; the cumulative beam-on time is again equal to T, and D_n is given by $D_n = \dot{D}(T + n\tau_s)$ or $\dot{D} = D_n/(T + n\tau_s)$.

Solving the equation for the true dose rate $\dot{D} = D_1/(T+\tau_s) = D_n/(T + n\tau_s)$ for the shutter correction time τ_s gives:

$$\tau_s = (D_n - D_1)T/(nD_1 - D_n) \tag{6.81}$$

In Eq. (6.81) $\tau_s > 0$ for $D_n > D_1$; $\tau_s = 0$ for $D_n = D_1$; and $\tau_s < 0$ for $D_n < D_1$. The time set on the timer will be $(T_c - \tau_s)$. Typical shutter correction times are of the order of 1 s.

BIBLIOGRAPHY

BRITISH JOURNAL OF RADIOLOGY, Central Axis Depth Dose Data for Use in Radiotherapy, Suppl. 25 (1996).

BURNS, D.T., DING, G.X., ROGERS, D.W.O., R_{50} as beam quality specifier for selecting stopping power ratios and reference depths for electrons, Med. Phys. **23** (1996) 383–388.

HENDEE, W.R., IBBOTT, G.S., Radiation Therapy Physics, Mosby, St. Louis, MI (1996).

JOHNS, H.E., CUNNINGHAM, J.R., The Physics of Radiology, Thomas, Springfield, IL (1984).

KHAN, F.M., The Physics of Radiation Therapy, Lippincott, Williams and Wilkins, Baltimore, MD (2003).

WILLIAMS, J.R., THWAITES, D.I. (Eds), Radiotherapy Physics in Practice, Oxford University Press, Oxford (2000).

Chapter 7

CLINICAL TREATMENT PLANNING IN EXTERNAL PHOTON BEAM RADIOTHERAPY

W. PARKER, H. PATROCINIO
Department of Medical Physics,
McGill University Health Centre,
Montreal, Quebec, Canada

7.1. INTRODUCTION

External photon beam radiotherapy is usually carried out with more than one radiation beam in order to achieve a uniform dose distribution inside the target volume and an as low as possible a dose in healthy tissues surrounding the target. ICRU Report No. 50 recommends a target dose uniformity within +7% and –5% of the dose delivered to a well defined prescription point within the target. Modern photon beam radiotherapy is carried out with a variety of beam energies and field sizes under one of two set-up conventions: a constant source to surface distance (SSD) for all beams or an isocentric set-up with a constant source to axis distance (SAD).

- In an SSD set-up, the distance from the source to the surface of the patient is kept constant for all beams, while for an SAD set-up the centre of the target volume is placed at the machine isocentre;
- Clinical photon beam energies range from superficial (30–80 kVp), through orthovoltage (100–300 kVp), to megavoltage energies (^{60}Co–25 MV);
- Field sizes range from small circular fields used in radiosurgery, through standard rectangular and irregular fields, to very large fields used for total body irradiation (TBI).

7.2. VOLUME DEFINITION

Volume definition is a prerequisite for meaningful 3-D treatment planning and for accurate dose reporting. ICRU Reports No. 50 and 62 define and describe several target and critical structure volumes that aid in the treatment planning process and that provide a basis for comparison of

219

treatment outcomes. The following volumes have been defined as principal volumes related to 3-D treatment planning: gross tumour volume (GTV), clinical target volume (CTV), internal target volume (ITV) and planning target volume (PTV). Figure 7.1 shows how the different volumes are related to each other.

7.2.1. Gross tumour volume

"*The Gross Tumour Volume (GTV) is the gross palpable or visible/ demonstrable extent and location of malignant growth*" (ICRU Report No. 50).

The GTV is usually based on information obtained from a combination of imaging modalities (computed tomography (CT), magnetic resonance imaging (MRI), ultrasound, etc.), diagnostic modalities (pathology and histological reports, etc.) and clinical examination.

7.2.2. Clinical target volume

"*The clinical target volume (CTV) is the tissue volume that contains a demonstrable GTV and/or sub-clinical microscopic malignant disease, which has to be eliminated. This volume thus has to be treated adequately in order to achieve the aim of therapy, cure or palliation*" (ICRU Report No. 50).
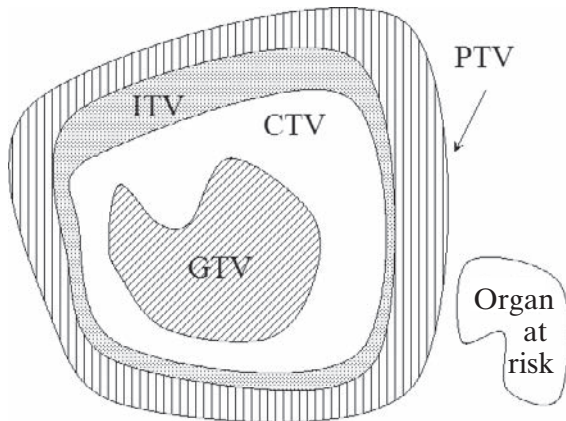
FIG. 7.1. Graphical representation of the volumes of interest, as defined in ICRU Reports No. 50 and 62.

The CTV often includes the area directly surrounding the GTV, which may contain microscopic disease and other areas considered to be at risk and requiring treatment (e.g. positive lymph nodes). The CTV is an anatomical–clinical volume and is usually determined by the radiation oncologist, often after other relevant specialists such as pathologists or radiologists have been consulted. The CTV is usually stated as a fixed or variable margin around the GTV (e.g. CTV = GTV + 1 cm margin), but in some cases it is the same as the GTV (e.g. prostate boost to the gland only).

There can be several non-contiguous CTVs, which may require different total doses to achieve treatment goals.

7.2.3. Internal target volume

The ITV consists of the CTV plus an internal margin. The internal margin is designed to take into account the variations in the size and position of the CTV relative to the patient's reference frame (usually defined by the bony anatomy); that is, variations due to organ motions such as breathing and bladder or rectal contents (ICRU Report No. 62).

7.2.4. Planning target volume

"*The planning target volume (PTV) is a geometrical concept, and it is defined to select appropriate beam arrangements, taking into consideration the net effect of all possible geometrical variations, in order to ensure that the prescribed dose is actually absorbed in the CTV*" (ICRU Report No. 50).

The PTV includes the internal target margin (ICRU Report No. 62) and an additional margin for set-up uncertainties, machine tolerances and intra-treatment variations. The PTV is linked to the reference frame of the treatment machine and is often described as the CTV plus a fixed or variable margin (e.g. PTV = CTV + 1 cm).

Usually a single PTV is used to encompass one or several CTVs to be targeted by a group of fields. The PTV depends on the precision of such tools as immobilization devices and lasers, but does not include a margin for the dosimetric characteristics of the radiation beam (i.e. penumbral areas and buildup region), as these will require an additional margin during treatment planning and shielding design.

7.2.5. Organ at risk

The organ at risk is an organ whose sensitivity to radiation is such that the dose received from a treatment plan may be significant compared with its tolerance, possibly requiring a change in the beam arrangement or a change in the dose.

Specific attention should be paid to organs that, although not immediately adjacent to the CTV, have a very low tolerance dose (e.g. the eye lens during nasopharyngeal or brain tumour treatments).

Organs with a radiation tolerance that depends on the fractionation scheme should be outlined completely to prevent biasing during treatment plan evaluation.

7.3. DOSE SPECIFICATION

A clearly defined prescription or reporting point along with detailed information regarding total dose, fractional dose and total elapsed treatment days allows for proper comparison of outcome results. Several dosimetric end points have been defined in ICRU Reports No. 23 and 50 for this purpose:

- Minimum target dose from a distribution or a dose–volume histogram (DVH).
- Maximum target dose from a distribution or a DVH.
- Mean target dose: the mean dose of all calculated target points (difficult to obtain without computerized planning).
- The ICRU reference point dose is located at a point chosen to represent the delivered dose using the following criteria:
  — The point should be located in a region where the dose can be calculated accurately (i.e. no buildup or steep gradients).
  — The point should be in the central part of the PTV.
  — The isocentre (or beam intersection point) is recommended as the ICRU reference point.
- Specific recommendations are made with regard to the position of the ICRU reference point for particular beam combinations:
  — For a single beam: the point on the central axis at the centre of the target volume.
  — For parallel opposed equally weighted beams: the point on the central axis midway between the beam entrance points.
  — For parallel opposed unequally weighted beams: the point on the central axis at the centre of the target volume.

— For other combinations of intersecting beams: the point at the intersection of the central axes (insofar as there is no dose gradient at this point).

7.4. PATIENT DATA ACQUISITION AND SIMULATION

7.4.1. Need for patient data

Patient data acquisition is an important part of the simulation process, since reliable data are required for treatment planning purposes and allow for a treatment plan to be properly carried out. The type of gathered data varies greatly, depending on the type of treatment plan to be generated (e.g. manual calculation of parallel opposed beams versus a complex 3-D treatment plan with image fusion). General considerations include:

- Patient dimensions are almost always required for treatment time or monitor unit (MU) calculations, whether read with a calliper, from CT slices or by other means;
- The type of dose evaluation dictates the amount of patient data required (e.g. DVHs require more patient information than a point dose calculation of organ dose);
- Landmarks such as bony or fiducial marks are required to match positions in the treatment plan with positions on the patient.

7.4.2. Nature of patient data

The patient information required for treatment planning varies from rudimentary to very complex, ranging from distances read on the skin, through manual determination of contours, to acquisition of CT information over a large volume, or even image fusion using various imaging modalities.

7.4.2.1. Two dimensional treatment planning

A single patient contour, acquired using lead wire or plaster strips, is transcribed on to a sheet of graph paper, with reference points identified. Simulation radiographs are taken for comparison with port films during treatment.

For irregular field calculations, points of interest can be identified on a simulation radiograph, and SSDs and depths of interest can be determined at

simulation. Organs at risk can be identified and their depths determined on simulator radiographs.

7.4.2.2. Three dimensional treatment planning

A CT data set of the region to be treated, with a suitable slice spacing (typically 0.5–1 cm for the thorax, 0.5 cm for the pelvis and 0.3 cm for the head and neck), is required.

An external contour (representative of the skin or immobilization mask) must be drawn on every CT slice used for treatment planning. The tumour and target volumes are usually drawn on CT slices by the radiation oncologist. Organs at risk and other structures should be drawn in their entirety if DVHs are to be calculated.

Figure 7.2 shows the typical outlining of target volume and organs at risk for a prostate treatment plan on one CT slice.

MRI or other studies are required for image fusion. With many contemporary treatment planning systems (TPSs), the user can choose to ignore inhomogeneities (often referred to as heterogeneities), perform bulk
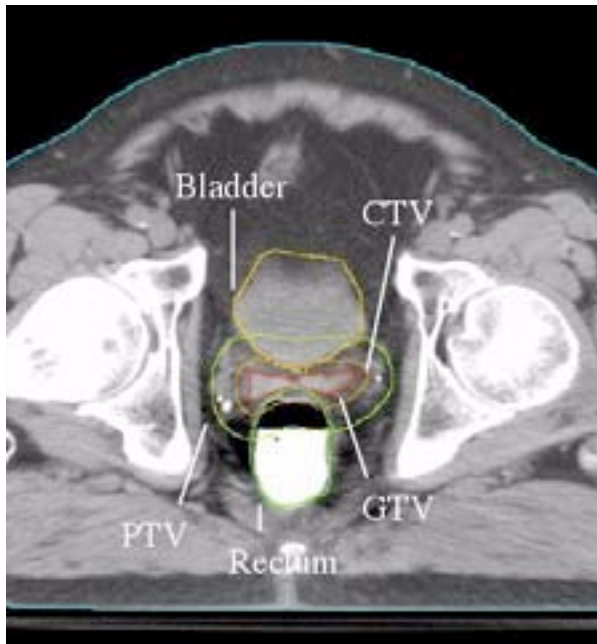
FIG. 7.2. Contours of GTV, CTV, PTV and organs at risk (bladder and rectum) have been drawn on this CT slice for a prostate treatment plan.

corrections on outlined organs or use the CT data themselves (with an appropriate conversion to electron density) for point to point correction.

Simulator radiographs or digitally reconstructed radiographs (DRRs) are used for comparison with portal films.

7.4.3. Treatment simulation

Patient simulation was initially developed to ensure that the beams used for treatment were correctly chosen and properly aimed at the intended target. At present, treatment simulation has a more expanded role in the treatment of patients, consisting of:

- Determination of the patient treatment position;
- Identification of the target volumes and organs at risk;
- Determination and verification of the treatment field geometry;
- Generation of simulation radiographs for each treatment beam for comparison with treatment port films;
- Acquisition of patient data for treatment planning.

The simplest form of simulation involves the use of port films obtained on the treatment machine prior to treatment in order to establish the treatment beam geometry. However, it is neither efficient nor practical to perform simulations on treatment units. Firstly, these machines operate in the megavoltage range of energies and therefore do not provide adequate quality radiographs for a proper treatment simulation, and, secondly, there is a heavy demand for the use of these machines for actual patient treatments, so using them for simulation is often considered an inefficient use of resources.

There are several reasons for the poor quality of port films obtained on treatment machines, such as the following:

— Most photon interactions with biological material in the megavoltage energy range are Compton interactions that are independent of atomic number and produce scattered photons that reduce contrast and blur the image.
— The large size of the radiation source (either the focal spot for a linac or the diameter of radioactive source in an isotope unit) increases the detrimental effects of beam penumbra on the image quality.
— Patient motion during the relatively long exposures required and the constraints on radiographic technique and equipment may contribute to poor image quality.

For the above reasons, dedicated equipment for radiotherapy simulation has been developed. Conventional simulation systems are based on treatment unit geometry in conjunction with diagnostic radiography and fluoroscopy systems. Modern simulation systems are based on CT or MR imagers and are referred to as CT simulators or MR simulators.

The clinical aspects of treatment simulation, be it with a conventional or CT simulator, rely on the positioning and immobilization of the patient as well as on the data acquisition and beam geometry determination.

7.4.4. Patient treatment position and immobilization devices

Depending on the patient treatment position or the precision required for beam delivery, patients may or may not require an external immobilization device for their treatment.

Immobilization devices have two fundamental roles:

● To immobilize the patient during treatment;
● To provide a reliable means of reproducing the patient's position from simulation to treatment, and from one treatment to another.

The simplest immobilization means include masking tape, Velcro belts or elastic bands. The basic immobilization device used in radiotherapy is the head rest, shaped to fit snugly under the patient's head and neck area, allowing the patient to lie comfortably on the treatment table. Figure 7.3 shows common headrests used for patient comfort and immobilization during treatment. Modern radiotherapy generally requires additional immobilization accessories during the treatment of patients.

FIG. 7.3. Headrests used for patient positioning and immobilization in external beam radiotherapy.

Patients to be treated in the head and neck or brain areas are usually immobilized with a plastic mask that, when heated, can be moulded to the patient's contour. The mask is affixed directly on to the treatment table or to a plastic plate that lies under the patient, thereby preventing movement. A custom immobilization mask is shown in Fig. 7.4.

For treatments to the thoracic or pelvic area, a variety of immobilization devices are available. Vacuum based devices are popular because of their reusability. Basically, a pillow filled with tiny Styrofoam balls is placed around the treatment area and a vacuum pump evacuates the pillow, leaving the patient's form as an imprint on the pillow. The result is that the patient can be positioned snugly and precisely on the pillow prior to every treatment. Another system, similar in concept, uses a chemical reaction between reagents in the pillow to form a rigid mould of the patient.

Special techniques, such as stereotactic radiosurgery, require such high precision that conventional immobilization techniques are inadequate. In radiosurgery, a stereotactic frame is attached to the patient's skull by means of screws and is used for target localization, patient set-up on the treatment machine and patient immobilization during the entire treatment procedure. The frame is bolted to the treatment table, thereby providing complete immobilization during the treatment.
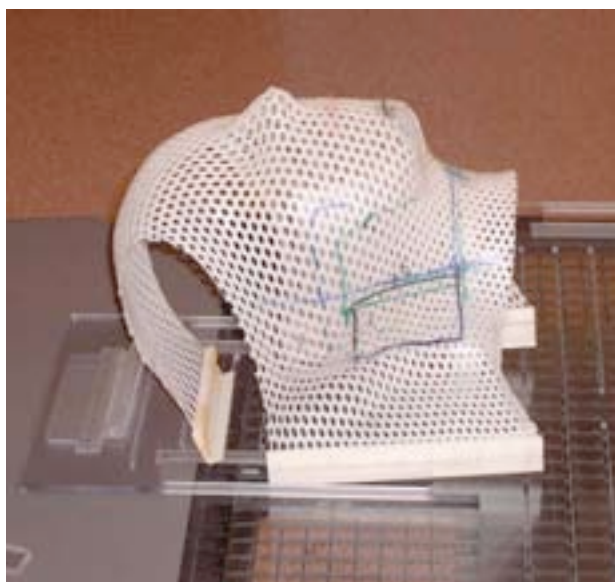
FIG. 7.4. Plastic mask used for immobilization of brain and head and neck patients.

7.4.5. Patient data requirements

In cases where only the dose along the central axis of the beam is sought (e.g. treatments with a direct field, or parallel and opposed fields, and a flat beam incidence), only the SSD is required, since a simple hand calculation for beam-on time or linac MUs may suffice.

Simple algorithms, such as Clarkson integration, may be used to determine the dosimetric effects of there being blocks in the fields, and to calculate the dose to off-axis points if their coordinates and SSD are measured. Since only point doses are calculated, the patient shape or contour off-axis is not required.

For simple computerized 2-D treatment planning, the patient's shape is represented by a single transverse skin contour through the central axis of the beams. This contour may be acquired by using lead wire or a plaster cast at the time of simulation.

The patient data requirements for more sophisticated TPSs, such as those used in conformal treatment planning, are more elaborate than those for 2-D treatment planning. They include the following:

- The external shape of the patient must be outlined in all areas where the beams enter and exit (for contour corrections) and in the adjacent areas (to account for scattered radiation);
- The targets and internal structures must be outlined in order to determine their shape and volume for dose calculation;
- The electron densities for each volume element in the dose calculation matrix must be determined if a correction for heterogeneities is to be applied;
- The attenuation characteristics of each volume element are required for image processing.

The nature and complexity of the data required for sophisticated treatment planning limits the use of manual contour acquisition. At the very best, patient external contour information can be obtained through this method.

Transverse CT scans contain all the information required for complex treatment planning and form the basis of CT simulation in modern radiotherapy treatment.

7.4.6. Conventional treatment simulation

7.4.6.1. Simulators

Simulators provide the ability to mimic most treatment geometries attainable on megavoltage treatment units and to visualize the resulting treatment fields on radiographs or under fluoroscopic examination of the patient. They consist of a gantry and table arrangement similar to that found on isocentric megavoltage treatment units, with the exception that the radiation source in a simulator is a diagnostic quality X ray tube rather than a high energy linac or a cobalt source. Some simulators have a special attachment that allows them to collect patient cross-sectional information similarly to a CT scanner; the combination is referred to as a CT simulator.

Figure 7.5 shows a photograph of a conventional treatment simulator.

The photons produced by the X ray tube are in the kilovoltage range and are preferentially attenuated by higher Z materials such as bone through photoelectric interactions. The result is a high quality diagnostic radiograph with limited soft tissue contrast but with excellent visualization of bony landmarks and high Z contrast agents.

A fluoroscopic imaging system may also be included and would be used from a remote console to view the patient's anatomy and to modify beam placement in real time.

FIG. 7.5. *A conventional treatment simulator has the capability to reproduce most treatment geometries available on radiotherapy treatment units. Simulators use a diagnostic X ray tube and fluoroscopic system to image the patient.*

7.4.6.2. Localization of the target volume and organs at risk

For the vast majority of sites the disease is not visible on the simulator radiographs, and therefore the block positions can be determined only with respect to anatomical landmarks visible on the radiographs (usually bony structures or lead wire clinically placed on the surface of the patient).

7.4.6.3. Determination of the treatment beam geometry

Typically, the patient is placed on the simulator table and the final treatment position of the patient is verified using the fluoroscopic capabilities of the simulator (e.g. the patient is straight on the table).

The position of the treatment isocentre, beam geometry (i.e. the gantry, table angles, etc.) and field limits are determined with respect to the anatomical landmarks visible under fluoroscopic conditions.

Once the final treatment geometry has been established, radiographs are taken as a matter of record and are used to determine shielding requirements for the treatment. Shielding can be drawn directly on the films, which may then be used as the blueprint for the construction of the blocks. A typical simulator radiograph is shown in Fig. 7.6.

Treatment time port films are compared with these radiographs periodically to ensure the correct set-up of the patient during the treatments.

7.4.6.4. Acquisition of patient data

After proper determination of the beam geometry, patient contours may be taken at any plane of interest to be used for treatment planning. Although more sophisticated devices exist, the simplest and most widely available method for obtaining a patient contour is through the use of lead wire. Typically, the wire is placed on the patient on a transverse plane parallel to the isocentre plane. The wire is shaped to the patient's contour and the shape is then transferred to a sheet of graph paper. Some reference to the room coordinate system must be marked on the contour (e.g. laser position) in order to relate the position of the beam geometry to the patient.

7.4.7. Computed tomography based conventional treatment simulation

7.4.7.1. Computed tomography based patient data acquisition

With the growing popularity of CT in the 1990s, the use of CT scanners in radiotherapy became widespread. Anatomical information on CT scans is

presented in the form of transverse slices, which contain anatomical images of very high resolution and contrast, based on the electron density.

CT images provide excellent soft tissue contrast, allowing for greatly improved tumour localization and definition in comparison with conventional simulation.

Patient contours can be obtained easily from the CT data — in particular, the patient's skin contour, target and any organs of interest. Electron density information, useful in the calculation of dose inhomogeneities due to the differing composition of human tissues, can also be extracted from the CT data set.

The target volume and its position are identified with relative ease on each transverse CT slice. The position of each slice and therefore the target can be related to bony anatomical landmarks through the use of scout or pilot images obtained at the time of CT scanning. Shown in Fig. 7.7 is a CT slice through a patient's neck used in CT based conventional simulation.

FIG. 7.6. A typical simulator radiograph for a head and neck patient. The field limits and shielding are clearly indicated on the radiograph.

FIG. 7.7. A CT image through a patient's neck. The target volume has been marked on the film by the physician.

Pilot or scout films relate CT slice position to anteroposterior (AP) and lateral radiographic views of the patient at the time of scanning (see Fig. 7.8). They are obtained by keeping the X ray source in a fixed position and moving the patient (translational motion) through the stationary slit beam. The result is a high definition radiograph that is divergent on the transverse axis but non-divergent on the longitudinal axis.

The target position relative to the bony anatomy on the simulator radiographs may then be determined through comparison with the CT scout or pilot films, keeping in mind the different magnifications between the simulator films and scout films. This procedure allows for a more accurate determination of tumour extent and therefore more precise field definition at the time of simulation.

If the patient is CT scanned in the desired treatment position prior to simulation, the treatment field limits and shielding parameters may be set with respect to the target position as determined from the CT slices.

7.4.7.2. Determination of the treatment beam geometry

The treatment beam geometry and any shielding required can now be determined indirectly from the CT data. The result is that the treatment port

more closely conforms to the target volume, reducing treatment margins around the target and increasing healthy tissue sparing.

7.4.8. Computed tomography based virtual simulation

7.4.8.1. Computed tomography simulator

Dedicated CT scanners for use in radiotherapy treatment simulation and planning are known as CT simulators. The components of a CT simulator include: a large bore CT scanner (with an opening of up to 85 cm to allow for a larger variety of patient positions and the placement of treatment accessories during CT scanning); room lasers, including a movable sagittal laser, allowing for patient positioning and marking; a flat table top to more closely match radiotherapy treatment positions; and a powerful graphics workstation, allowing for image manipulation and formation. An example of a modern CT simulator is shown in Fig. 7.9.

7.4.8.2. Virtual simulation

Virtual simulation is the treatment simulation of patients based solely on CT information. The premise of virtual simulation is that the CT data can be manipulated to render synthetic radiographs of the patient for arbitrary geometries. These radiographs, DRRs, can be used in place of simulator radiographs to determine the appropriate beam parameters for treatment. The

FIG. 7.8. Pilot or scout images relate slice position to radiographic landmarks.

FIG. 7.9. A dedicated radiotherapy CT simulator. Note the flat table top and the large bore (85 cm diameter). The machine was manufactured by Marconi, now Philips.

advantage of virtual simulation is that anatomical information may be used directly in the determination of treatment field parameters.

7.4.8.3. Digitally reconstructed radiographs

DRRs are produced by tracing ray lines from a virtual source position through the CT data of the patient to a virtual film plane. The sum of the attenuation coefficients along any one ray line gives a quantity analogous to optical density (OD) on a radiographic film. If the sums along all ray lines from a single virtual source position are then displayed on to their appropriate positions on the virtual film plane, the result is a synthetic radiographic image based wholly on the 3-D CT data set that can be used for treatment planning. Figure 7.10 provides an example of a typical DRR.

7.4.8.4. Beam's eye view

Beam's eye views (BEVs) are projections of the treatment beam axes, field limits and outlined structures through the patient on to the corresponding

FIG. 7.10. A DRR. Note that grey levels, brightness and contrast can be adjusted to provide an optimal image.

virtual film plane, and are frequently superimposed on to the corresponding DRRs, resulting in a synthetic representation of a simulation radiograph.

Field shaping is determined with respect to both the anatomy visible on the DRR and the outlined structures projected by the BEVs (see Fig. 7.11).

Multiplanar reconstructions (MPRs) are images formed from reformatted CT data. They are effectively CT images through arbitrary planes of the patient. Although typically sagittal or coronal MPR cuts are used for planning and simulation, MPR images through any arbitrary plane may be obtained.

7.4.8.5. Virtual simulation procedure

A CT simulation begins by placing the patient on the CT simulator table in the treatment position. The patient position is verified on the CT pilot or scout scans.

Prior to being scanned, it is imperative that patients be marked with a reference isocentre. Typically, a position near the centre of the proposed scan volume is chosen, radio-opaque fiducial markers are placed on the anterior and lateral aspects of the patient (with the help of the room lasers to ensure proper alignment) and the patient is tattooed to record the position of the fiducial markers to help with the subsequent patient set-up on the treatment machine.

FIG. 7.11. A DRR with superimposed BEV for a lateral field of a prostate patient.

This reference isocentre position can be used as the origin for a reference coordinate system from which the actual treatment isocentre position can be determined through translational motions of the table. The treatment isocentre can be identified on the patient through table motions and the use of a movable sagittal laser.

Target structures and organs of interest can be outlined directly on the CT images using tools available in the virtual simulation software. DRRs and BEVs created from the CT information and outlined data are used to simulate the treatment.

The determination of the treatment beam geometry and shielding is carried out with respect to the target position and critical organ location. Standard beam geometries (e.g. four field box, parallel opposed pair and lateral

oblique beams) can be used together with conformal shielding to increase the healthy tissue sparing. Alternatively, more unorthodox beam combinations can be used to maximize healthy tissue sparing in the event that a critical organ or structure is in the path of a beam.

It is imperative that when choosing beam geometries consideration be given to the prospective dose distributions. Additionally, the physical limitations of the treatment unit and its accessories with respect to patient position must be considered. For example, care must be taken that the gantry position does not conflict with the patient position.

Once a reasonable beam arrangement has been found, the field limits and shielding design may be obtained. Since the precise target location is known, the determination of the shielding design and treatment field limits becomes a matter of choosing an appropriate margin to account for physical and geometric beam effects such as beam penumbra.

Once the relevant treatment parameters have been obtained, the treatment beam geometry, the CT data including contours and the electron density information are transferred to the TPS for the calculation of the dose distribution.

7.4.9. Conventional simulator versus computed tomography simulator

The increased soft tissue contrast in combination with the axial anatomical information available from CT scans provides the ability to localize very precisely the target volumes and critical structures. The CT simulation phase allows for accurate identification and delineation of these structures directly on to the CT data set. This ability, in conjunction with the formation of DRRs and BEVs on which organs and targets are projected on to synthetic representations of simulator radiographs, allows the user to define treatment fields with respect to the target volume and critical structure location.

By contrast, conventional simulation requires knowledge of tumour position with respect to the visible landmarks on the diagnostic quality simulator radiographs. Since these radiographs provide limited soft tissue contrast, the user is restricted to setting field limits with respect to either the bony landmarks evident on the radiographs or anatomical structures visible with the aid of contrast agents such as barium.

Another important advantage of the CT simulation process over the conventional simulation process is the fact that the patient is not required to stay after the scanning has taken place. The patient only stays the minimum time necessary to acquire the CT data set, and this provides the obvious advantage that the radiotherapy staff may take their time in planning the
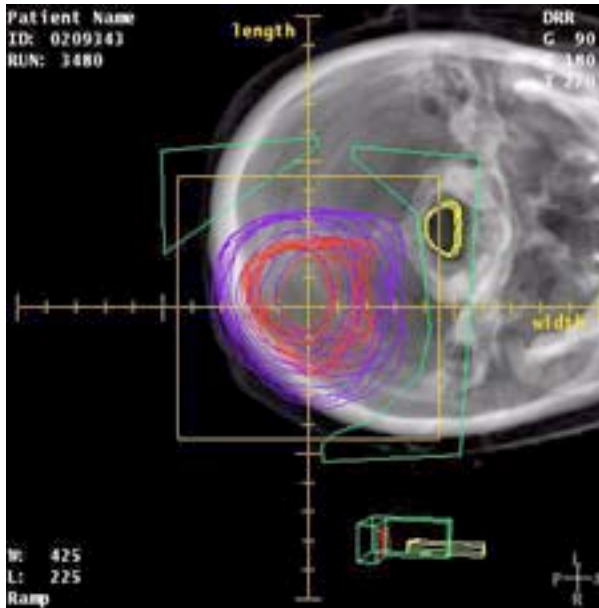
FIG. 7.12. A DRR with superimposed BEV for a vertex field of a brain patient. This treatment geometry would be impossible to simulate on a conventional simulator.

treatment as well as trying different beam configurations without the patient having to wait on the simulator table.

A CT simulator allows the user to generate DRRs and BEVs even for beam geometries that were previously impossible to simulate conventionally. Vertex fields, for example, obviously are impossible to plan on a conventional simulator because the film plane is in the patient (see Fig. 7.12).

There is some debate over whether there is a place in the radiotherapy clinic for a conventional simulator if a CT simulator is in place. Aside from the logistics and economics of having to CT scan every patient, there are certain sites where the use of CT simulation is not necessary (e.g. cord compression and bone and brain metastases). In addition, it is useful to perform a fluoroscopic simulation of patients after CT simulation in order to verify the isocentre position and field limits as well as to mark the patient for treatment. When patient motion effects such as breathing are of particular concern, a conventional simulation may be preferable.

7.4.10. Magnetic resonance imaging for treatment planning

The soft tissue contrast offered by MRI in some areas, such as the brain, is superior to that of CT, and allows small lesions to be seen with greater ease.

MRI alone, however, cannot be used for radiotherapy simulation and planning, for several reasons:

- The physical dimensions of the MRI scanner and its accessories limit the use of immobilization devices and compromise treatment positions;
- Bone signal is absent and therefore DRRs cannot be generated for comparison with portal films;
- There is no electron density information available for heterogeneity corrections on the dose calculations;
- MRI is prone to geometrical artefacts and distortions that may affect the accuracy of the dose distribution calculation and the treatment.

Many modern virtual simulation systems and TPSs have the ability to combine the information from different imaging studies using the process of image fusion or registration.

CT–MR image registration or fusion combines the accurate volume definition from MR with the electron density information available from CT. The MR data set is superimposed on the CT data set through a series of translations, rotations and scaling. This process allows the visualization of both studies side by side in the same imaging plane even if the patient has been scanned in a completely different treatment position. An example of CT–MR image fusion is presented in Fig. 7.13.
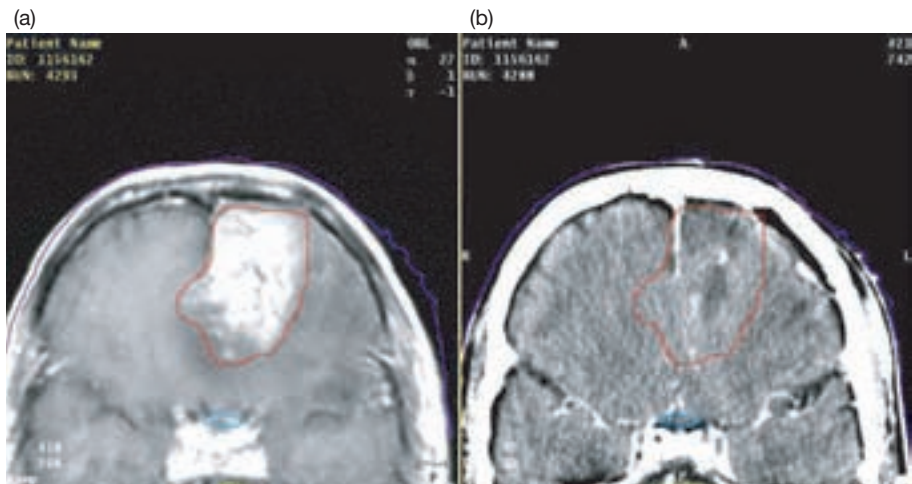
FIG. 7.13. (a) An MR image of a patient with a brain tumour. The target has been outlined and the result was superimposed on the patient's CT scan (b). Note that the particular target is clearly seen on the MR image but only portions of it are observed on the CT scan.

7.4.11. Summary of simulation procedures

Tables 7.1–7.3 summarize the conventional and virtual simulation processes.

TABLE 7.1. SUMMARY OF THE CONVENTIONAL SIMULATION PROCEDURE FOR A TYPICAL PATIENT (SIX STEPS)

Step	Conventional simulation procedure
1	Determination of patient treatment position with fluoroscopy
2	Determination of beam geometry
3	Determination of field limits and isocentre
4	Acquisition of contour
5	Acquisition of BEV and set-up radiographs
6	Marking of patient

TABLE 7.2. SUMMARY OF THE PROCEDURE FOR A TYPICAL PATIENT COMPUTED TOMOGRAPHY SIMULATION (NINE STEPS)

Step	CT simulation procedure
1	Determination of patient treatment position with pilot/scout films
2	Determination and marking of reference isocentre
3	Acquisition of CT data and transfer to virtual simulation workstation
4	Localization and contouring of targets and critical structures
5	Determination of treatment isocentre with respect to target and reference isocentre
6	Determination of beam geometry
7	Determination of field limits and shielding
8	Transfer of CT and beam data to the TPS
9	Acquisition of BEV and set-up DRRs

TABLE 7.3. GOALS OF PATIENT TREATMENT SIMULATION, AND THE TOOLS AVAILABLE FOR ACHIEVING THE GOALS IN CONVENTIONAL AND COMPUTED TOMOGRAPHY SIMULATION

Goal of patient simulation	Conventional simulation	CT simulation
Treatment position	Fluoroscopy	Pilot/scout views
Identification of target volume	Bony landmarks	From CT data
Determination of beam geometry	Fluoroscopy	BEV/DRR
Shielding design	Bony landmarks	Conformal to target
Contour acquisition	Manual	From CT data

7.5. CLINICAL CONSIDERATIONS FOR PHOTON BEAMS

7.5.1. Isodose curves

Isodose curves are lines that join points of equal dose. They offer a planar representation of the dose distribution and easily show the behaviour of one beam or a combination of beams with different shielding, wedges, bolus, etc.

Isodose curves can be measured in water directly or can be calculated from PDD and beam profile data. A set of isodose curves is valid for a given treatment machine, beam energy, SSD and field size.

While isodose curves can be made to display the actual dose in grays, it is more common to present them normalized to 100% at a fixed point. Two such common point normalizations are as follows:

- Normalization to 100% at the depth of dose maximum on the central axis;
- Normalization at the isocentre.

Figure 7.14 shows isodose curves superimposed on a transverse contour of a patient for the same beam. Figure 7.14(a) illustrates a distribution normalized at the depth of dose maximum z_{max}; the distribution in Fig. 7.14(b) is normalized at the isocentre.

7.5.2. Wedge filters

Three types of wedge filter are currently in use: manual, motorized and dynamic.

- A physical wedge is an angled piece of lead or steel that is placed in the beam to produce a gradient in radiation intensity. Manual intervention is required to place physical wedges on the treatment unit's collimator assembly.
- A motorized wedge is a similar device, a physical wedge integrated into the head of the unit and controlled remotely.
- A dynamic wedge produces the same wedged intensity gradient by having one jaw close gradually while the beam is on.

A typical isodose distribution for a wedged beam is shown is Fig. 7.15.

(a) (b)
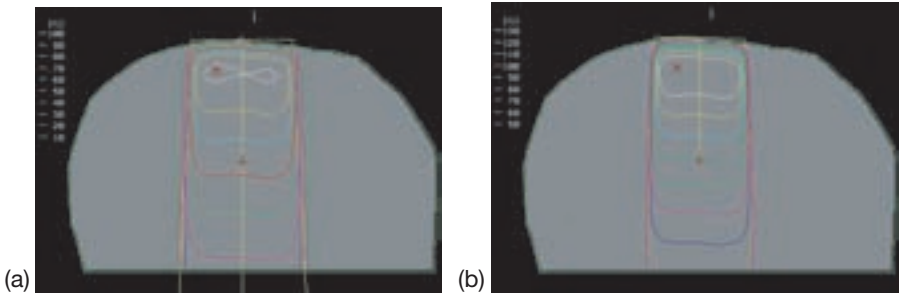
FIG. 7.14. A single 18 MV photon beam incident on a patient contour. Isodose curves are for (a) a fixed SSD beam normalized at the depth of dose maximum z_{max} and (b) an isocentric beam normalized at the isocentre.
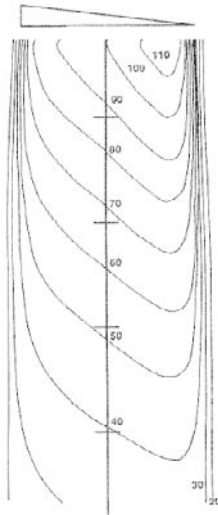
FIG. 7.15. Isodose curves for a wedged 6 MV photon beam. The isodoses have been normalized to z_{max} with the wedge in place.

(a)   (b)
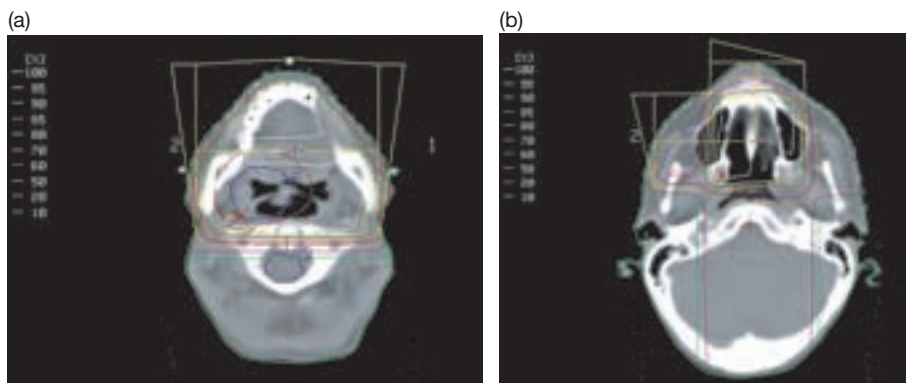
FIG. 7.16. Treatment plans illustrating two uses of wedge filters. In (a) two 15° wedges are used to compensate for the decreased thickness anteriorly. In (b) a wedged pair of beams is used to compensate for the hot spot that would be produced, with a pair of open beams at 90° to each other.

The following applies to all wedges:

- The thick end of the wedge is called the heel: the dose is lowest underneath this end. The other end is called the toe.
- The wedge angle is commonly defined as the angle between the 50% isodose line and the perpendicular to the beam central axis. Wedge angles in the range from 10° to 60° are commonly available.

There are two main uses of wedges:

— Wedges can be used to compensate for a sloping surface, as, for example, in nasopharyngeal treatments, in which wedges are used to compensate for decreased thickness anteriorly, as shown in Fig. 7.16. Figure 7.16(a) shows two wedged beams in a parallel opposed configuration, with the wedges used to compensate for missing tissue. Figure 7.16(b) shows two wedged beams at 90° to one another, with the wedges compensating for the hot spot near the surface.
— A wedge pair of beams is also useful in the treatment of relatively low lying lesions, in which two beams are placed at an angle (of less than 180°) called the hinge angle (see Fig. 7.17). The optimal wedge angle (assuming a flat patient surface) may be estimated from: 90° – 1/2 (hinge angle).

The wedge factor (WF) is defined as the ratio of dose at a specified depth (usually z_{max}) on the central axis with the wedge in the beam to the dose under

the same conditions without the wedge. This factor is used in MU calculations to compensate for the reduction in beam transmission produced by the wedge. The WF depends on the depth and field size.

7.5.3. Bolus

Bolus is a tissue equivalent material placed in contact with the skin to achieve one or both of the following: increase the surface dose and/or compensate for missing tissue.

To increase the surface dose, a layer of uniform thickness bolus is often used (0.5–1.5 cm), since it does not significantly change the shape of the isodose curves at depth. Several flab-like materials have been developed commercially for this purpose; however, cellophane wrapped wet towels or gauze offer low cost substitutes.

To compensate for missing tissue or a sloping surface, a custom made bolus can be built that conforms to the patient's skin on one side and yields a flat perpendicular incidence to the beam (see Fig. 7.18). The result is an isodose distribution that is identical to that produced on a flat phantom; however, skin sparing is not maintained. A common material used for this kind of bolus is wax, which is essentially tissue equivalent and when heated is malleable and can be fitted precisely to the patient's contour.

Bolus can also be used to compensate for lack of scatter, such as near the extremities or the head during TBI. Saline or rice bags can be used as bolus in these treatments.
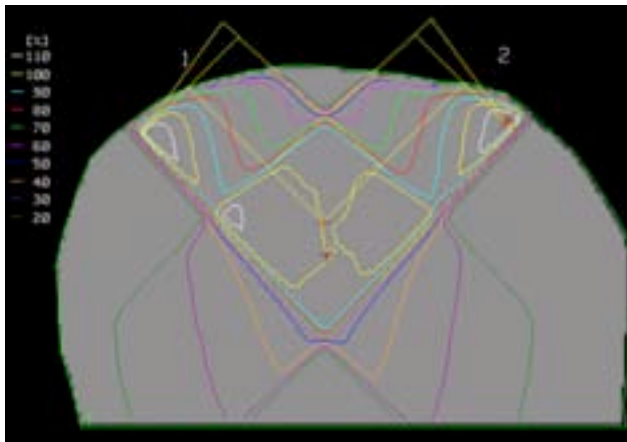
*FIG. 7.17. A wedge pair of 6 MV beams incident on a patient. The hinge angle is 90°
(orthogonal beams), for which the optimal wedge angle would be 45°. However, the additional obliquity of the surface requires the use of a higher wedge angle of 60°.*
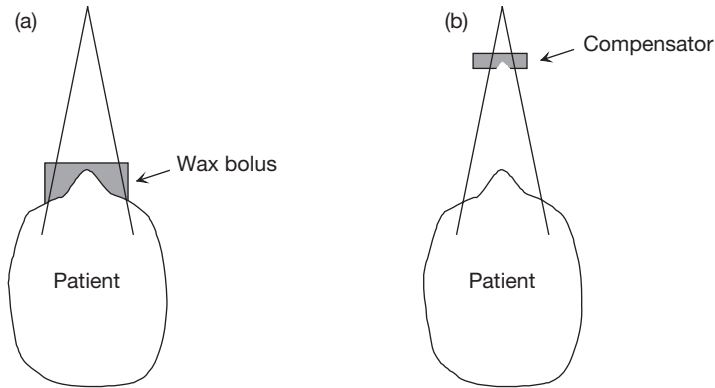
FIG. 7.18. Difference between a bolus and a compensating filter. In (a) a wax bolus is placed on the skin, producing a flat radiation distribution. Skin sparing is lost with bolus. In (b) a compensator achieving the same dose distribution as in (a) is constructed and attached to the treatment unit. Due to the large air gap, skin sparing is maintained.

7.5.4. Compensating filters

A compensating filter or compensator achieves the same effect on the dose distribution as a shaped bolus but does not cause a loss of skin sparing.

Compensating filters can be made of almost any material, but metals such as lead are the most practical and compact. They are usually placed in a shielding slot on the treatment unit head and can produce a gradient in two dimensions (such compensators are more difficult to make and are best suited for a computer controlled milling machine).

The closer to the radiation source the compensator is placed, the smaller the compensator. It is a simple case of demagnification with respect to the patient and source position to compensate for beam divergence. The dimensions of the compensator are simply scaled in length and width by the ratio of the SSD to the distance from the source to the compensator, as shown schematically in Fig. 7.18.

The thickness of the compensator is determined on a point by point basis depending on the reduction of the dose that is required at a certain depth of interest in the patient. The thickness of compensator x along the ray line above that point can be solved from the attenuation law $I/I_0 = \exp(-\mu x)$, where μ is the linear attenuation coefficient for the radiation beam and material used to construct the compensator.

The reduction in beam output through a custom compensator at z_{max} on the central axis needs to be measured and accounted for in MU/time calculations.

The use of compensating filters instead of bolus is generally more laborious and time consuming. Additionally, the resulting dose distribution cannot be readily calculated on most TPSs without measurement of the beam profile under the compensator and additional beam data entry into the TPS. Bolus, on the other hand, can be considered part of the patient contour, thus eliminating the need for measurement. The major advantage of a compensating filter over bolus is the preservation of the skin sparing effect.

7.5.5. Corrections for contour irregularities

Measured dose distributions apply to a flat radiation beam incident on a flat homogeneous water phantom. To relate such measurements to the actual dose distribution in a patient, corrections for irregular surface and tissue inhomogeneities have to be applied. Three methods for contour correction are used: the isodose shift method, the effective attenuation coefficient method and the tissue–air ratio (TAR) method.

7.5.5.1. Isodose shift method

A simple method, called the isodose shift method, can be used, in the absence of computerized approaches, for planning on a manual contour. The method is illustrated in Fig. 7.19.

- Grid lines are drawn parallel to the beam central axis all across the field.
- The tissue deficit (or excess) h is the difference between the SSD along a gridline and the SSD on the central axis.

TABLE 7.4. PARAMETER k USED IN THE ISODOSE SHIFT METHOD FOR CORRECTING ISODOSE DISTRIBUTIONS FOR AN IRREGULAR SURFACE

Photon energy (MV)	k (approximate)
<1	0.8
^{60}Co–5	0.7
5–15	0.6
15–30	0.5
>30	0.4

- k is an energy dependent parameter given in Table 7.4 for various photon beam energies.
- The isodose distribution for a flat phantom is aligned with the SSD central axis on the patient contour.
- For each gridline, the overlaid isodose distribution is shifted up (or down) such that the overlaid SSD is at a point $k \times h$ above (or below) the central axis SSD.
- The depth dose along the given gridline in the patient can now be read directly from the overlaid distribution.
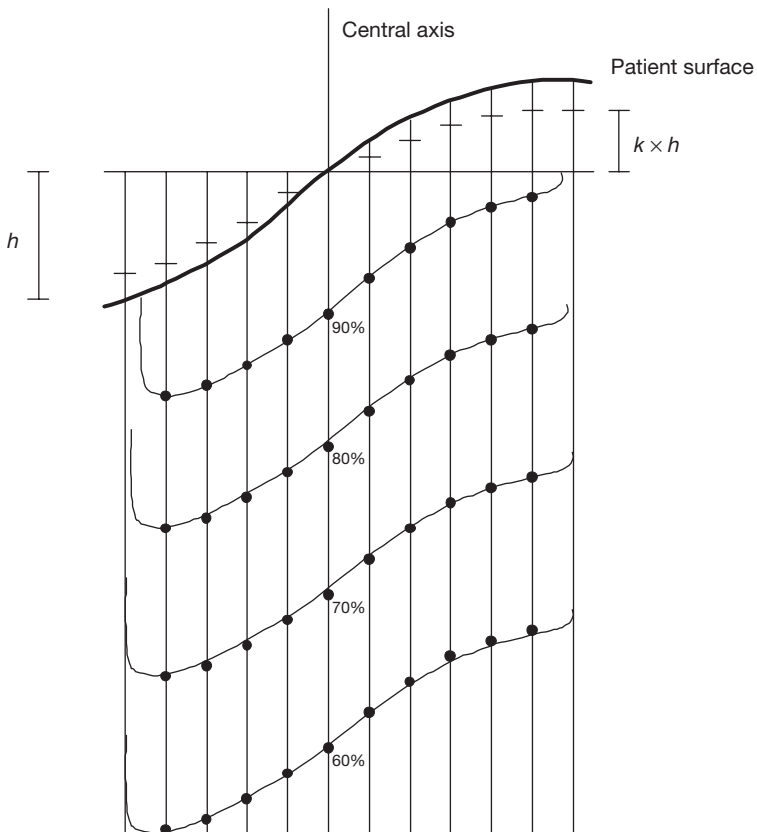
FIG. 7.19. Application of the isodose shift method for contour irregularity correction. The isodoses shown join the dose points calculated using the method (shown as solid black circles).

7.5.5.2. *Effective attenuation coefficient method*

A second method uses a correction factor known as the effective attenuation coefficient. The correction factor is determined from the attenuation factor $\exp(-\mu x)$, where x is the depth of missing tissue above the calculation point and μ is the linear attenuation coefficient of tissue for a given energy. For simplicity, the factors are usually precalculated and supplied in graphical or tabular form.

7.5.5.3. *Tissue–air ratio method*

The TAR correction method is also based on the attenuation law, but takes the depth of the calculation point and the field size into account. Generally, the correction factor C_F as a function of depth z, thickness of missing tissue h and field size A is given by:

$$C_F = \frac{TAR(z-h, A_Q)}{TAR(z, A_Q)} \tag{7.1}$$

7.5.6. Corrections for tissue inhomogeneities

In the most rudimentary treatment planning process, isodose charts and PDD tables are applied under the assumption that all tissues are water equivalent. In actual patients, however, the photon beam traverses tissues, such as fat, muscle, lung, air and bone, with varying densities and atomic numbers. Tissues with densities and atomic numbers different from those of water are referred to as tissue inhomogeneities or heterogeneities. Inhomogeneities in the patient result in:

- Changes in the absorption of the primary beam and associated scattered photons;
- Changes in electron fluence.

The importance of each effect depends on the position of the point of interest relative to the inhomogeneity. In the megavoltage range the Compton interaction dominates and its cross-section depends on the electron density (in electrons per cubic centimetre). The following four methods correct for the presence of inhomogeneities within certain limitations: the TAR method; the Batho power law method; the equivalent TAR method; and the isodose shift method. A sample situation is shown in Fig. 7.20, in which a layer of tissue of
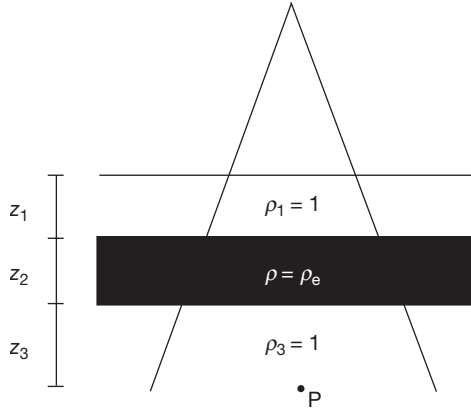
FIG. 7.20. An inhomogeneity nested between two layers of water equivalent tissue. Point P is on the central axis of the beam.

electronic density ρ_e relative to water is located between two layers of water equivalent tissue.

7.5.6.1. Tissue–air ratio method

The dose at an arbitrary point P below the inhomogeneity is corrected by:

$$C_F = \frac{TAR(z',r_d)}{TAR(z,r_d)} \tag{7.2}$$

where:

$$z' = z_1 + \rho_e z_2 + z_3$$

and

$$z = z_1 + z_2 + z_3$$

This method does not account for the position relative to the inhomogeneity. It also assumes that the homogeneity is infinite in lateral extent.

7.5.6.2. Batho power law method

The Batho power law method was initially developed by Batho and later generalized by Sontag and Cunningham.

The dose at an arbitrary point P below the inhomogeneity is corrected by:

$$C_F = \frac{\mathrm{TAR}(z_3, r_d)^{\rho_3 - \rho_2}}{\mathrm{TAR}(z, r_d)^{1 - \rho_2}} \qquad (7.3)$$

where, similarly to Eq. (7.2):

$$z = z_1 + z_2 + z_3$$

This method accounts for the position relative to the inhomogeneity. It still assumes that the homogeneity is infinite in lateral extent.

7.5.6.3. Equivalent tissue–air ratio method

The equivalent TAR method is similar to the TAR method outlined above, with the exception that the field size parameter is modified as a function of the relative density to correct for the geometrical position of the inhomogeneity with respect to the calculation point. The new dose at arbitrary point P is corrected by:

$$C_F = \frac{\mathrm{TAR}(z', r_d')}{\mathrm{TAR}(z, r_d)} \qquad (7.4)$$

where:

$$z' = z_1 + \rho_e z_2 + z_3$$

and

$$z = z_1 + z_2 + z_3$$

7.5.6.4. Isodose shift method

The isodose shift method for the dose correction due to the presence of inhomogeneities is essentially identical to the isodose shift method outlined in the previous section for contour irregularities.

Isodose shift factors for several types of tissue have been determined for isodose points beyond the inhomogeneity. The factors are energy dependent but do not vary significantly with field size.

The factors for the most common tissue types in a 4 MV photon beam are: air cavity: –0.6; lung: –0.4; and hard bone: 0.5. The total isodose shift is the thickness of inhomogeneity multiplied by the factor for a given tissue. Isodose curves are shifted away from the surface when the factor is negative.

7.5.7. Beam combinations and clinical application

Single photon beams are of limited use in the treatment of deep seated tumours, since they give a higher dose near the entrance at the depth of dose maximum than at depth. The guidelines for the use of a single photon beam in radiotherapy are as follows:

- A reasonably uniform dose to the target (±5%);
- A low maximum dose outside the target (<110%);
- No organs exceeding their tolerance dose.

Single fields are often used for palliative treatments or for relatively superficial lesions (depth < 5–10 cm, depending on the beam energy). For deeper lesions, a combination of two or more photon beams is usually required to concentrate the dose in the target volume and spare the tissues surrounding the target as much as possible.

7.5.7.1. Weighting and normalization

Dose distributions for multiple beams can be normalized to 100%, just as for single beams: at z_{max} for each beam or at the isocentre for each beam. This implies that each beam is equally weighted.

A beam weighting is applied at the normalization point for the given beam. A wedged pair with z_{max} normalization weighted 100:50% will show one beam with the 100% isodose at z_{max} and the other one with 50% at z_{max}. A similar isocentric weighted beam pair would show the 150% isodose at the isocentre.

7.5.7.2. Fixed source to surface distance versus isocentric techniques

Fixed SSD techniques require moving the patient such that the skin is at the correct distance (nominal SSD) for each beam orientation. Isocentric techniques require placing the patient such that the target (usually) is at the
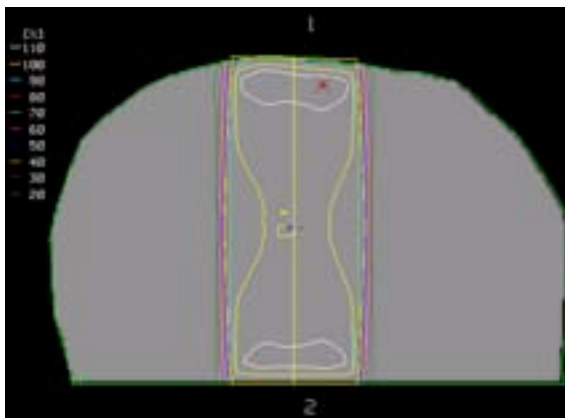
FIG. 7.21. *A parallel opposed beam pair is incident on a patient. Note the large rectangular area of relatively uniform dose (<15% variation). The isodoses have been normalized to 100% at the isocentre. This beam combination is well suited to a large variety of treatment sites (e.g. lung, brain, head and neck).*

isocentre. The machine gantry is then rotated around the patient for each treatment field.

Dosimetrically, there is little difference between these two techniques: fixed SSD arrangements are usually used at a greater SSD (i.e. the machine isocentre is on the patient's skin) than isocentric beams and therefore have a slightly higher PDD at depth. Additionally, beam divergence is smaller with SSD due to the larger distance.

These advantages are small and, with the exception of very large fields exceeding 40×40 cm^2, the advantages of a single set-up point (i.e. the isocentre) greatly outweigh the dosimetric advantage of SSD beams.

7.5.7.3. Parallel opposed beams

Parallel opposed beams overcome the difficulty of a decreasing dose gradient due to each individual beam. A decrease in the depth dose of one beam is partially compensated by an increase in the other. The resulting distribution has a relatively uniform distribution along the central axis. Figure 7.21 shows a distribution for parallel opposed beams normalized to the isocentre.

For small separations (<10 cm), low energy beams are well suited, since they have a sharp rise to a maximum dose and a relatively flat dose plateau in the region between both maximums.

For large separations (>15 cm), higher energy beams provide a more homogeneous distribution, whereas low energy beams can produce significant hot spots at the z_{max} locations of the two beams (>30%).

Many anatomical sites, such as lung lesions and head and neck lesions, can be adequately treated with parallel opposed beams.

7.5.7.4. Multiple coplanar beams

Multiple coplanar beams can be planned using a 2-D approach on a single plane, but their use allows for a higher dose in the beam intersection region. Common field arrangements include (see the two examples in Fig. 7.22):

- Wedge pair. Two beams with wedges (often orthogonal) are used to achieve a trapezoid shaped high dose region. This technique is useful in relatively low lying lesions (e.g. maxillary sinus and thyroid lesions).
- Four field box. A technique of four beams (two opposing pairs at right angles) producing a relatively high dose box shaped region. The region of highest dose now occurs in the volume portion that is irradiated by all four fields. This arrangement is used most often for treatments in the pelvis, where most lesions are central (e.g. prostate, bladder and uterus).
- Opposing pairs at angles other than 90° also result in the highest dose around the intersection of the four beams; however, the high dose area here has a rhombic shape.

(a)   (b)
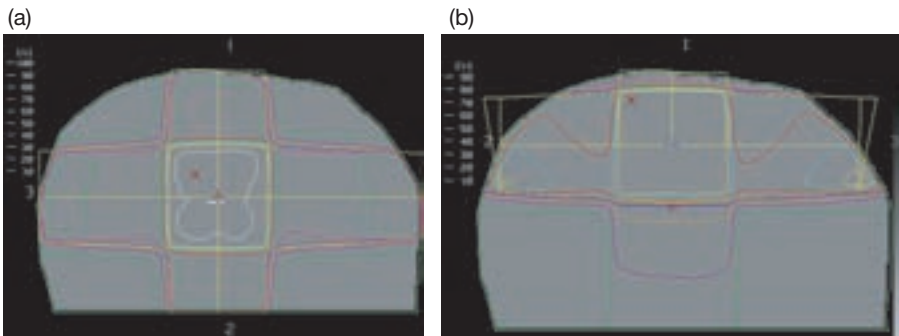
FIG. 7.22. Comparison of different beam geometries. A four field box (a) allows for a very high dose to be delivered at the intersection of the beams. A three field technique (b), however, requires the use of wedges to achieve a similar result. Note that the latter can produce significant hot spots near the entrance of the wedged beams and well outside the targeted area.

- Occasionally, three sets of opposing pairs are used, resulting in a more complicated dose distribution, but also in a spread of the dose outside the target over a larger volume (i.e. in more sparing of tissues surrounding the target volume).
- Three field box. A technique similar to a four field box for lesions that are closer to the surface (e.g. rectum). Wedges are used in the two opposed beams to compensate for the dose gradient in the third beam.

7.5.7.5. Rotational techniques

Rotational techniques produce a relatively concentrated region of high dose near the isocentre, but also irradiate a greater amount of normal tissue to lower doses than fixed field techniques. The target is placed at the isocentre, and the machine gantry is rotated about the patient in one or more arcs while the beam is on. A typical distribution achieved with two rotational arcs is shown in Fig. 7.23. It is a useful technique used mainly for prostate, bladder, cervix and pituitary lesions, particularly boost volumes.

The dose gradient at the edge of the field is not as sharp as that for multiple fixed field treatments. Skipping an angular region during the rotation allows the dose distribution to be pushed away from the region; however, this often requires that the isocentre be moved closer to this skipped area so that the resulting high dose region is centred on the target .
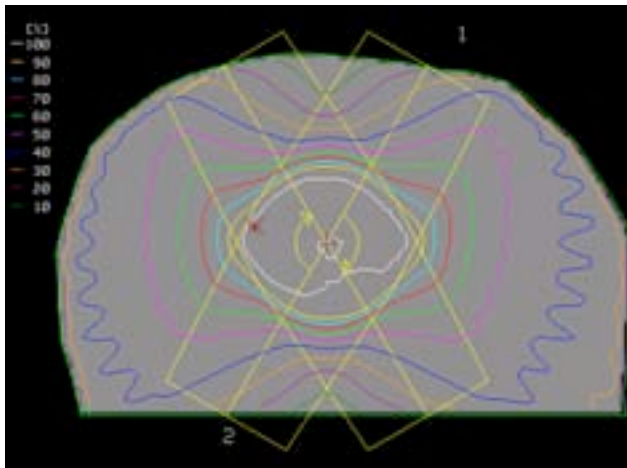
FIG. 7.23.   Isodose curves for two bilateral arcs of 120º each. The isodoses are tighter along the angles avoided by the arcs (anterior and posterior). The isodoses are normalized at the isocentre. Pelvic lesions such as prostate have been popular sites for the application of arc techniques.

The MU/time calculation uses the average TMR or TAR for the entire range of angles that the gantry covers during each arc.

7.5.7.6. Multiple non-coplanar beams

Non-coplanar beams arise from non-standard table angles coupled with gantry angulations; they may be useful when there is inadequate critical structure sparing from a conventional coplanar beam arrangement. Dose distributions from non-coplanar beam combinations yield similar dose distributions to conventional multiple field arrangements. Care must be taken when planning the use of non-coplanar beams to ensure that no collisions occur between the gantry and the patient or table.

Non-coplanar beams are most often used for treatments of the brain as well as of head and neck disease, where the target volume is frequently surrounded by critical structures.

Non-coplanar arcs are also used, the best known example being the multiple non-coplanar converging arcs technique used in radiosurgery.

7.5.7.7. Field matching

Field matching at the skin is the easiest field junctioning technique. However, due to beam divergence, this will lead to significant overdosing of tissues at depth and is only used in regions where tissue tolerance is not compromised. For most clinical situations field matching is performed at depth.

To produce a junction dose similar to that in the centre of open fields, beams must be junctioned such that their diverging edges match at the desired depth (i.e. their respective 50% isodose levels add up at that depth).

For two adjacent fixed SSD fields of different lengths L_1 and L_2, the surface gap g required to match the two fields at a depth z is (see Fig. 7.24):

$$\text{GAP} = 0.5L_1\left(\frac{z}{\text{SSD}}\right) + 0.5L_2\left(\frac{z}{\text{SSD}}\right) \tag{7.5}$$

For adjacent fields with isocentric beams and a sloping surface, a similar expression can be developed using similar triangle arguments.

7.6. TREATMENT PLAN EVALUATION

After the dose calculations are performed by dosimetrists or medical physicists on a computer or by hand, a radiation oncologist evaluates the plan. The dose distribution may be obtained for:

- A few significant points within the target volume;
- A grid of points over a 2-D contour or image;
- A 3-D array of points that covers the patient's anatomy.

The treatment plan evaluation consists of verifying the treatment portals and the isodose distribution for a particular treatment:

— The treatment portals (usually through simulation radiographs or DRRs) are verified to ensure that the desired PTV is targeted adequately.
— The isodose distribution (or the other dose tools discussed in this section) is verified to ensure that target coverage is adequate and that critical structures surrounding the PTV are spared as necessary.

The following tools are used in the evaluation of the planned dose distribution:

(i) Isodose curves;
(ii) Orthogonal planes and isodose surfaces;
(iii) Dose distribution statistics;
(iv) Differential DVHs;
(v) Cumulative DVHs.
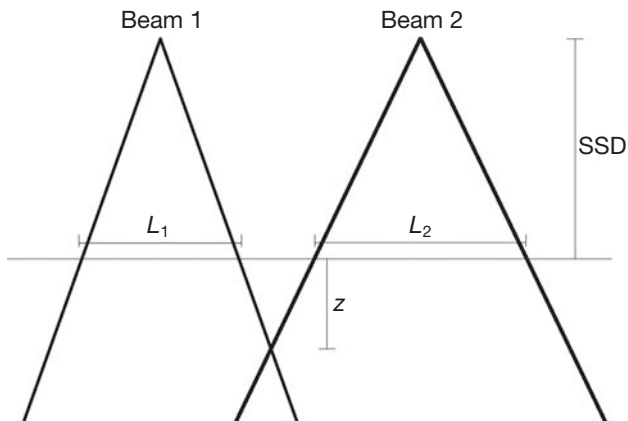
FIG. 7.24. Two adjacent fields matched at a depth z.

7.6.1. Isodose curves

Isodose curves, of which several examples were given in Section 7.5, are used to evaluate treatment plans along a single plane or over several planes in the patient. The isodose covering the periphery of the target is compared with the isodose at the isocentre. If the ratio is within a desired range (e.g. 95–100%), the plan may be acceptable provided that critical organ doses are not exceeded. This approach is ideal if the number of transverse slices is small.

7.6.2. Orthogonal planes and isodose surfaces

When a larger number of transverse planes are used for calculation (such as with a CT scan) it may be impractical to evaluate the plan on the basis of axial slice isodose distributions alone. In such cases, isodose distributions can also be generated on orthogonal CT planes, reconstructed from the original axial data. Sagittal and coronal plane isodose distributions are available on most 3-D TPSs, and displays on arbitrary oblique planes are becoming increasingly common.

An alternative way to display isodoses is to map them in three dimensions and overlay the resulting isosurface on a 3-D display featuring surface renderings of the target and/or other organs. An example of such a display is shown in Fig. 7.25. While such displays can be used to assess target coverage, they do not convey a sense of distance between the isosurface and the anatomical volumes and give no quantitative volume information.

7.6.3. Dose statistics

In contrast to the previous tools, the plan evaluation tools described here do not show the spatial distribution of dose superimposed on CT slices or on anatomy that has been outlined based on CT slices. Instead, they provide quantitative information on the volume of the target or critical structure and on the dose received by that volume. From the matrix of doses to each volume element within an organ, key statistics can be calculated. These include:

- The minimum dose to the volume;
- The maximum dose to the volume;
- The mean dose to the volume;
- The dose received by at least 95% of the volume;
- The volume irradiated to at least 95% of the prescribed dose.

The final two statistics are only relevant for a target volume. Organ dose statistics such as these are especially useful in dose reporting, since they are simpler to include in a patient chart than the DVHs described below.

7.6.4. Dose–volume histograms

A 3-D treatment plan consists of dose distribution information over a 3-D matrix of points over the patient's anatomy. DVHs summarize the information contained in the 3-D dose distribution and are extremely powerful tools for quantitative evaluation of treatment plans.

In its simplest form a DVH represents a frequency distribution of dose values within a defined volume that may be the PTV itself or a specific organ in the vicinity of the PTV. Rather than displaying the frequency, DVHs are usually displayed in the form of 'per cent volume of total volume' on the ordinate against the dose on the abscissa.
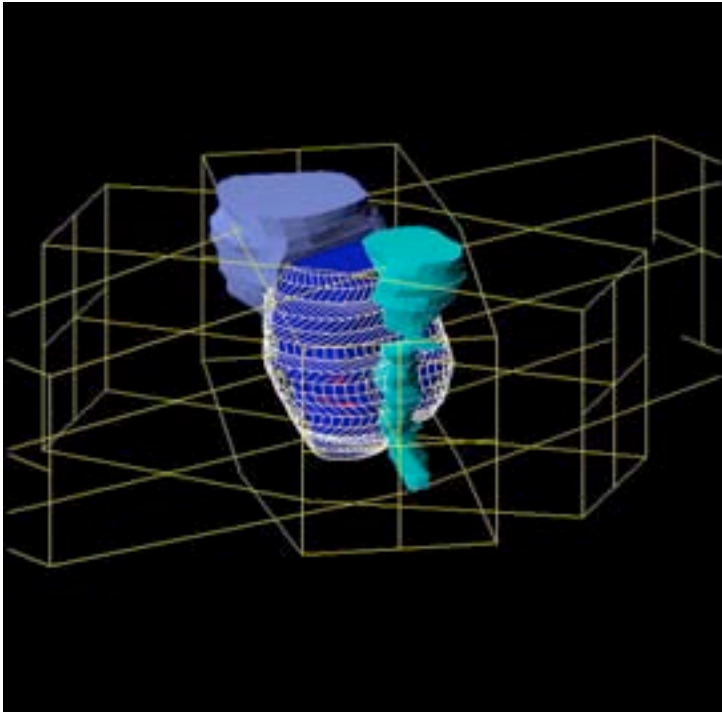
FIG. 7.25. A 3-D plot of the prescription isodose (white wireframe) is superimposed on the target volume, with the bladder and the rectum shown. The individual beams are also shown.

Two types of DVH are in use:

- Direct (or differential) DVHs;
- Cumulative (or integral) DVHs.

The main drawback of DVHs is the loss of spatial information that results from the condensation of data when DVHs are calculated.

7.6.4.1. Direct dose–volume histogram

To create a direct DVH, the computer sums the number of voxels with an average dose within a given range and plots the resulting volume (or more frequently the percentage of the total organ volume) as a function of dose. An example of a direct DVH for a target is shown in Fig. 7.26(a). The ideal DVH for a target volume would be a single column indicating that 100% of the volume receives the prescribed dose. For a critical structure, the DVH may contain several peaks, indicating that different parts of the organ receive different doses. In Fig. 7.26(b) an example of a DVH for a rectum in the treatment of the prostate using a four field box technique is shown.

7.6.4.2. Cumulative dose–volume histogram

Traditionally, physicians have sought to answer questions such as: "How much of the target is covered by the 95% isodose line?" In 3-D treatment planning this question is equally relevant and the answer cannot be extracted directly from a direct DVH, since it would be necessary to determine the area
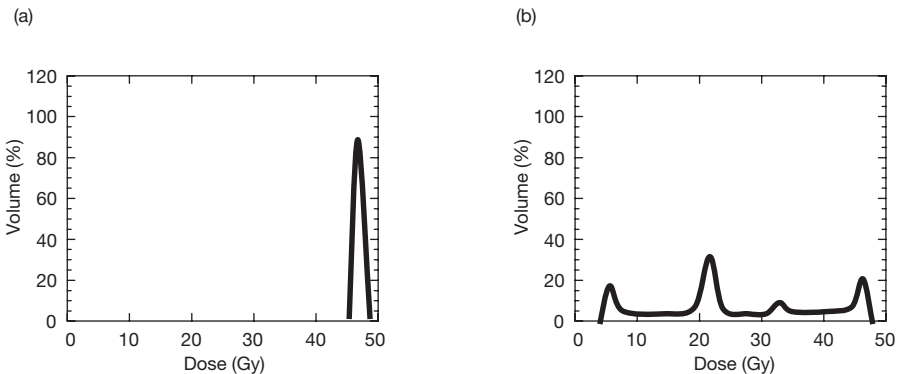
FIG. 7.26. Differential DVHs for a four field prostate treatment plan for (a) the target volume and (b) the rectum. The ideal target differential DVHs would be infinitely narrow peaks at the target dose for the PTV and at 0 Gy for the critical structure.

under the curve for all dose levels above 95% of the prescription dose. For this reason, cumulative DVH displays are more popular.

- The computer calculates the volume of the target (or critical structure) that receives at least the given dose and plots this volume (or percentage volume) versus dose;
- All cumulative DVH plots start at 100% of the volume for 0 Gy, since all of the volume receives at least no dose.

For the same organs as indicated in the example of Fig. 7.26, Fig. 7.27 shows the corresponding cumulative DVH (both structures are now shown on the same plot). While displaying the per cent volume versus dose is more popular, it is useful in some circumstances to plot the absolute volume versus dose. For example, if a CT scan does not cover the entire volume of an organ such as the lung, and the unscanned volume receives very little dose, then a DVH showing the percentage volume versus dose for that organ will be biased, indicating that a larger percentage of the volume receives dose. Furthermore, in the case of some critical structures, tolerances are known for irradiation of fixed volumes specified in cubic centimetres.

7.6.5. Treatment evaluation

Treatment evaluation consists of:

- Verifying the treatment portals (through port films or on-line portal imaging methods) and comparing these with simulator radiographs or DRRs;
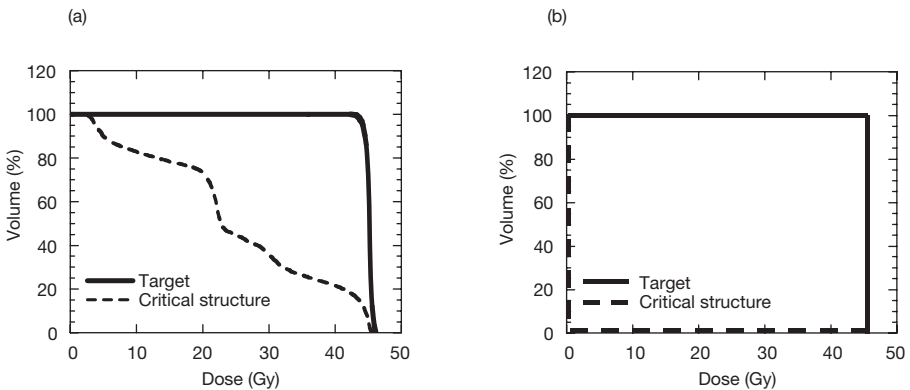
FIG. 7.27. Cumulative DVHs for the same four field prostate treatment plan used in Fig. 7.26. The ideal cumulative DVHs are shown in (b).

● Performing in vivo dosimetry through the use of diodes, thermoluminescent dosimeters (TLDs) and other detectors.

The latter methods are complex, often difficult to use in vivo and are beyond the scope of this section. Portal imaging, either through port films or on-line systems, provides relatively simpler ways of ensuring that the treatment has been successfully delivered.

7.6.5.1. Port films

A port film is usually an emulsion type film, often still in its light-tight paper envelope, that is placed in the radiation beam beyond the patient. Depending on the sensitivity to radiation (or speed), port films can be used in one of two ways:

● Localization: a fast film (requiring only a few centigrays to expose) is placed in each beam at the beginning or end of the treatment to verify that the patient installation is correct for the given beam.
● Verification: a slow film is placed in each beam and left there for the duration of the treatment. In this case any patient or organ movement during treatment will most likely affect the quality of the film.

Fast films generally produce a better image and are recommended for verifying small or complex beam arrangements. Slow films are recommended for larger fields, for example where as many as four films may be required to verify the treatment delivery.

Localization films used in radiotherapy do not require intensifying screens such as those used in diagnostic radiology. Instead, a single thin layer of a suitable metal (such as copper or aluminium) is used in front of the film (beam entry side) to provide electronic buildup, which will increase the efficiency of the film. A backing layer is sometimes used with double emulsion films to provide backscatter electrons. Since there is no conversion of X rays to light photons, as in diagnostic films, the films need not be removed from the envelope.

Port films can be taken either in single or double exposure techniques.

— Single exposure: the film is irradiated with the treatment field alone. This technique is well suited to areas where the anatomical features can clearly be seen inside the treated field. Practically all verification films are single exposure.

— Double exposure: the film is irradiated with the treatment field first, then the collimators are opened to a wider setting (usually 5–10 cm beyond each field limit) and all shielding is removed. A second exposure of typically 1–2 MUs is then given to the film. The resulting image shows not only the treated field but also some of the surrounding anatomy, which may be useful in verifying the beam position. Figure 7.28 shows a typical double exposure port film.

7.6.5.2. On-line portal imaging

On-line portal imaging systems consist of a suitable radiation detector, usually attached through a manual or semirobotic arm to the linac, and are capable of transferring the detector information to a computer that will process it and convert it to an image. These systems use a variety of detectors, all producing computer based images of varying degrees of quality.
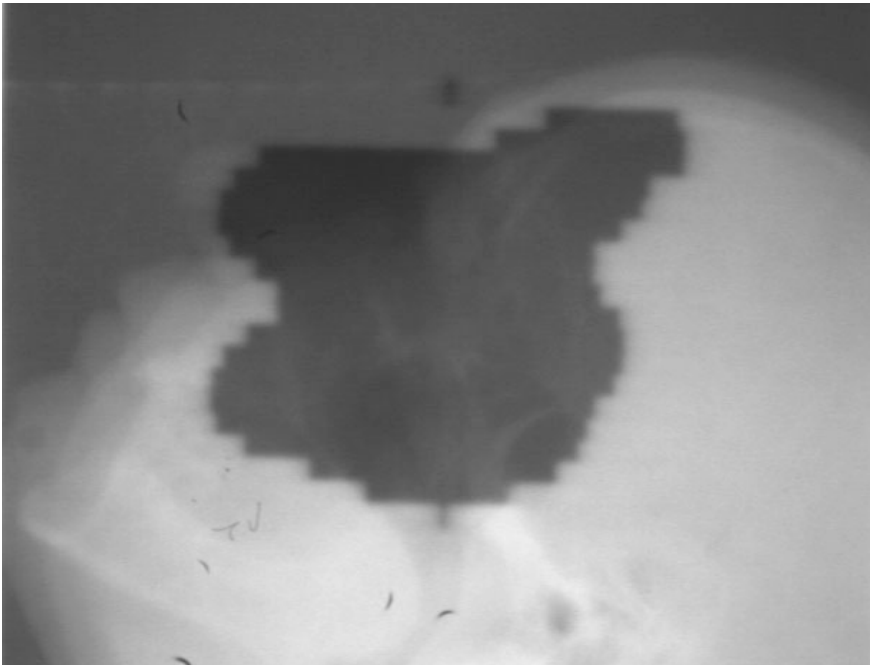
FIG. 7.28. Port film for a lateral field used in a treatment of the maxillary sinus. This double exposure radiograph allows the physician to visualize both the treatment field and the surrounding anatomy.

Currently these systems include:

- Fluoroscopic detectors;
- Ionization chamber detectors;
- Amorphous silicon detectors.

Fluoroscopic portal imaging detectors have the following characteristics:

— They work on the same principle as a simulator image intensifier system.
— The detector consists of a combination of a metal plate and fluorescent phosphor screen, a 45º mirror and a television camera.
— The metal plate converts incident X rays to electrons and the fluorescent screen converts electrons to light photons.
— The mirror deflects light to the TV camera, reducing the length of the imager, and the TV camera captures a small fraction (<0.1%) of the deflected light photons to produce an image.
— They have good spatial resolution (depending on phosphor thickness).
— They require only a few MUs to produce an image.
— They use technology that has been used in many other fields.

Matrix ionization chamber detectors have the following characteristics:

 (i) They are based on a grid of ionization chamber type electrodes that measure ionization from point to point.
 (ii) The detector consists of two metal plates, 1 mm apart, with the gap filled with isobutene. Each plate is divided into 256 electrodes and the plates are orientated such that the electrodes on one plate are at 90º to the electrodes on the other.
(iii) A voltage is applied between two electrodes across the gap and the ionization at the intersection is measured. By selecting each electrode on each plate in turn, a 2-D ionization map is obtained and converted to a greyscale image of 256×256 pixels.
(iv) The maximum image size is usually smaller than that of fluoroscopic systems.

Amorphous silicon detectors have the following characteristics:

(a) They have a solid state detector array consisting of amorphous silicon photodiodes and field effect transistors arranged in a large rectangular matrix.

(b) They use a metal plate–fluorescent phosphor screen combination like the fluoroscopic systems. Light photons produce electron–hole pairs in the photodiodes, whose quantity is proportional to the intensity, allowing an image to be obtained.

(c) They produce an image with a greater resolution and contrast than the other systems.

7.7. TREATMENT TIME AND MONITOR UNIT CALCULATIONS

Treatment time and MU calculations are an important component of the dose delivery process since they determine the number of MUs (for linacs) and time (for isotope teletherapy and orthovoltage machines) of beam-on for each individual beam of the treatment plan.

The patient treatments are carried out with either a fixed SSD or an isocentric technique. Each of the two techniques is characterized with a specific dose distribution and treatment time or MU calculation. The fixed SSD technique results in an isodose distribution that is governed by PDDs resulting from a well defined dose delivery to points P at the depth of dose maximum for each of the beams in the treatment plan. The weight (W) ranging from 0 to 1.0 applied for a given beam actually determines the dose delivered to point P for the particular beam. $W = 1$ implies a dose of 100 cGy to point P, $W = 0.65$ implies a dose of 65 cGy to point P, etc.

The isocentric technique, on the other hand, results in a dose distribution that is most often governed by TMRs normalized in such a way that each beam of the treatment plan delivers a prescribed fraction of the total dose at the isocentre. Other functions, such as TARs or tissue–phantom ratios (TPRs), are also sometimes used in isocentric dose distribution calculations.

Calculations of treatment time or MUs for both the fixed SSD and the isocentric technique depend on the basic treatment machine output calibration, which is discussed in Chapter 9. For megavoltage photon machines, the output is most commonly stipulated in cGy/MU for linacs and in cGy/min for cobalt units under conditions that may be summarized as follows:

- Measured in a water phantom;
- Measured on the central axis of the radiation beam;
- Stated for point P at the depth of maximum dose;
- Measured with a field size of 10×10 cm^2;
- Measured at the nominal SSD f of the unit (most commonly 100 cm).
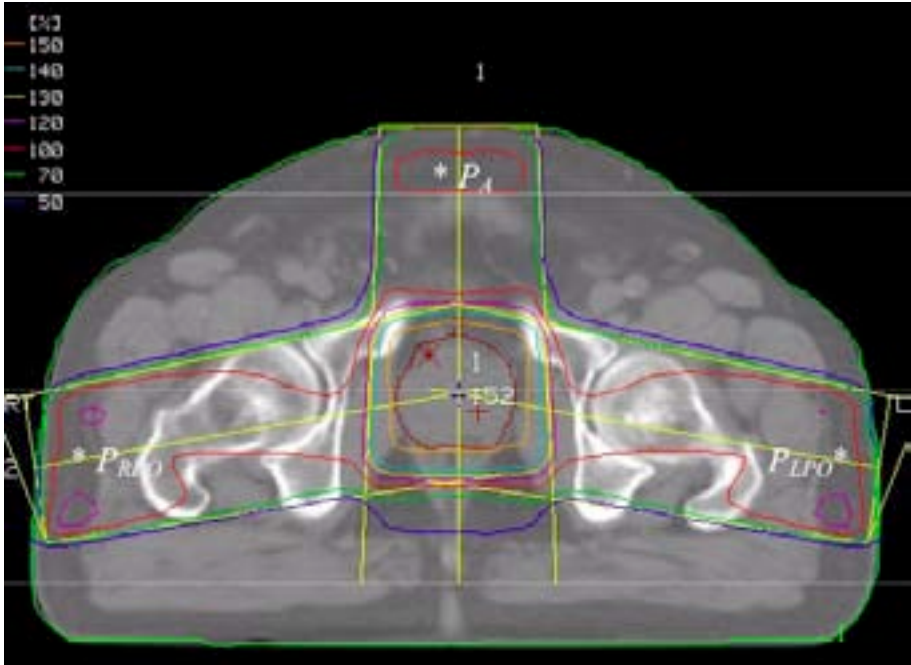
FIG. 7.29. Fixed SSD isodose distribution for a three field treatment of the prostate.

The output may be designated by $\dot{D}(z_{max}, 10, f, h\nu)$ and is used directly in meter-set calculations involving fixed SSD techniques.

For cobalt units the output $\dot{D}(z_{max}, 10, f, h\nu)$ is measured and quoted as the dose rate in cGy/min. The sensitivity of linac monitor chambers, on the other hand, is usually adjusted in such a way that $\dot{D}(z_{max}, 10, f, h\nu) = 1$ cGy/MU.

When used in isocentric calculations, $\dot{D}(z_{max}, 10, f, h\nu)$ must be corrected by the inverse square factor (ISF) unless the machine is actually calibrated at the isocentre:

$$\text{ISF} = \left(\frac{f + z_{max}}{f} \right)^2 \tag{7.6}$$

7.7.1. Treatment time and monitor unit calculations for a fixed source to surface distance set-up

Figure 7.29 shows a typical dose distribution obtained for a three field prostate boost treatment with a fixed SSD (100 cm) technique on a 6 MV linac. The three treatment fields have the following characteristics:

- Anterior field: 7.5×7.5 cm^2 open field with $W = 1.0$.
- Left posterior oblique (LPO) field: 6.5×7.5 cm^2 wedged field with $W = 0.8$ and WF = 0.53.
- Right posterior oblique (RPO) field: 6.5×7.5 cm^2 wedged field with $W = 0.8$ and WF = 0.53.

The dose $D(Q)$ of 200 cGy is prescribed at the ICRU reference point, located at the intersection of the three fields.

As shown in Fig. 7.29, the isodose line (IL) through the ICRU reference point is 152%, the maximum dose is 154% and the 150% isodose curve completely covers the PTV.

The PTV dose is thus between +2% and –2% of the $D(Q)$ dose, fulfilling well the recommendation that the target doses should lie between +7% and –5% of the dose prescribed at the ICRU reference point.

The dose distribution shown in Fig. 7.29 delivers a dose of 152 cGy to the ICRU reference point Q under the following conditions:

— A dose of 100 cGy is delivered at a point P_A ($W = 1$ for the anterior field);
— A dose of 80 cGy is delivered at a point P_{LPO} ($W = 0.8$ for the LPO field);
— A dose of 80 cGy is delivered at a point P_{RPO} ($W = 0.8$ for the RPO field).

Thus to obtain the prescribed dose of 200 cGy rather than 152 cGy at point Q, doses of $D(P_A) = 131.6$ cGy, $D(P_{LPO}) = 105.3$ cGy and $D(P_{RPO}) = 105.3$ cGy should be delivered to points P_A, P_{LPO} and P_{RPO}, respectively. The doses at points P for individual beams are often referred to as the given doses for a particular field in the fixed SSD treatment plan and are determined as follows:

$$D(P_A) = \frac{D(Q) \times 100 \times W_A}{IL} = \frac{200 \text{ cGy} \times 100 \times 1.0}{152} = 131.6 \text{ cGy} \qquad (7.7)$$

$$D(P_{LPO}) = \frac{D(Q) \times 100 \times W_{LPO}}{IL} = \frac{200 \text{ cGy} \times 100 \times 0.8}{152} = 105.3 \text{ cGy} \qquad (7.8)$$

$$D(P_{RPO}) = \frac{D(Q) \times 100 \times W_{RPO}}{IL} = \frac{200 \text{ cGy} \times 100 \times 0.8}{152} = 105.3 \text{ cGy} \qquad (7.9)$$

The next step is to calculate the linac monitor chamber setting in MUs required for the delivery of the given doses for each of the three fields constituting the fixed SSD treatment plan. The given dose rates for points P_A, P_{LPO} and P_{RPO} are obtained by multiplying the basic linac output with the RDF(A),

where A refers to the appropriate field size (see Section 6.6.4), and any other applicable transmission factors (such as the WF or the tray factor).

The monitor settings $\mathcal{MU}$ for points P_A, P_{LPO} and P_{RPO} are calculated as follows:

$$\mathcal{MU}(A) = \frac{D(P_A)}{\dot{D}(z_{max}, 10, 100, hv) \times RDF(A, hv)}$$

$$= \frac{131.6 \text{ cGy}}{1.0 \text{ cGy/MU} \times 0.98} = 134 \text{ MU} \tag{7.10}$$

$$\mathcal{MU}(LPO) = \frac{D(P_{LPO})}{\dot{D}(z_{max}, 10, 100, hv) \times RDF(A, hv) \times WF}$$

$$= \frac{105.3 \text{ cGy}}{1.0 \text{ cGy/MU} \times 0.97 \times 0.53} = 205 \text{ MU} \tag{7.11}$$

$$\mathcal{MU}(RPO) = \frac{D(P_{RPO})}{\dot{D}(z_{max}, 10, 100, hv) \times RDF(A, hv) \times WF}$$

$$= \frac{105.3 \text{ cGy}}{1.0 \text{ cGy/MU} \times 0.97 \times 0.53} = 205 \text{ MU} \tag{7.12}$$

7.7.2. Monitor unit and treatment time calculations for isocentric set-ups

Figure 7.30 shows a typical isodose distribution obtained for a three field prostate boost treatment with an isocentric (100 cm) technique on a 6 MV linac.

For the isocentric distribution, all field sizes (A_Q) are defined at the isocentre, and wedges are used for the two oblique fields, as in the fixed SSD example:

- Anterior 8×8 cm^2 open field with $W = 1.0$;
- LPO and RPO 7×8 cm^2 fields both with $W = 0.7$, and WF $= 0.53$.

A dose D_Q of 200 cGy is prescribed at the ICRU reference point, which is located at the treatment isocentre. The IL at this point is 240% (sum of the weights in per cent), the maximum dose in the distribution is 242% and the 235% isodose completely covers the PTV.

The dose distribution shown in Fig. 7.30 that delivers a dose of 240 cGy to the ICRU reference point Q is achieved under the following conditions:

— 100 cGy is delivered by the anterior field at the isocentre ($W = 1$);
— 70 cGy is delivered by the LPO field at the isocentre ($W = 0.7$);
— 70 cGy is delivered by the RPO field at the isocentre ($W = 0.7$).

Thus to obtain the prescribed dose of 200 cGy at point Q, doses of 83.4 cGy, 58.3 cGy and 58.3 cGy should be delivered by the respective beams at the isocentre. These doses are obtained by considering the relative weight of each beam, such that:

$$D(Q)_A = \frac{D(Q) \times 100 \times W_A}{IL} = \frac{200 \text{ cGy} \times 100 \times 1.0}{240} = 83.4 \text{ cGy} \tag{7.13}$$

$$D(Q)_{LPO} = \frac{D(Q) \times 100 \times W_{LPO}}{IL} = \frac{200 \text{ cGy} \times 100 \times 0.7}{240} = 58.3 \text{ cGy} \tag{7.14}$$
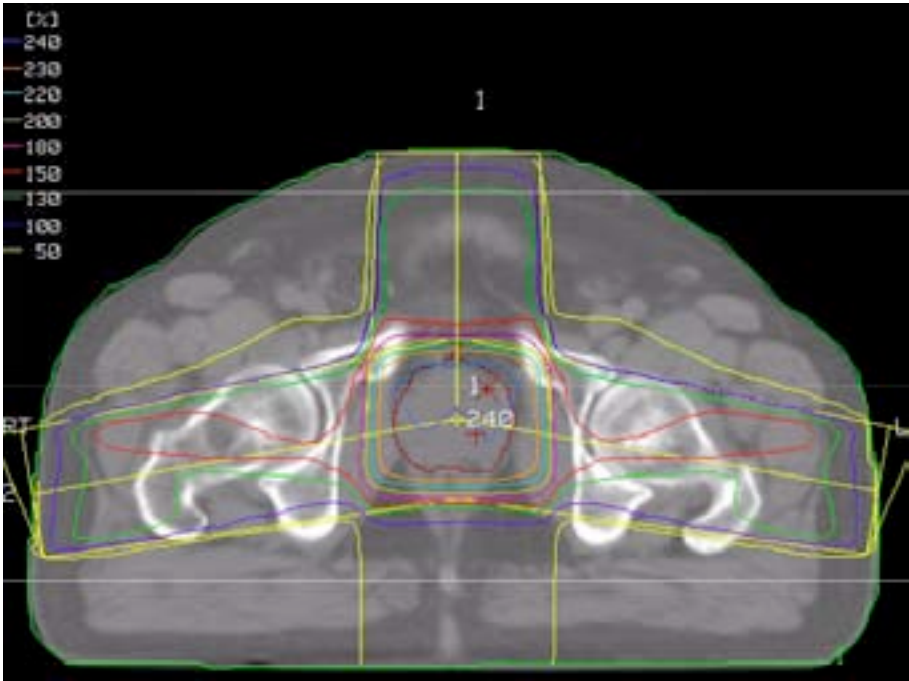
FIG. 7.30. Isocentric isodose distribution for a three field treatment of the prostate.

$$D(Q)_{RPO} = \frac{D(Q) \times 100 \times W_{RPO}}{IL} = \frac{200 \text{ cGy} \times 100 \times 0.7}{240} = 58.3 \text{ cGy} \qquad (7.15)$$

To calculate the linac monitor chamber setting in MUs, it is first necessary to calculate the doses from each beam at the isocentre at a depth of maximum dose $D(Q_{max})$, where $SSD = SAD - z_{max}$. The TMR is obtained for each field and used in the calculation as follows:

$$D(Q_{max})_A = \frac{D(Q)_A}{TMR(8 \times 8, 11.5)} = \frac{83.4 \text{ cGy}}{0.72} = 97.2 \text{ cGy} \qquad (7.16)$$

$$D(Q_{max})_{LPO} = \frac{D(Q)_{LPO}}{TMR(7 \times 8, 18.5)} = \frac{58.3 \text{ cGy}}{0.54} = 108.3 \text{ cGy} \qquad (7.17)$$

$$D(Q_{max})_{RPO} = \frac{D(Q)_{RPO}}{TMR(7 \times 8, 18.5)} = \frac{58.3 \text{ cGy}}{0.54} = 108.3 \text{ cGy} \qquad (7.18)$$

Once the dose at $D(Q_{max})$ is known for each beam it is possible to calculate the MU setting ($\mathcal{MU}$) from the basic linac output $\dot{D}(z_{max}, 10, f, hv)$ multiplied by the $RDF(A_Q)$, the ISF and other transmission factors as applicable, such that:

$$\mathcal{MU}(A) = \frac{D(Q_{max})_A}{\dot{D}(z_{max}, 10, 100, hv) \times ISF \times RDF(8 \times 8)}$$

$$= \frac{97.2 \text{ cGy}}{1.0 \text{ cGy/MU} \times \left(\frac{101.5}{100}\right)^2 \times 0.982} = 96 \text{ MU} \qquad (7.19)$$

$$\mathcal{MU}(LPO) = \frac{D(Q_{max})_{LPO}}{\dot{D}(z_{max}, 10, 100, hv) \times ISF \times RDF(7 \times 8) \times WF}$$

$$= \frac{108.3 \text{ cGy}}{1.0 \text{ cGy/MU} \times \left(\frac{101.5}{100}\right)^2 \times 0.975 \times 0.53} = 203 \text{ MU} \qquad (7.20)$$

$$\mathcal{MU}(\text{RPO}) = \frac{D(\text{Q}_{\text{max}})_{\text{RPO}}}{\dot{D}(z_{\text{max}}, 10, 100, h\nu) \times \text{ISF} \times \text{RDF}(7 \times 8) \times \text{WF}}$$

$$= \frac{108.3 \text{ cGy}}{1.0 \text{ cGy/MU} \times \left(\frac{101.5}{100}\right)^2 \times 0.975 \times 0.53} = 203 \text{ MU} \qquad (7.21)$$

7.7.3. Normalization of dose distributions

It is important to note that dose distributions can be normalized in a variety of different ways. The ICRU recommends normalization of the dose distribution to 100% at the prescription point Q. Clearly, the calculation of MUs must reflect the normalization technique employed for each particular case.

- If the dose distribution is normalized to 100% at the isocentre, an adjustment must be made to the calculation when calculating the relative dose contribution to the isocentre from each beam.
- For the isocentric example above, the isodose value at the isocentre is simply the sum of the absolute weights of each beam. If the dose distribution was normalized to 100% at the isocentre, with $D(\text{Q}) = 200$ cGy and a prescription isodose value (IL) of 100%, the relative contribution for beam A would amount to:

$$D(\text{Q})_A = \frac{D(\text{Q}) \times 100}{\text{IL}} \times \left(\frac{W_A}{W_A + W_{\text{LPO}} + W_{\text{RPO}}}\right)$$

$$= \frac{200 \text{ cGy} \times 100}{100} \times \left(\frac{1.0}{1.0 + 0.7 + 0.7}\right) = 83.4 \text{ cGy} \qquad (7.22)$$

The remainder of the calculation remains the same.

7.7.4. Inclusion of output parameters in the dose distribution

Modern TPSs give the user the ability to take into account several dosimetric parameters in the dose distribution affecting the beam output, thereby relieving the need to correct the beam output when performing the

monitor setting calculation. Obviously, large errors in monitor calculations could occur if the outputs were corrected without need. Frequently, for example, the isodose values in a dose distribution may already include:

- Inverse square law factors for extended distance treatments;
- Effects on dose outputs from blocks in the field; or
- Tray factors and WFs.

It is of the utmost importance to know exactly what the isodose lines mean on a dose distribution obtained from a given TPS.

7.7.5.   Treatment time calculation for orthovoltage and cobalt-60 units

Treatment time calculations for orthovoltage units and ^{60}Co teletherapy units are carried out similarly to the above examples, except that machine outputs are stated in cGy/min and the treatment timer setting in minutes replaces the monitor setting in MUs. A correction for shutter error should be included in the time set.

BIBLIOGRAPHY

BENTEL, G.C., Radiation Therapy Planning, McGraw-Hill, New York (1996).

BENTEL, G.C., NELSON, C.E., NOELL, K.T., Treatment Planning and Dose Calculation in Radiation Oncology, Pergamon Press, New York (1989).

HENDEE, W.R., IBBOTT, G.S., Radiation Therapy Physics, Mosby, St. Louis, MI (1996).

INTERNATIONAL COMMISSION ON RADIATION UNITS AND MEASUREMENTS, Measurement of Absorbed Dose Measured in a Phantom Irradiated by a Single Beam of X or Gamma Rays, Rep. 23, ICRU, Bethesda, MD (1973).

— Prescribing, Recording and Reporting Photon Beam Therapy, Rep. 50, ICRU, Bethesda, MD (1993).

— Prescribing, Recording and Reporting Photon Beam Therapy (Supplement to ICRU Report 50), Rep. 62, ICRU, Bethesda, MD (1999).

JOHNS, H.E., CUNNINGHAM, J.R., The Physics of Radiology, Thomas, Springfield, IL (1985).

KHAN, F.M., The Physics of Radiation Therapy, 3rd edn, Lippincott, Williams and Wilkins, Baltimore, MD (2003).

KHAN, F.M., POTTISH, R.A., Treatment Planning in Radiation Oncology, Williams and Wilkins, Baltimore, MD (1998).

MOULD, R.F., Radiotherapy Treatment Planning, Adam Hilger, Bristol (1981).

WILLIAMS, J.R., THWAITES, D.I., Radiotherapy Physics in Practice, Oxford Univ. Press, Oxford (1993).

Chapter 8

ELECTRON BEAMS:
PHYSICAL AND CLINICAL ASPECTS

W. STRYDOM
Department of Medical Physics,
Medical University of Southern Africa,
Pretoria, South Africa

W. PARKER, M. OLIVARES
Department of Medical Physics,
McGill University Health Centre,
Montreal, Quebec, Canada

8.1. CENTRAL AXIS DEPTH DOSE DISTRIBUTIONS IN WATER

Megavoltage electron beams represent an important treatment modality in modern radiotherapy, often providing a unique option in the treatment of superficial tumours (less than 5 cm deep). Electrons have been used in radiotherapy since the early 1950s, first produced by betatrons and then by microtrons and linacs. Modern high energy linacs typically provide, in addition to two megavoltage photon energies, several electron beam energies in the range from 4 to 22 MeV.

8.1.1. General shape of the depth dose curve

The general shape of the central axis depth dose curve for electron beams differs from that of photon beams (see Fig. 8.1). Figure 8.1(a) shows depth doses for various electron beam energies and Fig. 8.1(b) shows depth doses for 6 and 15 MV X ray beams.

Typically, the electron beam central axis depth dose curve exhibits a high surface dose (compared with megavoltage photon beams), and the dose then builds up to a maximum at a certain depth referred to as the electron beam depth of dose maximum z_{max}. Beyond z_{max} the dose drops off rapidly and levels off at a small low level dose component referred to as the bremsstrahlung tail. These features offer a distinct clinical advantage over the conventional X ray modalities in the treatment of superficial tumours.
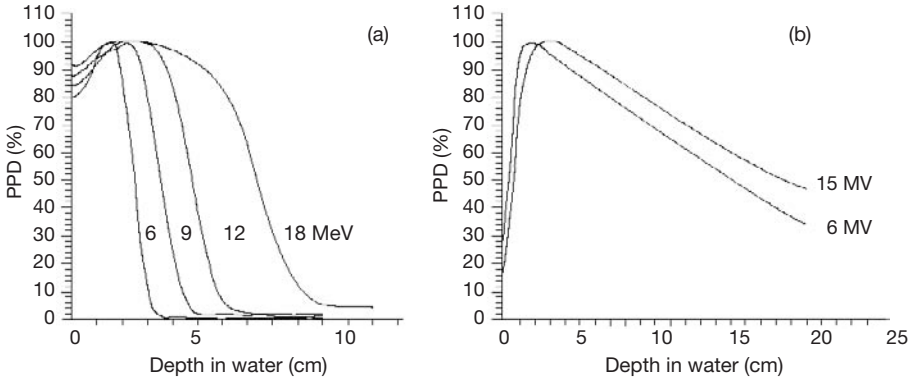
FIG. 8.1. Typical central axis PDD curves in water for a 10 × 10 cm² field size and an SSD of 100 cm for (a) electron beams with energies of 6, 9, 12 and 18 MeV and (b) photon beams with energies of 6 and 15 MV.

A typical high energy linac may produce electron beams with discrete energies in the range from 4 to 25 MeV.

Electron beams can be considered almost monoenergetic as they leave the accelerator; however, as the electron beam passes through the accelerator exit window, scattering foils, monitor chambers, collimators and air, the electrons interact with these structures, resulting in:

- A broadening of the beam's electron energy spectrum;
- Bremsstrahlung production contributing to the bremsstrahlung tail in the electron beam percentage depth dose (PDD) distribution.

On initial contact with the patient, the clinical electron beam has an incident mean energy $\bar{E}_0$ that is lower than the electron energy inside the accelerator.

The ratio of the dose at a given point on the central axis of an electron beam to the maximum dose on the central axis multiplied by 100 is the PDD, which is normally measured for the nominal treatment distance (i.e. the distance between the accelerator exit window and the patient's skin) and depends on field size and electron beam energy.

8.1.2. Electron interactions with an absorbing medium

As electrons travel through a medium, they interact with atoms by a variety of Coulomb force interactions that may be classified as follows:

● Inelastic collisions with atomic electrons, resulting in ionization and excitation of atoms and termed collisional or ionizational loss;
● Elastic collisions with atomic nuclei, resulting in elastic scattering that is characterized by a change in direction but no energy loss;
● Inelastic collisions with atomic nuclei, resulting in bremsstrahlung production and termed radiative loss;
● Elastic collisions with atomic electrons.

The kinetic energy of electrons is lost in inelastic collisions that produce ionization or is converted to other forms of energy, such as photon energy or excitation energy. In elastic collisions kinetic energy is not lost; however, the electron's direction may be changed or the energy may be redistributed among the particles emerging from the collision.

The typical energy loss for a therapy electron beam, averaged over its entire range, is about 2 MeV/cm in water and water-like tissues.

The rate of energy loss for collisional interactions depends on the electron energy and on the electron density of the medium. The rate of energy loss per gram per square centimetre, $MeV \cdot g^{-1} \cdot cm^{-2}$ (called the mass stopping power), is greater for low atomic number materials than for high atomic number materials. This is because high atomic number materials have fewer electrons per gram than lower atomic number materials and, moreover, high atomic number materials have a larger number of tightly bound electrons that are not available for this type of interaction.

The rate of energy loss for radiative interactions (bremsstrahlung) is approximately proportional to the electron energy and to the square of the atomic number of the absorber. This means that X ray production through radiative losses is more efficient for higher energy electrons and higher atomic number materials.

When a beam of electrons passes through a medium the electrons suffer multiple scattering, due to Coulomb force interactions between the incident electrons and predominantly the nuclei of the medium. The electrons will therefore acquire velocity components and displacements transverse to their original direction of motion. As the electron beam traverses the patient, its mean energy decreases and its angular spread increases.

The scattering power of electrons varies approximately as the square of the atomic number and inversely as the square of the kinetic energy. For this reason high atomic number materials are used in the construction of scattering foils used for the production of clinical electron beams in a linac. The scattering power variations in heterogeneous tissues are also responsible for the production of local hot and cold spots.

8.1.3. Inverse square law (virtual source position)

In contrast to a photon beam, which has a distinct focus located at the accelerator X ray target, an electron beam appears to originate from a point in space that does not coincide with the scattering foil or the accelerator exit window. The term 'virtual source position' was introduced to indicate the virtual location of the electron source.

The effective source to surface distance (SSD) for electron beams (SSD_{eff}) is defined as the distance from the virtual source position to the point of the nominal SSD (usually the isocentre of the linac). The inverse square law may be used for small SSD differences from the nominal SSD to make corrections to the absorbed dose for variations in air gaps between the patient surface and the applicator.

There are various methods to determine the SSD_{eff}. One commonly used method consists of measuring the dose at various distances from the electron applicator by varying the gap between the phantom surface and the applicator (with gaps ranging from 0 to 15 cm). In this method, doses are measured in a phantom at the depth of maximum dose z_{max}, with the phantom first in contact with the applicator (zero gap) and then at various distances g from the applicator. Suppose I_0 is the dose with zero gap ($g = 0$) and I_g is the dose with gap distance g. It follows then from the inverse square law that:

$$\frac{I_0}{I_g} = \left(\frac{SSD_{eff} + z_{max} + g}{SSD_{eff} + z_{max}} \right)^2 \tag{8.1}$$

or

$$\sqrt{\frac{I_0}{I_g}} = \frac{g}{SSD_{eff} + z_{max}} + 1 \tag{8.2}$$

A plot of $\sqrt{I_0 / I_g}$ against the gap distance g will give a straight line with a slope of:

$$\frac{1}{SSD_{eff} + z_{max}}$$

and the SSD_{eff} will then be given by:

$$SSD_{eff} = \frac{1}{slope} - z_{max} \tag{8.3}$$

Although the effective SSD is obtained from measurements at z_{max}, its value does not change with the depth of measurement. However, the effective SSD changes with beam energy, and has to be measured for all energies available in the clinic.

8.1.4. Range concept

A charged particle such as an electron is surrounded by its Coulomb electric field and will therefore interact with one or more electrons or with the nucleus of practically every atom it encounters. Most of these interactions individually transfer only minute fractions of the incident particle's kinetic energy, and it is convenient to think of the particle as losing its kinetic energy gradually and continuously in a process often referred to as the continuous slowing down approximation (CSDA).

The path length of a single electron is the total distance travelled along its actual trajectory until the electron comes to rest, regardless of the direction of movement. The projected path range is the sum of individual path lengths projected on to the incident beam direction (i.e. the central axis). The CSDA range (or the mean path length) for an electron of initial kinetic energy E_0 can be found by integrating the reciprocal of the total stopping power:

$$R_{CSDA} = \int_{0}^{E_0} \left[\frac{S(E)}{\rho} \right]_{tot}^{-1} dE \tag{8.4}$$

The CSDA range is purely a calculated quantity that represents the mean path length along the electron's trajectory and not the depth of penetration in a defined direction. The CSDA range for electrons in air and water is given in Table 8.1 for various electron kinetic energies.

The following two concepts of range are also defined for electron beams: maximum range and practical range.

The maximum range R_{max} (cm or g/cm^2) is defined as the depth at which extrapolation of the tail of the central axis depth dose curve meets the bremsstrahlung background, as shown in Fig. 8.2. It is the largest penetration depth of electrons in the absorbing medium. The maximum range has the drawback of not giving a well defined measurement point.

The practical range R_p (cm or g/cm^2) is defined as the depth at which the tangent plotted through the steepest section of the electron depth dose curve intersects with the extrapolation line of the background due to bremsstrahlung, as shown in Fig. 8.2.

TABLE 8.1.   CSDA RANGES IN AIR AND WATER FOR VARIOUS ELECTRON ENERGIES

Electron energy (MeV)	CSDA range in air (g/cm^2)	CSDA range in water (g/cm^2)
6	3.255	3.052
7	3.756	3.545
8	4.246	4.030
9	4.724	4.506
10	5.192	4.975
20	9.447	9.320
30	13.150	13.170

The depths R_{90} and R_{50} (cm or g/cm^2) are defined as depths on the electron PDD curve at which the PDDs beyond z_{max} attain values of 90% and 50%, respectively.

The depth R_q (cm or g/cm^2) is defined as the depth where the tangent through the dose inflection point intersects the maximum dose level, as shown in Fig. 8.2.

It is evident that the CSDA range is of marginal usefulness in characterizing the depth of penetration of electrons into an absorbing medium.
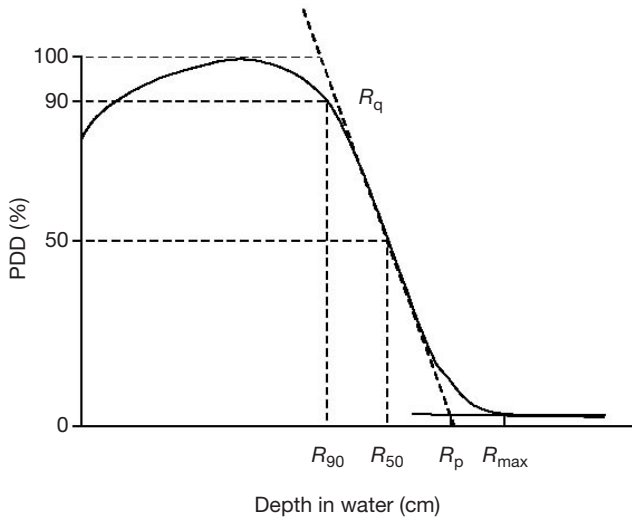
FIG. 8.2. Typical electron beam PDD curve illustrating the definition of R_q, R_p, R_{max}, R_{50} and R_{90}.

Scattering effects, predominantly between the incident electrons and nuclei of the absorbing medium, cause electrons to follow very tortuous paths, resulting in large variations in the actual path of electrons in the absorbing medium.

8.1.5. Buildup region (depths between the surface and z_{max} (i.e. $0 \leq z \leq z_{max}$))

The dose buildup in electron beams is much less pronounced than that of megavoltage photon beams and results from the scattering interactions that the electrons experience with atoms of the absorber. Upon entry into the medium (e.g. water), the electron paths are approximately parallel. With depth their paths become more oblique with regard to the original direction, due to multiple scattering, resulting in an increase in electron fluence along the beam central axis.

In the collision process between electrons and atomic electrons, it is possible that the kinetic energy acquired by the ejected electron is large enough (hard collision) to cause further ionization. In such a case, these electrons are referred to as secondary electrons or δ rays, and they also contribute to the buildup of dose.

As seen in Fig. 8.1, the surface dose of electron beams (in the range from 75% to 95%) is much higher than the surface dose for photon beams, and the rate at which the dose increases from the surface to z_{max} is therefore less pronounced for electron beams than for photon beams.

Unlike in photon beams, the per cent surface dose for electron beams increases with electron energy. This can be explained by the nature of electron scatter. At lower energies, electrons are scattered more easily and through larger angles. This causes the dose to build up more rapidly and over a shorter distance, as shown in Fig. 8.3. The ratio of surface dose to maximum dose is therefore lower for lower energy electrons than for higher energy electrons.

In contrast to the behaviour of megavoltage photon beams, the depth of maximum dose in electron beams z_{max} does not follow a specific trend with electron beam energy; rather, it is a result of the machine design and accessories used.

8.1.6. Dose distribution beyond z_{max} ($z > z_{max}$)

Scattering and continuous energy loss by electrons are the two processes responsible for the sharp drop-off in the electron dose at depths beyond z_{max}.

Bremsstrahlung produced in the head of the accelerator, in the air between the accelerator window and the patient, and in the irradiated medium is responsible for the tail in the depth dose curve.
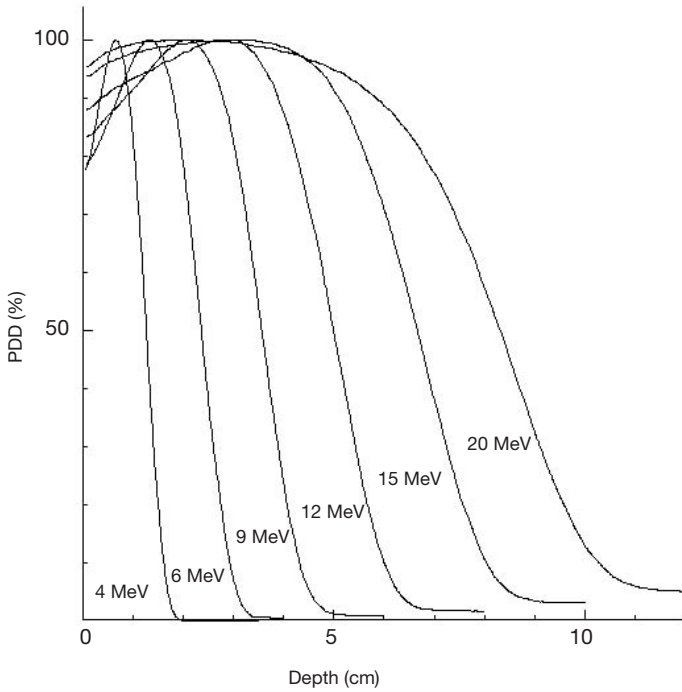
FIG. 8.3. *Central axis PDD curves for a family of electron beams from a high energy linac. All curves are normalized to 100% at z_{max}.*

The range of electrons increases with increasing electron energy. The electron dose gradient is defined as follows:

$$G = R_p/(R_p - R_q)$$

The dose gradient for lower electron energies is steeper than that for higher electron energies, since the lower energy electrons are scattered at a greater angle away from their initial directions. The stopping powers at low and high energy also affect the dose gradient.

The bremsstrahlung contamination (e.g. the tail sections of Fig. 8.1(a)) depends on electron beam energy and is typically less than 1% for 4 MeV and less than 4% for 20 MeV electron beams for an accelerator with dual scattering foils.

8.2. DOSIMETRIC PARAMETERS OF ELECTRON BEAMS

8.2.1. Electron beam energy specification

Owing to the complexity of the spectrum, there is no single energy parameter that will fully characterize an electron beam. Several parameters are used to describe a beam, such as the most probable energy $E_{p,0}$ on the phantom surface, the mean energy $\bar{E}_0$ on the phantom surface, and R_{50}, the depth at which the absorbed dose falls to 50% of the maximum dose.

The most probable energy $E_{p,0}$ on the phantom surface is empirically related to the practical range R_p in water as follows:

$$E_{p,0} = 0.22 + 1.09R_p + 0.0025R_p^2 \qquad (8.5)$$

where $E_{p,0}$ is in megaelectronvolts and R_p is in centimetres.

The mean electron energy $\bar{E}_0$ at the phantom surface is related to the half-value depth R_{50} as follows:

$$\bar{E}_0 = CR_{50} \qquad (8.6)$$

where $C = 2.33$ MeV/cm for water.

The depth R_{50} is the beam quality index in electron beam dosimetry as specified in IAEA TRS 398. R_{50} is calculated from the measured $R_{50,\text{ion}}$, the depth at which the ionization curve falls to 50% of its maximum, by:

$$R_{50} = 1.029R_{50,\text{ion}} - 0.06 \ (\text{g/cm}^2) \ (\text{for } R_{50,\text{ion}} \leq 10 \ \text{g/cm}^2) \qquad (8.7)$$

$$R_{50} = 1.059R_{50,\text{ion}} - 0.37 \ (\text{g/cm}^2) \ (\text{for } R_{50,\text{ion}} > 10 \ \text{g/cm}^2) \qquad (8.8)$$

$\bar{E}_z$, the mean energy at a depth z in a water phantom, is related to the practical range R_p by the Harder equation as follows:

$$\bar{E}_z = \bar{E}_0 \ (1 - z/R_p) \qquad (8.9)$$

8.2.2. Typical depth dose parameters as a function of energy

Some typical values for electron depth dose parameters as a function of energy are shown in Table 8.2. These parameters should be measured for each electron beam before it is put into clinical service.

TABLE 8.2. TYPICAL DEPTH DOSE PARAMETERS OF ELECTRON BEAMS

Energy (MeV)	R_{90} (cm)	R_{80} (cm)	R_{50} (cm)	R_p (cm)	$\bar{E}_0$ (MeV)	Surface dose (%)
6	1.7	1.8	2.2	2.9	5.6	81
8	2.4	2.6	3.0	4.0	7.2	83
10	3.1	3.3	3.9	4.8	9.2	86
12	3.7	4.1	4.8	6.0	11.3	90
15	4.7	5.2	6.1	7.5	14.0	92
18	5.5	5.9	7.3	9.1	17.4	96

8.2.3. Percentage depth dose

Typical central axis PDD curves for various electron beam energies are shown in Fig. 8.3 for a field size of 10×10 cm^2.

When diodes are used in PDD measurements, the diode signal represents the dose directly, because the stopping power ratio water to silicon is essentially independent of electron energy and hence depth.

If an ionization chamber is used in the determination of electron beam depth dose distributions, the measured depth ionization distribution must be converted to a depth dose distribution by using the appropriate stopping power ratios water to air at depths in a phantom. For more information on the ionization chamber measurements see IAEA TRS 398.

8.2.3.1. Percentage depth doses for small electron field sizes

When the distance between the central axis and the field edge is more than the lateral range of scattered electrons, lateral scatter equilibrium exists and the depth dose for a specific electron energy will be essentially independent of the field dimensions, as shown in Fig. 8.4 for field sizes larger than 10×10 cm^2 and an electron energy of 20 MeV.

With decreasing field size the decreasing degree of lateral electronic equilibrium will be present at the central axis, and the depth dose and output factors will show large sensitivity to field shape and size (see also Section 8.3.2), as shown in Fig. 8.4 for a 20 MeV electron beam and field sizes smaller than 10 $\times$ 10 cm^2.

When the length of one side of the electron field decreases to below the R_p value for a given electron energy, the depth of dose maximum decreases and
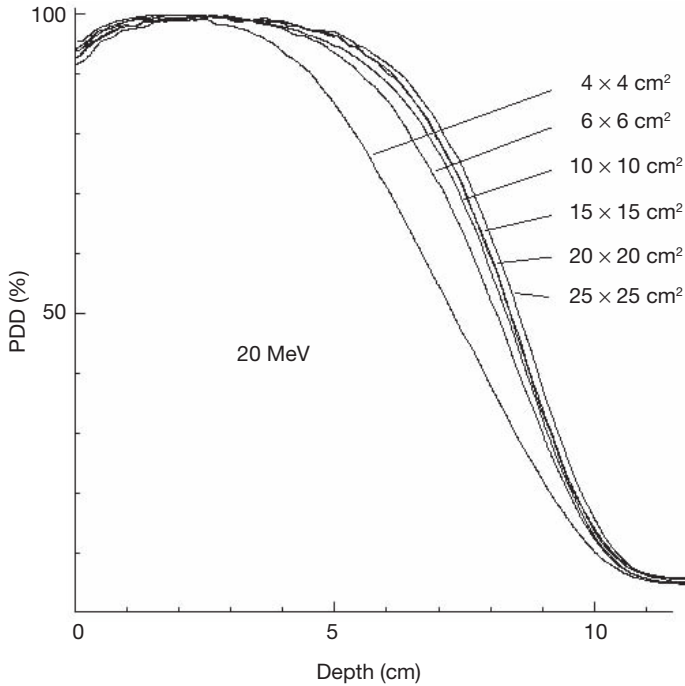
FIG. 8.4. PDD curves for different field sizes for a 20 MeV electron beam from a linac. It is clearly illustrated that for field sizes larger than the practical range of the electron beam (R_p is about 10 cm for this 20 MeV electron beam), the PDD curve remains essentially unchanged.

the relative surface dose increases with decreasing field size. The R_p, on the other hand, is independent of electron beam field size, as also shown in Fig. 8.4, and depends only on electron beam energy.

8.2.3.2. *Percentage depth doses for oblique beam incidence*

The distributions in Fig. 8.3 are given for normal (perpendicular) beam incidence on the phantom or patient surface. For oblique beam incidences with angles α between the beam central axis and the normal to the phantom or patient surface exceeding 20º, there are significant changes to the PDD characteristics of the electron beam, in contrast to the behaviour observed in photon beams.
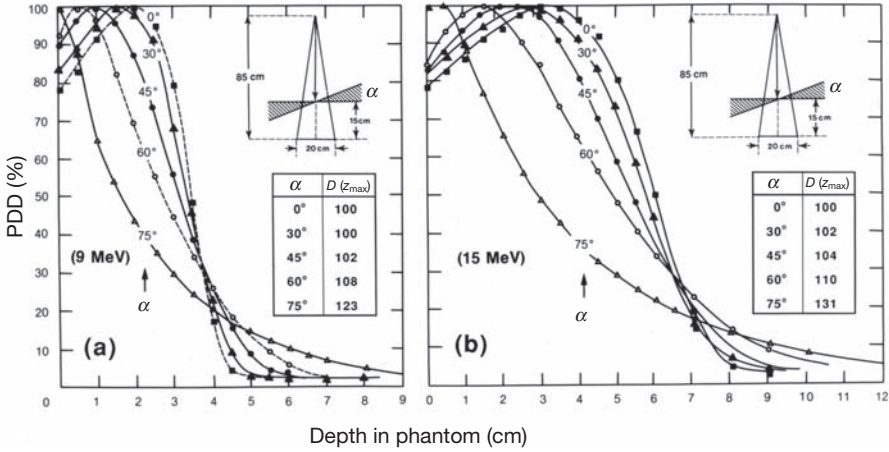
FIG. 8.5. PDD curves for various beam incidences for a (a) 9 MeV and (b) 15 MeV electron beam. α = 0 represents normal beam incidence. The inset shows the geometry of the experimental set-up and the doses at z_{max} for various angles α relative to the dose at z_{max} for α = 0.

Figure 8.5 illustrates the effect of the beam incidence angle α on PDD distributions. Angle α = 0 represents normal incidence. The larger the angle α, the shallower is z_{max} and the larger is the dose at z_{max}. All dose values are normalized to 100% at z_{max} for α = 0.

For small angles of incidence α, the slope of the PDD curve decreases and the practical range is essentially unchanged from that for normal beam incidence. When the angle of incidence α exceeds 60º, the PDD looses its characteristic shape and the definition of R_p can no longer be applied. For large angles of incidence, the dose at z_{max} increases significantly. This effect is due to the increased electron fluence through the central axis from the oblique beam angle.

8.2.4. Output factors

An important parameter that determines the electron beam output is the collimator jaw setting. For each electron applicator (cone) there is an associated jaw setting that is generally larger than the field size defined by the applicator (electron beam cone). Such an arrangement minimizes the variation of collimator scatter and therefore the output variation with field size is kept reasonably small. Typical electron applicator sizes are 6×6, 10×10, 15×15, 20×20 and 25×25 cm^2.

The output factor for a given electron energy is the ratio of the dose for any specific field size (applicator size) to the dose for a 10×10 cm^2 reference applicator, both measured at z_{max} in a phantom at an SSD of 100 cm.

The square field defined by the applicator will not adequately shield all normal tissues in most clinical situations. For this reason collimating blocks fabricated from lead or a low melting point alloy are routinely inserted into the end of the applicator to shape the fields. Output factors must also be measured for these irregular fields shaped by cut-outs.

For small field sizes this extra shielding will affect the PDD and the output factors due to lack of lateral scatter. The change in z_{max} as well as changes in the PDDs with small field sizes must be accounted for when measuring output factors.

8.2.5. Therapeutic range R_{90}

The depth of the 90% dose level (R_{90} (cm)) beyond z_{max} is defined as the therapeutic range for electron beam therapy. The R_{90} depth should, if possible, coincide with the distal treatment margin. This depth is approximately given by $E/4$ in centimetres of water, where E is the nominal energy in megaelectron-volts of the electron beam. R_{80} (cm), the depth that corresponds to the 80% PDD beyond z_{max}, is also a frequently used parameter for defining the therapeutic range, and can be approximated by $E/3$ in centimetres of water.

8.2.6. Profiles and off-axis ratios

A typical dose profile for a 6 MeV electron beam and a 25×25 cm^2 field at z_{max} is shown in Fig. 8.6. The off-axis ratio (OAR) relates the dose at any point in a plane perpendicular to the beam direction to the dose on the central axis in that plane. A plot of the OAR against the distance from the central axis is referred to as a dose profile.

8.2.7. Flatness and symmetry

The specification for the flatness of electron beams according to the IEC is given at z_{max} and consists of two requirements:

- The flatness specification requires that the distance between the 90% dose level and the geometrical beam edge should not exceed 10 mm along the major axes and 20 mm along the diagonals;
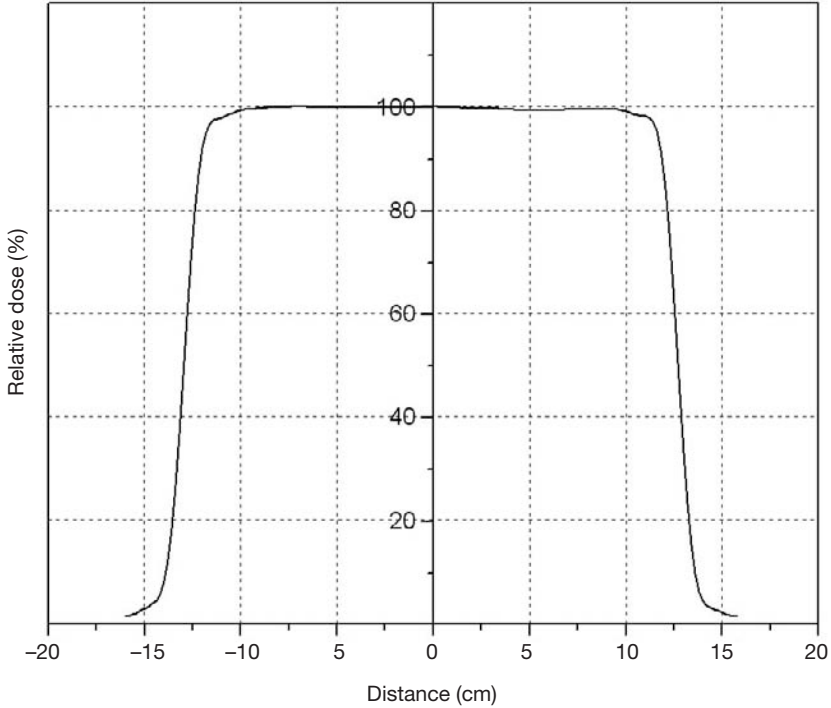
FIG. 8.6. *Dose profile at depth z_{max} for a 12 MeV electron beam and $25 \times 25\ cm^2$ field.*

- The maximum value of the absorbed dose anywhere within the region bounded by the 90% isodose contour should not exceed 1.05 times the absorbed dose on the axis of the beam at the same depth.

The specification for symmetry of electron beams according to the IEC at z_{max} is that the cross-beam profile should not differ by more than 3% for any pair of symmetric points with respect to the central ray.

8.3. CLINICAL CONSIDERATIONS IN ELECTRON BEAM THERAPY

8.3.1. Dose specification and reporting

Electron beam therapy is usually applied for the treatment of superficial or subcutaneous disease. Treatments are usually delivered with a single direct

electron field at a nominal SSD of 100 cm. The dose specification for treatment is commonly given at a depth that lies at, or beyond, the distal margin of the disease, and the energy chosen for the treatment depends on the depth of the lesion to be treated.

To maximize healthy tissue sparing beyond the tumour, while at the same time providing relatively homogeneous target coverage, treatments are usually prescribed at either z_{max}, R_{90} or R_{80}. If the treatment dose is specified at either R_{80} or R_{90}, the skin dose will often be higher than the prescription dose. The maximum dose to the patient could be up to 20% higher than the prescribed dose. The maximum dose should therefore always be reported for electron beam therapy.

8.3.2. Small field sizes

For field sizes larger than the practical range of the electron beam, the PDD curve remains constant with increasing field size, since the electrons from the periphery of the field are not scattered sufficiently to contribute to the central axis depth dose. When the field is reduced below that required for lateral scatter equilibrium, the dose rate decreases, z_{max} moves closer to the surface and the PDD curve becomes less steep (see Fig. 8.4). Therefore, for all treatments involving small electron beam field sizes, the beam output as well as the full PDD distribution must be determined for a given patient treatment.

8.3.3. Isodose curves

Isodose curves (see Fig. 8.7) are lines passing through points of equal dose. Isodose curves are usually drawn at regular intervals of absorbed dose and are expressed as a percentage of the dose at a reference point, which is normally taken as the z_{max} point on the beam central axis. As an electron beam penetrates a medium, the beam expands rapidly below the surface, due to scattering. However, the individual spread of the isodose curves varies depending on the isodose level, energy of the beam, field size and beam collimation.

A particular characteristic of electron beam isodose curves is the bulging of the low value curves (<20%) as a direct result of the increase in electron scattering angle with decreasing electron energy. At energies above 15 MeV, electron beams exhibit a lateral constriction of the higher value isodose curves (>80%).

Isodose curves for a 9 and 20 MeV electron beam are shown in Fig. 8.7. The phenomena of bulging and constricting isodose curves are clearly visible.
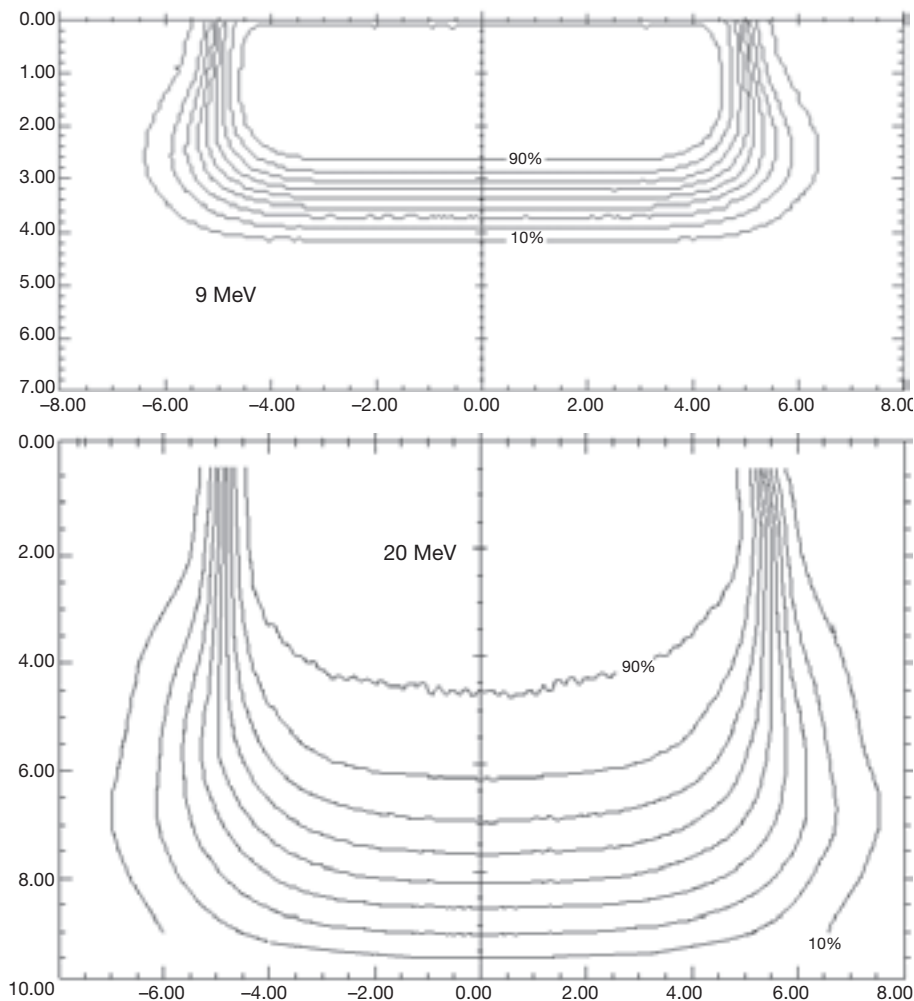
FIG. 8.7. *Measured isodose curves for 9 and 20 MeV electron beams. The field size is 10 × 10 cm^2 and SSD = 100 cm. Note the bulging low value isodose lines for both beam energies. The 80% and 90% isodose lines for the 20 MeV beam exhibit a severe lateral constriction. The abscissa and the ordinate represent distance from the central axis and depth in a water phantom, respectively, measured in centimetres.*

The term penumbra generally defines the region at the edge of a radiation beam over which the dose rate changes rapidly as a function of distance from the beam central axis. The physical penumbra of an electron beam may be defined as the distance between two specified isodose curves at a specified depth. A penumbra defined in this way is a rapidly varying function of depth.

The ICRU has recommended that the 80% and 20% isodose lines be used in the determination of the physical penumbra, and that the specified depth of measurement be $R_{85}/2$, where R_{85} is the depth of the 85% dose level beyond z_{max} on the electron beam central axis.

The low value isodose lines (e.g. below the 50% isodose line) diverge with increasing air gap between the patient and the end of the applicator (cone), while the high value isodose lines converge towards the central axis. This means that the penumbra will increase if the distance from the applicator increases.

8.3.4. Field shaping

Field shaping for electron beams is always achieved with electron applicators (cones), which may be used alone or in conjunction with shielding blocks or special cut-outs.

8.3.4.1. Electron applicators

Normally the photon beam collimators on the accelerator are too far from the patient to be effective for electron field shaping. After passing through the scattering foil, the electrons scatter sufficiently with the other components of the accelerator head, and in the air between the exit window and the patient, to create a clinically unacceptable penumbra.

Electron beam applicators or cones are usually used to collimate the beam, and are attached to the treatment unit head such that the electron field is defined at distances as small as 5 cm from the patient. Several cones are provided, usually in square field sizes ranging from 5×5 cm^2 to 25×25 cm^2.

8.3.4.2. Shielding and cut-outs

For a more customized field shape, a lead or metal alloy cut-out may be constructed and placed on the applicator as close to the patient as possible. Standard cut-out shapes may be preconstructed and ready for use at the time of treatment. Custom cut-out shapes may also be designed for patient treatment. Field shapes may be determined from conventional or virtual simulation, but are most often prescribed clinically by the physician prior to the first treatment.

The lead thickness required for the shielding of various electron energies with transmissions of 50%, 10% and 5% is given in Table 8.3. As a rule of thumb, simply divide the practical range R_p by 10 to obtain the approximate thickness of lead required for shielding (<5% transmission).

TABLE 8.3.   LEAD THICKNESS (mm) REQUIRED FOR VARIOUS
TRANSMISSION LEVELS FOR A 12.5×12.5 cm^2 ELECTRON FIELD

Transmission (%)	Energy (MeV)						
	6	8	10	12	14	17	20
50	1.2	1.8	2.2	2.6	2.9	3.8	4.4
10	2.1	2.8	3.5	4.1	5.0	7.0	9.0
5	3.0	3.7	4.5	5.6	7.0	8.0	10.0

8.3.4.3. Internal shielding

For certain treatments, such as treatments of the lip, buccal mucosa, eyelids or ear lobes, it may be advantageous to use an internal shield to protect the normal structures beyond the target volume. Care must be taken to consider the dosimetric effects of placing lead shielding directly on the patient's surface. A high dose may inadvertantly be delivered to healthy tissue in contact with the shield owing to electron backscattering from the shield. This dose enhancement can be appreciable and may reach levels of 30–70%, but drops off exponentially with distance from the interface on the entrance side of the beam.

Aluminium or acrylic materials have been used around lead shields to absorb the backscattered electrons. Often, these shields are dipped in wax to form a 1 or 2 mm coating around the lead. This not only protects the patient from the toxic effects of the lead, but also absorbs any scattered electrons, which are usually low in energy.

8.3.4.4. Extended source to surface distance treatments

In clinical situations in which a set-up at the nominal SSD is precluded, an extended SSD might be used, although, as a general rule, such treatments should be avoided unless absolutely necessary.

Extending the SSD typically produces a large change in output, a minimal change in PDD and a significant change in beam penumbra. The beam penumbra can be restored by placing collimation on the skin surface. The inside edge of the skin collimation has to be well within the penumbra cast by the normal treatment collimator. Clinical electron beams are not produced at a single source position in the head of the linac, but rather as an interaction of a pencil beam with the scattering foil and other components.

In general, the inverse square law, as used for photon beams, cannot be applied to electron beams without making a correction.

A virtual source position for electron beams can be determined experimentally as the point in space that appears to be the point source position for the electron beam. An 'effective' SSD, based on the virtual source position, is used when applying the inverse square law to correct for a non-standard SSD.

8.3.5. Irregular surface correction

A frequently encountered situation in electron beam therapy is that where the end of the treatment cone is not parallel to the skin surface of the patient. This could result in an uneven air gap, and corrections would have to be made to the dose distribution to account for the sloping surface. Corrections to isodose lines can be applied on a point by point basis through the use of the following equation:

$$D(\text{SSD}_{\text{eff}} + g, z) = D_0(\text{SSD}_{\text{eff}}, z)\left(\frac{\text{SSD}_{\text{eff}} + z}{\text{SSD}_{\text{eff}} + g + z}\right)^2 \times \text{OF}(\theta, z) \qquad (8.10)$$

where

SSD_{eff}	is the effective SSD;
g	is the air gap;
z	is the depth in the patient;
θ	is the obliquity angle between the tangent to the skin surface and the beam central axis;
$D_0(\text{SSD}_{\text{eff}}, z)$	is the dose at depth z for a beam incident normally on a flat phantom;
$\text{OF}(\theta, z)$	is a correction factor for the obliquity of the beam that tends to unity for beams of perpendicular incidence. This factor may either be measured or looked up in the literature.

8.3.6. Bolus

Bolus, made of a tissue equivalent material such as wax, is often used in electron beam therapy for the following purposes:

- To increase the surface dose;
- To flatten out irregular surfaces;
- To reduce the electron beam penetration in some parts of the treatment field.

For very superficial lesions, the practical range of even the lowest energy beam available from a linac may be too large to provide adequate healthy tissue sparing beyond the tumour depth. To overcome this problem, a tissue equivalent bolus material of specified thickness is placed on the surface of the patient with the intent to shorten the range of the beam in the patient.

Bolus may also be used to define more precisely the range of the electron beam. The difference between the available electron beam energies from a linac is usually no less than 3 or 4 MeV. If the lower energy is not penetrating enough and the next available energy is too penetrating, bolus may be used with the higher energy beam to fine tune the electron beam range. Bolus can also be used to shape isodose lines to conform to tumour shapes.

Sharp surface irregularities, where the electron beam may be incident tangentially, give rise to a complex dose distribution with hot and cold spots. Tapered bolus around the irregularity may be used to smooth out the surface and reduce the dose inhomogeneity.

Although labour intensive, the use of bolus for electron beam treatments is very practical, since treatment planning software for electron beams is limited and empirical data are normally collected only for standard beam geometries.

The use of computed tomography (CT) for treatment planning enables accurate determination of the tumour shape and depth and the patient contour. If a wax bolus can be constructed such that the total distance from the surface of the bolus to the required treatment depth is constant along the length of the tumour, then the shape of the resulting isodose curves should approximate the shape of the tumour (see Fig. 8.8).

8.3.7. Inhomogeneity corrections

The dose distribution from an electron beam can be greatly affected by the presence of tissue inhomogeneities such as lung or bone. The dose within these inhomogeneities is difficult to calculate or measure, but the effect on the distribution beyond the inhomogeneity is quantifiable.

8.3.7.1. Coefficient of equivalent thickness

The simplest correction for tissue inhomogeneities involves the scaling of the inhomogeneity thickness by its density relative to water, and the determination of a coefficient of equivalent thickness (CET).

The CET of a material is given by its electron density relative to the electron density of water and is essentially equivalent to the mass density of the
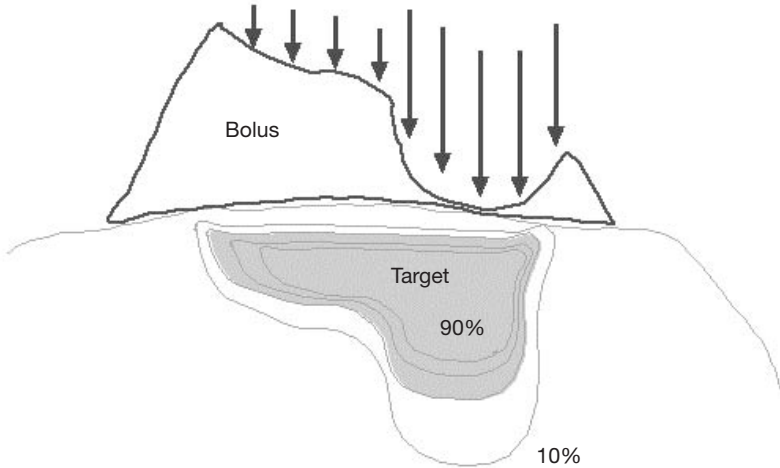
FIG. 8.8. Construction of a custom bolus to conform isodose lines to the shape of the target.

inhomogeneity; for example, lung has an approximate density of 0.25 g/cm^3 and a CET of 0.25. Thus a thickness of 1 cm of lung is equivalent to 0.25 cm of tissue. Solid bone has a CET of approximately 1.6.

The CET can be used to determine an effective depth in water equivalent tissue z_{eff} through the following expression:

$$z_{eff} = z - t(1 - \text{CET}) \tag{8.11}$$

where z is the actual depth of the point in the patient and t is the thickness of the inhomogeneity.

Figure 8.9 illustrates the effect of a lung inhomogeneity on the PDD curve of an electron beam.

8.3.7.2. Scatter perturbation (edge) effects

If an electron beam strikes the interface between two materials either tangentially or at a large oblique angle, the resulting scatter perturbation will affect the dose distribution at the interface. The lower density material will receive a higher dose, due to the increased scattering of electrons from the higher density side.
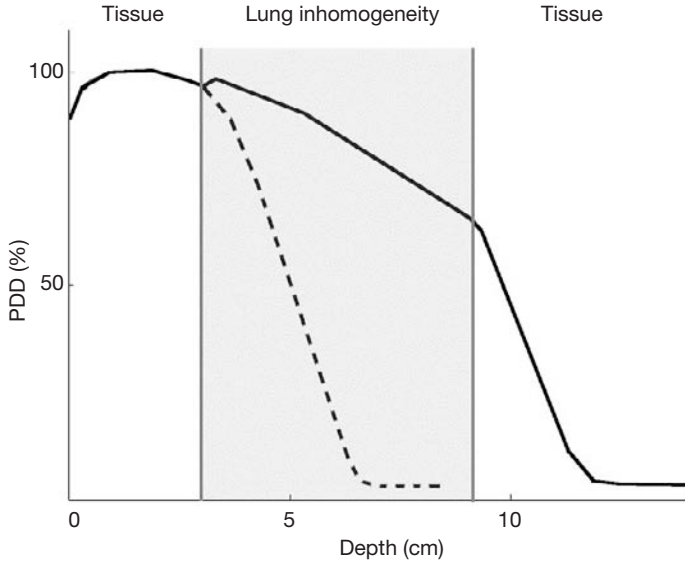
FIG. 8.9. Effect of a 5 cm lung inhomogeneity on a 15 MeV, 10 × 10 cm² electron beam PDD. The dashed curve represents the PDD in tissue without the inhomogeneity present.

Edge effects need to be considered in the following situations:

- Inside a patient, at the interfaces between internal structures of different density;
- On the surface of the patient, in regions of sharp surface irregularity;
- On the interface between lead shielding and the surface of the patient, if the shielding is placed superficially on the patient or if it is internal shielding.

The enhancement in dose at the tissue–metal interface is dependent on the beam energy at the interface and on the atomic number of the metal. In the case of a tissue–lead interface, the electron backscatter factor (EBF) is empirically given by:

$$\text{EBF} = 1 + 0.735e^{-0.052\bar{E}_\text{d}} \tag{8.12}$$

where $\bar{E}_\text{d}$ is the average energy of the electrons incident on the interface. This equation, given by Klevenhagen, represents the best fit to the experimental data.

8.3.8. Electron beam combinations

Electron beams may be abutted to adjacent electron fields or to adjacent photon fields.

8.3.8.1. Matched (abutted) electron fields

When abutting electron fields, it is important to take into consideration the dosimetric characteristics of electron beams at depth. The large penumbra and bulging isodose lines make hot spots and cold spots in the target volume practically unavoidable. Contiguous electron beams should be parallel to each other, in order to avoid significant overlapping of the high value isodose curves at depth.

In general, it is best to avoid adjacent electron fields, but if treatment with these fields is absolutely necessary, some basic film dosimetry should be carried out at the junction prior to treatment to verify that no hot or cold spots in dose are present.

8.3.8.2. Matched photon and electron fields

Electron–photon field matching is easier than electron–electron field matching. A distribution for photon fields is usually available from a treatment planning system (TPS), and the location of the electron beam treatment field as well as the associated hot and cold spots can be determined relative to the photon field treatment plan. The matching of electron and photon fields on the skin will produce a hot spot on the photon side of the treatment.

8.3.9. Electron arc therapy

Electron arc therapy is a special radiotherapeutic technique in which a rotational electron beam is used to treat superficial tumour volumes that follow curved surfaces. While the technique is well known and accepted as clinically useful in the treatment of certain tumours, it is not widely used because it is relatively complicated and its physical characteristics are poorly understood. The dose distribution in the target volume depends in a complicated fashion on the electron beam energy, field width, depth of the isocentre, source to axis distance (SAD), patient curvature, tertiary collimation and field shape as defined by the secondary collimator.

The excellent clinical results achieved by the few pioneers in this field during the past two decades have certainly stimulated an increased interest in electron arc therapy, both for curative treatments and for palliation. In fact,

manufacturers of linacs now offer the electron arc therapy mode as one of the standard treatment options. While this option is usually purchased with a new linac, since it is relatively inexpensive, it is rarely used clinically because of the technical difficulties involved.

Two approaches to electron arc therapy have been developed: the simpler is referred to as electron pseudo arc and is based on a series of overlapping stationary electron fields, and the other uses a continuous rotating electron beam. The calculation of dose distributions in electron arc therapy is a complicated procedure and usually cannot be performed reliably with the algorithms used for standard stationary electron beam treatment planning.

The angle β concept offers a semiempirical technique for treatment planning for electron arc therapy. The characteristic angle β for an arbitrary point A on the patient's surface (Fig. 8.10) is measured between the central axes of two rotational electron beams positioned in such a way that at point A the frontal edge of one beam crosses the trailing edge of the other beam.

The angle β is uniquely determined by three treatment parameters: f, the SAD; d_i, the depth of the isocentre; and w, the field width. Electron beams with combinations of d_i and w that give the same characteristic angle β actually exhibit very similar radial PDDs, even though they may differ considerably in individual d_i and w (see Fig. 8.11). Thus the PDDs for rotational electron beams depend only on the electron beam energy and on the characteristic angle β.
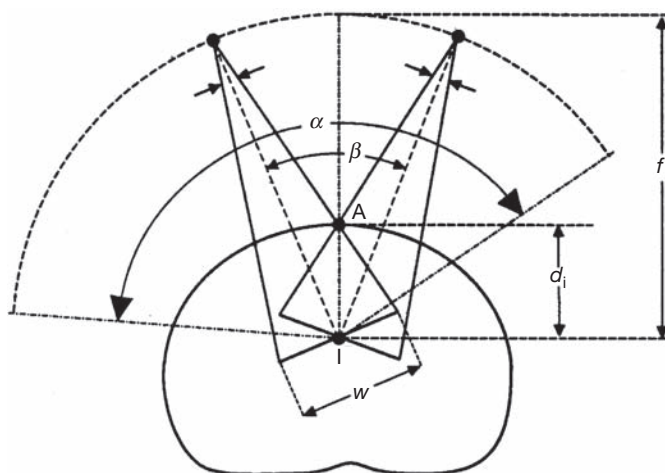
FIG. 8.10. Arc therapy geometry: f is the SAD; d_i is the depth of the isocentre; w is the field width defined at the isocentre; α is the arc angle or the angle of treatment; and β is the characteristic angle for the particular treatment geometry.

Photon contamination is of concern in electron arc therapy, since the photon contribution from all beams is added at the isocentre and the isocentre might be placed on a critical structure. Figure 8.12 shows a comparison between two dose distributions measured with film in a humanoid phantom. Figure 8.12(a) is for a small β of 10º (i.e. a small field width) and clearly exhibits a large photon dose at the isocentre, while Fig. 8.12(b) was taken for a large β of 100º and exhibits a low photon dose at the isocentre. In arc therapy the isocentre bremsstrahlung dose is inversely proportional to the characteristic angle β.
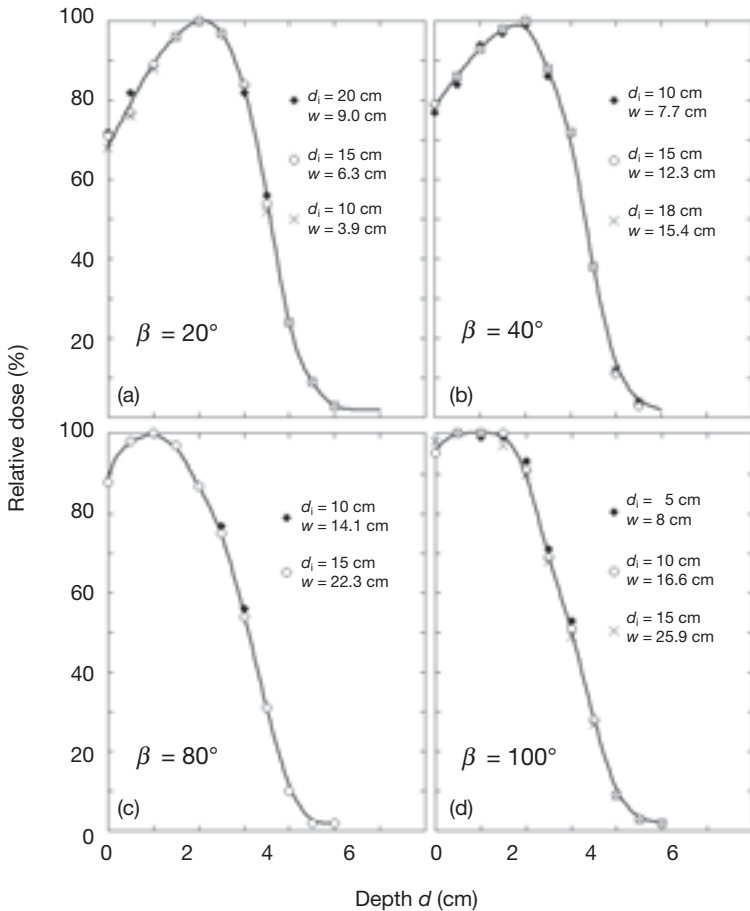
FIG. 8.11. Radial PDDs in electron arc therapy measured in a phantom for various combinations of w and d_i, giving characteristic angles β of (a) 20º, (b) 40º, (c) 80º and (d) 100º. The electron beam energy is 9 MeV.
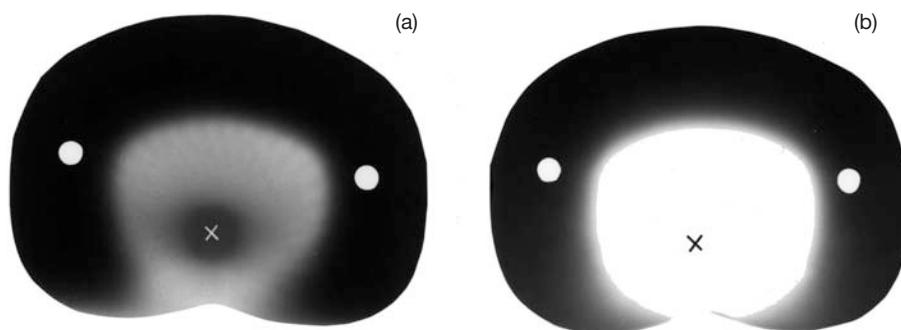
FIG. 8.12. Dose distributions for a 15 MeV rotational electron beam with an isocentre depth d_i of 15 cm, (a) for a β of 10° and (b) for a β of 100°.

One of the technical problems related to electron arc treatment involves the field shape of the moving electron beam defined by secondary collimators. For the treatment of sites that can be approximated with cylindrical geometry (e.g. the chest wall), the field width can be defined by rectangular photon collimators. When treating sites that can only be approximated with a spherical geometry (e.g. the scalp), a custom built secondary collimator defining a non-rectangular field of appropriate shape has to be used to provide a homogeneous dose in the target volume.

8.3.10. Electron therapy treatment planning

The complexity of electron–tissue interactions does not make electron beams well suited to conventional treatment planning algorithms. Electron beams are difficult to model, and look-up table type algorithms do not predict well the dose for oblique incidences or tissue interfaces.

The early methods of electron dose distribution calculations were empirical and based on water phantom measurements of PDDs and beam profiles for various field sizes, similarly to the Milan–Bentley method developed in the late 1960s for use in photon beams. Inhomogeneities were accounted for by scaling the depth dose curves using the CET technique. This technique provides useful parameterization of the electron depth dose curve but has nothing to do with the physics of electron transport, which is dominated by the theory of multiple scattering.

The Fermi–Eyges multiple scattering theory considers a broad electron beam as being made up of many individual pencil beams that spread out laterally in tissue, approximately as a Gaussian function, with the amount of spread increasing with depth. The dose at a particular point in tissue is calculated by an addition of contributions of spreading pencil beams.

The pencil beam algorithm can account for tissue inhomogeneities, patient curvature and irregular field shape. Rudimentary pencil beam algorithms deal with lateral dispersion but ignore angular dispersion and backscattering from tissue interfaces. Subsequent analytical advanced algorithms refined the multiple scattering theory through applying both the stopping powers and the scattering powers but nevertheless generally fail to provide accurate dose distributions in general clinical conditions.

The most accurate way to calculate electron beam dose distributions is through Monte Carlo techniques. The main drawback of the current Monte Carlo approach as a routine dose calculation engine is its relatively long calculation time. However, with ever increasing computer speeds combined with decreasing hardware costs, it can be expected that in the near future Monte Carlo based electron dose calculation algorithms will become available for routine clinical applications.

BIBLIOGRAPHY

INTERNATIONAL ATOMIC ENERGY AGENCY, The Use of Plane Parallel Ionization Chambers in High Energy Electron and Photon Beams, Technical Reports Series No. 381, IAEA, Vienna (1997).

— Absorbed Dose Determination in External Beam Radiotherapy, Technical Reports Series No. 398, IAEA, Vienna (2000).

INTERNATIONAL COMMISSION ON RADIATION UNITS AND MEASUREMENTS, Radiation Dosimetry: Electron Beams with Energies Between 1 and 50 MeV, Rep. 35, ICRU, Bethesda, MD (1984).

JOHNS, H.E., CUNNINGHAM, J.R., The Physics of Radiology, Thomas, Springfield, IL (1985).

KHAN, F.M., The Physics of Radiation Therapy, Lippincott, Williams and Wilkins, Baltimore, MD (2003).

KLEVENHAGEN, S.C., Physics and Dosimetry of Therapy Electron Beams, Medical Physics Publishing, Madison, WI (1993).

VAN DYK, J. (Ed.), Modern Technology of Radiation Oncology: A Compendium for Medical Physicists and Radiation Oncologists, Medical Physics Publishing, Madison, WI (1999).

Chapter 9

CALIBRATION OF PHOTON AND ELECTRON BEAMS

P. ANDREO
Department of Medical Radiation Physics,
University of Stockholm, Karolinska Institute,
Stockholm, Sweden

J.P. SEUNTJENS, E.B. PODGORSAK
Department of Medical Physics,
McGill University Health Centre,
Montreal, Quebec, Canada

9.1. INTRODUCTION

Modern radiotherapy relies on accurate dose delivery to the prescribed target volume. The ICRU has recommended an overall accuracy in tumour dose delivery of ±5%, based on an analysis of dose response data and on an evaluation of errors in dose delivery in a clinical setting. Considering all uncertainties involved in the dose delivery to the patient, the ±5% accuracy recommendation is by no means easy to attain.

Before clinical use, the output of photon and electron beams produced by external beam radiotherapy machines must be calibrated. This basic output calibration is but one, albeit very important, of the links constituting the chain representing an accurate dose delivery to the patient. The other links refer to: the procedures for measurement of relative dose data, equipment commissioning and quality assurance; treatment planning; and the actual patient set-up on the treatment machine.

- The basic output for a radiotherapy machine is usually stated as the dose rate for a point P at a reference depth z_{ref} (often the depth of dose maximum z_{max}) in a water phantom for a nominal source to surface distance (SSD) or source to axis distance (SAD) and a reference field size (often 10×10 cm^2) on the phantom surface or the isocentre. The output for kilovoltage X ray generators and teletherapy units is usually given in Gy/min, while for clinical accelerators it is given in Gy/MU.
- For superficial and orthovoltage beams and occasionally for beams produced by teletherapy radioisotope machines, the basic beam output

may also be stated as the air kerma rate in air (Gy/min) at a given distance from the source and for a given nominal collimator or applicator setting.

The basic output calibration of photon and electron beams is carried out with radiation dosimeters and special radiation dosimetry techniques. Radiation dosimetry refers to a determination by measurement and/or calculation of the absorbed dose or some other physically relevant quantity, such as air kerma, fluence or equivalent dose, at a given point of interest in a given medium.

A radiation dosimeter is defined as any device that is capable of providing a reading M that is a measure of the dose D deposited in the dosimeter's sensitive volume V by ionizing radiation.

— A dosimeter that produces a signal from which the dose in its sensitive volume can be determined without requiring calibration in a known field of radiation is referred to as an absolute dosimeter;
— Dosimeters requiring calibration in a known radiation field are called relative dosimeters.

The basic output calibration of a clinical radiation beam, by virtue of a direct measurement of dose or dose rate in water under specific reference conditions, is referred to as reference dosimetry. Three types of reference dosimetry technique are currently known:

(a) Calorimetry;
(b) Fricke dosimetry;
(c) Ionization chamber dosimetry.

These dosimeters can be used as absolute dosimeters but are seldom used as such in clinics, because their use in absolute dosimetry is cumbersome and, moreover, calibration in a known radiation field offers certain advantages, such as traceabilty to a standards laboratory. When an absolute dosimeter is used independently, it relies on its own accuracy instead of referring to a standard in common with other radiation users.

9.1.1. Calorimetry

Calorimetry is the most fundamental of the three reference dosimetry techniques, since it relies on basic definitions of either electrical energy or temperature. In principle, calorimetric dosimetry is simple; in practice,

however, the need for measuring extremely small temperature differences makes the technique very complex and relegates it to sophisticated standards laboratories.

Two main types of absorbed dose calorimeter are currently used in standards laboratories:

- Graphite calorimeters;
- Sealed water calorimeters.

In graphite calorimeters the average temperature rise is measured in a body that is thermally insulated from surrounding bodies ('jackets') by evacuated vacuum gaps. Gap corrections and dose transfer procedures are used in conjunction with graphite calorimeters to allow for the transfer of absorbed dose from graphite to water.

In stagnant sealed water calorimeters use is made of the low thermal diffusivity of water, which enables the temperature rise to be measured directly at a point in (continuous) water. Dose transfer procedures are not needed, but the measurement and analysis are complicated by the presence of conductive heat loss (or gain) and by the heat defect induced by radiolysis.

9.1.2. Fricke dosimetry

The energy of ionizing radiation absorbed in certain media produces a chemical change in the absorbing medium, and the amount of this chemical change may be used as a measure of absorbed dose. The best known chemical radiation dosimeter is the Fricke dosimeter, which relies on oxidation of ferrous ions into ferric ions in an irradiated ferrous sulphate solution. The amount of ferric ion produced in the solution is measured by absorption spectrometry with ultraviolet light at 304 nm, which is strongly absorbed by the ferric ion.

Fricke dosimetry (sometimes referred to as chemical dosimetry or ferrous sulphate dosimetry) depends on an accurate knowledge of the radiation chemical yield of ferric ions, measured in moles produced per 1 J of energy absorbed in the solution. The chemical yield is related to an older parameter, the G value, defined as the number of ferric molecules produced in the ferrous sulphate solution by 100 eV of absorbed energy. An accurate value of the chemical yield is difficult to ascertain because the chemical yield is affected to a certain degree by the energy of the radiation, dose rate and temperature of the solution during irradiation and readout. The best G value for ^{60}Co γ rays is 15.6 molecules per 100 eV, corresponding to a chemical yield of 1.607×10^{-6} mol/J. The typical dynamic range for ferrous sulphate Fricke dosimeters is from a few

grays to about 400 Gy, making Fricke dosimetry impractical for routine use in a clinic.

9.1.3. Ionization chamber dosimetry

The ionization chamber is the most practical and most widely used type of dosimeter for accurate measurement of machine output in radiotherapy. It may be used as an absolute or a relative dosimeter. Its sensitive volume is usually filled with ambient air and the dose related or dose rate related measured quantities are the ionization charge Q or ionization current I, respectively, produced by radiation in the chamber sensitive air mass m_{air}. Charge Q and air mass m_{air} are related to absorbed dose in air D_{air} by:

$$D_{air} = \frac{Q}{m_{air}}\left(\frac{W_{air}}{e}\right)$$

(9.1)

where (W_{air}/e) is the mean energy required to produce an ion pair in air per unit charge (the current value for dry air is 33.97 eV/ion pair or 33.97 J/C).

The subsequent conversion of the air cavity dose D_{air} to dose to medium (usually water) D_w is based on the Bragg–Gray or Spencer–Attix cavity theories (see Chapter 2 and Section 9.4 in this chapter).

The sensitive air volume or mass in an ionization chamber is determined:

- Directly by measurement (the chamber becomes an absolute dosimeter under special circumstances);
- Indirectly through calibration of the chamber response in a known radiation field (the chamber is used as a relative dosimeter).

9.1.4. Mean energy expended in air per ion pair formed

It is generally assumed that a constant value of (W_{air}/e) can be used for the complete photon and electron energy range used in radiotherapy dosimetry. However, there is no direct experimental support for such an assumption, as the data available have been obtained only from measurements with ^{60}Co and [137]Cs γ ray beams and 2 MV X rays. The value $(W_{air}/e) = (33.85 \pm 0.15)$ J/C early recommended by the ICRU came from a weighted mean value of the available experimental data, obtained mainly from absorbed dose measurements using a graphite calorimeter and a graphite ionization chamber in a graphite phantom. The two methods for deriving the absorbed dose to graphite must yield the same dose value, and one obtains:

$$(W_{air}/e) = \frac{D_{calorimetry}}{(Q/m_{air})s_{graphite,air}}$$ (9.2)

where Q is the charge collected in air mass m_{air} and corrected for influence quantities; and $s_{graphite,air}$ is the ratio of collision stopping powers for graphite and air calculated for the photon or electron beam energy used.

This method of evaluation requires a change in (W_{air}/e) when the stopping power ratio $s_{graphite,air}$ is changed. Following the introduction of new electron stopping power data by the ICRU in 1984, the value of (W_{air}/e) has been modified to (33.97 ± 0.06) J/C for dry air.

Analysis of the available experimental data at higher energies, mainly for electron beams, has suggested that energy dependence in (W_{air}/e) cannot be ruled out, but experimental uncertainties, and the use of different stopping power ratios over the years, do not allow a definitive conclusion to be reached on this question.

It is known that the (W_{air}/e) value for air at a temperature of 20ºC, pressure of 101.325 kPa and 50% relative humidity is 0.6% lower than that for dry air at the same temperature and pressure, resulting in a value of 33.77 J/C instead of 33.97 J/C. Thus for the same amount of energy available for creating charge, 0.6% more charge will be created in air at 50% relative humidity than in dry air (at 20ºC and 101.325 kPa).

9.1.5. Reference dosimetry with ionization chambers

Three types of ionization chamber may be used in reference dosimetry as absolute dosimeters:

- Standard free air ionization chambers;
- Cavity ionization chambers;
- Phantom embedded extrapolation chambers.

9.1.5.1. Standard free air ionization chambers

Standard free air ionization chambers measure the air kerma in air according to its definition by collecting all ions produced by the radiation beam that result from the direct transfer of energy from photons to primary electrons in a defined volume of air. Determination of the air kerma in air or air kerma rate in air requires accurate knowledge of (W_{air}/e). For practical reasons related to the range of charge carriers in air, the use of the standard free air ionization chamber is limited to photon energies below 0.3 MeV.

9.1.5.2. Cavity ionization chambers

Cavity ionization chambers measure the air kerma in air for energies in the range from 0.6 to 1.5 MeV by making use of the Bragg–Gray cavity relationship. Analogously to standard free air ionization chambers, ions are collected in air, but this time inside a cavity with a known cavity volume surrounded by a graphite wall thick enough to provide full buildup of secondary electrons. The Bragg–Gray equation relates the dose to air in the cavity of known volume to the dose to medium in which the secondary electron spectrum is being built up (i.e. the graphite wall (for the thick walled chambers used in primary standards dosimetry laboratories (PSDLs)). The absorbed dose to the wall is related to the collision air kerma in air through the mass–energy absorption coefficient ratio, wall to air. The collision air kerma in air is related to the total air kerma in air by correcting for the fractional energy expended in radiative interactions.

In addition to the need for an accurate knowledge of the sensitive air volume, wall correction factors are required to account for the effect of photon attenuation and scattering in the chamber wall. An accurate knowledge of (W_{air}/e) as well as the cavity volume and radiative fraction is required to determine the air kerma (rate) in air. Finally, standards laboratories implement additional correction factors such as the point source non-uniformity correction factor and factors that account for deviations from the Spencer–Attix cavity theory.

9.1.5.3. Phantom embedded extrapolation chambers

Phantom embedded extrapolation chambers are uncalibrated variable air volume extrapolation chambers built as an integral part of a water equivalent phantom in which the dose is measured, and can serve as radiation dosimeters in the measurement of absorbed dose for megavoltage photon and electron beams. Standard dosimetry protocols are based on the Bragg–Gray or Spencer–Attix cavity theories (see Chapter 2 for details), which provide a simple linear relationship between the dose at a given point in the medium and the ratio Q/m, where Q is the ionization charge collected in mass m of air in the measuring cavity inside the medium. In extrapolation chambers, the ratio Q/m is constant and may be replaced in the cavity relationship by the derivative dQ/dm, which can be measured accurately through a controlled variation in the electrode separation. The conversion of cavity dose to dose to medium is based on the Spencer–Attix cavity theory. As in the case of the standard free air ionization chamber and the cavity ionization chamber, extrapolation chamber dosimetry relies on an accurate knowledge of the value of (W_{air}/e).

9.1.6. Clinical beam calibration and measurement chain

The theoretical aspects of the three reference dosimetry techniques discussed above are all well understood; however, none of the three techniques, for one reason or another, is practical for routine clinical use. Clinical photon and electron beams are therefore most commonly calibrated with ionization chambers that are used as relative dosimeters and have calibration coefficients determined either in air or in water and are traceable to a national PSDL. The chamber calibration coefficient essentially obviates the need for an accurate knowledge of the chamber sensitive air volume.

The standard ISO 31-0, on quantities and units, has provided guidelines with regard to the use of the terms 'coefficient' and 'factor'. The former should be used for a multiplier possessing dimensions; the latter should be reserved for a dimensionless multiplier. For consistency, the widely disseminated practice of using the term 'calibration factor' is updated here to using 'calibration coefficient'.

The traceability of a calibration coefficient to a national PSDL implies that:

- The chamber was calibrated directly at the PSDL in terms of the air kerma in air or absorbed dose to water; or
- The chamber was calibrated directly at an accredited dosimetry calibration laboratory (ADCL) or secondary standards dosimetry laboratory (SSDL) that traces its calibration to a PSDL; or
- The chamber calibration coefficient was obtained through a cross-calibration with another ionization chamber (user's secondary standard), the calibration coefficient of which was measured directly at a PSDL, an ADCL or an SSDL.

9.1.7. Dosimetry protocols

The procedures to be followed when calibrating a clinical photon or electron beam are described in international or national radiation dosimetry protocols or dosimetry codes of practice; the choice of which protocol to use is largely left to individual radiotherapy departments. Dosimetry protocols are generally issued by national or regional organizations such as the American Association of Physicists in Medicine (AAPM) (North America), Institution of Physics and Engineering in Medicine and Biology (IPEMB) (UK), Deutsches Institut für Normung (DIN) (Germany), Nederlandse Commissie voor Stralingsdosimetrie (NCS) (the Netherlands and Belgium) and Nordic Association of Clinical Physics (NACP) (Scandinavia), or by international bodies such as the IAEA. This procedure ensures a high level of consistency in

dose determination among different radiotherapy clinics in a given country and between one country and another.

9.2. IONIZATION CHAMBER BASED DOSIMETRY SYSTEMS

As shown schematically in Fig. 9.1, ionization chamber based dosimetry systems are in principle quite simple and consist of three main components:

- A suitable ionization chamber;
- An electrometer;
- A power supply.

The circuitry of a simple ionization chamber based dosimetry system resembles a capacitor (ionization chamber) connected to a battery (power supply), with the electrometer measuring the 'capacitor' charging or discharging current.

9.2.1. Ionization chambers

Ionization chambers incorporate three electrodes, which define the chamber sensitive air volume. The sensitive air volume is typically of the order
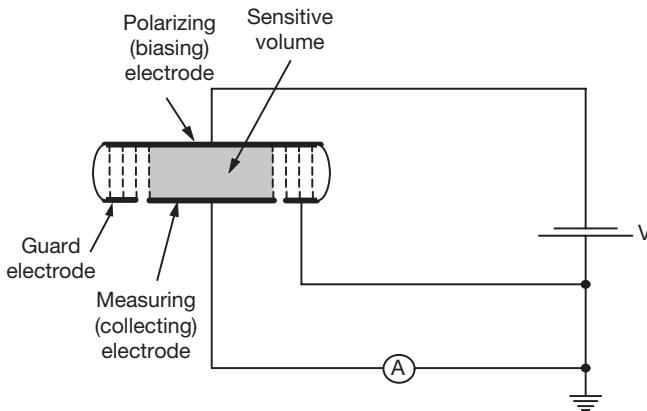
FIG. 9.1. Circuitry of an ionization chamber based dosimetry system. A represents the electrometer, V the power supply. The ionization chamber is usually connected to the electrometer through a shielded low noise triaxial cable, with the central wire carrying the signal from the measuring electrode to the electrometer, the first shield connecting the guard electrode to ground and the outer shield connecting the polarizing electrode to the power supply.

of 0.1 to 1 cm^3 in ionization chambers used for the calibration of clinical photon and electron beams. The three electrodes are the:

- Polarizing electrode, which is connected directly to the power supply.
- Measuring electrode, which is connected to ground through the low impedance electrometer to measure the charge or current produced in the chamber sensitive volume.
- Guard electrode, which is directly grounded and serves two purposes: it defines the chamber sensitive volume and prevents the measurement of chamber leakage currents.

Two types of ionization chamber are used in routine beam calibration:

— Cylindrical (often referred to as thimble) chambers;
— Parallel-plate (sometimes called end window or plane-parallel) chambers.

The more common cylindrical chambers are used in the calibration of orthovoltage and megavoltage X ray beams and electron beams of 10 MeV and above, while parallel-plate chambers are used in calibrations of superficial X ray beams, in calibrations of low energy electron beams and in surface dose measurements as well as dose measurements in the buildup region of megavoltage photon beams. Examples of typical ionization chambers used in radiotherapy are given in Fig. 9.2.

Air is usually used as the sensitive gas in an ionization chamber. The initial event of interaction of indirectly ionizing radiation with the chamber is characterized by a release of high energy electrons in the chamber wall or phantom through the photoelectric effect, Compton effect or pair production. Some of these electrons enter the chamber sensitive volume and ionize air molecules, producing positive ions and low energy electrons in the chamber sensitive volume. The low energy electrons attach themselves to electronegative oxygen molecules in air, forming negative ions. Thus in an air based ionization chamber the charged particles collected are the positive and negative ions (ion pairs) rather than positive ions and electrons.

9.2.2. Electrometer and power supply

An ionization chamber is essentially a capacitor in which leakage current or leakage charge is induced through the action of the radiation beam. The charge or current that is induced in the chamber is very small and must be measured by a very sensitive charge or current measuring device (electrometer). The power supply in ionization chamber/electrometer circuits
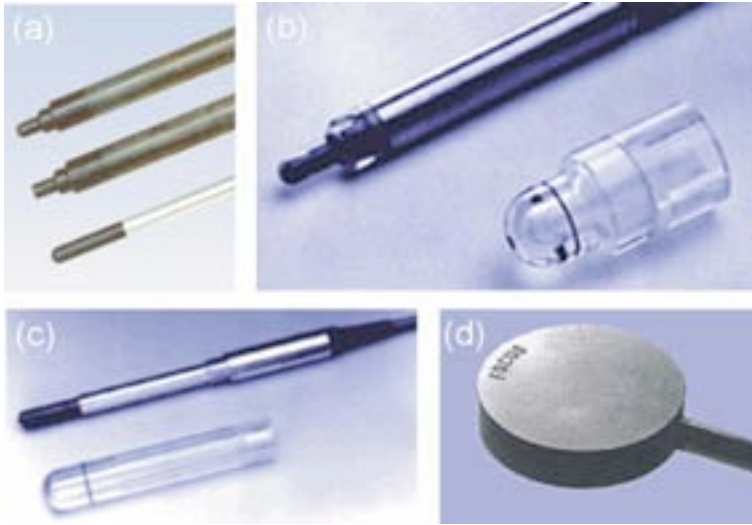
FIG. 9.2. Examples of typical ionization chambers used in radiotherapy: (a) cylindrical ionization chambers used for relative dosimetry; (b) pinpoint mini-chamber and ^{60}Co buildup cap; (c) Farmer type cylindrical chamber (top) with a ^{60}Co buildup cap (bottom); (d) parallel plate Roos type electron beam ionization chamber.

is either a stand-alone unit or forms an integral part of the electrometer. In either case it is important that one can change the magnitude and polarity of the voltage produced by the power supply, so that the ion collection efficiency of the chamber may be determined for a particular radiation beam (see Section 9.3).

9.2.3. Phantoms

Water is the standard phantom material for dosimetry measurements of photon and electron beams; however, dosimetric measurements are often carried out in more practical solid materials, such as polystyrene, Lucite, A-150 tissue equivalent plastic, Solid Water (WT1), Solid Water (RMI-457), Plastic Water or Virtual Water, that mimic water in terms of three parameters: mass density, number of electrons per gram and effective atomic number.

The effective atomic number Z_{eff} depends on the atomic composition of the mixture as well as on the type and quality of the radiation beam.

For low energy photons, for which the photoelectric effect is dominant over the Compton process and pair production events cannot occur, Z_{eff} of a mixture is defined by:

$$Z_{\text{eff}} = \sqrt[3.5]{\sum_i a_i Z_i^{3.5}}$$

(9.3)

where

a_i is the mass fraction of constituent element i;
Z_i is the atomic number of constituent element i.

Using Eq. (9.3) we obtain a Z_{eff} of 7.8 for air and 7.5 for water.

For megavoltage photon and electron beams Z_{eff} of a mixture is defined by:

$$Z_{\text{eff}} = \frac{\displaystyle\sum_i a_i \frac{Z_i^2}{A_i}}{\displaystyle\sum_i a_i \frac{Z_i}{A_i}}$$

(9.4)

where

a_i is the mass fraction of constituent element i;
Z_i is the atomic number of constituent element i;
A_i is the atomic mass of constituent element i.

Water is the most universal soft tissue substitute material, useful in both photon and electron beam measurements. Plastic solid materials are often used in phantom measurements; however, they are not universal tissue substitutes, since not all three required equivalency parameters for plastics can be matched adequately with those of water.

For photon beams, tissue equivalency or water equivalency implies a match in mass–energy absorption coefficient, mass stopping power and mass scattering power.

For a phantom to be water equivalent for electron dosimetry, it must match the linear stopping power and the linear scattering power of water. This is approximately achieved if the phantom material has the same electron density and the same atomic number as water.

Generally, water is recommended as the phantom material for the calibration of megavoltage photon and electron beams. The depth of calibration for megavoltage X ray beams is 10 cm, while for electron beams it is at a reference depth z_{ref}. The margin on the phantom around the nominal field size must be at least 5 cm of water in all directions, and there should be at least 10 cm of water beyond the chamber to provide adequate scattering conditions.

For kilovoltage X ray beams, the current plastics used in dosimetry cannot be considered truly water equivalent, and their use for calibration of X ray beam output should be approached with care.

9.3. CHAMBER SIGNAL CORRECTION FOR INFLUENCE QUANTITIES

For each ionization chamber, reference conditions are described by a set of influence quantities for which a chamber calibration coefficient is valid without any further corrections. Influence quantities are defined as quantities that are not the subject of a measurement but yet influence the quantity being measured. Examples of influence quantities in ionization chamber dosimetry are:

- Ambient air temperature, pressure and humidity;
- Applied chamber voltage and polarity;
- Chamber leakage currents;
- Chamber stem effects.

If the chamber is used under conditions that differ from the reference conditions, then the measured signal must be corrected for the influence quantities to obtain the correct signal.

9.3.1. Air temperature, pressure and humidity effects: $k_{T,P}$

The mass of air contained in the sensitive volume of the chamber is equal to $\rho_{air}V_{eff}$, where ρ_{air} is the air density and V_{eff} is the effective sensitive volume of the chamber. Since most ionization chambers are open to the ambient atmosphere, the air density ρ_{air} is a function of the atmospheric pressure, temperature and humidity, and so is the charge collected by the chamber, as both the air density and the collected charge are correlated.

It is common practice to fix the value of ρ_{air} to certain conditions and convert the chamber reading to these conditions. Most standards laboratories use the value of 1.2930 kg/m^3 for the dry air density value at standard conditions of 0ºC and 101.325 kPa. Considering air as an ideal gas, the density $\rho_{air}(T, P)$ at an arbitrary temperature T (ºC) and pressure P (kPa) is then given by:

$$\rho_{air}(T,P) = \rho_{air}(0\,^{\circ}\mathrm{C}, 101.325\text{ kPa})\frac{273.2}{(273.2+T)}\frac{P}{101.325} \tag{9.5}$$

When calibrating an ionization chamber, the charge measured by the chamber depends on the air temperature, pressure and humidity, and therefore the calibration coefficient must be given for stated reference values of these parameters. At most standards laboratories the chamber signal is corrected to normal conditions of 20ºC (22ºC in North America) and 101.325 kPa, but no correction is applied for humidity. Instead, the relative humidity during calibration is controlled within the range from 45% to 55%, so that the calibration coefficient applies for relative humidities around 50%.

In the user's beam, the correction factor for air temperature and air pressure $k_{T,P}$ is given as :

$$k_{T,P} = \frac{(273.2+T)}{(273.2+T_0)} \frac{P_0}{P}$$ (9.6)

and is applied to convert the measured signal to the reference conditions used for the chamber calibration at the standards laboratory. Note that P and T (ºC) are chamber air pressure and temperature, respectively, at the time of measurement, while P_0 and T_0 (ºC) are the normal conditions used in the standards laboratory.

The temperature of the air in a chamber cavity should be taken as that of the phantom, which is not necessarily the same as the temperature of the surrounding air. For measurements in a water phantom the chamber waterproof sleeve should be vented to the atmosphere in order to obtain a rapid equilibrium between the ambient air and the air in the chamber cavity.

(W_{air}/e) and stopping powers that are used in dosimetry protocols are stated for dry air but are affected by chamber air humidity. This results in an overall humidity correction factor of 0.997 for a ^{60}Co beam, correcting measurements at the 50% humidity level to those that would be obtained under dry air conditions and consisting of a 0.994 correction to the (W_{air}/e) dry air value of 33.97 J/C and a 1.003 correction to stopping powers.

9.3.2. Chamber polarity effects: polarity correction factor k_{pol}

Under identical irradiation conditions the use of polarizing potentials of opposite polarity in an ionization chamber may yield different readings, a phenomenon that is referred to as the polarity effect. For most ionization chamber types, the effect is practically negligible at phantom depths exceeding the depth of dose maximum in megavoltage photon beams, but in the buildup region of megavoltage photon beams and in electron beams, notably at low energies, as well as in very low energy X ray beams, the effect may be significant.

In electron beams the polarity effect is considered a charge balance effect that depends on the energy and angular distribution of the incident radiation, measurement depth in a phantom and field size. The polarity effect may actually change its sign with depth in a phantom.

When a chamber is used in a beam that produces a measurable polarity effect, the true reading is taken to be the mean of the absolute values of readings taken at the two polarities.

The polarity correction factor k_{pol} is thus given by the following relationship:

$$k_{pol} = \frac{|M_+| + |M_-|}{2M} \tag{9.7}$$

where M_+ and M_- are the chamber signals obtained under identical irradiation conditions at positive and negative chamber polarities, respectively, and M is the signal obtained at the polarity used routinely (either positive or negative).

If the polarity effect for a particular chamber is larger than 3%, the chamber should not be used for absolute dose measurement.

Whenever the polarity has been changed, charge equilibrium and stable operating conditions should be re-established by preirradiating the chamber and waiting several minutes before the next measurement.

9.3.3. Chamber voltage effects: recombination correction factor k_{sat}

The response of a given ionization chamber depends not only on the radiation dose, dose rate and chamber polarity but also on the voltage applied between the measuring and collecting electrodes of the chamber. The charges produced in the chamber by radiation may differ from the charges that are actually collected, and these discrepancies (charge losses or excess charges) occur as a result of constraints imposed by the physics of ion transport in the chamber sensitive volume and the chamber electrical design.

Charge losses in the chamber are caused by ion recombination; excess charges are caused by charge multiplication and electrical breakdown. Both charge recombination and charge multiplication are influenced by the potential applied to the ionization chamber.

A plot of chamber response (i.e. current I or charge Q against the applied voltage V for a constant dose rate or dose, respectively) is called a saturation curve, first rising linearly with voltage at low voltages, then reaching a saturation at high voltages and eventually breaking down at even higher voltages. A sketch of a typical saturation curve is shown in Fig. 9.3.
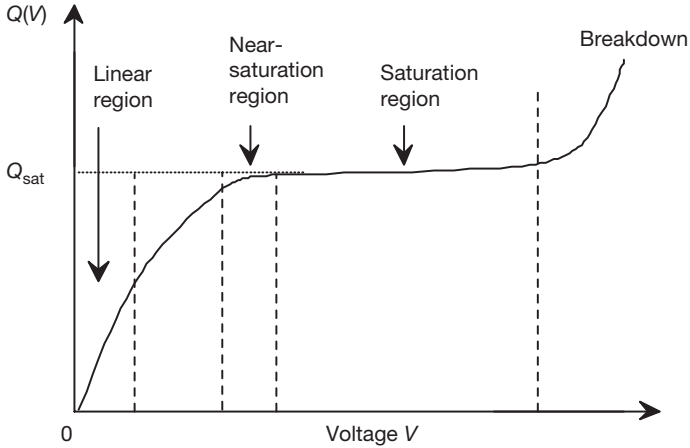
FIG. 9.3. Typical saturation curve for an ionization chamber. The saturation charge is represented by Q_{sat} and is used in dosimetry protocols as the appropriate parameter describing the radiation signal. Ionization chambers are usually operated in the near-saturation region and Q_{sat} is calculated by dividing the measured signal by the collection efficiency f.

The ratio $Q(V)/Q_{sat}$ or $I(V)/I_{sat}$, where Q_{sat} and I_{sat} are the saturation values of Q and I, respectively, is referred to as the collection efficiency f of the ionization chamber at the applied voltage V. In radiation dosimetry, ionization chambers are commonly used in the near-saturation region where $f > 0.98$, or even in the saturation region, where $f \approx 1$.

In saturation, all charges produced by radiation are collected and produce directly the Q_{sat} and I_{sat} for use in dosimetry protocols. When the chamber is used below saturation, some of the charges produced by radiation actually recombine and are lost to the dosimetric signal. This charge loss occurs through three different mechanisms:

- General recombination: opposite charges from different tracks collide and recombine.
- Initial recombination: opposite charges from same tracks collide and recombine.
- Ionic diffusion loss: charges diffuse against the electric field.

For studies of ionic recombination losses, ionizing radiations are placed into three categories:

— Continuous radiation (e.g. cobalt beams and orthovoltage X rays);
— Pulsed beams (e.g. non-scanned linac X ray beams and electrons);
— Scanned pulsed beams (e.g. scanned linac beams).

The ionic recombination correction factor k_{sat} (labelled P_{ion} in the AAPM TG 21 and TG 51 notation and equal to $1/f$ in recombination theory) accounts for the loss of ions in the chamber sensitive volume due to initial recombination, general recombination and diffusion against the electric field. General recombination is by far the predominant of the three effects.

According to Boag, in the near-saturation region f_g^c the collection efficiency for general recombination in a continuous radiation beam may be written as:

$$f_g^c = \frac{Q}{Q_{sat}} = \frac{1}{1+\dfrac{\Lambda_g}{V^2}} \tag{9.8}$$

or

$$\frac{1}{Q} = \frac{1}{Q_{sat}} + \frac{\Lambda_g/Q_{sat}}{V^2} = \frac{1}{Q_{sat}} + \frac{\lambda_g}{V^2} \tag{9.9}$$

and in a pulsed beam:

$$f_g^p = \frac{Q}{Q_{sat}} = \frac{V}{C}\ln\left(1+\frac{C}{V}\right) \tag{9.10}$$

or

$$\frac{1}{Q} = \frac{1}{Q_{sat}} + \frac{C/Q_{sat}}{2V} = \frac{1}{Q_{sat}} + \frac{C'}{V} \tag{9.11}$$

where Λ_g, C and C' are constants, Q is the measured signal and Q_{sat} is the saturation value of the signal.

The relationship for $1/Q$ suggests a linear behaviour when plotted against $1/V^2$ for continuous beams (Eq. (9.9)) and against $1/V$ for pulsed beams (Eq. (9.11)), with $1/Q_{sat}$ the intercept of the linear plot with the ordinate (i.e. for $1/V \rightarrow 0$ or $V \rightarrow \infty$).

Assuming the predominance of general recombination and based on the linear relationship of $1/Q$ with either $1/V^2$ in continuous radiation or $1/V$ in pulsed radiation, one can determine the collection efficiencies f_g^c and f_g^p for continuous and pulsed beams, respectively, with the so called two voltage technique. Chamber signals M are determined under the same irradiation conditions at two voltages, the normal operating voltage V_N and a lower

voltage V_L. The collection efficiencies at the normal chamber operating voltage V_N are then expressed as:

$$f_g^c(V_N) = \frac{M_N}{M_{sat}} = \frac{\dfrac{M_N}{M_L} - \left(\dfrac{V_N}{V_L}\right)^2}{1 - \left(\dfrac{V_N}{V_L}\right)^2} \tag{9.12}$$

for continuous beams and

$$f_g^p(V_N) = \frac{M_N}{M_{sat}} = \frac{\dfrac{M_N}{M_L} - \dfrac{V_N}{V_L}}{1 - \dfrac{V_N}{V_L}} \tag{9.13}$$

as an approximation for pulsed beams, where

M_N is the chamber signal determined at the normal operating voltage V_N;
M_L is the chamber signal determined at a lower voltage V_L;
M_{sat} is the saturation signal at $V = \infty$.

The polarity effect will change with the voltage, and both M_N and M_L should be corrected for this effect using Eq. (9.7).

For pulsed and pulsed–scanned megavoltage radiation beams, dosimetry protocols recommend that the recombination correction factor $k_{sat}(V_N)$ be determined:

(i)   Assuming a linear relationship between $1/M$ and $1/V$;
(ii)   Using the two voltage technique and the following quadratic polynomial:

$$k_{sat}(V_N) = a_0 + a_1 \frac{M_N}{M_L} + a_2 \left(\frac{M_N}{M_L}\right)^2 \tag{9.14}$$

where a_i are constants tabulated for pulsed and pulsed–scanned beams (see, for example, IAEA TRS 398, p. 52).

For $k_{sat}(V_N) \leq 1.03$ (i.e. $f \geq 0.97$) the recombination correction factor may be approximated to within 0.1% using the following relationship obtained from general recombination theory:

$$k_{\text{sat}}(V_N) = 1 + \frac{\dfrac{M_N}{M_L} - 1}{\dfrac{V_N}{V_L} - 1}$$

(9.15)

where, as defined above, M_N and M_L are the chamber signals obtained with the normal applied potential V_N and low applied potential V_L, respectively.

The ratio V_N/V_L should be equal to or larger than 3, and V_N must not be too large in order to ensure that charge multiplication effects do not contribute to the measured chamber signal.

It is important to re-establish charge equilibrium after the bias voltage has been changed. This can be achieved by preirradiating the chamber with a dose of 2 to 5 Gy before the next measurement.

9.3.4. Chamber leakage currents

Leakage currents present a difficult challenge in the design of ionization chamber based dosimetric systems. Their effects on the true radiation induced currents are minimized with guard electrodes, low noise triaxial cables and sophisticated electrometers. Leakage currents fall into three categories:

- Intrinsic (dark) leakage currents;
- Radiation induced leakage currents;
- Mechanical stress induced and friction induced spurious cable currents.

No matter how well an ionization chamber dosimetric system is designed, there will always be a small, non-radiation related signal present when the system is in a ready mode to respond to radiation. This intrinsic (dark) current results from surface and volume leakage currents flowing between the polarizing and measuring electrodes of the ionization chamber.

In a well designed ionization chamber system the intrinsic leakage currents are at least two orders of magnitude lower than the measured radiation induced signals, and are thus either negligible or can be suppressed from the actual radiation signal.

Electric leakage in the ionization chamber and electrometer may also occur as a consequence of the irradiation of insulators and chamber parts, cables and electronics of the measuring equipment. This is termed post-irradiation leakage, an effect that continues after the irradiation has ceased and commonly decreases exponentially with time.

IEC 60731 recommends that within 5 s after the end of a 10 min irradiation the leakage current should have decreased to ±1.0% or less of the ionization current produced in the measuring volume during the irradiation (i.e. it will fall to the intrinsic leakage current level of the dosimetric system).

Another effect in insulators, which received considerable attention in the mid-1980s, is the charge accumulation in non-conductive plastic phantoms. This charge accumulation causes a very large electric field around the chamber directing the flow of electrons towards the chamber cavity, yielding an increased signal and an erroneous result for the collection efficiency.

Mechanical stress on cable insulators can also cause a leakage current, and for this reason unnecessary bending and twisting of the cables should be avoided.

9.3.5. Chamber stem effects

Irradiating the chamber stem often cannot be avoided, but it results in a different type of leakage current, which is generally referred to as the stem effect. Two mechanisms have been described by the IEC, namely stem scatter and stem leakage:

- Stem scatter arises from the effect of scattered radiation in the stem that reaches the chamber volume. This effect can be determined using a dummy stem, and the chamber is irradiated successively with and without the presence of the dummy stem; the ratio of the readings allows a correction factor for the effect to be determined.
- Stem leakage arises as a consequence of a direct irradiation of this chamber volume as well as of the insulators and cables in the chamber. The effect can be determined by irradiating a chamber twice with a narrow rectangular field, once in a parallel orientation and then perpendicularly to the chamber central axis. A correction factor can be derived as above.

9.4. DETERMINATION OF ABSORBED DOSE USING CALIBRATED IONIZATION CHAMBERS

For practical reasons, outputs of clinical photon and electron beams are usually measured with ionization chambers that have calibration coefficients traceable to a standards laboratory and are thus used as relative dosimeters. Before such a chamber is used in radiotherapy machine output calibration, the user must identify a dosimetry protocol (code of practice) appropriate for the

given radiation beam. A dosimetry protocol provides the formalism and the data to relate a calibration of a chamber at a standards laboratory to the measurement of absorbed dose to water under reference conditions in the clinical beam. Two types of dosimetry protocol are available:

- Protocols based on air kerma in air calibration coefficients;
- Protocols based on absorbed dose to water calibration coefficients.

Most current megavoltage dosimetry protocols rely on chamber calibration coefficients determined in ^{60}Co beams at standards laboratories. It is expected that the use of megavoltage beam calibration qualities (X rays and electrons), today available only in a few PSDLs, will become more widespread in the future.

Conceptually, both types of protocol are similar and are based on several steps in the process of determining the absorbed dose or dose rate from a charge or current measurement, respectively, with an ionization chamber.

The first step in the use of dosimetry protocols involves the determination of the chamber signal M_Q through correction of the measured chamber charge or current for influence quantities known to affect the measured chamber signal, as discussed in Section 9.3. The subscript Q denotes the quality index of the beam being calibrated, as discussed in Section 9.8.

It should be noted that the formalisms presented here, based on a ^{60}Co calibration coefficient, work well for megavoltage photon and electron beams. The calibration of superficial and orthovoltage X ray beams, on the other hand, relies on different principles and the chamber calibration coefficient should be obtained for the particular X ray beam quality that is being calibrated. The physics of kilovoltage dosimetry is discussed in more detail in Section 9.10.

9.4.1. Air kerma based protocols

Air kerma based protocols use the air kerma in air calibration coefficient $N_{K,Co}$ obtained for a local reference ionization chamber in a ^{60}Co beam at a standards laboratory. Routine ionization chambers are then cross-calibrated with the reference ionization chamber in a local ^{60}Co beam. Two steps are involved in an air kerma based protocol for the calibration of megavoltage photon and electron beams:

- The cavity air calibration coefficient $N_{D,air}$ is calculated from the $N_{K,Co}$ calibration coefficient.

● Absorbed dose to water is determined using the Bragg–Gray relationship in conjunction with the chamber signal M_Q and the cavity air calibration coefficient $N_{D,air}$.

In a ^{60}Co beam at a standards laboratory the mean absorbed dose to air in the cavity is determined from the total air kerma in air $(K_{air})_{air}$ using the relationship:

$$D_{air} = (K_{air})_{air}(1-g)k_m k_{att} k_{cel} \qquad (9.16)$$

where

g is the fraction of the total transferred energy expended in radiative inter-actions on the slowing down of secondary electrons in air;

k_m is a correction factor for the non-air equivalence of the chamber wall and buildup cap needed for an air kerma in air measurement;

k_{att} is a correction factor for photon attenuation and scatter in the chamber wall;

k_{cel} is a correction factor for the non-air equivalence of the central electrode of the cylindrical ionization chamber.

The cavity air calibration coefficient $N_{D,air}$ is defined as:

$$N_{D,air} = D_{air}/M_Q \qquad (9.17)$$

where M_Q is the chamber signal corrected for influence quantities.

The air kerma in air calibration coefficient $N_{K,Co}$ is defined as:

$$N_{K,Co} = (K_{air})_{air}/M_Q \qquad (9.18)$$

If the electrometer device has its readout in nano-coulombs, both the cavity calibration coefficient and the air kerma in air calibration coefficient are given in units of cGy/nC.

By dividing the left and right hand sides of Eq. (9.16) by the corrected chamber signal in the calibration beam M_Q, the cavity air calibration coefficient can be determined from the air kerma in air calibration coefficient, determined at the ^{60}Co beam quality, using the relationship:

$$N_{D,air} = N_{K,Co}(1-g)k_m k_{att} k_{cel} \qquad (9.19)$$

The cavity air calibration coefficient is also directly related to the effective volume V_{eff} of the chamber by:

$$N_{\text{D,air}} = \frac{D_{\text{air}}}{M_Q} = \frac{1}{m_{\text{air}}}\frac{W_{\text{air}}}{e} = \frac{1}{\rho_{\text{air}}V_{\text{eff}}}\frac{W_{\text{air}}}{e} \qquad (9.20)$$

where

(W_{air}/e) is the average energy required to produce an ion pair in air;
m_{air} is the mass of air in the chamber cavity;
ρ_{air} is the air density at standard conditions of temperature and pressure;
V_{eff} is the effective air volume in the chamber collecting ions.

Equation (9.20) shows clearly that $N_{\text{D,air}}$ is a characteristic of the dosimetric device and depends only on the effective mass of air in the chamber cavity and does not depend on radiation quality as long as (W_{air}/e) is independent of the radiation quality. Hence the $N_{\text{D,air}}$ calibration coefficient determined at the ^{60}Co beam quality at the standards laboratory is also valid at the user's megavoltage beam quality Q.

If the effective chamber cavity volume V_{eff} were accurately known, the $N_{\text{D,air}}$ calibration coefficient could in principle be determined using Eq. (9.20). This is the case for cavity ionization chambers used to establish the air kerma in air for cobalt units at standards laboratories (see Section 9.1.4). For typical ionization chambers used in the clinic, however, V_{eff} is not known with sufficient accuracy and $N_{\text{D,air}}$ must be determined from the air kerma in air calibration coefficient $N_{\text{K,Co}}$ using Eq. (9.19).

The absorbed dose to air $D_{\text{air},Q}$ in the air cavity can be converted into absorbed dose to medium (e.g. water) $D_{\text{w},Q}$ by making use of the Bragg–Gray cavity relationship. With a known value of $N_{\text{D,air}}$ for a specific chamber, the fully corrected chamber signal M_Q at a point in a phantom allows determination of the absorbed dose to water as follows:

$$D_{\text{w},Q} = D_{\text{air},Q}(s_{\text{w,air}})_Q p_Q = M_Q N_{\text{D,air}}(s_{\text{w,air}})_Q p_Q \qquad (9.21)$$

where

$(s_{\text{w,air}})_Q$ is the ratio of restricted collision stopping powers of water to air;
p_Q is a perturbation correction factor accounting for perturbations caused by the chamber inserted into the medium, as discussed in detail in Section 9.7.

9.4.2. Absorbed dose to water based protocols

All dosimetry protocols aim at determination of the quantity absorbed dose to water. It is therefore logical to provide ionization chambers directly with a calibration coefficient in terms of this quantity, rather than in terms of the air kerma in air, if at all possible. Recent developments have provided support for a change in the quantity used at present to calibrate ionization chambers and provide calibration coefficients in terms of absorbed dose to water $N_{D,w}$ for use in radiotherapy beams. Many PSDLs now provide $N_{D,w}$ calibrations in ^{60}Co γ ray beams and some laboratories have already extended these calibration procedures to high energy photon and electron beams.

The absorbed dose to water $D_{w,Q0}$ at the reference depth z_{ref} in water for a reference beam of quality Q_0 and in the absence of the chamber is directly given by:

$$D_{w,Q0} = M_{Q0}N_{D,w,Q0} \tag{9.22}$$

where M_{Q0} is the fully corrected chamber reading under the reference conditions used in the standards laboratory and $N_{D,w,Q0}$ is the calibration coefficient in terms of the absorbed dose to water of the chamber obtained from the standards laboratory.

When a chamber is used in a beam of quality Q that differs from the quality Q_0 that was used in its calibration, the absorbed dose to water is given by:

$$D_{w,Q0} = M_{Q0}N_{D,w,Q0}k_{Q,Q0} \tag{9.23}$$

where the factor $k_{Q,Q0}$ corrects for the differences between the reference beam quality Q_0 and the actual user quality Q.

The beam quality correction factor $k_{Q,Q0}$ is defined as the ratio, at beam qualities Q and Q_0, of the calibration coefficients in terms of absorbed dose to water of the ionization chamber:

$$k_{Q,Q0} = \frac{N_{D,w,Q}}{N_{D,w,Q0}} \tag{9.24}$$

Currently, the common reference quality Q_0 used for the calibration of ionization chambers is the ^{60}Co γ radiation, and the symbol $k_{Q,Co}$, abbreviated to k_Q, is often used for the beam quality correction factor.

At some PSDLs high energy photon and electron beams are directly used for calibration purposes and the symbol $k_{Q,Q0}$ is used in these cases, with Q_0

specifying the calibration beam. Ideally, the beam quality correction factor should be measured directly for each chamber at the same quality as the user's beam. However, this is not achievable in most standards laboratories. Such measurements can be performed only in laboratories having access to the appropriate beam qualities; for this reason the technique is at present restricted to a few PSDLs around the world, as the procedure requires the availability of an energy independent dosimetry system, such as a calorimeter, operating at these beam qualities.

When no experimental data are available, or when it is difficult to measure $k_{Q,Q0}$ directly for realistic clinical beams, the correction factors can, in many cases, be calculated theoretically. By comparing Eq. (9.24) with the $N_{D,air}$ formalism given above, $k_{Q,Q0}$ can be written as:

$$k_{Q,Q0} = \frac{(s_{w,air})_Q}{(s_{w,air})_{Q0}} \frac{p_Q}{p_{Q0}}$$

(9.25)

including the following ratios, at beam qualities Q and Q_0:

- Spencer–Attix water to air restricted stopping power ratios $s_{w,air}$;
- The perturbation factors p_Q and p_{Q0} for departures from the ideal Bragg–Gray detector conditions.

The calculations of $k_{Q,Q0}$ are based on exactly the same data used in the calculations in the air kerma based approach, but the parameters are used as ratios, which have reduced uncertainties compared with individual values.

Most protocols provide a modified formalism for electron beams for use when a chamber is cross-calibrated (i.e. does not have a direct $N_{D,w,Co}$ calibration coefficient). The details can be found in the IAEA TRS 398 and AAPM TG 51 protocols.

A still frequently used quantity is the exposure calibration coefficient N_X, which is related to the air kerma in air calibration coefficient N_K through the following relationship:

$$N_K = N_X \frac{W_{air}}{e} \frac{1}{1-g}$$

(9.26)

where g is the fraction of the energy loss in air expended in radiative interactions (the radiative fraction). For ^{60}Co γ rays in air $g = 0.003$, for superficial X rays in air $g < 0.0002$.

Typical units of N_X and N_K are R/nC and Gy/nC, respectively. A typical unit for both $N_{D,air}$ and $N_{D,w}$ is Gy/nC.

Air kerma based   **Absorbed dose based**

Calibration beam

$(K_{air})_{air}$ is known in the calibration beam. $N_{K,Co}$ is determined for the user chamber

D_w is known in the calibration beam. $N_{D,w}$ is determined for the user chamber

$$N_{D,air} = N_{K,Co}(1-g)k_m k_{att} k_{cel}$$

$$N_{D,air} = \frac{N_{D,w}}{(s_{w,air} P_Q)_{Q_0}}$$

$N_{D,air}$

User's beam

Air kerma based route
$$D_w = M_Q N_{D,air} s_{w,air} P_Q$$

Absorbed dose based route
$$D_w = M_Q N_{D,w} k_{Q,Q_0}$$
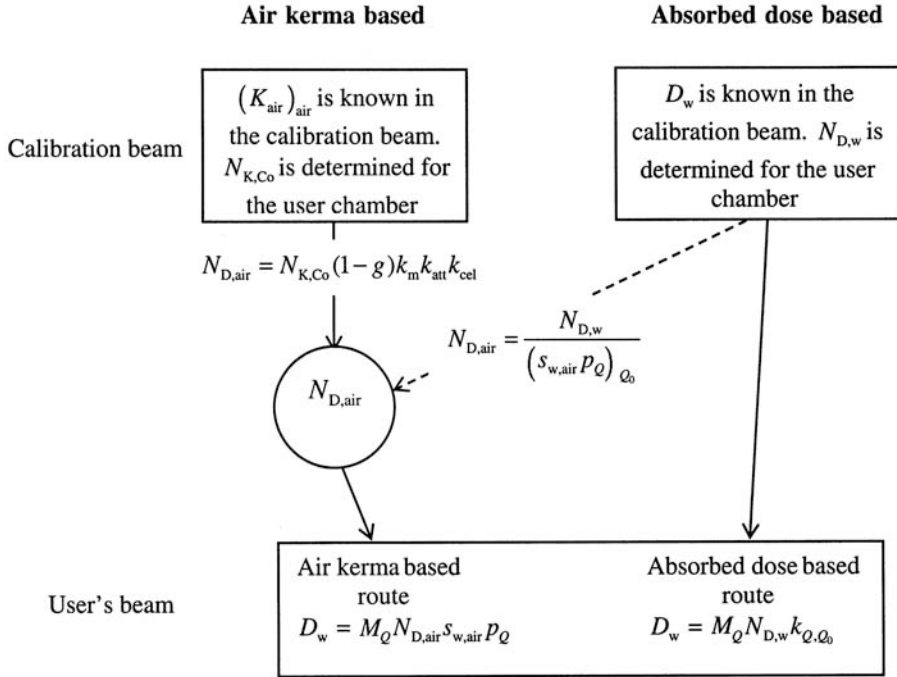
FIG. 9.4. Steps involved in ionization chamber based reference dosimetry: (a) air kerma in air based, (b) absorbed dose to water based.

A schematic summary of the steps involved in air kerma in air based and absorbed dose to water based calibration routes is given in Fig. 9.4. The physics and characteristics of stopping power ratios and perturbation correction factors are discussed in more detail in Sections 9.5 and 9.7.

The air kerma in air based formalism as well as the absorbed dose to water based formalism for the determination of absorbed dose to water in reference conditions includes stopping power ratios and correction factors for perturbation effects, the latter being detector dependent. Some of the analytical models available for the calculation of perturbation correction factors also include mass–energy absorption coefficient ratios.

Although ideally the formalism in terms of absorbed dose to water is based on experimentally determined quantities, the approach most common today relies on theoretically determined beam quality factors $k_{Q,Q0}$, which are also based on stopping power ratios (see Section 9.5) and perturbation correction factors (see Section 9.7).

9.5. STOPPING POWER RATIOS

The determination of absorbed dose in a medium using an ionization chamber is based on the Bragg–Gray principle relating the absorbed dose at a point in the medium (water) D_w to the mean absorbed dose in the detector (air) $\bar{D}_{air}$ through a proportionality factor that classically has been identified as the ratio of the mass (collision) stopping powers water to air:

$$D_w = \bar{D}_{air} s_{w,air} \tag{9.27}$$

The key Bragg–Gray assumption is that the electron fluence present in the detector is identical to that in the (undisturbed) medium at the point of interest in the water phantom. The gas filled ionization chamber in a high energy photon or electron beam behaves to a good approximation as a Bragg–Gray detector. Any deviations from perfect Bragg–Gray behaviour are accounted for by perturbation factors, which are discussed in detail in Section 9.7. The stopping power ratio applies to the electron spectrum at the point of interest in the undisturbed medium and is independent of the detector (except for the minor influence of the Spencer–Attix cut-off).

9.5.1. Stopping power ratios for electron beams

The most important characteristic of the water/air stopping power ratios for monoenergetic electrons is their strong dependence on energy and depth, as shown in Fig. 9.5, resulting mainly from the considerable variation in energy spectra at the various depths in water.

Until lately, the selection of stopping power ratios for the user's beam in electron dosimetry protocols has relied on the use of monoenergetic data using Harder's procedure based on the characterization of the electron beam through the mean electron energy at the phantom surface $\bar{E}_0$ together with depth of measurement z. Clinical beams are, however, far from monoenergetic and monodirectional at the phantom surface and even less so at depths in a phantom.

The validity of the $s_{w,air}(\bar{E}_0, z)$ selection procedure has been reviewed in detail in the IAEA protocol for parallel-plate ionization chambers (IAEA TRS 381) and a conclusion was reached that, even for beams with large energy and angular spread, the maximum error produced by such a procedure is always within 1%. For most beams used in clinical practice, even for those with a certain degree of photon contamination, the agreement was within the estimated uncertainty of the calculated stopping power ratios, being of the order of 0.6%.
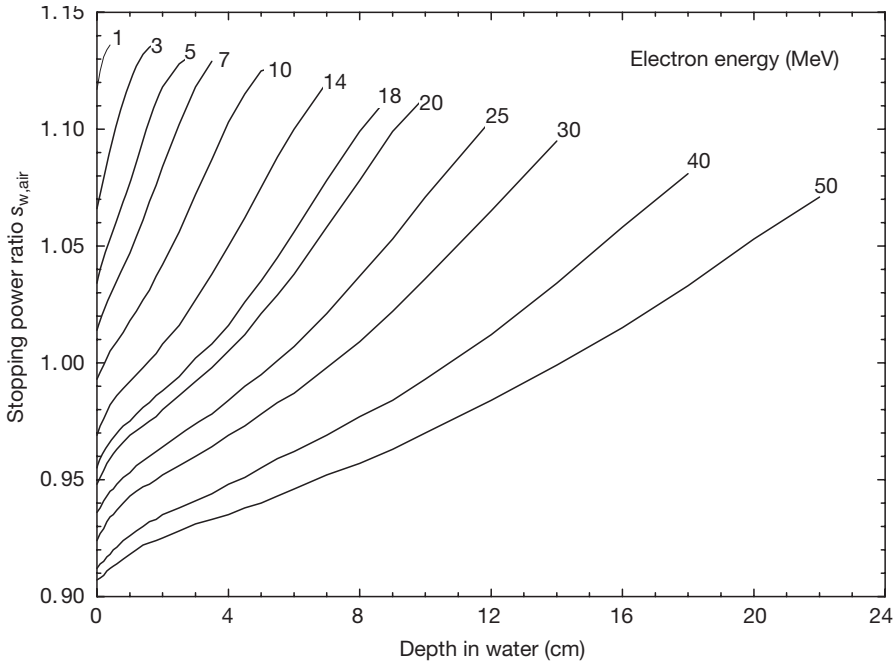
FIG. 9.5. Depth variation of the ratio of the mean restricted mass stopping powers of water and air $s_{w,air}$ for a cut-off energy Δ of 10 keV, derived from Monte Carlo generated electron spectra for monoenergetic, plane-parallel broad electron beams.

Stopping power ratios for realistic electron beams, obtained by simulating in detail the treatment head of some clinical accelerators, have become available and are used in the most recent dosimetry protocols based on standards of absorbed dose to water. However, it has been verified that no dramatic changes occur in electron beam dosimetry solely due to this improvement in the calculation of stopping power ratios.

9.5.2. Stopping power ratios for photon beams

The most important characteristic of the depth variation of the stopping power ratios of monoenergetic photons is that the ratios are almost constant beyond the depth of dose maximum (i.e. in the region of the transient electronic equilibrium), as Fig. 9.6 clearly shows. The range of variation of the stopping power ratio data with energy is also much smaller than in the case of electrons with similar energies. In the case of photon bremsstrahlung spectra produced by clinical accelerators the constancy of the stopping power ratio is
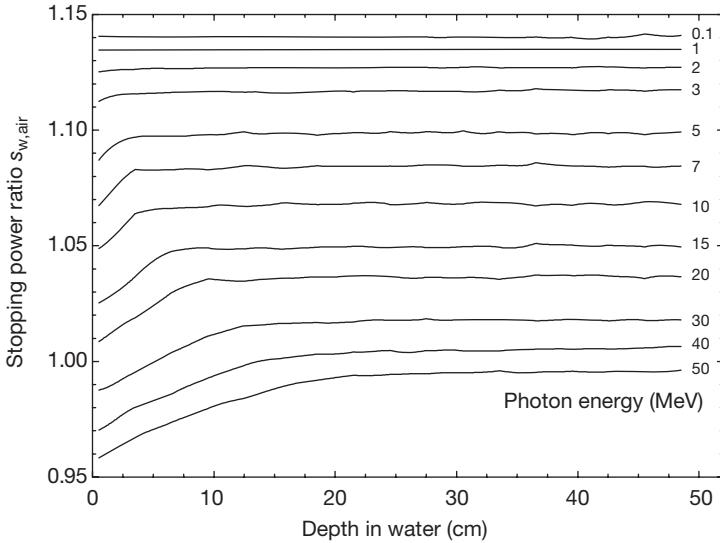
FIG. 9.6. *Depth variation of the ratio of the mean restricted mass stopping powers of water and air $s_{w,air}$ for a cut-off energy Δ of 10 keV, derived from Monte Carlo generated electron spectra for monoenergetic, plane-parallel monoenergetic and plane-parallel photon beams.*

reached at shallower depths, due to the presence of low energy photons in the spectrum.

9.6. MASS–ENERGY ABSORPTION COEFFICIENT RATIOS

The role of spectrum averaged mass–energy absorption coefficient ratios in modern dosimetry protocols is mainly restricted to their use in calculating perturbation and other correction factors for ionization chambers in ^{60}Co and high energy photon beams. In general, they are associated with the fraction of energy deposited within a detector due to electrons generated by photon interactions in the detector material itself.

Depending on the medium, the photon fluence spectra may change appreciably with depth or material thickness, and they also depend on the field size of the incident beam. It has been shown that the effects of spectral changes within a phantom on the mean mass–energy absorption coefficients are of importance only for large field sizes or for low energy photon beams, for which there is a more than 0.5% variation in $(\mu_{en}/\rho)_{w,m}$, the ratio of mass–energy absorption coefficients, for tissue-like materials (m) with respect to water (w) because of this effect.

A consistent set of mass–energy absorption coefficient ratios for photon dosimetry used in most dosimetry protocols was given in the IAEA TRS 277 protocol. These data have not yet been superseded by any other new set of data.

9.7. PERTURBATION CORRECTION FACTORS

For a detector to behave as a Bragg–Gray cavity, the electron fluence in the sensitive medium of the detector must be identical to that at a specified point in the uniform medium. The only possible true Bragg–Gray detector would be an exceedingly small air bubble; all protocols for absolute dose determination are, in fact, based on air filled ionization chambers.

For megavoltage photon radiation the Bragg–Gray conditions are adequately fulfilled for air cavities of the size encountered in practical ionization chambers (i.e. the ranges in air of the secondary electrons generated in megavoltage photon beams are much greater than the cavity dimensions). However, an ionization chamber does not consist only of an air cavity. There will always be a wall that, in general, is not perfectly medium equivalent. Often this wall is made of graphite, whereas the medium is water. Moreover, for cylindrical chambers there must be a central electrode, which is frequently made of aluminium, and there may be other materials around the chamber, such as a stem for cylindrical chambers and a back wall in the case of parallel-plate designs. All of these features can introduce deviations from perfect Bragg–Gray behaviour.

These deviations are generally dealt with by introducing one or more correction factor, often known as perturbation factors, into the expression for the absorbed dose (i.e. the factor p_Q in Eq. (9.21)). This overall factor is often written as a product of four perturbation factors, each one accounting for a different effect, assumed to be independent of the others, as follows:

$$p_Q = (p_{dis} p_{wall} p_{cel} p_{cav})_Q \tag{9.28}$$

where

p_{dis} is a factor that accounts for the effect of replacing a volume of water with the chamber cavity (cylindrical chambers);

p_{wall} is a factor that corrects the response of the ionization chamber for the non-water equivalence of the chamber wall and any waterproofing material;

p_{cel} is a factor that corrects the response of the chamber for the effect of the central electrode during in-phantom measurements;

p_{cav} is a factor that corrects the response of the ionization chamber for effects related to the air cavity, predominantly the in-scattering of electrons, which makes the electron fluence inside a cavity different from that in water in the absence of the cavity.

The word perturbation here means a perturbation by the detector of the electron fluence $\phi_{med}(P)$ present at the point of interest P in a uniform medium where the relevant fluence in the detector, inevitably a mean value over a finite volume $\bar{\phi}_{det}$, is that which gives rise to the signal (i.e. the fluence in the air in the case of an ionization chamber).

Sections 9.7.1–9.7.4 deal with the four different sources of the Bragg–Gray cavity perturbation. The emphasis here is on the physics of these correction factors. A complete account of numerical values for the particular chamber and radiation quality of interest can be taken from the particular protocol being followed, and a concise summary of the protocol recommendations is given in Section 9.9.

9.7.1. Displacement perturbation factor p_{dis} and effective point of measurement

An ionization chamber placed into a phantom will displace a certain volume of the phantom medium. Even if the chamber wall is medium equivalent, one still must consider the effect of the volume occupied by the air cavity. In general the dimensions of this volume are not negligible compared with any changes in the radiation field and hence in the dose distribution. For example, the dose may change by a few per cent within a distance equal to the diameter of the chamber. Clearly the chamber reading will be affected by this 'missing' medium. In simple terms one can expect that the reduced attenuation, in the case of photon beams, will result in a higher chamber reading compared with that in a very small 'air bubble' situated at the centre of the detector.

However, there is another effect: the missing material means that there is less scatter. This will counterbalance the first effect. The net result is still generally an increase in the signal that results in a correction factor known as the displacement perturbation factor, usually denoted by p_{dis}, which will thus be less than unity.

The value of p_{dis} will in general depend on both the radiation quality and the physical dimensions of the air cavity in the direction of the beam, as well as on the depth of measurement. In photon beams p_{dis} will be practically constant beyond the depth of dose maximum, due to the exponential fall-off in dose;

however, in the buildup region it will vary in a complicated fashion with depth. For a Farmer chamber, which has an internal radius of 3 mm, the value is close to 0.988 in a ^{60}Co beam.

The correction for displacement can be viewed in an alternative way. Instead of applying a factor to correct the chamber reading by assuming that the chamber is positioned so that its centre is at the depth of interest, a shift in the position of the chamber can be made. For a cylindrical chamber the electrons enter the wall at various depths, generally forward of its centre, and hence the electron fluence in the air cavity is representative of that existing at some point in the uniform medium shifted forward of the chamber centre. In fact, it was found that the readings of different chambers could be brought into coincidence with one another by performing shifts depending on the chamber dimensions. Thus the concept of the effective point of measurement P_{eff} was developed.

The newer absorbed dose to water based dosimetry protocols favour the p_{dis} approach. However, air kerma in air based protocols use the P_{eff} concept in preference to p_{dis}. The IAEA TRS 277 protocol recommended a shift of 0.5r for ^{60}Co γ rays, increasing to 0.75r for all higher energy photon beams. More recent reviews of the experimental evidence on the magnitude of the shift led the IAEA to recommend a single value of 0.6r for all high energy photon beams (IAEA TRS 398), as indicated schematically by the parameter z_c in Fig. 9.7(a).

In electron beams the use of p_{dis} is impractical, since the depth dose curve is very irregular in shape, in contrast to the quasi-exponential decrease in photon beams at depths beyond the buildup region. Since p_{dis} would vary rapidly and in an irregular way with depth in an electron beam, the P_{eff} concept is universally employed in electron beams.

- For cylindrical chambers the recommended shift is 0.5r (IAEA TRS 277 and IAEA TRS 398).
- For parallel-plate chambers P_{eff} is assumed to be situated in the centre of the inside face of the front wall, as illustrated in Fig. 9.7; this is logical since, in a well guarded chamber, it can be assumed that all the electrons entering the sensitive air volume do so through the front window.

9.7.2. Chamber wall perturbation factor p_{wall}

Compliance with the Bragg–Gray conditions implies that the electron fluence in the sensitive volume of the detector is identical (strictly in magnitude, energy and angular distribution) to that present in the undisturbed medium at the position of interest. However, an ionization chamber has a wall
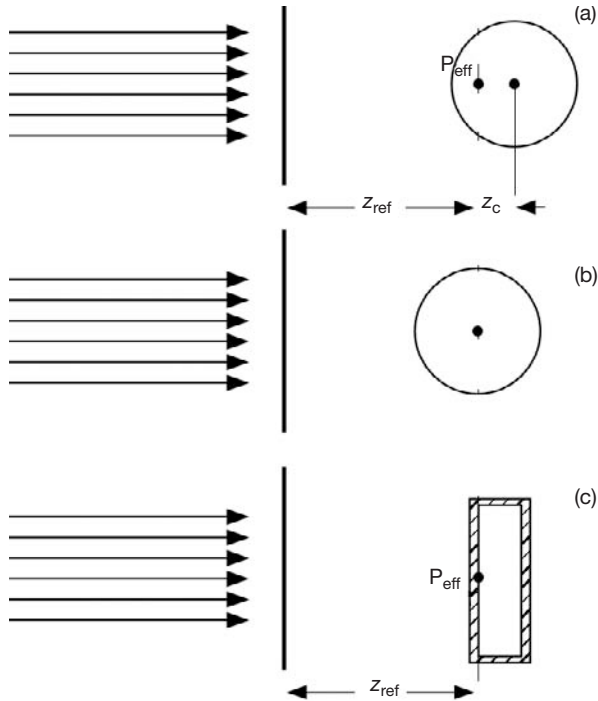
FIG. 9.7. (a) In most N_K based dosimetry protocols the effective point of measurement of a cylindrical ionization chamber is positioned at the reference depth z_{ref}, where the absorbed dose is required; the chamber centre is deeper than z_{ref} a distance z_c. (b) Except in electron and heavy ion beams, in $N_{D,w}$ based protocols the centre of a cylindrical chamber is positioned at the reference depth z_{ref} and the absorbed dose is determined at this position. (c) For plane-parallel chambers all protocols position the effective point of measurement (front of the air cavity) at the reference depth z_{ref}.

that in general is not made of medium equivalent material. In the case of photon beams the electron fluence in the air cavity in an ionization chamber, assumed cylindrical with a wall of a typical thickness, will consist partly of electrons generated in the (uniform) medium surrounding the wall that have travelled through the wall and partly of electrons generated by photon interactions with the wall material.

Quite clearly the number and energy distribution of these wall generated secondary electrons will be characteristic of photon interactions with the material of the wall and not of the medium, as demanded by Bragg–Gray conditions.

For ionization chambers with walls of intermediate thickness, in practical use in radiotherapy an approximate empirical two-component expression is in common use:

$$p_{wall} = \frac{\alpha s_{wall,air}(\mu_{en}/\rho)_{w,wall} + (1-\alpha)s_{w,air}}{s_{w,air}} \quad (9.29)$$

where α is the fraction of the dose to the air in the cavity due to electrons generated in the chamber wall; thus if this is zero, p_{wall} reduces to unity as expected.

An additional small correction has been implemented for the case when a waterproofing sleeve is used, where Eq. (9.29) is extended to a three-component model, with a third term $\tau s_{sleeve,air}(\mu_{en}/\rho)_{w,sleeve}$, where τ is the fraction of the ionization due to electrons generated in the sheath, as follows:

$$p_{wall} = \frac{\alpha s_{wall,air}(\mu_{en}/\rho)_{w,wall} + \tau s_{sleeve,air}(\mu_{en}/\rho)_{w,sleeve} + (1-\alpha-\tau)s_{w,air}}{s_{w,air}}$$

$$(9.30)$$

with α and τ the fractional contributions to ionization resulting from photon interactions in the wall and sleeve, respectively.

The two parameters α and τ can be estimated for ^{60}Co beams from the thickness of the wall t_{wall} and the waterproofing sleeve t_{sleeve} (g/cm^2), if present, using:

$$\alpha = 1 - \exp(-11.88t_{wall}) \quad (9.31)$$

and

$$\tau = \exp(-11.88t_{wall}) - \exp[-11.88(t_{wall} + t_{sleeve})] \quad (9.32)$$

For high energy beams, the fractional ionizations α and τ are derived from the data given by the IAEA TRS 398 protocol. In the case of electron beams, it is generally assumed that the effect of the chamber wall is negligible.

9.7.3. Central electrode perturbation p_{cel}

Cylindrical chambers have a central electrode, which is usually made of aluminium but can be made of graphite. The central electrode will produce an increase in the chamber signal compared with what would be obtained in an air

bubble, and a correction for the non-air equivalence of the electrode is in principle necessary; this is denoted by p_{cel}.

The effect of a central electrode made of graphite has been shown to be practically negligible in photon beams but decreases with energy from 1.008 to 1.004 for a 1 mm diameter aluminium electrode.

In electron beams the effect is negligible for graphite, and never greater than 0.2% at any energy (5–20 MeV) or depth for a 1 mm diameter aluminium electrode.

9.7.4. Cavity or fluence perturbation correction p_{cav}

An ionization chamber introduces a low density heterogeneity into a medium. In an electron beam, density changes can cause hot or cold spots as a result of electron scattering. The reason for this is clear from Fig. 9.8, attributed to Harder.

As a result of (elastic nuclear) scattering, the angular distribution of electrons broadens with depth; a low density cavity will consequently scatter out fewer electrons than are scattered in, resulting in an increase in the electron fluence towards the downstream end of the cavity in comparison with the fluence in a uniform medium at that depth.
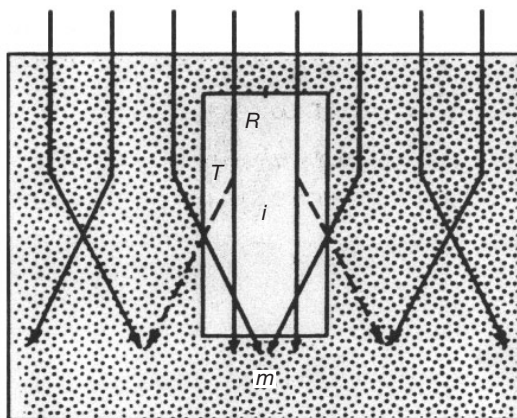
FIG. 9.8. Perturbation of the electron fluence caused by a gas filled cavity in a solid or liquid phantom. Electron tracks are idealized to emphasize the effects being shown. The dominance of in-scattering over out-scattering gives rise to an increase in the fluence towards the back of the cavity, and hence this produces an increase in the chamber signal.

All modern air kerma in air based dosimetry protocols include values of perturbation factors determined experimentally.

The magnitude of the in-scattering perturbation exceeds 3% for Farmer type chambers for E_z, the electron energy at depth z, below 8 MeV. This is one of the principal reasons why parallel-plate chambers are recommended in low energy electron beams. In a parallel-plate chamber the diameter of the air cavity (typically between 13 and 20 mm) is deliberately made very much greater than its thickness (the electrode spacing), which is 2 mm in almost all commercial designs. Thus most of the electrons enter the air cavity through the front face of the chamber and only a small fraction through the side walls.

Furthermore, well designed parallel-plate chambers have a relatively wide guard ring, 3 mm or more, which ensures that almost no electrons entering through the short side walls can contribute to the chamber signal. Consequently, in-scattering is virtually eliminated. The electron fluence in the sensitive volume of such a chamber is therefore that existing in the uniform medium at the depth of the inside face of the front window, which is the position of the effective point of measurement P_{eff}. For cylindrical chambers this guarding capability is virtually absent and the electron fluence is significantly perturbed. For these chambers the cavity perturbation correction factor p_{cav} is given by:

$$p_{cav} (\bar{E}_0, r) = 1 - 0.02155r \exp(-0.1224 \bar{E}_z) \tag{9.33}$$

where r is the cavity inner radius in millimetres and $\bar{E}_z$ is the mean electron energy at depth z as obtained from the Harder relationship (see Eq. (9.36)).

In photon beams there is generally charged particle equilibrium (CPE) (or a very good approximation to it), and therefore no change in either the energy or the angular distribution of the secondary electrons with position in the irradiated medium. The electron fluence perturbation effect is therefore negligible in photon beams. However, in the buildup region in photon beams, where there is no CPE, significant perturbation effects have been demonstrated.

9.8. BEAM QUALITY SPECIFICATION

The signal (current or charge) that is produced by an ionization chamber and measured by an electrometer must be multiplied by factors correcting for influence quantities (see Section 9.3) and the various dosimetric physical quantities described in the previous sections to yield the absorbed dose to water at a reference point in water, the quantity in terms of which radiotherapy

machine output is specified. Some of these quantities depend upon photon or electron beam energy, thus the beam quality needs to be specified for dosimetric calculations.

The most logical means to characterize the quality of a clinical radiation beam is to state its spectral distribution. However, since beam spectra are difficult to measure directly and cumbersome to determine in an absolute sense with Monte Carlo techniques, other, more practical, approaches to beam quality specification have been developed. These approaches are specific to three distinct ionizing radiation beam categories:

- Kilovoltage (superficial and orthovoltage) X ray beams;
- Megavoltage X ray beams;
- Megavoltage electron beams.

9.8.1. Beam quality specification for kilovoltage photon beams

For low energy photon beams the quality of the beam is most conveniently expressed in terms of the half-value layer (HVL) of the beam, with HVL representing the thickness of an attenuator that decreases the measured air kerma rate in air to half of its original value.

To minimize the effects of radiation scattered in the attenuator the HVL must be measured under 'good geometry' conditions that imply the use of:

- A narrow beam geometry to minimize scattering from the attenuator;
- A reasonable distance between the attenuator and the measuring device (ionization chamber) to minimize the number of scattered photons reaching the detector;
- An ionization chamber with air equivalent walls and with a flat photon energy response for the spectrum of radiations comprising the beam.

For superficial X ray beams (10–100 kVp) HVLs are usually given in millimetres of pure aluminium (typical HVLs from 0.01 to 10 mm of aluminium), while for orthovoltage X ray beams (above 100 kVp) HVLs are usually given in millimetres of pure copper (typical HVLs from 0.5 to 4 mm of copper).

The specification of beam quality in terms of the HVL is really a very crude beam specification, since it tells little about the energy distribution of the photons present in the beam. However, the beam specification through the HVL provides a general idea of the effective energy of the photon beam, which may be used to assess the beam penetration into tissue and to determine the appropriate values of the quantities used in dosimetry protocols.

Since two beams with widely differing potentials can have similar HVLs, due to the marked effect of different filtrations, it is customary to state, in addition to the HVL, the X ray potential and total filtration used in generating a given X ray beam.

Often low energy X ray beams are also characterized by stating their homogeneity coefficient κ, which is defined as the ratio between the first and second HVL (i.e. = HVL_1/HVL_2). For heterogeneous low energy X ray beams $HVL_2 > HVL_1$, resulting in $\kappa < 1$; for monochromatic beams, on the other hand, $HVL_2 = HVL_1$ and $\kappa = 1$.

Another quantity that is often used in beam quality specification is the equivalent or effective photon energy, defined as the quantum energy of a monoenergetic beam having an HVL equal to HVL_1 of the heterogeneous beam being specified.

9.8.2. Beam quality specification for megavoltage photon beams

In the megavoltage photon energy range, HVLs vary little with photon energy, making HVLs unsuitable for beam quality specification. Other indices were therefore developed, relating to the energy of the electron beam as it strikes the target (nominal accelerating potential (NAP)) and to radiation beam attenuation as the beam penetrates into water or tissue. Older radiation protocols were based on the NAP, while the recent ones are based on quantities that are related to beam penetration into water, such as the tissue–phantom ratio (TPR) or percentage depth dose (PDD).

A considerable improvement was made to air kerma in air based dosimetry protocols when stopping power ratios and mass–energy absorption coefficient ratios were correlated with clinically measured ionization ratios, such as the $TPR_{20,10}$, rather than with NAPs.

The parameter $TPR_{20,10}$ is defined as the ratio of doses on the beam central axis at depths of 20 cm and 10 cm in water obtained with a constant source to detector distance of 100 cm and a field size of 10×10 cm^2 at the position of the detector. The $TPR_{20,10}$ is a measure of the effective attenuation coefficient describing the approximately exponential decrease of a photon depth dose curve beyond the depth of maximum dose z_{max}, and, more importantly, it is independent of electron contamination of the incident photon beam.

The $TPR_{20,10}$ can be related to the measured $PDD_{20,10}$ using the following relationship:

$$TPR_{20,10} = 1.2661 PDD_{20,10} - 0.0595 \qquad (9.34)$$

where $PDD_{20,10}$ is the ratio of PDDs at depths of 20 cm and 10 cm for a field of 10×10 cm^2 defined at the water phantom surface with an SSD of 100 cm. This empirical relationship was obtained from a sample of almost 700 linacs.

Other beam quality indices have been proposed for megavoltage photon dosimetry; they are, in most cases, related to the depth of maximum dose z_{max}, making them susceptible to the electron contamination of the beam at this depth in a water phantom.

Based on PDD distributions, a widely disseminated recommendation for specifying the quality of high energy photon beams was made in British Journal of Radiology Supplement 17, which defined a parameter d_{80} as the depth of the 80% depth dose for a 10×10 cm^2 field at an SSD of 100 cm.

British Journal of Radiology Supplement 17 clearly points out that electron contamination of the photon beam should be considered a practical shortcoming of the d_{80} method. The use of $TPR_{20,10}$ as a photon beam quality index has also been endorsed by the recent British Journal of Radiology Supplement 25, although other beam quality specifiers, such as the PDD(10), are also considered.

The parameter PDD(10), the PDD at 10 cm depth in water, determined under the same conditions of field size and SSD as the parameter d_{80}, has in principle the same limitation with regard to the effect of electron contamination as d_{80}. A recommendation has been made that a 1 mm thin lead foil be used in measurements to remove the unknown electron contamination from the reading at z_{max} and to replace it by a known amount of electron contamination to arrive at the PDD with the presence of the lead foil, $PDD(10)_{Pb}$. A correction formula is provided to convert $PDD(10)_{Pb}$ into $PDD(10)_x$, the PDD at a depth of 10 cm in water in a pure photon beam excluding the electron contamination at z_{max}.

The advantages and limitations of the different photon beam quality indices have been discussed at great lengths in the scientific literature. The general conclusion is that there is no unique beam quality index that works satisfactorily in all possible conditions for the entire energy range of megavoltage photon energies used in radiotherapy and for all possible linacs used in hospitals and standards laboratories.

Most recent dosimetry protocols based on in-water calibrations of ionization chambers use the $TPR_{20,10}$ as the beam quality index (IPEM, IAEA TRS 398, etc.); the AAPM TG 51 protocol, however, uses the $PDD(10)_x$. For a user in a hospital or clinic there is no advantage of one specifier (index) over the other, as both lead to the same dose conversion factors and hence yield the same dose to water in the user's beam. However, the choice of the beam quality index should not be governed by user preference but should follow the

dosimetry protocol used in order to ensure uniformity and consistency in radiotherapy dosimetry.

9.8.3. Beam quality specification for megavoltage electron beams

Electron beams are essentially monoenergetic when exiting the accelerator waveguide; however, the electron beam striking the phantom or patient surface at a nominal SSD exhibits a spectrum that results from the energy spread caused by interactions between electrons and air as well as interactions between electrons and the linac components, such as the collimator, scattering foil, ionization chamber and treatment cone. A typical electron beam PDD distribution is shown in Fig. 9.9.

Until lately, the quality of clinical electron beams has been specified in practically all dosimetry protocols by $\bar{E}_0$, the mean electron energy of the incident spectrum striking the phantom surface. This beam quality index was derived from measurement of the half-value depth R_{50}, defined as the depth at which the electron beam depth dose decreases to 50% of its maximum value.
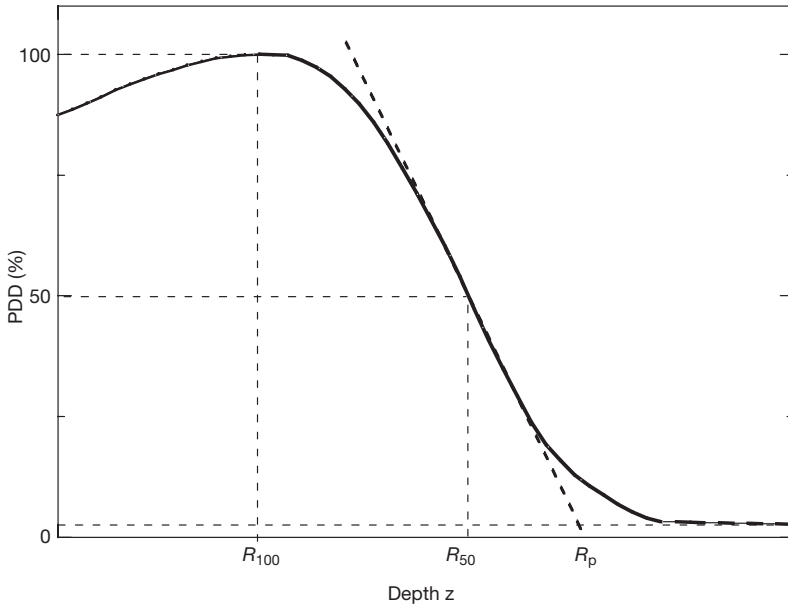
FIG. 9.9. Typical electron beam depth dose distribution with R_{100} the depth of dose maximum, R_{50} the depth of the 50% dose and R_p the practical range of electrons. The dose beyond R_p is contributed by the bremsstrahlung contamination of the electron beam produced in the linac components, air and water phantom.

The empirical relationship between $\bar{E}_0$ and R_{50} is:

$$\bar{E}_0 = CR_{50} \qquad\qquad (9.35)$$

where

C is a constant (2.33 MeV/cm);
R_{50} is the half-value depth in centimetres.

Strictly speaking, Eq. (9.35) is valid only for large field sizes (broad beams), for electron energies between 5 and 30 MeV, and for R_{50} determined from depth dose distributions measured in water with a constant source to chamber distance. The criterion for a broad beam is satisfied when the depth dose distribution is independent of field size, and this is achieved for field sizes exceeding 12×12 cm^2 for electron beam energies below 15 MeV and at least 20×20 cm^2 for energies above 15 MeV.

The mean energy at depth z in a phantom, $\bar{E}_z$, is also a quantity of general use in electron beam dosimetry. An empirical relationship, originally proposed for the most probable energy of an electron spectrum at a depth z in a water phantom, has been recommended by many electron dosimetry protocols to determine $\bar{E}_z$ according to:

$$\bar{E}_z = \bar{E}_0(1 - z/R_{\mathrm{p}}) \qquad\qquad (9.36)$$

where R_{p} is the practical range of the electron beam defined as the depth where the tangent at the steepest point (the inflection point) on the almost straight descending portion of the depth dose curve meets the extrapolated bremsstrahlung background.

Equation (9.36) is only an acceptable approximation of the mean energy at depth in water for electron beams with incident energies of less than 10 MeV or for small depths at higher energies. In other situations the mean electron energy $\bar{E}_z$ is obtained from tabulated data of $\bar{E}_z/\bar{E}_0$ versus the scaled depth z/R_{p} (IAEA TRS 277).

Much of the available data for electron dosimetry that were originally given in terms of $\bar{E}_z$ determined from Eq. (9.36) have been recast to Monte Carlo determined $\bar{E}_z$ in recent dosimetry protocols.

When R_{50} and R_{p} have been determined in a plastic phantom rather than in water, the electron ranges in plastic R_{pl} should be converted into ranges in water as follows:

$$R_{\mathrm{water}} = R_{\mathrm{pl}}C_{\mathrm{pl}} \qquad\qquad (9.37)$$

where C_{pl} is a material dependent scaling factor that was defined by the IAEA TRS 381 protocol as the ratio of average electron penetrations in water and plastic and is equivalent to the effective density of the AAPM TG 25 dosimetry protocol.

PDD distributions for clinical electron beams are most commonly determined from ionization measurements carried out in water or water equivalent phantoms with diodes or ionization chambers.

- Percentage depth ionization curves measured with a diode represent the PDD curve, since the mass collision stopping power ratios silicon to water are essentially constant with depth in a phantom (i.e. with electron beam energy).
- Percentage depth ionization curves measured with an ionization chamber, on the other hand, must be corrected for gradient effects as well as for variations in mass collision stopping power ratios water to air with electron energy when determining the PDDs from ionization measurements.

R_{50} may be determined from I_{50}, the 50% value on the percentage depth ionization curve measured with an ionization chamber in water, as follows:

$$R_{50} = 1.029 I_{50} \text{ (cm)} - 0.06 \text{ cm (for 2 cm} \leq I_{50} \leq 10 \text{ cm)} \tag{9.38}$$

and

$$R_{50} = 1.059 I_{50} \text{ (cm)} - 0.37 \text{ cm (for } I_{50} > 10 \text{ cm)} \tag{9.39}$$

$\bar{E}_0$ and $\bar{E}_z$ are determined from the measured R_{50} and R_p, respectively, and their use in electron beam dosimetry should be considered an approximation that facilitates the selection of dosimetric quantities and correction coefficients, rather than being an accurate statement on the energy parameters of clinical electron beams.

To avoid potential misunderstandings of the meaning of the energy based relationships, the recent dosimetry protocols use R_{50} directly as a beam quality index for selecting stopping power ratios and reference depths. This parallels the long standing practice in photon dosimetry in which beam qualities are expressed in terms of the penetration of the beam into a water phantom.

The choice of R_{50} as the beam quality index is a change from the previous practice of specifying beam quality in terms of the mean energy at the phantom surface. Since $\bar{E}_0$ is normally derived from R_{50}, this change in beam quality index is merely a simplification that avoids the need for a conversion to energy.

By choosing a specific reference depth z_{ref} for the calibration in water the stopping power ratio water to air has been shown to depend only on R_{50}.

The recent dosimetry protocols based on in-water calibration by the IAEA (TRS 398) and the AAPM (TG 51) have endorsed this approach, and all data are expressed in terms of R_{50}. The reference depth z_{ref} for electron beam calibration in water is expressed in terms of R_{50} as follows:

$$z_{ref} = 0.6R_{50} \text{ (cm)} - 0.1 \text{ cm} \qquad (9.40)$$

The reference depth in water is close to the depth of dose maximum z_{max} for beams with $R_{50} < 4$ cm ($\bar{E}_0 < 10$ MeV); however, for beams with $R_{50} \geq 4$ cm, z_{ref} is deeper than z_{max}. This choice of reference depth may be less convenient than that recommended in previous protocols, since for a given linac no two reference beams will have the same reference depth. However, the new reference depth defined by Eq. (9.40) has been shown to reduce significantly machine to machine variations in chamber calibration coefficients, and the gained accuracy justifies its use.

9.9. CALIBRATION OF MEGAVOLTAGE PHOTON AND ELECTRON BEAMS: PRACTICAL ASPECTS

This section summarizes the practical aspects of the recommendations made in air kerma in air based and absorbed dose to water based codes of practice or protocols for the calibration of megavoltage photon and electron beams. For numerical values on the various correction and conversion factors we refer to the IAEA TRS 277 or the IAEA TRS 398 protocols. For background on the physical meaning of the factors we refer to the previous sections.

9.9.1. Calibration of megavoltage photon beams based on the air kerma in air calibration coefficient $N_{K,Co}$

A cylindrical ionization chamber is used at a given depth z in a water phantom (typically z is 5 or 10 cm). The calibration is based on an air kerma in air calibration coefficient $N_{K,Co}$ obtained in a ^{60}Co beam at a standards laboratory.

Beam quality is specified with a ratio of TPRs, TPR_{20} at depths of 20 cm and 10 cm in water or with the PDD at a depth of 10 cm in water with electron contamination removed, $PDD(10)_x$, as discussed in Section 9.8.2.

The Bragg–Gray or Spencer–Attix cavity theory is used to determine the absorbed dose $D_w(z)$ or dose rate at the point of interest at depth z in the water phantom from the measured signal M_Q (charge or current) as follows:

$$D_w(z) = M_Q N_{D,air} s_{w,air} p_{wall} p_{cel} \tag{9.41}$$

where

M_Q is the chamber current or charge corrected for influence quantities and measured at beam quality Q;

$N_{D,air}$ is related to N_K through Eq. (9.19);

$s_{w,air}$ is the restricted stopping power ratio between water and air averaged over the electron slowing down spectrum resulting from the photon spectrum;

p_{wall} is the wall correction factor that accounts for the non-equivalence of the medium and wall;

p_{cel} is the central electrode correction factor that accounts for scatter and absorption of radiation on the central electrode (the factor was ignored in the AAPM TG 21 protocol but introduced in the IAEA TRS 277 and subsequent IAEA dosimetry protocols).

In the IAEA air kerma in air based protocols, the displacement effect resulting from the insertion of an air cavity into a phantom is accounted for by defining an effective point of measurement while the cavity perturbation effect is negligible. For cylindrical chambers in high energy photon beams the effective point of measurement is located $0.6r$ upstream of the chamber centre, r being the cavity inner radius.

For the purpose of absorbed dose measurements, in the absorbed dose to water based protocols the point of measurement is defined as the centre of the chamber and the displacement effects are accounted for by the introduction of the 'gradient correction factor' equivalent to p_{dis}.

The cavity fluence perturbation correction factor p_{cav} is unity in high energy photon beams.

9.9.2. Calibration of megavoltage photon beams based on the dose to water calibration coefficient $N_{D,w,Co}$

A cylindrical ionization chamber is used at a given depth z in a water phantom (typically z is 10 cm). The calibration is based on a dose to water chamber calibration coefficient $N_{D,w,Co}$ obtained from a standards laboratory

with the chamber irradiated with a ^{60}Co beam at a reference depth z_{ref} in a water phantom.

The absorbed dose to water $D_{w,Co}$ at a given depth in a phantom in a cobalt beam in the absence of the ionization chamber is given by:

$$D_{w,Co} = M_{co}N_{D,w,Co} \tag{9.42}$$

where M_{co} is the chamber signal (charge or current) corrected for influence quantities, as discussed in Section 9.3.

When the ionization chamber is used in a beam quality Q different from the ^{60}Co used in its calibration, the absorbed dose to water is given by:

$$D_{w,Q} = M_Q N_{D,w,Co} k_{Q,Co} \tag{9.43}$$

where the correction factor $k_{Q,Co}$ corrects for the effects of the difference between the reference ^{60}Co beam quality (Co) and the actual user beam quality Q, and the chamber signal M_Q has been corrected to the reference values of influence quantities, other than beam quality, for which the calibration coefficient is valid.

The beam quality Q of megavoltage photon beams is specified, as discussed in Section 9.8.2, either with a ratio of TPRs ($TPR_{20,10}(Q)$) or with the PDD ($PDD(10, 10 \times 10, SSD, Q)_x$.

The IAEA TRS 398 dosimetry protocol recommends the use of the ratio of TPRs, while the AAPM TG 51 protocol recommends the use of PDD_x, for megavoltage photon beam quality specification. Despite considerable polemics on the merits of each of the two approaches, in practice they both give essentially the same results for the megavoltage photon beams currently used in clinical practice.

The beam quality correction factor $k_{Q,Co}$ is defined as the ratio, at the beam qualities Q and Co, of the calibration coefficients in terms of the absorbed dose to water of the ionization chamber:

$$k_{Q,Co} = \frac{N_{D,w,Q}}{N_{D,w,Co}} \tag{9.44}$$

Ideally, the beam quality correction factors should be measured directly for each ionization chamber at the same quality as the user's beam. In practice, this is generally not possible, so the factors are calculated theoretically assuming the validity of Bragg–Gray cavity theory and using the $N_{D,air}$ concept (see Section 9.4).

9.9.3. Calibration of megavoltage electron beams based on the air kerma in air calibration coefficient $N_{K,Co}$

For electron beams with energies equal to or above 10 MeV a cylindrical or a parallel-plate ionization chamber is used at a reference depth in a water phantom (usually close to z_{max}). For electron energies below 10 MeV a parallel-plate ionization chamber must be used. The calibration is based on air kerma in air calibration coefficient N_K obtained in a ^{60}Co beam at the standards laboratory, but for parallel-plate chambers a cross-calibration against a cylindrical chamber allows a direct determination of the $N_{D,air}$ coefficient.

$\bar{E}_0$, the mean electron energy on a phantom surface, is used for specifying the electron beam quality (Eq. (9.35)).

The Spencer–Attix cavity relationship is used to determine the absorbed dose at the reference point in a water phantom as follows:

$$D_w(z) = M_Q N_{D,air} s_{w,air} p_{cav} p_{cel} \tag{9.45}$$

where

M_Q is the corrected measured chamber current or charge.

$N_{D,air}$ is related to N_K through Eq. (9.19).

$s_{w,air}$ is the restricted stopping power ratio between water and air.

p_{cav} is the cavity fluence perturbation correction factor accounting for the in-scattering effect as discussed in Section 9.7. It is unity for well guarded parallel-plate chambers and is given by Eq. (9.33) for Farmer type cylindrical chambers.

p_{cel} is the central electrode correction factor that accounts for scatter and absorption of radiation on the central electrode of a cylindrical chamber. The factor was ignored in the AAPM TG 21 protocol but was taken into account in the IAEA TRS 277 and subsequent IAEA protocols, as well as in the AAPM TG 51 protocol.

For parallel-plate chambers the effective point of measurement is located on the inner surface of the window at its centre, and no gradient correction is required.

For cylindrical ionization chambers, on the other hand, the effective point of measurement is located $0.5r$ upstream from the chamber centre. In the AAPM protocols, in the latter case, the point of measurement is defined as the centre of the chamber and the gradient effects are to be accounted for by the introduction of the gradient or displacement correction factor p_{dis}.

The wall correction factor p_{wall} is considered unity in electron beam dosimetry.

9.9.4. Calibration of high energy electron beams based on the dose to water calibration coefficient $N_{D,w,Co}$

The output calibration is based on a dose to water chamber calibration coefficient $N_{D,w,Co}$ obtained from a standards laboratory with the chamber irradiated in a reference beam of quality Q_0. This reference quality is most commonly a ^{60}Co γray beam ($N_{D,w,Co}$), but may also be an electron beam.

Parallel-plate ionization chambers are recommended for all electron beam qualities and must be used for electron beams of energies below 10 MeV. At electron energies equal or above 10 MeV the use of cylindrical chambers is allowed.

The reference point for parallel-plate chambers is taken to be on the inner surface of the entrance window, at the centre of the window.

Water is recommended as the reference medium. The water phantom should extend to at least 5 cm beyond all four sides of the largest field size employed. For electron energies below 10 MeV a plastic phantom may be used, but all depths must be scaled appropriately.

The beam quality index for electron beams is R_{50}, the half-value depth in water, measured with a field size of at least 10×10 cm^2 for $R_{50} \leq 7$ g/cm^2 and at least 20×20 cm^2 for $R_{50} > 7$ g/cm^2. The preferred choice of detector for the measurement of R_{50} is a well guarded parallel-plate ionization chamber, the preferred choice of phantom medium is water.

Output calibration is carried out in a water phantom at a reference depth z_{ref} with a field of 10×10 cm^2. The reference depth is given by:

$$z_{ref} = 0.6R_{50} - 0.1 \text{ g/cm}^2 \tag{9.46}$$

with R_{50} given in g/cm^2. This depth is close to the depth of dose maximum z_{max} at beam qualities $R_{50} < 4$ g/cm^2 ($E_0 \leq 10$ MeV); at higher beam energies it is deeper than z_{max}.

The absorbed dose to water at the reference depth z_{ref} in an electron beam of quality Q, in the absence of the chamber, is given by:

$$D_{w,Q} = M_Q N_{D,w,Co} k_{Q,Co} \tag{9.47}$$

where

M_Q is the chamber signal corrected for influence quantities;

$N_{D,w,Co}$ is the calibration coefficient in terms of absorbed dose to water for the chamber irradiated in a ^{60}Co beam at a standards laboratory;

$k_{Q,Co}$ is a chamber correction factor for differences between the reference beam quality (Co) and the actual electron beam quality Q.

Calculated values of $k_{Q,Co}$ against R_{50} are available in dosimetry protocol documents for a wide variety of parallel-plate and cylindrical ionization chambers. They are tabulated directly in the IAEA TRS 398 protocol or determined as a product of conversion and correction factors termed k_{ecal}, k'_{R50} and P_{gr} in the AAPM TG 51 protocol.

9.10. KILOVOLTAGE DOSIMETRY

During the past 30 years there has been a great deal of development in the dosimetry of high energy (i.e. megavoltage photon and electron) beams. The dosimetry of kilovoltage X ray beams (low and medium energy or orthovoltage X ray beams), on the other hand, remained more or less static in that period until the late 1980s. Despite this, kilovoltage beams are still in widespread use for the treatment of superficial lesions.

The IAEA TRS 277 protocol devoted a separate, detailed section to kilovoltage X rays, setting out a new air kerma in air based formalism, and this has recently been followed by several national dosimetry protocols on kilovoltage X ray dosimetry. Note that the second edition of the IAEA TRS 277 protocol provided substantial changes to the numerical data given in the original publication of 1987.

9.10.1. Specific features of kilovoltage beams

When kilovoltage X rays interact with a medium, the secondary electrons have extremely short ranges due to their low initial energy coupled with the rapid increase of the collision stopping power at subrelativistic energies. This results in several important differences between kilovoltage and megavoltage beams as far as radiation dosimetry is concerned:

- The Bragg–Gray principle can no longer be applied to such beam qualities (i.e. the electron fluence in the air cavity of the ionization chamber is not exclusively determined by electron interactions in the surrounding medium);
- Owing to the short electron ranges, absorbed dose can be equated to the collision kerma to a very good approximation;

● Radiative losses can be ignored in low atomic number materials, so that absorbed dose and kerma are essentially equivalent.

An ionization chamber calibration coefficient in kilovoltage X rays is determined with reference to a free air ionization chamber at a set of kilovoltage radiation qualities, in contrast to a single air kerma in air calibration coefficient at ^{60}Co for megavoltage beams. Since the wall thickness of a typical cylindrical ionization chamber is larger than the range of secondary electrons created in it, CPE is established in the wall without a buildup cap. For this reason, and since the chamber calibration coefficient is given in terms of air kerma in air, the calibrated chamber acts as a kerma detector even when used in a phantom.

The amount of photon scatter in a tissue equivalent phantom at kilovoltage energies is much larger than in high energy photon beams. This fact makes ratios of mass–energy absorption coefficients and, to a lesser extent, other, detector related dosimetric quantities depth and field size dependent.

Kilovoltage beam quality is specified differently than megavoltage beam quality. As discussed in Section 9.8, for kilovoltage beams the beam quality is specified in terms of the HVL, generally expressed in millimetres of aluminium or, at the top end of the energy range, in millimetres of copper.

It should be noted that beams with widely differing tube potentials may have similar HVLs, due to the marked effect of different filtrations. Thus the user determines the HVL of the beams of interest and then chooses N_K values for the calibrated chamber for the beam using the calibration curve supplied by the standards laboratory.

9.10.2. Air kerma based in-phantom calibration method (medium energies)

For medium energy X ray beams, typically above 100 kV, various dosimetry protocols recommend that the dose be determined at a depth in a water phantom, similarly to recommendations for megavoltage beam qualities. The various dosimetry protocols differ, however, in their specification of the reference depth.

The IAEA TRS 277 protocol followed early recommendations of the ICRU and specifies a depth of 5 cm in water.

The UK protocol (IPEMB, 1996) chose instead a depth of 2 cm in water for the reference depth, considering this to be much more representative of clinical practice; this has also been adopted in several other recent protocols.

The formalism for the determination of the absorbed dose to water is:

$$D_{w,Q} = M_Q N_{K,Q}[(\mu_{en}/\rho)_{w,air}]_Q p_Q \qquad (9.48)$$

where, for the HVL of the user's beam (Q):

M_Q is the instrument reading corrected for influence quantities (see Section 9.3);

$N_{K,Q}$ is the air kerma in air chamber calibration coefficient for beam quality Q;

$(\mu_{en}/\rho)_{w,air}$ is the mass–energy absorption coefficient ratio water to air for the photon spectrum at the depth of measurement in water and for the field size of the user's beam;

p_Q is an overall perturbation correction factor, which is not to be confused with the p_Q factor of Eq. (9.28) and which consists of multiplicative components of a different nature than those involved in Eq. (9.28).

For a detailed description of these components please refer to, for example, the AAPM TG 61 protocol.

There is only a weak dependence on field size or depth in the values of $(\mu_{en}/\rho)_{w,air}$ in general and in the p_Q values for Farmer type chambers. Cylindrical chambers of the Farmer type are commonly used at this energy range. All recent kilovoltage dosimetry protocols agree to within about 1.5% in the determination of the absorbed dose to water at 2 cm depth in a water phantom.

9.10.3. Air kerma based backscatter method (low and medium photon energies)

Clinically, for these beams, the dose is most often prescribed for the skin surface (strictly just below the surface, where CPE is established). This has led to the most important and widely used method of determining the absorbed dose. The principle is straightforward. A chamber is positioned free in air (i.e. with no phantom involved) at a position corresponding to the centre of the field on the patient's skin surface. The reading of the (calibrated) chamber yields the air kerma in air $(K_{air})_{air}$. This is then converted into dose to water at the surface of a phantom at the field size of interest. The energy or quality range for this method differs slightly from protocol to protocol, but all of the protocols denote it by the term low energy; in the IAEA TRS 277 protocol this range is 10–160 kV.

The theoretical route is as follows:

- The air kerma in air $(K_{air})_{air}$ is converted into water kerma in air $(K_w)_{air}$ through the mass–energy absorption coefficient ratio water to air, but still under free in air conditions (i.e. for the primary spectrum); this has the advantage that $(\mu_{en}/\rho)_{w,air}$ is independent of field size.
- Next, the backscatter factor (BSF) converts the water kerma in air $(K_w)_{air}$ into the water kerma in water $(K_w)_w$ at the surface of a water phantom.

The formalism for this procedure is:

$$D_{w,Q}^{surface} = M_{free\,air,Q} N_{K,Q} BSF [(\mu_{en}/\rho)_{w,air}]_{free\,air,Q} \tag{9.49}$$

where, for the HVL of the user's beam (Q):

$M_{free\,air,Q}$ is the instrument reading corrected for influence quantities;
N_K is the air kerma in air chamber calibration coefficient;
BSF is the backscatter factor for the field size, HVL and SSD;
$[(\mu_{en}/\rho)_{w,air}]_{free\,air,Q}$ is the mass–energy absorption coefficient ratio water to air for the free in air (primary) spectrum.

Note that, in principle, the type of ionization chamber has no significance when using the backscatter method to determine the surface dose; one is merely using the chamber as a means of transferring the air kerma in air from the standards laboratory to the user's beam. In practice, however, the chamber is required to exhibit a small variation in N_K with the HVL over the full quality range.

The IAEA TRS 277 protocol recommends a thin window parallel-plate ionization chamber for this low energy range.

In the IPEMB protocol a secondary standard graphite cylindrical chamber, 0.3 cm^3, of the type NE 2561 or NE 2611 is to be used over the complete medium and low energy range.

The AAPM TG 61 protocol explicitly incorporates in an equation of the Eq. (9.49) type a chamber stem correction termed $P_{stem,air}$, which accounts for the change in the chamber calibration coefficient for the difference in field size between the standards laboratory beam and the clinical beam. For an ideal stem free ionization chamber this correction is unity. For a cylindrical Farmer type chamber the correction is less than 1%, but it can be very significant for certain types of thin window chamber, due to their significant chamber bodies.

9.10.4. Air kerma in air based calibration method for very low energies

In German and UK protocols there is a third method at the lowest energies, the Bucky therapy range, which corresponds approximately to 8–50 kV. In this energy range a thin window parallel-plate chamber is recommended for calibration purposes.

The backscatter method may be invalid for the very small field sizes sometimes employed clinically in such low energy beams (i.e. the field size can be insufficient to completely cover the chamber and hence the value of the product MN_K will no longer yield the correct value for air kerma in air in the user's beam).

For these beams the parallel-plate chamber is placed at the surface of a phantom and the dose at the surface is determined. The relevant expression is identical to that for the in-phantom medium energy method, except that now the factor p_Q (denoted as k_{ch}) refers to the specific parallel-plate chamber employed and pertains to the surface dose rather than to the dose at 2 cm depth.

The lack of data available for the k_{ch} factor led to the assumption that it is equal to unity. However, this assumption cannot be correct, since it assumes that the scatter from the body of the chamber is negligible. Recent experiments have found that it varies from about 1.01 to 1.08 for a field diameter of 5.4 cm (at a focal distance of 50 cm), depending on the chamber, beam quality and phantom. An update to the IPEMB protocol will recommend specific values for these significant correction factors.

9.10.5. Absorbed dose to water based calibration method

Standards of absorbed dose to water in the kilovoltage X ray range are not generally available. However, it is possible to derive calibration coefficients in terms of absorbed dose to water from air kerma in air calibration coefficients using one of the accepted dosimetry protocols (e.g. IAEA TRS 398). Thus any calibration laboratory with standards of air kerma in air can in this way provide (derived) calibration coefficients in terms of absorbed dose to water. Even though this is formally equivalent to the user obtaining an air kerma in air calibration and individually applying the same air kerma protocol, it has the advantage of permitting the widespread use of the unified methodology of absorbed dose to water standards in an area of dosimetry in which standard methods are notably lacking.

9.11. ERROR AND UNCERTAINTY ANALYSIS FOR IONIZATION CHAMBER MEASUREMENTS

9.11.1. Errors and uncertainties

An error is defined as the difference between the measured value of a measurand and the true value. An error has a sign, and a correction factor can be associated with it. When the error is known, the true value of the measurand can be calculated from the measured value. An uncertainty associated with a measurement is a parameter that characterizes the dispersion of the values that can be attributed to the measurand. The value of the uncertainty is usually an estimated standard deviation, has no sign and is assumed to be symmetrical with respect to the estimated value of the quantity. It is a measure of our lack of exact knowledge after all recognized systematic effects have been eliminated by applying appropriate corrections.

9.11.2. Classification of uncertainties

Uncertainties of measurements are expressed as relative standard uncertainties, and the evaluation of standard uncertainties is classified into two types: type A and type B.

- Type A uncertainties are inherently random and are obtained by a statistical analysis of a series of observations. A 1σ type A uncertainty corresponds to the standard error on the mean of a set of observations at the 68% confidence level.
- Type B uncertainties are determined through other than statistical, but often subjective, methods and account for systematic effects in the determination of a quantity.

Although of a totally different nature, type A and type B uncertainties are often combined assuming they are independent, using the propagation law of uncertainties without cross-correlation (i.e. relative standard uncertainties are quadratically summed).

9.11.3. Uncertainties in the calibration chain

The IAEA TRS 398 dosimetry code of practice describes an extensive uncertainty analysis on the calculated values of the beam quality conversion factors k_Q for photon and electron beams. For photon beams the estimated relative standard uncertainty for the calculated beam quality conversion factors

is 1.0%. For electron beams the value amounts to 1.2% for cylindrical chambers and 1.7% for parallel-plate chambers when based on a ^{60}Co calibration technique and to 0.9% for cylindrical chambers and 0.6% for plane-parallel chambers when based on a cross-calibration technique in an electron beam.

In order to obtain the uncertainty on a beam calibration, the above mentioned uncertainties need to be combined with the uncertainties on:

- The absorbed dose calibration coefficient at ^{60}Co or in a high energy electron beam, if a cross-calibration technique is used.
- Issues related to the in-phantom measurement of absorbed dose in the clinic. These comprise type A and type B uncertainties on the positioning of the chamber in the water phantom, the temperature and pressure measurement, the ion recombination, polarity and electrometer correction factor (if present), and the linac stability during the measurements of absorbed dose. For a detailed analysis we refer to the IAEA TRS 398 protocol.

BIBLIOGRAPHY

AMERICAN ASSOCIATION OF PHYSICISTS IN MEDICINE, A protocol for the determination of absorbed dose from high-energy photon and electron beams, Task Group 21, Radiation Therapy Committee, Med. Phys. **10** (1983) 741–771.

— AAPM's TG-51 protocol for clinical reference dosimetry of high energy photon and electron beams, Task Group 51, Med. Phys. **26** (1999) 1847–1870.

— AAPM protocol for 40–300 kV x-ray beam dosimetry in radiotherapy and radiobiology, Task Group 61, Med. Phys. **28** (2001) 868–892.

BRITISH JOURNAL OF RADIOLOGY, Central Axis Depth Dose Data for Use in Radiotherapy, Supplement 17 (1983).

— Central Axis Depth Dose Data for Use in Radiotherapy, Supplement 25 (1996).

INSTITUTE OF PHYSICAL SCIENCES IN MEDICINE, Code of practice for high-energy photon therapy dosimetry based on the NPL absorbed dose calibration service, Phys. Med. Biol. **35** (1990) 1355–1360.

INSTITUTION OF PHYSICS AND ENGINEERING IN MEDICINE AND BIOLOGY, The IPEMB code of practice for electron dosimetry for radiotherapy beams of initial energy from 2 to 50 MeV based on air-kerma calibration, Phys. Med. Biol. **41** (1996) 2557–2603.

— The IPEMB code of practice for the determination of absorbed dose for x-rays below 300 kV generating potential (0.035 mm Al–4 mm Cu HVL; 10–300 kV generating potential), Phys. Med. Biol. **41** (1996) 2605–2625.

INTERNATIONAL ATOMIC ENERGY AGENCY, Absorbed Dose Determination in Photon and Electron Beams, Technical Reports Series No. 277, IAEA, Vienna (1987).

— Absorbed Dose Determination in Photon and Electron Beams, 2nd edn, Technical Reports Series No. 277, IAEA, Vienna (1997).

— Calibration of Dosimeters Used in Radiotherapy, Technical Reports Series No. 374, IAEA, Vienna (1994).

— The Use of Plane Parallel Ionization Chambers in High Energy Electron and Photon Beams, Technical Reports Series No. 381, IAEA, Vienna (1997).

— Absorbed Dose Determination in External Beam Radiotherapy, Technical Reports Series No. 398, IAEA, Vienna (2000).

INTERNATIONAL ELECTROTECHNICAL COMMISSION, Medical Electrical Equipment — Dosimeters with Ionization Chambers as Used in Radiotherapy, IEC 60731, IEC, Geneva (1997).

INTERNATIONAL ORGANIZATION FOR STANDARDIZATION, Quantities and Units — Part 0: General Principles, ISO 31-0, ISO, Geneva (1992).

Chapter 10

ACCEPTANCE TESTS AND COMMISSIONING MEASUREMENTS

J.L. HORTON
Department of Radiation Physics,
University of Texas MD Anderson Cancer Center,
Houston, Texas, United States of America

10.1. INTRODUCTION

Following the installation of a therapy machine, be it an orthovoltage X ray unit, cobalt unit, linac or brachytherapy machine, in a radiotherapy clinic, the medical physicist must perform a series of measurements and tasks prior to placing the unit into clinical operation. These duties include acceptance testing and commissioning. Although calibration of the treatment beams is a part of the acceptance tests and commissioning, calibration is not discussed in this chapter, as it is fully covered in Chapter 9.

10.2. MEASUREMENT EQUIPMENT

10.2.1. Radiation survey equipment

A Geiger counter and a large volume ionization chamber survey meter are required to carry out a radiation survey of all treatment rooms. For facilities with a treatment unit operated above 10 MeV, neutron survey equipment such as Bonner spheres, long counters and BF_3 counters are necessary. However, it may be appropriate to contract neutron measurements to a medical physics consulting service, since this may be a less expensive option than developing the specialized skills and knowledge required for most neutron measurements and acquiring the expensive neutron detection equipment that is typically required only during acceptance testing.

10.2.2. Ionometric dosimetry equipment

A variety of ionization chambers are required to compile the radiation beam properties measured during the acceptance testing and commissioning of a radiation treatment unit. Thimble ionization chambers with volumes of the order of 0.1–0.2 cm^3 are used to measure a number of relative quantities and factors. These relative factors, including central axis percentage depth doses (PDDs), output factors and penumbra, may exhibit a rapidly changing dose gradient. In this situation small volume ionization chambers are preferred to reduce the uncertainty in the effective point of measurement. For measurements in the buildup region, which exhibits the greatest change in dose gradient, a parallel-plate or extrapolation chamber is required. Calibration measurements are typically performed with a thimble ionization chamber with a volume of the order of 0.5 cm^3 to increase the signal to noise ratio. A single electrometer that can be used with all these ionization chambers is a wise choice.

10.2.3. Film

Radiographic film has a long history of use in radiotherapy physics measurements. It has been used most successfully for quality control and electron beam measurements. However, the composition of radiographic film is very different from that of tissue, which makes it difficult for use in photon beam dosimetry.

In the past decade radiochromic film has been introduced into radiotherapy physics practice. This film is more tissue equivalent than radiographic film and is becoming more widely used for photon beam dosimetry.

Film dosimetry also requires a densitometer to evaluate the darkening of the film and to relate the darkening to the radiation received. It should be noted that different densitometers are suggested for radiochromic film than for conventional radiographic film, as the absorption peaks occur at different wavelengths for these different films.

10.2.4. Diodes

Owing to their small size, silicon diodes are convenient for measurements in small photon radiation fields. Diodes are also used for electron beam measurements because the stopping power ratio of silicon to water is almost constant over the energies measured in radiotherapy. The response of diodes should be checked against ionometric measurements before routine use.

10.2.5. Phantoms

10.2.5.1. Radiation field analyser and water phantom

A water phantom that scans ionization chambers or diodes in the radiation field is required for acceptance testing and commissioning. This type of water phantom is frequently referred to as a radiation field analyser (RFA) or an isodose plotter. Although a 2-D RFA is adequate, a 3-D RFA is preferable, as it allows the scanning of the radiation field in orthogonal directions without changing the phantom set-up.

The traversing mechanism for the ionization chambers or diodes may also be used to move the film densitometer. The traversing mechanism should have an accuracy of movement of 1 mm and a precision of 0.5 mm. A 3-D scanner of an RFA should be able to scan 50 cm in both horizontal dimensions and 40 cm in the vertical dimension. The water tank should be at least 10 cm larger than the scan in each dimension.

The RFA should be filled with water and then positioned with the radiation detector centred on the central axis of the radiation beam. The traversing mechanism should move the radiation detector along the principal axes of the radiation beam. After the gantry has been levelled with the beam directed vertically downwards, levelling of the traversing mechanism can be accomplished by scanning the radiation detector along the central axis of the radiation beam, indicated by the image of the cross-hair. Any deviation of the radiation detector from the central axis, as the detector is moved away from the water surface, indicates that the traversing mechanism is not levelled.

10.2.5.2. Plastic phantoms

For ionometric measurements in the buildup region a polystyrene or water equivalent plastic phantom is convenient. A useful configuration for this phantom consists of ten blocks of $25 \times 25 \times 5$ cm^3. One block should be drilled to accommodate a Farmer type ionization chamber with the centre of the hole 1 cm from one surface. A second block should be machined to place the entrance window of a parallel-plate chamber at the level of one surface of the block. This arrangement allows measurements with the parallel-plate chamber with no material between the window and the radiation beam. An additional seven blocks of the same material as the rest of the phantom should be 25×25 cm^2. These blocks should be 0.5, 1, 2, 4, 8, 16 and 32 mm thick. These seven blocks combined with the 5 cm thick blocks allow measurement of depth ionization curves in 0.5 mm increments to any depth from the surface to 40 cm with the parallel-plate chamber and from 1 to 40 cm with the Farmer chamber.

The depth of 40 cm is the limit, because 10 cm of backscatter should be maintained downstream from the measurement point.

A plastic phantom for film dosimetry is also required. It is convenient to design one section of the phantom to serve as a film cassette. Other phantom sections can be placed adjacent to the cassette holder to provide full scattering conditions.

Use of ready pack film irradiated parallel to the central axis of the beam requires that the edge of the film be placed at the surface of the phantom and that the excess paper be folded down and secured to the entrance surface of the phantom. Pinholes should be placed in a corner of the downstream edge of the paper package so that air can be squeezed out before placing the ready pack in the phantom, otherwise air bubbles will be trapped between the film and the paper. Radiation will be transmitted unattenuated through these air bubbles, producing incorrect data.

Plastic phantoms are also commonly used for routine quality control measurements. The design of these phantoms will depend on the requirements of the quality control programme.

10.3. ACCEPTANCE TESTS

Acceptance tests assure that the specifications contained in the purchase order are fulfilled and that the environment is free of radiation and electrical hazards to staff and patients. The tests are performed in the presence of a manufacturer's representative. Upon satisfactory completion of the acceptance tests, the physicist signs a document certifying that these conditions are met. When the physicist accepts the unit, the final payment is made for the unit, ownership of the unit is transferred to the institution and the warranty period begins. These conditions place a heavy responsibility on the physicist for the correct performance of these tests.

Acceptance tests may be divided into three groups:

- Safety checks;
- Mechanical checks;
- Dosimetry measurements.

A number of national and international protocols exist to guide the physicist in the performance of these tests.

10.3.1. Safety checks

Acceptance tests begin with safety checks to assure a safe environment for the staff and public.

10.3.1.1. *Interlocks, warning lights and patient monitoring equipment*

The initial safety checks should verify that all interlocks are functioning properly. These interlock checks should include the door interlock, all radiation beam-off interlocks, all motion disable interlocks and all emergency-off interlocks.

The door interlock prevents irradiation from occurring when the door to the treatment room is open. The radiation beam-off interlocks halt irradiation but they do not halt the motion of the treatment unit or patient treatment table. The motion disable interlocks halt motion of the treatment unit and patient treatment table but they do not stop machine irradiation. Emergency-off interlocks typically disable power to the motors that drive the treatment unit and treatment table motions and disable power to some of the radiation producing elements of the treatment unit. The idea is both to prevent collisions between the treatment unit and personnel, patients or other equipment and to halt undesirable irradiation.

The medical physicist must verify the proper functioning of all these interlocks and ensure that all personnel operating the equipment have a clear understanding of each. After verifying that all interlocks and emergency-off switches are operational, all warning lights should be checked. Next, the proper functioning of the patient monitoring audiovideo equipment can be verified. The audiovideo equipment is normally used for patient monitoring but is often also useful for monitoring equipment or gauges during acceptance testing and commissioning involving radiation measurements.

10.3.1.2. *Radiation survey*

After completion of the interlock checks, the medical physicist should perform a radiation survey in all areas outside the treatment room. For cobalt units and linacs operated below 10 MeV a photon survey is required; for linacs operated above 10 MeV the physicist must survey for neutrons in addition to photons. The survey should be conducted using the highest energy photon beam. To ensure meaningful results the physicist should perform a preliminary calibration of the highest energy photon beam before conducting the radiation survey. Photon measurements will require both a Geiger counter and an ionization chamber survey meter. Neutron measurements will require a

neutron survey meter. Several types are available, including Bonner spheres, long counters and BF_3 counters.

The fast response of the Geiger counter is advantageous in performing a quick initial survey to locate the areas of highest radiation leakage through the walls. After the location of these hot spots is determined, the ionization chamber type survey meter may be used to quantify leakage currents.

- All primary barriers should be surveyed with the largest field size, with the collimator rotated to 45º and with no phantom in the beam;
- All secondary barriers should be surveyed with the largest field size, with a phantom in the beam;
- The first area surveyed should be the control console area, where an operator will be located to operate the unit for all subsequent measurements.

10.3.1.3. Collimator and head leakage

Shielding surrounds the target on a linac or the source on a ^{60}Co unit. Most regulations require this shielding to limit the leakage radiation to 0.1% of the useful beam at 1 m from the source. The adequacy of this shielding must be verified during acceptance testing.

This verification may be accomplished by closing the collimator jaws and covering the head of the treatment unit with film. The films should be marked to permit the determination of their position on the machine after they are exposed and processed. The exposure should be long enough to yield an optical density (OD) of 1 on the films.

For example, assume that an exposure of 10 cGy yields an OD of 1 on the film and the films are secured to the head of the treatment unit at a distance of 25 cm from the source. Then the expected radiation level at the position of the films is 1.6% of the useful beam (0.1% of the useful beam at 1 m inverse squared to 25 cm). An exposure of 625 cGy at the isocentre (10 cGy divided by 1.6%) should yield an OD of 1 on the film.

Any hot spots revealed by the film can be quantified by using an ionization chamber style survey meter. The survey meter can be positioned 1 m from the hot spot with a ring stand and clamps. The reading may be viewed remotely with the closed circuit television camera to be used for patient monitoring.

10.3.2. Mechanical checks

The mechanical checks establish the precision and accuracy of the mechanical motions of the treatment unit and patient treatment table.

10.3.2.1. Collimator axis of rotation

The photon collimator jaws rotate on a circular bearing attached to the gantry. The central axis of the photon, electron and light fields should be aligned with the axis of rotation of this bearing and the photon collimator jaws should open symmetrically about this axis. This axis is an important aspect of any treatment unit and must be carefully determined.

The collimator rotation axis can be found with a rigid rod attached to the collimator housing. This rod should terminate in a sharp point and be long enough to reach from where it will be attached to the collimator housing to the approximate position of the isocentre.

The gantry should be positioned to point the collimator axis vertically downwards and then the rod is attached to the collimator housing. Millimetre graph paper is attached to the patient treatment table and the treatment table is raised to contact the point of the rod. With the rod rigidly mounted, the collimator is rotated through its range of motion. The point of the rod will trace out an arc as the collimator is rotated. The point of the rod is adjusted to be near the centre of this arc. This point should be the collimator axis of rotation. This process is continued until the minimum radius of the arc is obtained. This minimum radius provides an indication of the precision of the collimator axis of rotation. In most cases this arc will reduce to a point, but should not exceed 1 mm in radius in any event.

10.3.2.2. Photon collimator jaw motion

The photon collimator jaws should open symmetrically about the collimator axis of rotation. A dial indicator can be used to verify this. The indicator is attached to a point on the collimator housing that remains stationary during rotation of the collimator jaws. The feeler of the indicator is brought into contact with one set of jaws and the reading is recorded. The collimator is then rotated through 180° and again the indicator is brought into contact with the jaws and the reading is recorded. The collimator jaw symmetry about the rotation axis is one half of the difference in the two readings. This value projected to the isocentre should be less than 1 mm. This procedure is repeated for the other set of collimator jaws.

The two sets of collimator jaws should be perpendicular to each other. To check this, the gantry is rotated to orientate the collimator axis of rotation horizontally. Then the collimator is rotated to place one set of jaws horizontally. A spirit level is placed on the jaws to verify that they are horizontal. Then the spirit level is used to verify that the vertically positioned jaws are vertical.

With the jaws in this position the collimator angle indicators are verified. These indicators should be reading a cardinal angle at this point, either 0º, 90º, 180º or 270º, depending on the collimator position. This test is repeated with the spirit level at all cardinal angles by rotating the collimator to verify the collimator angle indicators.

10.3.2.3. *Congruence of light and radiation field*

At this point the alignment of the light field is to be verified. With millimetre graph paper attached to the patient treatment table, the table is raised to the nominal isocentre distance. The gantry is orientated to point the collimator axis of rotation vertically downwards. The position of the collimator axis of rotation is indicated on this graph paper. The projected image of the cross-hair should be coincident with the collimator axis of rotation and should not deviate more than 1 mm from this point as the collimator is rotated through its full range of motion. The projected images of the jaws should open and close symmetrically about this point. The symmetry of the collimator jaw images about this point should be better than 1 mm at all cardinal angles of the collimator.

The congruence of the light and radiation field can now be verified. A ready pack of radiographic film is placed perpendicularly to the collimator axis of rotation. The edges of the light field are marked with radio-opaque objects or by pricking holes with a pin through the ready pack film at the corners of the light field. The film is positioned near z_{max} by placing plastic on top of it and is irradiated to yield an OD of between 1 and 2. The light field edge should correspond to the radiation field edge within 2 mm. This test should be repeated over the range of field sizes and at two different distances to verify that the virtual light and photon sources are the same distance from the isocentre.

At this point the light field has been aligned to the collimator axis of rotation. Any misalignment between the light and radiation field may indicate that the central axis of the radiation field is not aligned to the collimator axis of rotation. The alignment of the photon field is a complex procedure that should only be performed by factory personnel. Any misalignment must be evaluated for its magnitude, effect on treatment and whether factory personnel should be called in to verify and correct the problem.

10.3.2.4. *Gantry axis of rotation*

The gantry axis of rotation can be found with any rigid rod that has a telescoping capability. Many treatment machines are supplied with a mechanical front pointer that may be used for this purpose. The axis of the front pointer should be aligned along the collimator axis of rotation and its tip should be at the nominal isocentre distance. The gantry is positioned to point the central axis of the beam vertically downwards; a second rigid rod that terminates in a small diameter tip off the end of the patient treatment table is then affixed and the treatment table is adjusted to bring the rod affixed to the treatment table to contact the point of the rod fixed to the gantry. The treatment table is then shifted along its longitudinal axis to move the point of the rod out of contact with the rod affixed to the gantry. Care should be taken not to change the vertical or lateral positions of the rod.

The gantry is rotated through 180º and the treatment table is moved back to a position where the two rods contact. If the front pointer correctly indicates the isocentre distance, the points on the two rods should contact in the same relative position at both angles. If not, the treatment table height and the length of the front pointer are adjusted until this condition is achieved as closely as possible. Owing to flexing of the gantry, it may not be possible to achieve the same position at both gantry angles. If so, the treatment table height is positioned to minimize the overlap at both gantry angles. This overlap is a 'zone of uncertainty' of the gantry axis of rotation. This zone of uncertainty should not be more than 1 mm in radius. The tip of the rod affixed to the treatment table now indicates the height of the gantry axis of rotation. This procedure is repeated with the gantry at parallel opposed horizontal angles to establish the right/left position of the gantry axis of rotation.

The collimator axis of rotation indicated by the cross-hair image, aligned before, should pass through this point. Patient positioning lasers are then aligned to pass through this point.

10.3.2.5. *Patient treatment table axis of rotation*

The patient treatment table axis of rotation can be found by positioning the gantry with the collimator axis of rotation pointed vertically downwards. Millimetre graph paper is attached to the treatment table and the image of the cross-hair marked on this graph paper. As the treatment table is rotated, the movement of the cross-hair image on the graph paper is noted. The cross-hair image should trace an arc with a radius of less than 1 mm.

The collimator axis of rotation, the gantry axis of rotation and the treatment table axis of rotation should all intersect in a sphere. The radius of

this sphere determines the isocentre uncertainty. This radius should be no greater than 1 mm, and for machines used in radiosurgery should not exceed 0.5 mm.

10.3.2.6. Radiation isocentre

The radiation isocentre should be determined for all photon energies. To locate the radiation isocentre a ready pack film is taped to one of the plastic blocks that comprise a plastic phantom. The plane of the film should be placed in the plane traced out by the central axis of the X ray beam as the gantry is rotated. The film should be perpendicular to and approximately centred on the gantry axis of rotation. A pin prick is made in the film to indicate the gantry axis of rotation. A second block is then placed against the film, sandwiching it between the two blocks, and the collimator jaws are closed to approximately 1 mm × 1 mm.

The film is then exposed to produce an OD of 0.3–0.5. Without touching the film, the film is exposed again at a number of different gantry angles in all four quadrants. Gantry angles that are not 180º apart should be chosen to avoid having the entrance of one beam overlap the exit of another. The processed film should show a multiarmed cross, referred to as a 'star shot'. The point where all central axes intersect is the radiation isocentre. Owing to gantry flex, it may be a few millimetres wide but should not exceed 4 mm. This point should be within 1–2 mm of the mechanical isocentre indicated by the pin prick on the film.

Verification of the radiation isocentre can be accomplished by centring an ionization chamber with an appropriate buildup cap on this point. The ionization collected for a fixed number of monitor units (MUs) on a linac or for time on a ^{60}Co unit should be independent of the gantry angle.

10.3.2.7. Optical distance indicator

A convenient method to verify the accuracy of the optical distance indicator (ODI) over the range of its readout uses the plastic phantom discussed in Section 10.2.5. With the gantry positioned with the collimator axis of rotation pointing vertically downwards, five of the 5 cm thick blocks are placed on the treatment table, with the top of the top block at the isocentre. The ODI should read the isocentre distance. By adding and removing 5 cm blocks the ODI can be easily verified at other distances in 5 cm increments.

10.3.2.8. Gantry angle indicators

The accuracy of the gantry angle indicators can be determined by placing a spirit level across the rails that hold the blocking tray. At each of the cardinal angles the level should indicate level. Some spirit levels also have an indicator for 45º angles that can be used to check angles of 45º, 135º, 225º and 315º. The gantry angle indicators should be accurate to within 0.5º.

10.3.2.9. Collimator field size indicators

The collimator field size indicators can be checked by comparing the indicated field sizes with values measured on a piece of graph paper fixed to the treatment table with the top of the table raised to the isocentre height. The range of field size should be checked for both symmetric and asymmetric field settings.

10.3.2.10. Patient treatment table motions

The patient treatment table should move in the vertical and horizontal planes. The vertical motion can be checked by attaching a piece of millimetre graph paper to the treatment table and, with the gantry positioned with the collimator axis of rotation pointing vertically downwards, marking the position of the image of the cross-hair on the paper. As the treatment table is moved through its vertical range, the cross-hair image should not deviate from this mark. The horizontal motion can be checked in a similar fashion, with the gantry positioned with the collimator axis in a horizontal plane. A piece of graph paper is affixed to the treatment table, the position of the cross-hair is marked and the treatment table is moved through its range of lateral motion. By rotating the treatment table 90º from its 'neutral' position, the longitudinal motion can be verified with the collimator axis orientated in a horizontal plane.

10.3.3. Dosimetry measurements

Dosimetry measurements establish that the central axis PDDs and off-axis characteristics of clinical beams meet the specifications. The characteristics of the monitor ionization chamber of a linac or the timer of a ^{60}Co unit are also determined.

10.3.3.1. Photon energy

The energy specification of an X ray beam is usually stated in terms of the central axis PDD. Typical specifications are in terms of the value of the 100 cm source to surface depth (SSD) central axis PDD for a 10×10 cm^2 field at a depth of 10 cm in a water phantom. This value is compared with values given in the British Journal of Radiology Supplement 25 to determine the nominal energy of the photon beam. During acceptance testing this value will be determined with a small volume ionization chamber in a water phantom in accordance with the acceptance test protocol.

10.3.3.2. Photon beam uniformity

The uniformity of a photon beam is typically specified in terms of either transverse beam profiles or the uniformity index. For the case in which transverse beam profiles are used, the flatness and symmetry of the beam are specified over the central 80% of the beam profile at a depth of 10 cm in a water phantom. The beam uniformity should also be specified at the depth of maximum dose z_{max} in a water phantom. Specification at z_{max} prevents the off-axis peaking of the beam profile becoming too large at this depth. The off-axis peaking is a product of the design of the flattening filter to produce a flat profile at a depth of 10 cm. The flattening filter also produces a differential hardening across the transverse direction of the beam that results in off-axis peaking at a depth shallower than 10 cm. Beam profiles are measured along the principal planes as well as along a diagonal of the beam.

The uniformity index is a measure of the beam uniformity over the entire area of the beam, not just the principal planes. The uniformity index is measured in a plane perpendicular to the central axis. It is defined to be the area enclosed by the 90% isodose curve divided by the area enclosed by the 50% isodose curve.

The IEC definition of the flattened area of the beam depends on the field size. According to the IEC, the flattened area is defined by straight lines joining points on the major axes and diagonals of the square fields given in Table 10.1.

10.3.3.3. Photon penumbra

The photon penumbra is typically defined as the distance between the 80% and 20% dose points on a transverse beam profile measured 10 cm deep in a water phantom. However, there are also other definitions of the penumbra,

TABLE 10.1. INTERNATIONAL ELECTROTECHNICAL COMMIS-SION'S DEFINITION OF THE FLATTENED AREA OF THE BEAM

Side of square field a (cm)	d_m[a]	d_d[b]
$5 \le a \le 10$	1 cm	2 cm
$10 < a \le 30$	$0.1a$	$0.2a$
$30 < a$	3 cm	6 cm

[a] The distance from the contour of the 50% of the absorbed dose on the beam central axis to the flattened area of the beam. It is on a major axis of the beam.
[b] Defined on a beam diagonal.

such as the distance between the 90% and 10% dose points on the beam profile at a given depth in a phantom. Whenever penumbra values are quoted, the depth of the profile and the spread in the percentage dose should be stated.

10.3.3.4. Electron energy

The electron energy is typically determined from measurements of the practical range in a water phantom. The most probable electron energy at the phantom surface $E_{p,0}$ can be determined from the practical range with the following equation:

$$E_{p,0} = 0.0025R_p^2 + 1.98R_p + 0.22 \tag{10.1}$$

where R_p is the practical range.

Another energy of interest for calibration purposes is the average energy on the phantom surface. Further discussion of the determination of the average energy is found in Chapters 8 and 9. Although the manufacturers state nominal electron energies, the central axis PDD characteristics of electron beams are really the values of clinical interest.

10.3.3.5. Electron beam bremsstrahlung contamination

The radiation measured beyond the practical range of the electrons in the phantom material is the bremsstrahlung contamination of the electron beam. All electron beams have bremsstrahlung contamination that results from inter-actions between electrons and materials in the scattering foils, collimators, air and patients. The bremsstrahlung contamination increases with electron energy, as discussed in Section 1.3.2.

10.3.3.6. Electron beam uniformity

The beam uniformity of an electron beam is typically specified in terms of either transverse beam profiles or the uniformity index. Beam profiles are measured along the principal planes and along a diagonal of the beam. For the case in which beam profiles are used, the flatness and symmetry of the beam are typically specified over the central 80% of the beam profile at a stated depth in a water phantom. The depth of measurement will depend on the machine specifications. If the vendor supplied specifications are inadequate, the physicist should propose an alternative set. The IEC definition of electron field uniformity includes measuring beam profiles at depths of 1 mm, the depth of the 90% dose and one half of the depth of the 80% dose.

10.3.3.7. Electron penumbra

The electron penumbra is usually defined as the distance between the 80% and 20% dose points along a major axis at a given depth. The IEC defines this depth as one half of the depth of the 80% dose on the central axis. Machine vendors specify other depths, such as depth of z_{max} or depth of the 90%, for the definition of electron penumbra.

10.3.3.8. Monitor characteristics

The amount of radiation delivered by a treatment unit is determined by the setting of an MU device on the treatment unit. A timer serves this purpose on a cobalt unit and an ionization chamber that intercepts the entire treatment beam is used on a linac. This MU device should be calibrated according to an appropriate national or international protocol for all energies, dose rates and modalities that will be used clinically.

The linearity of the MU device should be verified by placing an ionization chamber at a fixed depth in a phantom and recording the ionization collected during irradiations with different time or MU settings over the range of the monitor. The collected ionization can be plotted on the y axis and the monitor or time setting on the x axis. These data should produce a straight line indicating a linear response of the MU device or timer.

If these data produce a straight line that does not pass through the origin, then the monitor is linear but has an end effect. A negative x intercept indicates that more radiation is delivered than indicated by the MU setting. Similarly a positive x intercept indicates that less radiation is delivered than indicated by the MU setting. The end effect should be determined for each energy and

modality on the treatment unit. For teletherapy units and orthovoltage X ray units this effect is referred to as the shutter error.

An alternative means of determining the end effect is the multiple start–stop method. With this technique an ionization chamber is placed in the beam and irradiated for a given time or number of MUs. The irradiation is repeated for the same time or number of MUs, but with the irradiation interrupted a fixed number of times. If there is no end effect, the collected ionization should be the same for both irradiations. If the collected ionization is less for the irradiation that was interrupted, less radiation is delivered than indicated by the monitor setting. The end effect can be calculated from the following relationship:

$$\alpha \; = \; \left(\frac{I_n - I_1}{nI_1 - I_n} \right) T \tag{10.2}$$

where

α is the end effect;
I_n is the ionization collected after $(n - 1)$ interruptions;
I_1 is the ionization collected after no interruptions;
T is the total MUs or timer setting.

Note that a negative end effect determined with the multiple start–stop method corresponds to a positive x intercept determined from plotting the data for different monitor settings. In both instances less radiation is delivered than indicated by the monitor setting.

Most linac manufacturers design the monitor chamber to be either sealed so that the monitor chamber calibration is independent of temperature–pressure fluctuations or with a temperature–pressure compensation circuit. The effectiveness of either method should be evaluated by determining the long term stability of the monitor chamber calibration. This evaluation can be performed during commissioning by measuring the output each morning in a plastic phantom in a set-up designed to reduce set-up variations and increase precision of the measurement.

Linacs usually provide the capability of irradiating at several different dose rates. Different dose rates may change the collection efficiency of the monitor ionization chamber, which would change the calibration (cGy/MU) of the monitor ionization chamber. The calibration of the monitor ionization chamber should be determined at all available dose rates of the treatment unit. The constancy of output with the gantry angle should also be verified.

10.3.3.9. Arc therapy

The verification of the arc or rotational therapy specification is accomplished by setting a number of MUs on a linac or time on a ^{60}Co unit and a number of degrees for the desired arc. Radiation is then initiated. Termination of radiation and treatment unit motion should agree with the specification. Typical values are within 1 MU and 3º of the set values. This test should be performed for all energies and modalities of treatment and over the range of arc therapy geometry for which arc therapy will be used.

10.4. COMMISSIONING

Commissioning of an external beam radiotherapy or brachytherapy device includes a series of tasks that generally should consist of the following:

- Acquiring all radiation beam data (including beam output) required for treatment;
- Organizing these data into a dosimetry data book;
- Entering these data into a computerized treatment planning system (TPS);
- Developing all dosimetry, treatment planning and treatment procedures;
- Verifying the accuracy of these procedures;
- Establishing quality control tests and procedures;
- Training all personnel.

An abbreviated commissioning process will be required following any major repair of the unit.

10.4.1. Photon beam measurements

10.4.1.1. Central axis percentage depth doses

Typically the first commissioning measurements are of the central axis PDDs. To measure these, the surface of the water phantom is placed at the nominal SSD or at the isocentre. The vertical depth of the ionization chamber in the water phantom is determined by measuring from the bottom of the meniscus of the water to the centre of the chamber.

Central axis PDD values should be measured over the range of field sizes from 4×4 cm^2 to 40×40 cm^2. Increments between field sizes should be no greater than 5 cm, but are typically 2 cm. Measurements should be made to a

depth of 35 or 40 cm. Field sizes smaller than 4×4 cm^2 require special attention. Although 0.1 cm^3 chambers typically have diameters of 3–4 mm, the length is of the order of 1.5 cm. Owing to a lack of lateral electronic equilibrium and penumbral effects for ionization field sizes smaller than 4×4 cm^2, the dose varies significantly across the length of the chamber. Detectors of small dimensions are required for these measurements; several solutions are possible. A 0.1 cm^3 chamber orientated with its central electrode parallel to the central axis of the beam or a diode may be used in a water phantom. Alternatively, it may be possible to use a polystyrene phantom with a parallel-plate chamber that has a small collecting electrode.

These techniques should be validated by first measuring a central axis PDD of a 10×10 cm^2 field and then comparing these results with the results determined with conventional measurement techniques. By comparing the 10×10 cm^2 depth dose curves obtained with the two methods one can ascertain the validity of the method and the effective point of measurement of the diode or the ionization chamber.

Many photon central axis PDDs reveal a shift in z_{max} towards the surface as the field size increases. This shift results from an increasing number of secondary electrons and photons generated from the increasing surface area of the collimator jaws and the flattening filter. Some of these electrons and photons strike the detector and, since they have a lower energy than the primary photons, they cause a z_{max} degradation for large field sizes.

10.4.1.2.   Output factors

The radiation output at z_{max}, in cGy/MU for a linac and cGy/min for a cobalt unit, increases with an increase in collimator opening or field size. This increase in output can be measured at z_{max} of each field size. Alternatively, the increase in output can be measured at a fixed depth for each field size and the output at z_{max} determined by using the appropriate central axis PDD values.

Regardless of which measurement technique is used, the increasing output is normalized to the radiation output of the calibration field size, typically a 10×10 cm^2 field. The resulting ratios are referred to as output factors (or relative dose factors (RDFs) or total scatter factors).

Output factors are usually presented graphically as a function of equivalent square fields. This approach assumes that the output for rectangular fields is equal to the output for the equivalent square field. This assumption must be verified by measuring the output for a number of rectangular fields at their z_{max}. Outputs for rectangular fields with high and low aspect ratios should be measured. If the outputs for rectangular fields vary from the output for their

equivalent square fields by more than 2%, it may be necessary to have a table or graph of output factors for each rectangular field.

This matter can be further complicated, as linacs may exhibit a dependence on jaw orientation. For example, the output for a rectangular field may depend on whether the upper or lower jaw forms the long side of the field. This effect is sometimes referred to as the collimator exchange effect and should be investigated as part of the commissioning process.

Most modern linacs have collimators that open asymmetrically about the central axis of the X ray beam. Treatment with asymmetric fields requires knowledge of the output factors for these fields, if this effect is not accounted for in the TPS. The output factors for asymmetric fields can usually be approximated by:

$$[OF(r)]_{a,y} = [OF(r)]_s OAR(z_{max}, y) \qquad (10.3)$$

where $[OF(r)]_{a,y}$ is the output factor for an $r \times r$ field formed with an asymmetric collimator opening. The central ray of this field is y centimetres from the central axis of the symmetric field. $[OF(r)]_s$ is the output factor for an $r \times r$ field formed with a symmetric collimator opening and $OAR(z_{max}, y)$ is the off-axis ratio (OAR) measured at z_{max} and y centimetres from the central axis of the symmetric field.

The collimator scatter factor is measured in air with a buildup cap large enough to provide electronic equilibrium. Typically, these values are normalized to a 10×10 cm^2 field. A problem arises for small high energy photon field sizes, as the size of the buildup cap approaches or exceeds the size of the field. A significant portion of the measured signal represents scatter occurring in the buildup cap. This scatter has been estimated to be in the range of 1% to 10% of X ray energies between 2 and 30 MV.

Using a buildup cap constructed of higher density material such as aluminium or copper may solve the problem. This stratagem reduces the size of the cap, permitting measurement of fields down to 4×4 cm^2.

Alternatively the collimator scatter correction factor may be determined by placing the ionization chamber at an extended SSD but with the field defined at the nominal SSD. With the chamber at 200 cm the collimator scatter correction factor can be measured for fields with dimensions down to 4×4 cm^2 at 100 cm. These relative measurements should all be performed under the same conditions. In other words, if one chooses to measure with a high density buildup cap, measurements for all field sizes should be performed with the same buildup cap.

As the output factor is the product of the collimator scatter correction factor and the phantom scatter correction factor, the phantom scatter

correction factor may be found by dividing the output factor by the collimator scatter correction factor.

10.4.1.3. Blocking tray factors

Most treatment units have collimators that form rectangular fields. Since treatment volumes are rarely rectangular, high density shielding blocks are used to protect normal critical structures within the irradiated area. The blocks are either individually designed blocks fabricated from a low melting point alloy, such as Lipowitz's alloy, or standard 'library' blocks that may be purchased from the vendor of the treatment machine. In either case these blocks are supported on a plastic tray to correctly position them within the radiation field. This tray attenuates the radiation beam. The amount of beam attenuation provided by the tray must be known to calculate the dose received by the patient. The attenuation for solid trays is easily measured by placing an ionization chamber on the central axis of the beam at 5 cm depth in a phantom in a 10×10 cm^2 field. The ratio of the ionization chamber signal with the tray in the beam to the signal without the tray is the blocking tray transmission factor.

Although the tray transmission factor should be measured for several depths and field sizes, this factor usually has only a weak dependence on these variables and typically one may use one value for all depths and field sizes.

10.4.1.4. Multileaf collimators

On most current treatment machines multileaf collimators (MLCs) are finding widespread application for conventional field shaping as a replacement for shielding blocks. The advantages of an MLC include a reduction in the amount of storage space needed in the treatment room, elimination of the need for the treatment technologists to lift heavy blocks and the ability to treat multiple fields without re-entering the treatment room. Disadvantages include the discrete step size of the leaves and additional quality assurance requirements. Additional data are also required to characterize the output factors, central axis PDDs and penumbra of the MLC fields and the leakage through and between the leaves.

Typically the central axis PDDs of MLC defined fields are not significantly different from fields defined with collimator jaws. The penumbra of MLC defined fields should be measured for both the leaf ends and edges. The penumbra will depend on the leaf design and on whether the leaves are singly or doubly focused. Generally, the MLC penumbra is within 2 mm of the penumbra of fields defined with collimator jaws, with the greatest difference

being for singly focused MLC fields not centred on the collimator axis of rotation.

The output factor for fields shaped by MLC systems added downstream from the conventional four jaw collimator system are closely approximated by the product of the collimator scatter factor for the collimator setting and the phantom scatter factor for the irradiated area. This relation is the same as for fields formed with conventional blocks. Some MLC systems replace at least one set of conventional jaws. For these MLC systems the product of the collimator scatter factor and phantom scatter factor for the irradiated area approximates the output factor. Of course, the physicist should verify these relationships for central axis PDDs, penumbra and output factors on each machine.

Leakage through the MLC consists of transmission through the leaves and leakage between the leaves. Leakage between the leaves is easily demonstrated by exposing a film placed perpendicularly to the collimator axis of rotation with the leaves fully closed. Leakage through the leaves can be determined by comparing the umbra region of transverse beam profiles for fields defined by the MLC with fields defined by the collimator jaws. Typical values of MLC leakage through the leaves are in the range of 3% to 5% of the isocentre dose.

10.4.1.5.   Central axis wedge transmission factors

Wedges are used to shape the dose distribution of radiation treatment fields. The central axis wedge transmission factor is the ratio of the dose at a specified depth on the central axis of a specified field size with the wedge in the beam to the dose for the same conditions without the wedge in the beam. Central axis wedge transmission factors determined for one field size at one depth are frequently used to calculate beam-on times or MU settings for all wedged fields and depths. However, central axis wedge transmission factors may be a function of both depth and field size.

The field size variation may depend not only on the width of the field along the gradient of the wedge but also on the length of the field. In other words, the central axis wedge transmission factor for a given wedge for a 10×10 cm^2 field may differ from the central axis wedge transmission factor for a 10×20 cm^2 field even when the 10 cm is along the wedge gradient in both cases. These dependencies require measuring central axis PDDs with the wedge in the beam for a range of field sizes. The dose with the wedge in the beam can then be related to the calibrated dose rate by measuring the central axis wedge transmission factor at one depth for each field size.

To measure the central axis wedge transmission factor for a given field size at one depth the ionization chamber should be placed on the central axis of the beam with its axis aligned parallel to a constant thickness of the wedge. Measurements should be performed with the wedge in its original position and with the wedge rotated through 180º. This set of measurements verifies that the wedge and the ionization chamber are correctly positioned. The wedge position may be rotated through 180º by rotating the collimator or by rotating the wedge itself.

Rotation of the wedge itself reveals whether the side rails are symmetrically positioned about the collimator axis of rotation. Rotation of the collimator verifies that the ionization chamber is positioned on the collimator axis of rotation. The measured values should be the same for the two wedge orientations. If the values differ by more than 5% for a 60º wedge or 2% for a 30º wedge, then the wedge or ionization chamber is not positioned correctly and the situation should be corrected. Otherwise it is usually adequate to take the average value of the two wedge orientations as the correct value.

10.4.1.6. Dynamic wedge

Linacs are available with an option allowing independent movement of the collimator jaws. This option may be used to create wedged shaped dose distributions by moving one of the independent collimator jaws while the opposite jaw remains stationary during irradiation. This technique is referred to as a dynamic wedge. Clinical implementation of dynamic wedges requires measurement of central axis PDDs, central axis wedge transmission factors and transverse beam profiles of the dynamic wedges. These measurements are complicated by the modulation of the photon fluence during the delivery of the radiation field.

The central axis PDD may be measured by integrating the dose at each point during the entire irradiation of the dynamic wedge field. The central axis wedge transmission factors are determined by taking the ratio of the collected ionization at a specified depth for the dynamic wedge field to the collected ionization at the same specified depth for the open field with the same collimator and MU settings.

It is important to note that the central axis wedge transmission factors for dynamic wedges may have much larger field size dependence than physical wedges and the field size dependence for dynamic wedges may not be asymptotic. Some manufacturers' implementations of the dynamic wedge technique show a significant change in the trend of the central axis wedge transmission factor as the field width changes between 9.5 and 10 cm. This change in the central axis wedge transmission ratio has been demonstrated to

approach 20%. This characteristic should be carefully investigated on each machine. Dynamic wedge transverse beam profiles can be measured with a detector array or an integrating dosimeter such as radiochromic film. When a detector array is used, the sensitivity of each detector must be determined.

10.4.1.7. Transverse beam profiles/off-axis energy changes

The distribution of dose at any point within a radiation beam is required to be known for treatment planning. Transverse beam profiles are measured to characterize the dose at points off the central axis. Frequently off-axis data are normalized to the dose on the central axis at the same depth. These data are referred to as OARs, which are combined with central axis data to generate isodose curves.

The number of profiles and the depths at which these profiles are measured will depend on the requirements of the TPS. Some systems require these profiles at a few equally spaced depths, others require several profiles at specified depths and some require only one off-axis profile for the largest field size measured in air with a buildup cap. Transverse beam profiles should be measured in addition to those on which the beam model was determined to verify the accuracy of the TPS algorithms.

Of course, these profiles should be measured for both open and wedged fields. The profiles of the wedged field can then be combined with the central axis PDD values for wedged fields to generate wedged isodose curves. Any change in wedge factor (WF) with depth is then included in the isodose curves.

10.4.1.8. Entrance dose and interface dosimetry

Knowledge of interface dosimetry, such as the entrance dose between the patient surface and z_{max}, is important in a variety of clinical situations. Other areas of interface dosimetry that may be important are interfaces at small air cavities such as the nasopharynx, at the exit surface of the patient, at bone–tissue interfaces and between a metallic prosthesis and tissue.

These measurements are usually time consuming because they are not easily automated with a water phantom and scanner. The rapidly changing dose gradient demands measurement with a thin window parallel-plate chamber. The requirement for a thin window makes water phantom measurements difficult because of the need to waterproof the chamber and to avoid deformation of the window by hydrostatic pressure.

Measurements are typically carried out in a polystyrene phantom in a constant SSD geometry. They begin with the block containing the chamber upstream, backed by two 5 cm blocks of backscattering material with all the

buildup sheets placed downstream from these blocks. The first measurement is made with no buildup material upstream from the chamber. The next depth is measured by moving the appropriate sheet of buildup material from the bottom to the top of the phantom. This scheme maintains a constant SSD as buildup material is added.

Interface dosimetry measurements should always be performed with both polarities on the entrance window of the ionization chamber. Large differences in the signal at the interface will be observed when the polarity is reversed. Measurements further from the interface exhibit smaller differences than measurements nearer the interface. For depths beyond the transition zone readings with either polarity should be the same. The true value Q_T of the measured ionization at each depth is:

$$Q_T = (Q_+ - Q_-)/2 \tag{10.4}$$

The positive or negative signs refer to the polarity of the signal, and the sign of the signal is maintained in this operation. The value computed with Eq. (10.4) is the same as the average of the absolute magnitudes of Q_+ and Q_-, unless they have the same sign. This will occur in low signal to noise situations in which the cable or stem contributes a significant spurious current that does not change sign with a change in polarity, while the true signal from the sensitive volume of the chamber does change sign with a change in polarity.

10.4.1.9. Virtual source position

Knowledge of the virtual source position is required for treatment at extended SSDs. A common technique to determine the virtual source position is to make in-air ionization measurements at several distances from the nominal source position to the chamber. The data are plotted with the distance to the nominal source position on the *x* axis and the reciprocal of the square root of the ionization on the *y* axis.

These data should follow a straight line; if not, the radiation output does not follow the inverse square law. If the straight line passes through the origin, the virtual and nominal source positions are the same. If the straight line has a positive *x* intercept, the virtual source position is downstream from the nominal source position, while a negative *x* intercept indicates an upstream virtual source position.

For example, consider a machine with a nominal source to axis distance (SAD) of 100 cm. Assume for this machine that these measurements demonstrated that the reciprocal of the square root of the measured ionization followed a straight line but that the *x* intercept was +1 cm. This situation reveals

that the inverse square law applies but that the virtual source is 99 cm from the isocentre. In this case the inverse square calculation should be from 99 cm rather than 100 cm.

This analysis should be performed for the range of field sizes, as collimator scatter may change the virtual source position. Of course, if the data do not follow a straight line, the inverse square law is not applicable and special calibrations will be required at each distance.

Measurement of the beam divergence at various distances from the source is a less commonly used technique to determine the virtual source position. This measurement is performed by exposing films orientated perpendicularly to the central axis of the beam at a depth of z_{max}. The full width at half maximum (FWHM) of the beam is determined at each distance. The FWHM at each distance can be plotted and will form a straight line if the inverse square law is valid. The x intercept indicates the virtual source position. This measurement should be performed for a range of field sizes. One problem is that the range of field sizes and distances for which this technique may be used is limited by the size of the film.

10.4.2. Electron beam measurements

10.4.2.1. Central axis percentage depth dose

Electron central axis PDD values have been measured with cylindrical and parallel-plate ionization chambers, diodes and film; however, the ionometric method remains the gold standard.

The effective point of measurement for parallel-plate chambers is the inside surface of the entrance window. The effective point of measurement with cylindrical chambers, on the other hand, is shifted from the centre of the chamber, and the shift is one half the inside radius of the cavity towards the source.

Cylindrical chambers perturb the electron fluence more than parallel-plate chambers. This perturbation is corrected with a replacement correction. This factor is less than 1 for cylindrical chambers, and the value of the factor decreases (further from unity) as the energy of the electron beam decreases and the depth in the phantom increases.

Most thin window parallel-plate chambers with a plate separation of 2 mm or less have a replacement correction of unity. However, some of these chambers have a replacement correction different from unity. The replacement factor is dependent on the guard ring design, as well as on the plate separation distance. Chambers with narrow guard rings tend to have replacement factors further removed from unity than those with wider guard rings.

Parallel-plate chambers can be difficult to waterproof if used in a water phantom. Hydrostatic pressure in a water phantom can also deform a thin entrance window of a parallel-plate chamber if a thin waterproof sheath is used. This deformation changes the chamber's sensitivity.

Use of a parallel-plate chamber in a phantom can lead to a dosimetric mismatch if the phantom material differs from the material of the chamber. This mismatch can result in a change in the number of backscattered electrons with the chamber in place from what would occur in a homogeneous phantom. Depending on the materials involved this change may be either an increase or a decrease.

Medical physics societies recommend calibration of low energy electrons with specially designed parallel-plate chambers, because the replacement correction factor is much more significant for cylindrical chambers for electrons less than 10 MeV. Higher energy electrons can be measured with cylindrical chambers.

Water is the phantom material generally recommended for high energy electrons, because it is nearly tissue equivalent and has uniform composition regardless of its origin.

Plastic phantoms are recommended for low energy electron measurements with a thin window parallel-plate chamber that cannot be readily waterproofed, in order to prevent hydrostatic deformation of the window. Plastic phantoms are also useful for film dosimetry measurements.

Several plastic materials are acceptable for phantoms. However, these plastics are not exactly water equivalent (i.e. they do not necessarily have the same linear collision and radiative stopping powers and the same linear angular scattering power as water). This lack of exact water equivalence requires that depths of measurements made in plastic phantoms be corrected to water equivalent depths by scaling. The AAPM TG 25 dosimetry protocol recommends a scaling factor based on the ratios of the depth of the 50% ionization measured in the two materials:

$$z_{water} \; = \; z_{med}(R_{50}^{water}/R_{50}^{med}) \tag{10.5}$$

where

z_{water} is the depth in water that is equivalent to the measurement depth z_{med};
R_{50}^{water} is the depth of the 50% ionization in water;
R_{50}^{med} is the depth of the 50% ionization in a phantom medium.

In reference to plastic phantoms, it must be noted that polystyrene is an ambiguous term. Some medical physicists refer to clear polystyrene as

polystyrene and to white polystyrene with a 3% loading of TiO_2 as 'high impact' polystyrene. Other physicists refer to white polystyrene as polystyrene and to the clear version as clear polystyrene. When using tables for depth scaling factors one should ascertain which polystyrene is listed. Also, the density of any plastic should be verified, as it can vary between production batches.

Additionally, unlike photons, electron percentage depth ionization curves are not equivalent to PDD curves. Electron ionization measurements must be multiplied by the replacement factor and the restricted mass stopping power ratio to determine dose. These factors are energy dependent, and thus depth dependent, because the electron beam loses energy as it penetrates the phantom.

The therapeutic dose is frequently chosen to be the 90% dose at a depth beyond the depth of dose maximum z_{max}. For fields with dimensions similar to or smaller than the range of the electrons, loss of side scatter equilibrium will result in a shift of the depth of z_{max} towards the surface and a decrease in the depth of the 90% dose. The range will remain approximately the same as for larger fields. For field sizes larger than the range, the depth of the therapeutic dose remains constant.

The electron PDD should be measured in field size increments small enough to permit accurate interpolation to intermediate field sizes. Although skin sparing is much less than for photon beams, skin dose remains an important consideration in many electron treatments. Surface dose is best measured with a thin window parallel-plate ionization chamber. The central axis PDD should be measured to depths large enough to determine the bremsstrahlung contamination in the beam.

10.4.2.2. Output factors

The radiation output (cGy/MU) is a function of field size and is determined at z_{max} at the standard SSD. The output is measured with a small volume ionization chamber at z_{max} on the central axis of the field. The output depends on the method used to define the field. Three types of collimation are used to define an electron field: secondary collimators (cones) in combination with the X ray jaws; irregularly shaped lead or low melting point alloy metal cut-outs placed in the secondary collimators; and skin collimation.

(a) Secondary collimators

Cones, or electron collimators, are available for a limited number of square fields, typically 5×5 cm^2 to 25×25 cm^2 in 5 cm increments. Circular and rectangular cones are available, but they are not as common as square cones.

The purpose of the cone depends on the manufacturer. Some use cones only to reduce the penumbra, while others use the cone to scatter electrons off the side of the cone to improve field flatness. The output for each cone must be determined for all electron energies. These values are frequently referred to as cone ratios rather than output factors.

(b) Metal cut-outs

Irregularly shaped electron fields are formed by placing metal cut-outs of lead or low melting point alloy in the end of the cone nearest the patient. The penumbra produced by these cut-outs is essentially the same as the penumbra produced by the cones themselves. A thickness of 12 mm of a low melting point alloy, such as Lipowitz's metal, is adequate for electrons up to 20 MeV. The output factors for fields defined with these cut-outs depend on the electron energy, the cone and the area of the cut-out. The dependence of output should be determined for square field inserts down to 4×4 cm^2 for all energies and cones.

As with photons, fields smaller than 4×4 cm^2 require special precautions because the size of the ionization chamber may approach the size of the field, and smaller detectors are required. A parallel-plate chamber with a small collecting electrode may be used in a polystyrene phantom or a diode used in a water phantom. In either case the same set-up should be used to measure both the small field and the 10×10 cm^2 field.

Since z_{max} shifts towards the surface in electron fields with dimensions smaller than the range of the electrons, it must be determined for each small field size when measuring output factors. The output factor is the ratio of the dose at z_{max} for the small field to the dose at z_{max} for the 10×10 cm^2 field. For ionometric data this requires converting the ionization to the dose at each z_{max} before determining the output factor, rather than simply taking the ratio of the ionizations. If central axis PDD data measured with diodes agree with the central axis PDD data determined from ionometric data, the diode data can be used directly to determine the depth of z_{max}.

Use of film is an alternative solution. It can be exposed in a polystyrene or water equivalent plastic phantom in an orientation parallel to the central axis of the beam. One film should be exposed to a 10×10 cm^2 field, the other film to the smaller field. The films should be scanned to find the central axis z_{max} for each field. The ratio of the dose at z_{max} of the small field to the dose at z_{max} of the large field is the output factor. This requires that the dose has been determined from the net OD with a characteristic curve and that good agreement has been demonstrated between the PDD measured with film to that determined from ionization chamber data for a 15×15 cm^2 field.

The output factor (or cone ratio) is a function of energy, cone size and insert size. Typically, all values are normalized to an open 10×10 cm^2 cone. For rectangular fields formed by placing inserts in cones the equivalent square can be approximated with a square root method. The validity of this method should be checked on each machine for which the approximation is used.

$$OF(E, x, y, f) = [OF(E, x, x, f) \times OF(E, y, y, f)]^{1/2} \qquad (10.6)$$

where

f is the SSD;

$OF(E, x, y, f)$ is the output factor for an x cm $\times$ y cm rectangular field of energy E;

$OF(E, x, x, f)$ is the output factor for an x cm $\times$ x cm rectangular field of energy E;

$OF(E, y, y, f)$ is the output factor for a y cm $\times$ y cm rectangular field of energy E.

(c) Skin collimation

Skin collimation is used to minimize the penumbra for very small electron fields, to protect critical structures near the treatment area and to restore the penumbra when treatment at an extended distance is required. When designing skin collimation the cone insert chosen should be larger than the area to be treated. The skin collimation then collimates this larger field to the treatment area. The skin collimation should also extend a distance beyond the area collimated by the cone insert, to protect the patient from scattered electrons.

The thickness required for any electron shielding can be estimated by:

t_{pb} (mm) $= 0.5E_{p,0}$ (MeV) $+ 1$ for lead and
t_{Lm} (mm) $= 1.2t_{pb}$ (mm) for Lipowitz's metal $\qquad (10.7)$

where

$E_{p,0}$ (MeV)   is the most probable electron energy at the surface of the patient;
t_{pb} (mm)   is the thickness of the lead;
t_{Lm} (mm)   is thickness of Lipowitz's metal.

Some clinical situations may require minimizing the weight of the skin collimation on the patient, resulting in somewhat thinner masks. In these situations it is recommended that the degree of shielding be assessed. This

assessment can be performed with a thin window parallel-plate chamber in a polystyrene phantom at a depth of 1 mm.

As for any small field, skin collimation may affect the PDD as well as the penumbra if the dimensions of the treatment field are smaller than the electron range. The field size dependence of the PDD is principally a result of scattering in the patient.

The PDD for a field defined by skin collimation can be approximated as the PDD of the field determined by secondary collimation, such as a cone. The field size dependence of the output results from electron scattering from the X ray jaws and in air. In most cases for cones that are 5 cm or more from the skin, the output for a field defined with skin collimation is the same as the output defined by the secondary collimator for that treatment. However, if the skin collimation defines a field so small that the PDD changes, then the output may be affected and a measurement may be required.

10.4.2.3. Transverse beam profiles

As for photon beams, transverse electron beam profiles are measured to determine the off-axis dose distribution of electron beams. This information is combined with the central axis PDD to yield the isodose distribution. The number of transverse profiles and the depths at which they must be measured depend on the requirements set by the treatment planning computer.

These profiles are measured in a water phantom with a small volume ionization chamber. The surface of the phantom is placed at 100 cm or the nominal SSD and the ionization chamber is scanned perpendicularly to the central axis.

An alternative film dosimetry technique is to measure isodose curves rather than beam profiles. The film is exposed parallel to the central axis of the beam. Optical isodensity is converted to isodose. However, the PDD determined with film is typically 1 mm shallower than ionometric determination for depths greater than 10 mm, and for depths shallower than 10 mm the differences may be as great as 5 mm. Isodose curves may also be measured with small volume ionization chambers or diodes.

10.4.2.4. Virtual source position

Frequently, electron fields must be treated at extended distances because the surface of the patient prevents positioning of the electron applicator at the normal treatment distance. A common example of this occurs during the treatment of posterior neck fields for head and neck carcinoma. The shoulder typically interferes with positioning of the electron applicator at the normal

treatment distance to the neck. Additional scattering in the extended air path increases the penumbral width and decreases the output (cGy/MU). Knowledge of the virtual electron source is required to predict these changes. The virtual source position is the point from which the electrons appear to emanate.

Determination of the virtual source position is similar to the verification of the inverse square law for photons. Treatment planning computers use the virtual source position to calculate the divergence of electron beams at extended SSDs. Correction of the output at an extended SSD requires an air gap correction factor in addition to the inverse square factor. The air gap factor corrects the deviations from the inverse square law resulting from the collimator and air scatter of the electrons. The air gap correction factor may be either greater or less than unity, as the output may either increase or decrease at extended distances, depending on the collimator design, electron energy, field size and air gap. However, for SSDs up to 110 cm and energies up to 25 MeV this correction is typically less than 2%.

There can be significant changes in the PDD at extended SSDs if the electron cone scatters electrons to improve the field flatness. For these machines it may be necessary to measure isodose curves over a range of SSDs.

Treatment at an extended SSD will also increase the penumbra width. At lower energies the width of the penumbra (the distance between the 80% and 20% dose values on a beam profile normalized to 100% on the central axis) increases approximately proportionally with the air gap. As electron energy increases the increase in the penumbra width is less dramatic at depth than for lower energies, but at the surface the increase in penumbra remains approximately proportional to the air gap. Since a large number of clinical situations demand treatment at an extended SSD, it is advisable to measure a sample of isodose curves at extended SSDs to evaluate the algorithms in the TPS in use. The penumbra can be restored when treating at extended distances by the use of skin collimation, as discussed in Chapter 9.

10.5.   TIME REQUIRED FOR COMMISSIONING

Acceptance testing and commissioning of megavoltage treatment units has been discussed in this chapter. The completion of all the tasks associated with placing a treatment unit in clinical service can be estimated to require from 1.5 weeks to 3 weeks per energy following completion of the acceptance tests. The time will depend on machine reliability, amount of data measurement, sophistication of the treatments planned and experience of the physicist. Highly specialized techniques, such as stereotactic radiosurgery,

intraoperative treatment, intensity modulated radiotherapy (IMRT) and total skin electron treatment, have not been discussed and are not included in these time estimates.

Commonly used methods to estimate data that have not been measured from measured data have been discussed. The accuracy of all these techniques must be verified on each machine, as variations exist between machines.

BIBLIOGRAPHY

FOOD AND AGRICULTURE ORGANIZATION OF THE UNITED NATIONS, INTERNATIONAL ATOMIC ENERGY AGENCY, INTERNATIONAL LABOUR ORGANISATION, OECD NUCLEAR ENERGY AGENCY, PAN AMERICAN HEALTH ORGANIZATION, WORLD HEALTH ORGANIZATION, International Basic Safety Standards for Protection against Ionizing Radiation and for the Safety of Radiation Sources, Safety Series No. 115, IAEA, Vienna (1996).

INTERNATIONAL ELECTROTECHNICAL COMMISSION, Safety of Medical Electrical Equipment, Part 2: Particular Requirements for Medical Electron Accelerators in the Range 1 MeV to 50 MeV, Section 1: General, Section 2: Radiation Safety for Equipment, IEC 601-2-1, IEC, Geneva (1996).

PODGORSAK, E.B., METCALFE, P., VAN DYK, J., "Medical accelerators", Modern Technology of Radiation Oncology: A Compendium for Medical Physicists and Radiation Oncologists (VAN DYK, J., Ed.), Medical Physics Publishing, Madison, WI (1999).

Chapter 11

COMPUTERIZED TREATMENT PLANNING SYSTEMS FOR EXTERNAL PHOTON BEAM RADIOTHERAPY

M.D.C. EVANS
Department of Medical Physics,
McGill University Health Centre,
Montreal, Quebec, Canada

11.1. INTRODUCTION

Computerized treatment planning systems (TPSs) are used in external beam radiotherapy to generate beam shapes and dose distributions with the intent to maximize tumour control and minimize normal tissue complications. Patient anatomy and tumour targets can be represented as 3-D models. The entire process of treatment planning involves many steps and the medical physicist is responsible for the overall integrity of the computerized TPS to accurately and reliably produce dose distributions and associated calculations for external beam radiotherapy. The planning itself is most commonly carried out by a dosimetrist, and the plan must be approved by a radiation oncologist before implementation in actual patient treatments.

Treatment planning prior to the 1970s was generally carried out through the manual manipulation of standard isodose charts on to patient body contours that were generated by direct tracing or lead wire representation, and relied heavily on the judicious choice of beam weight and wedging by an experienced dosimetrist.

The simultaneous development of computed tomography (CT), along with the advent of readily accessible computing power from the 1970s on, led to the development of CT based computerized treatment planning, providing the ability to view dose distributions directly superimposed upon a patient's axial anatomy.

The entire treatment planning process involves many steps, beginning from beam data acquisition and entry into the computerized TPS, through patient data acquisition, to treatment plan generation and the final transfer of data to the treatment machine.

Successive improvements in treatment planning hardware and software have been most notable in the graphics, calculation and optimization aspects of current systems. Systems encompassing the 'Virtual Patient' are able to display

beam's eye views (BEVs) of radiation beams and digitally reconstructed radiographs (DRRs) for arbitrary dose distributions. Dose calculations have evolved from simple 2-D models through 3-D models to 3-D Monte Carlo techniques, and increased computing power continues to increase calculation speed.

Traditional forward based treatment planning, which is based on a trial and error approach by experienced professionals, is giving way to inverse planning, which makes use of dose optimization techniques to satisfy the user specified criteria for the dose to the target and critical structures. Dose optimization is possible by making use of dose–volume histograms (DVHs) based on CT, magnetic resonance imaging (MRI) or other digital imaging techniques. These optimized plans make use of intensity modulated radiotherapy (IMRT) to deliver the required dose to the target organ while respecting dose constraint criteria for critical organs.

Computerized treatment planning is a rapidly evolving modality, relying heavily on both hardware and software. Thus it is necessary for related professionals to develop a workable quality assurance programme that reflects the use of the TPS in the clinic and that is sufficiently broad in scope to ensure proper treatment delivery.

11.2. SYSTEM HARDWARE

11.2.1. Treatment planning system hardware

The principal hardware components of a TPS include a central processing unit (CPU), a graphics display, memory, digitizing devices, output devices, and archiving and network communication devices. As hardware capabilities tend to change quickly, the general approach is to acquire equipment having the highest current specifications while allowing for future upgrades.

The CPU must have at least the memory and processor speed required by the operating system and treatment planning software. In particular, the specifications for the system speed, random access memory (RAM) and free memory, as well as networking capabilities, must be considered.

The graphics display is normally sufficient for accommodating the patient transverse anatomy on a 1:1 scale, typically 17–21 in. (43–53 cm) or larger. The resolution is submillimetre or better so as not to distort the input. Graphics speed can be enhanced with video cards and hardware drivers.

Memory and archiving functions are carried out through either removable media or networking. Removable media may include floppy disks, rewritable hard disks, optical disks or digital video disks (DVDs). Mass

archiving may also be accomplished with slower digital audio tape (DAT); however, these devices have been reported to suffer from long term instability. Archiving may be carried out over a network on a remote computer or server; these archiving operations may be carried out automatically during low use periods of the day. Archiving operations can include beam data and parameters, patient related data such as CT scans and dose distributions, and data used for setting up the patient for treatment on a linac with record and verify systems.

Digitizing devices are used to acquire manually entered patient data such as transverse contours and BEVs of irregular field shapes. These devices are typically backlit tablets with either a magnetic or acoustic stylus for manually tracing shapes. Scanners, either flatbed or upright, can be used to digitize images from hard copies such as paper or radiographic film. Videoframe grabbers may also be used to digitize images.

Output devices include colour laser printers and plotters for text and graphics. Printers and plotters can be networked for shared access. Hard copies can be in the form of paper or film via a laser camera.

Uninterruptible power supplies (UPSs) are recommended for the CPU, data servers and other critical devices, such as those used for storage and archiving. UPSs can provide backup power so that a proper shutdown of the computer can be accomplished during power failures of the regular power distribution grid, and they also act as surge suppressors for the power.

Communications hardware includes modem or Ethernet cards on local workstations and multiple hubs for linking various peripheral devices and workstations. Large networks require fast switches running at at least 100 Mb/s for file transfer of images. Physical connections on both small and large networks are run through coaxial cable, twisted pairs or optical fibre, depending upon the speed requirements.

The environmental conditions under which the TPS hardware runs may be subject to temperature and humidity requirements. Thus the physical location of the equipment associated with the TPS within a department is of importance.

11.2.2. Treatment planning system configurations

Smaller TPS configurations may have a stand-alone layout whereby one central CPU handles most functions and communications requests. In this configuration there may only a be few users, and access to the peripheral devices used for printing and archiving is not shared. Network requirements may also be limited; however, even stand-alone TPSs now routinely require

network switches to communicate with digital imaging devices such as CT scanners.

Larger systems often operate within a hospital-wide network, and may also make use of Internet based communications systems. Many of the devices operated and accessed by the large TPS configuration will not have a direct connection and must be accessed through a number of network switches using a communications protocol such as transmission control protocol/internet protocol (TCP/IP). These larger systems may also have a remote server for various file handling tasks related to patient data, digital images, beam data and dose calculation. Large area TPS configurations having many users and remote workstations may require the services of an administrator to maintain security, user rights, networking, backup and archiving.

11.3. SYSTEM SOFTWARE AND CALCULATION ALGORITHMS

Dose calculation algorithms are the most critical software component in a computerized TPS. These modules are responsible for the correct representation of dose in the patient, and may be linked to beam time or monitor unit (MU) calculations. Dose calculations have evolved from simple 2-D calculations, to partial 3-D point kernel methods, to full 3-D dose models in which the histories of the primary and scattered radiation in the volume of interest are considered.

11.3.1. Calculation algorithms

There are numerous dose calculation algorithms used by computerized TPSs, and due to the rapidly changing nature of computer power the implementation of these techniques is a constantly evolving process. Specific details of treatment planning dose algorithms can be found throughout the literature, and a small selection is included in the bibliography section of this chapter.

Prior to understanding sophisticated computerized treatment planning algorithms, a proper understanding of manual dose calculations is essential, and there are many texts that adequately discuss these methods, including Johns and Cunningham, Khan, and Hendee and Ibbot.

ICRU Report No. 42 lists the chronological development of dose calculation algorithms for photon and electron beams. It provides representative examples for calculation of the central axis depth dose and the cross-beam or off-axis ratio (OAR) for photon beams. Representative examples of electron beam calculations, including the empirical and semi-empirical

formalism for calculation of the central axis depth dose, and the empirical formalism for calculation of the cross-beam or OARs, are also provided.

Early TPSs generated dose distributions through the manipulation of relatively simple 2-D beam data for a range of square fields in water. These data sets comprised matrices of central axis percentage depth doses (PDDs) and several OARs (profiles) at a number of depths.

To speed up calculation, central axis data were converted and stored as infinite PPD data, while the profiles were stored along ray lines backprojected to an arbitrary source to surface depth (SSD). In this manner, data could be rapidly manipulated using look-up tables to generate dose distributions on to external patient contours. These types of algorithm were used for both photon and electron beam treatment planning and led to very fast dose calculations. However, in general they were not truly representative of the 3-D scattering conditions in the patient.

Prior to the advent of widespread CT use in treatment planning, irregular field dosimetry was accomplished using BEV films of treatment fields obtained with conventional simulators. Using the central axis and profile data sets, the primary and scatter components of the beam could be separated using the zero area tissue–air ratio (TAR) and scatter–air ratio (SAR) at depth to generate Clarkson sector integration calculations for points of interest in the irregular field.

The approach of current beam calculation algorithms is to decompose the radiation beam into primary and secondary or scatter components, and to handle each component independently. In this manner, changes in scattering due to changes in beam shape, beam intensity, patient geometry and tissue inhomogeneities can be incorporated into the dose distribution.

One such model uses convolution methods whereby the dose at any point in the medium can be expressed as the sum of the primary and scatter components. These models use superposition principles to account for both local changes in the primary fluence and changes in the spread of energy due to local scattering caused by the patient and beam geometry. Under specific conditions of non-divergent sources and homogeneous phantoms, convolution type integrals can be used to simplify and speed up these calculations.

Monte Carlo or random sampling techniques are used to generate dose distributions by following the histories of a large number of particles as they emerge from the source of radiation and undergo multiple scattering interactions both inside and outside the patient.

Monte Carlo techniques are able to accurately model the physics of particle interactions by accounting for the geometry of individual linacs, beam shaping devices such as blocks and multileaf collimators (MLCs) and patient surface and density irregularities. They allow a wide range of complex patient

treatment conditions to be considered. In order to achieve a statistically acceptable result, Monte Carlo techniques require the simulation of a large number of particle histories, and are only now becoming practical for routine treatment planning as computing power reduces the calculation time to an acceptable level, of the order of a few minutes for a given treatment plan.

Pencil beam algorithms are common for electron beam dose calculations. In these techniques the energy spread or dose kernel at a point is summed along a line in a phantom to obtain a pencil type beam or dose distribution. By integrating the pencil beam over the patient's surface to account for changes in primary intensity and by modifying the shape of the pencil beam with depth and tissue density, a dose distribution can be generated.

As pointed out by Cunningham, treatment planning algorithms have progressed chronologically to include analytical, matrix, semi-empirical and 3-D integration methods.

The analytical technique as developed by Sterling calculated the dose in the medium as the product of two equations, one of which modelled the PDD, while the other modelled the beam's off-axis component. The model has been extended to incorporate field shielding and wedge hardening.

Treatment planning computer systems developed in the 1970s began using the diverging matrix method of beam generation based on measured data.

The Milan–Bentley model was used to calculate diverging fan lines that radiate from a source and intersect depth lines located at selected distances below the patient's surface. Dose distributions are made by rapidly manipulating measured data sets consisting of central axis PDD and OAR data sets stored as a function of field size. These techniques continue to be used in treatment planning algorithms (Storchi and Woudstra), although they suffer from the perceived disadvantage of requiring large amounts of measured data, and from their limited ability to properly model scatter and electron transport conditions.

Semi-empirical dose calculation methods model the dose to a point by considering the contribution from the primary and scattered radiation independently. Based originally on the Clarkson scatter integration technique, these models have been refined by combining the formalism of basic physics with data derived from measurement. Correction factors to account for penumbra, block transmission and flattening filters have improved in these models.

These methods have been further refined by applying differential SAR techniques to allow for variations in the intensity of scatter radiation throughout the field due to the presence of wedges or non-uniform surface contours.

3-D integration methods represent the transport of electrons and photons away from the primary site of interaction so as to have an accurate description of the deposition of absorbed energy while considering the geometry and composition of the entire volume being irradiated. Monte Carlo techniques for computing dose spread arrays or kernels used in convolution–superposition methods are described by numerous authors, including Mackie, and in the review chapters in Khan and Potish, and Van Dyk provides a detailed summary of treatment planning algorithms in general.

11.3.2. Beam modifiers

Treatment planning software for photon beams and electron beams must be capable of handling the many diverse beam modifying devices found on linac models. Some of these devices are generic to all linacs, whereas others are specific to certain manufacturers. Some of these devices and specific considerations for incorporation into the TPS are listed below, separated into two main groups: photon beam modifiers (consisting of jaws, blocks, compensators, MLCs, wedges) and electron beam modifiers (consisting of cones, blocks, bolus, etc.).

11.3.2.1. Photon beam modifiers

Jaws: The field size is defined by motorized collimating devices (jaws). Jaws can move independently or in pairs and are usually located as an upper and lower set. Jaws may over-travel the central axis of the field by varying amounts. The travel motion (transverse or arced) will determine the junction produced by two abutting fields. The TPS will account for the penumbra produced by the location of these jaws, and differences in radial and transverse open beam symmetry due to the jaw design may also be considered.

Blocks: Field shielding is accounted for in the TPS by considering the effective attenuation of the block to reduce the total dose under the shielded region. The dose through a partially shielded calculation volume, or voxel, is calculated as a partial sum of the attenuation proportional to the region of the voxel shielded. The geometry of straight edge and tapered blocks can be considered separately so as to more accurately model the penumbra through the region of the block edge. TPSs are able to generate files for blocked fields that can be exported to commercial block cutting machines.

MLC: An MLC is a beam shaping device that can replace almost all conventional mounted blocks, with the exception of island blocking and excessively curved field shapes. Most modern linacs are now equipped with MLCs. There are various designs; however, MLCs with a leaf width of the order

of 0.5–1.0 cm at the isocentre are typical: MLCs providing smaller leaf widths are referred to as micro MLCs. The MLC may be able to cover all or part of the entire field opening, and the leaf design may be incorporated into the TPS to model transmission and penumbra. The MLC may also have varying degrees of dynamic motion that can be invoked while the beam is on in order to enhance dose delivery.

Wedges: Static wedges remain the principal devices for modifying dose distributions. The TPS can model the effect of the dose both along and across the principal axes of the physical wedge, as well as account for any PDD change due to beam hardening and/or softening along the central axis ray line. The clinical use of wedges may be limited to field sizes smaller than the maximum collimator setting. More recently, wedging may be accomplished by the use of universal or sliding wedges incorporated into the linac head, or, even more elegantly, by dynamic wedging accomplished by the motion of a single jaw while the beam is on.

Custom compensators may be designed by TPSs to account for missing tissue or to modify dose distributions to conform to irregular target shapes. TPSs are able to generate files for compensators that can be read by commercial compensator cutting machines.

11.3.2.2. Electron beam modifiers

Electron beams are used with external collimating devices known as cones or applicators that reduce the spread of the electron beam in the air. The design of these cones is dependent on the manufacturer and affects the dosimetric properties of the beam.

Electron shielding for irregular fields may be accomplished with the use of thin lead or low melting point alloy inserts. These shielding inserts can have significant effects upon the electron beam dosimetry (especially the PDD and output), and these effects may be modelled by the TPS.

The design of the linac head may be important for electron dosimetry, especially for Monte Carlo type calculations. In these conditions particular attention is paid to the scattering foil. The effective or virtual SSD will appear to be shorter than the nominal SSD, and may be taken into consideration by the TPS.

Bolus may be used to increase the surface dose for both photon and electron treatments. Bolus routines incorporated into TPS software will usually permit manual or automatic bolus insertion in a manner that does not modify the original patient CT data. It is important that the TPS can distinguish between the bolus and the patient so that bolus modifications and removal can be achieved with ease.

11.3.3. Heterogeneity corrections

Heterogeneity or inhomogeneity corrections generally account for the differences between the standard beam geometry of a radiation field incident upon a large uniform water phantom and the beam geometry encountered by the beam incident upon the patient's surface. Beam obliquity and regions where the beam does not intersect the patient's surface will affect the dose distribution. Inside the patient, the relative electron density of the irradiated medium can be determined from the patient CT data set.

Most TPS algorithms apply either a correction factor approach or a model based approach. Generalized correction factors, such as the power law or the equivalent TAR methods, lead to fast calculations, but are based on a correction of the initial dose calculated in water. Model based approaches such as the differential SAR approach and Monte Carlo based algorithms consider the transport and scatter in the irradiated medium directly, but have historically involved longer calculation times. Most methods are still having difficulties with dose calculations at tissue interfaces.

11.3.4. Image display and dose–volume histograms

BEVs and room eye views (REVs) are used by modern TPSs. The BEV is often used in conjunction with DRRs to aid in assessing tumour coverage and for beam shaping with blocks or an MLC.

The REV gives the user a perception of the relationship of the gantry and table to each other and may help in avoiding potential collisions when moving from the virtual plan to the actual patient set-up. DRRs are projection images generated by mathematically passing ray lines through the patient CT data. Digitally composite radiographs (DCRs) may be generated by differentially weighting ranges of CT numbers to selectively discriminate between tissue densities on the projected image.

Portal image generation can be accomplished by TPSs by substituting energy shifted attenuation coefficients for CT data sets. These virtual portal images with the treatment field superimposed can be used for comparison with the portal images obtained with the patient in the treatment position on the treatment machine.

Image registration routines can help match simulator, MR, positron emission tomography (PET), single photon emission computed tomography (SPECT), ultrasound and other image sources to planning CT and treatment acquired portal images.

DVHs are calculated by the TPS with respect to the target and critical structure volumes in order to establish the adequacy of a particular treatment

plan and to compare competing treatment plans. DVHs may be displayed as differential DVHs, whereby the ordinate represents the volume receiving the dose specified on the abscissa, or as cumulative DVHs, whereby the ordinate represents the volume or percentage volume receiving a dose equal to or greater than that indicated on the abscissa. Overlapping DVHs aid in evaluating different treatment plans, although no information with respect to the dose location is presented.

The natural DVH is encountered more commonly in brachytherapy, whereby the inherent effects of the inverse square law are reduced in the display to aid in DVH interpretation. TPSs can employ logic to help define volumes when dealing with overlapping structures; for example, when a volumetric margin is defined around a target, the TPS can establish a volume equal to the margin minus the target, and DVHs can be calculated for this virtual volume around the target.

11.3.5. Optimization and monitor unit calculations

Optimization routines including inverse planning are provided by TPSs with varying degrees of complexity. Algorithms can modify beam weights and geometry or calculate beams with a modulated beam intensity to satisfy the user criteria. These criteria may be based on a number of discrete points of interest or be specified as minimum/maximum doses to targets and critical structures. DVHs are used in optimization routines to specify the required dose criteria for various volumes. These routines can make use of 'class solutions' using a predefined beam geometry specific to a clinical site (e.g. prostate) to shorten calculation times.

Beam time and MU calculation by TPSs is optional. The calculation process is directly related to the normalization method. Relative field size output factors, wedge factors (WFs), tray factors and other machine specific factors are required. The absolute output at a reference point (e.g. SSD of 100 cm, depth of dose maximum for a reference field) will be required, as well as decay data for cobalt units. Total prescription dose and fractionation information can be incorporated.

11.3.6. Record and verify systems

Networked TPSs allow for interface between linac record and verify systems, either through a direct connection or through a remote server using fast switches. Record and verify systems may be provided by the TPS manufacturer, the linac manufacturer or third party software. They may require a mapping between various accessories on the linac and the TPS so that devices such as the jaws and wedges are orientated correctly with respect to the

patient's anatomy. Communication between the TPS and the linac avoids the errors associated with manual transcription of paper printouts to the linac and can help in the treatment of complex cases involving asymmetric jaws and custom MLC shaped fields.

11.3.7. Biological modelling

Distributions modelled on biological effects may in the future become more clinically relevant than those based upon dose alone. Such distributions will aid in predicting both the tumour control probability (TCP) and the normal tissue complication probability (NTCP). These algorithms can account for specific organ dose response and aid in assessing the dose fractionation and volume effects. Patient specific data can be incorporated in the biological model to help predict individual dose response to a proposed treatment regime.

11.4. DATA ACQUISITION AND ENTRY

11.4.1. Machine data

Prior to entering radiation data into the TPSs, the various mechanical components of the treatment machines must be obtained so that the TPS model of the machine agrees with the possible mechanical motions and limits of the machine. The gantry, table and collimator rotation conventions used in a particular institution must be described accurately and the angle convention fully understood. The TPS must also be able to distinguish between jaw pairs and to accurately model the limits of the jaw over-travel.

Static and virtual wedge use by the TPS will be limited to field sizes that correspond to the maximum field setting in both the transverse and longitudinal directions. Dynamic wedge use may also be limited by the jaw over-travel and by the maximum dose rate available on the linac. Specific files used by the linac to generate jaw movements, such as segmented treatment tables (STTs), may also be used directly by the TPS.

The TPS models the MLC leaf design and leaf motion. Blocking trays may reside at several distances, and this is accounted for by the TPS for penumbra generation. Blocks with straight or tapered edges may be modelled separately.

Linacs capable of producing IMRT fields may do so via step and shoot or fully dynamic techniques. For these types of treatment the TPS requires data regarding the maximum leaf speed and the characteristics of the maximum rise in the beam-on time and information on maximum dose rates.

Missing tissue compensators and dose compensators can be calculated by the TPS, and physical data related to the attenuation coefficients of the materials used to fabricate physical compensators are required.

The electron cone design varies from one linac manufacturer to another. The TPS may require information regarding the distance from the cone to the nominal SSD, as well as the external dimensions of the electron cone, in order to produce REVs so as to avoid potential patient–machine collisions.

11.4.2. Beam data acquisition and entry

The beam data required by the TPS must be well understood. This is especially true when acquiring beam data from the treatment units. Special consideration must be given to the geometry of the radiation detector (typically ionization chambers or diodes) and to any geometrical correction factors that must be applied to the data. Beam data are often smoothed and renormalized both following measurement and prior to data entry into the treatment planning computer.

Typical photon beam data sets include central axis PDDs and OARs (profiles) for open and wedged fields for a range of square fields. Diagonal field profiles to account for radial and transverse open beam asymmetry and wedged field lateral profiles to account for the variation in wedge hardening off-axis may also be required. In the case of diagonal profiles it may only be possible to acquire half-field scans, depending upon the size of the water tank.

The penumbra may be fitted to, or extracted from, measured data. In either case it is important that scan lengths be of sufficient length, especially for profiles at large depths, where field divergence can become considerable.

Relative or absolute field size factors are required for TPSs. These values are used both in treatment time calculations and in the calculation of dose distributions involving dynamic beams (e.g. dynamic wedges, dynamic MLCs). Particular care must be taken with respect to the reference field size, reference depth and nominal SSD, as these will have a global effect on time and MU calculations. Central axis WFs, tray factors and other accessory factors (normally the ratio of dose with and without the accessory) are also required by the TPS.

Measured beam data relevant to the MLC can include transmission through the leaf, inter-leaf transmission between adjacent leaves and intra-leaf transmission occurring when leaves from opposite carriage banks meet end on.

Beam measurement for electrons is more difficult than for photons because of the continuously decreasing energy of the beam with depth. Electron beam data measured with ionization chambers must be first converted to dose with an appropriate method, typically using a look-up table of stopping

power ratios. Measurements with silicon diodes are often considered to be tissue equivalent and give a reading directly proportional to dose.

Monte Carlo TPSs require accurate information concerning the geometry and composition of linac beam line components such as the waveguide exit window, target, flattening filter, scattering foil, transmission ionization chamber, jaws, MLC, blocks and trays, and any other items the electron or photon beam is likely to encounter.

Beam data acquired from a linac may be entered manually using a digitizer tablet and tracing stylus. A hard copy of beam data is used, and it is important that both the beam data printout and the digitizer be routinely checked for calibration.

Beam data may also be entered via a keyboard. This may be required for text, parameters such as transmission and field size factors, or for more detailed data sets such as the PDD and profiles. Other parameters may be required on a trial and error basis by TPSs that fit beam models to measured data. Keyboard data entry is inherently prone to operator error and requires independent verification.

Beam data entry via file transfer from the beam acquisition computer to the TPS is common. The digital nature of the computer acquired beam data makes them readily available to the TPS; however, careful attention must be paid to the file format. File headers contain formatting data concerning the direction of measurement, SSD, energy, field size, wedge type and orientation, detector type and other relevant parameters. Special attention must be paid to these labels to ensure that they are properly passed to the TPS. Data transfer can also occur via removable media or over a network.

11.4.3. Patient data

The patients' anatomical information may be entered via the digitizer using one or more contours obtained manually or it may come from a series of transverse slices obtained via a CT scan. In both cases, isodose distributions are calculated and displayed in patient transverse planes; this mode of radiation treatment planning is referred to as conventional 2-D treatment planning.

Three dimensional treatment planning delivers tumouricidal doses in volumes of tissue rather than in individual planes. The 3-D information data required to localize the tumour volume and normal tissues may be obtained from various imaging modalities. The patient's volumetric anatomical information is likely to be derived from multislice CT or MR scanning. It may also be the result of image registration and fusion techniques in which the volume described in one data set (MRI, PET, SPECT, ultrasound, digital

subtraction angiography (DSA)) is translated or registered with another data set, typically CT.

The patient image data may be transferred to the TPS via the DICOM 3 (Digital Imaging and Communications in Medicine) or DICOM RT (radiotherapy) format. Both formats were adopted by the American College of Radiology (ACR) and the National Electrical Manufacturers Association (NEMA) in 1993.

To ensure accurate dose calculation, the CT numbers must be converted to electron densities and scattering powers. The conversion of CT numbers to electron density and scattering power is usually performed with a user defined look-up table, which in turn is generated using a water equivalent circular phantom containing various inserts of known densities simulating normal body tissues such as bone and lung.

Patient data can undergo image segmentation whereby the region within an image data set that belongs to an organ or tumour is defined. Manual contouring on the TPS can be achieved by using copy and edit tools for convenience. Automatic contouring routines can help in outlining organs or regions of bulk density.

Standard volumes, such as those defined by the ICRU Report No. 50 and the ICRU Report No. 62, including the gross target volume (GTV), clinical target volume (CTV) and planning target volume (PTV), are used by the TPS, along with automatic margin generation. Image segmentation is used in the determination of the beam geometry to irradiate the target volume while sparing normal tissues and in the evaluation of treatment plans using DVHs.

Patient anatomy may be displayed using the BEV capability of the TPS. The rendering of patient anatomy from the point of view of the radiation source is useful in viewing the path of the beam, the structures included in the beam and the shape of the blocks or MLC defined fields.

11.5. COMMISSIONING AND QUALITY ASSURANCE

11.5.1. Errors

Uncertainties and errors in TPSs may arise from any of the many steps involved in the treatment planning process. Expected and acceptable errors may be expressed either as a percentage error in high dose regions of the dose distribution such as the irradiated volume or as distance in high dose gradient regions such as the buildup or penumbra regions of the distribution. A statement of acceptable uncertainty should also address the probability of practically achieving these levels.

11.5.2. Verification

Data verification entails a rigorous comparison between measured or input data and data produced by the TPS. Standard test data sets such as the AAPM TG 23 data set can be used to assess TPS performance. TPS data can also be compared with published data, although this can only serve as an approximation. AAPM TG 53 provides a detailed description of quality assurance tests that may be carried out by the clinical physicist.

Hard copy plots of basic TPS data and measured beam data are kept in logbooks for ready access. Comparisons for situations of varying degrees of complexity such as open and wedged fields with and without blocks can be used to initially assess TPS performance. More complex set-ups involving partial fields and inhomogeneous phantoms may also be considered. Geometrical verification of the accuracy of the TPS to produce shielded regions, as either blocks or apertures, can be performed by overlaying a hard copy. When designing shields with an MLC, the leaf intersection on the region of interest may occur on the outer corner, centre or inner corner. This must be verified in order to assess the amount of over- or undershielding that occurs.

Certain 3-D beam algorithms are not based on directly measured beam data but are based on the linac design and component composition. Verification with respect to the stated manufacturers' specifications will therefore be necessary.

The digitizer and plotter (printer) can be verified by using the digitizer to enter a contour of known dimensions and comparing it with the final hard copy.

Commissioning tests will include geometry with oblique fields and fields using asymmetrical jaws. Beam junctioning as calculated by the TPS, for either abutting fields or those junctioned with independent jaws, can be compared with test cases measured with film or detector arrays.

Calculations of rotational beams for both photons and electrons can be compared with measured or published data. Special attention must be given to the beam weighting and normalization used for rotational and arced beams.

To confirm file compatibility between the CT scanner and the TPS, a file transfer process must be performed. CT using helical scans may require separate transfer software.

The transfer of image data is checked by performing an analysis of the input data for a known configuration and density, such as a phantom, to detect any error in magnification and in spatial coordinates. Special attention should be given to the pixel values, scan size and matrix size. The images must be checked for the integrity of surface rendering, especially for unlinked structures such as arms.

The large amount of data used by a TPS can make routine verification of all data difficult or impossible. Scheduled checks of dose distributions and beam time/MU calculations using a standard geometrical phantom with a variety of fields and beam modifiers are recommended for all TPSs; the frequency and scope of these procedures are described in the publications in the bibliography. The use of check sum programmes can ensure file and data integrity and alert the user to the possibility of inadvertent data changes or file corruption.

11.5.3. Spot checks

Spot checks of measured data versus those obtained from the TPS are required; these spot checks can involve calculations of fields shielded by blocks or MLCs. Spot checks of static and dynamic wedged fields with respect to measured data points are also recommended. A detector array may be used to verify wedged and, even more importantly, dynamically wedged dose distributions produced by the TPS. Wedge distributions produced by the TPS must be verified for identification, orientation, beam hardening and field size limitations.

11.5.4. Normalization and beam weighting

Dose normalization and beam weighting options vary from one TPS to another and have a direct impact on the representation of patient dose distributions. Normalization may be referred to a specific point such as the isocentre, to the intersection of several beam axes or to a minimum or maximum value in a slice or entire volume. Normalization can be referred to an arbitrary isodose line in a volume or to a minimum or maximum isosurface or related to a target or organ. Beam weighting may depend on whether the technique is SSD or source to axis distance (SAD).

Common TPS weightings for SSD set-ups relate the 100% value to the given dose at the depth of dose maximum per beam. SAD set-up options employ either an isocentric type weighting, whereby the beam weight is summed at the isocentre, or a tissue–phantom ratio (TPR) weighting, whereby a 100% beam weight produces a distribution having a value at the isocentre in the patient equal to the sum of the beams' TPRs.

Manual checks of all dose distributions as well as beam time or MU calculations used for treatment are recommended. Since many treatment plans involve complex beam delivery, these manual checks do not need to be precise, yet they serve as a method of detecting gross errors on the part of the TPS.

11.5.5. Dose–volume histograms and optimization

DVHs must be verified for both geometric and calculative accuracy. By drawing geometric targets such as spheres or cubes in a phantom, volume calculations can be verified. A dose distribution displaying a single beam passing through the sphere or cube can be used to verify the DVH calculation for both the differential and cumulative representations.

Optimization routines are provided by many TPSs, and intensity modulated beams having complex dose distributions may be produced. As these set-ups involve partial or fully dynamic treatment delivery, spot checks of absolute dose to a point, as well as a verification of the spatial and temporal aspects of the dose distributions using either film or detector arrays, are a useful method of evaluating the TPS beam calculations.

11.5.6. Training and documentation

Training and a reasonable amount of documentation for both the hardware and software are essential. Typically the training is given on the site and at the manufacturer's facility. Ongoing refresher courses are available to familiarize dosimetrists and physicists with 'bug fixes' and system upgrades. Documentation regarding software improvements and fixes is kept for reference by users at the clinic. TPS manufacturers have lists of other users and resource personnel to refer to.

Most manufacturers of TPSs organize users' meetings, either as stand-alone meetings or in conjunction with national or international scientific meetings of radiation oncologists or radiation oncology physicists. During these meetings special seminars are given by invited speakers and users describing the particular software systems, new developments in hardware and software as well as problems and solutions to specific software problems.

11.5.7. Scheduled quality assurance

Following acceptance and commissioning of a computerized TPS a scheduled quality assurance programme should be established to verify the output of the TPS (see also Section 12.3.7).

The frequency of these tests and the acceptance criteria should be established based on the user's specific needs or on national or international norms. Owing to the complexity and changing nature of TPSs, quality assurance tests found in the literature (suggested in the bibliography) may not be sufficient; however, they can give the basis for a scheduled programme.

Scheduled quality assurance tests for TPSs will validate data relating to routine treatments using photon beams, electron beams and brachytherapy programmes. The tests should not only verify the output of physical data (such as PDDs, TPRs, OARs, the effects of blocked fields, the inverse square law, decay and half-life), but should also verify the final machine monitor or time settings. The tests must also consider the role of the CT scanner or CT simulator in the planning process and as much as possible should mimic the use of the TPS in determining the use of the therapy unit for delivering patient treatments.

Particular attention may be paid to tests for TPSs that deal with specialized techniques such as stereotactic and 3-D TPSs. In addition, care must be given to in-house systems that are undocumented and undergo routine development. These TPSs may require quality assurance tests at a higher frequency.

There is a common thread of continuity that runs from machine acceptance and commissioning to data acquisition, data entry into the TPS, the production of patient specific dosimetry and treatment delivery. The medical physicist must be able to link all these steps together, and a well planned and scheduled set of quality assurance tests for the TPS is an important link in the safe delivery of therapeutic radiation.

11.6. SPECIAL CONSIDERATIONS

TPSs can be dedicated for special techniques as stand-alone systems. In addition, there are various clinical procedures that require careful consideration, owing to their inherent complexity.

A list of techniques that require special consideration and that may result in dedicated TPSs includes:

- Brachytherapy;
- Orthovoltage radiotherapy;
- IMRT;
- Dynamic MLC;
- Total body irradiation (TBI) (photon and electron);
- Micro MLC;
- Stereotactic radiosurgery with a linac or Gamma Knife;
- Tomotherapy;
- Intraoperative radiotherapy;
- D shaped beams for choroidal melanoma;
- Electron beam arc therapy;
- Total skin electron irradiation (TSEI).

BIBLIOGRAPHY

AMERICAN ASSOCIATION OF PHYSICISTS IN MEDICINE, Comprehensive QA for radiation oncology: Report of AAPM Radiation Therapy Committee Task Group 40, Med. Phys. **21** (1994) 581–618.

— American Association of Physicists in Medicine Radiation Therapy Committee Task Group 53: Quality assurance for clinical radiotherapy treatment planning, Med. Phys. **25** (1998) 1773–1829.

— Radiation Treatment Planning Dosimetry Verification, AAPM Task Group 55 Report, American Institute of Physics, New York (1995).

CHAO, K.S., PEREZ, C.A., BRADY, L.W., Radiation Oncology Management Decisions, Lippincott-Raven, New York (1999).

CLARKSON, J., A note on depth doses in fields of irregular shape, Br. J. Radiol. **14** (1941) 265.

CUNNINGHAM, J.R., Keynote address: Development of computer algorithms for radiation treatment planning, Int. J. Radiol. Oncol. Biol. Phys. **16** (1989) 1367–1376.

INTERNATIONAL COMMISSION ON RADIATION UNITS AND MEASUREMENTS, Use of Computers in External Beam Radiotherapy Procedures with High-energy Photons and Electrons, Rep. 42, ICRU, Bethesda, MD (1987).

— Prescribing, Recording and Reporting Photon Beam Therapy, Rep. 50, ICRU, Bethesda, MD (1993).

— Prescribing, Recording and Reporting Photon Beam Therapy (Supplement to ICRU Report 50), Rep. 62, ICRU, Bethesda, MD (1999).

JOHNS, H.E., CUNNINGHAM, J.R., The Physics of Radiology, Thomas, Springfield, IL (1983).

KHAN, F.M., The Physics of Radiation Therapy, Lippincott, Williams and Wilkins, Baltimore, MD (2003).

KHAN, F.M., POTISH, R.A., Treatment Planning in Radiation Oncology, Lippincott, Williams and Wilkins, Baltimore, MD (1998).

MACKIE, T.R., SCRIMGER, J.W., BATTISTA, J.J., A convolution method of calculating dose for 15-MV x rays, Med. Phys. **47** (1985) 188–196.

MILAN, J., BENTLEY, R.E., The storage and manipulation of radiation dose data in a small digital computer, Br. J. Radiol. **47** (1974) 115–121.

STERLING, T.D., PERRY, H., KATZ, L., Automation of radiation treatment planning, Br. J. Radiol. **37** (1964) 544–550.

STORCHI, P., WOUDSTRA, E., Calculation models for determining the absorbed dose in water phantoms in off-axis planes of rectangular fields of open and wedged photon beams, Phys. Med. Biol. **40** (1995) 511–527.

VAN DYK, J., BARNETT, R.B., BATTISTA, J., "Computerized radiation treatment planning systems", The Modern Technology of Radiation Oncology: A Compendium for Medical Physicists and Radiation Oncologists (VAN DYK, J., Ed.), Medical Physics Publishing, Madison, WI (1999) 231–286.

VAN DYK, J., BARNETT, R.B., CYGLER, J.E., SHRAGGE, P.C., Commissioning and quality assurance of treatment planning computers, Int. J. Radiol. Oncol. Biol. Phys. **26** (1993) 261–273.

Chapter 12

QUALITY ASSURANCE OF EXTERNAL BEAM RADIOTHERAPY

D.I. THWAITES
Department of Oncology Physics,
Edinburgh Cancer Centre, University of Edinburgh,
Western General Hospital,
Edinburgh, United Kingdom

B.J. MIJNHEER
Department of Radiotherapy,
Netherlands Cancer Institute,
Amsterdam, Netherlands

J.A. MILLS
Department of Clinical Physics and Bioengineering,
Walsgrave Hospital,
Coventry, United Kingdom

12.1. INTRODUCTION

12.1.1. Definitions

12.1.1.1. Quality assurance

'Quality assurance' is all those planned and systematic actions necessary to provide adequate confidence that a product or service will satisfy the given requirements for quality (ISO 9000:1994). As such it is wide ranging, covering all relevant procedures, activities and actions, and hence all groups of staff involved in the process under consideration.

12.1.1.2. Quality assurance in radiotherapy

'Quality assurance in radiotherapy' is all procedures that ensure consistency of the medical prescription, and safe fulfilment of that prescription, as regards the dose to the target volume, together with minimal dose to normal tissue, minimal exposure of personnel and adequate patient monitoring aimed

at determining the end result of the treatment. Again, it must be stressed that quality assurance in radiotherapy is concerned with all aspects of the radiotherapy process and should involve all groups of staff in a cooperative approach, since quality activities are interdependent.

12.1.1.3. Quality control

'Quality control' is the regulatory process through which the actual quality performance is measured, compared with existing standards, and the actions necessary to keep or regain conformance with the standards. Quality control is one part of overall quality assurance. It is concerned with operational techniques and activities used:

● To check that quality requirements are met;
● To adjust and correct performance if the requirements are found not to have been met.

12.1.1.4. Quality standards

'Quality standards' is the set of accepted criteria against which the quality of the activity in question can be assessed. Various national or international organizations, such as the World Health Organization (WHO) in 1988, AAPM in 1994, European Society for Therapeutic Radiation Oncology (ESTRO) in 1995 and Clinical Oncology Information Network (COIN) in 1999, have issued recommendations for standards in radiotherapy. Other organizations, such as the IEC in 1989 and the Institute of Physics and Engineering in Medicine (IPEM) in 1999, have issued recommendations for certain parts of the radiotherapy process. Where recommended standards are not available, local standards need to be developed, based on a local assessment of requirements.

12.1.2. Need for quality assurance in radiotherapy

An assessment of clinical requirements in radiotherapy shows that a high accuracy is necessary to produce the desired result of tumour control rates that are as high as possible, consistent with maintaining complication rates within acceptable levels. Quality assurance procedures in radiotherapy can be characterized as follows:

● Quality assurance reduces uncertainties and errors in dosimetry, treatment planning, equipment performance, treatment delivery, etc., thereby improving dosimetric and geometric accuracy and the precision

of dose delivery. This improves radiotherapy results (treatment outcomes), raising tumour control rates as well as reducing complication and recurrence rates.

● Quality assurance not only reduces the likelihood of accidents and errors occurring, it also increases the probability that they will be recognized and rectified sooner if they do occur, thereby reducing their consequences for patient treatment. This is the case not only for larger incidents but also for the higher probability minor incidents.

● Quality assurance allows a reliable intercomparison of results among different radiotherapy centres, ensuring a more uniform and accurate dosimetry and treatment delivery. This is necessary for clinical trials and also for sharing clinical radiotherapy experience and transferring it between centres.

● Improved technology and more complex treatments in modern radiotherapy can only be fully exploited if a high level of accuracy and consistency is achieved.

The objective of patient safety is to ensure that exposure of normal tissue during radiotherapy be kept as low as reasonably achievable (ALARA) consistent with delivering the required dose to the planning target volume (PTV). This forms part of the objective of the treatment itself. The measures to ensure quality of a radiotherapy treatment inherently provide for patient safety and for the avoidance of accidental exposure. Patient safety is therefore automatically integrated with quality assurance of radiotherapy treatments.

12.1.3. Requirements on accuracy in radiotherapy

Definitions of accuracy and precision as applied in a radiotherapy context, as well as discussions of dosimetric and geometric uncertainty requirements, can be found in various publications (see, for example, publications by Dutreix in 1984, Mijnheer et al. in 1987, Dobbs and Thwaites in 1999 and Van Dyk in 1999).

In modern statistical analysis, uncertainties are classified as either type A, meaning that they have been assessed by statistical means, or type B, meaning that they have been assessed by some other means. In earlier textbooks, and still in common practice, uncertainties are frequently described as random (a posteriori) or systematic (a priori).

Random uncertainties can be assessed by repeated observations or measurements and can be expressed as the standard deviation (SD) of their random distribution. The underlying distribution is frequently unknown, but for the Gaussian distribution 68% of occurrences are within 1 SD of the mean.

The 95% confidence level (CL) or confidence interval is frequently taken to be approximately equivalent to 2 SD.

Systematic uncertainties, however, can only be assessed by an analysis of the process. Possible distributions may well be very different. However, it may be possible to estimate the effective SD, within which the correct value is expected to lie in around 70% of cases.

Irrespective of how uncertainties are assessed, the uncertainties at different steps are usually combined in quadrature to estimate overall values; for example, if two steps are involved and the uncertainty on each is estimated to be 5%, then the combined uncertainty is approximately 7%.

The clinical requirements for accuracy are based on evidence from dose response (dose effect) curves for the tumour control probability (TCP) and normal tissue complication probability (NTCP). Both of these need careful consideration in designing radiotherapy treatments for a good clinical outcome.

The steepness of a given TCP or NTCP curve against dose defines the change in response expected for a given change in delivered dose. Thus uncertainties in delivered dose translate into either reductions in the TCP or increases in the NTCP, both of which worsen the clinical outcome. The accuracy requirements are defined by the most critical curves (i.e. very steeply responding tumours and normal tissues).

From consideration of the available evidence on clinical data, various recommendations have been made about the required accuracy in radiotherapy:

- The ICRU in its Report No. 24 reviewed TCP data and concluded that an uncertainty of 5% is required in the delivery of absorbed dose to the target volume. This has been widely quoted as a standard; however, it was not stated explicitly what confidence level this represented. It is generally interpreted as 1.5 SD or 2 SD, and this assumption has been broadly supported by more recent assessments; for example, Mijnheer et al. in 1987, considering the NTCP, and Brahme et al. in 1988, considering the effect of dose variations on the TCP, recommend an uncertainty of 3–3.5% (1 SD) (i.e. 6% or 7% at the 95% CL). In general, the smallest of these numbers (6% at the 95% CL) might be applicable to the simplest situations, with the minimum number of parameters involved, while the larger figure (7%) is more realistic for practical clinical radiotherapy when more complex treatment situations and patient factors are considered.
- Geometric uncertainty, for example systematic errors on the field position, block position, etc., relative to target volumes or organs at risk, also leads to dose problems, either underdosing of the required volume

(decreasing the TCP) or overdosing of nearby structures (increasing the NTCP). Consideration of these effects has led to recommendations on geometric (or spatial) uncertainty of between 5 and 10 mm (at the 95% CL). The figure of 5 mm is generally applied to overall equipment related mechanical/geometric problems, while larger figures (typically 8 or 10 mm) are used to indicate the overall spatial accuracy, including representative contributions for problems related to the patient and to the clinical set-up. The latter factors obviously depend on the site involved, the method of immobilization and the treatment techniques employed.

Thus the recommended accuracy of dose delivery is generally 5–7% (95% CL), depending on the factors intended to be included. Figures of 5–10 mm (95% CL) are usually given on spatial accuracy, depending on the factors intended to be included. These are general requirements for routine clinical practice.

In some specialist applications better accuracy might be demanded, requiring an increased quality assurance effort, for example if doses are escalated above normal values (e.g. high dose conformal radiotherapy) or if smaller geometric tolerances are required (e.g. stereotactic radiotherapy).

These recommendations are for the end point of the radiotherapy process (i.e. for the treatment as delivered to the patient). Therefore in each of the steps that contribute to the final accuracy, correspondingly smaller values are required, such that when all are combined the overall accuracy is met. Many analyses have shown that this is not easy to achieve. The aim of a quality assurance programme is to maintain each individual step within an acceptable tolerance. Very careful attention is required at all levels and for each process and substage within each process. The more complex the treatment technique, the more stages, substages, parameters and factors are involved, and correspondingly more complex quality assurance is required.

12.1.4. Accidents in radiotherapy

Treatment of disease with radiotherapy represents a twofold risk for the patient:

- Firstly, and primarily, there is the potential failure to control the initial disease, which, when it is malignant, is eventually lethal to the patient;
- Secondly, there is the risk to normal tissue from increased exposure to radiation.

Thus in radiotherapy an accident or a misadministration is significant if it results in either an underdose or an overdose, whereas in conventional radiation protection (and in radiation protection legislation and protocols) only overdoses are generally of concern.

When is a difference between the prescribed and delivered dose considered to be at the level of an accident or a misadministration in external beam radiotherapy? From the general aim of an accuracy approaching 5% (95% CL), about twice this seems to be an accepted limit for the definition of an accidental exposure (i.e. a 10% difference); for example, in several jurisdictions levels are set for reporting to regulatory authorities if equipment malfunctions are discovered that would lead to a 10% difference in a whole treatment or a 20% difference in a single fraction. In addition, from clinical observations of outcome and of normal tissue reactions, there is good evidence that differences of 10% in dose are detectable in normal clinical practice. Additional dose applied incidentally outside the proposed target volume may lead to increased complications.

In 2000 the IAEA analysed a series of accidental exposures in radiotherapy to draw lessons for the prevention of such occurrences. Criteria for classifying radiological accidents include:

- Direct causes of misadministrations;
- Contributing factors;
- Preventability of misadministration;
- Classification of the potential hazard.

Table 12.1 shows some examples of the direct causes of misadministrations in external beam radiotherapy catalogued and analysed in the IAEA report.

These incidents are representative of typical causes. Recording, categorizing and analysing differences in delivered and prescribed doses in radiotherapy can be carried out at many levels. Table 12.1 gives examples of the relatively small number of events reported that resulted in misadministrations (i.e. in large discrepancies between the prescribed and delivered doses).

Other evaluations have been reported from the results of in vivo dosimetry programmes or other audits of radiotherapy practice in which smaller deviations, or 'near misses', have been analysed. Similar lists of causes with similar relative frequencies have been observed. In any wide ranging analysis of such events, at whatever level, a number of general observations can be made:

TABLE 12.1. SOME EXAMPLES OF THE DIRECT CAUSES OF MISAD-
MINISTRATIONS IN EXTERNAL BEAM RADIOTHERAPY IN THE
2000 IAEA REPORT

Cause	Number of accidents
Calculation error of exposure time or dose	15
Inadequate review of patient chart	9
Error in anatomical area to be treated	8
Error in identifying the correct patient	4
Error involving lack of or misuse of a wedge	4
Error in calibration of ^{60}Co source	3
Transcription error of prescribed dose	3
Decommissioning of teletherapy source error	2
Human error during simulation	2
Error in commissioning of the TPS[a]	2
Technologist misread the treatment time or MUs[b]	2
Malfunction of accelerator	1
Treatment unit mechanical failure	1
Accelerator control software error	1
Wrong repair followed by human error	1

[a] TPS: treatment planning system.
[b] MU: monitor unit.

- Errors may occur at any stage of the process and be made by every staff group involved. Particularly critical areas are interfaces between staff groups, or between processes, where information is passed across the interface.
- Most of the immediate causes of accidental exposure are also related to a lack of an adequate quality assurance programme or a failure in its application.
- General human causes of errors include complacency, inattention, lack of knowledge, overconfidence, pressures on time, lack of resources and failures in communication.

Human error will always occur in any organization and in any activity. However, one aim of the existence of a comprehensive, systematic and consistently applied quality assurance programme is to minimize the number of

occurrences and to identify them at the earliest possible opportunity, thereby minimizing their consequences.

12.2. MANAGING A QUALITY ASSURANCE PROGRAMME

A number of organizations and publications have given background discussion and recommendations on the structure and management of a quality assurance programme, or quality system management, in radiotherapy or radiotherapy physics (e.g. the WHO in 1988, the AAPM in 1994, ESTRO in 1995 and 1998, the IPEM in 1999, Van Dyk and Purdy in 1999 and McKenzie et al. in 2000).

12.2.1. Multidisciplinary radiotherapy team

Radiotherapy is a process of increasing complexity involving many groups of professionals. Responsibilities are shared between the different disciplines and must be clearly defined. Each group has an important part in the output of the entire process, and their overall roles, as well as their specific quality assurance roles, are interdependent, requiring close cooperation. Each staff member must have qualifications (education, training and experience) appropriate to his or her role and responsibility and have access to appropriate opportunities for continuing education and development.

The exact roles and responsibilities or their exact interfaces or overlaps (and possibly also the terminology for different staff groups) may depend on:

- National guidelines, legislation, etc.;
- Systems of accreditation, certification, licensing or registration, although such schemes may not exist for all the different groups in all countries;
- Local departmental structures and practice.

The following list of radiotherapy team members is based on publications from various organizations (e.g. the WHO in 1988, the AAPM in 1994 and ESTRO in 1995):

- Radiation oncologists (in some systems referred to as radiotherapists or clinical oncologists) are almost always certified (or accredited) in the radiation oncology specialty by recognized national boards and are at least responsible for:
  — Consultations;
  — Dose prescriptions;

— On-treatment supervision and evaluations;
— Treatment summary reports;
— Follow-up monitoring and evaluation of treatment outcome and morbidity.

- Medical physicists (or radiation oncology physicists, radiotherapy physicists, clinical physicists) are in many countries certified by a recognized national board and are generally responsible for:
  — Specification, acceptance, commissioning, calibration and quality assurance of all radiotherapy equipment;
  — Measurement of beam data;
  — Calculation procedures for the determination and verification of patient doses;
  — The physics content of treatment planning and patient treatment plans;
  — Supervision of therapy equipment maintenance, safety and performance;
  — Establishment and review of quality assurance procedures;
  — Radiation safety and radiation protection in the radiotherapy department.

- Radiotherapy technologists (in some systems referred to as radiation therapists, therapy radiographers, radiation therapy technologists, radiotherapy nurses) are in many countries certified by recognized national boards and are responsible for:
  — Clinical operation of simulators, computed tomography (CT) scanners, treatment units, etc.;
  — Accurate patient set-up and delivery of a planned course of radiation therapy prescribed by a radiation oncologist;
  — Documenting treatment and observing the clinical progress of the patient and any signs of complication.

  Radiotherapy technologists may also often be involved in:
  — Undertaking daily quality assurance of treatment equipment in accordance with physics quality assurance procedures and protocols;
  — Treatment planning;
  — Construction of immobilization devices, etc.

  In many, but by no means all, countries radiotherapy technologists constitute an independent professional group, distinct from general nursing staff.

- Dosimetrists (in many systems there is no separate group of dosimetrists, and these functions are carried out variously by physicists, medical physics technicians or technologists, radiation dosimetry technicians or

technologists, radiotherapy technologists or therapy radiographers). The specific responsibilities of staff operating in this role include:

— Accurate patient data acquisition;
— Radiotherapy treatment planning;
— Dose calculation;
— Patient measurements.

Dosimetrists may be involved in machine calibrations and regular equipment quality assurance under the supervision of a medical physicist and may construct immobilization and other treatment devices. In jurisdictions where the distinct profession of dosimetrist exists, dosimetrists may be certified by recognized national boards.

● Engineering technologists (in some systems medical physics technicians or technologists, clinical technologists, service technicians, electronic engineers or electronic technicians) have specialized expertise in the electrical and mechanical maintenance of radiotherapy equipment. Their services may be in-house or via a service contract for equipment maintenance. They also provide a design and build capability for specialized patient related devices and are usually supervised by medical physicists.

12.2.2. Quality system/comprehensive quality assurance programme

A quality system is the organizational structure, responsibilities, procedures, processes and resources required for implementing quality management. A quality system in radiotherapy is a management system that:

● Should be supported by the department management in order to work effectively.
● May be formally accredited (e.g. to ISO 9000).
● Should be as comprehensive as is required to meet the overall quality objectives.
● Must have a clear definition of its scope and of all the quality standards to be met.
● Must be consistent in standards for different areas of the programme.
● Requires collaboration between all members of the radiotherapy team.
● Must incorporate compliance with all the requirements of national legislation, accreditation, etc.
● Requires the development of a formal written quality assurance programme that details the quality assurance policies and procedures, quality control tests, frequencies, tolerances, action criteria, required records and personnel.

- Must be regularly reviewed as to operation and improvement. To this end a quality assurance committee is required, which should represent all the different disciplines within radiation oncology.
- Requires control of the system itself, including:
  — Responsibility for quality assurance and the quality system: quality management representatives.
  — Document control.
  — Procedures to ensure that the quality system is followed.
  — Ensuring that the status of all parts of the service is clear.
  — Reporting all non-conforming parts and taking corrective action.
  — Recording all quality activities.
  — Establishing regular review and audits of both the implementation of the quality system (quality system audit) and its effectiveness (quality audit).

The quality assurance committee must be appointed by the department management/head of department with the authority to manage quality assurance and should:

- Involve the heads of all the relevant groups in the department (radiation oncology, medical physics, radiation therapy, maintenance, nursing, etc.) or their nominees;
- Establish and support the quality assurance team;
- Assist the entire radiation oncology staff to apply quality assurance recommendations and standards to the local situation;
- Approve quality assurance policies and procedures and the assignment of quality assurance responsibilities in the department;
- Establish its own remit, meeting frequency, reporting routes and accountability;
- Monitor and audit the quality assurance programme to ensure that each component is being performed appropriately and is documented and that feedback from this process is used to improve the quality system and to improve quality generally;
- Regularly review the operation and progress of the quality assurance system and maintain records of this process and of all its own meetings, decisions and recommendations;
- Investigate and review all non-conformances, and give feedback to the system;
- Review and recommend improvements in quality assurance procedures, documentation, etc.

The comprehensive quality assurance team:

— Is responsible for performing quality assurance related tasks;
— Is an integrated team from all groups, including radiation oncologists, medical physicists, radiotherapy technologists, dosimetrists, health physicists, nurses, service engineers, data entry managers, administration staff, etc., as all areas of the process should be covered.

Each member should be clear on his or her responsibilities and be adequately trained to perform them, and should also know which actions are to be taken in the event that any result is observed outside the limits of established acceptable criteria. A subgroup of the team can be trained to act as internal auditors of the quality system.

Increasingly, international bodies such as the IAEA recommend the establishment of a quality system in radiotherapy to ensure patient radiation safety, and many national nuclear and/or health regulatory commissions are demanding the implementation of such a quality system as a requirement for hospital licensing and accreditation.

12.3. QUALITY ASSURANCE PROGRAMME FOR EQUIPMENT

Within the context of radiotherapy, equipment covers all devices from megavoltage treatment machines to the electrical test equipment used to monitor signals within the machine. This section, however, concentrates on the major items and systems and should be read in conjunction with the appropriate chapters concerned with each of these categories of equipment.

There are many sets of national and international recommendations and protocols covering quality assurance and quality control requirements for various radiotherapy equipment items (see, for example, IEC of 1989, AAPM of 1994 and IPEM of 1999) that should be referred to where available. These give recommended tests, test frequencies and tolerances. Some give test methods, while others give practical advice on quality assurance and quality control tests for many items of equipment.

12.3.1. Structure of an equipment quality assurance programme

A general quality assurance programme for equipment includes:

● Initial specification, acceptance testing and commissioning for clinical use, including calibration where applicable (see Chapter 10).

- Quality control tests. At the conclusion of the commissioning measurements, before the equipment is put into clinical use, quality control tests should be established and a formal quality control programme initiated that will continue for the entire clinical lifetime of the equipment.
- Additional quality control tests after any significant repair, intervention or adjustment or when there is any indication of a change in performance as observed during use or during planned preventive maintenance or routine quality control programmes.
- A planned preventive maintenance programme, in accordance with the manufacturer's recommendations.

12.3.1.1. Equipment specification

In preparation for procurement of equipment, a detailed specification document must be prepared. This should set out the essential aspects of the equipment operation, facilities, performance, service, etc., as required by the customer.

A multidisciplinary team from the department should be involved in contributing to the specification, including input from radiotherapy physicists, radiation oncologists, radiotherapy technologists, engineering technicians, etc. It would generally be expected that liaison between the department and the suppliers would be the task of a radiotherapy physicist.

In response to the specifications, the various interested suppliers should indicate how the equipment they offer will meet the specifications and whether there are any areas that cannot be met or whether there are any limiting conditions under which specified requirements can or cannot be met, etc.

Decisions on procurement should be made by a multidisciplinary team, comparing specifications as well as considering costs and other factors.

12.3.1.2. Acceptance

Acceptance of equipment is the process in which the supplier demonstrates the baseline performance of the equipment to the satisfaction of the customer. Acceptance is against the specification, which should be part of the agreed contract of what the supplier will provide to the customer. The essential performance required and expected from the machine should be agreed upon before acceptance of the equipment begins.

As an example, methods of declaring the functional performance of megavoltage treatment machines are given in the IEC 976 and IEC 977 documents. It is a matter of the professional judgement of the medical physicist responsible for accepting the equipment to decide whether any aspect of the

agreed acceptance criteria is to be waived. This waiver should be recorded along with an agreement from the supplier, for example to correct the equipment should performance deteriorate further.

Acceptance provides a baseline set of equipment performance measurements that should encompass the essential aspects of the equipment's operation. During the acceptance of a treatment machine the supplier should demonstrate that the control parameters of the machine are operating well within their range and that none are at an extreme value.

The aspects covered in acceptance will depend on the equipment involved. However, these would generally include at least any settings, baseline machine running parameters, operations and devices that are critical to safety or clinical accuracy.

The equipment can only be formally accepted to be transferred from the supplier to the customer when the medical physicist responsible for the customer side of acceptance either is satisfied that the performance of the machine fulfils all specifications as listed in the contract document or formally accepts any waivers as stated above.

12.3.1.3. Commissioning

Following acceptance of the equipment, a full characterization of its performance for clinical use over the whole range of possible operation should be undertaken. This is referred to as commissioning. Depending on the type of equipment, acceptance and commissioning may partially overlap. Together they will establish the baseline recorded standards of performance to which all future performance and quality control tests will be referred.

Where appropriate, commissioning will incorporate calibration to agreed protocols and standards. For critical parts of commissioning, such as calibration, an independent second check is recommended. Commissioning includes the preparation of procedures, protocols, instructions, data, etc., on the clinical use of the equipment.

Clinical use can only begin when the physicist responsible for commissioning is satisfied that all the above aspects have been completed and that the equipment and any necessary data, etc., are safe to use on patients.

12.3.1.4. Quality control

It is essential that the performance of treatment equipment remain consistent within accepted tolerances throughout its clinical life, as patient treatments will be planned and delivered on the basis of the performance measurements at acceptance and commissioning. An ongoing quality control

programme of regular performance checks is therefore begun immediately after commissioning to test this.

If these quality control measurements identify departures from expected performance, corrective actions are required. An equipment quality control programme should specify the following:

- The parameters to be tested and the tests to be performed;
- The specific equipment to be used to perform the tests;
- The geometry of the tests;
- The frequency of the tests;
- The staff group or individual performing the tests, as well as the individual supervising and responsible for the standards of the tests and for actions that may be necessary if problems are identified;
- The expected results;
- The tolerance and action levels;
- The actions required when the tolerance levels are exceeded.

No one programme is necessarily suitable in all circumstances. Programmes may need tailoring to the specific equipment and departmental situation; for example, frequencies may need to be adjusted in the light of experience with a given machine.

The test content should be kept as simple as possible, consistent with the defined aims, in order to optimize the time and effort with the return required. Frequencies normally follow a hierarchy ranging from frequent simple tests of critical parameters, up to complex extended annual tests, where the latter are subsets of the original acceptance and commissioning tests. Various levels lie between these two extremes.

Quality control programmes must be flexible to permit additional testing whenever it seems necessary following repair, observed equipment behaviour or indications of problems from the regular quality control tests.

To minimize treatment interruption due to non-regular interventions or additional quality control measurements, it is essential to maintain the test and measurement equipment in good order and for it to be subject to its own quality control programme, and to have adequate equipment readily available.

12.3.2. Uncertainties, tolerances and action levels

Performance to within the tolerance level gives acceptable accuracy in any situation. Performance outside the action level is unacceptable and demands action to remedy the situation.

Any quality control test should use measuring equipment appropriate to the task. All such equipment should itself be subject to an appropriate maintenance and quality control programme. Irradiation conditions and measuring procedures should be designed to be appropriate to the task. In these circumstances the quality control measurement is expected to give the best estimate of the particular measured parameter. However, this will have an associated uncertainty, dependent upon the measurement technique. The tolerance set for the parameter must take into account the uncertainty of the measurement technique employed.

If the measurement uncertainty is greater than the tolerance level set, random variations in the measurement will lead to unnecessary intervention, increased downtime of equipment and inefficient use of staff time. Tolerances should be set with the aim of achieving the overall uncertainties desired, as summarized in Section 12.1.3.

Variances can be combined in quadrature for combined factors, which can be used to determine specific tolerance limits for individual parameters.

Action levels are related to tolerances but provide flexibility in monitoring and adjustment; for example, if a measurement on the constancy of dose/MUs indicates a result between the tolerance and action levels, it may be permissible to allow clinical use to continue until this is confirmed by measurement the next day before taking any further action. Thus:

- If a daily measurement is within tolerance, no action is required;
- If the measurement exceeds the action level, immediate action is necessary and the machine must not be used clinically until the problem is corrected and the correction is verified by measurement;
- However, if the measurement falls between tolerance and action levels, this may be considered acceptable until the next daily measurement;
- If repeated measurements remain consistently between tolerance and action levels, adjustment is required;
- Any measurement at any time outside the action level requires immediate investigation and, if confirmed, rectification.

Action levels are often set at approximately twice the tolerance level, although some critical parameters may require tolerance and action levels to be set much closer to each other or even at the same value.

Different sets of recommendations may use rather different approaches to set tolerance levels and/or action levels, and this should be borne in mind in comparing values from different sources. In some, the term tolerance level is used to indicate values that in others may be closer to action levels (i.e. some workers use the term tolerance to indicate levels at which adjustment or

correction is necessary). Some recommendations explicitly list performance standards under the two headings.

Test frequencies need to be considered in the context of the acceptable variation throughout a treatment course and also considering the period of time over which a parameter varies or deteriorates. Frequencies may be modified in the light of experience of the performance and stability of a given piece of equipment, initially setting a nominal frequency that may be subsequently reviewed in the light of observation. As machines get older this may need further review.

The staff resources available to undertake the tests may limit what can be checked, which may have an effect on the structure of the quality control programme. Tests should be designed to provide the required information as rapidly as possible with minimal time and equipment. Customized devices are often very useful to make tests easier.

Where available, national organizations' own quality control protocols should be applied. The following sections give some examples of parameters, test frequencies and tolerances for different items of radiotherapy equipment.

For consistency, the values are almost all taken from AAPM TG 40, with some additional comments from the IPEM report on quality control in radiotherapy published in 1999; while broadly similar, there are some differences in tolerances and frequencies. The protocols should be referred to for more details. Where local protocols are not available, existing recommendations such as these should be consulted and adapted for local circumstances.

12.3.3. Quality assurance programme for cobalt-60 teletherapy machines

A sample quality assurance programme for a ^{60}Co teletherapy machine with recommended test procedures, test frequencies and action levels is given in Table 12.2.

The IPEM report on quality control in radiotherapy published in 1999 recommends that an output check be undertaken weekly and that the source position be monitored monthly. The source positioning may be monitored by measuring the uniformity of the field in the appropriate direction or by inspection of an external mark on the source carrying mechanism. In addition, the IPEM requires more dosimetric and geometric checks at monthly intervals and, in its annual recommendations, it emphasizes more safety tests, for example radiation wipe tests and tests on head leakage and electrical safety, etc.

TABLE 12.2. SAMPLE QUALITY ASSURANCE PROGRAMME FOR A COBALT-60 UNIT (AAPM TG 40)

Frequency	Procedure	Action level[a]
Daily	Door interlock	Functional
	Radiation room monitor	Functional
	Audiovisual monitor	Functional
	Lasers	2 mm
	Distance indicator	2 mm
Weekly	Check of source position	3 mm
Monthly	Output constancy	2%
	Light/radiation field coincidence	3 mm
	Field size indicator	2 mm
	Gantry and collimator angle indicator	1º
	Cross-hair centring	1 mm
	Latching of wedges and trays	Functional
	Emergency off	Functional
	Wedge interlocks	Functional
Annually	Output constancy	2%
	Field size dependence of output constancy	2%
	Central axis dosimetry parameter constancy (PDD[b], TAR[c], TPR[d])	2%
	Transmission factor constancy for all standard accessories	2%
	Wedge transmission factor constancy	2%
	Timer linearity and error	1%
	Output constancy versus gantry angle	2%
	Beam uniformity with gantry angle	3%
	Safety interlocks: follow test procedures of manufacturer	Functional
	Collimator rotation isocentre	2 mm diameter
	Gantry rotation isocentre	2 mm diameter
	Table rotation isocentre	2 mm diameter
	Coincidence of collimator, gantry and table axis with the isocentre	2 mm diameter
	Coincidence of the radiation and mechanical isocentre	2 mm diameter

TABLE 12.2. SAMPLE QUALITY ASSURANCE PROGRAMME FOR A COBALT-60 UNIT (AAPM TG 40) (cont.)

Frequency	Procedure	Action level[a]
	Table top sag	2 mm
	Vertical travel of table	2 mm
	Field light intensity	Functional

[a] AAPM TG 40 lists these values as tolerances. However, the protocol makes it plain that they are action levels; that is, they should be interpreted to mean that, for any parameter, if the difference between the measured value and the expected value is greater than the figure above (e.g. the measured isocentre under the gantry rotation exceeds 2 mm diameter), or the change is greater than the figure above (e.g. the output changes by more than 2%), an action is required. The distinction between absolute differences and changes is emphasized by the use of the term 'constancy' for the latter case. For constancy, the per cent values are the deviation of the parameter with respect to its nominal value; distances are referenced to the isocentre or nominal source to surface distance (SSD).

[b] PDD: percentage depth dose.

[c] TAR: tissue–air ratio.

[d] TPR: tissue–phantom ratio.

12.3.4. Quality assurance programme for linacs

Although there is considerable variation in the practice of quality control on linacs, the three major publications (IEC 977, IPEM 81 and AAPM TG 40) are broadly consistent. However, in particular the IEC 977 document does not specify daily checks. Typical quality assurance procedures for a dual mode linac with frequencies and action levels are given in Table 12.3.

IPEM 81 recommends a simple field size check daily and has a wider tolerance on daily output constancy but a weekly check with a tighter tolerance than AAPM TG 40. It has a frequency structure of daily, weekly, two weekly, monthly, six monthly and annually and includes tests on some parameters not listed in the AAPM protocols. It also provides a specific quality control protocol for electron beams. As a more recent publication than AAPM TG 40, it gives recommendations for the quality control of dynamic wedges and multileaf collimators (MLCs).

12.3.5. Quality assurance programme for treatment simulators

Treatment simulators replicate the movements of isocentric ^{60}Co and linac treatment machines and are fitted with identical beam and distance

TABLE 12.3. SAMPLE QUALITY CONTROL PROGRAMME FOR A DUAL MODE LINAC (AAPM TG 40)

Frequency	Procedure	Action level[a]
Daily	X ray output constancy	3%
	Electron output constancy[b]	3%
	Lasers	2 mm
	Distance indicator	2 mm
	Door interlock	Functional
	Audiovisual monitor	Functional
Monthly	X ray output constancy[c]	2%
	Electron output constancy[c]	2%
	Backup monitor constancy	2%
	X ray central axis dosimetry parameter constancy (PDD, TAR, TPR)	2%
	Electron central axis dosimetry parameter constancy (PDD)	2 mm at therapeutic depth
	X ray beam flatness constancy	2%
	Electron beam flatness constancy	3%
	X ray and electron symmetry	3%
	Emergency off switches	Functional
	Wedge and electron cone interlocks	Functional
	Light/radiation field coincidence	2 mm or 1% on a side[d]
	Gantry/collimator angle indicators	1º
	Wedge position	2 mm (or 2% change in transmission factor)
	Tray position and applicator position	2 mm
	Field size indicators	2 mm
	Cross-hair centring	2 mm diameter
	Treatment table position indicators	2 mm/1º
	Latching of wedges and blocking tray	Functional
	Jaw symmetry[e]	2 mm
	Field light intensity	Functional
Annually	X ray/electron output calibration constancy	2%
	Field size dependence of X ray output constancy	2%
	Output factor constancy for electron applicators	2%
	Central axis parameter constancy (PDD, TAR, TPR)	2%
	Off-axis factor constancy	2%
	Transmission factor constancy for all treatment accessories	2%
	Wedge transmission factor constancy[f]	2%
	Monitor chamber linearity	1%
	X ray output constancy with the gantry angle	2%
	Electron output constancy with the gantry angle	2%

TABLE 12.3. SAMPLE QUALITY CONTROL PROGRAMME FOR A DUAL MODE LINAC (AAPM TG 40) (cont.)

Frequency	Procedure	Action level[a]
Annually	Off-axis factor constancy with the gantry angle	2%
	Arc mode	Manufacturer's specifications
	Safety interlocks: follow manufacturer's test procedures	Functional
	Collimator rotation isocentre	2 mm diameter
	Gantry rotation isocentre	2 mm diameter
	Table rotation isocentre	2 mm diameter
	Coincidence of collimator, gantry and table axes with the isocentre	2 mm diameter
	Coincidence of the radiation and mechanical isocentre	2 mm diameter
	Table top sag	2 mm
	Vertical travel of the table	2 mm

[a] AAPM TG 40 lists these values as tolerances. However, the protocol makes it plain that they are action levels; that is, they should be interpreted to mean that, for any parameter, if the difference between the measured value and the expected value is greater than the figure above (e.g. the measured isocentre under the gantry rotation exceeds 2 mm diameter), or the change is greater than the figure above (e.g. the output changes by more than 2%), an action is required. The distinction between absolute differences and changes is emphasized by the use of the term 'constancy' for the latter case. For constancy, the per cent values are plus or minus the deviation of the parameter with respect to its nominal value; distances are referenced to the isocentre or nominal SSD.

[b] All electron energies need not be checked daily, but all electron energies are to be checked at least twice weekly.

[c] A constancy check with a field instrument using temperature and pressure corrections.

[d] Whichever is greater; should also be checked after a change in the light field source.

[e] Jaw symmetry is defined as the difference in distance of each jaw from the isocentre.

[f] Most wedge transmission factors are field size and depth dependent, and should be checked. In particular, the field size variations for dynamic wedges can be very large.

indicators. Hence all measurements that concern these aspects of ^{60}Co and linac machines also apply to the simulator and should be quality controlled in a similar manner.

It should be noted that, if mechanical/geometric parameters are out of tolerance on the simulator, this will affect treatments of all patients, whichever treatment machine they are subsequently treated on.

In addition, the performance of the imaging components on the simulator is of equal importance to its satisfactory operation. For this reason, quality control on simulators requires critical measurements of the imaging system. The imaging system consists of a diagnostic X ray tube, an image intensifier with manual and automatic kV–mA facilities and an imaging chain that may include digital image capture. Typical quality assurance procedures for a conventional simulator with test frequencies and action levels are given in Table 12.4.

TABLE 12.4. SAMPLE QUALITY CONTROL PROGRAMME FOR A SIMULATOR (AAPM TG 40)

Frequency	Procedure	Action level[a]
Daily	Safety switches	Functional
	Door interlock	Functional
	Lasers	2 mm
	Distance indicator	2 mm
Monthly	Field size indicator	2 mm
	Gantry/collimator angle indicators	1º
	Cross-hair centring	2 mm diameter
	Focal spot axis indicator	2 mm
	Fluoroscopic image quality	Baseline
	Emergency collision avoidance	Functional
	Light/radiation field coincidence	2 mm or 1%
	Film processor sensitometry	Baseline
Annually	Collimator rotation isocentre	2 mm diameter
	Gantry rotation isocentre	2 mm diameter
	Table rotation isocentre	2 mm diameter
	Coincidence of the collimator, gantry and table axes with the isocentre	2 mm diameter
	Table top sag	2 mm
	Vertical travel of the table	2 mm
	Exposure rate	Baseline
	Table top exposure with fluoroscopy	Baseline
	kVp and mAs calibration	Baseline
	High and low contrast resolution	Baseline

[a] AAPM TG 40 lists these values as tolerances. However, they are action levels; that is, they should be interpreted to mean that, for any parameter, if the difference between the measured value and the expected value is greater than the figure above (e.g. the measured isocentre under gantry rotation exceeds 2 mm diameter), an action is required.

TABLE 12.5.   SAMPLE OF A ROUTINE REGULAR QUALITY CONTROL PROGRAMME FOR A COMPUTED TOMOGRAPHY SCANNER OR COMPUTED TOMOGRAPHY SIMULATOR (IPEM 81)

Frequency	Procedure	Action level[a]
Daily	Safety switches	Functional
Monthly	Scan plane to alignment laser	2 mm
	Indication of x axis	1º
	Table position registration	1 mm
	Distance between known points in the image	2 mm
	Left and right registration	Correct operation
	CT number for water	1%
	CT number for lung and bone	2%
	Reconstructed slice location	1 mm
Annually	Table deflection under load	2 mm

[a] IPEM 81 lists these values as tolerances but implies that at least some of them would require action if exceeded.

IPEM 81 includes cross-wire checks and simpler field size and field alignment checks in the daily test schedule, with fuller checks at monthly intervals.

12.3.6.   Quality assurance programme for computed tomography scanners and computed tomography simulation

For dose prediction as part of the treatment planning process there is an increasing reliance upon CT image data with the patient in a treatment position. Since CT data are used for a more comprehensive indication of the patient's anatomy and to provide tissue density information, which is essential for accurate dose prediction, it is essential that the geometry and CT densities be accurate.

Typical quality assurance procedures with frequencies and action levels are listed in Table 12.5. The protocol also lists the tests to be carried out after new software is installed (scanner or TPS).

AAPM TG 66 provides extensive coverage of quality assurance in CT simulation.

12.3.7. Quality assurance programme for treatment planning systems

As an integral part of the radiotherapy process the TPS provides computer predictions of the dose distributions that can be achieved both in the target volume and in normal tissue. As this information is used to provide guidance to the clinician on the best treatment for an individual patient, these systems are critical to the treatment process and hence their performance must be assured.

The major aspect of the acceptance and commissioning of the system is to test its fundamental performance and gain an understanding of the algorithms used for dose prediction. This provides knowledge of the limitations of the system; a considerable part of this understanding should be gained by comparison with experimental measurements in phantoms for test cases of varying complexity. Some information on this should also be obtainable from the manufacturer, from the literature and from users groups.

Following software upgrades, a more limited acceptance and commissioning programme should be undertaken; the extent of this will depend upon the extent of change made to the system. However, it is prudent to take a cautious approach in order to try to ensure that the performance of the system remains satisfactory. Testing should not be deferred in order simply to speed up the introduction of new software into clinical use.

Generic tolerances of 2% have often been quoted for isodose distributions where dose gradients are not steep and of 2 mm where dose gradients are steep. These may typically be applied to single field or single source isodose distributions. However, these will not necessarily be applicable in less simple situations. A similar generic tolerance of 2% is often quoted on MU calculations, which again may need careful consideration in complex situations. Discussion of the acceptable tolerances for different situations has been given by various authors, for example Van Dyk and colleagues and Venselaar (see also Chapter 11).

Acceptance, commissioning and quality control recommendations are given, for example, by the AAPM (TG 40 and TG 43) and the IPEM (in Reports 68 and 81); these should be referred to for more details. The exact requirements will depend on the level of complexity of the system and on the treatment planning techniques used clinically. Any uncertainty concerning the operation or output of a TPS should be tested by comparing the performance of the TPS with measurements in suitable phantoms. A sample of a routine regular quality control programme for a TPS is given in Table 12.6.

TABLE 12.6. SAMPLE OF A ROUTINE REGULAR QUALITY CONTROL PROGRAMME FOR A TREATMENT PLANNING SYSTEM, FROM IPEM 68 AND 81 AND AAPM TG 40

Frequency	Procedure	Tolerance[a]
Daily	Input and output devices	1 mm
Monthly	Checksum	No change
	Reference subset of data[b]	2%[c] or 2 mm[d]
	Reference prediction subset	2% or 2 mm
	Processor tests	Pass
	CT transfer	1 mm
Annually	MU calculations	2%
	Reference quality assurance test set[e]	2% or 2 mm

[a] These may be action levels in simple situations, but tolerances in more complex situations (see discussion above).

[b] These refer to the comparison of dose calculations at commissioning to the same calculations subsequently.

[c] Per cent difference between calculation by the TPS and measurement (or independent calculation).

[d] In regions of high dose gradient the distance between isodose lines is more appropriate than per cent differences. In addition, less accuracy may be obtained near the end of single sources for brachytherapy calculations.

[e] These tests refer to the comparison of calculations with measurement in a water tank.

12.3.8. Quality assurance programme for test equipment

Test equipment in radiotherapy concerns all the additional equipment required to measure radiation doses and to perform electrical measurements of machine signals and mechanical measurements of machine devices. The details of the quality control programme will depend on the equipment and its use.

Some examples of considerations for a quality control programme for test and measuring equipment (tolerances given in brackets where applicable) include the following:

- Local standard ionization chamber and electrometer. These must be calibrated in accordance with national protocols at an accredited dosimetry standards laboratory at between one and three years' frequency, depending on national guidelines and procedures. This must include checks on linearity, scale corrections, etc. Venting should be checked before recalibration and corrected if faulty.

- Recombination and stem effects may be checked at this time. If not, they should be checked independently by the user at least when new and after any malfunction or repair. The applied voltage and leakage should be checked at each use. Before and after any use to calibrate field instruments, a ^{90}Sr or similar check of constancy (to 1%) should be carried out.

- Field instrument ionization chamber and electrometers. These should be calibrated against the local standard, typically yearly, depending on national guidelines and procedures (to 1%). Linearity, venting and stem effects should be checked at the same time. Recombination corrections should be determined when the chamber is new and after any malfunction or repair. The applied voltage and leakage should be checked at each use. It is recommended to carry out constancy checks monthly, for example comparing response against another chamber or using a ^{90}Sr or similar check source (agreement is expected to be within 1%).

- Thermometer. When new, the calibration should be checked (to 0.5ºC). Regular comparisons of thermometers against each other help to identify damage. Electronic thermometers may require more frequent checks.

- Barometer. When new, pressure calibration should be checked (to 1 mm Hg or 1 mbar). This should be regularly checked by comparison against an independent system. If comparison is against a local airport system, beware that the airport pressures quoted are normally corrected to sea level and will therefore need a height correction to the hospital height.

- Linear rulers. Check the scale when new (to 0.3%).

- Phantoms. Check dimensions, densities, etc., when new. Regularly check for damage with time.

- Automated beam scanning systems. When new, test the software and hardware functions, for example the accuracy of data analysis (to 1%), accuracy of printouts (to 1 mm), etc. When new and regularly before use, check electrical and mechanical safety; the geometric accuracy of drives and detector positioning (to 1 mm); reproducibility (to 1 mm); backlash/hysteresis (to 1 mm); and orthogonality of drives (to 0.5º). Check the dosimetry systems in a similar way to the guidance given for checking ionization chambers and electrometers, or other dosimetry systems, depending on the specific measuring devices being used with the plotting tank.

- Other dosimetry systems. Systems for relative dosimetry (e.g. thermoluminescent dosimeters (TLDs), diodes, diamonds and film), in vivo dosimetry (e.g. TLDs and diodes) and for radiation protection measurements, for example, should be tested to tolerances and at frequencies consistent with their particular uses in the department. All such systems

will require careful assessment when new to determine their range of applicability and any corrections and calibrations required. Usually this will involve comparison and calibration against ionization chamber systems. After that, quality control tests and checks will be required to ensure that they perform acceptably and that any changes in behaviour with time or with radiation damage are measured and corrected for. In particular, performance checks (including recalibration, where appropriate) will be required after any observed malfunction or after any repair.

● Electrical test equipment. Any equipment used for testing the running parameters of treatment equipment should be suitably calibrated and quality controlled.

12.4. TREATMENT DELIVERY

12.4.1. Patient charts

Besides describing disease related items, a patient chart should also contain all information related to the prescribed and actual treatment. The basic components of a patient treatment chart are:

● The patient's name and identification;
● A photograph;
● An initial physical evaluation of the patient;
● Treatment planning data;
● Treatment execution data;
● Clinical assessment during treatment;
● The treatment summary and follow-up;
● A quality assurance checklist.

Any mistakes made in the data entry of the patient chart are likely to be carried through the whole treatment; quality assurance of the patient chart is therefore essential. All planning data should be independently checked ('redundant checking'), including the plan integrity, MU calculations, irradiation parameters, etc. (see Chapters 7 and 11). All data entered as the interface between the planning process and the treatment delivery process should be independently checked.

Regular chart checks should be carried out through the treatment course. The frequency of chart checking should be at least weekly, starting before the third fraction of a new treatment course or after each modification of the

treatment. Chart checking should be performed by a team consisting of a radiation oncologist, a physicist and radiographers. The review should be signed and dated by the checkers.

Particular care must be taken to ensure that items such as wedge orientation and block positioning are correct, as they may not be correctly set on the simulator. Data transferred automatically, for example from the TPS, should also be verified to check that no data corruption has occurred.

All errors that are traced during chart checking should be thoroughly investigated and evaluated by the quality assurance team, which should include a quality assurance system manager (quality management representative), if available. The causes should be eradicated and may result in (written) changes in the various procedures of the treatment process.

Electronic treatment charts are applied in some institutions to replace at least part of the patient chart; they allow direct input of treatment data from the simulator or from a TPS.

12.4.2. Portal imaging

Besides dosimetric errors, geometric errors are also of extreme importance in determining the outcome of a radiotherapy treatment. Geometric accuracy is limited by:

- Uncertainties in a particular patient set-up;
- Uncertainties in the beam set-up;
- Movement of the patient or the target volume during treatment.

In order to verify the patient set-up with respect to the position of the radiation beam, portal imaging is applied at one of the first treatment fractions, is repeated if the fields are modified and is sometimes repeated during the course of treatment.

The purpose of portal imaging is:

— To verify the field placement, characterized by the isocentre or another reference point relative to anatomical structures of the patient during the actual treatment;
— To verify that the beam aperture produced by blocks or by an MLC has been properly produced and registered.

Sometimes it is useful to have more than one check during one treatment fraction, for example to observe the influence of swallowing and breathing or organ motion on the patient set-up.

Portal images are compared with reference images, which can be either (orthogonal) simulator images, digitally reconstructed radiographs (DRRs) or the first portal image made during a treatment series. A double exposure technique can be useful if only limited anatomical information is present in the treatment field. An example is provided in Fig. 12.1, in which DRRs of anterior and lateral pelvic treatments and electronic portal imaging device (EPID) fields are shown for comparison with images obtained with an EPID.

If unusual oblique or non-coplanar fields are used, making it difficult to interpret the images, it may be necessary to set up additional orthogonal portal images for comparison with reference images.

Sequences of portal image series for the same patient throughout the treatment can provide verification of day to day variations in the patient set-up and can give information on changes throughout the treatment; the frequency depends on the site, the type of immobilization, the patient conditions, the intended degree of reproducibility, the other quality assurance systems in use and the resources and portal imaging systems available.

Local protocols must be established to specify who has the responsibility for verification of portal images (generally a clinician) and what criteria are used as the basis to judge the acceptability of information conveyed by portal images.
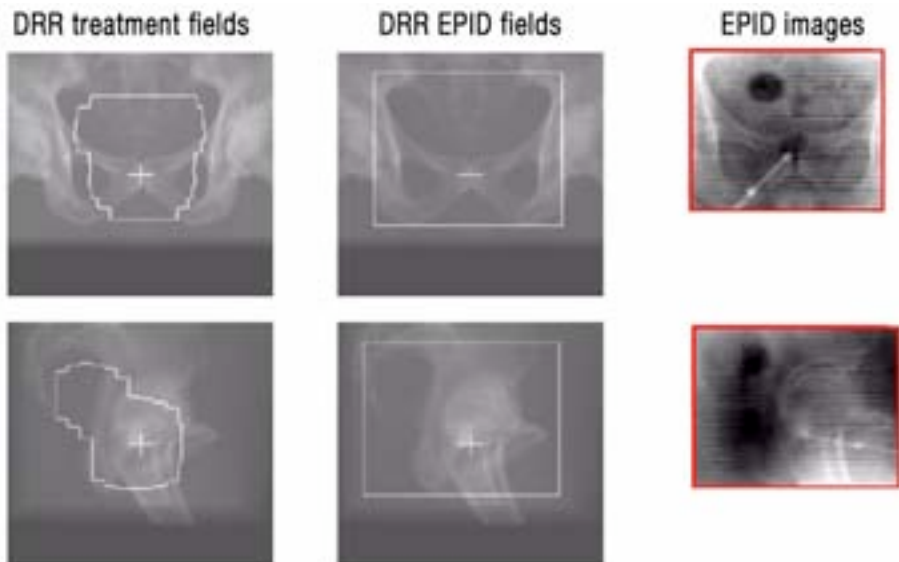
FIG. 12.1. DRRs from treatment fields and large fields to verify the position of the isocentre and the corresponding EPID fields.

12.4.2.1. Portal imaging techniques

At present, photographic film is still a commonly used modality for portal imaging. The quality of film images produced by high energy photons is, however, rather poor compared with conventional X ray images. Portal film enhancement can be performed after digitizing the image, for example by means of a video camera or a laser scanner, thus yielding a better visibility of relevant anatomical landmarks.

Special therapy verification films are commercially available, while cassettes with lead or copper screens are used to reduce the dose needed to form an image.

A technique that gives portal images of improved quality compared with normal photographic film is the use of photostimulated phosphors. After exposure the phosphor plate is scanned with a laser beam. By erasing the image with another light source, the plate can be reused.

A disadvantage of these film techniques is their off-line character, which requires a certain amount of time before the result can be applied clinically. For this reason on-line EPIDs have been developed. Reviews of the physics of portal imaging and portal imaging systems, as well as of their operating principles and clinical applications, can be found in AAPM TG 58.

Two main EPID approaches have been widely applied clinically:

- In the first method a metal plate–phosphor screen combination is used to convert the photon beam intensity into a light image. The screen is viewed by a sensitive video camera using an angled mirror. A drawback of this approach is the bulkiness of the device as a result of the use of a mirror.
- The second approach uses a matrix of liquid filled ionization chambers. This type of EPID has similar dimensions to a film cassette (see Fig. 12.2).

A recent, third method is based on amorphous silicon flat panel systems. A typical example is shown in Fig. 12.3.

For both film and EPID use, tables with recommended, site specific MU values are necessary. The MU values are a function of beam energy, patient thickness and field size, and must be established by each centre for its systems and techniques.

Retrospective analysis of portal films demonstrates that the frequency of field placement errors can be quite high, although more recent studies indicate both a lower frequency of errors and smaller errors if careful patient positioning is applied.

FIG. 12.2. Liquid filled matrix ionization chamber type of EPID connected via a retractable arm to a linac.

Gross set-up errors, for example the wrong placement of shielding blocks, can be detected by visual inspection of the portal image and comparison with a reference image, and corrected immediately.

Correction of field placement errors must be carried out with care. Only the systematic component has to be corrected. Decision rules have to be formulated for what magnitude of deviation a correction has to be performed for and how often measurements have to be repeated for an individual patient.

Various sources of random and systematic set-up errors can be detected by portal imaging; for example, Hurkmans and colleagues, in a review of set-up errors, tabulated the values observed by various authors for different treatment sites. These include the following, given as 1 SD in each specific orthogonal or other relevant direction: head and neck, 1.3–4.6 mm systematic, 1.1–2.5 mm random; prostate, 1.2–3.8 mm systematic, 1.2–3.5 mm random; general pelvic region, 0.6–4.5 mm systematic, 1.1–4.9 mm random; thoracic region, 2.0–5.1 mm systematic, 2.2–5.4 mm random; breast, 1.8–15.5 mm overall;

FIG. 12.3. Amorphous silicon type of EPID installed on the gantry of a linac.

mantle field and total body irradiation (TBI), typically 4–9 mm overall. The range of values is given to accommodate different techniques, immobilization methods and quality assurance procedures on set-up, etc. The smaller values indicate what may be achievable in best practice. Such studies indicate significant improvement in observed systematic deviations when comparing treatments before and after correction of field placement errors.

Portal imaging may lead to various strategies for improvement of positioning accuracy by the radiation technologist through improvement of patient immobilization, introduction of correction rules, adjustment of margins in combination with dose escalation, incorporation of set-up uncertainties in treatment planning, etc. Routine use of EPIDs is currently increasing rapidly, although in many centres it still requires a certain amount of development work and staff training, resulting in a still limited clinical implementation.

The clinical applications of electronic portal imaging can be separated into off-line and on-line analysis:

— Off-line analysis can be used to quantify and separate random and systematic uncertainties for individual patients;

— On-line imaging allows, in principle, a quick decision about continuation of treatment by comparing the portal image with the reference image and looking for unacceptable discrepancies.

12.4.2.2. Future developments in portal imaging

The field of on-line portal imaging is in rapid development. The currently available EPID systems are still mainly used in larger institutions, demonstrating the usefulness of these systems for verifying patient positioning during intensity modulated radiotherapy (IMRT) or other conformal radiotherapy techniques.

Specific questions, such as the effect of immobilization devices on the accuracy of patient set-up, the measurement of organ motion during treatment and the use of EPIDs for quality assurance of the functioning of radiotherapy equipment (e.g. MLCs) and for beam and patient dosimetry, have been studied. However, much work still needs to be done before automated treatment set-up analysis by on-line portal imaging can be used on a routine basis in the clinic.

A disadvantage of the current techniques of portal imaging is their poor contrast and limited spatial resolution. Recent developments have allowed the creation of new types of flat panel detector for X ray imaging, both for diagnostic purposes and for use as an EPID, based on amorphous silicon (a-Si). They have been tested in various centres and are now being increasingly supplied with new treatment units; their use is expected to become widespread. The spatial and contrast information content of the a-Si detector array and film images is quite similar.

12.4.3.   In vivo dose measurements

There are many steps in the chain of processes that determine the dose delivery to a patient undergoing radiotherapy, and each of these steps may introduce an uncertainty. It is therefore worth while, and may even be necessary, for specific patient groups or for unusual treatment conditions to be given an ultimate check of the actual treatment by using in vivo dosimetry.

In vivo dose measurements can be divided into entrance dose measurements, exit dose measurements and intracavitary dose measurements.

- Entrance dose measurements serve to check the output and performance of the treatment apparatus as well as the accuracy of patient set-up;
- Exit dose measurements serve, in addition, to check the dose calculation algorithm and to determine the influence of shape, size and density variations of the body of the patient on the dose calculation procedure;

● Sometimes it is also possible to determine the intracavitary dose in readily accessible body cavities such as the oral cavity, oesophagus, vagina, bladder and rectum.

In vivo dose measurements not only serve to check the dose delivery to the target volume but are also applied to assess the dose to organs at risk (e.g. the eye lens, gonads and lungs during TBI) or in situations in which the dose is difficult to predict (e.g. non-standard SSD or using bolus).

If entrance dose measurements alone are applied, the entrance dose has to be converted to the corresponding target dose using patient and treatment set-up information. A combination of entrance and exit dose measurements is a more accurate method of obtaining the target dose. Various methods are available to obtain the midline dose from entrance and exit dose values. These methods give generally good results for homogeneous situations but in the presence of inhomogeneities considerable deviations can occur.

12.4.3.1. In vivo dose measurement techniques

TLDs and semiconductor detectors (silicon diodes) are the types of dosimeter most commonly employed for in vivo dosimetry purposes. Other systems have also been used, including film, gel dosimeters, ionization chambers, electronic devices (e.g. metal oxide semiconductor field effect transistors (MOSFETs)) and alanine. The characteristics of the main detectors are reviewed in detail in Chapter 3.

TLDs have the advantage that they are small, reasonably tissue equivalent and not attached to measuring equipment with cables or wires. TLDs can be calibrated either individually or as part of a batch having the same mean sensitivity. It is recommended to perform a calibration during each series of in vivo dose measurements for the conditions of the TLD material, readout equipment and anneal procedure at the time.

All thermoluminescent materials suffer from fading of the stored signal to some extent. By applying the same procedure during patient irradiation and calibration, the loss of signal due to fading can easily be taken into account.

The variation of the thermoluminescent sensitivity of LiF with photon energy is rather small. Correction factors due to variations in field size, patient thickness or beam hardening by wedges will therefore also be very small or negligible.

Diodes have the advantage that they have a high sensitivity, give an instant readout and require only simple instrumentation. An example of a diode dosimetry system is given in Fig. 12.4.

FIG. 12.4. Diodes applied for in vivo dosimetry.

The entrance dose and the exit dose can be derived from diode readings by multiplication with an absorbed dose to water calibration coefficient and a number of correction factors that depend on the specific irradiation parameters used. For entrance and exit dose measurements, separate calibrations are required, with the diodes irradiated in both orientations. Owing to the decrease in sensitivity with integrated dose, it is necessary to recalibrate the diodes frequently, for example once every few weeks, depending on the diode workload.

For accurate dose determinations a number of small correction factors, at both the entrance and exit side, are required to correct for variation in response of the diode with field size, focus to skin distance, patient thickness, wedge filter thickness and temperature. Three basic physical properties of the diodes are responsible for these correction factors: the energy dependence, the dose per pulse dependence and the temperature dependence of the sensitivity. The latter correction is dependent on the diode type, but may amount to 0.3%/°C. Note that the temperature of a diode on the skin of a patient is about 30°C, which requires a correction factor of about 3% if calibrated at room temperature.

Diodes may exhibit a directional dependence that is related to the construction of the diode and its buildup cap. The sensitivity in the direction of the cable is generally lower than in the direction perpendicular to it, depending on the details of design and construction and the beam energy it is being used for.

The entrance dose and the exit dose are generally defined at the depth of dose maximum below the surface. In vivo dosimetry detectors should therefore be covered with a buildup cap appropriate to the photon beam energy. The use of such a 'thick' detector eliminates the skin sparing effect and introduces an underdosage, up to 5%, in the shadow of the detector.

The accuracy of entrance and exit dose measurements in open beams, after proper calibration of the diodes, is of the order of 1% and 2% (1 SD), respectively. For wedged beams an additional uncertainty has to be introduced due to the positioning of the diode with respect to the wedge profile.

For specific dose estimates for eyes, skin, etc. (i.e. not at full buildup), appropriately designed dosimeters are required, with buildup to match the clinical situation.

Errors traced by in vivo dosimetry are related to the set-up of the patient, human errors in the data transfer during the consecutive steps of treatment preparation, unstable accelerator performance and inaccuracies in dose calculation, for example by the TPS. In vivo dosimetry during TBI is often applied to verify the midline dose at various parts of the body and to assess the dose in organs at risk such as the lungs and kidneys.

The workload involved in an in vivo dosimetry programme depends on many factors, such as the accuracy required, the frequency of checks, the time devoted to the analysis of the results and the personnel.

Accurate in vivo dosimetry as part of a dosimetric quality assurance programme during a clinical trial of conformal therapy of patients treated for prostate cancer has been reported. For patient groups for which such a high accuracy in dose delivery is required, routine in vivo dosimetry during a few treatment sessions is highly recommended. After every change in the treatment procedure, in vivo dosimetry for a limited number of patients should again be performed.

If the action level is, for example, 5%, then one or a few measurements are sufficient to trace discrepancies larger than this threshold. If the goal is to discover smaller deviations between the intended and actual dose values, then a larger number of measurements might be required in order to separate systematic from random uncertainties.

Other practical aspects, such as the workload on accelerators and availability of staff, might also be limiting factors for in vivo dosimetry. The goal of an in vivo dosimetry programme has therefore to be well defined.

As part of the quality assurance of treatment planning calculations, it is recommended that an independent MU calculation programme be used to check the routine dose calculations. It has been shown that some of the errors found by in vivo dosimetry would also have been traced by independent MU calculations. It can therefore be concluded that a combination of a separate check of the MU calculations for all patients with in vivo dosimetry for a representative subgroup is an effective method of quality assurance.

12.4.3.2. Use of electronic portal imaging systems for in vivo dosimetry

A very interesting development is the use of portal imaging for in vivo dosimetry, or 'transit dosimetry', purposes. Portal images can be transformed to 'dose images', which can then be correlated with exit dose values. Various groups are currently studying the usefulness of films or EPIDs for in vivo dosimetry. Two different approaches (forwards and backwards) are described schematically in Fig. 12.5.

It should be noted that the relationship between the exit dose and the transmission dose at the position of the portal imaging detector is not simple and depends on many factors, such as the skin to detector distance, field size, patient thickness and photon beam energy.

Since a relatively large number of images can be made during one treatment fraction, EPIDs can be used to measure the influence of organ and patient motion on the dose distribution during one treatment session.

Portal dose measurements are extremely useful in detecting differences between actual patient data as encountered during treatment and those applied during treatment planning. EPIDs are likely to become very useful for dosimetric quality assurance of intensity modulated beams.

12.4.4. Record and verify systems

Both portal imaging and in vivo dosimetry studies have traced a number of mistakes in treatment set-ups. Computer verification of treatment parameters allows some such errors to be identified and corrected for before the machine is turned on. Such record and verify systems have been developing in scope for some time, and, based on this experience, electronic patient information systems (or radiotherapy information systems) are rapidly becoming commonplace in the clinic.

A record and verify system aims to compare the set-up parameters with the prescribed values. Patient identification data, machine parameters and dose prescription data are entered into the computer beforehand. At the time of
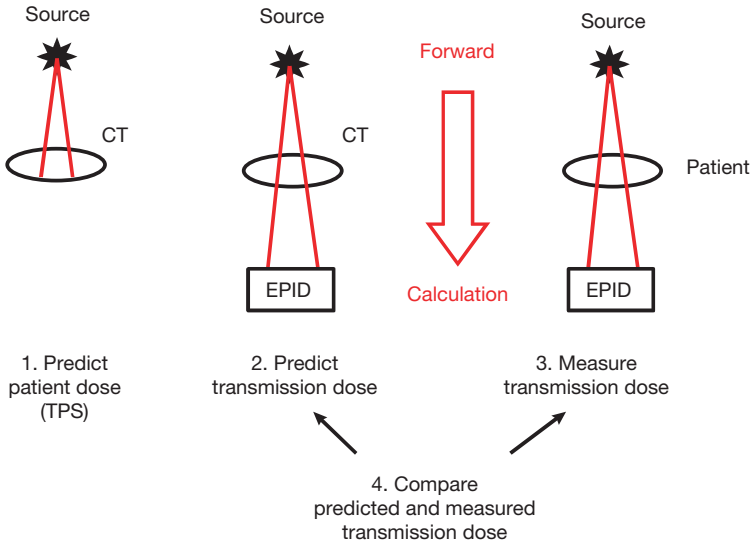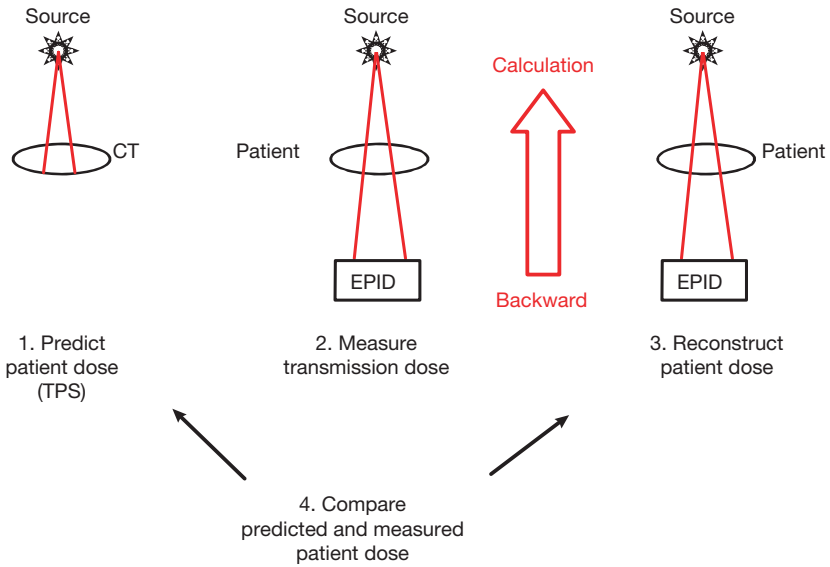
FIG. 12.5. *Two different approaches for applying portal imaging for in vivo dosimetry.*

treatment, these parameters are identified at the treatment machine, and, if there is no difference, the treatment can start. If discrepancies are present, this is indicated and the parameters concerned are highlighted.

Tolerances for verification of machine parameters should be provided by the manufacturer. Clinical tolerance tables must also be defined locally in the department for each set of techniques in order to allow for patient/set-up variations day to day. It is recommended not to have too many tolerance tables.

Record and verify systems must have the flexibility to be overridden. This feature must be used with care and only when reasons are clear and properly documented.

These systems, containing radiation field information for each specific patient, allow the use of assisted set-up (i.e. letting the computer set the machine parameters once the patient is positioned on the table). This facility is particularly useful if isocentric treatments are performed and can help to optimize set-up times, particularly for complex treatments. A dummy run should be carried out because of the increased risk of collision.

The computer can also keep a record of the actual machine settings used. A printed record can be kept on a patient record card or on a daily record sheet of all treatments carried out. This can help to optimize time.

The treatment delivered, if relying on a record and verify system setting or verifying the parameters, is only as good as the information input to the system. It is therefore vital that the data in the record and verify system be quality controlled, using independent (redundant) checking to verify the input and to sanction its clinical use.

The performance of the record and verify system should be included in an appropriate quality assurance programme. The details of such quality assurance tests will be specific to the system in question.

12.5. QUALITY AUDIT

12.5.1. Definition

A quality audit is a systematic and independent examination to determine whether quality activities and results comply with planned arrangements and whether the arrangements are implemented effectively and are suitable to achieve the stated objectives.

Quality audits:

- Are performed by personnel not directly responsible for the areas being audited, preferably in cooperative discussion with the responsible personnel.
- Evaluate the need for improvement or corrective action.
- Should not be confused with surveillance or inspection.
- Can be conducted for internal or external purposes.
- Can be applied at any level of a quality assurance programme.
- Must be against predetermined standards, linked to those that the quality assurance programme is trying to achieve.
- Should require action if those standards are not met.
- Should be regular and form part of a quality feedback loop to improve quality.
- Can be of the implementation, or operation, of a quality system or quality assurance programme (i.e. can be mainly procedural), looking at quality assurance procedures, protocols, quality control programmes, quality control and quality assurance results and records, etc.: procedural quality audit.
- Can also verify the effectiveness, or performance, of a quality system or quality assurance programme (i.e. can be mainly practical): practical quality audit.
- May be voluntary and cooperative, or may be regulatory (e.g. for accreditation of the department or hospital or for quality system certification).

12.5.2. Practical quality audit modalities

12.5.2.1. Postal audit with mailed dosimeters

Postal audits with mailed dosimeters (usually TLDs) are generally organized by secondary standards dosimetry laboratories (SSDLs), agencies such as the IAEA, the Radiological Physics Center (RPC) in the USA and ESTRO (EQUAL), national societies or national quality networks. They can be applied at various levels in the clinical dosimetry chain and can include procedural audits by using a questionnaire.

12.5.2.2. Quality audit visits

Quality audit visits can audit practical aspects in detail, limited only by time. They can audit procedural aspects by questioning staff and by inspection of procedures and records.

12.5.3. What should be reviewed in a quality audit visit?

The content of a quality audit visit should be predefined and will depend on the purpose of the visit; for example, is it a routine regular visit within a national or regional quality audit network, is it regulatory or cooperative between peer professionals, is it a visit following a possible misadministration, or is it a visit following an observed higher than expected deviation in a mailed TLD audit programme that the centre cannot explain?

An example of the contents of a quality audit visit is the following:

- Check documentation, for example the contents of policies and procedures, quality assurance programme structure and management, patient dosimetry procedures, simulation procedures, patient positioning, immobilization and treatment delivery procedures, equipment acceptance and commissioning records, dosimetry system records, machine and treatment planning data, quality control programme content, tolerances and frequencies, quality control and quality assurance records of results and actions, preventive maintenance programme records and actions and patient data records, follow-up and outcome analysis.
- Check infrastructure, for example equipment, personnel, patient load, existence of policies and procedures, quality assurance programme in place, quality improvement programme in place, radiation protection programme in place and data and records.
- Carry out check measurements of beam calibration, field size dependence, electron cone factors, depth dose, electron gap corrections, wedge transmission (with field size), tray, etc., factors, mechanical characteristics, patient dosimetry, dosimetry equipment and temperature and pressure measurement comparison.
- Carry out check measurements on other equipment, such as the simulator and CT scanner.
- Assess treatment planning data and procedures. Measure some planned distributions in phantoms.

This is a simple outline of possible items to check and measure. Depending on the type and purpose of the audit visit and the time available, some or all of these may be assessed. Alternatively, assessment of only a small subset may be appropriate. Additionally, the auditor should be flexible in approach and be prepared to audit extra aspects if this appears necessary from the results of the initial measurements carried out. Some preplanned audit tasks may need to be modified or reduced if it becomes clear that there are higher priority aspects that need to be followed up in the time available.

BIBLIOGRAPHY

AMERICAN ASSOCIATION OF PHYSICISTS IN MEDICINE, Physical Aspects of Quality Assurance in Radiation Therapy, AAPM Task Group 24 Report, AAPM, New York (1984).

— Comprehensive QA for radiation oncology: Report of AAPM Radiation Therapy Committee Task Group 40, Med. Phys. **21** (1994) 581–618.

— American Association of Physicists in Medicine Radiation Therapy Committee Task Group 53: Quality assurance for clinical radiotherapy treatment planning, Med. Phys. **25** (1998) 1773–1829.

— Clinical use of electronic portal imaging: Report of AAPM Radiation Therapy Committee Task Group 58, Med. Phys. **28** (2001) 712–737.

— Quality assurance for computed-tomography simulators and the computed-tomography-simulation process: Report of the AAPM Radiation Therapy Committee Task Group No. 66, Med. Phys. **30** (2003) 2762–2790.

BRAHME, A., et al., Accuracy requirements and quality assurance of external beam therapy with photons and electrons, Acta Oncol. Suppl. 1 **27** (1988).

CLINICAL ONCOLOGY INFORMATION NETWORK, ROYAL COLLEGE OF RADIOLOGISTS, Guidelines for external beam radiotherapy, Clin. Oncol. **11** (1999) S135–S172.

DUTREIX, A., When and how can we improve precision in radiotherapy? Radiother. Oncol. **2** (1984) 275–292.

ESSERS, M., MIJNHEER, B.J., In-vivo dosimetry during external photon beam radiotherapy, Int. J. Radiat. Oncol. Biol. Phys. **43** (1999) 245–259.

EUROPEAN SOCIETY FOR THERAPEUTIC RADIOLOGY AND ONCOLOGY, Quality assurance in radiotherapy, Radiother. Oncol. **35** (1995) 61–73.

— Practical Guidelines for the Implementation of a Quality System in Radiotherapy, Physics for Clinical Radiotherapy Booklet No. 4, ESTRO, Brussels (1998).

HURKMANS, C.W., REMEIJER, P., LEBESQUE, J.V., MIJNHEER, B.J., Set-up verification using portal imaging: Review of current clinical practice, Radiother. Oncol. **58** (2001) 105–226.

INTERNATIONAL ATOMIC ENERGY AGENCY, Quality Assurance in Radiotherapy, IAEA-TECDOC-1040, IAEA, Vienna (1997).

— Lessons Learned from Accidental Exposures in Radiotherapy, Safety Reports Series No. 17, IAEA, Vienna (2000).

INTERNATIONAL COMMISSION ON RADIOLOGICAL UNITS AND MEASUREMENTS, Determination of Dose in a Patient Irradiated by Beams of X or Gamma Rays in Radiotherapy Procedures, Rep. 24, ICRU, Bethesda, MD (1976).

INTERNATIONAL ELECTROTECHNICAL COMMISSION, Medical Electrical Equipment — Medical Electron Accelerators: Functional Performance Characteristics, IEC 976, IEC, Geneva (1989).

— Medical Electrical Equipment — Medical Electron Accelerators in the Range 1 MeV to 50 MeV: Guidelines for Performance Characteristics, IEC 977, IEC, Geneva (1989).

INSTITUTE OF PHYSICS AND ENGINEERING IN MEDICINE, A Guide to Commissioning and Quality Control of Treatment Planning Systems, Rep. 68, IPEM, York, United Kingdom (1996).

— Physics Aspects of Quality Control in Radiotherapy, Rep. 81, IPEM, York, United Kingdom (1998).

INTERNATIONAL ORGANIZATION FOR STANDARDIZATION, Quality Management and Quality Assurance Standards — Part I. Guidelines for Selection and Use, ISO 9000, ISO, Geneva (1994).

MIJNHEER, B., BATTERMANN, J., WAMBERSIE, A., What degree of accuracy is required and can be achieved in photon and neutron therapy, Radiother. Oncol. **8** (1987) 237–252.

VAN DYK, J. (Ed.), The Modern Technology for Radiation Oncology: A Compendium for Medical Physicists and Radiation Oncologists, Medical Physics Publishing, Madison, WI (1999).

VAN DYK, J., BARNET, R., CYGLER, J., SHRAGGE, P., Commissioning and quality assurance of treatment planning computers, Int. J. Radiat. Oncol. Biol. Phys. **26** (1993) 261–273.

VENSELAAR, J., WELLEWEERD, H., MIJNHEER, B., Tolerances for the accuracy of photon beam dose calculation of treatment planning systems, Radiother. Oncol. **60** (2001) 203–214.

WORLD HEALTH ORGANIZATION, Quality Assurance in Radiotherapy, WHO, Geneva (1988).

WILLIAMS, J.R., THWAITES, D.I. (Eds), Radiotherapy Physics in Practice, Oxford Univ. Press, Oxford (2000).

Chapter 13

BRACHYTHERAPY:
PHYSICAL AND CLINICAL ASPECTS

N. SUNTHARALINGAM
Department of Radiation Oncology,
Thomas Jefferson University Hospital,
Philadelphia, Pennsylvania,
United States of America

E.B. PODGORSAK
Department of Medical Physics,
McGill University Health Centre,
Montreal, Quebec,
Canada

H. TÖLLI
Division of Human Health,
International Atomic Energy Agency,
Vienna

13.1. INTRODUCTION

Brachytherapy (sometimes referred to as curietherapy or endocurie therapy) is a term used to describe the short distance treatment of cancer with radiation from small, encapsulated radionuclide sources. This type of treatment is given by placing sources directly into or near the volume to be treated. The dose is then delivered continuously, either over a short period of time (temporary implants) or over the lifetime of the source to a complete decay (permanent implants). Most common brachytherapy sources emit photons; however, in a few specialized situations β or neutron emitting sources are used.

There are two main types of brachytherapy treatment:

- Intracavitary, in which the sources are placed in body cavities close to the tumour volume;
- Interstitial, in which the sources are implanted within the tumour volume.

Intracavitary treatments are always temporary, of short duration, while interstitial treatments may be temporary or permanent. Temporary implants are inserted using either manual or remote afterloading procedures. Other, less common forms of brachytherapy treatments include surface plaque, intra-luminal, intraoperative and intravascular source applications; for these treatments either γ or β emitting sources are used.

The physical advantage of brachytherapy treatments compared with external beam radiotherapy is the improved localized delivery of dose to the target volume of interest. The disadvantage is that brachytherapy can only be used in cases in which the tumour is well localized and relatively small. In a typical radiotherapy department about 10–20% of all radiotherapy patients are treated with brachytherapy.

Several aspects must be considered when giving brachytherapy treatments. Of importance is the way in which the sources are positioned relative to the volume to be treated, and several different models have been developed over the past decades for this purpose. The advantage of using a well established model is that one benefits from the long experience associated with such models and that one can take advantage of published results. The use of uniform models and methods in brachytherapy treatments simplifies comparison of treatment results.

A typical treatment in which a model may be used is, for example, the treatment of cancer of the cervix, in which the dose is given to a specific point A, or low dose rate (LDR) treatments of head and neck cancers using ^{192}Ir wires. In this latter case the Paris model provides suitable guidelines for calculation of the treatment dose and time.

For treatments in which dose optimization techniques are used, the treatment times depend on how the sources are positioned relative to the dose calculation points and on the source strength. In situations in which the system to be used is not obvious, the scientific literature should be consulted in order to take full advantage of already existing experience.

With the use of a specific method for the brachytherapy treatment and a model for the dose distribution calculation, comparison of results is simplified. The use of a well established dosimetric system for the treatment of cancer gives a common point for such comparisons. However, the use of a model alone is not sufficient to validate results; it is necessary to have a reliable method for determination of the source strength in order for the dose calculation to be accurate. This means that it is necessary for brachytherapy sources to be calibrated, with the calibration traceable to a national or international standards laboratory.

The important aspects of any brachytherapy treatment are:

● Use of a suitable dosimetric model for the treatment time and dose calculation;
● Use of calibrated sources.

These are by no means all the necessary components. A treatment does not reach its goals if the source misses its aimed positions by a large margin; that is, if there are severe geographical misses in placing the sources relative to their intended positions. Owing to the steep dose gradient that characterizes brachytherapy, such geometrical misses may be seriously detrimental to the intended treatment. Thus there is a need for a quality control programme guaranteeing that the treatment is given in accordance with its purposes.

From a radiobiological point of view brachytherapy dose delivery can result in complex dose rate effects that may influence the therapeutic outcome. The continuous delivery of dose will influence the repair of sublethal and potentially lethal damage, cell proliferation and other cell kinetics, all of which can modify the radiation response of tumour and normal tissues.

Tables 13.1–13.4 summarize brachytherapy treatments with regard to the type of implant, duration of implant, method of source loading and dose rate.

TABLE 13.1. VARIOUS TYPES OF BRACHYTHERAPY IMPLANT

Type of implant	Description
Intracavitary	Sources are placed into body cavities close to the tumour volume
Interstitial	Sources are implanted surgically within the tumour volume
Surface (mould)	Sources are placed over the tissue to be treated
Intraluminal	Sources are placed in a lumen
Intraoperative	Sources are implanted into the target tissue during surgery
Intravascular	A single source is placed into small or large arteries

TABLE 13.2. BRACHYTHERAPY TREATMENTS CLASSIFIED WITH RESPECT TO TREATMENT DURATION

Type of implant	Description
Temporary	Dose is delivered over a short period of time and the sources are removed after the prescribed dose has been reached
Permanent	Dose is delivered over the lifetime of the source until complete decay

TABLE 13.3. BRACHYTHERAPY TREATMENTS CLASSIFIED WITH RESPECT TO SOURCE LOADING

Method of loading	Description
Hot loading	The applicator is preloaded and contains radioactive sources at the time of placement into the patient
Afterloading	The applicator is placed first into the target position and the radioactive sources are loaded later, either by hand (manual afterloading) or by a machine (automatic remote afterloading)

TABLE 13.4. BRACHYTHERAPY TREATMENTS CLASSIFIED WITH RESPECT TO DOSE RATE[a]

Dose rate	Numerical value of the dose rate at the dose specification point(s)
Low dose rate (LDR)	0.4–2 Gy/h
Medium dose rate (MDR)[b]	2–12 Gy/h
High dose rate (HDR)	>12 Gy/h

[a] The definitions here are according to the ICRU. In practice, HDR treatments are given with a substantially higher dose rate than that given by the lower limit of 12 Gy/h.

[b] MDR is not in common use. In those few cases in which it has been used, the treatment results have been rather poor compared with LDR or HDR treatments.

13.2. PHOTON SOURCE CHARACTERISTICS

13.2.1. Practical considerations

Brachytherapy sources are usually encapsulated; the capsule serves several purposes:

- Containing the radioactivity;
- Providing source rigidity;
- Absorbing any α and, for photon emitting sources, β radiation produced through the source decay.

The useful radiation fluence from a brachytherapy source generally consists of:

— γ rays, which form the most important component of the emitted radiation;
— Characteristic X rays emitted incidentally through electron capture or internal conversion that occurs in the source;
— Characteristic X rays and bremsstrahlung that originate in the source capsule.

The choice of an appropriate photon emitting radionuclide for a specific brachytherapy treatment depends on several relevant physical and dosimetric characteristics, the most important of which are the:

 (i) Photon energies and photon beam penetration into tissue and the shielding materials;
 (ii) Half-life;
(iii) Half-value layer (HVL) in shielding materials such as lead;
(iv) Specific activity;
 (v) Source strength;
(vi) Inverse square fall-off of dose with distance from the source (this is the dominant dosimetric effect, because of the very short treatment distances used in brachytherapy).

The photon energy influences penetration into tissue as well as the radiation protection requirements. Dose distributions in tissue, within the short treatment distances of interest, are not influenced much by photon scattering when photon energies are above 300 keV. This is due to the attenuation by tissue being compensated for by scatter buildup of the dose. However, tissue

attenuation is highly significant for low photon energies of the order of 30 keV and below.

The HVL required to shield against high energy photons from brachytherapy sources is several millimetres of lead. For low energy photons the required thickness is much smaller, usually less than 0.1 mm of lead.

13.2.2. Physical characteristics of some photon emitting brachytherapy sources

Over a dozen radioactive nuclides have a history of use as sealed sources in brachytherapy, but only six are commonly used today, while a few others are used under special circumstances. The common sources are ^{60}Co, ^{137}Cs, ^{192}Ir, ^{125}I, ^{103}Pd and ^{90}Sr/^{90}Y; the less common sources are ^{198}Au, ^{106}Ru and ^{252}Cf. The use of ^{226}Ra and ^{222}Rn was discontinued because of safety concerns, but their long history of clinical use still influences modern brachytherapy concepts. Some physical characteristics of common brachytherapy sources are listed in Table 13.5.

13.2.3. Mechanical source characteristics

Brachytherapy photon sources are available in various forms (needles, tubes, seeds, wires, pellets) but are generally used as sealed sources. Usually they are doubly encapsulated in order to provide adequate shielding against the α and β radiation emitted from the source and to prevent leakage of the radioactive material.

- Caesium-137 is available in several forms, such as needles, tubes and pellets.
- Iridium-192 is available in the form of wires, the radioactive core being an iridium–platinum alloy with an outer sheath of 0.1 mm thick platinum. Iridium-192 sources are also available as seeds, again doubly encapsulated with an outer sheath of stainless steel, and as strands of nylon ribbon. HDR remote afterloading units use specially designed ^{192}Ir sources with typical activities of 370 GBq (10 Ci).
- Iodine-125, ^{103}Pd and ^{198}Au sources are only available as seeds. They are usually inserted into the tumour volume using special delivery 'guns'.
- Cobalt-60 brachytherapy sources are available as pellets with a typical activity of 18.5 GBq (0.5 Ci) per pellet.

TABLE 13.5.   SOME CHARACTERISTICS OF ISOTOPES USED IN BRACHYTHERAPY

Isotope	Average[a] photon energy (MeV)	Half-life	HVL in lead (mm)	Γ_{AKR} [b, d] $\left(\dfrac{\mu Gy \cdot m^2}{GBq \cdot h} \right)$	Λ [c, d] $\left(\dfrac{cGy \cdot h^{-1}}{cGy \cdot cm^2 \cdot h^{-1}} \right)$
Co-60	1.25	5.26 a	11	309	1.11
Cs-137	0.66	30 a	6.5	77.3	1.11
Au-198	0.41	2.7 d	2.5	56.2	1.13
Ir-192	0.38	73.8 d	3	108	1.12
I-125	0.028	60 d	0.02	—	—
Pd-103	0.021	17 d	0.01	—	—

[a]   These are only approximate values, depending on the source make and filtration.
[b] Γ_{AKR} is the air kerma rate constant.
[c] Λ is the dose rate constant.
[d]   Using generic values of the air kerma rate constant or dose rate constant for a low energy photon source may lead to substantial errors in dose calculations. They are therefore not given here for ^{125}I and [103]Pd.

13.2.4.   Source specification

The following two sections provide the recommended quantities for brachytherapy source specification: Section 13.2.4.1 for γ ray sources and Section 13.2.4.2 for β ray sources. Older quantities are still used, mainly by manufacturers and in some older treatment planning systems (TPSs). When a conversion from one quantity to another is made, great care must be taken in the selection of appropriate factors. For a full description of the conversion procedure the interested reader is referred to IAEA-TECDOC-1274.

13.2.4.1. Specification of γ ray sources

The recommended quantity for the specification of γ ray sources is the reference air kerma rate $\dot{K}_{air}(d_{ref}))_{air}$, which is defined by the ICRU as the air kerma rate in air at a reference distance of 1 m, corrected for air attenuation and scattering. The definition given in this report agrees with that given in ICRU Report No. 38 and No. 58.

For needles, tubes and other similar rigid sources, the direction from the source centre to the reference point should be at right angles to the long axis of the source. The SI unit of the reference air kerma rate is Gy/s, but for the

purposes of source specification it is more convenient to use μGy/h for LDR brachytherapy sources, progressing to μGy/s and mGy/h for HDR applications.

The AAPM recommends photon emitting sources to be specified in terms of the air kerma strength S_K. The relationship between $(\dot{K}_{air}(d_{ref}))_{air}$ and S_K is given by:

$$S_K = (\dot{K}_{air}(d_{ref}))_{air}\, d_{ref}^2 \qquad (13.1)$$

where d_{ref} is the reference distance at which the reference air kerma rate is defined (1 m).

It is apparent from the above equation that the numerical values of the source strength, whether expressed in air kerma strength or in reference air kerma rate, are identical. The only difference between these two quantities is the unit in which the source strength is expressed. If the reference air kerma rate of a source is 1 μGy/h, then its strength, expressed in air kerma strength, is 1 μGy·m^2·h^{-1}. AAPM TG 43 recommends a shorthand notation of 1 U = 1 μGy·m^2·h^{-1} = 1 cGy·cm^2·h^{-1}.

In the past, the strength of a brachytherapy source was specified in terms of activity (i.e. the number of disintegrations per unit time), or, for carrier free sources, such as ^{226}Ra, simply as mass of a nuclide. The original definition of the curie (Ci) as the unit of activity was that 1 Ci equals the activity produced by 1 g of ^{226}Ra (3.7×10^{10} s^{-1}). Refined measurements determined the activity of 1 g of ^{226}Ra as 3.655×10^{10} s^{-1} or 0.988 Ci.

Measurement of source activity presented problems, in particular for sources with filtration material surrounding the source, due to attenuation and scattering effects. Other alternative quantities that were introduced for specifying source strengths but are no longer recommended for use are the apparent activity and the milligram radium equivalence.

In the past the exposure rate produced at a given distance from the source was also used as a measure of source strength.

The exposure rate $\dot{X}_P$ at point P in air at a distance d from the source was the original parameter of interest in brachytherapy and is expressed as follows:

$$\dot{X}_P = \frac{\mathcal{A}\, \Gamma_X}{d^2} \qquad (13.2)$$

where

$\mathcal{A}$ is the source activity (Ci);
Γ_X is the exposure rate constant (R·m^2·Ci^{-1}·h^{-1}).

The currently used approach is to state the air kerma rate in air $(\dot{K}_{air}(d))$ at point P in air a distance d from the source as follows:

$$(\dot{K}_{air}(d))_{air} = \frac{\mathcal{A}_{app}\Gamma_{AKR}}{d^2} \tag{13.3}$$

where

$\mathcal{A}_{app}$ is the apparent activity of the source;
Γ_{AKR} is the air kerma rate constant related to Γ_X through the following relationship:

$$\Gamma_{AKR} = \frac{\Gamma_X 0.876 \times 10^{-2} \text{ Gy/R}}{3.7 \times 10^{10} \text{ Bq/Ci}} = 236.8 \frac{\mu\text{Gy/R}}{\text{GBq/Ci}} \Gamma_X \tag{13.4}$$

with Γ_X given in $\text{R·m}^2\text{·Ci}^{-1}\text{·h}^{-1}$ and Γ_{AKR} in $\mu\text{Gy·m}^2\text{·GBq}^{-1}\text{·h}^{-1}$.
Example: For the ^{60}Co isotope:

$$\Gamma_X = 1.31 \frac{\text{R·m}^2}{\text{Ci·h}} \quad \text{and} \quad \Gamma_{AKR} = 310 \frac{\mu\text{Gy·m}^2}{\text{GBq·h}} \tag{13.5}$$

The apparent activity $\mathcal{A}_{app}$ for a given brachytherapy source is defined as the activity of a hypothetical unfiltered point source of the same radionuclide that would give the same air kerma rate in air at a reference distance (typically 1 m) along the perpendicular bisector of the source. The SI unit of apparent activity is the becquerel (1 Bq = 1 s^{-1}), the old unit is the curie (1 Ci = 3.7 × 10^{10} s^{-1} = 3.7 × 10^{10} Bq). The apparent activity is sometimes called the equivalent activity.

Accurate measurements of the radiation intensity (energy fluence rate) at a specified point are possible, and hence the reference air kerma rate in air and the air kerma strength are now the recommended quantities for specifying source strength.

13.2.4.2. Specification of β ray sources

The recommended quantity for the specification of β ray sources is the reference absorbed dose rate in water at a reference distance from the source. The reference distance differs from one type of source to another and is generally between 0.5 and 2 mm from the source.

13.3. CLINICAL USE AND DOSIMETRY SYSTEMS

13.3.1. Gynaecology

Intracavitary brachytherapy is mostly used for cancers of the uterine cervix, uterine body and vagina. Various applicators are in use to hold the sources in an appropriate configuration. A cervix applicator consists of a central tube (tandem) and lateral capsules (ovoids or colpostats).

13.3.1.1. Types of source

The most widely used source for the treatment of gynaecological cancers is ^{137}Cs. It is often necessary to use sources of different strengths in order to achieve the desired dose distribution. In modern remote afterloading devices ^{192}Ir is the commonly used radionuclide.

13.3.1.2. Dose specification

Numerous systems have been devised for dose specification in the treatment of the cervix: the two most commonly used are the Manchester system and the ICRU system.

The Manchester system is characterized by doses to four points: A, B, bladder and rectum. The duration of the implant is based on the dose rate at point A, which is located 2 cm superior to the cervical os and 2 cm lateral to the cervical canal. Point B is defined 3 cm laterally to point A if the central canal is not displaced. If the tandem displaces the central canal, point A moves with the canal, but point B remains fixed at 5 cm from the midline.

The system recommended by the ICRU relates the dose distribution to the target volume rather than to a specific point. The ICRU system for dose specifications for brachytherapy of the cervix is given in Section 13.4 (see ICRU Report No. 38).

13.3.1.3. Source arrangement

Intracavitary radiation therapy of cervical cancer requires careful placement of sources with respect to the target volume and any surrounding critical structures. The clinical guidelines usually followed result in adequate dose delivery to the paracervical tissues and avoidance of underdose in regions around the cervix while respecting mucosal tolerance.

13.3.1.4. Applicators

Several rigid applicators have been used in the treatment of cancer of the cervix. The most commonly used applicator is the Fletcher–Suit–Delcos system. When using this type of rigid applicator system, the dose distribution can be optimized by a careful selection and relative placement of the sources in the tandem and the colpostats/ovoids.

13.3.1.5. Rectal and bladder dose monitoring

The most frequent clinical complications of intracavitary radiation treatments of cervical cancer result from a high dose delivered to the portions of the rectum and bladder that are in close proximity to the sources. Applicator placement with respect to the location of the rectum and bladder is therefore very important, in order to keep the dose to these critical structures as low as possible. In many instances surgical cotton gauze is used to displace the sensitive structures away from the applicators.

Direct measurement of rectal dose has been attempted using miniature ionization chambers or scintillation detector dose rate meters. However, these rigid systems give unacceptable variability in the results and correlate poorly with calculated values.

13.3.2. Interstitial brachytherapy

Various preplanning dosimetry systems have been developed for clinical use. In the early years of brachytherapy, tables of total dose delivered as a function of area or volume to be treated were calculated and made available. These tables were used to calculate the required number of sources and to preplan their placement within the target volume so as to achieve an adequate treatment. This required following well defined rules for the placement of the sources. Two systems that were widely used were the Patterson–Parker (Manchester) system and the Quimby (Memorial) system. A more recent and currently widely used system is the Paris system.

13.3.2.1. Patterson–Parker system

The aim of the Patterson–Parker dosimetry system is to plan and deliver a uniform dose (±10% from the prescribed or stated dose) throughout the volume to be treated. The sources are distributed non-uniformly following certain rules, based on the size of the target volume, with more source strength concentrated in the periphery. Usually the prescribed dose is about 10% higher

than the minimum dose within the treated volume. The Patterson–Parker dose tables give the cumulative source strength required to deliver 900 cGy, using current factors and dose units, as a function of area (planar implants) or volume.

Single plane: The source arrangement treats a slab of tissue 1 cm thick. The prescribed dose is on a parallel plane, 0.5 cm away from the source plane.

Double plane: Thicker slabs of tissue, usually up to about 2.5 cm, are treated with sources placed in two parallel planes. The required total source strength is equally divided between the two planes, following the distribution rules for single plane implants. Correction factors are used for plane separations larger than 1 cm in order to achieve a minimum dose that is no more than 10% lower than the prescribed dose. The prescribed dose is in each of the interior planes, which are 0.5 cm from the source planes. Note that the midplane dose for thick target volumes may be as much as 20–30% lower than the prescribed dose.

Other volumes: Distribution rules follow the rind to core ratio concept for different shapes of volume (cylinder, sphere, rectangular solid). Typically 75% of the source strength is placed on the rind and 25% in the core.

13.3.2.2. Quimby system

The Quimby system is based on a uniform distribution of source strength, accepting a non-uniform delivery of dose. Usually, the dose in the centre of the treatment volume is higher than the dose near the periphery. The dose value obtained from the Quimby tables is the minimum dose within the implanted volume. Note that for surface applicators the stated dose is the maximum dose in the treatment plane.

Typically, for equal dose delivery to similar size planar or volume implants, the total source strength required when using the Quimby system will be much greater than that required by the Patterson–Parker system.

13.3.2.3. Paris system

The Paris system is used primarily for single and double plane implants and does not address the other types of volume implant. It is necessary to follow a set of general rules for the selection and placement of the sources in order to achieve the desired dose distributions. The general rules are as follows:

- Sources must be linear and their placement parallel;
- The centres of all sources must be located in the same plane (central plane);

● The linear source strength (activity) must be uniform and identical for all sources;
● Adjacent sources must be equidistant from each other;
● The spacing between sources should be wider when using long sources.

The stated (reference) dose rate is a fixed percentage (85%) of the basal dose rate. The basal dose rate is the average of the minimum dose rates located between the sources inside the implanted volume. The individual minimum dose rates should be within ±10% of the average (basal dose rate), thus restricting the number of sources to be used.

13.3.3. Remote afterloading systems

Generally, the radiation sources are manually afterloaded into applicators or catheters that have been placed within the target volume. At the end of the treatment the sources are removed, again manually. These procedures result in some radiation exposure to the medical and support staff. Several computer driven remote afterloading systems have been developed to help minimize this radiation exposure.

There are three distinct types of remote afterloading device:

● LDR;
● HDR;
● Pulsed dose rate (PDR).

The use of remote afterloading devices offers several practical advantages over manual procedures, such as:

— Increased patient treatment capacity;
— Consistent and reproducible treatment delivery;
— Reduced radiation exposure of staff.

Remote afterloading devices are used in both interstitial and intracavitary clinical applications. The anatomic sites commonly treated with these devices are similar to those treated with conventional brachytherapy procedures.

The essential components of all remote afterloading systems are:

 (i)   A safe to house the radioactive source;
 (ii) Radioactive sources, single or multiple;
(iii) A local or remote operating console;

(iv) A source control and drive mechanism;
(v) Source transfer guide tubes and treatment applicators;
(vi) A treatment planning computer.

The three commonly used radioactive sources in remote afterloading devices are ^{60}Co, ^{137}Cs and ^{192}Ir. Currently the most commonly used source for afterloading is ^{192}Ir, because of its medium average γ ray energy (~400 keV) and its high specific activity. However, its relatively short half-life is a distinct disadvantage, since frequent replacement of sources is required (typically three to four times per year).

LDR devices use multiple sources, together with inactive spacers, to achieve typical treatment dose rates of about 0.4–2 Gy/h. In contrast, HDR systems use a single source of ^{192}Ir, with a typical activity of 10–20 Ci (370–740 GBq), delivering treatment dose rates exceeding 2 Gy/min.

PDR devices use a single 1 Ci (37 GBq) ^{192}Ir source and are programmed to deliver short duration HDR treatments, usually at hourly intervals, to simulate continuous LDR treatments. The dose distributions in both HDR and PDR treatments are optimized to accomplish the clinical goals by varying the distance between dwell positions and dwell times of the source. Both LDR and HDR systems are used clinically for intracavitary, interstitial and intraluminal treatments.

The advantages of using HDR systems over LDR systems are: optimization of dose distribution; outpatient treatments; and elimination of staff radiation exposure.

However, there are some disadvantages in the use of HDR systems, such as: uncertainty in biological effectiveness; potential for accidental high exposures and serious errors; and increased staff commitment.

13.3.4. Permanent prostate implants

Brachytherapy has gained wide acceptance as a treatment modality for early stage prostate cancer, in which the disease is confined to the prostate gland. The permanent placement of short lived radionuclide sources, emitting low energy photons, is often used as the primary treatment, and some attempts are also being made to use fractionated or single session HDR brachytherapy treatments as a boost to external beam radiotherapy.

Several factors must be considered in the use of permanent seed implants, such as the choice of radionuclide, planning technique, source delivery technique and total prescribed dose.

13.3.4.1. Choice of radionuclide for prostate implants

The use of permanent radioactive seed implants for the treatment of early prostate cancer has gained renewed interest with the introduction of ^{125}I and [103]Pd seeds, which emit low energy (~30 keV) photons.

Gold-198 seeds, which emit medium energy photons (~400 keV), were used in the past, but the unnecessary radiation exposure hazard prevented the use of this radionuclide from gaining wide acceptance.

Palladium-103, which has a shorter half-life (17 days) than [125]I (60 days), delivers a higher initial dose rate and hence has been found useful in treating fast growing high grade tumours.

13.3.4.2. Planning technique: ultrasound or computed tomography

There are two surgical approaches to performing seed implantation of the prostate: retropubic (open) and transperineal (closed), with ultrasound or computed tomography (CT) guidance. The transperineal approach with ultrasound guidance has become the technique of choice, in part because it is carried out as an outpatient one day procedure.

13.3.4.3. Preplanning, seed placement and dose distributions

Preplanning of the implant is based on either ultrasound or CT cross-sectional (axial) images. The intended treatment volume generally is the whole prostate gland with a small margin of periprostatic tissue. The number of seeds required and their geometric placement in the target volume is determined through optimized computer dose planning or precalculated nomograms.

The recommended total dose to the periphery of the target volume is 150–160 Gy for ^{125}I and 115–120 Gy for [103]Pd when a brachytherapy implant is the sole modality of radiation treatment.

13.3.4.4. Post-implant dose distributions and evaluation

Post-implant CT imaging is usually performed two to three weeks post-implantation to allow for reduction in oedema and any migration of seeds. Using CT images, dose calculations are performed and compared with pre-implant dose distributions.

13.3.5. Eye plaques

Intraocular melanoma is the most common eye tumour. An eye plaque, loaded with ^{125}I seeds, is applied externally to the scleral (outer) surface over the tumour base. The number of seeds to be used is related to the size of the plaque, and ranges from 7 to 24 for plaque diameters of 12–20 mm. The typical activity used is 0.5–5 mCi per seed so as to achieve treatment dose rates of 0.5–1.25 Gy/h, with a prescription dose of 100 Gy delivered in 5–12 consecutive days.

The prescription point is defined as the tumour apex if the apical height exceeds 5 mm, and 5 mm depth from the interior sclera if the apex is less than 5 mm high. Tumour localization is usually performed using fundoscopy, fundus photography and ultrasound A and B scans. CT and magnetic resonance imaging (MRI) may also be used. Post-implant, plaque placement verification is carried out with ultrasound imaging.

A less common approach to the treatment of lesions in the eye is based on β emitting sources: ^{90}Sr/^{90}Y (maximum electron energy: 2.27 MeV; penetration into tissue: 12 mm) and more recently ^{106}Ru (maximum electron energy: 3.4 MeV; penetration into tissue: 20 mm).

13.3.6. Intravascular brachytherapy

The potential role of radiation in preventing restenosis after angioplastic treatment or stent placement is being studied using brachytherapy techniques. Pre-clinical and clinical investigations have used catheter based radiation sources or radioactive stents to deliver dose to the affected coronary artery vessel wall. Iridium-192 has been the choice for a medium energy γ emitting source and is being used both at medium and high dose rates. Strontium-90/^{90}Y, ^{90}Y and ^{32}P are in use as β emitting sources. Several factors, such as the adequacy of dose delivery, depth of penetration, dose coverage and radiation dose received by attending staff, are considered in the selection of the appropriate radioactive source for this treatment.

A typical treatment prescription dose is 14 Gy at 2 mm from the centre of the source, with the inner surface of the lumen not to exceed a dose of 30 Gy. Measurements and calculations of dose rates at very short distances (<5 mm) from the sources are required for their clinical use.

13.4. DOSE SPECIFICATION AND REPORTING

The prescription of the treatment dose and the reporting of the delivered dose in brachytherapy treatments, using standardized and uniform methodology, have been recommended recently by the ICRU in two separate reports. The intent of these recommendations is to specify the minimum information that must be reported by everyone performing brachytherapy treatments.

These reports give recommendations for the definition of the different volumes of interest, description of the implant and specification of delivered dose. The reference air kerma rate in air (cGy/h at 1 m) is the ICRU recommended quantity for specifying source strength.

13.4.1. Intracavitary treatments

The data recommended in ICRU Report No. 38 for reporting of gynaecological brachytherapy are:

- A description of the technique (source, applicator);
- The total reference air kerma rate;
- The time dose pattern;
- A description of the reference volume;
- The dose at reference points (bladder, rectum, lymphatic trapezoid, pelvic wall).

The major thrust of this report was to identify an absorbed dose level of 60 Gy as the appropriate reference dose level for LDR treatments, resulting in the requirement to specify the dimensions (width, height and thickness) of the pear shaped 60 Gy isodose reference volume. If the treatment also includes some external beam radiotherapy, the reference isodose for brachytherapy is obtained by subtracting the external beam dose from a total dose of 60 Gy.

13.4.2. Interstitial treatments

The dosimetry information recommended in ICRU Report No. 58 for reporting of interstitial implant treatments consists of:

- A description of clinical target volumes.
- The sources, technique and implant time.
- The total reference air kerma.

- A description of the dose: prescription point/surface, prescription dose, reference doses in the central plane, mean central dose and peripheral dose.
- A description of the high and low dose region and dose uniformity indices.
- Dose–volume histograms (DVHs).

The report emphasizes the need to report, as a minimum, four different dose related quantities to adequately describe an implant treatment. In addition to the total reference air kerma, the next significant parameter is the mean central dose, which is representative of the plateau dose region inside the target volume. The minimum dose is important in tumour control — hence the need to report the peripheral dose. To help correlate dose and any late damage, high dose regions (>150% of the mean central dose) and low dose regions (<90% of the peripheral dose) are also to be reported.

13.5. DOSE DISTRIBUTIONS AROUND SOURCES

Dose calculations are presented in this section for photon emitting sources only. The dose calculations are divided into two categories:

- The first category represents the AAPM TG 43 formalism, which can be considered as the most complete formalism available today. This approach is used in modern TPSs and is suitable as a method for commissioning.
- The second category may be used for quick checks and verification of treatment plans.

13.5.1. AAPM TG 43 algorithm

In 1995 the AAPM introduced in TG 43 a dose calculation formalism to establish the 2-D dose distribution around cylindrically symmetric sources. For such sources the dose distribution can be described in terms of a polar coordinate system with its origin at the source centre, where r is the distance from the origin to the point of interest P and θ is the angle with respect to the long axis of the source, as shown in Fig. 13.1. Point $P(r_0, \theta_0)$ is the reference point that lies on the transverse bisector of the source at a distance of 1 cm from the origin (i.e. at $r_0 = 1$ cm and $\theta_0 = \pi/2$).

FIG. 13.1. Geometry used in the calculation of dose distribution near a linear source.

The dose rate $\dot{D}(r,\theta)$ at the point of interest P(r, θ) in water is then written as:

$$\dot{D}(r,\theta) = S_K \Lambda \frac{G(r,\theta)}{G(r_0,\theta_0)} g(r) F(r,\theta) \qquad (13.6)$$

where

r is the distance (cm) from the origin to the point of interest P;

θ is the angle between the direction of radius vector r and the long axis of the source;

θ_0 defines the source transverse plane and is equal to $\pi/2$ radians;

S_K is the air kerma strength of the source ($\mu Gy \cdot m^2 \cdot h^{-1}$);

Λ is the dose rate constant in water;

$G(r, \theta)$ is the geometry function;

$g(r)$ is the radial dose function;

$F(r, \theta)$ is the anisotropy function.

The dose rate constant Λ is defined as the dose rate to water at a distance of 1 cm on the transverse axis per unit air kerma strength source in water:

$$\Lambda = \frac{D(r_0, \theta_0)}{S_K} \tag{13.7}$$

The dose rate constant Λ with units of:

$$\frac{cGy \cdot h^{-1}}{cGy \cdot cm^2 \cdot h^{-1}} = cGy \cdot h^{-1} \cdot U^{-1}$$

(or actually cm^{-2}) includes the effects of source geometry, the spatial distribution of radioactivity within the source encapsulation, self-filtration within the source and scattering in water surrounding the source (1 U = 1 $\mu Gy \cdot m^2 \cdot h^{-1}$ = 1 $cGy \cdot cm^2 \cdot h^{-1}$).

The geometry function $G(r, \theta)$ accounts for the variation of the relative dose due to the spatial distribution of activity within the source. $G(r, \theta)$ reduces to $1/r^2$ for point source approximation and to $\beta/(Lr \sin \theta)$ for a line source approximation with β and L as defined in Fig. 13.1.

The radial dose function $g(r)$ accounts for the effects of attenuation and scatter in water on the transverse plane of the source ($\theta = \pi/2$), excluding fall-off, which is included by the geometry function $G(r, \theta)$. It may also be influenced by filtration of photons by the encapsulation and source materials.

The anisotropy function $F(r, \theta)$ accounts for the anisotropy of dose distribution around the source, including the effects of absorption and scatter in water. $F(r, \theta)$ is defined as unity on the transfer plane; however, its value off the transfer plane decreases: (i) as r decreases; (ii) as θ approaches 0º or 180º; (iii) as the source encapsulation thickness increases; and (iv) as the photon energy decreases.

The dose distributions around brachytherapy sources are calculated assuming photon interactions only, and are influenced by the emitted radiation and the surrounding media. The dose at any point from a single finite source can be considered as a summation of doses from multiple point sources. When the source is in free space, no absorption or scattering effects are present; however, when the source is placed in water, absorption and scatter will influence the dose rate at any point away from the source.

In 2004 the AAPM updated and revised the original TG 43 protocol for calculation of dose rate distributions around photon emitting brachytherapy sources. The updated protocol (TG 43U1) includes the elimination of apparent activity for specification of source strength and a revised definition of the air kerma strength S_K.

The air kerma strength is now defined as the air kerma rate in a vacuum $(\dot{K}_\delta(d))_{\text{vac}}$ and is attributed to all photons of energy larger than a cut-off energy δ at a distance d from the source centre. The distance d can be any distance that is large relative to the maximum dimension of the source and the detector.

The stipulation 'in a vacuum' means that the measurement should be corrected for photon attenuation and scattering in air as well as in encapsulation material and for photon scattering from nearby objects, such as walls, floor and ceiling.

The cut-off energy δ (typically 5 keV) excludes all low energy and contaminating photons that increase $(\dot{K}_\delta(d))_{\text{vac}}$ without contributing to the dose in tissue at distances exceeding 1 mm in tissue.

13.5.2. Other calculation methods for point sources

The formalism given by the AAPM represents an accurate method for absorbed dose calculations for general source geometries. This section presents dose calculation methods for point sources based on knowledge of air kerma in air. Such calculations can be used as convenient methods for checking a treatment plan. Air kerma based methods, as presented here, are also sometimes used in older type TPSs.

With knowledge of the apparent activity $\mathcal{A}_{\text{app}}$ and the air kerma rate constant, the air kerma rate in air at a distance d can be calculated with Eq. (13.3). From knowledge of the air kerma rate in air, the next step is to calculate the air kerma rate in water $(\dot{K}_{\text{air}})_{\text{wat}}$ at the same distance d between the source and the point of interest.

For photon emitting sources with energies at or above those of ^{192}Ir, the ratio $(\dot{K}_{\text{air}})_{\text{wat}}/(\dot{K}_{\text{air}})_{\text{air}}$ is a slowly varying function of the distance and may be represented quite accurately by a polynomial of third or fourth degree, $M(d)$. Thus:

$$(\dot{K}_{\text{air}}(d))_{\text{wat}} = (\dot{K}_{\text{air}}(d))_{\text{air}} M(d) \tag{13.8}$$

Figure 13.2 shows the absorption and scatter correction for two commonly used brachytherapy sources, ^{192}Ir and ^{137}Cs. The curves shown in the figure were calculated with the use of Meisberger polynomials.

The original work by Meisberger assumes that the correction factors are valid at distances between 1 and 10 cm. However, it has been shown that different methods for this correction show relatively large differences at distances above approximately 5 cm.
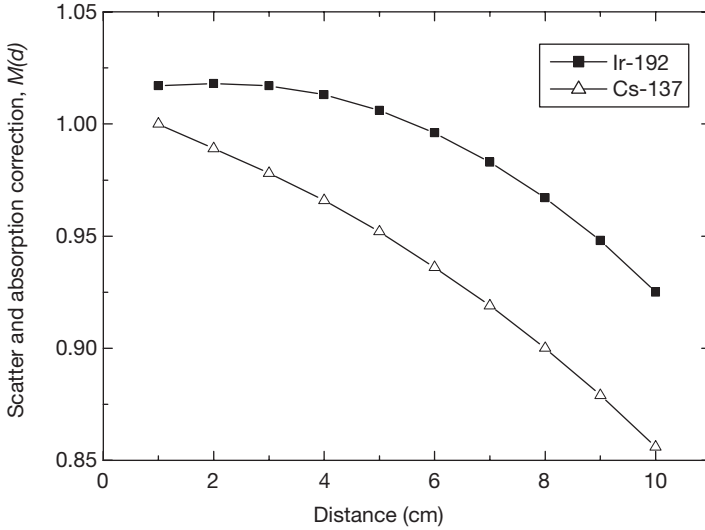
FIG. 13.2. Scatter and absorption corrections for ^{192}Ir and ^{137}Cs.

At first glance, it seems that the radial dose function $g(r)$, as given in the AAPM TG 43 formalism, is identical to the scatter and absorption correction given by $M(d)$ in Eq. (13.8). This, however, is not the case and one should not mix correction factors between different models for dose calculations. The $g(r)$ function is normalized at 1 cm, whereas $M(d)$ is normalized at zero distance.

The water kerma rate in water is related to the air kerma rate in water via the ratio of the mass–energy transfer coefficient:

$$(\dot{K}_{wat})_{wat} = (\dot{K}_{air})_{wat} (\mu_{tr}/\rho)_{air}^{wat} \tag{13.9}$$

For most radionuclides used in brachytherapy with photon energies above 200 keV the ratio of the mass–energy transfer coefficient is almost constant at 1.11; for ^{125}I and ^{103}Pd, however, it is ~1.01.

Finally, the absorbed dose rate to water at a distance d between the source and the point of interest is given by:

$$\dot{D}_{wat} = (\dot{K}_{wat})_{wat} (1 - g) \tag{13.10}$$

where g is the radiative fraction. The radiative fraction is generally ignored, because for the radionuclides used in brachytherapy it is very small (less than 0.3%).

Equation (13.10) can now be written fully as follows:

$$\dot{D}_{wat}(d) = (\dot{K}_{air})_{air} \, M(d)(\mu_{tr}/\rho)_{air}^{wat}(1-g) \tag{13.11}$$

where the distance d is now inserted explicitly.

If the source is calibrated in terms of reference air kerma rate in air $(\dot{K}_{air}(d_{ref}))_{air}$, the air kerma rate in air at the distance d is given by:

$$(\dot{K}_{air}(d))_{air} = (\dot{K}_{air}(d_{ref}))(d_{ref}/d)^2 \tag{13.12}$$

The dose rate can therefore be calculated using the following expression:

$$\dot{D}_{wat}(d) = (\dot{K}_{air}(d_{ref}))_{air} M(d)(\mu_{tr}/\rho)_{air}^{wat}(1-g)(d_{ref}/d)^2 \tag{13.13}$$

For an easy and quick check of the dose at a short distance (e.g. 1 cm) from a single source, the approximations $g = 0$ and $M(d) = 1$ may be made. The dose rate at 1 cm can then be approximated with $\dot{D}(d) \approx (\dot{K}_{air}(d_{ref}))_{air} \times 1.11 \times (1/0.01)^2$.

Note that if the source is specified in terms of reference air kerma rate, there is no need to know the air kerma rate constant. Owing to the uncertainty in the latter constant, proper specification of brachytherapy sources reduces the uncertainty in the calculated dose.

13.5.3. Linear sources

For purposes of dose distribution calculation, linear sources are assumed to consist of a number of point sources, each contributing to the total dose at the point of interest P. Two situations must be considered: the simpler unfiltered line source and the more complicated filtered line source.

13.5.3.1. Unfiltered line source in air

The air kerma rate in air is given by:

$$(\dot{K}_{air})_{air} = \frac{A\Gamma_{AKR}}{Lh}(\theta_2 - \theta_1) \tag{13.14}$$

where

A is the total activity of the line source.
L is the length of the line source.

h is the perpendicular distance between point P and the line source and angles θ_1 and θ_2, as shown in Fig. 13.1, are the integration limits. The angles must be given in radians and not in degrees.

13.5.3.2. Filtered line source in air

The air kerma rate in air is given by:

$$(\dot{K}_{air})_{air} = \frac{A\Gamma_{AKR}}{Lh}\left(\int_0^{\theta_2} e^{-\mu t/\cos\theta}\,\mathrm{d}\theta - \int_0^{\theta_1} e^{-\mu t/\cos\theta}\,\mathrm{d}\theta\right) \qquad (13.15)$$

where

$\displaystyle\int_0^{\theta} e^{-\mu t/\cos\theta}\,\mathrm{d}\theta$ is the Sievert integral accounting for photon attenuation in the source capsule;

t is the thickness of the source capsule;

μ is the attenuation coefficient for photons in the source capsule material, as illustrated in Fig. 13.1.

Sievert integrals are available in tabulated forms, but they may also be solved using numerical methods. For $\theta < 0.35$ radian (20º) the following approximation may be used:

$$\int_0^{\theta} e^{-\mu t/\cos\theta}\,\mathrm{d}\theta \approx \theta e^{-\mu t} \qquad (13.16)$$

It should be noted that the analytic form, as given by the Sievert integral, usually underestimates the air kerma or dose at points along or near the source axis. The reason for this is that the Sievert integral does not account for multiple scattering of photons in the source or its capsule. In the Sievert integral approach, photons emitted from every infinitesimal source element are assumed to be subject to the narrow beam geometry. A far more accurate approach is to use Monte Carlo techniques for the calculation of filtration effects.

13.5.3.3. Filtered line source in water

The dose rate at point P in water $\dot{D}_w(d,\theta)$ for a filtered line source may now be stated as:

$$\dot{D}_w(d,\theta) = \frac{A\Gamma_{AKR}}{Lh}\left(\int_0^{\theta_2} e^{-\mu t/\cos\theta} M(d,\theta)\mathrm{d}\theta - \int_0^{\theta_1} e^{-\mu t/\cos\theta} M(d,\theta)\mathrm{d}\theta\right)$$

$$\times \left(\frac{\mu_{tr}}{\rho}\right)_{air}^w (1-g) \qquad (13.17)$$

where

$M(d, \theta)$ is the absorption and scatter correction varying over the source length;
d is the distance between point P and the source segment.

The integrals of Eq. (13.17) can be readily calculated with computer algorithms that carry out the calculations by summation over a large number of source segments.

13.6. DOSE CALCULATION PROCEDURES

13.6.1. Manual dose calculations

13.6.1.1. Manual summation of doses

As a first approximation, each source can be assumed to be a point source if the distance between the dose calculation point and the source centre is at least twice the active length of the source. The total dose at any point will be a summation of the doses from each individual source. For most seed sources (~3 mm length) this approximation is good to within 5% at distances larger than 5 mm. For linear sources (~2 cm length) precalculated tables should be used to calculate the dose at points close to the source (0.5–5 cm).

13.6.1.2. Precalculated dose distributions (atlases)

For some clinical situations, in which the arrangement of sources for the required implant follows a standard pattern (linear array, tandem and ovoids,

vaginal cylinder), precalculated dose distributions (available in atlases) may be used with the appropriate scaling of source strength (activity).

13.6.2. Computerized treatment planning

13.6.2.1. Source localization

Accurate calculation of dose distributions is possible only if the position coordinates of each source with respect to an arbitrary origin can be accurately established. The impact of the inverse square distance factor in calculating dose is dominant at short distances. Source localization can be established by the use of one of several radiographic methods:

- Two orthogonal films;
- Two stereoshift films;
- Two/three isocentric films;
- CT.

It is usually difficult and very time consuming to perform manual matching of sources, especially when large numbers of seeds are used. Several automatic matching algorithms are now available in most brachytherapy TPSs.

13.6.2.2. Dose calculation

Basic dose calculation algorithms use the point source model and/or the line source model. In most instances the computation is based on a table look-up of 2-D precalculated doses for standard length linear sources and summation of the contribution from each source. For seed implants it is usual to use the point source 1-D approximation for each source. New dose calculation algorithms are now in use based on the AAPM TG 43 formalism for linear sources.

13.6.2.3. Dose distribution display

The most common display is a 2-D distribution of dose in a single cross-sectional plane, usually the central plane that contains or is close to the centres of most sources. Since the calculation is performed for a matrix of points in 3-D, it is possible to display 2-D distributions in any arbitrary plane. The display usually includes isodose rate lines, the target of interest and the location of the sources.

Three dimensional calculations offer improved analysis of dose distributions with respect to target volume coverage and the dose to normal tissues. The calculated dose values are used to display isodose surfaces and also to calculate and display DVHs.

Three dimensional displays of dose distributions offer a major advantage in their ability to help visualize dose coverage in 3-D, as seen from any orientation.

13.6.2.4. Optimization of dose distribution

Optimization of dose distribution in brachytherapy is usually achieved by establishing the relative spatial or temporal distribution of the sources and by weighting the strength of individual sources. The results of any optimization depend heavily on the number of points selected for the dose calculation and their relative locations.

The current optimization approaches fall into one of the following categories:

- Source distribution rules;
- Geometry;
- Specified dose points;
- Trial and adjustment.

In most instances, when computer algorithms are not available, optimization is performed by trial and adjustment. Optimization in HDR and PDR treatment planning, where a single stepping source is used, involves manipulation of the source dwell positions and the relative dwell times to produce the desired result. Most optimization methods in current use are analytic, in that the solutions come from equations. Another approach uses random search techniques in which the performance of a system is made to improve, as determined by an objective function.

13.6.3.   Calculation of treatment time

13.6.3.1. Use of Patterson–Parker tables

The original Patterson–Parker (Manchester system) tables for planar and volume implants relate the treatment time required to deliver a certain dose with the area or volume of an implant. The area or volume of the implant has to be established from orthogonal radiographs. Corrections need to be made for uncrossed ends in determining the treated area or volume. Treatment time is

calculated from knowing the total activity used in the implant and the cumulative source strength (total reference air kerma) required to deliver the prescribed dose.

13.6.3.2. Choice of reference points

The choice of the reference points for the calculation of treatment dose rates and dose should follow, if possible, the ICRU recommendations. In general, the points are representative of the target volume and other tissues of interest. The dose prescription point is usually representative of the periphery of the target volume.

13.6.3.3. Decay corrections

In calculating the total dose delivered in the time duration of the implant, one must consider the exponential decay of the source activity. The cumulative dose D_{cum} delivered in time t is given by:

$$D_{cum} = \dot{D}_0 \int_0^t e^{-\lambda t} dt = \frac{\dot{D}_0}{\lambda}(1 - e^{-\lambda t}) = 1.44 t_{1/2} \dot{D}_0 (1 - e^{-(\ln 2)t/t_{1/2}}) \qquad (13.18)$$

where

$\dot{D}_0$ is the initial dose rate;
λ is the decay constant of the source equal to $\lambda = (\ln 2)/t_{1/2}$;
$t_{1/2}$ is the half-life of the source.

If the treatment time t is very short in comparison with the half-life $t_{1/2}$ (i.e. $t \ll t_{1/2}$), then $\exp[-(\ln 2)t/t_{1/2}] \approx 1 + (\ln 2)t/t_{1/2}$ in Eq. (13.18) and:

$$D_{cum} = \dot{D}_0 t \qquad (13.19)$$

For permanent implants $t = \infty$ in Eq. (13.18) and the following relationship is used to determine the cumulative dose (to complete source decay):

$$D_{cum} = \dot{D}_0/\lambda = 1.44 t_{1/2} \dot{D}_0 \qquad (13.20)$$

where $\dot{D}_0$ again is the initial dose rate.

13.7. COMMISSIONING OF BRACHYTHERAPY COMPUTER TREATMENT PLANNING SYSTEMS

13.7.1. Check of the reconstruction procedure

Besides the computer, the major hardware devices associated with a planning system are the digitizer and the plotter. Their accuracy should be routinely checked. Simple test cases with a small number of sources placed in a known geometry, as seen on two orthogonal radiographs, should be run to check the accuracy of source reconstruction. The verification test should include translation from film to Cartesian coordinates, rotations and corrections for magnification.

13.7.2. Check of consistency between quantities and units

A major source of error in dose distribution calculations is the incorrect use of quantities and units as required by the dose calculation software. It is essential to verify the correct labelling of the input and output quantities and units. The strength of the sources (activity) may be specified in one of several alternative units, and the user should pay particular attention to this important parameter. An inconsistent use of units for this parameter could lead to serious errors in treatment.

13.7.3. Computer versus manual dose calculation for a single source

The computer calculated dose distribution around a linear source should be compared with published dose rate values for a similar source or to the Sievert integral. When comparing with the Sievert integral, scatter and attenuation corrections should not be included. Additional tests should include:

- The inverse square law for point sources;
- Summing of the dose for multiple sources;
- Scaling of the dose rate with source strength;
- Scaling of the dose with time.

13.7.4. Check of decay corrections

Computer calculations of dose rates at specific times within the duration of the implant should be verified with manual calculations. Similarly, the

computer calculated dose to total decay for permanent implants should be verified. A proper choice of units should be made for these calculations.

13.8. SOURCE COMMISSIONING

13.8.1. Wipe tests

A package containing a shipment of a radionuclide must be monitored immediately upon receipt for any physical damage or excessive radiation levels. Wipe tests for any contamination should be carried out on the package surface. Radiation levels should be measured and recorded both at the surface and at 1 m distance.

Individual encapsulated sources should be wipe tested for possible leakage or contamination. This should be performed at the time of receipt of new sources and at six monthly intervals for sources with a long half-life that are kept in the permanent inventory. A source is considered to be leaking if ~200 Bq (~5 nCi) of removable contamination is measured. The measurement is usually performed using a sensitive scintillation well counter.

13.8.2. Autoradiography and uniformity checks of activity

Radiography and autoradiography using a single film exposure with a simulator can be used to check the uniform distribution of the radioactive material within an encapsulated source. The film is scanned with a densitometer to determine isodensity and isodose profiles. Autoradiographs are useful to check a batch of seeds or ribbons with seeds, for both uniformity of activity and for presence of any inadvertent 'cold' (non-radioactive) seeds.

13.8.3. Calibration chain

It is recommended that brachytherapy sources have their source strength calibrations traceable to a national standards laboratory. In some instances it may be necessary to establish a second level of traceability by comparison with the same type of calibrated source. These comparison calibrations are best done in a well type ionization chamber. Re-entrant or well type ionization chambers are convenient for calibration of either high or low strength sources.

Calibrated stem type ionization chambers may also be used for the measurement of high strength sources. Most standards laboratories will calibrate these chambers for different quality radiations, and an interpolation or extrapolation method is then used to obtain the calibration factor for a given

radioisotope source; for example, a calibration coefficient for ^{192}Ir is obtained as the mean between the calibration factors for 250 kV orthovoltage X rays and ^{60}Co γ rays. The activity of all sources should be measured on receipt with a local dosimeter and compared with the manufacturer's certificate of source strength.

13.9. QUALITY ASSURANCE

13.9.1. Constancy check of a calibrated dosimeter

The constancy of the response of the calibrated dosimeter system may be checked by periodic measurement of a long half-life source, such as ^{137}Cs in the case of a well type chamber. It is necessary to use a special source holder that will position the check source in a reproducible manner, since the ionization chamber response is very dependent on source position and orientation. This periodic measurement also provides a good quality assurance check of the entire measuring system.

13.9.2. Regular checks of sources and applicators

13.9.2.1. Mechanical properties

The mechanical integrity of a source must be checked at regular intervals by visual inspection, leak testing and activity measurement. Applicators, because of their repeated clinical use, undergo severe handling, cleaning and sterilization. Visual inspection and radiographic evaluation of all applicators should be performed at some pre-established frequency. For gynaecological applicators it is necessary to check that the assembly is structurally sound, that all clamps, screws and retaining devices are functioning properly and that the source insert carriers seat correctly in the colpostats.

13.9.2.2. Source strength

Long half-life sources maintained within a permanent inventory should be checked at some established frequency for their change in source strength (activity) with time. Calculated values, often obtained by decaying a prior calibration, should be compared with measurements. Short half-life sources, used either in temporary or permanent implants, should have their activity measured at the time of receipt and compared with the manufacturer's value.

13.9.2.3. Wipe tests

All sources that are maintained in a permanent inventory are required to be wipe tested for any leakage of radiation. The frequency of leak testing is usually on a semi-annual basis.

13.9.3. Checks of source positioning with afterloading devices

The position of sources placed within afterloading devices can be determined with autoradiographs. It is necessary to check that the unit will position the source with millimetre accuracy at predetermined programmed positions along treatment catheters. The use of appropriate radiographic markers and combination of a radiographic image with an autoradiograph is a convenient method for checking source positioning.

13.9.4. Radiation monitoring around patients

After implantation of sources in a patient, a radiation survey must be performed in areas within and around the patient's room. Radiation levels should be measured and recorded so as to assist in maintaining minimum exposure of hospital staff and visitors. The radiation levels in adjoining patients' rooms should be very low, such that no individual would receive more than 0.2 mSv in any one hour.

Prior to release of an implant patient from hospital, the patient and the room must be surveyed. For temporary implants a survey must be done upon removal of the sources so as to confirm removal of all sources. Patients with permanent implants may be discharged from the hospital if at the time of discharge the radiation level at 1 m is less than 0.5 mSv/h.

13.9.5. Quality management programme

All facilities performing brachytherapy procedures should have in place some form of a quality management programme, with well defined objectives, to ensure compliance with standard good practices. The programme should include written procedures for prescribing, recording and documenting each treatment. Most programmes have as their main objectives:

● The preparation of a physician's written directive before administration of treatment;
● Clear identification of the patient;
● Documentation of treatment and related calculations;

- Compliance of each treatment with the written directive;
- The identification and evaluation of any unintended deviation from the prescription.

13.10. BRACHYTHERAPY VERSUS EXTERNAL BEAM RADIOTHERAPY

Brachytherapy is an important modality in the treatment of malignant disease; a modality that allows conformal treatment without heavy technological involvement. However, since it generally involves invasive procedures (interstitial brachytherapy), except for special instances in which intracavitary techniques may be employed, brachytherapy is relegated to second place behind external beam radiotherapy in the treatment of malignant disease. A typical radiation oncology department will treat about 80% of its patients with the various external beam techniques and about 10–20% of its patients with brachytherapy. The basic principles of brachytherapy have not changed much during the past 100 years of radiotherapy; however, the advent of remote afterloading brachytherapy has made brachytherapy much more efficient for the patient and safer for staff from the radiation protection point of view. In terms of physics human resource needs, a brachytherapy patient requires considerably more involvement than an average external beam patient.

Nearly every malignant disease in the human body has been treated with brachytherapy; however, gynaecological cancer treatments provide the greatest success and permanent prostate implants are becoming increasingly common. There are also various sites for which brachytherapy has proven a complete failure. The newest application of brachytherapy is intravascular (also referred to as endovascular) brachytherapy, used for the prevention of restenosis in arteries following coronary arterial angioplasty.

BIBLIOGRAPHY

AIRD, E.G., WILLIAMS, J.R., REMBOWSKA, A., "Brachytherapy", Radiotherapy Physics in Practice (WILLIAMS, J.R., THWAITES, D.I., Eds), Oxford Univ. Press, Oxford (2000).

AMERICAN ASSOCIATION OF PHYSICISTS IN MEDICINE, Dosimetry of interstitial brachytherapy sources: Recommendations of the AAPM Radiation Therapy Committee Task Group No. 43, Med. Phys. **22** (1995) 209–239.

— Update of AAPM Task Group No. 43 Report: A revised AAPM protocol for brachytherapy dose calculations, Med. Phys. **31** (2004) 633–674.

GLASGOW, G.P., "Brachytherapy", Modern Technology in Radiation Oncology: A Compendium for Teachers and Students (VAN DYK, J., Ed.), Medical Physics Publishing, Madison, WI (1999).

INTERNATIONAL ATOMIC ENERGY AGENCY, Calibration of Photon and Beta Ray Sources Used in Brachytherapy, IAEA-TECDOC-1274, IAEA, Vienna (2002).

INTERNATIONAL COMMISSION ON RADIATION UNITS AND MEASUREMENTS, Dose and Volume Specification for Reporting Intracavitary Therapy in Gynecology, Rep. 38, ICRU, Bethesda, MD (1985).

— Dose and Volume Specification for Reporting Interstitial Therapy, Rep. 58, Bethesda, MD (1997).

INTERSTITIAL COLLABORATIVE WORKING GROUP, Interstitial Brachytherapy: Physical, Biological, and Clinical Considerations, Raven, New York (1990).

JOHNS, H.E., CUNNINGHAM, J.R., The Physics of Radiology, Thomas, Springfield, IL (1984) Ch. 13.

KHAN, F.M., The Physics of Radiation Therapy, Lippincott, Williams and Wilkins, Baltimore, MD (2003) Ch. 15.

PIERQUIN, B., MARINELLO, G., A Practical Manual of Brachytherapy, Medical Physics Publishing, Madison, WI (1997).

WILLIAMSON, J.F., THOMADSEN, B.R., NATH, R. (Eds), Brachytherapy Physics (AAPM 1994 Summer School), Medical Physics Publishing, Madison, WI (1994).

Chapter 14

BASIC RADIOBIOLOGY

N. SUNTHARALINGAM
Department of Radiation Oncology,
Thomas Jefferson University Hospital,
Philadelphia, Pennsylvania,
United States of America

E.B. PODGORSAK
Department of Medical Physics,
McGill University Health Centre,
Montreal, Quebec, Canada

J.H. HENDRY
Division of Human Health,
International Atomic Energy Agency,
Vienna

14.1. INTRODUCTION

Radiobiology, a branch of science concerned with the action of ionizing radiation on biological tissues and living organisms, is a combination of two disciplines: radiation physics and biology. All living things are made up of protoplasm, which consists of inorganic and organic compounds dissolved or suspended in water. The smallest unit of protoplasm capable of independent existence is the cell.

Cells contain inorganic compounds (water and minerals) as well as organic compounds (proteins, carbohydrates, nucleic acids and lipids). The two main constituents of a cell are the cytoplasm, which supports all metabolic functions within the cell, and the nucleus, which contains the genetic information (DNA).

Human cells are either somatic cells or germ cells.

Cells propagate through division: division of somatic cells is called mitosis, while division of germ cells is called meiosis. When a somatic cell divides, two cells are produced, each carrying a chromosome complement identical to that of the original cell. The new cells themselves may undergo further division, and the process continues.

Somatic cells are classified as:

- Stem cells, which exist to self-perpetuate and produce cells for a differentiated cell population (e.g. stem cells of the haematopoietic system, epidermis and mucosal lining of the intestine);
- Transit cells, which are cells in movement to another population (e.g. a reticulocyte that is differentiating to become an erythrocyte);
- Mature cells, which are fully differentiated and do not exhibit mitotic activity (e.g. muscle cells and nervous tissue).

A group of cells that together perform one or more functions is referred to as tissue. A group of tissues that together perform one or more functions is called an organ. A group of organs that perform one or more functions is a system of organs or an organism.

14.2. CLASSIFICATION OF RADIATIONS IN RADIOBIOLOGY

For use in radiobiology and radiation protection the physical quantity that is useful for defining the quality of an ionizing radiation beam is the linear energy transfer (LET). In contrast to the stopping power, which focuses attention on the energy loss by an energetic charged particle moving through a medium, the LET focuses attention on the linear rate of energy absorption by the absorbing medium as the charged particle traverses the medium.

The ICRU defines the LET as follows:

"*LET of charged particles in a medium is the quotient dE/dl, where dE is the average energy locally imparted to the medium by a charged particle of specified energy in traversing a distance of dl.*"

In contrast to the stopping power, which has a typical unit of MeV/cm, the unit usually used for the LET is keV/μm. The energy average is obtained by dividing the particle track into equal energy increments and averaging the length of track over which these energy increments are deposited.

Typical LET values for commonly used radiations are:

- 250 kVp X rays: 2 keV/μm.
- Cobalt-60 γ rays: 0.3 keV/μm.
- 3 MeV X rays: 0.3 keV/μm.
- 1 MeV electrons: 0.25 keV/μm.

LET values for other, less commonly used radiations are:

— 14 MeV neutrons: 12 keV/μm.
— Heavy charged particles: 100–200 keV/μm.
— 1 keV electrons: 12.3 keV/μm.
— 10 keV electrons: 2.3 keV/μm.

X rays and γ rays are considered low LET (sparsely ionizing) radiations, while energetic neutrons, protons and heavy charged particles are high LET (densely ionizing) radiations. The demarcation value between low and high LET is at about 10 keV/μm.

14.3. CELL CYCLE AND CELL DEATH

The cell proliferation cycle is defined by two well defined time periods:

● Mitosis (M), where division takes place;
● The period of DNA synthesis (S).

The S and M portions of the cell cycle are separated by two periods (gaps) G_1 and G_2 when, respectively, DNA has not yet been synthesized or has been synthesized but other metabolic processes are taking place.

The time between successive divisions (mitoses) is called the cell cycle time. For mammalian cells growing in culture the S phase is usually in the range of 6–8 h, the M phase less than an hour, G_2 is in the range of 2–4 h and G_1 is 1–8 h, making the total cell cycle of the order of 10–20 h. In contrast, the cell cycle for stem cells in certain tissues is up to about 10 days.

In general, cells are most radiosensitive in the M and G_2 phases, and most resistant in the late S phase.

The cell cycle time of malignant cells is shorter than that of some normal tissue cells, but during regeneration after injury normal cells can proliferate faster.

Cell death of non-proliferating (static) cells is defined as the loss of a specific function, while for stem cells and other cells capable of many divisions it is defined as the loss of reproductive integrity (reproductive death). A surviving cell that maintains its reproductive integrity and proliferates almost indefinitely is said to be clonogenic.

14.4. IRRADIATION OF CELLS

When cells are exposed to ionizing radiation the standard physical effects between radiation and the atoms or molecules of the cells occur first and the possible biological damage to cell functions follows later. The biological effects of radiation result mainly from damage to the DNA, which is the most critical target within the cell; however, there are also other sites in the cell that, when damaged, may lead to cell death. When directly ionizing radiation is absorbed in biological material, the damage to the cell may occur in one of two ways: direct or indirect.

14.4.1. Direct action in cell damage by radiation

In direct action the radiation interacts directly with the critical target in the cell. The atoms of the target itself may be ionized or excited through Coulomb interactions, leading to the chain of physical and chemical events that eventually produce the biological damage. Direct action is the dominant process in the interaction of high LET particles with biological material.

14.4.2. Indirect action in cell damage by radiation

In indirect action the radiation interacts with other molecules and atoms (mainly water, since about 80% of a cell is composed of water) within the cell to produce free radicals, which can, through diffusion in the cell, damage the critical target within the cell. In interactions of radiation with water, short lived yet extremely reactive free radicals such as H_2O^+ (water ion) and OH• (hydroxyl radical) are produced. The free radicals in turn can cause damage to the target within the cell.

The free radicals that break the chemical bonds and produce chemical changes that lead to biological damage are highly reactive molecules because they have an unpaired valence electron.

About two thirds of the biological damage by low LET radiations (sparsely ionizing radiations) such as X rays or electrons is due to indirect action.

Indirect action can be modified by chemical sensitizers or radiation protectors.

The steps involved in producing biological damage by the indirect action of X rays are as follows:

- Step 1: Primary photon interaction (photoelectric effect, Compton effect and pair production) produces a high energy electron.

● Step 2: The high energy electron in moving through tissue produces free radicals in water.
● Step 3: The free radicals may produce changes in DNA from breakage of chemical bonds.
● Step 4: The changes in chemical bonds result in biological effects.

Step (1) is in the realm of physics; step (2) is in chemistry; steps (3) and (4) are in radiobiology.

14.4.3. Fate of irradiated cells

Irradiation of a cell will result in one of the following nine possible outcomes:

● No effect.
● Division delay: The cell is delayed from going through division.
● Apoptosis: The cell dies before it can divide or afterwards by fragmentation into smaller bodies, which are taken up by neighbouring cells.
● Reproductive failure: The cell dies when attempting the first or subsequent mitosis.
● Genomic instability: There is a delayed form of reproductive failure as a result of induced genomic instability.
● Mutation: The cell survives but contains a mutation.
● Transformation: The cell survives but the mutation leads to a transformed phenotype and possibly carcinogenesis.
● Bystander effects: An irradiated cell can send signals to neighbouring unirradiated cells and induce genetic damage in them.
● Adaptive responses: The irradiated cell is stimulated to react and become more resistant to subsequent irradiation.

14.5. TYPE OF RADIATION DAMAGE

14.5.1. Timescale

The timescale involved between the breakage of chemical bonds and the biological effect may be hours to years, depending on the type of damage.

If cell kill is the result, it may happen in hours to days, when the damaged cell attempts to divide (early effects of radiation). This can result in early tissue reactions (deterministic effects) if many cells are killed.

If the damage is oncogenic (cancer induction), then its expression may be delayed for years (late effects of radiation). Ionizing radiation has been proven to cause leukaemia and has been implicated in the development of many other cancers in tissues such as bone, lung, skin, thyroid and breast.

In addition to carcinogenesis (induction of cancer), the late effects of radiation include: delayed tissue reactions (deterministic effects) such as fibrosis and other reactions mediated by vascular deficiencies; life span shortening (due largely to cancer lethalities); genetic damage, where the effects may be expressed in subsequent generations; and potential effects to the foetus.

14.5.2. Classification of radiation damage

Radiation damage to mammalian cells is divided into three categories:

- Lethal damage, which is irreversible, irreparable and leads to cell death;
- Sublethal damage, which can be repaired in hours unless additional sublethal damage is added that eventually leads to lethal damage;
- Potentially lethal damage, which can be manipulated by repair when cells are allowed to remain in a non-dividing state.

14.5.3. Somatic and genetic effects

The effects of radiation on the human population can be classified as either somatic or genetic:

- Somatic effects are harm that exposed individuals suffer during their lifetime, such as radiation induced cancers (carcinogenesis), sterility, opacification of the eye lens and life shortening.
- Genetic or hereditary effects are radiation induced mutations to an individual's genes and DNA that can contribute to the birth of defective descendants.

Carcinogenesis expresses itself as a late somatic effect in the form of acute or chronic myeloid leukaemia or some solid tumours, for example in the skin, bone, lung, thyroid or breast. Human data on carcinogenesis have been collected from the following sources:

— Low level occupational exposure;
— Atomic bomb survivors in Hiroshima and Nagasaki;
— Medical radiation exposure of patients (e.g. during treatment of ankylosing spondylitis, treatment of thyroid abnormalities and radio-

therapy of cancer) and staff (e.g. radiologists in the early part of the last century).

14.5.4. Stochastic and deterministic (non-stochastic) effects

The harmful effects of radiation may be classified into two general categories: stochastic and deterministic (previously called non-stochastic). The National Council on Radiation Protection and Measurements (NCRP) defines these effects as follows:

- A stochastic effect is one in which the probability of occurrence increases with increasing dose but the severity in affected individuals does not depend on the dose (induction of cancer, radiation carcinogenesis and genetic effects). There is no threshold dose for effects that are truly stochastic, because these effects arise in single cells and it is assumed that there is always some small probability of the event occurring even at very small doses.
- A deterministic effect (tissue reaction) is one that increases in severity with increasing dose, usually above a threshold dose, in affected individuals (organ dysfunction, fibrosis, lens opacification, blood changes and decrease in sperm count). These are events caused by damage to populations of cells, hence the presence of a threshold dose.

14.5.5. Acute versus late tissue or organ effects

An organ or tissue expresses response to radiation damage either as an acute effect or as a late (chronic) effect.

Acute effects manifest themselves soon after exposure to radiation and are characterized by inflammation, oedema, denudation of epithelia and haemopoietic tissue, and haemorrhage. Late effects are delayed and are, for example, fibrosis, atrophy, ulceration, stenosis or obstruction of the intestine. Late effects may be generic and caused by absorption of radiation directly in the target tissue, or consequential to acute damage in overlying tissues such as mucosa or the epidermis.

14.5.6. Total body radiation response

The response of an organism to acute total body radiation exposure is influenced by the combined response to radiation of all organs constituting the organism. Depending on the actual total body dose above 1 Gy, the response is described as a specific radiation syndrome:

● 1 Gy < dose < 10 Gy: bone marrow syndrome.
● 10 Gy < dose < 100 Gy: gastrointestinal syndrome.
● Dose > 100 Gy: central nervous system syndrome.

Human data on specific radiation syndromes have been collected from the following sources:

— Accidents in industry and research laboratories;
— Exposure to radioactive fallout from the testing of nuclear weapons or the Chernobyl nuclear power plant accident;
— Exposure of humans to high levels of radiation in Hiroshima and Nagasaki;
— Medical exposure of humans to total body irradiations (TBIs).

14.5.7. Foetal irradiation

Between conception and birth the foetus passes through three basic stages of development:

● Pre-implantation (day 1 to 10);
● Organogenesis (day 11 to 42);
● Growth stage (day 43 to birth).

Radiation is a known teratogen (i.e. it causes birth defects). The effects of radiation on the foetus depend on two factors: the dose and the stage of development at the time of exposure. The principal effects of radiation on a foetus are foetal or neonatal death, malformations, growth retardation, congenital defects and cancer induction.

An abortion to avoid the possibility of radiation induced congenital abnormalities should be considered only when the foetal dose has exceeded 10 cGy.

14.6. CELL SURVIVAL CURVES

A cell survival curve describes the relationship between the surviving fraction of cells (i.e. the fraction of irradiated cells that maintain their reproductive integrity (clonogenic cells)) and the absorbed dose. Cell survival as a function of radiation dose is graphically represented by plotting the surviving fraction on a logarithmic scale on the ordinate against dose on a linear scale on the abscissa.

Cell surviving fractions are determined with in vitro or in vivo techniques. Examples of survival curves for cells irradiated by densely and sparsely ionizing radiation beams are shown in Fig. 14.1.

The type of radiation influences the shape of the cell survival curve. Densely ionizing radiations exhibit a cell survival curve that is almost an exponential function of dose, shown by an almost straight line on the log–linear plot. For sparsely ionizing radiation, however, the curves show an initial slope followed by a shoulder region and then become nearly straight at higher doses. Factors that make cells less radiosensitive are: removal of oxygen to create a hypoxic state, the addition of chemical radical scavengers, the use of low dose rates or multifractionated irradiation, and cells synchronized in the late S phase of the cell cycle.

Several mathematical methods of varying degrees of complexity have been developed to define the shape of cell survival curves, all based on the concept of the random nature of energy deposition by radiation.

The linear quadratic model is now most often used to describe the cell survival curve, assuming that there are two components to cell kill by radiation (Fig. 14.1(b)):

$$S(D) = e^{-\alpha D - \beta D^2} \qquad\qquad (14.1)$$

where

$S(D)$ is the fraction of cells surviving a dose D;

α is a constant describing the initial slope of the cell survival curve;

β is a smaller constant describing the quadratic component of cell killing.

The ratio α/β gives the dose at which the linear and quadratic components of cell killing are equal (8 Gy in the example shown in Fig. 14.1(b)).

For completeness, the earlier multitarget single hit model described the slope of the survival curve by D_0 (the dose to reduce survival to 37% of its value at any point on the final near exponential portion of the curve) and the extrapolation number n (the point of intersection of the slope on the log survival axis). D_q was the quasi-threshold dose. However, this model (Fig. 14.1(a)) does not have any current biological basis.
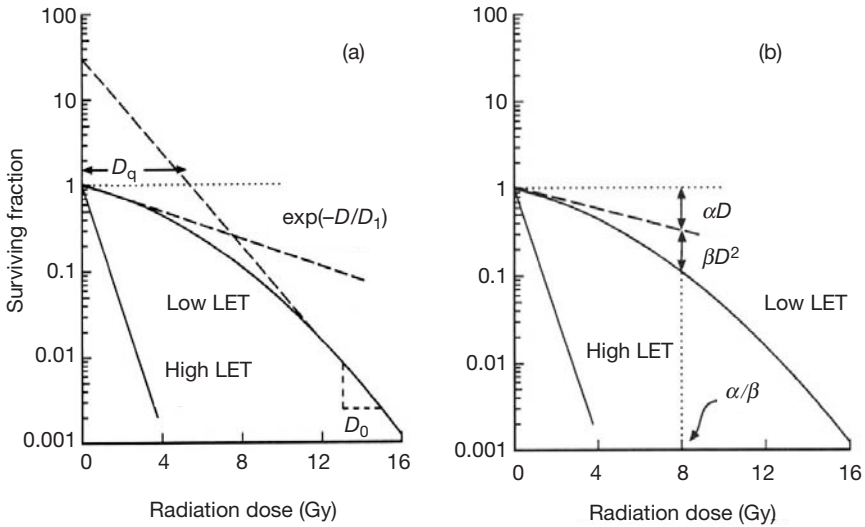
FIG. 14.1. Typical cell survival curves for high LET (densely ionizing) radiation and low LET (sparsely ionizing) radiation. (a) The earlier multitarget single hit model; (b) the current linear quadratic model.

14.7. DOSE RESPONSE CURVES

A plot of a biological effect observed (e.g. tumour induction or tissue response) against the dose given is called a dose response curve. Generally, as dose increases so does the effect.

Three types of dose response relationship are known:

- Linear;
- Linear quadratic;
- Sigmoid.

Dose response curves may or may not have a threshold. A threshold dose is the largest dose for a particular effect studied below which no effect will be observed.

Various dose response curves are shown in Fig. 14.2, with:

— A linear relationship with no threshold;
— A linear relationship with a threshold;
— A linear quadratic relationship with no threshold;
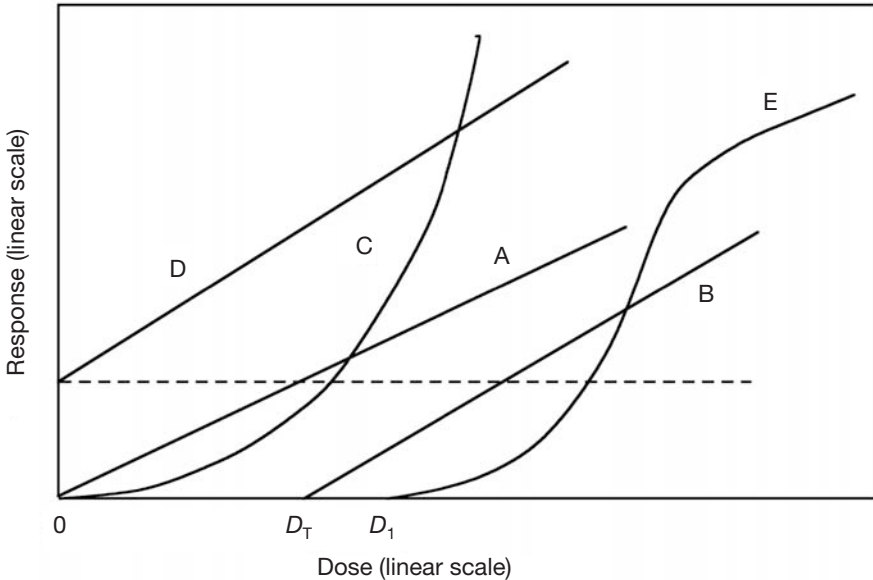
FIG. 14.2. Typical dose response curves for cancer induction (curves A, B, C and D) and for tissue response (curve E). Curve A represents a linear relationship with no threshold; curve B represents a linear relationship with threshold D_T; curve C represents a linear quadratic relationship with no threshold (assumed for stochastic effects, for example carcinogenesis); curve D represents a linear relationship with no threshold (the area below the dashed line represents the natural incidence of the effect, for example carcinogenesis); and curve E represents a sigmoid relationship with threshold D_1, as is common for deterministic effects in tissues, for example tumour control or treatment morbidity. The curves are diagrammatic only and are separated for clarity (in practice the dashed line would be lower).

— A linear relationship (the area below the dashed line indicates the natural incidence of the effect);
— A sigmoid relationship with a threshold.

The response of different tissues or organs to radiation varies markedly, depending primarily on two factors: the inherent sensitivity of the individual cells and the kinetics of the population.

There is a clear distinction in radiation response between tissues that are early responding (skin, mucosa and intestinal epithelium) and those that are late responding (spinal cord), as shown schematically in Fig. 14.3 for the surviving fraction against the dose.

The cell survival curves for late responding tissues are more curved than those for early responding tissues. For early effects the ratio α/β is large and

495
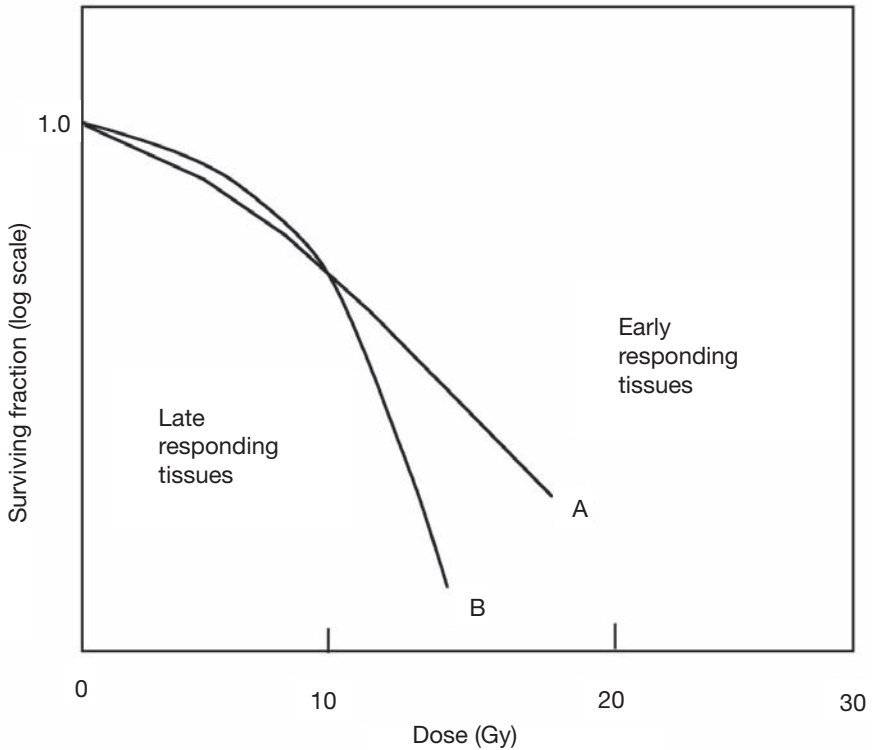
FIG. 14.3. Hypothetical target cell survival curves for (curve A) early responding tissues and (curve B) late responding tissues.

α dominates at low doses. For late effects α/β is small and β has an influence at doses lower than for early responding tissues. The α and β components of mammalian cell killing are equal at approximately $\alpha/\beta = 10$ Gy and $\alpha/\beta = 3$ Gy for early and late effects, respectively.

14.8. MEASUREMENT OF RADIATION DAMAGE IN TISSUE

The effects of radiation on tissue as a function of dose are measured with assays and the measurement results are given in the form of cell survival curves or dose response curves. Three categories of tissue assay are in use:

- Clonogenic assays measure the reproductive integrity of the clonogenic stem cells in tissue, and the measurements result in cell survival curves.

- Functional assays measure functional end points for various tissues and produce dose response curves in which the response is measured on a graded reaction scale or expressed as a proportion of cases in which reactions are greater than a specified level.
- Lethality assays quantify the number of animal deaths after irradiation of the whole animal or of a specific organ with a given dose. The experiments usually result in deduced values of the parameter LD50, where LD stands for 'lethal dose', defined as the dose to animals or to a specific organ of animals that kills 50% of the animals.

14.9. NORMAL AND TUMOUR CELLS: THERAPEUTIC RATIO

The aim of radiotherapy is to deliver enough radiation to the tumour to destroy it without irradiating normal tissue to a dose that will lead to serious complications (morbidity). As shown in Fig. 14.4, the principle is usually illustrated by plotting two sigmoid curves, one for the tumour control probability (TCP) (curve A) and the other for the normal tissue complication probability (NTCP) (curve B).
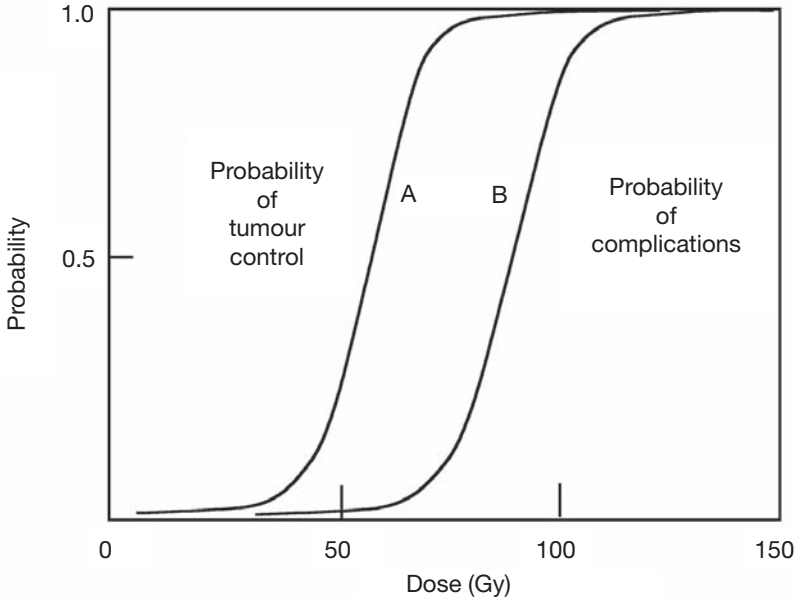
FIG. 14.4. The principle of therapeutic ratio. Curve A represents the TCP, curve B the probability of complications. The total clinical dose is usually delivered in 2 Gy fractions.

The optimum choice of radiation dose delivery technique in the treatment of a given tumour is such that it maximizes the TCP and simultaneously minimizes the NTCP. For a typical good radiotherapy treatment, TCP ≥ 0.5 and NTCP ≤ 0.05.

The further curve B (NTCP) is to the right of curve A (TCP) in Fig. 14.4, the easier it is to achieve the radiotherapeutic goal, the larger is the therapeutic ratio and the less likely will it be that the treatment causes complications. The therapeutic ratio generally refers to the ratio of the TCP and NTCP at a specified level of response (usually 0.05) for normal tissue.

Figure 14.4 shows an ideal situation; in reality, the TCP curve is often shallower than the NTCP curve, partly because tumours are more heterogeneous than normal tissues. Moreover, the TCP curve for regional control of certain tumours never reaches a value of 1.0, as a result of microscopic or metastatic spread of the disease beyond the primary tumour site. It is imperative that the average doses to normal tissues be kept lower than the doses to tumours in order to minimize treatment complications and optimize treatment outcomes. In modern radiotherapy this is achieved through sophisticated 3-D treatment planning (forward or inverse) and dose delivery (conformal or intensity modulated).

In the early days of radiotherapy it was usually assumed that normal cells were less sensitive to single doses of radiation than tumour cells; however, currently it is accepted that both malignant cells and those normal cells responsible for early reactions exhibit similar values (albeit with individual variations) for D_0 of around 1.3 Gy, with α/β of about 10 Gy.

It is for late reactions in general that the shoulder on the target cell survival curve is effectively greater than it is for target cells in tumours or early reacting tissues, with α/β of about 3 Gy, thus providing a differential that is exploited in hyperfractionation protocols to spare (reduce) late reactions using small dose fractions.

The therapeutic ratio varies with many factors, such as the dose rate and LET of the irradiation, the presence of radiosensitizers or radioprotectors, the design of the treatment plan and the precision of implementation of the treatment plan.

14.10. OXYGEN EFFECT

The presence or absence of molecular oxygen within a cell influences the biological effect of ionizing radiation: the larger the cell oxygenation above anoxia, the larger is the biological effect of ionizing radiation. Especially for low LET radiations, the larger the cell oxygenation above anoxia, the larger the
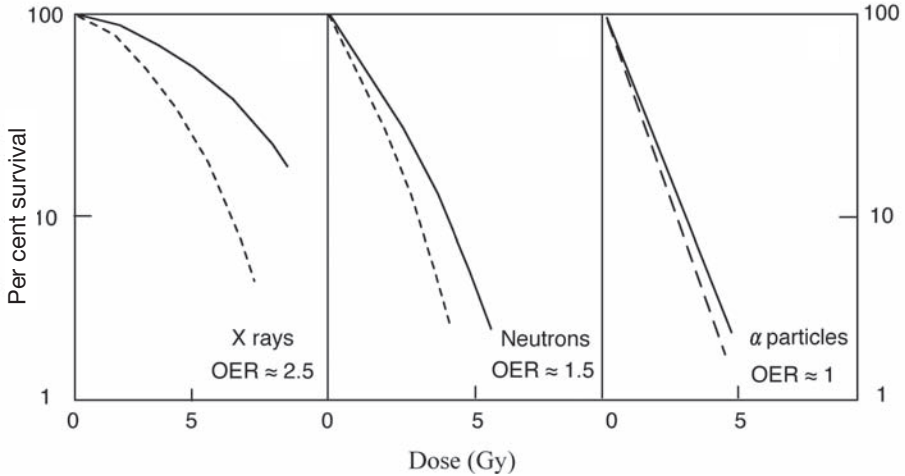
FIG. 14.5. *Typical cell surviving fractions for X rays, neutrons and α particles: dashed curves are for well oxygenated cells, solid curves for hypoxic cells.*

biological effect until saturation of the effect of oxygen occurs. As shown in Fig. 14.5, the effect is quite dramatic for low LET (sparsely ionizing) radiations, while for high LET (densely ionizing) radiations it is much less pronounced. The ratio of doses without and with oxygen (hypoxic versus well oxygenated cells) to produce the same biological effect is called the oxygen enhancement ratio (OER).

$$OER = \frac{\text{Dose to produce a given effect without oxygen}}{\text{Dose to produce the same effect with oxygen}} \qquad (14.2)$$

The OER for X rays and electrons is about three at high doses and falls to about two for doses of 1–2 Gy. The OER decreases as the LET increases and approaches OER = 1 at about LET = 150 keV/μm, as shown in Fig. 14.6.

Cells at the periphery of tumour cords growing around blood vessels become chronically hypoxic because of the consumption of most of the oxygen near the blood vessel. The transient closing of blood vessels can also make the whole tumour cord hypoxic for a few minutes at a time. Reoxygenation is the process by which cells that are hypoxic become oxygenated after irradiation, through the killing and removal of oxic radiosensitive cells from the tumour.
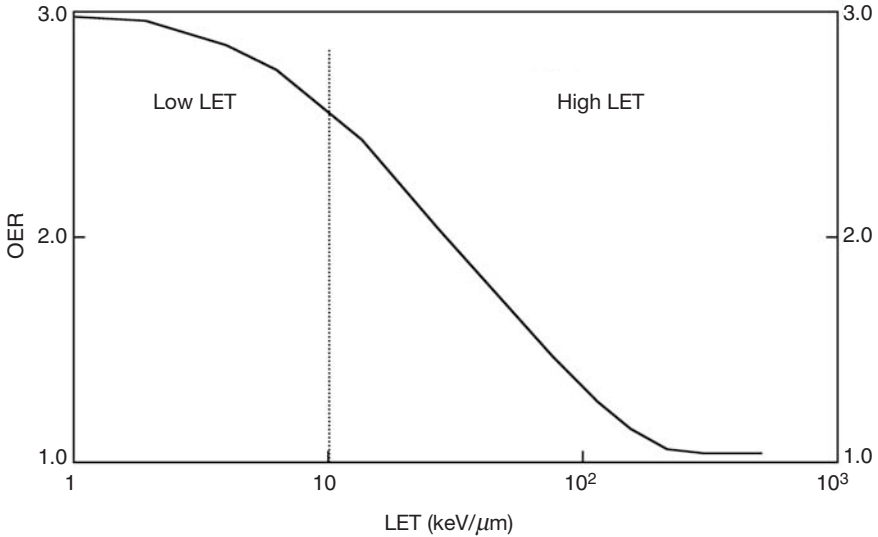
FIG. 14.6. OER plotted against LET. The vertical dashed line separates the low LET region, where LET < 10 keV/μm, from the high LET region, where LET > 10 keV/μm.

14.11. RELATIVE BIOLOGICAL EFFECTIVENESS

As the LET of radiation increases, the ability of the radiation to produce biological damage also increases. The relative biological effectiveness (RBE) compares the dose of test radiation to the dose of standard radiation to produce the same biological effect. The standard radiation has been taken as 250 kVp X rays for historical reasons, but is now recommended to be ^{60}Co γ rays. The RBE is defined by the following ratio:

$$RBE = \frac{\text{Dose from standard radiation to produce a given biological effect}}{\text{Dose from test radiation to produce the same biological effect}}$$

(14.3)

The RBE varies not only with the type of radiation but also with the type of cell or tissue, biologic effect under investigation, dose, dose rate and fractionation. In general, the RBE increases with the LET to reach a maximum RBE of 3–8 (depending on the level of cell kill) at LET ≈ 200 keV/m and then decreases because of energy overkill, as shown in Fig. 14.7.

An increase in the RBE in itself offers no therapeutic advantage unless there is a differential effect making the RBE for normal tissue smaller than that for the tumour, increasing the relative level of tumour cell killing and the therapeutic ratio.

14.12. DOSE RATE AND FRACTIONATION

For the same radiation dose, radiation delivered at a lower dose rate may produce less cell killing than radiation delivered at a higher dose rate, because sublethal damage repair occurs during the protracted exposure. As the dose rate is reduced, the slope of the survival curve becomes shallower and the shoulder tends to disappear, since in the linear quadratic model α does not change significantly; however, $\beta \rightarrow 0$.

The typical dose rates used in radiotherapy are of the order of:

- 1 Gy/min in standard radiotherapy and high dose rate (HDR) brachytherapy;
- 0.1 Gy/min in TBI;
- 0.01 Gy/min in low dose rate (LDR) brachytherapy.
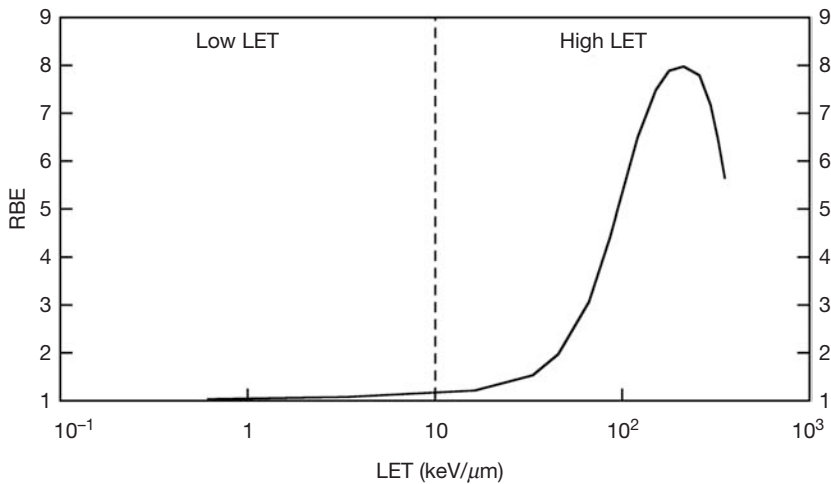
FIG. 14.7. RBE against LET. The vertical dashed line separates the low LET region, where RBE ≈ 1, from the high LET region, where the RBE first rises with the LET, reaches a peak of about 8 for LET ≈ 200 keV/μm, and then drops with a further increase in the LET.

Fractionation of radiation treatment so that it is given over a period of weeks rather than in a single session results in a better therapeutic ratio. However, to achieve the desired level of biological damage the total dose in a fractionated treatment must be much larger than that in a single treatment.

The basis of fractionation is rooted in five primary biological factors called the five Rs of radiotherapy:

— Radiosensitivity. Mammalian cells have different radiosensitivities.
— Repair. Mammalian cells can repair radiation damage. This is a complex process that involves repair of sublethal damage by a variety of repair enzymes and pathways.
— Repopulation. Cells repopulate while receiving fractionated doses of radiation.
— Redistribution. Redistribution in proliferating cell populations throughout the cell cycle phases increases the cell kill from a fractionated treatment relative to a single session treatment.
— Reoxygenation. Reoxygenation of hypoxic cells occurs during a fractionated course of treatment, making them more radiosensitive to subsequent doses of radiation.

Conventional fractionation is explained as follows: division of dose into multiple fractions spares normal tissues through repair of sublethal damage between dose fractions and repopulation of cells. The former is greater for late reacting tissues and the latter for early reacting tissues. Concurrently, fractionation increases tumour damage through reoxygenation and redistribution of tumour cells. A balance is achieved between the response of tumour and early and late reacting normal tissues, so that small doses per fraction spare late reactions preferentially, and a reasonable schedule duration allows regeneration of early reacting tissues and tumour reoxygenation to likely occur.

The current standard fractionation is based on five daily treatments per week and a total treatment time of several weeks. This regimen reflects the practical aspects of dose delivery to a patient, successful outcome of patient treatments and convenience to the staff delivering the treatment.

Other fractionation schemes are being studied with the aim of improving the therapeutic ratio. Some of these are hyperfractionation, accelerated fractionation and CHART:

(i) Hyperfractionation uses more than one fraction per day with a smaller dose per fraction (<1.8 Gy) to reduce long term complications and to allow delivery of higher total tumour dose.

(ii) Accelerated fractionation reduces the overall treatment time, minimizing tumour cell repopulation during the course of treatment.

(iii) CHART (continuous hyperfractionated accelerated radiation therapy) is an experimental programme used with three fractions per day for 12 continuous days.

14.13. RADIOPROTECTORS AND RADIOSENSITIZERS

Various chemical agents may alter cell response to ionizing radiation, either reducing or enhancing the cell response.

Chemical agents that reduce cell response to radiation are called radioprotectors. They generally influence the indirect effects of radiation by scavenging the production of free radicals. The dose modifying factor (DMF) is defined as follows:

$$DMF = \frac{\text{Dose to produce an effect with radioprotector}}{\text{Dose to produce the same effect without radioprotector}} \quad (14.4)$$

Chemical agents that enhance cell response to radiation are called radiosensitizers and generally promote both the direct and indirect effects of radiation. Examples are halogenated pyrimidines, which intercalate between the DNA strands and inhibit repair, and hypoxic cell radiosensitizers, which act like oxygen.

Another type of radiosensitizer is compounds containing boron, which enhances the effects of thermal neutron radiation therapy. Boron-10 has a high cross-section for reaction with thermal neutrons (kinetic energy of the order of 0.025 eV). When a thermal neutron interacts with ^{10}B an unstable nuclide ^{11}B is formed that undergoes fission and produces α particles delivering a high dose in the immediate vicinity of the compound that contains boron. This boron neutron capture therapy (BNCT) has been investigated since the 1950s; however, successful clinical applications have so far been elusive.

BIBLIOGRAPHY

HALL, E.J., Radiobiology for the Radiologist, Lippincott, Philadelphia, PA (2000).

NIAS, A.H.W., An Introduction to Radiobiology, Wiley, New York (1998).

STEEL, G.G., Basic Clinical Radiobiology, Arnold, London (2002).

Chapter 15

SPECIAL PROCEDURES AND TECHNIQUES IN RADIOTHERAPY

E.B. PODGORSAK
Department of Medical Physics,
McGill University Health Centre,
Montreal, Quebec, Canada

M.B. PODGORSAK
Department of Radiation Medicine,
Roswell Park Cancer Institute,
Buffalo, New York,
United States of America

15.1. INTRODUCTION

In addition to the routine conventional radiotherapy techniques used in standard radiotherapy departments and clinics, several specialized techniques are known and used for special procedures, be it in dose delivery or target localization. These techniques deal with specific problems that usually require equipment modifications, special quality assurance procedures and heavy involvement and support from clinical physicists. Owing to their increased complexity, these specialized techniques are usually available only in larger, regional centres.

The radiotherapy techniques that currently fall into the specialized category are listed below; the first six are special dose delivery techniques, the last three are special target localization techniques:

- Stereotactic irradiation;
- Total body irradiation (TBI) with photon beams;
- Total skin electron irradiation (TSEI);
- Intraoperative radiotherapy (IORT);
- Endorectal irradiation;
- Conformal radiotherapy and intensity modulated radiotherapy (IMRT);
- Image guided radiotherapy (IGRT);
- Respiratory gated radiotherapy;

● Positron emission tomography (PET)/computed tomography (CT) fused images.

15.2. STEREOTACTIC IRRADIATION

From an obscure irradiation technique practised in the 1960s and 1970s in only a few specialized centres, stereotactic irradiation has during the past 15 years developed into a mainstream radiotherapeutic technique practised in most major radiotherapy centres around the world. Stereotactic irradiation is the term used to describe focal irradiation techniques that use multiple non-coplanar photon radiation beams and deliver a prescribed dose of ionizing radiation to preselected and stereotactically localized lesions, primarily in the brain, although attempts have been made to extend the technique to other parts of the body.

The main characteristics of stereotactic irradiation are as follows:

● Total prescribed doses are of the order of 10–50 Gy, and the planning targets are small, with typical volumes ranging from 1 to 35 cm^3.
● The requirements for positional and numerical accuracy in dose delivery are ±1 mm and ±5%, respectively.
● The dose in stereotactic irradiation may be delivered through a stereotactic implantation of radioactive sources (stereotactic brachytherapy) or, more commonly, with one or several external radiation sources (stereotactic external beam irradiation).
● With regard to dose fractionation, stereotactic external beam irradiation (SEBI) is divided into two categories:
  — Stereotactic radiosurgery: the total dose is delivered in a single session.
  — Stereotactic radiotherapy: like in standard radiotherapy, the total dose is delivered in multiple fractions.
● From a technical point of view there is essentially no difference between stereotactic radiosurgery and stereotactic radiotherapy, and often the term radiosurgery is used to describe both techniques.
● Essentially any radiation beam that has been found useful for external beam radiotherapy has also found use in radiosurgery (cobalt γ rays, megavoltage X rays, proton and heavy charged particle beams, and even neutron beams).

15.2.1. Physical and clinical requirements for radiosurgery

The physical and clinical requirements for radiosurgery are as follows:

- Accurate determination of the target volume and its location with stereotactic techniques;
- Calculation of 3-D dose distributions inside and outside the target volume;
- Calculation of dose–volume histograms (DVHs) for the target and specific sensitive organs;
- Dose distributions that conform to target shapes and give a sharp dose fall-off outside the target volume;
- Direct superposition of isodose distributions on diagnostic images, showing the anatomical location of the target and surrounding structures;
- Accurate knowledge of the total dose and fractionation scheme required for treatment of the particular disease;
- Accurate positional (within ±1 mm) delivery of dose to the predetermined target;
- Accurate numerical (within ±5%) delivery of dose to the predetermined target;
- Dose delivery accomplished within a reasonable amount of time;
- Low skin dose (to avoid epilation) and low eye lens dose (to avoid cataracts);
- Low or negligible scatter and leakage dose to radiosensitive organs (to avoid subsequent somatic and genetic effects of radiation).

15.2.2. Diseases treated with stereotactic irradiation

The diseases treated with stereotactic irradiation are:

- Functional disorders;
- Vascular lesions;
- Primary benign and malignant tumours;
- Metastatic tumours.

15.2.3. Equipment used for stereotactic radiosurgery

The following equipment is used for stereotactic radiosurgery:

- A stereotactic frame, which defines a fixed coordinate system for an accurate localization and irradiation of the planning target volume (PTV). The stereotactic frame is also used for patient set-up on the treatment machine and for patient immobilization during the actual treatment procedure.

- Imaging equipment (CT, magnetic resonance (MR) and digital subtraction angiography (DSA)) with which the structures, lesions and PTVs are visualized, defined and localized.
- Target localization software, which is used in conjunction with the stereotactic frame system and imaging equipment to determine the coordinates of the target in the stereotactic frame reference system.
- A treatment planning system (TPS) with which the 3-D dose distribution for the radiosurgical treatment is calculated and superimposed on to the patient's anatomical information.
- An appropriate radiation source and radiosurgical treatment technique.

15.2.4. Historical development

The combined use of stereotaxy and irradiation in the treatment of disease was introduced in the early 1950s by the Swedish neurosurgeon Leksell, who also coined the term 'radiosurgery' to describe the technique. Leksell initially used 200 kVp X rays to deliver, in a single session, a high radiation dose (of the order of 100 Gy) to an intracranial target. He approached the target from several directions to focus the dose on the target within the brain and spare the surrounding vital structures.

Radiosurgery based on orthovoltage X rays was discontinued in the late 1950s but the idea of focal brain irradiation was carried over to other, more suitable, radiation beams, first to protons from cyclotrons, then to focused ^{60}Co γ rays and more recently to megavoltage X rays from linacs.

Linacs were proposed as viable radiation sources for radiosurgery in 1974 by Larsson. In 1984 Betti and Derechinsky reported on the development and clinical application of the linac based multiple non-coplanar arcs technique. Soon thereafter, the technique was introduced clinically in Vicenza (Italy) by Colombo and colleagues and in Heidelberg (Germany) by Hartmann and colleagues.

In 1986, Harvard University in Boston and McGill University in Montreal were the first two institutions to use linac based radiosurgery in North America. Harvard adopted the multiple non-converging arcs technique, while McGill developed its own radiosurgical technique, referred to as dynamic stereotactic radiosurgery.

15.2.5. Radiosurgical techniques

15.2.5.1. Gamma Knife

The Gamma Knife (also referred to as the gamma unit) is a radiosurgical device that has been associated with, and dedicated to, radiosurgery for the past four decades. Despite great technological advances during this time, the fundamental design and principles of the gamma unit have not changed much since Leksell introduced the prototype gamma unit in the late 1960s. The unit incorporates 201 ^{60}Co sources housed in the central body of the unit. These sources produce 201 collimated beams directed to a single focal point at a source to focus distance of about 40 cm. The final definition of the circular beam field size is provided by one of four helmets delivering circular fields with nominal diameters between 4 and 18 mm at the machine focal point. The main components of the gamma unit are:

- A radiation unit with an upper hemispherical shield and a central body;
- An operating table and sliding cradle;
- A set of four collimator helmets providing circular beams with diameters of 4, 8, 14 and 18 mm at the isocentre;
- A control unit.

A typical Gamma Knife installation depicting the main body of the machine, the treatment table and a collimator helmet is shown in Fig. 15.1.

15.2.5.2. Linac based radiosurgery

Linac based radiosurgery uses a standard isocentric linac with tight mechanical and electrical tolerances, modified for radiosurgery. The modifications are relatively simple and consist of:

— Supplementary collimation either in the form of a set of collimators to define small diameter circular radiosurgical beams or a micro multileaf collimator (MLC) to define small area irregular fields;
— A remotely controlled motorized table or treatment chair rotation;
— Table brackets or a floor stand for immobilizing the stereotactic frame during treatment;
— Interlocked readouts for angular and height position of the table;

FIG. 15.1. State of the art Gamma Knife (Model 4C) showing the main body of the unit containing 201 ^{60}Co sources (each nominally with an activity of 30 Ci = 1.11 × 10^{12} Bq), the treatment table and a collimator helmet deployed for treatment. The inset shows an up-close image of the automatic positioning system used to position the patient for treatment. (Courtesy of Elekta AB.)

— Special brakes to immobilize the vertical, longitudinal and lateral table motions during treatment.

Isocentric linac based radiosurgical techniques currently fall into three categories: multiple non-coplanar converging arcs, dynamic stereotactic radiosurgery and conical rotation. Each technique is characterized by a particular set of individual rotational motions of the linac gantry and the patient support assembly (table or chair) from given start to stop angles.

In the multiple non-coplanar converging arcs technique the patient is stationary either on the treatment table or chair while the gantry moves through a given arc. In the dynamic stereotactic radiosurgery technique both the gantry and the patient rotate simultaneously during the dose delivery (gantry 300º from 30º to 330º and table 150º from 75º to –75º). Figure 15.2 shows a patient being treated with the dynamic stereotactic radiosurgery technique.
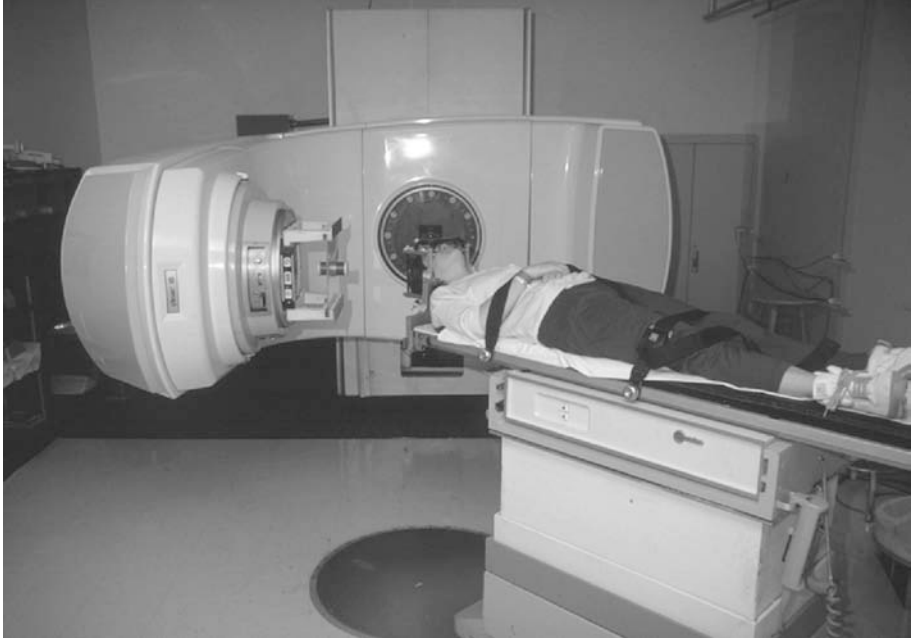
FIG. 15.2. Patient being treated with the dynamic stereotactic radiosurgery technique.

In conical rotation the patient rotates on a treatment chair while the gantry is stationary during the dose delivery. Of the three approaches, the multiple converging arcs technique is the most common, followed by dynamic rotation.

15.2.5.3. Miniature linac on robotic arm

A miniature linac on a robotic arm (CyberKnife) provides a radically new approach to linac based radiosurgery, both in target localization and in beam delivery. Instead of the conventional frame based stereotaxy, the system uses non-invasive image guided target localization, and instead of a conventional isocentric linac, the system uses a miniature 6 MV linac, operated in the X band at 10^4 MHz and mounted on an industrial robotic manipulator. A typical installation of a robotic arm mounted linac is shown in Fig. 15.3.

The CyberKnife stereotactic radiosurgery system broadens the range of traditional stereotactic radiosurgery and offers the following improvements over standard radiosurgical techniques:
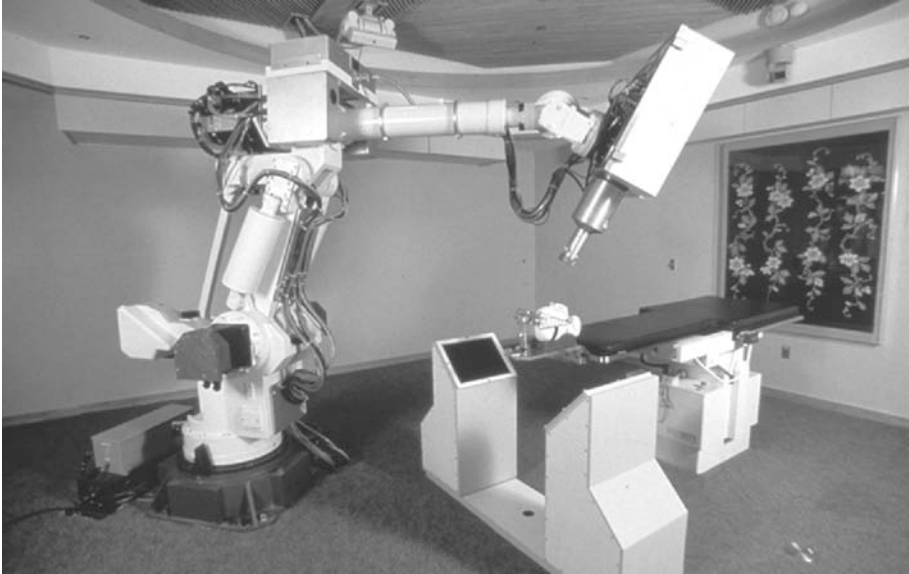
FIG. 15.3. Miniature linac mounted on an industrial robotic arm (CyberKnife). (Courtesy of Accuray, Inc.)

 (i) It allows frameless radiosurgery (i.e. it dispenses with the need for a rigid and invasive stereotactic frame).
 (ii) It monitors and tracks the patient's position continuously and uses on-line images for finding the exact position of the target in the treatment room coordinate system.
 (iii) It aims the radiation beam into the on-line determined target position and achieves a dose delivery accuracy of the order of 1 mm through this image guided dose delivery method.
 (iv) It allows for frameless radiosurgical dose delivery to extracranial targets such as the spine, lung and prostate through using the body skeleton or surgically implanted fiducial markers as a frame of reference for targeting.

15.2.6. Uncertainty in radiosurgical dose delivery

The minimum uncertainty in target localization achievable with modern imaging equipment combined with a frame based stereotactic technique is of the order of ±1 mm. The possible motion of brain tissues, when moving the patient from the imaging equipment to the therapeutic machine, is of the order of a fraction of a millimetre; thus of little concern.

The measured uncertainty in radiosurgical dose delivery for a linac in an excellent mechanical condition is of the order of ±0.5 mm, while for a gamma unit it is somewhat smaller, at ±0.3 mm. Both the gamma unit and the linac provide very similar overall accuracies in dose delivery; however, achieving and maintaining the optimal accuracy with an isocentric linac in comparison with a gamma unit requires a much larger effort as well as a very stringent and disciplined quality assurance programme. Owing to the intricacies of the specific dose delivery methods, the potential for serious problems, like a geographic miss, is greater on a linac than on a gamma unit. However, radiosurgery with isocentric linacs has a much greater potential for new developments than do gamma units; for example, computer controlled micro MLCs are already commercially available, allowing single isocentre treatments with irregularly shaped radiation fields.

A miniature linac mounted on a robotic arm not only offers a real potential for frameless radiosurgery and actual image guided dose delivery, with obvious benefits to the patient and staff, but also enables the use of stereotactic treatment techniques on organs other than the brain.

In comparison with multiple isocentre treatments, micro MLC treatments are simpler, use a single isocentre and result in dose distributions that are more homogeneous inside the target, conform better to the target shape and contribute a much lower scatter and leakage dose to radiation sensitive organs. Three dimensional conformal radiosurgery with modulated intensity fields produced with micro MLCs will become routinely used in clinics as soon as inverse treatment planning (ITP) software for radiosurgery becomes available.

15.2.7. Dose prescription and dose fractionation

The prescribed dose and fractionation of stereotactic dose delivery depend on the disease treated as well as on the volume and location of the intracranial target. Benign diseases are typically treated with a single session, while malignant tumours are treated with fractionated regimens.

Stereotactic radiosurgery (single session treatment):

- Is used in the treatment of functional disorders, vascular malformations, some benign tumours and metastatic lesions.
- Is occasionally used as a boost in conjunction with standard treatments of malignant intracranial lesions.
- Employs prescribed doses of 12–25 Gy; the larger the lesion, the lower the dose.

In stereotactic radiotherapy (fractionated treatment with stereotactic techniques) either the stereotactic frame is left attached to the patient's cranium for the duration of the treatment course or a relocatable stereotactic frame is used for individual treatments. The dose per fraction is typically larger than that of the standard treatment because of the complexities of radiosurgical treatments. Typical dose/fractionation regimens are: 6×7 Gy (total dose 42 Gy), with treatment given every second day, or 10×4 Gy (total dose 40 Gy), with treatment given daily.

15.2.8. Commissioning of radiosurgical equipment

The basic principles involved in the commissioning of radiosurgical devices are very similar for all such devices, despite the large variations in dose delivery techniques that they entail. The following issues should be considered before embarking on a clinical radiosurgical service:

- The properties of radiation beams must be measured to ensure radiation safety of the patient and accurate treatment planning;
- The mechanical integrity of the radiosurgical device must be within acceptable tolerances to provide reliable and accurate delivery of the prescribed dose;
- All steps involved in the radiosurgical procedure, from the target localization, through treatment planning to dose delivery, must be verified experimentally to ensure reliable and accurate performance of the hardware and software used in the radiosurgical procedure.

15.2.9. Quality assurance in radiosurgery

Stereotactic radiosurgery is a very complex treatment modality requiring not only close collaboration among the members of the radiosurgical team but also careful target localization and treatment planning, as well as strict adherence to stringent quality assurance protocols. The core radiosurgical team consists of a neurosurgeon, a radiation oncologist, a medical physicist and a radiotherapy technologist (radiation therapist).

The quality assurance protocols for radiosurgery fall into three categories:

- The basic quality assurance protocols covering the performance of all equipment used for target localization, 3-D treatment planning and radiosurgical dose delivery;

- The treatment quality assurance protocols dealing with the calibration and preparation of equipment immediately preceding the radiosurgical treatment;
- Treatment quality assurance during the radiosurgical procedure on a patient.

15.2.10. Gamma Knife versus linac based radiosurgery

The introduction of linac based radiosurgery in radiation oncology departments during the late 1980s has very rapidly transformed radiosurgery into a mainstream radiotherapeutic technique and has stimulated great advances in its technical and clinical utility. However, the move of radiosurgery into radiation oncology departments has also caused some problems and differences of opinion between neurosurgeons, who were the inventors and until then the principal users of radiosurgery, and radiation oncologists, who are the professionals trained and licensed in the treatment of disease with ionizing radiation.

Radiation oncologists are quite comfortable with the clinical use of isocentric linacs. They embraced the new linac based radiosurgical techniques with great enthusiasm, but had some reservations about the use of single high dose irradiation in radiosurgery, in contrast to the multifractionated schemes used in conventional radiotherapy. Neurosurgeons, however, had previous favourable experience with gamma unit radiosurgery and expressed serious concerns about the mechanical stability of isocentric linacs when used in radiosurgery.

An unstable linac isocentre could adversely affect the accuracy of dose delivery and result in substandard treatments in comparison with treatments provided by the 201 stationary beams from the gamma unit. These concerns are valid, and clearly not all isocentric linacs are suitable for conversion to radiosurgery. However, a well designed, well aligned and properly maintained isocentric linac will have a stable and small enough isocentre sphere (of the order of 1 mm diameter) to make it suitable for use in radiosurgery.

The general consensus among radiation oncologists and medical physicists is that linac based radiosurgical treatments with regard to treatment outcomes are equivalent to those provided by gamma units and that linac based techniques, in comparison with gamma units, are considerably more complicated but have a much greater potential for new and exciting developments.

The consensus among the majority of neurosurgeons is that the use of gamma units is superior to that of any linac based radiosurgical technique.

During the past decade this consensus has resulted in over 100 new gamma unit installations worldwide.

15.2.11. Frameless stereotaxy

In recent years great advances have been made in frameless stereotaxy, which aims to dispense with the invasiveness of the stereotactic frame fixation to the skull without losing the inherent accuracy of the frame based stereotactic approach. New techniques have been developed for image guided neuro-surgery and radiosurgery based either on surgical implantation of fiducial markers (gold wire or screws) or on on-line planar imaging (linac on a robotic arm (see Section 15.2.5.3)).

The accuracy of target localization achieved with these new frameless techniques approaches that attainable with invasive stereotactic frames. Frameless radiosurgery relies heavily upon modern digital imaging and on-line monitoring, and is likely to replace the current frame based approach in the future.

15.3. TOTAL BODY IRRADIATION

TBI is a special radiotherapeutic technique that delivers to a patient's whole body a dose uniform to within ±10% of the prescribed dose. Megavoltage photon beams, either ^{60}Co γ rays or megavoltage X rays, are used for this purpose. In a broader sense, the treatment concepts of whole body irradiation encompass all irradiations with large photon fields, such as half-body irradiation, total nodal irradiation and irradiation of the whole body except for a few specific organs, which are partially or fully shielded from the prescribed dose.

15.3.1. Clinical total body irradiation categories

Depending on the specific clinical situation, TBI techniques are divided into the following four categories:

- High dose TBI, with dose delivery in a single session or in up to six fractions of 200 cGy each in three days (total dose 1200 cGy);
- Low dose TBI, with dose delivery in 10–15 fractions of 10–15 cGy each;
- Half-body irradiation, with a dose of 8 Gy delivered to the upper or lower half body in a single session;

● Total nodal irradiation, with a typical nodal dose of 40 Gy delivered in 20 fractions.

15.3.2. Diseases treated with total body irradiation

TBI is used primarily as part of a preparatory cytoreductive conditioning regimen prior to bone marrow transplantation (BMT). The source of marrow may be the patient (autologous transplant), an identical twin (syngeneic transplant) or a histocompatile donor (allogeneic transplant). In the near future, bioengineering promises to produce a supply of stem cells originating from unrelated and unmatched donors for use in bone marrow transplantation. The cells will be engineered so as to make rejection highly improbable, greatly expanding the usefulness and reliability of BMT.

Before engraftment of donor bone marrow, pretransplant conditioning is applied to eradicate the tumour cells or cells with genetic disorders. Although the conditioning regimen may be based on chemotherapy alone, the most common form of pretransplant conditioning is a combination of high dose chemotherapy and TBI. The latter is included in BMT protocols because it results in immunosuppression, which helps prevent the failure of the graft, a serious, usually fatal, complication of BMT, referred to as graft versus host disease. Thus an optimal application of TBI is a very important component of a successful BMT procedure.

The most notable diseases treated with BMT are:

● Various types of leukaemia (acute non-lymphoblastic, acute lymphoblastic and chronic myelogenous);
● Malignant lymphoma;
● Aplastic anaemia.

15.3.3. Technical aspects of total body irradiation

All contemporary TBI techniques use megavoltage photon beams produced by either ^{60}Co teletherapy units or linacs. The beams are either stationary, with field sizes of the order of 70×200 cm^2 encompassing the whole patient, or moving, with smaller field sizes, in some sort of translational or rotational motion to cover the whole patient with the radiation beam. Usually, parallel opposed irradiations are used by delivering each fractional dose in two equal instalments and switching the patient's position between the two instalments.

15.3.4. Total body irradiation techniques

TBI treatment techniques are carried out either with dedicated irradiators (Fig. 15.4(a) and (b) and Fig. 15.5) or, more commonly, with modified conventional megavoltage radiotherapy equipment. Currently, four methods are in use to administer TBI with modified conventional radiotherapy equipment:

- Treatment at extended source to surface distances (SSDs) (Fig. 15.4(c) and (d));
- Treatment at standard SSDs after the ^{60}Co machine collimator is removed (Fig. 15.5);
- Treatment with a translational beam (Fig. 15.6(a));
- Treatment with a sweeping beam (Fig. 15.6(b) and Fig. 15.7).

The first two techniques use large stationary beams and a stationary patient, while the latter two use moving beams produced by translating the
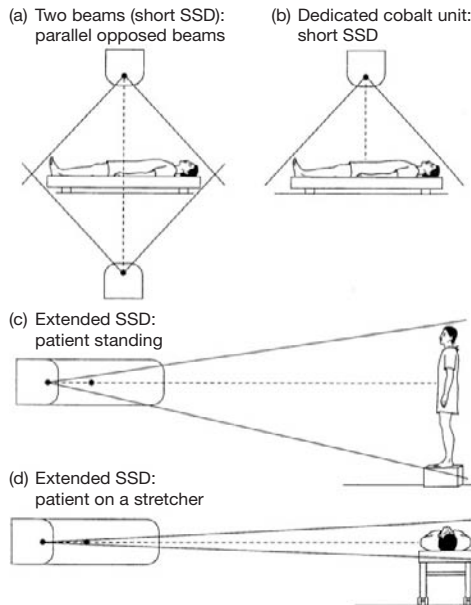
FIG. 15.4. Stationary beam TBI techniques: (a) two short SSD parallel opposed beams; (b) dedicated cobalt unit; (c) extended SSD — patient standing; (d) extended SSD — patient on a stretcher.

FIG. 15.5. A ^{60}Co teletherapy unit dedicated to TBI. The source to floor distance is 250 cm; the patient is treated on a floor mattress in a prone and supine position to obtain a parallel opposed beam.

patient through a stationary beam or through sweeping the beam over a stationary patient.

15.3.5. Dose prescription point

The TBI dose is prescribed to a point inside the body, referred to as the dose prescription point (usually at the midpoint at the level of the umbilicus). The TBI procedure must deliver the prescribed dose to the dose prescription point and should maintain the dose throughout the body within ±10% of the prescription point dose. Uniformity of dose is achieved with the use of bolus or compensators.

15.3.6. Commissioning of total body irradiation procedure

Once a particular treatment machine and TBI technique have been selected, a thorough commissioning of the proposed TBI procedure must be carried out. The basic dosimetric parameters for TBI are the same as those for standard radiotherapy, including absolute beam output calibration, percentage depth doses (PDDs) and beam profiles (off-axis ratios (OARs)). However,

(a) Translational beam: patient moves through the beam
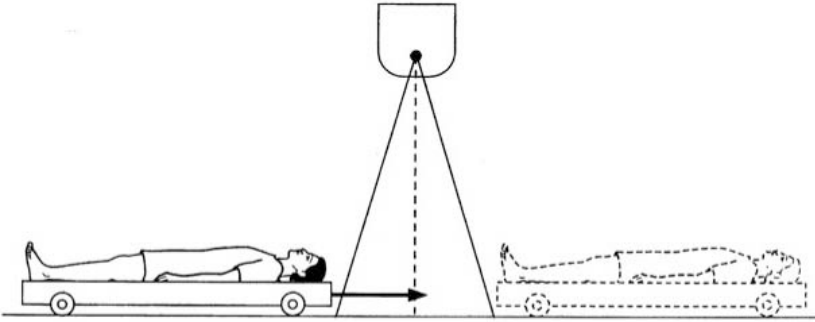
(b) Sweeping beam: patient on a stretcher
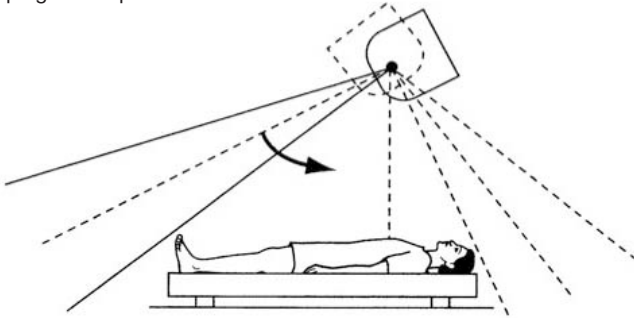
FIG. 15.6. Moving beam TBI techniques: (a) translational beam — patient moves transla-tionally through a stationary beam; (b) sweeping beam — the beam sweeps over a stationary patient.

these parameters must be measured under the specific TBI conditions in order to obtain reliable data for use in clinical TBI.

Several dosimetric problems specific to large field dosimetry but not occurring in standard radiotherapy must be considered. These problems are related to the phantoms and ionization chambers that are used in the measurement of the dosimetric parameters. In contrast to standard radio-therapy, in TBI the phantoms are generally smaller than the actual field size and smaller than the patient. This causes different scattering conditions that might adversely affect the beam output as well as the PDDs required in the determination of the treatment times or monitor units (MUs) required to achieve the prescribed tumour dose.

The accuracy of the TBI dosimetric data might be adversely affected by the relatively large portion of the ionization chamber cable irradiated with the

FIG. 15.7. Patient being treated with the sweeping beam TBI technique on a 4 MV linac.

large TBI field as well as by the chamber leakage currents and saturation characteristics, which become more problematic at the relatively low dose rates used in TBI.

15.3.7. Test of total body irradiation dosimetry protocol

Once the basic dosimetric data for a particular TBI technique to be used clinically are available, several TBI irradiation 'dry runs' should be carried out to verify the TBI dosimetry protocol.

15.3.8. Quality assurance in total body irradiation

TBI is a complex treatment modality requiring careful treatment planning, accurate localization of the organs that are to receive a reduced dose or to be shielded completely from the radiation beam and strict adherence to quality assurance protocols. These protocols fall into three categories: basic quality assurance, pretreatment quality assurance and treatment quality assurance.

- Basic quality assurance protocols cover the performance of the equipment used for TBI treatment planning and dose delivery. In addition to the dose delivery machine, which is either a cobalt unit or a linac, the TBI equipment may also include a CT scanner, which provides data on lung geometry and density as well as the geometry of other critical organs, and a TPS, which is used for the determination of lung dose.

- Pretreatment quality assurance protocols deal with calibration and with the preparation of equipment and the treatment room immediately preceding the TBI treatment. This includes positioning the equipment and any special TBI components such as flattening or compensating filters in the appropriate position as well as ensuring the proper functioning of any special dosimetric equipment that will be used for measuring the dose delivered to the prescription point or determining the transmission of radiation through the lung.

- Treatment quality assurance protocols deal with measurement of the dose delivered to the patient during the TBI procedure. The requirements for accurate dose delivery in TBI are as stringent as those in conventional external beam radiotherapy. It is important that in departments delivering TBI in vivo dose measurement techniques be available to verify the patient dose directly during the treatment or immediately after the first fractionated treatment.

15.4. TOTAL SKIN ELECTRON IRRADIATION

TSEI is a special radiotherapeutic technique that aims to irradiate the patient's whole skin with the prescribed radiation dose while sparing all other organs from any appreciable radiation dose. Since skin is a superficial organ, the choice of electron beams for the treatment of generalized skin malignancies (most commonly mycosis fungoides) is obvious, even though superficial X rays also could be, and actually were in the past, used for this purpose.

The patient population requiring TSEI is relatively small, therefore the technique is available only in major radiotherapy centres. In the past, superficial X ray machines, van de Graaff generators and even machines incorporating β particle emitting sources were used for TSEI. All contemporary TSEI procedures, however, are based on electron linacs, which are used for conventional radiotherapy and modified for delivery of the large and uniform electron fields required for TSEI.

Photon contamination of electron beams used in TSEI is a potential detriment to the patient. Its magnitude must therefore be known accurately for each particular TSEI technique to ensure that the total prescribed electron

beam dose to the patient's skin is not accompanied with an unacceptably high total body photon dose. Certain areas of the patient's skin as well as some organs (such as nails and eyes) may have to be shielded in order to avoid treatment morbidity. The typical dose/fractionation regimen is 40 Gy in 20 fractions.

15.4.1. Physical and clinical requirements for total skin electron irradiation

All clinical TSEI procedures are governed by three categories of specification:

- A physical specification of the large stationary electron field:
  - Electron field size of the order of 80×200 cm^2;
  - Dose uniformity at z_{max} in a water equivalent phantom for at least 80% of the central nominal field area (typically ±5% from dose at z_{max} in a phantom on the central ray);
  - Nominal SSD of 300–500 cm;
  - Beam energy at the waveguide exit window of 6–10 MeV;
  - Beam energy on the phantom surface of 4–7 MeV;
  - Dose rate on the beam central ray at z_{max} in a water equivalent phantom;
  - Photon contamination of the electron beam.
- A physical specification of the dose distribution resulting from the superposition of multiple stationary electron fields:
  - Dose rate at z_{max} on the central ray (usually on the skin surface, which becomes the dose prescription point);
  - Bremsstrahlung contamination dose rate at the patient's midpoint at the level of the umbilicus.
- Clinical specifications:
  - Dose/fractionation regimen;
  - Actual total body photon dose received by the patient during the course of the TSEI treatment;
  - Prescription for boosts to underdosed areas;
  - Prescription for any special shielding (eyes, nails, etc.).

15.4.2. Current total skin electron irradiation techniques

The TSEI techniques in use today may be grouped into three main categories:
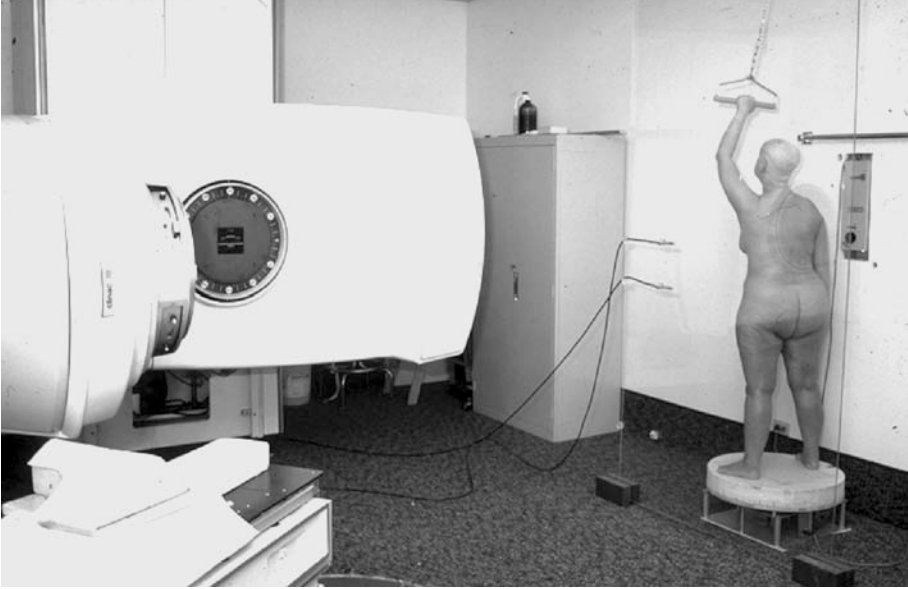
FIG. 15.8. Patient being treated for mycosis fungoides with the rotational TSEI technique.

- Translational techniques, in which the patient is translated on a stretcher through an electron beam of sufficient width to cover the patient's transverse dimensions;
- Large electron field techniques, in which a standing stationary patient is treated at a large SSD with a single large electron beam or a combination of large electron beams;
- Rotational techniques, in which the patient is standing on a rotating platform in a large electron field. A patient being treated with the rotational TSEI technique is shown in Fig. 15.8.

15.4.3. Selection of total skin electron irradiation technique

Once an institution decides to provide the TSEI treatment modality, an adequate TSEI technique must be chosen and commissioned, and quality assurance procedures for the clinical use of TSEI must be developed. The large electron field used for TSEI is produced either with single or dual electron fields; the patients will either be treated with multiple large electron beams or they will be rotated in a large electron beam.

15.4.4. Dose calibration point

The output of the large TSEI radiation field is specified at the dose calibration point, which is found on the electron beam central ray at z_{max} in a tissue equivalent phantom. Often the beam output and flatness are monitored directly on-line with two ionization chambers, one placed on the beam central axis to monitor the beam output and the other placed off-axis to monitor the flatness.

15.4.5. Skin dose rate at the dose prescription point

The TSEI dose is prescribed on the patient's skin surface at the level of the umbilicus (dose prescription point), which is usually on the axial slice containing the central ray. The dose rate at the dose prescription point is the skin dose rate resulting from the particular TSEI technique used in the treatment, be it with multiple stationary electron beams or with a rotational electron beam. The skin dose rate is related to the beam output at the dose calibration point, but the actual relationship for a particular technique must be determined experimentally.

15.4.6. Commissioning of the total skin electron irradiation procedure

Based on current TSEI standards, the TSEI technique, newly introduced into a clinic, will use a large and uniform stationary electron field and will treat the patient at a large SSD either with multiple beams in varying upright positions or by rotating an upright patient in a stationary electron beam. Various techniques involving the use of beam spoilers (to degrade the electron beam energy striking the patient) or special filters (to improve the electron beam flatness through electron beam scattering) are used to produce the large and uniform electron fields in the patient treatment plane.

For the purposes of TSEI procedure commissioning, a complete set of relevant dosimetric data must be collected, first for the large stationary electron field and then for the actual dose delivery with the multiple beams or the rotational beam.

The basic dosimetric parameters of the large TSEI electron field are:

- The field flatness measured at z_{max} in a tissue equivalent phantom and normalized to 100 at the dose calibration point;
- The electron beam output at the dose calibration point;
- PDDs measured to a depth of 15 cm in a tissue equivalent phantom.

The PDDs are normalized to 100 at the dose calibration point and measured on the beam central ray as well as on various directions parallel to the central ray. The physical characteristics of the clinical TSEI beam are measured with a modular cylindrical polystyrene or water phantom of 30 cm diameter and height. The skin dose rate is typically measured with thermoluminescence dosimetry or film on the phantom surface. The skin dose rate at the TSEI dose prescription point is given as a fraction of the calibration point dose rate, typically ranging from 0.4 to 0.5.

15.4.7. Measurement of clinical total skin electron irradiation dose distributions

In addition to the basic cylindrical dosimetry phantom, commissioning of the TSEI procedure should also involve measurements of dose distributions with an anthropomorphic body and head phantom augmented by various cylindrical tissue equivalent phantoms to simulate a complete patient, including legs and arms. This allows a thorough measurement of the skin dose distribution, of electron beam penetration into the body and of X ray contamination.

The shielding effects of legs upon each other and arms upon the head, neck and trunk should be evaluated, underdosed skin areas should be identified and boost irradiation methods should be developed to ensure that the whole patient's skin dose is as close as possible to the prescription skin dose.

15.4.8. Quality assurance in total skin electron irradiation

TSEI is a special technique that, much like any other irradiation procedure, requires strict adherence to quality assurance protocols. These protocols fall into three categories, similarly to the discussion in Section 15.3.8:

- A basic quality assurance protocol dealing with the equipment used in TSEI;
- A pretreatment quality assurance protocol dealing with the calibration and preparation of equipment immediately prior to the TSEI treatment;
- A treatment quality assurance protocol that deals with measurements of the actual dose delivered to the patient during the TSEI procedure.

15.5. INTRAOPERATIVE RADIOTHERAPY

IORT is a special radiotherapeutic technique that delivers in a single session a radiation dose of the order of 10–20 Gy to a surgically exposed internal organ, tumour or tumour bed. Thus IORT combines two conventional modalities of cancer treatment, surgery and radiotherapy, but, despite its long tradition, it is still a developing modality whose role in the management of many tumour sites remains to be determined.

Often IORT is applied as part of a treatment protocol that includes other modalities, such as chemotherapy and external beam radiotherapy. The initial treatments attempt to shrink the tumour, possibly simplifying the subsequent surgical resection. Typically, when surgical resection of a tumour mass is finally attempted, not all the tumour can be removed without significant morbidity. To improve local regional control, a large dose of radiation is delivered during the surgical procedure, with all or most radiosensitive normal tissues either shielded or displaced out of the radiation field.

15.5.1. Physical and clinical requirements for intraoperative radiotherapy

The IORT team consists of a surgeon, radiation oncologist, medical physicist, anaesthesiologist, nurse, pathologist and radiation therapist. IORT requires an operating room for the surgical procedure and a treatment room for delivery of the radiation dose. Often both rooms are merged into one, resulting in a specially shielded operating suite in which a dedicated radiation treatment unit is installed permanently.

Once a radiation modality and the location in which the treatment unit is to be installed are selected, an applicator system must be chosen. Applicators are important for three reasons:

- To define the target area;
- To shield tissues outside the target area from radiation;
- To keep sensitive tissues from falling into the target area during irradiation.

15.5.2. Intraoperative radiotherapy radiation modalities and techniques

There are three different radiation modalities that may be used to deliver radiation dose intraoperatively:

- Orthovoltage X rays;
- Megavoltage electron beams;
- High dose rate (HDR) [192]Ir brachytherapy sources.

The first treatment units used for delivering IORT were superficial and orthovoltage X ray units. While the initial treatment results were encouraging, the relatively poor penetration of X rays into tissue prevented a widespread development of X ray machine based IORT.

Most IORT programmes today are based on electron beams produced by megavoltage linacs, since electrons provide several advantages over X rays for the purposes of IORT:

— The electron dose is deposited over a definite range, thus sparing tissue downstream from the target;
— Depending on the target thickness and electron energy, the dose can be deposited homogeneously throughout the target volume;
— In contrast to low energy X rays, there is not much difference between the tissue and bone absorption of megavoltage electron beams.

15.5.3. Commissioning of an intraoperative radiotherapy programme

Once a decision is made on introducing an IORT service into an institution, an IORT team must be assembled, an IORT technique chosen and IORT equipment ordered.

Upon delivery of the equipment, the commissioning of the IORT procedure must be carried out:

● Radiation beam parameters must be measured and dosimetry data summarized so that they may be quickly understood and readily used. Dosimetry measurements that may be necessary, depending upon the IORT modality used, include: the absolute dose output at the end of treatment applicators; central axis depth dose data; the surface dose and buildup; bremsstrahlung contamination of electron beams if using the modality; and dose distribution data.
● The transition between the surgical procedure and irradiation must be carefully planned and all steps involved properly worked out and practised as part of the commissioning procedure. Irrespective of the radiation modality used for the IORT, the set of dosimetry data must be documented in an easily readable format to permit quick and accurate dosimetric calculations.

15.5.4. Quality assurance in intraoperative radiotherapy

Quality assurance for IORT treatments is in some respects even more important than that for standard radiotherapy, since IORT treatments are

almost always given in a single session, making it essentially impossible to correct a misadministration of dose.

Quality assurance in IORT consists of three components, similarly to the discussion in Section 15.3.8:

- Basic quality assurance dealing with all IORT equipment;
- Pretreatment quality assurance dealing with equipment preparation and verification immediately prior to the IORT treatment;
- Treatment quality assurance during the IORT dose delivery to the patient.

15.6. ENDOCAVITARY RECTAL IRRADIATION

In recent years increasing efforts have been directed towards the development of organ saving therapeutic approaches for malignant neoplasms, which were traditionally treated by radical surgery. For malignancies of the rectum and anal canal, sphincter saving procedures are successful in achieving not only a high probability of local control but also an improved quality of life by avoiding the permanent colostomy and male impotence that may result from abdominoperineal resection.

Endocavitary rectal (endorectal) irradiation is a sphincter saving procedure used in the treatment of selected rectal carcinomas with superficial X rays. The technique was introduced in the 1930s by Chaoul and subsequently developed and practised by others, most notably Papillon.

15.6.1. Physical and clinical requirements for endorectal irradiation

The main physical requirement for the technique to be successful is that the X ray beam should have a low effective energy, giving a PDD in tissue of 100% on the surface and about 50%, 30% and 10% at depths of 5, 10 and 25 mm, respectively. This implies an X ray tube potential of ~50 kVp and a short SSD treatment distance.

Selection criteria for endocavitary rectal irradiation are as follows:

- A biopsy proven, well or moderately well differentiated rectal adeno-carcinoma;
- A mobile lesion with a maximum diameter of 3 cm;
- The location of the lesion within 10 cm from the anal canal;
- No evidence of lymph node or distant metastases.

Two techniques have been used for endorectal treatments:

— The short SSD technique, with the SSD of the order of 4 cm and the X ray tube inserted into the proctoscopic cone;
— The long SSD technique, with the SSD of the order of 20 cm and the X ray tube coupled to the cone externally.

Most of the published accounts of endorectal irradiation deal with the short SSD technique, which, in honour of its main proponent, is referred to as the Papillon technique. Both the proctoscopic cone and the inserted X ray tube are handheld during the treatment, making the treatment cumbersome, potentially unreliable because of possible cone movement during the treatment (geographical miss of the tumour) and, from the radiation protection point of view, potentially hazardous if proper radiation safety procedures are not followed.

The long SSD technique has been developed for use of superficial X ray tubes, the design of which does not allow insertion into a proctoscopic cone. However, there are in fact several advantages of long over short SSDs in endorectal irradiation:

 (i)   The X ray tube can be connected to the ~20 cm long proctoscopic cone externally, allowing the use of smaller diameter cones;
 (ii) The X ray tube and the proctoscope do not have to be handheld during treatment, thereby improving positioning and treatment accuracy as well as solving the radiation protection problem;
(iii) The dose uniformity over the tumour volume is improved, since a change in SSD of a few millimetres on an irregular tumour surface affects the surface dose uniformity much more at an SSD of 4 cm than of 20 cm.

15.6.2. Endorectal treatment technique

The endorectal treatment technique consists of the following steps:

• The patient is positioned on the proctoscopic table and the proctoscopic cone with a plunger is inserted into the rectum;
• The plunger is removed, a proctoscopic viewing device is attached to the cone and the cone is placed over the tumour;
• In the short SSD technique the X ray tube is then inserted into the cone, and both the cone and the X ray tube are handheld for the duration of the treatment;

- In the long SSD technique the cone is then immobilized with an adjustable hydraulic clamp and the X ray tube is coupled with an electromagnetic lock to the cone and also immobilized;
- The X ray machine is turned on and the prescribed target dose is delivered.

The total tumour dose is of the order of 80 Gy and is delivered in two or three fractions of 20–30 Gy in each fraction. The fractions are typically given two weeks apart.

15.6.3. Quality assurance in endorectal treatments

Quality assurance in endorectal treatments is at least as important as in standard radiotherapy, since the number of fractions is relatively low and the prescribed dose per fraction is high.

The quality assurance in rectal irradiation consists of three components, similarly to the discussion in Section 15.3.8:

- Basic quality assurance dealing with the complete equipment consisting of the superficial X ray tube, treatment proctoscopic cone and obturator, and visualization device. The output of the X ray tube should be measured with a parallel-plate ionization chamber that is suitable for calibration of superficial X rays and has a calibration coefficient traceable to a standards laboratory. The effect of the chamber body on the chamber signal when the field size used in the calibration laboratory differs from the field size used clinically should be considered.
- Pretreatment quality assurance dealing with equipment preparation immediately prior to endocavitary treatment. Calibration of the X ray beam and operation of all other treatment components should be verified.
- Treatment quality assurance during the delivery of the endorectal treatment.

15.7. CONFORMAL RADIOTHERAPY

15.7.1. Basic aspects of conformal radiotherapy

The basic premise of conformal radiotherapy is that, in comparison with standard dose delivery techniques, tumour control can be improved by using special techniques that allow the delivery of a higher tumour dose while

maintaining an acceptable level of normal tissue complications. Conformal radiotherapy conforms or shapes the prescription dose volume to the PTV while at the same time keeping the dose to specified organs at risk below their tolerance dose. The conformal radiotherapy chain is based on 3-D target localization, 3-D treatment planning and 3-D dose delivery techniques.

Target localization is achieved through anatomical and functional imaging: CT, MRI, single photon emission computed tomography (SPECT), PET and ultrasound. Treatment planning is achieved either with standard forward planning techniques, which design uniform intensity beams shaped to the geometrical projection of the target, or, for more advanced conformal radiotherapy techniques, with inverse planning, which, in addition to beam shaping, uses intensity modulated beams to improve target dose homogeneity and spare organs at risk.

Dose delivery techniques range from the use of standard regular and uniform coplanar beams to intensity modulated non-coplanar beams produced with MLCs.

15.7.2. Multileaf collimators

Modern linacs can be equipped with MLCs that incorporate from 20 to 60 pairs of narrow, closely abutting tungsten leaves, each leaf projecting a typical width of 10 mm or less at the linac isocentre. MLCs projecting leaf widths of less than 5 mm at the isocentre are referred to as micro MLCs. They are used to shape irregular fields of less than 10 cm in maximal field dimension, such as head and neck fields, or irregular fields with less than 3 cm in maximal dimension, such as fields used in radiosurgery.

The MLCs may be an integral part of the linac head, replacing upper or lower secondary collimator jaws, or they may be attached to the linac head and used in conjunction with both the upper and lower collimator jaws. A typical MLC attached to a linac head and used in conjunction with the upper and lower collimator jaws is shown in Fig. 15.9.

Each leaf is individually motorized and computer controlled, allowing positioning with an accuracy better than 1 mm and the generation of irregular radiation fields, shaped to conform to the beam's eye view (BEV) target cross-section. A separate, miniature DC motor drives each leaf independently. Positional control and verification of the leaves is achieved by a sophisticated servomechanism using electronic or optical/video techniques to sense the position.
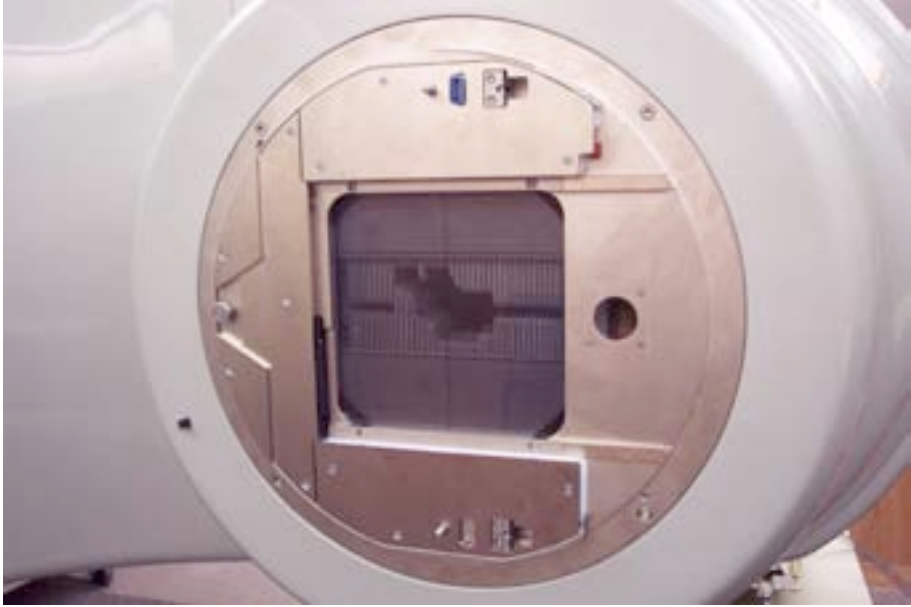
FIG. 15.9. MLC with 60 pairs of abutting tungsten leaves (Millenium MLC, Varian).

15.7.3.   Acceptance testing of multileaf collimators

Before using an MLC clinically it is important that the user first carry out an elaborate acceptance testing protocol. Acceptance testing must cover the mechanical, radiation and software aspects of the MLC operation:

- Mechanical: the motion of the leaves and their maximum travel, abutting of the leaves on and off the central field axis, the alignment of MLC axes with axes of the linac secondary collimators, the positional reproducibility of the leaves, the interlocks for the leaves and jaw positional tolerances.
- Radiation: the transmission of the leaves, the leakage between the leaves, the leakage in the junction of two abutting leaves, both on the field axis and off the field axis, and the leaf penumbra both along the leaf and perpendicularly to it.
- Software: verification of the field shaper, the linkage between the TPS and the MLC and the accuracy of the field shaping and functioning of the controller.

15.7.4. Commissioning of multileaf collimators

The commissioning protocol involves obtaining a collection of beam data for all beam energies produced by the linac and various irregular fields produced by the MLC. The essence of the MLC commissioning is to verify that the physical characteristics of the MLC do not affect appreciably the basic dosimetric parameters of the open beams, such as field flatness, symmetry, collimator factor, output factor, scatter factor and PDD.

The in-phantom dosimetric parameters, such as the relative dose factor, scatter factor, PDD and tissue–maximum ratio (TMR), are determined by the field shape created by the MLC collimator. The in-air dosimetric parameter, the collimator factor, in linac configurations in which the MLC is essentially a tertiary collimator, is determined by the square or rectangular field shaped by the secondary linac collimator jaws and is considered independent of MLC shaping. In linac configurations in which the MLC replaces the upper or lower collimator jaws, the collimator factor is a function of the radiation field determined by the MLC.

15.7.5. Quality assurance programme for multileaf collimators

A quality assurance programme must be implemented for the clinical use of MLCs to ensure the reliable and safe operation of software and all mechanical components. The programme should cover positional accuracy, leaf motion reliability, leaf leakage, interlocks, networking and data transfer.

15.7.6. Intensity modulated radiotherapy

In addition to field shaping in 2-D conformal radiotherapy, in which the radiation fields are irregularly shaped but of uniform intensity, an MLC may also be used to achieve beam intensity modulation for use in 3-D conformal radiotherapy. From an obscure, highly specialized radiotherapeutic technique practised in only a few specialized centres around the world, IMRT has developed into a mainstream radiotherapeutic technique already available in most major radiotherapy centres around the world.

The IMRT technique is currently the most advanced form of conformal radiotherapy and holds great promise for improving radiotherapy both through increased tumour control probability and decreased treatment morbidity (i.e. decreased normal tissue complication probability (NTCP)). It relies on ITP for determination of the required intensity modulated beam maps and on 3-D multimodality imaging to define the target volumes.

In addition to CT, MRI and PET, ultrasound is beginning to play an important role because of its ease of incorporation into a treatment room, where the position of the target volume can be verified on a daily basis. However, the current routine clinical use of IMRT is still hindered by several difficulties, such as the:

- Complexity of the equipment used for dose delivery;
- Complexity of the ITP process;
- Quality assurance issues related to dose distribution calculation and dose delivery.

For IMRT planning the ITP techniques provide several advantages over the standard forward planning approaches, such as:

— Improved dose homogeneity inside the target volume and the potential for limited irradiation of surrounding sensitive structures;
— Increased speed and lesser complexity of the proposed solution;
— A quantitative introduction of cost functions, often incorporating dose volume constraints and biological functions;
— Adjustment of the optimal treatment planning to the actual dose delivery technique and accounting for all practical hardware limitations.

Various approaches to IMRT have been developed, ranging from simple standard physical compensators to scanned photon pencil beams. Between the two extremes are the currently used MLC based IMRT techniques, which fall into two categories: one uses multiple static MLC shaped fields and the other uses dynamic MLC dose delivery approaches.

Rudimentary IMRT treatments have been used clinically since the 1960s with wedges and physical compensators. Modern clinical IMRT, however, became possible in the latter part of the 1990s due to a synergistic effort among four areas that only then became well established:

(i) Three dimensional medical imaging by CT, MRI, SPECT and PET;
(ii) ITP;
(iii) Quality assurance techniques for verification of dose delivery;
(iv) Computer controlled dose delivery.

15.7.7. Commissioning of intensity modulated radiotherapy systems

The steps involved in the commissioning of an IMRT system will depend to some degree on the type of ITP system to be used. Some ITP systems are

simple modules within a standard 3-D TPS and use the regular dose calculation algorithm to evaluate the delivered dose from optimized fluence maps. To commission such a system it is necessary to first commission the standard TPS.

Extra measurements characterizing some basic properties of the MLC to be used must be made (e.g. leaf transmission and leakage, leaf maximum speed and other parameters specific to the ITP system). Other ITP algorithms are stand-alone systems that require complete beam data measurement, entry and possibly modelling, separate from a 3-D planning system. At least one manufacturer attempts to simplify the commissioning process by offering to carry out beam modelling for the customer, provided that all necessary beam data are supplied.

IMRT treatments can be delivered with the MLC operating in one of three basic modes:

- The segmented MLC (SMLC) mode, often referred to as the step and shoot mode;
- The dynamic MLC (DMLC) mode, sometimes referred to as the sliding window mode;
- Intensity modulated arc therapy (IMAT).

In the SMLC mode (static IMRT) the intensity modulated fields are delivered with a sequence of small segments or subfields, each subfield with a uniform intensity. The technique is also referred to as step and shoot, implying that the beam is only turned on when the MLC leaves are stationary in each of the prescribed subfield positions. There is no MLC motion while the beam is turned on.

In the DMLC mode (dynamic IMRT) the intensity modulated fields are delivered in a dynamic fashion with the leaves of the MLC moving during the irradiation of the patient. For a fixed gantry position the opening formed by each pair of opposing MLC leaves is swept across the target volume under computer control with the radiation beam turned on to produce the desired fluence map.

The new delivery method of IMAT has recently been proposed. In this method the sliding window approach is used as the gantry rotates around a patient. IMAT should result in the most conformal dose distributions possible with standard linac hardware.

Each method of delivery needs to be commissioned separately, as the MLC and linac performance is stressed differently depending on the method. IMRT treatments require tighter tolerances on MLC performance than required when the MLC is to be used only in static applications. Thus a set of commissioning tests separate from those described earlier for the MLC alone

needs to be developed. These tests must be able to verify the accuracy and reproducibility of MLC positioning and movement for each delivery technique to be used clinically.

Often a clinic will adopt a single delivery method to allow all staff members to become proficient in its principles and to avoid confusion. This simplifies the commissioning process, since only one delivery method needs to be tested.

Verification of the accuracy of the dose calculation algorithm of an inverse planning system is carried out using the standard dosimetry tools (radiographic or radiochromic film, thermoluminescence dosimetry, ionization chamber in conjunction with various phantoms). Most commercially available IMRT planning systems permit fluence maps optimized for a clinical application to be transferred to a representative phantom for calculation. The phantom can be then physically loaded with any of the above mentioned dosimeters and irradiated with the planned IMRT fields.

Many phantoms specially designed for verification of IMRT fields have recently become commercially available. These phantoms have various inhomogeneities built in that allow verification not only of IMRT plans but also of the algorithm used for tissue inhomogeneity corrections. It is also possible, however, to use simple phantoms made of Lucite, polystyrene or other water equivalent materials, in which dosimeters can be positioned but no inhomogeneities (heterogeneities) can be accounted for.

15.7.8. Quality assurance for intensity modulated radiotherapy systems

A comprehensive quality assurance programme must be developed to ensure accurate IMRT dose delivery. This programme must include standard verification of accelerator radiation output as well as testing of dynamic MLC positioning and movement. A good approach is to perform a subset of the commissioning tests on a regular basis. Owing to the added stress on MLC components, particularly the motors, it is recommended to augment the standard spare parts kit to include at least several additional motors.

15.7.9. Dose verification for intensity modulated radiotherapy treatment plans

It is strongly recommended to carry out an independent verification of all IMRT treatment plans, at least until the entire IMRT team is comfortable with the planning and treatment delivery processes. This is done through a transfer of each IMRT plan to a representative phantom for dose calculation. The phantom can then be loaded with various dosimeters and irradiated with the

IMRT fields planned for the patient. Actual dose delivery can then be compared with the plan and evaluated for accuracy. Several manufacturers have recently developed software and hardware that greatly simplify the evaluation of IMRT dose delivery. These systems should be seriously considered for purchase in addition to any IMRT software/hardware system.

15.8. IMAGE GUIDED RADIOTHERAPY

Over the past decade there have been substantial advances in the technology used to plan and deliver precision radiotherapy. ITP and virtual simulation, which are aided by fusion of multimodality images (CT, MRI and PET) of patient anatomies, have revolutionized the planning of radiotherapy treatments. In the near future determination of intratumoural volumes that need to be treated with extra high doses, such as hypoxic cells or cells with low intrinsic radiosensitivity, will become possible through the rapidly developing molecular imaging technology.

In parallel with developments in target localization, the efficacy of treatment delivery has been improved with the recent introduction of IMRT and tomotherapy. The accuracy of dose delivery with these new techniques has been limited by uncertainty in target localization at the time of treatment. Interfraction as well as intrafraction target movement relative to reference landmarks coupled with set-up errors and other inaccuracies add to this uncertainty. The standard approach has been to add margins to the target volume, usually at the expense of most of the potential benefits of the more precise treatment delivery techniques.

It has recently become possible to image patient anatomy just before delivery of a fraction of radiotherapy, thus gaining precise knowledge of the location of the target volume on a daily basis. This technique of dose delivery to the patient is known as IGRT and has the potential of ensuring that the relative positions of the target volume and some reference point for each fraction are the same as in the treatment plan. This may allow reduced treatment margins, fewer complications, dose escalation and the avoidance of geographical misses.

The ideal image guided system will allow the acquisition of soft tissue images at the time of each fraction of radiotherapy. The system must be fast and simple so as not to affect appreciably the patient throughput on the treatment machine, be accurate within the limits of target definition and have the ability to deliver a conformal dose.

Several IGRT systems are currently commercially available. All systems allow pretreatment imaging immediately after a patient is positioned on the

linac treatment table for therapy. These IGRT systems are based on direct integration of:

- A kilovoltage or megavoltage imaging system with an isocentric medical linac, referred to as cone beam computed tomography (CBCT) and offered by two linac manufacturers as onboard imaging options: Elekta (Synergy model) and Varian (Trilogy model).
- A CT scanner integrated with an isocentric medical linac, offered by Siemens (Primatom model).
- Megavoltage computed tomography (MVCT) with a tomotherapy machine that uses a miniature linac waveguide mounted on a CT type gantry, offered by TomoTherapy, Inc.
- A 2-D or 3-D ultrasound imaging system integrated with an isocentric medical linac, manufactured by Nomos (BAT system) and BrainLab (ExacTrac system).
- On-line imaging with paired orthogonal planar imagers with a miniature linac mounted on a robotic arm, offered by Accuray (CyberKnife system).

15.8.1. Cone beam computed tomography

CBCT imaging enables visualization of the exact tumour location just prior to patient treatment on a linac. The technique integrates CT imaging with a linac and involves acquiring multiple planar images produced by a kilovoltage or megavoltage cone beam rotating a full 360º about the patient in the treatment position on the linac table. A filtered backprojection algorithm similar to CT scanning algorithms is used to reconstruct the volumetric images of the target volume, sensitive structures and landmarks in the patient. The volumetric data are then compared with the planning CT data as well as the associated optimized dose distribution, and a decision is made on fine tuning the patient position to account for tumour motion or set-up error.

Both kilovoltage and megavoltage beams can be used for CBCT:

- The kilovoltage system consists of a conventional X ray tube mounted on a retractable arm at 90º to the high energy treatment beam and a flat panel X ray detector mounted on a retractable arm opposite the X ray tube. The X ray system can, in addition to cone beam images, produce radiographic and fluoroscopic images.
- The advantage of megavoltage beams for CBCT is that the beams come from the linac beam line and thus no additional equipment is required to produce the cone beam; however, kilovoltage beams produce better soft

tissue contrast and are thus deemed more useful. A megavoltage CBCT makes use of the detector panel that is already present for use in electronic portal imaging.

Elekta and Varian linacs equipped with onboard imaging for CBCT are shown in Figs 15.10 and 15.11.

15.8.2. Computed tomography Primatom

A system comprised of a linac and a CT unit at opposite ends of a standard radiotherapy treatment table has been developed and is marketed by Siemens. This system allows precise CT imaging of patient anatomy prior to each fraction of radiotherapy. Not only can the patient be shifted to compensate for target motion and set-up inaccuracies, but the system can also in principle allow clinicians to account for changes in target volume size and shape over a multifraction course of radiotherapy.

FIG. 15.10. The onboard X ray imaging system for CBCT integrated into an Elekta Synergy linac system. (Courtesy of Elekta AB.)
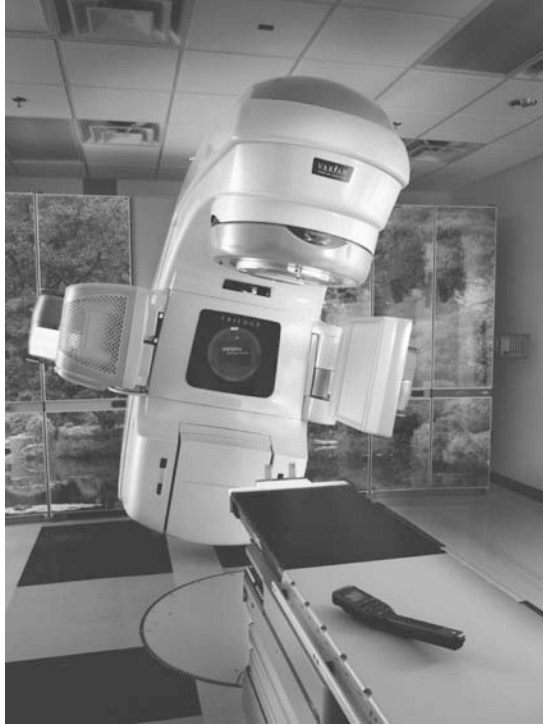
FIG. 15.11.   The onboard X ray imaging system for CBCT integrated into a Varian Trilogy linac system. (Courtesy of Department of Radiation Oncology, Emory University School of Medicine, Atlanta, Georgia, USA. Photo by Weinberg-Clark Photography.)

15.8.3.   Tomotherapy

The tomotherapy concept for delivering radiotherapy was introduced in the early 1990s at the University of Wisconsin. Since then many research publications have demonstrated the potential benefit of delivering radiation dose using this innovative approach. A commercial version, known as the TomoTherapy HI ART System, was released recently for clinical use and combines treatment planning, patient positioning and dose delivery into one system.

In the tomotherapy system, IMRT is delivered with a 6 MV linac that is mounted on a CT type gantry ring, allowing the linac to rotate around a patient. Beam collimation is accomplished with a computer controlled MLC, also on the rotating gantry, that has two sets of interlaced leaves that rapidly move in and out of the beam to constantly modulate the intensity of the radiation beam

as the linac rotates around the patient. During treatment, the table advances the patient through the gantry bore so that the radiation dose is delivered in a helical geometry around the target volume.

The system is designed to obtain an MVCT scan of patient anatomy at any time before, during or after treatment. The MVCT image data are acquired with a 738 element xenon ionization chamber array that rotates on the gantry opposite the linac. This image guidance allows fine adjustment of the patient's position at every fraction to ensure that the dose distribution will be delivered precisely to the target volume as planned. A CT scan can also be taken immediately after a fraction of therapy with the patient still in the treatment position, allowing, at least in principle, an evaluation of the true dose distribution delivered to the patient.

15.8.4. BAT system

Nomos introduced the BAT (B-Mode Acquisition and Targeting) system. The system consists a cart based ultrasound unit positioned next to a linac treatment table and is used by a radiotherapist to image the target volume prior to each fraction of a patient's radiotherapy. The relationship of the target volume to a reference point, usually the linac isocentre, is determined interactively by the user and compared with the target volume originally contoured in the CT data set. Suggestions for patient translation to move the target volume into the same position relative to the isocentre as in the treatment plan are made by the system, and the therapist can then move the patient, based on this information, to gain better treatment accuracy.

The BAT system has found its widest application in pelvic radiotherapy, particularly for prostate cancer. The prostate can move significantly from one day to another within the pelvis relative to bony anatomy. Imaging the prostate target volume transabdominally with an ultrasonic probe on a daily basis and fine tuning the patient position based on system suggestion permits an accurate delivery of conformal treatment plans and allows target dose escalation without causing unacceptable bladder and rectal complications.

15.8.5. ExacTrac ultrasonic module

BrainLab has also developed an ultrasound based system for IGRT to be used in conjunction with an isocentric linac. This system can be used with any ultrasound unit, and is comprised of a reflective marker array attached to an ultrasound probe. This array is calibrated by the ExacTrac infrared tracking system relative to reflective markers attached to the patient's body. In principle, the system works similarly to the BAT system described above, and

allows fine adjustment of the patient's position to compensate for target movement and set-up inaccuracies.

15.8.6. CyberKnife

The CyberKnife was developed in the mid 1990s by Accuray as an innovative tool for intracranial stereotactic radiosurgery (see Section 15.2.5.3). It delivers the dose with a miniature (10^4 MHz) linac mounted on an industrial robotic arm, a combination that offers excellent spatial accuracy in dose delivery and allows, in comparison with isocentric linacs and tomotherapy units, a great deal of flexibility in directing the beam towards the target.

Owing to its on-line target imaging and automatic adjustment of the radiation beam direction to compensate for target motion, the CyberKnife provides a frameless alternative to conventional radiosurgical procedures. The rigid invasive stereotactic frame, the essential component of standard radio-surgical treatments used for target localization, treatment set-up and patient immobilization during treatment, is not required for treatment with the CyberKnife.

The location of the lesion is predetermined through a family of axial CT images that serves as a base for the determination of a set of digitally recon-structed radiograph (DRR) images. A set of paired orthogonal X ray imagers determines the location of the lesion in the room coordinate system and communicates these coordinates to the robotic arm, which adjusts the pointing of the linac beam to maintain alignment with the target.

The CyberKnife radiosurgery system provides an innovative approach to image guided dose delivery that is based on an on-line orthogonal pair of digital X ray imagers, a patient CT data set fused with MR and/or PET images and a miniature linac mounted on an industrial robotic arm. This new approach to highly accurate intracranial as well as extracranial delivery of high radiation doses with small radiation fields opens the field of radiosurgery to very exciting new research directions, both in basic radiation physics and clinical cancer research.

Besides the obvious advantage of dispensing with the need for a stereo-tactic frame without compromising the treatment's spatial accuracy, the CyberKnife also offers several other advantages over conventional radio-surgery, such as:

- Veritable image guided dose delivery.
- Possibility for fractionated treatment of intracranial malignant tumours.
- Possibility for treatment of extracranial spinal lesions, relying on the skeleton to provide a reference frame.

● Possibility for radiosurgical treatment of other organs such as the lung and prostate using surgically implanted fiducial markers as a reference frame.

● Capability for on-line tracking of target motion, which results either from patient motion during treatment or from organ motion within the patient during treatment.

15.9. ADAPTIVE RADIOTHERAPY

A full implementation of IGRT will lead to the concept of adaptive radiotherapy (ART). In this process the dose delivery for subsequent treatment fractions of a course of radiotherapy can be modified to compensate for inaccuracies in dose delivery that cannot be corrected for by simply adjusting the patient's positioning. The causes of these inaccuracies may include tumour shrinkage, patient loss of weight and increased hypoxia resulting during the course of fractionated treatment.

15.10. RESPIRATORY GATED RADIOTHERAPY

In the current radiotherapy practice relatively large margins are added to tumour volumes in the chest and upper abdominal cavities to compensate for the effects of respiratory motion on tumour dose delivery. This results in compromises to prescribed tumour doses as well as treatment plans that adversely affect the treatment outcome and increase the incidence of radiation induced morbidity. The quest for ever increasing tumour doses to increase the tumour control probability (TCP) combined with the goal of low NTCP results in smaller margins around the tumour and a need to deal effectively with organ motion during the treatment.

The next big challenge in IGRT thus comes from the natural and unavoidable organ motion during treatment. To account for this organ motion 4-D imaging technology is required, which allows viewing of volumetric CT images changing over the fourth dimension, time. For example, image guided radiosurgery, discussed above, is an elegant, albeit not the only, approach to dealing with organ motion. A simpler means is provided by the respiratory gating system (RGS), which is a special accessory added to a linac to compensate automatically and instantly for the effects of respiratory movement on external beam radiotherapy to the chest and upper abdomen.

Respiratory gated treatment was developed in Japan for radiotherapy with heavy ions, and the idea was recently introduced to treatment with linacs.

Varian developed an RGS that is referred to as a real time position management RGS and is applicable to any organ or structure subject to respiration induced motion, such as the breast, lung, mediastinum, liver and pancreas. The system is non-invasive, allows dose escalation combined with tighter tumour margins and can also be used in IMRT and other 3-D conformal treatments. A reflective marker is placed on the patient's chest and a video camera tracks its up and down movement. The continuous marker signal is processed by a computer that initiates a beam hold in the linac when the breath movement exceeds parameters that were determined during the treatment simulation. The target motion is correlated with the motion of external markers in simulation and these markers are then used in the treatment to control appropriate beam-on times to limit treatment to those time periods when the target is static.

Elekta developed the Active Breathing Coordinator (ABC), which allows clinicians to deliver radiation dose to the patient during the breath hold. The breathing volume is measured by the machine's mouthpiece and the pattern is displayed on the control room monitor. When the breath hold volume is achieved, a balloon valve is actuated to block airflow to the patient for a predetermined period of time. The end result is a repeatable breath hold that provides the same volumes each time. The operator irradiates during this breath hold, reducing the motion of the tumour during irradiation.

15.11. POSITRON EMISSION TOMOGRAPHY/COMPUTED TOMOGRAPHY SCANNERS AND POSITRON EMISSION TOMOGRAPHY/COMPUTED TOMOGRAPHY IMAGE FUSION

PET/CT machines combining the strengths of two well established imaging modalities represent the most exciting innovation in cancer diagnosis and therapy of the late 1990s. Both PET and CT have been used as imaging modalities since the early 1970s. This section discusses some characteristics of each individual unit, demonstrating the rationale behind the development of the combined PET/CT scanner.

The CT scanner was invented by Hounsfield and Cormack and is based on acquisition of a large number of cone beam projections around a patient by a detector array and representation of transmission measurements of X rays through a patient. The measured transmission data are reconstructed to produce a tomographic image, most commonly through the filtered backprojection method.

The usefulness of CT in radiotherapy was recognized almost immediately after its development, and it has been used not only for providing a detailed

image of internal anatomy, including tumour volumes, but also for providing electron densities for the accurate treatment planning of tissues with heterogeneities.

CT yields a detailed image of the body's anatomical structures by producing cross-sectional X ray slices of the body. While CT is excellent in depicting structures and anatomy, it may miss small or early stage tumours, and, moreover, it does not provide any functional information on the tumours it detects.

PET provides information on the metabolic function of organs or tissues by detecting how cells process certain compounds such as glucose. Most cancer cells metabolize glucose at a much higher rate than normal tissues. By detecting increased radiolabelled glucose metabolism with a high degree of sensitivity, PET identifies cancerous cells, even at an early stage, when other imaging modalities may miss them.

Owing to its relatively poor spatial resolution, PET cannot pinpoint the exact size and location of tumours to the precision required for optimal diagnosis and treatment planning. This limitation until recently precluded a wider use of PET machines in radiotherapy.

In a typical PET study, one administers a positron emitting radionuclide by injection or inhalation. The radionuclide circulates through the bloodstream to reach a particular organ. The positrons emitted by the radionuclide have a very short range in tissue and undergo annihilation with an available electron. This process generally results in an emission of two γ rays, each with an energy of 0.511 MeV, moving away from the point of production in nearly opposite directions (at 180º to each other).

The PET machine generates transverse images depicting the distribution of positron emitting radionuclides in the patient and uses annihilation coincidence detection to obtain projections of the activity distribution. The transverse images are obtained through the process of filtered backprojection.

Detectors used for coincidence detection in modern PET machines are scintillators made of bismuth germanate (BGO) or lutetium oxyorthosilicate doped with cerium (LSO:Ce) that transform the 0.511 MeV γ ray energy into visible photons detected by photomultiplyer tubes (PMTs).

The radionuclides used in PET studies are produced by bombardment of an appropriate stable nuclide with protons from a cyclotron (see Section 5.4), thereby producing positron emitting radionuclides that are subsequently attached to clinically useful biological markers. The common positron emitting radionuclides used in PET imaging studies are listed in Table 15.1.

The ^{18}F radionuclide attached to the 2-fluoro-2-deoxy-D-glucose (FDG) molecule is the biological marker most commonly used in studies involving glucose metabolism in cancer diagnosis and treatment.

TABLE 15.1. COMMON POSITRON EMITTING RADIONUCLIDES USED IN POSITRON EMISSION TOMOGRAPHY

Radionuclide	Symbol	Half-life (min)	Maximum positron energy (keV)
Carbon-11	C-11	20.5	960
Nitrogen-13	N-13	10	1200
Oxygen-15	O-15	2	1732
Fluorine-18	F-18	110	634
Rubidium-82	Rb-82	1.2	3356

The relatively short half-life of the positron emitting radionuclides used in PET scanning requires that a cyclotron be available near the PET machine, making a routine PET scanning clinical service very costly.

PET and CT obviously complement each other in providing important diagnostic information. Separate PET and CT images are unfortunately difficult to fuse because the patient is generally not positioned identically on both machines. However, the recently introduced PET/CT machines, integrating PET and CT technologies into a single device, enable the collection of both anatomical and biological information simultaneously during a single examination, resulting in accurately fused PET and CT images that permit a more accurate tumour detection and tumour localization for a wide variety of cancers.

The main advantages of PET/CT machines are as follows:

● Earlier diagnosis of disease;
● Accurate staging and tumour localization;
● More precise treatment;
● Monitoring of response to treatment and early detection of recurrences;
● Reduction of biopsy sampling errors;
● Reduction of the number of invasive procedures required during follow-up.

BIBLIOGRAPHY

AMERICAN ASSOCIATION OF PHYSICISTS IN MEDICINE, Total Skin Electron Therapy: Techniques and Dosimetry, AAPM Task Group 30 Report, AAPM, New York (1987).

— Stereotactic Radiosurgery, AAPM Task Group 42 Report, AAPM, New York (1995).

GILDENBERG, P.L., TASKER, R.R. (Eds), Textbook of Stereotactic and Functional Neurosurgery, McGraw-Hill, New York (1998).

HARTMANN, G., et al., Quality Assurance Program on Stereotactic Radiosurgery, Springer, Berlin (1995).

KHAN, F.M., The Physics of Radiation Therapy, Lippincott, Williams and Wilkins, Baltimore, MD (2003).

McCULLOUGH, E.C., "Intraoperative electron beam radiation therapy (IORT)", Advances in Radiation Oncology Physics — Dosimetry, Treatment Planning, and Brachytherapy (PURDY, J., Ed.), American Institute of Physics, New York (1992).

PODGORSAK, E.B., PODGORSAK, M.B., "Stereotactic irradiation", The Modern Technology in Radiation Oncology: A Compendium for Medical Physicists and Radiation Oncologists (VAN DYK, J., Ed.), Medical Physics Publishing, Madison, WI (1999) 589–640.

— "Special techniques in radiotherapy", ibid., pp. 641–693.

STERNICK, E.S. (Ed.), The Theory and Practice of Intensity Modulated Radiation Therapy, Advanced Medical Publishing, Madison, WI (1997).

VEETH, J.M., "Intraoperative radiation therapy in treatment of cancer", Frontiers of Radiation Therapy and Oncology, Vol. 31, Karger, Basle (1997).

VAN DYK, J., GALVIN, J.M., GLASGOW, G.P., PODGORSAK, E.B., Physical Aspects of Total and Half Body Irradiation, Report of Task Group 29, Report No. 17, American Association of Physicists in Medicine, New York (1986).

WEBB, S., The Physics of Conformal Radiotherapy, Institute of Physics Publishing, Bristol, United Kingdom (1997).

WOLKOV, H.B., "Intraoperative radiation therapy", Textbook of Radiation Oncology (LEIBEL, S.A., PHILIPS, T.L., Eds), W.B. Saunders, Philadelphia, PA (1998).

Chapter 16

RADIATION PROTECTION AND SAFETY IN RADIOTHERAPY

P. ORTIZ LÓPEZ
Division of Radiation, Transport and Waste Safety,
International Atomic Energy Agency,
Vienna

G. RAJAN
Medical Physics and Safety Section,
Bhabha Atomic Research Centre,
Mumbai, Maharashtra, India

E.B. PODGORSAK
Department of Medical Physics,
McGill University Health Centre,
Montreal, Quebec, Canada

16.1. INTRODUCTION

Soon after the discovery of X rays by Roentgen in 1895 and of natural radioactivity by Becquerel in 1896 it became apparent that ionizing radiation was not only useful for the diagnosis and treatment of disease but also harmful to human tissues. It has been recognized since early studies on X rays and radioactive minerals that exposure to high levels of radiation can cause clinical damage to tissues of the human body. In addition, long term epidemiological studies of populations exposed to radiation, especially the survivors of the atomic bombings of Hiroshima and Nagasaki in Japan in 1945, have demonstrated that exposure to radiation also has a potential for delayed effects such as induction of malignancies or damage to genetic material.

Ionizing radiation and radioactive substances are natural and permanent features of the environment, and thus the risks associated with radiation exposure can only be restricted, not eliminated entirely. Additionally, the use of human-made radiation is now widespread. Sources of ionizing radiation are essential to modern health care: disposable medical supplies sterilized by intense radiation have been central to combating disease; radiology and nuclear medicine are a vital diagnostic tool; and radiotherapy is commonly part

of the treatment of malignancies. Applications of ionizing radiation are growing in industry, agriculture, medicine and many other fields of industry and research, benefiting humanity. Irradiation is used around the world to preserve foodstuffs and reduce wastage, and sterilization techniques have been used to eradicate disease carrying insects and pests. Industrial radiography is in routine use, for example to examine welds, detect cracks and help prevent failure of engineered structures.

The acceptance by society of the risks associated with radiation is conditional on the benefits to be gained from the use of radiation. Nonetheless, the risks must be restricted and protected against by the application of radiation safety standards. It is therefore essential that activities involving radiation exposure be subject to certain standards of safety in order to protect the individuals who are exposed to radiation, be it occupationally, for medical diagnostic or therapeutic purposes, or as members of the public.

16.2. RADIATION EFFECTS

Exposure to radiation can cause detrimental health effects that fall into one of two categories: deterministic or stochastic.

16.2.1. Deterministic effects

At large doses, radiation effects such as nausea, reddening of the skin or, in severe cases, more acute syndromes are clinically expressed in exposed individuals within a relatively short period of time after the exposure; such effects are called deterministic because they are certain to occur if the dose exceeds a threshold level.

Deterministic effects are the result of various processes, mainly cell death or delayed cell division, caused by exposure to high levels of radiation. If extensive enough, these effects can impair the function of the exposed tissues. The severity of a particular deterministic effect in an exposed individual increases with dose above the threshold for the occurrence of the effect.

16.2.2. Stochastic effects

Radiation exposure can also induce delayed effects such as malignancies, which are expressed after a latency period and may be epidemiologically detectable in a population; this induction is assumed to take place over the entire range of doses, without a threshold level. Hereditary effects due to radiation exposure have been statistically detected in other mammalian

populations and are presumed to occur in human populations also. These epidemiologically detectable effects (malignancies and hereditary effects) are termed stochastic effects because of their random nature.

Stochastic effects may ensue if an irradiated cell is modified rather than killed. Modified cells may, after a prolonged delay, develop into a cancer. The body's repair mechanisms make this a very improbable outcome at small doses; nevertheless, there is no evidence of a threshold dose below which cancer cannot result. The probability of occurrence of cancer is higher for higher doses, but the severity of any cancer that may result from irradiation is independent of dose. If the cell damaged by radiation exposure is a germ cell whose function is to transmit genetic information to progeny, it is conceivable that hereditary effects of various types may develop in the descendants of the exposed individual. The likelihood of stochastic effects is presumed to be proportional to the dose received, without a dose threshold.

The many aspects of the concept of radiation detriment make it undesirable to select any single quantity to represent it. The concept of detriment as recommended by the ICRP for stochastic effects includes the following quantities: the probability of fatal cancer attributable to radiation exposure; the weighted probability of incurring a non-fatal cancer; the weighted probability of severe hereditary effects; and the length of lifetime lost, if the harm occurs.

16.2.3. Effects on the embryo and foetus

In addition to deterministic and stochastic health effects in adults, other health effects may occur in infants due to exposure of the embryo or foetus to radiation. These effects include a greater likelihood of leukaemia (stochastic effect) and, for exposure above various threshold dose values during certain periods of pregnancy, severe mental retardation and congenital malformations (deterministic effect). For more details on effects on the foetus see ICRP Publication 84.

16.3. INTERNATIONAL CONSENSUS AND RADIATION SAFETY STANDARDS

Safety standards are based on knowledge of radiation effects and on the principles of protection described below. In this respect, the development of safety standards by the IAEA follows a well established approach. The United Nations Scientific Committee on the Effects of Atomic Radiation (UNSCEAR), a body set up by the United Nations in 1955, compiles, assesses

and disseminates information on the health effects of radiation and on levels of radiation exposure due to different sources; this information was taken into account in developing the standards. Following a decision made in 1960, the IAEA safety standards are based on the recommendations of the ICRP, which also take account of the scientific information provided by UNSCEAR.

Purely scientific considerations, however, are only part of the basis for decisions on protection and safety, and the safety standards implicitly encourage decision makers to make value judgements about the relative importance of risks of different kinds and about the balancing of risks and benefits. General acceptance of risk is a matter of consensus, and therefore international safety standards should provide a desirable international consensus for the purpose of protection.

For these reasons, international consensus is basic to the IAEA standards, which are prepared with the wide participation of and approval by its Member States and relevant international organizations. The current version of the safety standard entitled International Basic Safety Standards for Protection against Ionizing Radiation and for the Safety of Radiation Sources (hereinafter referred to as the BSS) was issued in 1996 under the joint sponsorship of the Food and Agriculture Organization of the United Nations, IAEA, International Labour Organisation, OECD Nuclear Energy Agency, Pan American Health Organization and World Health Organization.

The BSS was published as IAEA Safety Series No. 115 and comprises four sections: preamble, principal requirements, appendices and schedules. The purpose of the report is to establish basic requirements for protection against exposure to ionizing radiation and for the safety of radiation sources that may deliver such exposure.

16.4. TYPES OF RADIATION EXPOSURE

Certain industrial or medical practices will result in some radiation exposure with predictable magnitudes, albeit with some degree of uncertainty; such expected exposures are referred to in the BSS as normal exposures.

In addition, scenarios can be envisaged for which there is a potential for exposure, but no certainty that an exposure will in fact occur; such unexpected but feasible exposures are termed potential exposures. Potential exposures can become actual exposures if the unexpected situation does occur, for example as a consequence of equipment failure, design problems or operating errors.

The means specified in the BSS for controlling normal exposures is the restriction of the doses delivered. In the case of exposure of patients, exposures

are controlled through delivering only the doses that are necessary to achieve the diagnostic or therapeutic objective.

The primary means for controlling potential exposures is by optimizing the design of installations, equipment and operating procedures with the following aims:

- To restrict the probability of occurrence of events that could lead to unplanned exposures;
- To restrict the magnitudes of the exposures that could result if such events were to occur.

The radiation exposures covered by the BSS encompass the exposures, both normal and potential, of:

— Workers pursuing their occupations (occupational exposures);
— Patients in diagnosis or treatment (medical exposures);
— Members of the public.

The radiation exposures are therefore divided into three categories:

(i) Occupational exposure, which is defined as all exposures of workers incurred in the course of their work (with the exception of exposures excluded from the BSS and exposures from practices or sources exempted by the BSS).

(ii) Medical exposure, which is defined as exposure incurred:
— By patients as part of their own medical or dental diagnosis or treatment;
— By persons, other than those occupationally exposed, knowingly while voluntarily helping in the support and comfort of patients;
— By volunteers in a programme of biomedical research involving their exposure.

(iii) Public exposure, which is defined as exposure incurred by members of the public from radiation sources, excluding any occupational or medical exposure and the normal local natural background radiation but including exposure to authorized sources and practices and from intervention situations.

16.5. QUANTITIES AND UNITS USED IN RADIATION PROTECTION

16.5.1. Physical quantities

Although most of the requirements of the BSS are qualitative, they also establish quantitative limits and guidance levels. The main physical quantities used in safety standards are the activity and absorbed dose:

- The activity $\mathcal{A}$ of an amount of a radionuclide in a particular energy state at a given time is the quotient of dN by dt, where dN is the number of spontaneous nuclear transformations from that energy state in the time interval dt:

$$\mathcal{A} = dN/dt = \lambda N = ((\ln 2)/t_{1/2})N \qquad (16.1)$$

where

λ is the decay constant of the radioactive nucleus;
N is the number of radioactive nuclides (atoms);
$t_{1/2}$ is the half-life of the radioactive nucleus.

The SI unit of activity is $1 \ s^{-1}$ and its name is the becquerel (Bq), representing one nuclear transformation (disintegration or decay) per second (i.e. $1 \ Bq = 1 \ s^{-1}$). The older unit of activity is the curie (Ci), representing $3.7 \times 10^{10} \ s^{-1}$ (i.e. $1 \ Ci = 3.7 \times 10^{10} \ Bq$). The curie was initially defined as the activity of 1 g of ^{226}Ra; however, refined measurements have shown that the activity of 1 g of ^{226}Ra is 0.988 Ci.

- The absorbed dose D is defined as the quotient of $d\bar{\varepsilon}$ by dm, where $d\bar{\varepsilon}$ is the mean energy imparted to matter of mass dm:

$$D = \frac{d\bar{\varepsilon}}{dm} \qquad (16.2)$$

The SI unit for absorbed dose is 1 J/kg and its name is the gray (Gy). The older unit of dose is the rad, representing 100 erg/g (i.e. 1 Gy = 100 rad).

16.5.2. Radiation protection quantities

The absorbed dose is the basic physical dosimetry quantity, but it is not entirely satisfactory for radiation protection purposes because the effectiveness in damaging human tissue differs for different types of ionizing radiation. In addition to the physical quantities, other dose related quantities have been

introduced to account not only for the physical effects but also for the biological effects of radiation upon tissues. These quantities are organ dose, equivalent dose, effective dose, committed dose and collective dose.

16.5.2.1. Organ dose

The organ dose is defined as the mean dose D_T in a specified tissue or organ T of the human body, given by:

$$D_T = \frac{1}{m_T} \int_{m_T} D \, dm = \frac{\varepsilon_T}{m_T} \tag{16.3}$$

where

m_T is the mass of the organ or tissue under consideration;
ε_T is the total energy imparted by radiation to that tissue or organ.

16.5.2.2. Equivalent dose

The biological detriment (harm) to an organ depends not only on the physical average dose received by the organ but also on the pattern of the dose distribution that results from the radiation type and energy. For the same dose to the organ, α or neutron radiation will cause greater harm compared with γ rays or electrons. This is because the ionization events produced by α or neutron radiation will be much more closely spaced (densely ionizing radiations) and so there is a higher probability of irreversible damage to the chromosomes and less chance of tissue repair.

Consequently, the organ dose is multiplied by a radiation weighting factor w_R to account for the effectiveness of the given radiation in inducing health effects; the resulting quantity is called the equivalent dose H_T.

The equivalent dose H_T is defined as:

$$H_T = w_R D_{T,R} \tag{16.4}$$

where

$D_{T,R}$ is the absorbed dose delivered by radiation type R averaged over a tissue or organ T;
w_R is the radiation weighting factor for radiation type R.

For X rays, γ rays and electrons $w_R = 1$; for protons $w_R = 5$; for particles $w_R = 20$; and for neutrons w_R ranges from 5 to 20, depending on the neutron energy.

The SI unit of equivalent dose is J/kg and its name is the sievert (Sv); the old unit is the rem and the relationship between the two units is 1 Sv = 100 rem; for example, for 1 Gy of photon dose to an organ, the equivalent dose is 1 Sv. However, for the same dose of 20 keV neutrons, the equivalent dose is 10 Sv, since the detriment is ten times larger (i.e. $w_R = 10$ for 20 keV neutrons).

The organ dose $D_{T,R}$ is a measure of the energy absorption per unit mass averaged over the organ, while the equivalent dose H_T is a measure of the consequent biological harm (detriment) to the organ or tissue T.

If an organ is irradiated by more than one type of radiation, the equivalent dose is given by the sum:

$$H_T = \sum w_R D_{T,R} \tag{16.5}$$

In earlier ICRP recommendations, weighting factors related to the quality of radiation were applied to the absorbed dose to a point, and the radiation weighted absorbed dose was called the dose equivalent H (not referred to an organ, but to a point).

16.5.2.3. Effective dose

The relationship between the probability of stochastic effects and equivalent dose is also found to depend on the organ or tissue irradiated. This implies that for the same equivalent dose the detriments from the exposure of different organs or tissues are different. To take account of these differences, tissue weighting factors are needed.

Tissue weighting factors w_T should represent the relative contribution of an organ or tissue to the total detriment due to the effects resulting from a uniform irradiation of the whole body. For low doses, individual organ or tissue detriments can be treated as additive and the total detriment to the whole body is the summation of individual detriments. The relative contribution to the total detriment is therefore given by the quotient between the individual detriment and the total detriment resulting from a uniform irradiation of the whole body. Since the sum of relative contributions is normalized to unity, the sum $\Sigma w_T = 1$.

The effective dose E is defined as the summation of tissue equivalent doses, each multiplied by the appropriate tissue weighting factor w_T, to indicate the combination of different doses to several different tissues in a way that correlates well with all stochastic effects combined (ICRP Publication 60):

$$E = \sum w_T H_T \tag{16.6}$$

Tissue weighting factors w_T are tabulated in ICRP Publication 60 and in IAEA safety standards. Despite depending on the sex and age of the person, for the purposes of radiation protection the values for tissue weighting factors are taken as constants and are applicable to the average population; for example, $w_T = 0.20$ for gonads, $w_T = 0.12$ for lung or red bone marrow and $w_T = 0.01$ for skin. Thus for the same equivalent dose, the risk of a stochastic effect at low doses is higher for gonads than for the lungs or red bone marrow.

The unit of effective dose is J/kg and its name is the sievert (Sv).

A uniform equivalent dose over the whole body gives an effective dose that is numerically equal to the uniform equivalent dose.

The weighing factors w_T and w_R are mutually independent; that is, the tissue risk factors w_T are independent of radiation type and the radiation weighting factors w_R are independent of tissue type, allowing us to write:

$$E = \sum_T w_T \sum_R w_R \, D_{T,R} = \sum_R w_R \sum_T w_T \, D_{T,R} \tag{16.7}$$

When one deals with only one type of radiation in a given situation, the effective dose is given by:

$$E = \sum w_T D_{T,R} \tag{16.8}$$

The effective dose is a measure of dose designated to reflect the amount of radiation detriment likely to result from the dose. Effective doses from various radiation types and exposure modes may be compared directly.

Annual dose limits for occupational and public exposure are given in terms of the annual effective dose; in the case of exposure of an organ or of hands or feet they are given in terms of equivalent dose.

The term 'effective dose' replaces the term 'effective dose equivalent' defined in earlier ICRP reports.

For a well defined geometry of irradiation, the equivalent dose H to individual organs or the effective dose E can be computed for an anthropomorphic phantom that simulates the human body. However, these quantities are not directly measurable, since there are no primary standards established for them.

16.5.2.4. Committed dose

When radionuclides are taken into the body, the resulting dose is received throughout the period of time during which they remain in the body. The total

dose delivered during this period of time is referred to as the committed dose and is calculated as a specified time integral of the rate of receipt of the dose. Any relevant dose restriction is applied to the committed dose from the intake. The committed dose may refer to the committed effective dose and the committed equivalent dose.

16.5.2.5. *Collective dose*

The radiation protection quantities discussed above relate to the exposure of an individual. The collective dose relates to exposed groups or populations and is defined as the summation of the products of the mean dose in the various groups of exposed people and the number of individuals in each group. The unit of collective dose is the man-sievert (man-Sv).

16.5.3. Operational quantities

The organ dose D_T, equivalent dose H and effective dose E are not directly measurable and there are no laboratory standards to obtain traceable calibrations for the radiation monitors using these quantities. For this reason, the ICRU has defined a set of measurable operational quantities for protection purposes: the ambient dose equivalent, directional dose equivalent and personal dose equivalent; the latter is used for comparing with regulatory requirements such as dose limits.

16.5.3.1. *Ambient dose equivalent*

The ambient dose equivalent at a point in a radiation field $H*(d)$ is defined as the dose equivalent that would be produced by the corresponding aligned and expanded field in the ICRU sphere at a depth d on the radius opposing the direction of the aligned field. The ICRU sphere is a 30 cm diameter tissue equivalent sphere with a composition of 76.2% oxygen, 11.1% carbon, 10.1% hydrogen and 2.6% nitrogen. A depth d = 10 mm is recommended for strongly penetrating radiation.

16.5.3.2. *Directional dose equivalent*

The directional dose equivalent at a point in a radiation field $H'(d, \Omega)$ is defined as the dose equivalent that would be produced by the corresponding expanded field in the ICRU sphere at depth d on a radius in a specified direction $\tilde{\Omega}$. A depth d = 0.07 mm is recommended for weakly penetrating

radiation. Angle Ω is the angle between the beam direction and the radius of the ICRU sphere on which the depth d is defined.

16.5.3.3. *Personal dose equivalent*

The personal dose equivalent $H_p(d)$ is defined for both strongly and weakly penetrating radiations as the equivalent dose in soft tissue below a specified point on the body at an appropriate depth d. The relevant depth is generally d = 10 mm for penetrating radiations (photon energies above 15 keV), while depths d = 0.07 mm and d = 3 mm are used for weakly penetrating radiations (photon energies below 15 keV and β radiations) in skin and the eye lens, respectively.

The personal dose equivalent from exposure to penetrating radiation during the year is the radiation quantity to be compared with the annual dose limits (for effective dose) and to demonstrate compliance with the BSS recommendations as indicated below (see the BSS, Schedule II).

16.6. BASIC FRAMEWORK OF RADIATION PROTECTION

The principles of radiation protection and safety upon which the radiation safety standards are based are those developed by the ICRP. The detailed formulation of these principles can be found in the ICRP publications and they cannot easily be paraphrased without losing their essence. However, a brief, although simplified, summary of the principles is given in this section.

A practice that entails exposure to radiation should only be adopted if it yields sufficient benefit to the exposed individuals or to society to outweigh the radiation detriment it causes or could cause (i.e. the practice must be justified).

Individual doses due to the combination of exposures from all relevant practices should not exceed specified dose limits for occupational and public exposure; dose limits are not applicable to medical exposure.

Radiation sources and installations should be provided with the best available protection and safety measures under the prevailing circumstances, so that the magnitudes and likelihood of exposures and the numbers of individuals exposed be as low as reasonably achievable (ALARA), economic and social factors being taken into account, and the doses they deliver and the risk they entail be constrained (i.e. protection and safety should be optimized):

- In diagnostic medical exposure, optimization of protection is achieved by keeping the exposure of patients to the minimum necessary to achieve the required diagnostic objective;

- In therapeutic medical exposure, optimization is achieved by keeping exposure of normal tissue ALARA consistent with delivering the required dose to the planning target volume (PTV) (from the BSS requirements in Appendix II).

As indicated in Section 16.13, pregnant workers shall be protected so as to ensure that the embryo or foetus is afforded the same broad level of protection as required for members of the public.

A safety culture should be inculcated that governs attitudes and behaviour in relation to the protection and safety of all individuals and organizations dealing with sources of radiation; in depth defensive measures should be incorporated into the design and operating procedures for radiation sources to compensate for potential failures in protection or safety measures; and protection and safety should be ensured by sound management and good engineering, quality assurance, training and qualification of personnel, comprehensive safety assessments and attention to lessons learned from experience and research.

Dose limits do not apply to medical exposure and are not relevant for the control of potential exposures, nor are they relevant for decisions on whether and how to undertake an intervention, but workers undertaking an intervention shall be subject to the relevant requirements of Appendix V of the BSS. Table 16.1 summarizes the values of annual dose limits.

16.7. GOVERNMENTAL REGULATION AND NATIONAL INFRASTRUCTURE

The BSS place requirements on legal persons authorized to conduct practices that cause radiation exposure or to intervene in order to reduce existing exposures; these legal persons have the primary responsibility for applying the standards. Governments, however, have a responsibility for their enforcement, generally through a system that includes a regulatory authority.

The authorizations of the legal persons to conduct a practice may take the form of a registration or a licence. The difference between a registration and a licence is that the latter requires a more specific safety assessment. The authorized legal persons are therefore called registrants and licensees. In the case of radiotherapy, the authorization usually takes the form of a licence.

In addition, national infrastructures include certain essential services, such as personal dosimetry, and services for calibration and intercomparison of radiation measuring equipment. The provision of such services at the national

TABLE 16.1. SUMMARY OF ANNUAL DOSE LIMITS ACCORDING TO BSS SCHEDULE II AND ICRP REPORT 60 (TABLE 6, p. 46)

	Occupational exposure	Exposure to apprentices 16–18 years of age	Public exposure
Effective dose (whole body) (mSv)	20, averaged over five consecutive years 50 in a single year[a]	6	1, averaged over five consecutive years 5 in a single year[b]
Equivalent dose (eye lens) (mSv)	150	50	15
Equivalent dose (hands, feet, skin) (mSv)	500	150	50

[a] Provided that the average effective dose over five consecutive years does not exceed 2 mSv/a.
[b] Provided that the average effective dose over five consecutive years does not exceed 1 mSv/a.

level does not detract from the ultimate responsibility for radiation protection and safety borne by the legal persons authorized to conduct the practices.

16.8. SCOPE OF THE BASIC SAFETY STANDARDS

Paragraph 1.3 of the BSS (Principal Requirements, Scope) states, inter alia, that:

"*The Standards apply to practices, including any sources within the practices, and interventions which are:*

(a)   carried out in a State that chooses to adopt the Standards or requests any of the Sponsoring Organizations to provide for the application of the Standards;

(b)   undertaken by States with the assistance of the FAO, the IAEA, the ILO, the PAHO, or the WHO, in the light of relevant national rules and regulations;

(c)   carried out by the IAEA or involve the use of materials, services, equipment, facilities and non-published information made available by the IAEA or at its request or under its control or supervision;…"

16.9. RESPONSIBILITIES FOR IMPLEMENTATION OF BASIC SAFETY STANDARDS REQUIREMENTS

Paragraph 1.6 of the BSS (Principal Requirements, Responsible Parties) states that:

"*The principal parties having the main responsibilities for the application of the Standards shall be:*

(a)   registrants or licensees; and
(b)   employers."

Paragraph 1.7 of the BSS (Principal Requirements, Responsible Parties) states that:

"*Other parties shall have subsidiary responsibilities for the application of the Standards. These parties may include, as appropriate:*

(a)   suppliers;
(b)   workers;
(c)   radiation protection officers;
(d)   medical practitioners;
(e)   health professionals;
(f)   qualified experts;
(g)   Ethical Review Committees; and
(h)   any other party to whom a principal party has delegated specific responsibilities."

Specific responsibilities for medical exposure are given in Section 16.14 of this chapter.

16.10. SAFETY IN THE DESIGN OF RADIATION SOURCES AND EQUIPMENT

Paragraph II.11 of the BSS (Appendix II, Medical Exposure, Optimization of Protection for Medical Exposures) states, inter alia, that:

"*…equipment used in medical exposure shall be so designed that:*

(a)   *failure of a single component of the system be promptly detectable so that any unplanned medical exposure of patients is minimized; and*

(b)   *the incidence of human error in the delivery of unplanned medical exposure be minimized.*"

16.10.1. Equipment

Radiation sources, including radioactive material, equipment and accessories, should be purchased only from authorized suppliers and should have a valid type test. Procedures for the purchase, installation, acceptance, commissioning, use, maintenance and quality control of such material should be developed with the involvement of qualified experts and the quality assurance/radiation protection committee.

Paragraph II.13 of the BSS (Appendix II, Medical Exposure, Optimization of Protection for Medical Exposures) states, inter alia, that:

"*Registrants and licensees, in specific co-operation with suppliers, shall ensure that, with regard to equipment consisting of radiation generators and that containing sealed sources used for medical exposures:*

(a)   *whether imported into or manufactured in the country where it is used, the equipment conform to applicable standards of the International Electrotechnical Commission (IEC) and the ISO or to equivalent national standards;*

(b)   *performance specifications and operating and maintenance instructions, including protection and safety instructions, be provided in a major world language understandable to the users and in compliance with the relevant IEC or ISO standards with regard to 'accompanying documents', and that this information be translated into local languages when appropriate;*

(c)   *where practicable, the operating terminology (or its abbreviations) and operating values be displayed on operating consoles in a major world language acceptable to the user;…*"

Paragraph II.15 of the BSS (Appendix II, Medical Exposure, Optimization of Protection for Medical Exposures) states, inter alia, that:

"*Registrants and licensees, in specific co-operation with suppliers, shall ensure that:*

(a) *radiation installations using radioactive sources be fail-safe in the sense that the source will be automatically shielded in the event of an interruption of power and will remain shielded until the beam control mechanism is reactivated from the control panel;*

(b) *high energy radiotherapy equipment should:*

   (i)   *have at least two independent 'fail to safety' systems for terminating the irradiation; and*

   (ii) *be provided with safety interlocks or other means designed to prevent the clinical use of the machine in conditions other than those selected at the control panel;…"*

The IEC standards applicable to radiotherapy are:

- IEC 601-2-1, for medical electron accelerators;
- IEC 60601-2-11, for external beam radiotherapy;
- IEC 60601-2-17, for remote afterloading brachytherapy;
- IEC 601-2-8, for superficial therapy with X rays;
- IEC 60601-2-29, for therapy simulators;
- IEC 62C/62083, for treatment planning systems (TPSs);
- IEC 60601-1-4, for computer controlled or programmable medical systems.

Evidence of compliance with the IEC or equivalent national standards should be demonstrated. For type tests, sufficient evidence of compliance may be provided by the manufacturer's records with the results of the tests for the relevant equipment type and model. This should be supplemented by acceptance tests for the individual piece of equipment delivered. The relevant safety tests described in the IEC standards should be included in the acceptance protocol and be specified in the purchasing conditions. More detailed guidance is provided in IAEA-TECDOC-1040.

The IEC standards prescribe the tests to be carried out by the manufacturer for a given type of equipment and for site tests to be carried out at the hospital on every individual piece of equipment. The IEC distinguishes three grades of test:

- Grade A: this grade refers to an analysis of the equipment design related to an IEC safety requirement. It results in a written statement included in the technical description regarding the working principles or constructional means by which the IEC requirement is fulfilled.
- Grade B: visual inspection or functional test or measurement. For this test grade the relevant IEC standard specifies a procedure (see, for example,

IEC 60601-2-1). The test should then be performed according to the IEC procedure. Grade B tests may include fault conditions, which are achievable only without interference with the circuitry or construction of the equipment.

● Grade C: functional test or measurement, which may involve interference with circuitry or the construction of the equipment, and should be performed by, or under the direct supervision of, the manufacturer or its agent.

The equipment design should allow interruption of the irradiation from the control panel, and after the interruption resumption of irradiation should only be possible from the control panel. External beam radiotherapy equipment containing radioactive sources and high dose rate (HDR) brachytherapy equipment should be provided with a device to return sources manually to the shielded position in the event of an emergency. For Gamma Knifes it should be possible to close the shielding door manually.

Irradiation heads for external beam radiotherapy, source containers in brachytherapy and other devices containing radioactive sources should have a clear permanent sign indicating the existence of radioactive material (i.e. the ISO 361 symbol).

In addition, when outside the radiotherapy department all devices containing radioactive sources should be labelled with a warning that is recognized as 'danger' by any member of the public. The ISO radiation symbol, shown in Fig. 16.1, is not intended to be a warning signal of danger but only of the existence of radioactive material.

Accidents involving members of the public have occurred when the ISO symbol was present but not recognized as indicating danger. This prompted the IAEA to coordinate work on reaching an international agreement for a radiation danger warning sign.

16.10.2. Sealed sources

Paragraph II.15 of the BSS (Appendix II, Medical Exposure, Optimization of Protection for Medical Exposures) states, inter alia, that:

"*(e) Radioactive sources for either teletherapy or brachytherapy shall be so constructed that they conform to the definition of a sealed source;…*"

A sealed source is defined in the BSS glossary as radioactive material that is:

FIG. 16.1. The ISO 361 radiation symbol.

"(*a*) *permanently sealed in a capsule or (b) closely bounded and in a solid
   form.*"

The capsule or material of a sealed source shall be strong enough to maintain leaktightness under the conditions of use and wear for which the source was designed, and also under foreseeable mishap. To meet the requirements of BSS para. II.15, sealed sources used for external beam radiotherapy and brachytherapy should comply with ISO 2919.

Applicators for brachytherapy should be those manufactured specifically for the source or those with which they are compatible. The use of radioactive sources after their manufacturer-recommended working life should be continued only upon leak testing and with approval of the regulatory authority. The use of older teletherapy units containing ^{137}Cs and brachytherapy sources incorporating ^{226}Ra or old ^{137}Cs in preloaded applicators is no longer justified. Preloaded applicators and sources should be replaced as soon as practicable with afterloading sources not containing ^{226}Ra. Sources using β emitters should be provided with shielding of low atomic number materials to minimize bremsstrahlung production while in storage or while undergoing preparation for use.

16.10.3. Safety in the design of facilities and ancillary equipment

As a general rule, the design of a radiotherapy facility needs to make provisions for safety systems or devices associated with the equipment and treatment room. This includes electrical wiring related to emergency off switches, safety interlocks and warning signals.

Appropriate methods and data for shielding calculations are presented in ICRP Publication 33 and the NCRP 49 report. An appropriate qualified expert should carry out the overall design of the facility, including shielding calculations. Examples of shielding calculations are given in Section 16.17. Additional information on the design of radiotherapy facilities can be found in IAEA-TECDOC-1040, IEC Report 61859 and a report by the IPEM.

Radiation monitoring equipment should be available on the site in the vicinity of installations using sources of ionizing radiation.

Paragraph II.15 of the BSS (Appendix II, Medical Exposure, Optimization of Protection for Medical Exposures) states, inter alia, that:

"*(f) when appropriate, monitoring equipment be installed or be available to give warning of an unusual situation in the use of radiation generators and radionuclide therapy equipment.*"

16.10.3.1. Manual brachytherapy

Typical safety features for the storage and preparation of radioactive sealed sources for manual brachytherapy are the following:

- The room should be used only for source storage and preparation by designated and trained personnel.
- The room should be provided with a locked door to control access and maintain source security (see Section 16.12).
- A radiation sign should be posted on the door.
- There should be shielded storage (a safe) available for all sources. The outer surface of the storage shall be made of fireproof materials. The safe should be located near the preparation workbench to reduce the exposure of personnel during the handling and transfer of sources.
- The safe should have compartments for different source activities. Each compartment should be marked so as to permit immediate and easy identification of its contents from the outside with a minimum of exposure.
- The workbench should be provided with an L block shielding with a lead glass viewing window.

- The source handling area should be well illuminated and a magnifying glass in a fixed mounting should be available in order to handle sources efficiently and with a minimum of radiation exposure.
- Devices for handling sources, especially forceps, should be available. They should be as long as practicable and compatible with efficient source handling. A device should be provided for threading sources expeditiously, with the fingers protected by distance.
- Sources should be readily identifiable by sight. When radioactive sources of the same appearance but of different activities are used, they should be distinguishable, for example by different coloured threads or beads.
- The working surface for source preparation should be smooth and seamless to avoid loosing small sources such as ^{192}Ir wire fragments.
- The source storage and preparation laboratory should have a sink for cleansing sources, provided with a filter or trap suitable for preventing loss of sources through the drainage system.
- There should be a clear indication of the radiation level in the room. This may be achieved by an area radiation monitor that is visible on entering the room and during any handling of unshielded sources, or a survey meter should be available and in use during source handling.
- Space should be available for secure storage to enable the decay of short half-life sources such as ^{192}Ir.
- Hand carried transport containers must be provided with long handles and the lid of the container must be securely fastened to prevent tipping and dropping of sources during transport. Containers should bear the radiation symbol as well as a warning sign.
- Space should be available for source transport trolleys with source containers.

It is preferable that patient treatment rooms be for individual patients and adjacent to each other. If this is not possible, appropriate shielding between one patient and another is required.

— Shielding should be provided for nurses and visitors of brachytherapy patients, for which movable shields may be used within patient rooms, especially in manual brachytherapy.
— Prior to each treatment, movable shields should be placed close to the patient's bed in such a way that exposure of the nurses caring for the patient is minimized. This is achieved by anticipating the nurse's tasks, positions and movements throughout the room.

— The treatment room should contain a shielded storage container (large enough to accept applicators if necessary) and a remote handling tool (forceps) for the event of a dislodged source.

— Sterilization facilities for preloaded applicators, if they are still temporarily used until replacement by remote afterloading applicators, should be available in preparation or treatment rooms to ensure sufficient protection.

— An area monitor should be placed at the treatment room entrance so as to detect when a source or a patient with a source is leaving the room area. In order to ensure that no source remains within the patient, clothes or bed linen, or in the area after treatment, a portable monitor shall be available for monitoring these items.

16.10.3.2. Remote control brachytherapy and external beam radiotherapy

External beam radiotherapy and HDR brachytherapy should be carried out in specially designed treatment rooms within the radiotherapy department, while low dose rate (LDR) remote control brachytherapy can be performed in the ward in the area where manual brachytherapy is performed. The treatment room shielding should be designed in accordance with suitable recommendations (ICRP Publication 33 and the NCRP 49 report). The room should be large enough to accommodate the treatment machine, allowing the full range of motion of the treatment table and patient transport.

With regard to treatment rooms for HDR brachytherapy, IAEA-TECDOC-1040 states the following:

"*If the feasibility of sharing a shielded treatment room between an HDR unit and another currently-used treatment machine is considered, it should be carefully evaluated. To avoid scheduling problems considerations should include the anticipated number of HDR procedures as well as the number of external beam treatments. This report recommends against this strategy in most instances.*"

Access to the irradiation room shall be furnished with a visible signal indicating whether the radiation source is on or off. A door interlock or other suitable means to prevent unauthorized access should be provided and a power fail safe area radiation monitor should be visible on entering the room. The mechanism should be capable of maintaining irradiation interruption until the door is closed and locked and verification has been made that no person but the patient is inside the room. After an interruption, provided that no

operating parameters are changed or reselected, it should be possible to restart the irradiation, but only from the equipment control panel.

One or more emergency off switches should be conveniently placed inside the treatment room to allow interruption of the irradiation from inside the room. The control panel should be installed in such a way that the operator will have a total overview of the access to the irradiation room at all times. Adequate systems, devices or other means should be provided to allow the operator to have a clear and full view of the patient.

The systems for patient observation should be redundant and independent (e.g. closed circuit television or lead glass windows, depending on the type of treatment unit). Oral communication should be possible with the treatment rooms and patients by using an intercom or other communication system. Fire-fighting means should be available in order to preserve the integrity of radioactive sources in the event of a fire. An installed radiation monitor and/or a portable survey instrument should be used to confirm the safe condition of the source.

16.11. SAFETY ASSOCIATED WITH ACCEPTANCE TESTS, COMMISSIONING AND OPERATION

After equipment installation, acceptance tests should be conducted in order to verify that the equipment conforms to the technical specifications given by the manufacturer and to verify compliance with the safety requirements of the IEC standards. Usually the equipment belongs to the supplier until the acceptance process has been completed. The tests are usually performed by a manufacturer's representative in the presence of personnel representing the user (a qualified expert in radiotherapy physics), who will decide on acceptance. The first test in the acceptance procedure of a radiation emitting device must be a rigorous area survey of the surroundings of the treatment room that houses the radiation emitting machine.

As discussed in detail in Chapter 10, the tests to be included in the acceptance protocol should be specified in the purchasing conditions and contracts and should clearly establish the responsibility of suppliers for resolving any non-conformity identified during acceptance testing. The grade B and C tests specified in the IEC standard for a particular machine can be used as guidance for preparing the test protocol.

After acceptance and before starting operation, calibration of radiation sources and radiation beams as well as commissioning is performed. These phases are critical to patient safety, as shown in accidental exposures, involving in some instances a large number of patients, in which commissioning tests

were not carried out or were done poorly (see IAEA Safety Reports Series No. 17). During commissioning the qualified expert in radiotherapy physics measures all data required for the clinical use of the machine, including data used in TPSs.

Acceptance tests and commissioning should not be restricted to radiation emitting equipment or sources but should also be conducted for any system that has implications on safety, such as the TPS. Improper commissioning of TPSs has been the cause of several accidental medical overexposures or under-exposures, both detrimental to the treatment outcome.

Quality controls need to be carried out following formally established quality control protocols:

- Periodically under normal operating conditions;
- After the source has been installed or replaced;
- After repairs or maintenance work carried out on a treatment machine that have the potential to alter the radiation output.

An independent audit of the calibration of the source should be carried out before starting clinical use of the source. Quality assurance is dealt with in detail in Chapter 10. The BSS requirements on quality assurance for medical exposure are provided in Section 16.14.

Equipment should be operated in accordance with the technical documents, ensuring satisfactory operation at all times in respect of both the tasks to be accomplished and radiation safety. In particular, the manufacturer's operating manual, and any additional procedures, should be approved in accordance with the quality assurance system (see Section 16.10 for the BSS requirements on equipment) by a national or international body that is responsible for type approval of radiation emitting devices.

Sealed sources should be subject to leak tests prior to the first use and at regular intervals thereafter, in conformity with ISO 9978. Leak tests should be capable of detecting the presence of 0.2 kBq of removable contamination from the sealed source:

— For manual brachytherapy sources the typical method is the direct wet wipe test.
— For external beam radiotherapy and remote control brachytherapy the method to be used is the indirect wipe test of the nearest accessible surface.
— For ^{226}Ra sources immersion or gas emanation tests are adequate; however, ^{226}Ra should be replaced by other radionuclides as soon as practicable.

The sterilization process in brachytherapy should be appropriate for preventing damage to sources and applicators that could affect safety.

16.11.1. Safe operation of external beam radiotherapy

Safe operation of external beam treatment units requires procedures for wipe tests, area surveys and interlock checks and procedures for emergencies such as a source that becomes stuck in the on or partially on position. Such procedures require that the necessary equipment be available, calibrated and in working order.

The equipment includes:

● A radiation monitor of the Geiger–Müller (GM) type;
● A radiation monitor, ionization chamber type, with scales from microsieverts onwards;
● Equipment for wipe tests, such as well counters and multichannel analysers;
● Personal alarm dosimeters, especially for emergency intervention.

The procedures for the use of this equipment should recognize that some instruments will 'lock up' in a high radiation field and read erroneously. Hence the procedure should require a three step process:

— Checking the battery;
— Checking the monitor response with a check source;
— Turning the instrument on and starting to monitor from outside the room in which the source is located (i.e. from the lower to the higher dose rate areas).

During clinical operation the presence of other staff in the area of the control panel should be limited to the minimum in order to avoid distracting the operator.

16.11.2. Safe operation of brachytherapy

The source strength (usually in terms of the reference air kerma rate) of each brachytherapy source should be determined individually before it is used on a patient (see Chapter 13). The source documentation should be checked carefully. It is essential that the unit of activity used for source calibration be the same as the unit of activity used in the TPS. Some of the accidental exposures in brachytherapy have been caused by errors in the manufacturer's

specification of the activity of one or several sources and others by the unit of activity used in the hospital being different from the unit stated by the manufacturer (see IAEA Safety Reports Series No. 17 and ICRP Publication 86).

After verification of the source strength, the source or source holder should be marked with unique identifiers (e.g. a pre-established colour) to facilitate visual recognition and to prevent the possibility of confusion among different sources. Containers used for the transport of radioactive sources shall be in conformance with the requirements established in the IAEA Regulations for the Safe Transport of Radioactive Material.

The movements of the sources from the time they have left the safe until their return should be documented and signed by the person responsible for the move (using forms or a logbook). A person should be assigned to be in charge of accountability of the sources. This person should keep a record, with signatures, of the source order and issuance from and return to the safe (see requirements for source security below).

LDR and HDR sources have certain common operating procedures for safe use:

- Source inventories should be performed that show the location and current activity of each source at the facility, with a unique identifier for each source. This may be either a colour coded or a letter–number identifier.
- Sources should never be left on preparation surfaces. They must be in storage, in transit or inside the patient.
- Leak tests (using moist wipes) need to be performed and documented on a periodic basis and should have a sensitivity that is sufficient to detect a very low increase above the background radiation.
- For HDR units wipe tests are only performed on the afterloading drive assembly and transport containers, since the source itself has too high an activity to allow this sort of test.
- Area surveys are to be performed periodically around the source storage facilities for LDR and HDR sources.
- The storage facilities are to be marked to indicate that they contain radioactive material. The person responsible for radiation safety in the event of an emergency should be clearly indicated.
- The storage facilities are to be kept locked at all times.
- After every brachytherapy treatment, the patient has to be monitored with a radiation survey meter so as to ensure that no activity remains in the patient.

Specific precautions to be observed during the cutting and handling of ^{192}Ir wires should include ensuring that:

— Appropriate tools and equipment such as forceps, cutting devices, magnifying glasses and good illumination of the work surface are available and used; if ^{192}Ir wires are cut off for immediate use, a container to hold cut lengths should be provided and labelled.
— Radioactive waste is collected and stored in adequate containers.
— Surfaces and tools are properly decontaminated.

The following information should be posted for brachytherapy treatments: identification of the patient, sources, date and time of insertion and removal, nursing required, time allowance for nurses and visitors, and concise instructions for unplanned source and applicator removal and for emergency. A patient with a removable source in or upon his or her body should not leave the room unless accompanied by a hospital attendant.

Upon completion of treatment the licensee should ensure that all brachytherapy sources are removed from the patient, except in the case of permanent implants. The patient should be monitored with a portable detector to ensure that no source remains in or on the patient. Linen, dressings, clothing and equipment should be kept within the room where the removal of sources takes place until all sources are accounted for, and should be monitored with a radiation survey meter. Rubbish bins, soiled dressing bins and laundry baskets coming from a brachytherapy ward or other area where brachytherapy sources are employed should be monitored with a radiation survey meter.

Mobile containers and portable equipment containing radioactive sources should be moved to a storage room or to a secure place when not in use.

16.11.2.1. Safe operation of manual brachytherapy

The following is necessary for the safe operation of manual brachytherapy:

• The sources should be inspected visually for possible damage after each use by means of magnifying viewers and a leaded viewing window in a shielded work area.
• A diagram should be provided at the source storage safe showing the exact location of each source within the safe; this aids in reducing the time it takes to locate and identify a source.

- The sources should be handled only with long forceps or tongs, never directly with the fingers.
- When transporting the sources a mobile, shielded container is needed and the shortest route possible should be used.
- Sources that come into direct contact with body tissues require cleaning and possible sterilization after each use, which can subject the sources to possible damage from heat, abrasion, chemical attack and mechanical stresses. These sources must therefore be inspected after every use.
- The work surfaces should be easily cleaned and brightly lit to make it easy to find any sources that have been dropped.
- As indicated in Section 16.10, a filter should be used to prevent loss of sources to the drainage system while cleaning in the sink.

16.11.2.2. Safe operation of remote control afterloading brachytherapy

The following is necessary for the safe operation of remote control after-loading brachytherapy:

- Quality control of the afterloader including tests to be performed at the beginning of each treatment day.
- The couplings and transfer tubes need to be checked (for HDR brachytherapy it has to be done before each treatment) to ensure that there is nothing to prevent source motion.
- Remote afterloading equipment requires specific emergency procedures, which are especially critical in HDR brachytherapy. These procedures are dealt with in Section 16.16.

16.12. SECURITY OF SOURCES

Paragraph 2.34 of the BSS (Requirements for Practices, Technical Requirements) states, inter alia, that:

"*Sources shall be kept secure so as to prevent theft or damage and to prevent any unauthorized legal person from carrying out any of the actions specified in the General Obligations for practices of the Standards (see paras 2.7–2.9) by ensuring that:*

(a)   control of a source not be relinquished without compliance with all relevant requirements specified in the registration or licence and without immediate communication to the Regulatory Authority… of

information regarding any decontrolled, lost, stolen or missing source;

(b) *a source not be transferred unless the receiver possesses a valid authorization; and*

(c) *a periodic inventory of movable sources be conducted at appropriate intervals to confirm that they are in their assigned locations and are secure.*"

The objective of source security is to ensure continuity in the control and accountability of each source at all times in order to meet the requirement in para. 2.28 of the BSS. Specific provisions shall be made for situations in which loss of control could lead to accidents, such as:

- Storage of sources before installation;
- Temporary or permanent cessation in use;
- Storage after decommissioning awaiting a decision on source return or disposal;
- Brachytherapy sources remaining in the patient, clothes, bed linen or treatment area.

To comply with this requirement, the licensee needs to develop procedures to ensure the safe exchange and movement of radioactive sources within the institution and establish controls to prevent theft, loss, unauthorized withdrawal or damage of sources, or entrance of unauthorized personnel to the controlled areas.

The licensee also needs to check the number of sources in a container when removing and when returning the sources and should perform a physical inventory of all sealed sources to confirm that they are present and secure in their assigned locations. The licensee should maintain a source movement log with a record indicating the date of removal, the name of the patient and the return of the source.

Radiotherapy equipment should be equipped with safety systems capable of preventing their use by unauthorized personnel. A key should be required to energize the system, access to which should be restricted to authorized staff. Any loss of a source should be reported immediately to the radiation protection officer, who should report it to the regulatory authority. All linen, dressing, clothing, equipment and refuse containers should be kept within the brachytherapy patient's room until checks have been performed and documented that sources are not attached to them.

16.13. OCCUPATIONAL EXPOSURE

Detailed requirements for protection against occupational exposure are given in the BSS, while the recommendations on how to meet these require-ments are given in the IAEA Safety Guide on Occupational Radiation Protection, Safety Standards Series No. RS-G-1.1, and the IAEA Safety Guide on Assessment of Occupational Exposure Due to External Sources of Radiation, Safety Standards Series No. RS-G-1.3. A summary of the most relevant issues for radiotherapy is given in this section.

16.13.1. Responsibilities and conditions of service

The parties responsible for protection against occupational exposure are not only the licensees but also the employers. In some cases the employer and the licensee are the same legal person, but in other cases they may be different; for example, the employer of a maintenance engineer may be the maintenance company, while maintenance engineers work in many radiotherapy depart-ments, each one under a different licensee.

16.13.2. Use of dose constraints in radiotherapy

Dose constraints can be used for optimizing protection in the planning stage for each radiation source. Anticipated individual doses should be compared with the appropriate dose constraints and protective measures should be taken to keep doses below the dose constraints. The BSS definition of dose constraint is:

"*For occupational exposures, dose constraint is a source related value of individual dose used to limit the range of options considered in the process of optimization.*"

Since dose constraints are source related, the source should be specified; for example, when choosing source related dose constraints for the sources involved in a radiotherapy facility, consideration should be given to the fact that medical and paramedical staff may work in more than one hospital and be exposed to sources from two radiotherapy departments (e.g. in one hospital in the morning and in another hospital in the evening).

16.13.3. Investigation levels for staff exposure in radiotherapy

Investigation levels are a tool used to provide a 'warning' on the need to review procedures and performance, investigate what is not working as expected and take timely corrective action. In radiotherapy, a suitable quantity for use as the investigation level is the monthly effective dose itself, but the dose to the hands can be used as a quantity for the investigation level for staff in manual brachytherapy. In radiotherapy departments in which different staff members are dedicated to specific work or tasks, different investigation levels can be associated with the various tasks.

The following are examples of related tasks and their levels that are rarely exceeded, and therefore could be suitable as investigation levels:

- For staff working only with accelerators or remote control brachytherapy, a monthly investigation level of 0.2 mSv effective dose;
- For staff working with ^{60}Co external beam radiotherapy, brachytherapy nurses and persons inserting and removing manual brachytherapy sources, a monthly investigation level of 0.4 mSv effective dose.

16.13.4. Pregnant workers

Paragraph I.16 of the BSS (Appendix I, Occupational Exposure, Conditions of Service) states that:

"*A female worker should, on becoming aware that she is pregnant, notify the employer in order that her working conditions may be modified if necessary.*"

Paragraph I.17 of the BSS (Appendix I, Occupational Exposure, Conditions of Service) states that:

"*The notification of pregnancy shall not be considered a reason to exclude a female worker from work; however, the employer of a female worker who has notified pregnancy shall adapt the working conditions in respect to occupational exposure so as to ensure that the embryo or foetus is afforded the same broad level of protection as required for members of the public.*"

This is especially relevant, for example, in manual brachytherapy, where under normal conditions the dose to the foetus in certain workers may reach

the dose limit for members of the public established in the BSS (see Table 16.1).

16.13.5. Classification of areas

Relevant areas of a practice can be classified as either controlled or supervised, according to the BSS (paras I.21–I.25).

A controlled area is defined as an area in which specific protection measures and safety provisions are needed for controlling normal exposure and for preventing potential exposure. In radiotherapy practice, areas requiring specific protection measures (controlled areas) include:

- All irradiation rooms for external beam radiotherapy;
- Remote afterloading brachytherapy treatment rooms;
- Operating rooms during brachytherapy procedures using real sources;
- Brachytherapy patient rooms;
- All radioactive source storage and handling areas.

It is preferable to define controlled areas by physical boundaries such as walls or other physical barriers marked or identified with radiation area signs.

A supervised area is an area that should be kept under review even though specific protection measures and safety provisions are not normally needed. Supervised areas may include areas requiring a regular review of the radiological conditions to determine whether there has been some breakdown of control in the procedures. Supervised areas may involve areas surrounding brachytherapy patient rooms or around radioactive source storage and handling areas.

All areas designated as neither controlled nor supervised areas should be such that persons in them would receive the same level of protection as members of the public.

16.13.6. Local rules and supervision

The rules and procedures listed in Section 16.11 include those needed for occupational protection. Management should make the rules known to those to whom they apply and ensure that they are followed by assigning responsibilities for supervision of tasks.

16.13.7. Protective equipment and tools

Paragraph I.28 of the BSS (Appendix I, Occupational Exposure, Personal Protective Equipment) states, inter alia, that:

"*Employers… and licensees shall ensure that:*

(a)   workers be provided with suitable and adequate personal protective equipment…"

Protective equipment for radiotherapy is discussed in Section 16.10.

16.13.8. Individual monitoring and exposure assessment

The purpose of monitoring and exposure assessment is to gather and provide information on the actual exposure of workers and to confirm good working practices contributing to reassurance and motivation. The BSS requires individual monitoring for any worker who is normally employed in a controlled area and who may receive a significant occupational exposure.

Those radiotherapy professionals most likely to require individual monitoring are radiation oncologists, qualified experts in radiotherapy physics, radiation protection officers, radiotherapy technologists, source handlers, maintenance staff and any nursing or other staff who must spend time with patients who contain radioactive sources.

Monitoring includes more than just measuring and determining the equivalent dose; it includes interpretation and assessment. Individual external doses can be determined by using individual monitoring devices such as thermoluminescent dosimeters (TLDs) or film badges, which are usually worn on the front of the upper torso (in most radiotherapy procedures the whole body is assumed to be fairly uniformly exposed). When the possibility exists of exposure to the hands, such as in the handling of brachytherapy sources, extremity dosimeters need to be worn (if compatible with clinical practice).

In a radiotherapy department the personal dosimeters should be exchanged at regular intervals not exceeding three months. Moreover, the reports on read dosimeters should become available as soon as possible but no later than within three months after the exchange. Delays in the evaluation of a dosimeter can result in the loss of the stored information.

If an individual's dosimeter is lost, the licensee shall perform and document an assessment of the dose the individual received and add it to the worker's dose record. Often the most reliable method for estimating an individual's dose is to use his or her recent dose history, provided that nothing

unusual occurred in the period. Individual monitoring devices are to be calibrated, and this calibration shall be traceable to a standards dosimetry laboratory.

16.13.9. Monitoring of the workplace

The BSS requires licensees in cooperation with employers to develop programmes for monitoring the workplace (paras I.37–I.40). Initial monitoring is to be conducted immediately after the installation of new radiotherapy equipment and after the replacement of teletherapy sources and remote controlled brachytherapy sources. Initial monitoring should include measurements of radiation leakage from equipment within the acceptance tests and area monitoring of occupied space around irradiation rooms.

Monitoring of exposure levels should be conducted through the use of area monitors in teletherapy and HDR treatment rooms. Monitoring of the source storage and handling area is to be conducted with a survey meter immediately following the removal from or return to storage of brachytherapy sources.

Monitoring is to be conducted in association with brachytherapy procedures. Soon after implantation of the sources, a survey should be made of exposure rates in the vicinity of the patient. After removal of the brachytherapy sources from a patient, a survey is to be performed to confirm removal from the patient and return to shielding of all sources. The transport container should be surveyed before and after brachytherapy procedures.

Monitoring of packages containing radioactive sources upon receipt by the licensee is to be performed. All survey meters used for workplace monitoring must be calibrated, and this calibration shall be traceable to a standards dosimetry laboratory.

16.13.10. Health surveillance

Paragraph I.41 of the BSS (Appendix I, Occupational Exposure, Health Surveillance) states, inter alia, that:

"*Employers… and licensees shall make arrangements for appropriate health surveillance in accordance with the rules established by the Regulatory Authority.*"

The primary purpose of medical surveillance is to assess the initial and continuing fitness of employees for their intended tasks.

Health surveillance programmes shall be based on the general principles of occupational health. No specific health surveillance related to exposure to ionizing radiation is necessary for staff involved in the operation of a radiotherapy practice. Only in the case of overexposed workers at doses much higher than the equivalent dose limits (e.g. 0.2–0.5 Sv or higher) would special investigations involving biological dosimetry and further extended diagnosis and medical treatment be necessary.

Counselling should be available to workers such as women who are or may be pregnant, or are breastfeeding a child, individual workers who have or may have been exposed substantially in excess of the dose limits and workers who may be worried about their radiation exposure. This is particularly necessary for women who are or may be pregnant, such as female technologists working in radiotherapy and nurses working in brachytherapy wards.

16.13.11. Records

Paragraph I.44 of the BSS (Appendix I, Occupational Exposure, Records) states, inter alia, that:

"*Employers… and licensees shall maintain exposure records for each worker…*"

The exposure records shall include the following:

- Information on the general nature of work involving occupational exposure;
- Information on the doses and data upon which dose assessments have been based;
- When a worker is or has been occupationally exposed while in the employ of more than one employer;
- Information on the dates of employment with each employer and the doses, exposures and intakes in each such employment;
- Records of any doses due to emergency interventions or accidents, which shall be distinguished from doses incurred during normal work.

Employers and licensees shall provide for access by workers to information contained in their own exposure records, and give due care and attention to the maintenance of appropriate confidentiality of records.

16.14. MEDICAL EXPOSURE

The detailed requirements given in Appendix II of the BSS are applicable in particular to radiotherapy sources. In addition, the IAEA Safety Guide on Radiological Protection for Medical Exposure to Ionizing Radiation (Safety Standards Series No. RS-G-1.5) describes strategies to involve organizations outside the regulatory framework, such as professional bodies (those for radiation oncology and medical physics), whose cooperation is essential to ensure compliance with the BSS requirements for medical exposure. Examples that may illustrate this point include acceptance testing processes for radiation equipment, calibration of radiotherapy units and reporting of medical accidental exposure.

Requirements on justification and optimization of protection apply to medical exposure but not to the dose limits. Further, dose constraints do not apply to the exposure of patients as part of their own diagnosis and treatment, but specific dose constraints shall be defined for non-occupational comforters and for medical exposure of individuals exposed for medical research, if these individuals do not benefit directly from the exposure.

16.14.1. Responsibilities for medical exposure

Paragraph II.1 of the BSS (Appendix II, Medical Exposure, Responsibilities) states, inter alia, that:

"*Registrants and licensees shall ensure that:*

(a) *no patient be administered a diagnostic or therapeutic medical exposure unless the exposure is prescribed by a medical practitioner;*
(b) *medical practitioners be assigned the primary task and obligation of ensuring overall patient protection and safety in the prescription of, and during the delivery of, medical exposure;*
(c) *medical and paramedical personnel be available as needed, and either be health professionals or have appropriate training adequately to discharge assigned tasks in the conduct of the diagnostic or therapeutic procedure that the medical practitioner prescribes;*
(d) *for therapeutic uses of radiation (including teletherapy and brachytherapy), the calibration, dosimetry and quality assurance requirements of the Standards be conducted by or under the supervision of a qualified expert in radiotherapy physics;…*"

Furthermore, para. II.1 of the BSS requires that the licensee shall ensure that:

"*(f)* training criteria be specified or be subject to approval, as appropriate, by the Regulatory Authority in consultation with relevant professional bodies."

16.14.2. Justification of medical exposure

Paragraph II.4 of the BSS (Appendix II, Medical Exposure, Justification of Medical Exposures) states that:

"*Medical exposures should be justified by weighting the diagnostic or therapeutic benefits they produce against the radiation detriment they might cause, taking into account the benefits and risks of available alternative techniques that do not involve medical exposure.*"

With respect to medical research, para. II.8 of the BSS states that:

"*The exposure of humans for medical research is deemed to be not justified unless it is:*

(a)   in accordance with the provisions of the Helsinki Declaration and follows the guidelines for its application prepared by Council for International Organizations of Medical Sciences (CIOMS) and WHO; and

(b)   subject to the advice of an Ethical Review Committee (or any other institutional body assigned similar functions by national authorities) and to applicable national and local regulations."

Research on humans in therapeutic procedures should only be performed if there is a direct health benefit to the exposed person.

16.14.3. Optimization of exposure and protection

Paragraph II.18 of the BSS (Appendix II, Medical Exposure, Optimization of Protection for Medical Exposures) states, inter alia, that:

"*Registrants and licensees shall ensure that:*

(a)   *exposure of normal tissue during radiotherapy be kept as low as reasonably achievable consistent with delivering the required dose to the planning target volume, and organ shielding be used when feasible and appropriate;*

(b)   *radiotherapeutic procedures causing exposure of the abdomen or pelvis of women who are pregnant or likely to be pregnant be avoided unless there are strong clinical indications;…*

(d)   *any therapeutic procedure for pregnant women be planned to deliver the minimum dose to any embryo or foetus;…"*

The optimization of protection in the case of patients is complex and does not necessarily mean the reduction of doses to patients, as priority has to be given to the acquisition of reliable diagnostic information and the achievement of the desired therapeutic effect.

With regard to the exposure of pregnant patients, the ICRP in Publication 84, Pregnancy and Medical Radiation, states:

"*Termination of pregnancy is an individual decision affected by many factors. Foetal doses below 100 mGy should not be considered a reason for terminating a pregnancy. At foetal doses above this level, there can be foetal damage, the magnitude and type of which is a function of dose and stage of pregnancy.*"

16.14.4. Calibration of radiotherapy sources and machines

Paragraph II.19 of the BSS (Appendix II, Medical Exposure, Optimization of Protection for Medical Exposures) states, inter alia, that:

"*Registrants and licensees shall ensure that:*

(a)   *the calibration of sources used for medical exposure be traceable to a Standards dosimetry laboratory;*

(b)   *radiotherapy equipment be calibrated in terms of radiation quality or energy and either absorbed dose or absorbed dose rate at a predefined distance under specified conditions, e.g. following the recommendations given in IAEA Technical Reports Series No. 277;*

(c)   *sealed sources used for brachytherapy be calibrated in terms of activity, reference air kerma rate in air or absorbed dose rate in a specified medium, at a specified distance, for a specified reference date;…*

    (e)   the calibrations be carried out at the time of commissioning a unit, after any maintenance procedure that may have an effect on the dosimetry and at intervals approved by the Regulatory Authority."

At the time of publication of the BSS, the IAEA code of practice based on air kerma in air (IAEA TRS 277) was included in the requirements. More recent protocols (codes of practice) based on standards of absorbed dose to water, such as IAEA TRS 398, were not available at that time. However, it is possible to extend the BSS requirement to the new protocols (see Chapter 9).

Sealed sources used for external beam radiotherapy and brachytherapy need to have a calibration certificate provided by the manufacturer, in accordance with ISO 1677 or its national equivalent standard.

The licensee must implement a protocol for the calibration of radiation sources used for radiotherapy. The regulatory authority should encourage the professional bodies of medical physics to adopt a protocol and require its implementation by the licensees. It is advisable to use international protocols for calibration, as this would avoid confusion and help prevent mistakes. Examples are the calibration procedures described by the IAEA (TRS 277, TRS 381 and TRS 398 for external beams and IAEA-TECDOC-1097 for brachytherapy).

Calibration of new equipment and new radiation sources should be performed independently by at least two different qualified experts in radiotherapy physics and preferably using different dosimetry systems. The results should be compared only after the completion of both measurements.

The licensee should ensure that all teletherapy equipment outputs are compared at least once every two years in a national, regional or international programme for independent dose verification.

One of the simplest mechanisms for independent verifications of external beam calibration or physical dosimetry is participation in the IAEA–WHO thermoluminescence dosimetry postal dose quality audit. The regulatory authority should encourage registrants and licensees to participate in this programme or in similar programmes.

For new brachytherapy sources for which the measurement varies by more than 5% from the manufacturer's certified activity or air kerma rate in air, the source shall not be used for patient treatment until the difference is investigated further and resolved. The responsibility for the investigation and for further action remains with the licensee, and the investigation is usually performed by a qualified expert in radiotherapy physics, with or without external help.

16.14.5. Clinical dosimetry

Paragraph II.20 of the BSS (Appendix II, Medical Exposure, Optimization of Protection for Medical Exposures) states, inter alia, that:

"*Registrants and licensees shall ensure that the following items be determined and documented:…*

(b) for each patient treated with external beam radiotherapy equipment, the maximum and minimum absorbed doses to the planning target volume together with the absorbed dose to a relevant point, such as the centre of the planning target volume, plus the dose to other relevant points selected by the medical practitioner prescribing the treatment;

(c) in brachytherapy treatments performed with sealed sources, the absorbed doses at selected relevant points in each patient;…

(e) in all radiotherapeutic treatments, the absorbed doses to relevant organs."

To meet these requirements (i.e. the items to be determined and the way they are to be determined and documented), a protocol should be used. The ICRU reports are recommended for consultation on such determination and recording.

16.14.6. Quality assurance for medical exposure

Paragraph II.22 of the BSS (Appendix II, Medical Exposure, Optimization of Protection for Medical Exposures) states that:

"*Registrants and licensees, in addition to applying the relevant requirements for quality assurance specified elsewhere in the Standards, shall establish a comprehensive quality assurance programme for medical exposures with the participation of appropriate qualified experts in the relevant fields, such as radiophysics or radiopharmacy, taking into account the principles established by the WHO and the PAHO.*"

The regulatory authority should encourage licensees to work with professional associations in the development of such programmes. The licensee should ensure that the programmes are updated on a regular basis. As the development of a national programme may not be feasible in many Member States, a well established and proven international or national programme may

be followed (e.g. AAPM TG 40, ESTRO Booklet No. 2, IAEA-TECDOC-1151).

Paragraph II.23 of the BSS (Appendix II, Medical Exposure, Optimization of Protection for Medical Exposures) states that:

"*Quality assurance programmes for medical exposures shall include:*

(a)   *measurements of the physical parameters of the radiation generators, imaging devices and irradiation installations at the time of commissioning and periodically thereafter;*

(b)   *verification of the appropriate physical and clinical factors used in patient diagnosis or treatment;*

(c)   *written records of relevant procedures and results;*

(d)   *verification of the appropriate calibration and conditions of operation of dosimetry and monitoring equipment; and*

(e)   *as far as possible, regular and independent quality audit reviews of the quality assurance programme for radiotherapy procedures.*"

Following the acceptance of new radiotherapy equipment, sufficient data shall be measured at the commissioning to be used for clinical dosimetry and treatment planning:

● The measured data shall be clearly documented in the workbook;
● Before being issued for use in treatment planning, the documentation shall be independently verified, signed and dated;
● All dosimetry calibrations, clinical dosimetry data and methods of calculation for therapy equipment are to be reconfirmed at regular intervals.

The measurements and checks carried out for this purpose should be sufficient to detect any significant variations from the data in use. Verification of patient treatment through in vivo dosimetry is advisable under special circumstances. This procedure may not be available in all institutions, but nevertheless it is recommended for incorporation as soon as it becomes feasible.

A routine quality assurance programme is an integral component of modern radiotherapy practice; this programme should include auditing, both internal and external, and continual improvement. These principles need to be linked to the radiation protection programme in order to strengthen safety while at the same time improving quality and efficiency.

Feedback from operational experience and lessons learned from accidents or near misses can help to identify potential problems and correct deficiencies, and should therefore be used systematically as part of the quality assurance programme.

The maintenance of records is an important part of a quality assurance programme. When planning and developing an effective quality assurance programme, licensees need to recognize that it demands a strong managerial commitment and support in the form of training and resources of time, personnel and equipment.

16.14.7. Constraints for comforters and visitors

Dose constraints do not apply to patients. With regard to patients' comforters and visitors, para. II.27 of the BSS (Appendix II, Medical Exposure, Dose Constraints) recommends the following:

"*Registrants and licensees shall constrain any dose to individuals incurred knowingly while voluntarily helping (other than in their occupation) in the care, support or comfort of patients undergoing medical diagnosis or treatment, and to visitors to patients who have received therapeutic amounts of radionuclides or who are being treated with brachytherapy sources, to a level not exceeding that specified in Schedule II, para. II-9.*"

Schedule II, para. II-9, of the BSS states, inter alia, that:

"*…the dose of any such comforter or visitor of patients shall be constrained so that it is unlikely that his or her dose will exceed 5 mSv during the period of a patient's diagnostic examination or treatment. The dose to children visiting patients who have ingested radioactive materials should be similarly constrained to less than 1 mSv.*"

16.14.8. Discharge of patients

Paragraph II.28 of the BSS (Appendix II, Medical Exposure, Maximum Activity for Patients in Therapy on Discharge from Hospital) states that:

"*In order to restrict the exposure of any members of the household of a patient who has undergone a therapeutic procedure with sealed or unsealed radionuclides and members of the public, such a patient shall not be discharged from hospital before the activity of radioactive substances in the body falls below the level specified in Schedule III, Table III-VI. Written*"

instructions to the patient concerning contact with other persons and relevant precautions for radiation protection shall be provided as necessary."

Table III-VI in the BBS (Schedule III) only includes the value for ^{131}I and sets 1100 MBq as the guidance level for maximum activity for patients in therapy on discharge from hospital. The ICRP has an ongoing task group with the charge of developing guidance for other sources, including those used for permanent implants in brachytherapy, such as ^{125}I and [103]Pd.

16.14.9. Investigation of accidental medical exposure

Paragraph II.29 of the BSS (Appendix II, Medical Exposure, Investigation of Accidental Medical Exposures) states, inter alia, that:

"*Registrants and licensees shall promptly investigate any of the following incidents:*

(a) *any therapeutic treatment delivered to either the wrong patient or the wrong tissue, or using the wrong pharmaceutical, or with a dose or dose fractionation differing substantially from the values prescribed by the medical practitioner or which may lead to undue acute secondary effects;…*
(c) *any equipment failure, accident, error, mishap or other unusual occurrence with the potential for causing a patient exposure significantly different from that intended.*"

Paragraph II.30 of the BSS (Appendix II, Medical Exposure, Investigation of Accidental Medical Exposures) states that:

"*Registrants and licensees shall, with respect to any investigation required under para. II.29:*

(a) *calculate or estimate the doses received and their distribution within the patient;*
(b) *indicate the corrective measures required to prevent recurrence of such an incident;*
(c) *implement all the corrective measures that are under their own responsibility;*
(d) *submit to the Regulatory Authority, as soon as possible after the investigation or as otherwise specified by the Regulatory Authority, a*

> *written report which states the cause of the incident and includes the information specified in (a) to (c), as relevant, and any other information required by the Regulatory Authority; and*
>
> *(e) inform the patient and his or her doctor about the incident.*"

IAEA Safety Reports Series No. 17 and ICRP Publication 86 contain reviews and lessons to be learned from an extensive collection of accidental medical exposures.

16.15. PUBLIC EXPOSURE

16.15.1. Responsibilities

The licensee is responsible for controlling public exposure resulting from a radiotherapy practice. Public exposure is controlled by proper shielding design and, in large part, by ensuring that radiation sources are shielded and secured (e.g. located in a locked area), interlocks are functional and keys to the control panel are secured, to prevent unauthorized access or use. The presence of members of the public in and near the radiotherapy department shall be considered when designing shielding of storage and treatment facilities.

16.15.2. Access control for visitors

The licensee should make arrangements to control access of members of the public to radiotherapy irradiation rooms and to provide adequate information and instruction to these persons before they enter a controlled area so as to ensure appropriate protection (e.g. members of the public shall be accompanied by radiotherapy staff).

16.15.3. Radioactive waste and sources no longer in use

The licensee should notify the regulatory authority and submit a plan for the transfer and disposal of sources if they are no longer in use. The licensee maintains responsibility for the sources until the time of their transfer to another appropriate licensee or to an authorized waste disposal facility; in particular the licensee has to notify the regulatory authority of any intention to transfer or decommission ^{60}Co teletherapy equipment prior to initiating any action. Depleted uranium used as shielding material shall also be treated as radioactive waste; for example, a ^{60}Co teletherapy head may contain depleted uranium and is to be disposed of appropriately.

16.15.4. Monitoring of public exposure

Paragraph III.13 of the BSS (Appendix III, Public Exposure, Monitoring of Public Exposure) states, inter alia, that:

"*…and licensees shall, if appropriate:*

(a)   establish and carry out a monitoring programme sufficient to ensure that the requirements of the Standards regarding public exposure to sources of external irradiation be satisfied and to assess such exposure;…

(c)   keep appropriate records of the results of the monitoring programmes;…"

The programme for monitoring public exposure from radiotherapy shall include dose assessments in the surroundings of irradiation rooms for external beam radiotherapy, brachytherapy wards, source storage, source preparation rooms and waiting rooms.

16.16.   POTENTIAL EXPOSURE AND EMERGENCY PLANS

Requirements on the safety of sources and facilities are set out in Section 16.10. This section focuses on the identification of possible emergency situations or accidents, their prevention, and preparation for and mitigation of them.

16.16.1. Potential exposure and safety assessment

Paragraph IV.3 of the BSS (Appendix IV, Potential Exposure: Safety of Sources, Safety Assessment) states, inter alia, that:

"*…licensees shall conduct a safety assessment, either generic or specific for the sources for which they are responsible…*"

The assessment is to be provided to the regulatory authority, according to the BSS principal requirements on authorization (paras 2.11–2.13 of the BSS).

Generic safety assessments are suitable for types of equipment with a high degree of uniformity (para. IV.9 of the BSS). As experience in identifying accident scenarios by an individual licensee may be limited, arrangements

between licensees and manufacturers to provide for notification of malfunctions and dissemination by feedback to licensees should be encouraged.

16.16.2. Mitigation of consequences: emergency plans

Based on the events identified by the safety assessment, the licensee shall elaborate mitigation measures embodied in a set of emergency procedures. The responsibilities shall be allocated (para. V.2 of the BSS) and the relevant staff shall be trained in the mitigation measures, which shall be periodically rehearsed. The lessons learned from the rehearsals shall be used to review and update the emergency plans. The procedures shall identify the responsibilities of individuals and shall be concise, unambiguous and posted visibly in places where they could be needed.

Only maintenance staff trained and authorized for these tasks should carry out emergency procedures during source change of external beam radiotherapy units and remote control brachytherapy units. If participation of radiotherapy staff is necessary for any of these actions, the scope of this participation shall be restricted to operating the control panel, and responsibilities shall be clearly defined.

For emergency situations there need to be emergency plans that are concise and easily followed, and these should be developed before the startup of a radiation treatment programme. The most frequent types of emergency situation are given below.

16.16.2.1. Lost source

It is critical for this type of event that an up to date inventory exists so that the following can be determined immediately:

- Which sources are missing;
- What is their type and activity;
- Where they were last known to be, and when;
- Who last took possession of the sources.

The area where the sources were last known to be should be closed to entry and exit until a survey has been performed. This search needs to be performed with the most sensitive radiation detection survey meter.

16.16.2.2. Stuck source

Emergency procedures need to be short, concise, unambiguous and, if necessary, illustrated with drawings without any explanation text. They need to be suitable for being read at first sight and followed.

● External beam radiotherapy units. Emergency procedures for this event should be posted at the treatment unit. In general, the first step is to use the source driving mechanism to return the source to the shielded position. If this is not immediately successful and there is a patient on the treatment table, the patient should be removed from the area and the area must be secured from further entry. Emphasis should be placed on avoiding exposure of the staff to the primary beam. The radiation protection officer is then notified and takes over control of the situation.

● Remote control brachytherapy units. Emergency plans require an emergency container to be available in the treatment room, as well as an emergency kit containing long handled forceps for manipulation of the source guide tubes and applicators, if the source fails to return to the safe. The emergency container should be placed close to the patient and should be sufficiently large so that it can accept the entire applicator assembly that contains the source and is removed from the patient.

For HDR brachytherapy, the following remark is taken from IAEA-TECDOC-1040:

"*High dose rate brachytherapy is potentially a high risk technique and extreme accuracy and care are essential. The short response time required for emergency actions (minutes) imposes the need for the presence of both a physician and physicist trained in emergency procedures during all applications.*"

Manufacturers usually provide suggested emergency procedures for an event in which the source fails to return to the safe. They assume that the physical integrity of the applicator is maintained. These procedures are specific to the actual afterloading unit but generally involve the following sequence. Each step assumes that if the previous action fails to lead to recovery, then the following action is required. The generic sequence is as follows:

— Observation at the console of error message and emergency indicators (audible and visible alarms);
— Recovery from the console (e.g. pressing an emergency off button);

— Entry into the room with a portable radiation survey meter (opening the door activates the interlock that retracts the source);
— Monitoring radiation levels in the room;
— Recovery from the afterloading unit (by pressing an emergency off button on the remote afterloading unit);
— Manual retraction of the source (using a hand crank);
— Patient survey and remote afterloading unit survey (confirming that the source is in the safe);
— Applicator removal and placement in the emergency container;
— Patient survey and emergency container survey (to confirm that the source is not in the patient and is in the emergency container);
— Removal of the patient from the vault (with subsequent survey monitoring).

16.16.2.3. Contamination

There is a very low probability of contamination accidents in radiotherapy departments in which ^{226}Ra and powder form ^{137}Cs sources have been replaced. In the event of a contamination accident it is important that the area be closed to further entry and that all who were in the area remain there to be surveyed and decontaminated, if necessary. If there are windows or other ventilation present, these should be closed. A statement of how to contact the responsible radiation safety individual in the event of an emergency should be available.

16.16.2.4. Off-site accidents

Off-site accidents with major consequences have been caused by loss of security of teletherapy sources not in use. Some of them (in Mexico and Brazil) caused large scale contamination and others external irradiation only (in Thailand and Turkey). Off-site accidents require actions by national and international intervening organizations. Participation of radiotherapy licensees in national emergency plans may be required and should be integrated.

16.16.2.5. Patient accidental exposure

The requirements in the BSS on investigation of accidental medical exposure, including incident reporting and corrective measures to be taken, are referred to in Section 16.14.

16.17. GENERAL SHIELDING CALCULATIONS

The three important parameters that influence external radiation exposure are time, distance and shielding:

● The radiation dose received by individuals is proportional to the time they spend in the radiation field.
● The radiation dose generally follows an inverse square law, hence the dose is reduced substantially by increasing the distance from the source of radiation.
● The dose is reduced if shielding attenuates the radiation.

These parameters are involved in shielding design, which basically consists of three steps:

(1) Establishing a design value for the effective dose in the occupied area;
(2) Estimating the radiation field in the occupied area if there were no shielding;
(3) Obtaining the attenuation factor that is necessary to reduce the dose value from the effective dose in (2) to the effective dose in (1).

It is convenient to keep heavily occupied areas as far away as possible from the treatment rooms and to surround these rooms with no occupancy or low occupancy areas (e.g. the roof, with control of access). The treatment room itself should be large enough for easy patient transport in trolleys and also for ease of installation and servicing of the equipment. Design of the room with a maze facility makes a heavy motorized entry door unnecessary for shielding against photons; however, one must still consider shielding against neutrons in a high energy linac facility. With proper design, a maze can make both neutron shielding and a heavy motorized door unnecessary.

Treatment rooms in radiotherapy departments typically fall into one of the following six categories: linac; ^{60}Co teletherapy; orthovoltage X ray; superficial X ray; HDR brachytherapy; and LDR brachytherapy.

Shielding requirements for each of these rooms follow similar rules and conventions; however, each of the rooms introduces a few of its own specific requirements and constraints. If the source room contains only LDR type brachytherapy sources and they are always stored in a locked shielded safe within the room, except while preparing the sources behind a shield, the room may not require special shielding.

A patient room that houses manual afterloading LDR brachytherapy patients may not need shielding if mobile lead shields are used around the

patient's bed. Installations housing linacs, teletherapy machines, X ray machines or HDR remote afterloading devices all require special shielding to protect the operators, staff, patients and public in adjacent areas.

16.17.1. Step one: Design dose in occupied areas (annual dose and weekly dose)

The design effective dose rate P (in Sv/a or Sv/week) in a given occupied area (Table 16.2) is derived by constrained optimization (i.e. by selecting a source related dose constraint), with the condition that the individual effective doses from all relevant sources will be well below the prescribed effective dose limits for persons occupying the area to be shielded. However, when using constraints for shielding calculations, consideration should be given to the remark made in ICRP Publication 33 (para. 256) stating that actual dose values to individuals in the occupied areas are to be 1/10 (for equivalent dose) to 1/30 of the effective dose used as the shielding design parameter. This is due to a number of conservative assumptions made in the calculation. Typical conservative assumptions in the calculations are the following:

- The attenuation of the beam by the patient is usually not considered.
- The maximum possible leakage radiation is assumed.
- The workload, as well as the use and occupancy factors, is overestimated.
- An assumption is made that staff are always in the most exposed place of the occupied area.
- For linacs producing X rays and electrons an assumption is made that the linac always operates in the X ray mode.
- For dual energy linacs an assumption is made that the linac always runs in the higher energy mode.

Since some of these conservative assumptions may be unavoidable to cover uncertainties when using constraints, a critical review of conservative assumptions should be performed so as to achieve a balanced decision and avoid accumulation of over-conservative measures that may go far beyond optimization.

The use of $P = 0.01$ mSv/week corresponds to an area for permanent occupation by members of the public and may lead to a high value of shielding thickness (of the order of 230–250 cm of regular concrete for 20 MV photons in an area exposed to the primary beam at a distance of about 4 m from the source).

This thickness of regular concrete will be reduced by 50 cm or more if the area is designated as a controlled area and the dose constraint of 0.2 mSv/week

TABLE 1. TYPICAL VALUES FOR DESIGN EFFECTIVE DOSE P IN OCCUPIED AREAS ADJACENT TO A RADIOTHERAPY TREATMENT ROOM

	Annual effective dose (mSv/a)	Weekly effective dose (mSv/week)
Occupational worker	10	0.2
Member of the public	0.5	0.01

is used. This approach would be consistent with keeping the console area away from the public, who may cause distractions or have an effect on other safety aspects. This solution, however, requires individual monitoring of persons who work in or come frequently to the area of the console, but is not necessary for persons who work in the area only occasionally.

The relation between effective dose P and the air kerma in air values for the radiation field is made through the personal dose equivalent $H_p(d)$ for penetrating radiation, where $d = 10$ mm. An accepted conservative assumption is to make the personal dose equivalent numerically equal to the effective dose P and to the air kerma in air value (Gy/week) of the radiation field.

16.17.2. Step two: Calculation of the radiation field (air kerma in air) in the occupied area without shielding

The following parameters are used for calculation of the effective dose without shielding:

- Primary radiation, which is the radiation directly emitted from the treatment machine through the collimator opening in the case of external sources and from the radioactive source in the case of brachytherapy.
- Scatter radiation, which is the radiation produced by the scattering of the primary radiation beam from various media struck by the primary beam, such as the patient, collimators, beam shaping accessories and air.
- Leakage radiation, which is the radiation that escapes through the shielded head of the therapy unit (for accelerators leakage radiation only exists while the beam is on; for cobalt units leakage radiation is always present).

● The workload *W*, which is defined as the machine output per week or per year at a well defined point (usually the machine isocentre in the treatment room) and is expressed in Gy/week or Gy/a, respectively.

16.17.3. Step three: Attenuation by shielding barriers

The primary barrier is the portion of the treatment room walls or ceiling that may be irradiated directly by the primary beam. Therapy machines are usually located on the lowest floor of a building, so shielding of the floor against primary, scattered and leakage radiation is not of concern.

Secondary barriers are all portions of the treatment room walls, floor or ceiling that cannot be irradiated directly by the primary beam. These barriers provide shielding against the scatter and leakage radiation produced in the treatment room.

The use factor *U* is the fraction of the beam-on time during which the primary beam is directed towards a particular barrier. The following primary beam use factors are usually assumed for external beam machines: *U* (floor) = 1; *U* (walls) = 0.25; *U* (ceiling) = 0.25. For all secondary barriers *U* is always equal to 1, since secondary radiation is always present when the beam is on.

The occupancy factor *T* is a factor with which the workload is multiplied to account for the degree of occupancy of the area in question. Typical values are *T* (offices) = 1; *T* (corridors) = 0.25; *T* (waiting rooms) = 0.125.

The half-value layer (HVL) and the tenth-value layer (TVL) are those thicknesses of attenuating material that decrease the photon beam intensities to 50% and 10%, respectively, of the original value (100%).

The barrier transmission factor *B* provides the fraction of the incident beam air kerma in air transmitted through a given thickness of shielding material. Primary, scatter and leakage barrier transmission factors B_{pri}, B_{scat} and B_{leak}, respectively, must be calculated, and the required barrier thickness is then determined using published graphs of transmission factors against shielding material thickness for various beam energies and shielding materials.

Shielding materials are materials used in primary and secondary barriers to provide shielding against the primary, scatter and leakage radiation produced in the radiotherapy treatment room. The most common materials used for the shielding of external beam and brachytherapy treatment facilities are: ordinary concrete (density: 2.35 g/cm^3), barite concrete (density: up to 3.2 g/cm^3), high density concrete (density: up to 5 g/cm^3), steel (density: 7.9 g/cm^3) and lead (density: 11.3 g/cm^3).

To compute the radiation levels beyond the radiation barriers in areas adjacent to treatment rooms, transmission data are required, which take into

account not only the primary beam attenuation but also the radiation scattered in the shielding itself (broad beam geometry data).

Narrow beam geometry only includes primary radiation, so that the point of interest does not receive any scattered radiation; for example, to measure the primary beam intensity transmitted through an attenuator, a narrow beam geometry (with suitable collimation and barrier to detector distance) is set up so that the scatter does not reach the detector. Narrow beam geometry is useful to characterize beam quality in the kilovoltage photon range (see Chapter 9).

In broad beam geometry the detector (or the radiation worker) receives not only the transmitted beam but also the scatter from or through the barrier. Sets of broad beam transmission and graphics data for common use in radiotherapy installations are provided in ICRP Publication 33 and the NCRP 49 report.

If K_P and K_S represent the primary and the scattered air kerma in air 'seen' by the detector, respectively, the buildup B for a barrier is given by:

$$B = (K_P + K_S)/K_P \qquad (16.9)$$

For narrow beam geometry $B = 1$ and for broad beam geometry $B > 1$, where B refers to buildup, not to be confused with the transmission factors B_{pri}, B_{scat} and B_{leak} in the text below.

16.18. TYPICAL LINAC INSTALLATION

The main components of a typical linac installation are the treatment room, entrance maze, control room and optional mechanical–electrical room. The maze connects the treatment room with the control room, which houses the operational controls of the linac. The treatment room and maze together are called the linac bunker.

A schematic diagram of a typical installation for an isocentric high energy linac is given in Fig. 16.2. The thickness of the primary and secondary barriers is determined through first determining the transmission factors and then determining the barrier thickness required to achieve the calculated transmission.

16.18.1. Workload

Typical linac workload figures vary depending on initial assumptions. An example of slightly conservative assumptions is:
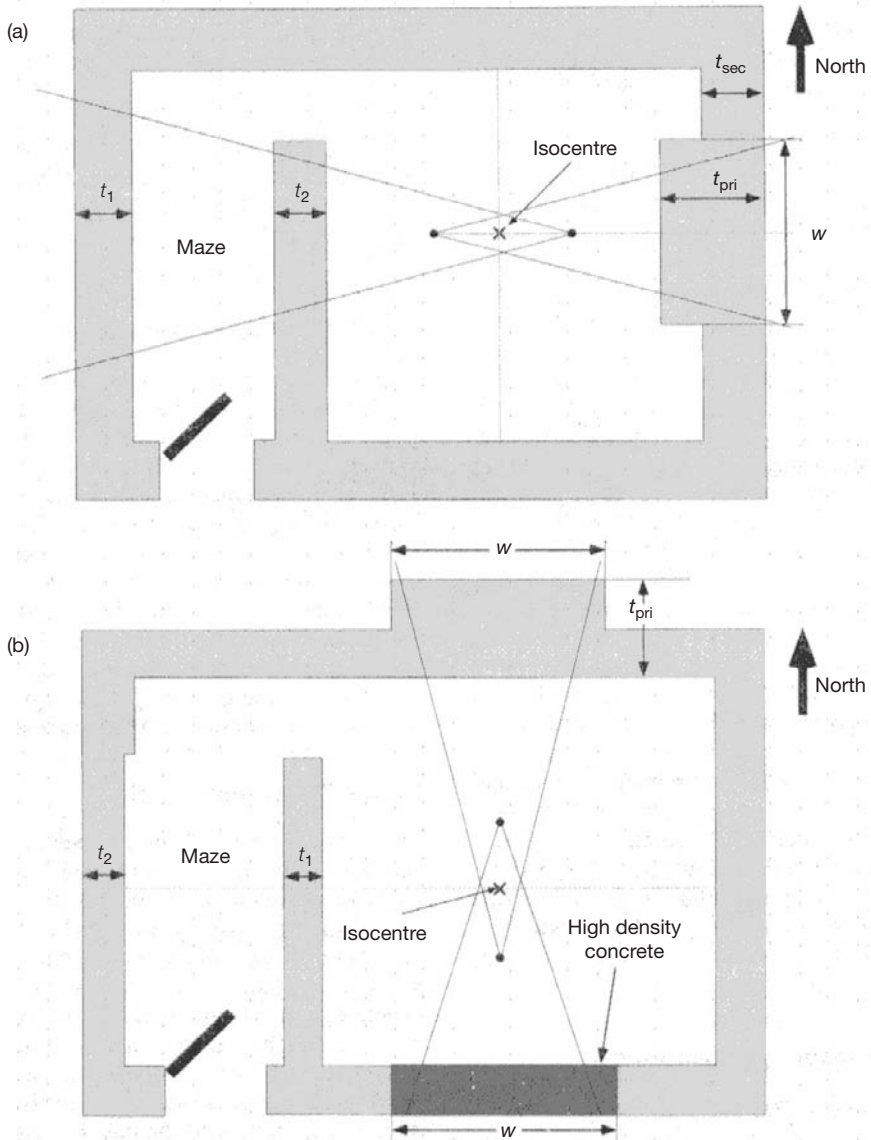
FIG. 16.2. Typical floor plan for an isocentric high energy linac bunker. (a) The machine gantry rotation axis is parallel to the maze entry corridor; the primary barriers are parts of the floor and ceiling, as well as parts of the east and west walls. (b) The machine gantry rotation axis is perpendicular to the maze entry corridor; the primary barriers are parts of the floor and ceiling and parts of the north and south walls. Normal density concrete (2.35 g/cm³) is used in all walls except for the south wall, which is made of high density concrete (5 g/cm³). The door to the treatment room maze is a neutron shielded door.

- The clinical workload W_{clin} for 50 patients per working day, 3.3 Gy delivered dose at the isocentre per patient (pt), five working days per week and 52 working weeks per year:

$$W_{clin} = 3.3\frac{Gy}{pt} \times 50\frac{pts}{day} \times 5\frac{days}{week} \times 52\frac{weeks}{year} = 42\,900\,\frac{Gy}{year} \tag{16.10}$$

- The physics workload W_{phys} includes use of the linac for calibration, quality assurance, phantom measurements, servicing and maintenance. A conservative estimate of this is W_{phys} = 7100 Gy/a, resulting in the following total linac workload. Total linac workload W_{tot} at the machine isocentre:

$$W_{tot} = W_{clin} + W_{phys} = 5 \times 10^4 \text{ Gy/a} \sim 10^3 \text{ Gy/week} \tag{16.11}$$

In shielding calculations for dual energy linacs a conservative assumption is usually made that the accelerator will operate at the higher energy 100% of the time.

16.18.2. Calculation of the primary barrier transmission factor

The primary barrier transmission factor B_{pri} is calculated from the following relationship:

$$B_{pri} = \frac{P(d_{pri}/d_0)^2}{WUT} \tag{16.12}$$

where

d_0 is the linac source to axis distance (SAD) (usually 1 m);
d_{pri} is the distance from the linac target (X ray source) to the point of interest (usually 0.3 m outside the wall or ceiling to be shielded);
W is the total workload of the linac;
U is the barrier use factor;
T is the occupancy factor at the point of interest.

The primary beam of an external beam unit should only be directed towards primary barriers with sufficient shielding. If part of the primary shielding is incorporated into the equipment with the use of a retractable beam stopper, electrical and/or mechanical interlocks should be provided to prevent the possibility that the radiation beam is directed towards the primary barriers when the beam stopper is not intercepting the beam.

The beam stopper is usually made of lead with a thickness adequate to attenuate the primary radiation beam to 0.1% of its original value (typically 3 TVLs or 10 HVLs, amounting to about 10–15 cm of lead for megavoltage photon beams). Treatment machines equipped with beam stoppers are cumbersome with regard to patient set-up on the treatment machine; however, the beam stoppers minimize the required thickness of the primary barriers and are thus used in installations in which space constraints prevent the use of adequate primary barrier thickness. With the use of beam stoppers, the primary barrier wall thickness becomes close to that required for secondary barriers.

16.18.3. Calculation of the scatter barrier transmission factor

The scatter barrier transmission factor B_{scat} is determined from:

$$B_{scat} = \frac{P(d_1/d_0)^2(d_2/d_0)^2(F_0/F)}{aWT} \qquad (16.13)$$

where

d_0 is the SAD of the linac;
d_1 is the distance from the patient to the point of interest;
d_2 is the distance from the target to the scattering volume (patient);
a is the ratio of the scattered radiation at 1 m from the scattering object (patient) to the primary radiation at 1 m;
F_0 is an average field area (400 cm^2);
F is the actual field size at the position of the patient.

The scattering coefficient a depends on the photon beam energy and scattering angle. Its typical value for 90º scatter is 10^{-4}–10^{-3}. The Compton scattering formula predicts a maximum energy of 0.511 keV (m_ec^2) for 90º scatter and a maximum energy of 0.255 keV (0.5 m_ec^2) for 180º scatter.

16.18.4. Calculation of the leakage barrier transmission factor

The leakage barrier transmission factor B_{leak} is calculated assuming a beam attenuation due to linac head shielding transmission of 0.1%. The energy of the leakage radiation is assumed to be the same as that of the primary radiation. Thus:

$$B_{\text{leak}} = \frac{10^3 P(d_3/d_0)^2}{WT} \tag{16.14}$$

where

d_0 is the SAD of the linac;
d_3 is the distance from the isocentre to the point of interest (average distance for all possible gantry positions);
W is the workload of the linac;
T is the occupancy factor.

16.18.5. Determination of barrier thickness

Using broad beam transmission data from ICRP Publication 33 or the NCRP 49 report, one can determine the required primary, leakage and scatter barrier thickness for the calculated transmission factors B_{pri}, B_{leak} and B_{scat}, respectively.

The barrier thickness determined for leakage radiation is usually larger than that determined for scatter radiation. One rule of thumb is that if the leakage barrier thickness exceeds the scatter barrier by more than 3 HVLs (i.e. ~1 TVL), then just the leakage barrier thickness is applied as the required wall thickness. However, if the thicknesses for the two barriers are within 3 HVLs, then one extra HVL is added to the leakage barrier thickness to determine the required secondary barrier thickness to account for the slight increase in effective dose due to the scattered component.

Ordinary concrete is the most common shielding material in megavoltage therapy installations (Table 16.3). Other materials may be used to conserve space, since for megavoltage beams the required primary barrier thickness is inversely proportional to the density of the shielding material (see the Compton effect, Section 1.4.6). It should be kept in mind, however, that

TABLE 16.3. TYPICAL SHIELDING THICKNESS OF ORDINARY CONCRETE TO PROTECT MEMBERS OF THE PUBLIC IN AREAS ADJACENT TO COBALT UNITS OR HIGH ENERGY LINAC BUNKERS

Radiation quality	Primary barrier (cm)	Secondary barrier (cm)
Co-60	130	65
10–25 MV	240	120

replacing ordinary concrete with other materials will have serious financial implications; for example, high density concrete (5 g/cm^3) will cut the barrier thickness roughly to half of that required for ordinary concrete, but on a per volume basis the costs of the shielding material will increase by a factor of 30. The difference is even more pronounced when steel or lead is used for shielding.

16.18.6. Consideration of neutron production in a high energy linac

In high energy (above 10 MV) linac installations, neutrons are produced by X ray–neutron (x, n) and electron–neutron (e, n) reactions. The neutron contamination is produced by high energy photons and electrons incident on the target, primary collimator, beam flattening filter, collimator jaws, beam accessories, air and the patient. The cross-section for a (x, n) reaction is at least an order of magnitude larger than that for an (e, n) reaction; hence neutrons produced by the linac X ray mode are of primary concern. For this reason, the maximum photon energy produced by a linac rather than the maximum electron energy is considered the more significant contributor to the neutron dose.

Neutrons can activate other elements, which remain radioactive and will contribute to the radiation exposure of radiotherapy staff entering the treatment room after a high energy photon beam treatment. The radionuclides from activated components of a linac are generally short lived (of the order of seconds to a few minutes).

A similar problem is posed by the direct activation of elements in (x, n) reactions, such as ^{15}O (half-life 2 minutes) and ^{13}N (half-life 10 minutes). The radioactivity in treatment room air is removed by efficient room ventilation. The ventilation also handles the removal of ozone and noxious gases, in addition to the removal of radioactive gases, through 6–8 air exchanges per hour.

The concrete primary and secondary barriers designed to protect against photon dose are quite adequate to protect against electrons and contamination neutrons. However, neutrons undergoing multiple scattering along the maze can present an unacceptable radiation level in the control area, thus requiring a specially designed door.

16.18.7. Door of a linac room

The door of a high energy linac installation may require shielding against X rays and neutrons scattered through the maze towards the linac control area. High energy neutrons are more of a problem than low energy photons.

Neutrons are thermalized and absorbed with a layer of about 12 cm of borated polyethylene in the door, which is followed by about 2.5 cm of lead to absorb the γ rays produced by neutron capture reactions in boron nuclei. An alternative to the special neutron shielding door is a double maze design, which avoids the need for a shielded door.

16.18.8. Other considerations

A 'radiation area' sign (along with a visible red light) needs to be provided above the door to the treatment room, and preferably also on the control room door, to indicate a beam-on condition. There should be audio communication with the patient and emergency switches inside the room to shut off the radiation in the event of an emergency.

In some cases (e.g. installation of a linac in an existing ^{60}Co room or in a small room) installation of the machine with a beam stopper may be necessary.

The manufacturer often quotes a primary beam stopper that attenuates the primary beam by a factor of 0.001 (about 3 TVLs), reducing the primary barrier thickness requirement by 3 TVLs. If the remaining primary barrier thickness is less than the thickness required for scatter and leakage, the whole wall can be made of a uniform thickness as required for a scattering and leakage barrier.

16.19. SHIELDING DESIGN FOR BRACHYTHERAPY FACILITIES

HDR brachytherapy treatment rooms are designed with similar constraints as are linac and teletherapy rooms. There is, however, one major difference: in brachytherapy rooms all walls are primary barriers, since the source can generally be positioned anywhere in the room and the radiation is emitted isotropically and uncollimated from the source. The attenuation in the patient is not considered in primary barrier transmission calculations. The workload specification is given in terms of air kerma in air per week or year.

The typical workload specification for a remote afterloading HDR ^{192}Ir facility is determined using the following data:

- Maximum source activity: 370 GBq (10 Ci).
- Maximum number of patients treated: 10/day.
- Number of working days (or treatment days) per week: 5 days/week.
- Maximum treatment time: 10 min (for 10 Ci) per patient.
- Air kerma rate constant for ^{192}Ir:

111 μGy·m^2/(GBq·h) = 4.1 μGy·m^2/(mCi·h)

● Workload:

$W = 10^4 \times 10 \times 5 \times 10 \times (1/60) \times 4.1$ μGy·m^2/week = 3.4×10^5 μGy·m^2/week

Although the treatment time increases due to decay, the product (activity × time) remains the same and hence the example for the computation is made for the maximum treatment time with a 370 GBq (10 Ci) source. All parameters are conservative, introducing a safety factor in the calculated workload. For older HDR units using ^{60}Co a maximum of 20 source pellets may be used, each pellet with a maximum activity of about 1.85 GBq (500 mCi/pellet) for a total source activity of 370 GBq (10 Ci). The maximum treatment time and the number of patients per day, however, remain the same for a ^{60}Co HDR remote afterloading unit as in the HDR ^{192}Ir case.

The workload for planning an HDR ^{60}Co brachytherapy room comes to about 1.1×10^6 μGy·m^2/week, using Γ_{AKR} of 308.5 (μGy·m^2)/(GBq·h).

In the case of LDR remote afterloading ^{137}Cs units, two patients may be treated simultaneously with a maximum of 18 sources per patient, the activity of each source being around 1110 GBq (30 mCi). The treatment time for LDR brachytherapy is assumed to be 40 h/week.

BIBLIOGRAPHY

AMERICAN ASSOCIATION OF PHYSICISTS IN MEDICINE, Comprehensive QA for radiation oncology: Report of AAPM Radiation Therapy Committee Task Group 40, Med. Phys. **21** (1994) 581–618.

EUROPEAN SOCIETY FOR THERAPEUTIC RADIOLOGY AND ONCOLOGY, Quality assurance in radiotherapy, Radiother. Oncol. **35** (1995) 61–73.

FOOD AND AGRICULTURE ORGANIZATION OF THE UNITED NATIONS, INTERNATIONAL ATOMIC ENERGY AGENCY, INTERNATIONAL LABOUR ORGANISATION, OECD NUCLEAR ENERGY AGENCY, PAN AMERICAN HEALTH ORGANIZATION, WORLD HEALTH ORGANIZATION, International Basic Safety Standards for Protection against Ionizing Radiation and for the Safety of Radiation Sources, Safety Series No. 115, IAEA, Vienna (1996).

INSTITUTE OF PHYSICS AND ENGINEERING IN MEDICINE, The Design of Radiotherapy Treatment Room Facilities (STEDEFORD, B., MORGAN, H.M., MAYLESS, W.P.M., Eds), IPEM, York, United Kingdom (1997).

CHAPTER 16

INTERNATIONAL ATOMIC ENERGY AGENCY (Vienna)

Absorbed Dose Determination in Photon and Electron Beams, 2nd Edition, Technical Reports Series No. 277 (1997).

Method for the Development of Emergency Response Preparedness for Nuclear or Radiological Accidents, IAEA-TECDOC-953 (1997).

The Use of Plane Parallel Chambers in High Energy Electron and Photon Beams, Technical Reports Series No. 381 (1997).

Design and Implementation of a Radiotherapy Programme: Clinical, Medical Physics, Radiation Protection and Safety Aspects, IAEA-TECDOC-1040 (1998).

Assessment of Occupational Exposure Due to External Sources of Radiation, IAEA Safety Standards Series No. RS-G-1.3 (1999).

Calibration of Brachytherapy Sources, IAEA-TECDOC-1079 (1999).

Occupational Radiation Protection, IAEA Safety Standards Series No. RS-G-1.1 (1999).

Absorbed Dose Determination in External Beam Radiotherapy, Technical Reports Series No. 398 (2000).

Aspectos Físicos de la Garantía de Calidad: Protocolo de Control de Calidad, IAEA-TECDOC-1151 (2000).

Lessons Learned from Accidental Exposures in Radiotherapy, Safety Reports Series No. 17 (2000).

Regulations for the Safe Transport of Radioactive Material, 1996 Edition (Revised), IAEA Safety Standards Series No. TS-R-1 (ST-1, Rev.) (2000).

Radiological Protection for Medical Exposure to Ionizing Radiation, IAEA Safety Standards Series No. RS-G-1.5 (2002).

INTERNATIONAL COMMISSION ON RADIOLOGICAL PROTECTION, Protection Against Ionizing Radiation from External Sources Used in Medicine, Publication 33, Pergamon Press, Oxford and New York (1982).

— 1990 Recommendations of the International Commission on Radiological Protection, Publication 60, Pergamon Press, Oxford and New York (1991).

— Pregnancy and Medical Radiation, Publication 84, Pergamon Press, Oxford and New York (2000).

— Prevention of Accidents to Patients Undergoing Radiation Therapy, Publication 86, Pergamon Press, Oxford and New York (2002).

INTERNATIONAL ELECTROTECHNICAL COMMISSION (Geneva)

Medical Electrical Equipment — Part 2: Particular Requirements for the Safety of Therapeutic X-ray Generators, IEC 601-2-8 (1987).

General Requirements for Safety. 4. Collateral Standard: Programmable Electrical Medical Systems, IEC 60601-1-4 (1997).

Guidelines for Radiotherapy Treatment Rooms Design, IEC 61859 (1997).

Medical Electrical Equipment — Part 2: Particular Requirements for the Safety of Gamma Beam Therapy Equipment, IEC 60601-2-11 (1997).

Medical Electrical Equipment — Part 2-1: Particular Requirements for the Safety of Electron Accelerators in the Range of 1 MeV to 50 MeV, IEC 60601-2-1 (1998).

Medical Electrical Equipment — Part 2-17: Particular Requirements for the Safety of Remote-controlled Automatically-driven Gamma-ray Afterloading Equipment, IEC 60601-2-17 (1998).

Medical Electrical Equipment — Part 2: Particular Requirements for the Safety of Radiotherapy Simulators, IEC 60601-2-29 (1999).

Medical Electrical Equipment: Requirements for the Safety of Treatment Planning Systems, IEC 62C/62083 (in preparation).

INTERNATIONAL ORGANIZATION FOR STANDARDIZATION, Basic Ionizing Radiation Symbol, ISO 361, ISO, Geneva (1975).

— Radiation Protection — Sealed Radioactive Sources — General Requirements and Classification, ISO 2919, ISO, Geneva (1998).

— Radiation Protection — Sealed Sources — Leakage Test Methods, ISO 9978, ISO, Geneva (1992).

McGINLEY, P.H., Shielding Techniques for Radiation Oncology Facilities, 2nd edn, Medical Physics Publishing, Madison, WI (1998).

NATIONAL COUNCIL ON RADIATION PROTECTION AND MEASURE-MENTS, Protection Against Radiation from Brachytherapy Sources, Rep. 40, NCRP, Bethesda, MD (1972).

— Structural Shielding Design and Evaluation for Medical Use of X Rays and Gamma Rays of Energies up to 10 MeV, Rep. 49, NCRP, Bethesda, MD (1976).

— Radiation Protection Design Guidelines for 0.1 MeV - 100 MeV Particle Accelerator Facilities, Rep. 51, NCRP, Bethesda, MD (1977).

INTERNATIONAL ORGANIZATIONS

The following international organizations' mission statements fully or partially address radiation protection and the use of ionizing radiation in medicine:

European Federation of Organisations for Medical Physics (EFOMP)
    Dijon, France   www.efomp.org

European Society for Therapeutic Radiology and Oncology (ESTRO)
    Brussels, Belgium   www.estro.be

International Atomic Energy Agency (IAEA)
    Vienna   www.iaea.org

International Commission on Radiation Units and Measurements (ICRU)
    Bethesda, Maryland, USA   www.icru.org

International Commission on Radiological Protection (ICRP)
    Stockholm, Sweden   www.icrp.org

International Electrotechnical Commission (IEC)
    Geneva, Switzerland   www.iec.ch

International Federation for Medical and Biological Engineering (IFMBE)
                            www.ifmbe.org

International Organization for Standardization (ISO)
    Geneva, Switzerland   www.iso.org

International Organization for Medical Physics (IOMP)
                            www.iomp.org

International Radiation Protection Association (IRPA)
    Fontenay-aux-Roses, France   www.irpa.net

International Society of Radiology (ISR)
    Bethesda, Maryland, USA   www.isradiology.org

International Union for Physical and Engineering Sciences in Medicine (IUPESM)
                            www.iupesm.org

Pan American Health Organization (PAHO)
Washington, DC   www.paho.org

Radiological Society of North America (RSNA)
Oak Brook, Illinois, USA   www.rsna.org

United Nations Scientific Committee on the Effects of Atomic Radiation (UNSCEAR)
Vienna   www.unscear.org

World Health Organization (WHO)
Geneva   www.who.int

ABBREVIATIONS

AAPM	American Association of Physicists in Medicine
ABC	Active Breathing Coordinator
ACR	American College of Radiology
ADCL	accredited dosimetry calibration laboratory
ALARA	as low as reasonably achievable
AP	anterioposterior
ART	adaptive radiotherapy
a-Si	amorphous silicon
BAT	B-Mode Acquisition and Targeting
BEV	beam's eye view
BGO	bismuth germanate
BIPM	Bureau international des poids et mesures
BMT	bone marrow transplantation
BNCT	boron neutron capture therapy
BSF	backscatter factor
BSS	International Basic Safety Standards for Protection against Ionizing Radiation and for the Safety of Radiation Sources
CBCT	cone beam computed tomography
CCPM	Canadian College of Physicists in Medicine
CET	coefficient of equivalent thickness
CF	collimator factor
CHART	continuous hyperfractionated accelerated radiotherapy
CL	confidence level
CNT	carbon nanotube
COIN	Clinical Oncology Information Network
COMP	Canadian Organization of Medical Physicists
CPE	charged particle equilibrium
CPU	central processing unit
CSDA	continuous slowing down approximation
CT	computed tomography
CTV	clinical target volume
DCR	digitally composited radiograph
DICOM	digital imaging and communications in medicine
DIN	Deutsches Institut für Normung
DMLC	dynamic multileaf collimator

DMF	dose modifying factor
DRR	digitally reconstructed radiograph
DSA	digital subtraction angiography
DVH	dose–volume histogram
EBF	electron backscatter factor
EFOMP	European Federation of Organisations for Medical Physics
EM	electromagnetic
EPD	electronic personal dosimeter
EPID	electronic portal imaging device
ESTRO	European Society for Therapeutic Radiology and Oncology
FDG	fluorodeoxyglucose
FWHM	full width at half maximum
GM	Geiger–Müller
GTV	gross tumour volume
HDR	high dose rate
HVL	half-value layer
ICRP	International Commission on Radiological Protection
ICRU	International Commission on Radiation Units and Measurements
IEC	International Electrotechnical Commission
IFMBE	International Federation for Medical and Biological Engineering
IGRT	image guided radiotherapy
IL	isodose line
IMAT	intensity modulated arc therapy
IMRT	intensity modulated radiotherapy
IOMP	International Organization for Medical Physics
IORT	intraoperative radiotherapy
IPEM	Institute of Physics and Engineering in Medicine
IPEMB	Institution of Physics and Engineering in Medicine and Biology
ISO	International Organization for Standardization
ITP	inverse treatment planning
ITV	internal target volume

IUPESM	International Union for Physical and Engineering Sciences in Medicine
LD	lethal dose
LDR	low dose rate
LET	linear energy transfer
linac	linear accelerator
LPO	left posterior oblique
MDR	medium dose rate
MLC	multileaf collimator
MOSFET	metal oxide semiconductor field effect transistor
MPR	multiplanar reconstruction
MR	magnetic resonance
MRI	magnetic resonance imaging
MU	monitor unit
MVCT	megavoltage computed tomography
NACP	Nordic Association of Clinical Physics
NAP	nominal accelerating potential
NCRP	National Council on Radiation Protection and Measurements
NCS	Nederlandse Commissie voor Stralingsdosimetrie
NEMA	National Electrical Manufacturers Association
NTCP	normal tissue complication probability
OAR	off-axis ratio
OER	oxygen enhancement ratio
OD	optical density
ODI	optical distance indicator
OSL	optically stimulated luminescence
PAHO	Pan American Health Organization
PDD	percentage depth dose
PDD(10)	percentage depth dose at 10 cm depth in water for a 10×10 cm^2 field
PDR	pulsed dose rate
PET	positron emission tomography
PMT	photomultiplier tube
PSDL	primary standards dosimetry laboratory
PSF	peak scatter factor

PTV	planning target volume
RAM	random access memory
RBE	relative biological effectiveness
RDF	relative dose factor
REF	relative exposure factor
REV	room's eye view
RF	radiofrequency
RFA	radiation field analyser
RGS	respiratory gating system
RPL	radiophotoluminescence
RPO	right posterior oblique
SAD	source to axis distance
SAR	scatter–air ratio
SD	standard deviation
SEBI	stereotactic external beam irradiation
SF	scatter factor
SI	Système international d'unités
SPECT	single photon emission computed tomography
SMLC	segmented multileaf collimator
SSD	source to surface distance
SSDL	secondary standards dosimetry laboratory
STP	standard temperature and pressure
STT	segmented treatment tables
TAR	tissue–air ratio
TBI	total body irradiation
TCP	tumour control probability
TCPE	transient charged particle equilibrium
TECDOC	technical document
TG	task group
TLD	thermoluminescent dosimeter
TMR	tissue–maximum ratio
TPR	tissue–phantom ratio
$TPR_{20,10}$	ratio of tissue–phantom ratio at depths of 20 cm and 10 cm in water
TPS	treatment planning system
TRS	Technical Reports Series
TSEI	total skin electron irradiation
TVL	tenth-value layer

UNSCEAR	United Nations Scientific Committee on the Effects of Atomic Radiation
UPS	uninterruptible power supply
WF	wedge factor
WHO	World Health Organization

SYMBOLS

Roman symbols

a	radius of atom; specific activity; scattering coefficient
a_0	Bohr radius of hydrogen atom
a_{eq}	side of equivalent square
A	ampere (SI unit of current)
Å	ångström (unit of distance: 1 Å = 10^{-10} m)
A	area; field size; atomic mass number
A_Q	field size at point Q in a phantom
$\mathcal{A}$	activity
b	impact parameter
B	buildup factor; barrier transmission factor; magnetic field
B_{leak}	leakage barrier transmission factor
B_{pri}	primary barrier transmission factor
B_{scat}	scatter barrier transmission factor
Bq	becquerel (SI unit of activity)
c	speed of light
C	coulomb (SI unit of charge)
C	capacitance; cema (converted energy per unit mass)
ºC	degree Celsius (unit of Celsius temperature)
Ci	curie (unit of activity: 1 Ci = 3.7×10^{10} Bq)
C_{pl}	material dependent scaling factor: plastic to water
C_E	dose to water correction factor for megavoltage electron beams (old concept)
C_λ	dose to water correction factor for megavoltage photon beams (old concept)
C/Z	shell correction in collision stopping power
d	distance; depth; cavity size parameter
d_i	isocentre depth
d_{pri}	distance from radiation source to point of interest
d_{80}	depth of the 80% percentage depth dose in water for photon beams
D	dose
$\dot{D}$	dose rate
D_{air}	absorbed dose to air
D_{cav}	dose to cavity
D_{gas}	dose to gas

D_{med}	dose to medium
D_T	organ dose
D_w	dose to water
D_{wall}	dose to wall
D'_{med}	dose to small mass of medium in air
$D_{\alpha-n}$	distance of closest approach between the α particle and the nucleus

e	electron
e	charge of electron ($1\,e = 1.602 \times 10^{-19}$ C)
E	total energy; effective dose
E_B	binding energy
$E_B(K)$	binding energy of the K shell electron
$\bar{E}_d$	average energy of electrons incident on an interface
E_K	kinetic energy
$\bar{E}_K$	average kinetic energy
E_K^{thr}	threshold kinetic energy
E_n	energy level of orbital electron with principal quantum number n
E_R	binding energy of electron in ground state of hydrogen (Rydberg energy)
E_0	rest energy
$\bar{E}_{ab}$	mean (average) absorbed energy
$\bar{E}_{tr}$	mean (average) transferred energy
$\bar{E}_0$	mean (average) electron energy on phantom surface
$\bar{E}_z$	mean (average) electron energy at depth z in water

f	source to surface distance; collection efficiency
f_g	collection efficiency in general recombination
fm	femtometre (unit of distance: 1 fm = 10^{-15} m)
f_{med}	roentgen to centigray conversion factor for medium
F	force
$F(r,\theta)$	anisotropy function

$g(r)$	radial dose function
$\bar{g}$	radiative fraction
G	gravitational constant
$G(r,\theta)$	geometry function
Gy	gray (SI unit of dose)

h	hour (unit of time)
h	Planck's constant; thickness of missing or excessive tissue
$\hbar$	reduced Planck's constant

620

H	equivalent dose
H^*	ambient dose equivalent
H'	directional dose equivalent
H_p	personal dose equivalent
I	current; intensity; mean excitation potential; measured ionization
I_{sat}	saturation current
I_{50}	50% value on the percentage depth ionization curve for electron beams
J	joule (SI unit of energy)
kg	kilogram (SI unit of mass)
k	correction factor; parameter in the isodose shift method
k_{att}	correction factor for photon attenuation and scatter in the chamber wall
k_{cell}	correction factor for central electrode
k_h	humidity correction factor
k_m	correction factor for non-air equivalence of the chamber wall
k_{pol}	polarity correction factor
$k(r_{med})$	correction factor accounting for photon beam attenuation in the buildup cap
k_q	ionization chamber correction factor
k_{sat}	saturation correction factor
$k_{T,P}$	temperature and pressure correction factor
K	kelvin (SI unit of thermodynamic temperature)
K	kerma
K_{col}	collision kerma
K_{rad}	radiative kerma
$(K_{air})_{air}$	air kerma in air
$(K_{air})_w$	air kerma in water
$(K_w)_{air}$	water kerma in air
$(K_w)_w$	water kerma in water
l	length
L	angular momentum; restricted linear collision stopping power
m	metre (SI unit of length)
m	mass
m_{air}	mass of air
m_e	electron mass

m_0	rest mass
m_p	proton mass
m_n	neutron mass
m_T	mass of organ or tissue
m_α	α particle mass
M	ionization chamber reading; atomic mass in atomic mass units u
$M(d)$	(Meisberger) polynomial of third or fourth degree
M_Q	ionization chamber reading at beam quality Q
MU	monitor unit (unit of quantity $\mathcal{MU}$)
$\mathcal{MU}$	monitor unit (quantity with unit MU)
n	neutron
n	principal quantum number
n_i	initial principal quantum number
n_f	final principal quantum number
N	newton (SI unit of force)
N	number of radioactive nuclei; ionization chamber calibration coefficient
N_A	Avogadro's number
N_a	number of atoms per mass
$N_{D,air}$	cavity air calibration coefficient
$N_{D,w}$	dose in water calibration coefficient
N_e	number of electrons per volume
N_K	air kerma in air calibration coefficient
$N_{K,co}$	air kerma in air calibration coefficient obtained in a ^{60}Co beam
N_X	exposure calibration coefficient
p	proton
p	perturbation correction factor; momentum
p_{cav}	cavity perturbation factor
p_{cel}	central electrode perturbation factor
p_{dis}	replacement correction factor
p_{fl}	electron fluence correction factor
p_q	overall perturbation correction factor for an ionization chamber
p_{wall}	chamber wall perturbation factor
P	pressure; power; design effective dose rate in a radiotherapy installation
Pa	pascal (SI unit of pressure)
P_{eff}	effective point of measurement
P_0	standard air pressure (101.325 kPa or 760 torr)

P_K fraction of all photoeffect events for $h\nu > E_B(K)$ occurring in the K shell

Q   point of interest in phantom
Q charge; beam quality
Q_{sat} saturation charge

r radius; distance
r_n radius of electron orbit with principal quantum number n
r_0 nuclear radius constant
r_e classical electron radius
r_{eq} equivalent radius
R   roentgen (unit of exposure)
R resistance; particle range in medium
R_P practical range
R_∞ Rydberg constant
R_{90} depth in water of the 90% percentage depth dose of an electron beam
R_{80} depth in water of the 80% percentage depth dose of an electron beam
R_{50} depth in water of the 50% percentage depth dose of an electron beam

s   second (unit of time)
s restricted mass collision stopping power; screening constant
$s_{w,air}$ ratio of restricted mass collision stopping powers water to air
S linear stopping power; scatter function; cell surviving fraction
S_c collimator scatter factor
S_K air kerma strength
S_P phantom scatter factor
$S_{c,p}$ total scatter factor
Sv   sievert (unit of equivalent dose and unit of effective dose)
(S/ρ) mass stopping power
$(S/\rho)_{col}$ mass collision stopping power
$(S/\rho)_{rad}$ mass radiative stopping power
$(S/\rho)_{tot}$ total mass stopping power
(S_Δ/ρ) restricted mass stopping power

t time; thickness
t_{max} time of maximum radioactive daughter activity
$t_{1/2}$ half-life
T   tesla (SI unit of magnetic flux density)
T temperature; linear scattering power; occupancy factor
(T/ρ) mass angular scattering power

T_0	standard air temperature (273.2K or 0ºC)
u	atomic mass unit
U	unit of air kerma strength given as: 1 U = 1 cGy·cm^2·h^{-1}
u_A	standard uncertainty of type A
u_B	standard uncertainty of type B
u_C	combined standard uncertainty of a quantity
U	use factor; expanded uncertainty
υ	velocity
V	volt (unit of voltage)
V	voltage; potential; volume
V_{eff}	effective volume
w	weighting factor
w_R	radiation weighting factor
w_T	tissue weighting factor
W	watt (SI unit of power); transmitted particle in weak interactions
W	workload
(W/e)	average energy required to produce an ion pair
(W_{air}/e)	average energy required to produce an ion pair in air
X	attenuator thickness; exposure
$x_{1/2}$	half-value layer
$x_{1/10}$	tenth-value layer
$\bar{x}$	mean value of all measurements x_i
y	year (unit of time)
Y	radiation (bremsstrahlung) yield
z	depth in a phantom
z_{max}	depth of dose maximum
z_{ref}	reference depth
z_α	atomic number of the α particle
Z	atomic number
Z_{eff}	effective atomic number
Z^0	transmitted particle in weak interaction

Greek symbols

α alpha particle; fine structure constant; initial slope of cell survival curve; fractional contribution to ionization by the chamber wall; electron arc angle

β beta particle; particle velocity normalized to the speed of light in a vacuum; quadratic component of the cell survival curve; characteristic angle in electron arc therapy; effective electron fluence correction factor; proportionality constant between the dose and kerma in air

γ gamma ray

Γ specific gamma ray constant

Γ_X exposure rate constant

Γ_{AKR} specific air kerma rate constant

δ delta ray

Δ cut-off energy

ε permittivity; photon energy normalized to the rest energy of the electron

ε_0 permittivity of vacuum

θ scattering angle

θ_{max} angle of maximum photon emission intensity

κ linear pair production attenuation coefficient; homogeneity coefficient

λ decay constant

λ_C Compton wavelength of the electron

Λ dose rate constant

μ permeability; linear attenuation coefficient

$_a\mu$ atomic attenuation coefficient

$_e\mu$ electronic attenuation coefficient

μ_0 permeability of vacuum

μ_{ab} linear energy absorption coefficient

μ_{en} linear energy absorption coefficient

μ_{tr} linear energy transfer coefficient

ν photon frequency

ρ density

σ cross-section

σ_C linear Compton attenuation coefficient

σ_R linear Rayleigh attenuation coefficient

τ average (mean) life of radioactive nucleus; linear photoelectric attenuation coefficient; fractional contribution to ionization by the chamber sleeve; kinetic energy normalized to rest energy

τ_s	shutter correction time
υ	velocity
ϕ	fluence
ψ	energy fluence
ω	angular frequency; fluorescent yield
ω_K	K shell fluorescent yield
Ω	solid angle

BIBLIOGRAPHY

AIRD, E.G., WILLIAMS, J.R., REMBOWSKA, A., "Brachytherapy", Radiotherapy Physics (WILLIAMS, J.R., THWAITES, D.I., Eds), Oxford Univ. Press, Oxford (2000).

AMERICAN ASSOCIATION OF PHYSICISTS IN MEDICINE (New York)

A protocol for the determination of absorbed dose from high-energy photon and electron beams, Task Group 21, Radiation Therapy Committee, Med. Phys. **10** (1983) 741–771.

Radiation Treatment Planning Dosimetry Verification, AAPM Task Group 23 Report, American Institute of Physics, New York (1995).

Physical Aspects of Quality Assurance in Radiation Therapy, AAPM Task Group 24 Report, AAPM (1984).

Physical Aspects of Total and Half Body Irradiation, AAPM Task Group 29 Report, AAPM (1986).

Total Skin Electron Therapy: Techniques and Dosimetry, AAPM Task Group 30 Report, AAPM (1987).

Medical accelerator safety considerations, Report of AAPM Radiation Therapy Committee Task Group No. 35, Med. Phys. **20** (1993) 1261–1275.

Comprehensive QA for Radiation Oncology: Report of AAPM Radiation Therapy Committee Task Group 40, Med. Phys. **21** (1994) 581–618.

Stereotactic Radiosurgery, AAPM Task Group 42 Report, AAPM (1995).

Dosimetry of interstitial brachytherapy sources: Recommendations of the AAPM Radiation Therapy Committee Task Group No. 43, Med. Phys. **22** (1995) 209–239.

AAPM's TG-51 protocol for clinical reference dosimetry of high energy photon and electron beams, Task Group 51, Med. Phys. **26** (1999) 1847–1870.

American Association of Physicists in Medicine Radiation Therapy Committee Task Group 53: Quality assurance for clinical radiotherapy treatment planning, Med. Phys. **25** (1998) 1773–1829.

Clinical use of electron portal imaging: Report of AAPM Radiation Therapy Committee Task Group 58, Med. Phys. **28** (2001) 712–737.

AAPM protocol for 40–300 kV x-ray beam dosimetry in radiotherapy and radiobiology, Task Group 61 Report, Med. Phys. **28** (2001) 868–892.

Quality assurance for computed-tomography simulators and the computed-tomography-simulation process: Report of the AAPM Radiation Therapy Committee Task Group No. 66, Med. Phys. **30** (2003) 2762–2790.

ATTIX, F.H., Introduction to Radiological Physics and Radiation Dosimetry, Wiley, New York (1986).

ATTIX, F.H., ROESCH, W.C., TOCHILIN, E., Radiation Dosimetry, Academic Press, New York (1968).

BENTEL, G.C., Radiation Therapy Planning, McGraw-Hill, New York (1996).

BENTEL, G.C., NELSON, C.E., NOELL, K.T., Treatment Planning and Dose Calculation in Radiation Oncology, Pergamon Press, Oxford and New York (1989).

BRAHME, A., et al., Accuracy requirements and quality assurance of external beam therapy with photons and electrons, Acta Oncol. Suppl. 1 **27** (1988).

BRITISH INSTITUTE OF RADIOLOGY, Central Axis Depth Dose Data for Use in Radiotherapy, Br. J. Radiol. Suppl. 17 (1983).

— Central Axis Depth Dose Data for Use in Radiotherapy, Br. J. Radiol. Suppl. 25 (1996).

CAMERON, J.R., SUNTHARALINGAM, N., KENNEY, G.K., Thermoluminescent Dosimetry, University of Wisconsin Press, Madison, WI (1968).

CHAO, K.S., PEREZ, C.A., BRADY, L.W., Radiation Oncology Management Decisions, Lippincott-Raven, New York (1999).

CLARK, M.J., et al., Dose quantities for protection against external radiations: Guidance on the 1990 recommendations of ICRP, Doc. NRPB **4** 3 (1993).

CLARKSON, J., A note on depth doses in fields of irregular shape, Br. J. Radiol. **14** (1941) 265.

CLINICAL ONCOLOGY INFORMATION NETWORK, ROYAL COLLEGE OF RADIOLOGISTS, Guidelines for external beam radiotherapy, Clin. Oncol. **11** (1999) S135–S172.

COIA, L., SCHULTHEISS, T.E., HANKS, G.E., A Practical Guide to CT-simulation, Advanced Medical Publishing, Madison, WI (1995).

CUNNINGHAM, J.R., Keynote address: Development of computer algorithms for radiation treatment planning, Int. J. Radiol. Oncol. Biol. Phys. **16** (1989) 1367–1376.

DOBBS, H., THWAITES, D.I., "Quality assurance and its conceptual framework", Physics Aspects of Quality Control in Radiotherapy (MAYLES, H.M., et al., Eds), Rep. 81, Institute of Physics and Engineering in Medicine, York, United Kingdom (1999) Ch. 1.

DUTREIX, A., When and how can we improve precision in radiotherapy? Radiother. Oncol. **2** (1984) 275–292.

ESSERS, M., MIJNHEER, B.J., In-vivo dosimetry during external photon beam radiotherapy, Int. J. Radiat. Oncol. Biol. Phys. **43** (1999) 245–259.

EUROPEAN SOCIETY FOR THERAPEUTIC RADIOLOGY AND ONCOLOGY, Quality assurance in radiotherapy, Radiother. Oncol. **35** (1995) 61–73.

— Practical Guidelines for the Implementation of a Quality System in Radiotherapy, Physics for Clinical Radiotherapy Booklet No. 4, ESTRO, Brussels (1998).

EVANS, R.D., The Atomic Nucleus, McGraw-Hill, New York (1955).

FOOD AND AGRICULTURE ORGANIZATION OF THE UNITED NATIONS, INTERNATIONAL ATOMIC ENERGY AGENCY, INTERNATIONAL LABOUR ORGANISATION, OECD NUCLEAR ENERGY AGENCY, PAN AMERICAN HEALTH ORGANIZATION, WORLD HEALTH ORGANIZATION, International Basic Safety Standards for Protection against Ionizing Radiation and for the Safety of Radiation Sources, Safety Series No. 115, IAEA, Vienna (1996).

GILDENBERG, P.L., TASKER, R.R. (Eds), Textbook of Stereotactic and Functional Neurosurgery, McGraw-Hill, New York (1998).

GLASGOW, G.P., "Brachytherapy", Modern Technology in Radiation Oncology: A Compendium for Medical Physicists and Radiation Oncologists (VAN DYK, J., Ed.), Medical Physics Publishing, Madison, WI (1999) 695–752.

GREENE, D., WILLIAMS, P.C., Linear Accelerators for Radiation Therapy, Institute of Physics Publishing, Bristol (1997).

GREENING, J.R., Fundamentals of Radiation Dosimetry, Adam Hilger, Bristol (1981).

HALE, J., The Fundamentals of Radiological Science, Thomas, Springfield, IL (1974).

HALL, E.J., Radiobiology for the Radiologist, Lippincott, Philadelphia, PA (2000).

HARTMANN, G., et al., Quality Assurance Program on Stereotactic Radiosurgery, Springer-Verlag, Berlin (1995).

HENDEE, W.R., IBBOTT, G.S., Radiation Therapy Physics, Mosby, St. Louis, MI (1996).

HORTON, J., Handbook of Radiation Therapy Physics, Prentice Hall, New York (1987).

INSTITUTE OF PHYSICAL SCIENCES IN MEDICINE, Code of practice for high-energy photon therapy dosimetry based on the NPL absorbed dose calibration service, Phys. Med. Biol. **35** (1990) 1355–1360.

INSTITUTE OF PHYSICS AND ENGINEERING IN MEDICINE (York, United Kingdom)

The IPEMB code of practice for electron dosimetry for radiotherapy beams of initial energy from 2 to 50 MeV based on air kerma calibration, Phys. Med. Biol. **41** (1996) 2557–2603.

The IPEMB code of practice for the determination of absorbed dose for x-rays below 300 kV generating potential (0.035 mm Al–4 mm Cu HVL; 10–300 kV generating potential), Phys. Med. Biol. **41** (1996) 2605–2625.

A Guide to Commissioning and Quality Control of Treatment Planning Systems (SHAW, J.E., Ed.), Rep. 68 (1996).

The Design of Radiotherapy Treatment Room Facilities (STEDEFORD, B., MORGAN, H.M., MAYLESS, W.P.M., Eds) (1997).

Physics Aspects of Quality Control in Radiotherapy (MAYLES, H.M., et al., Eds), Rep. 81 (1998).

INTERNATIONAL ATOMIC ENERGY AGENCY (Vienna)

Absorbed Dose Determination in Photon and Electron Beams, Technical Reports Series No. 277 (1987).

Calibration of Dosimeters Used in Radiotherapy, Technical Reports Series No. 374 (1995).

Absorbed Dose Determination in Photon and Electron Beams, 2nd edn, Technical Reports Series No. 277 (1997).

Method for the Development of Emergency Response Preparedness for Nuclear or Radiological Accidents, IAEA-TECDOC-953 (1997).

The Use of Plane Parallel Chambers in High Energy Electron and Photon Beams, Technical Reports Series No. 381 (1997).

Design and Implementation of a Radiotherapy Programme: Clinical, Medical Physics, Radiation Protection and Safety Aspects, IAEA-TECDOC-1040 (1998).

Assessment of Occupational Exposure Due to External Sources of Radiation, IAEA Safety Standards Series No. RS-G-1.3 (1999).

Occupational Radiation Protection, IAEA Safety Standards Series No. RS-G-1.1 (1999).

"Recommendations on standardized procedures for calibration of brachytherapy sources at SSDLs and hospitals", Calibration of Brachytherapy Sources, IAEA-TECDOC-1079 (1999).

Standardized Quality Audit Procedures for On-site Dosimetry Visits to Radiotherapy Hospitals, DMRP-199907-IU (1999).

Absorbed Dose Determination in External Beam Radiotherapy, Technical Reports Series No. 398 (2000).

Aspectos Físicos de la Garantía de Calidad en Radioterapia: Protocolo de Control de Calidad, IAEA-TECDOC-1151 (2000).

Calibration of Radiation Protection Monitoring Instruments, Safety Reports Series No. 16 (2000).

Lessons Learned from Accidental Exposures in Radiotherapy, Safety Reports Series No. 17 (2000).

Calibration of Photon and Beta Ray Sources Used in Brachytherapy, IAEA-TECDOC-1274 (2002).

Radiological Protection for Medical Exposure to Ionizing Radiation, IAEA Safety Standards Series No. RS-G-1.5, IAEA (2002).

Regulations for the Safe Transport of Radioactive Material, 1996 Edition (As Amended 2003), IAEA Safety Standards Series No. TS-R-1 (2003).

INTERNATIONAL COMMISSION ON RADIATION UNITS AND MEASUREMENTS (Bethesda, MD)

Measurement of Absorbed Dose Measured in a Phantom Irradiated by a Single Beam of X or Gamma Rays, Rep. 23 (1973).

Determination of Absorbed Dose in a Patient Irradiated by Beams of X or Gamma Rays in Radiotherapy Procedures, Rep. 24 (1976).

Radiation Dosimetry: Electron Beams with Energies Between 1 and 50 MeV, Rep. 35 (1984).

Stopping Powers for Electrons and Positrons, Rep. 37 (1984).

Dose and Volume Specification for Reporting Intracavitary Therapy in Gynecology, Rep. 38 (1985).

Use of Computers in External Beam Radiotherapy Procedures with High-energy Photons and Electrons, Rep. 42 (1987).

Determination of Dose Equivalents Resulting from External Radiation Sources, Rep. 43 (1988).

Measurement of Dose Equivalents from External Photon and Electron Radiations, Rep. 47 (1992).

Prescribing, Recording and Reporting Photon Beam Therapy, Rep. 50 (1993).

Quantities and Units in Radiation Protection Dosimetry, Rep. 51 (1993).

Dose and Volume Specification for Reporting Interstitial Therapy, Rep. 58 (1997).

Prescribing, Recording and Reporting Photon Beam Therapy (Supplement to ICRU Report 50), Rep. 62 (1999).

INTERNATIONAL COMMISSION ON RADIOLOGICAL PROTECTION

Protection Against Ionizing Radiation from External Sources Used in Medicine, Publication 33, Pergamon Press, Oxford and New York (1982).

1990 Recommendations of the International Commission on Radiological Protection, Publication 60, Pergamon Press, Oxford and New York (1991).

Conversion Coefficients for Use in Radiological Protection Against External Radiation: Adopted by the ICRP and ICRU in 1995, Publication 74, Pergamon Press, Oxford and New York (1997).

General Principles for the Radiation Protection of Workers, Publication 75, Pergamon Press, Oxford and New York (1997).

Pregnancy and Medical Radiation, Publication 84, Pergamon Press, Oxford and New York (2000).

Prevention of Accidental Exposure to Patients Undergoing Radiation Therapy, Publication 86, Pergamon Press, Oxford and New York (2002).

INTERNATIONAL ELECTROTECHNICAL COMMISSION (Geneva)

Medical Electrical Equipment — Part 2: Particular Requirements for the Safety of Therapeutic X-ray Generators, IEC 601-2-8 (1987).

Medical Electrical Equipment — Medical Electron Accelerators — Functional Performance Characteristics, IEC 976 (1989).

Medical Electrical Equipment — Medical Electron Accelerators in the Range 1 MeV to 50 MeV — Guidelines for Performance Characteristics, IEC 977 (1989).

Safety of Medical Electrical Equipment, Part 2: Particular Requirements for Medical Electron Accelerators in the Range 1 MeV to 50 MeV, Section 1: General, Section 2: Radiation Safety for Equipment, IEC 601-2-1 (1996).

General Requirements for Safety. 4. Collateral Standard: Programmable Electrical Medical Systems, IEC 60601-1-4 (1997).

Medical Electrical Equipment — Part 2: Particular Requirements for the Safety of Gamma Beam Therapy Equipment, IEC 60601-2-11 (1997).

Medical Electrical Equipment — Dosimeters with Ionization Chambers as Used in Radiotherapy, IEC 60731 (1997).

Guidelines for Radiotherapy Treatment Rooms, IEC 61859 (1997).

Medical Electrical Equipment — Part 2-1: Particular Requirements for the Safety of Electron Accelerators in the Range of 1 MeV to 50 MeV, IEC 60601-2-1, IEC (1998).

Medical Electrical Equipment — Part 2-17: Particular Requirements for the Safety of Remote-controlled Automatically-driven Gamma-ray Afterloading Equipment, IEC 60601-2-17 (1998).

Medical Electrical Equipment — Part 2: Particular Requirements for the Safety of Radiotherapy Simulators, IEC-60601-2-29 (1999).

Medical Electrical Equipment: Requirements for the Safety of Treatment Planning Systems, Publication IEC 62C/62083 (in preparation).

INTERNATIONAL ORGANIZATION FOR STANDARDIZATION (Geneva)

Basic Ionizing Radiation Symbol, ISO 361 (1975).

X and Gamma Reference Radiations for Calibrating Dosemeters and Dose Ratemeters and for Determining their Response as a Function of Energy, ISO 4037. See also High Rate Series of Filtered X-radiations, ISO 4037-1979/Addendum 1 (1983); and Low Rate Series of Filtered X-radiations, ISO 4037-1979/Amendment 1-1983 (E) (1979).

Reference Beta Radiations for Calibrating Dosimeters and Dose Rate Meters and for Determining their Response as a Function of Beta Radiation Energy, ISO 6980 (1984).

Dosimetry of the Reference Radiation Fields Used for Determining the Response of Protection Level Dosimeters and Dose-rate Meters at Photon Energies Between 4 and 9 MeV, ISO/DP 9991 (1988).

Dosimetry of X and Gamma Reference Radiations for Radiation Protection over the Energy Range from 9 keV to 1.3 MeV, ISO/DIS 8963 (1988).

Guide to Expression of Uncertainty in Measurement (1992).

Quantities and Units — Part 0: General Principles, ISO 31-0 (1992).

Radiation Protection — Sealed Sources — Leakage Test Methods, ISO 9978 (1992).

Quality Management and Quality Assurance Standards — Part I. Guidelines for Selection and Use, ISO 9000 (1994).

Radiation Protection — Sealed Radioactive Sources — General Requirements and Classification, ISO 2919 (1998).

JOHNS, H.E., CUNNINGHAM, J.R., The Physics of Radiology, Thomas, Springfield, IL (1984).

KARZMARK, C.J., NUNAN, C.S., TANABE, E., Medical Electron Accelerators, McGraw-Hill, New York (1993).

KASE, K.R., BJARNGARD, B.E., ATTIX, F.H. (Eds), The Dosimetry of Ionizing Radiation, Academic Press, San Diego, CA (1985).

KHAN, F., The Physics of Radiation Therapy, 4th edn, Lippincott, Williams and Wilkins, Baltimore, MD (2003).

KHAN, F.M., POTISH, R.A. (Eds), Treatment Planning in Radiation Oncology, Lippincott Williams and Wilkins, Philadelphia, PA (1998).

KLEVENHAGEN, S.C., Physics and Dosimetry of Therapy Electron Beams, Medical Physics Publishing, Madison, WI (1993).

KNOLL, G.F., Radiation Detection and Measurement, Wiley, New York (1979).

MACKIE, T.R., SCRIMGER, J.W., BATTISTA, J.J., A convolution method of calculating dose for 15-MV x rays, Med. Phys. **47** (1985) 188–196.

MAYLES, W.P.M., HEISIG, S., MAYLES, H.M.O., “Treatment verification and in-vivo dosimetry”, Radiotherapy Physics in Practice (WILLIAMS, J.R., THWAITES, D.I., Eds), Oxford Univ. Press, Oxford (2000) 220–246.

McCULLOUGH, E.C., “Intraoperative electron beam radiation therapy (IORT)”, Advances in Radiation Oncology Physics — Dosimetry, Treatment Planning, and Brachytherapy (PURDY, J., Ed.), American Institute of Physics, New York (1992).

McGINLEY, P.H., Shielding Techniques for Radiation Oncology Facilities, Medical Physics Publishing, Madison, WI (1998).

McKENZIE, A., KEHOE, T., THWAITES, D.I., “Quality assurance in radiotherapy physics”, Radiotherapy Physics in Practice (WILLIAMS, J.R., THWAITES, D.I., Eds), Oxford Medical Publishing, Oxford (2000).

MEIJER, G., VAN KLEFFENS, H., MIJNHEER, B., Consistency in quality control programmes for electron accelerators in radiotherapy centres, Radiother. Oncol. **48** (1998) 103–110.

MIJNHEER, B., BATTERMANN, J., WAMBERSIE, A., What degree of accuracy is required and can be achieved in photon and neutron therapy, Radiother. Oncol. **8** (1987) 237–252.

MILAN, J., BENTLEY, R.E., The storage and manipulation of radiation dose data in a small digital computer, Br. J. Radiol. **47** (1974) 115–121.

MOULD, R.F., Radiotherapy Treatment Planning, Adam Hilger, Bristol (1981).

MUNRO, P., "Megavoltage radiography for treatment verification", The Modern Technology in Radiation Oncology: A Compendium for Medical Physicists and Radiation Oncologists (VAN DYK, J., Ed.), Medical Physics Publishing, Madison, WI (1999) 481–508.

NATIONAL COUNCIL ON RADIATION PROTECTION AND MEASUREMENTS (Bethesda, MD)

Protection Against Radiation from Brachytherapy Sources, Rep. 40 (1972).

Structural Shielding Design and Evaluation for Medical Use of X Rays and Gamma Rays of Energies up to 10 MeV, Rep. 49 (1976).

Radiation Protection Design Guidelines for 0.1 MeV–100 MeV Particle Accelerator Facilities, Rep. 51 (1977).

NIAS, A.W., An Introduction to Radiobiology, Wiley, New York (1998).

NATIONAL RADIOLOGICAL PROTECTION BOARD, New Radiation Quantities Recommended by ICRU for Practical Use in Radiation Protection: Their Implementation in the United Kingdom, NRPB, Didcot (1986).

PODGORSAK, E.B., METCALFE, P., VAN DYK, J., "Medical accelerators", The Modern Technology in Radiation Oncology: A Compendium for Medical Physicists and Radiation Oncologists (VAN DYK, J., Ed.), Medical Physics Publishing, Madison, WI (1999) 349–435.

PODGORSAK, E.B., PODGORSAK, M.B., "Stereotactic irradiation", ibid., pp. 589–640.

— "Special techniques in radiotherapy", ibid., pp. 641–693.

STEEL, G.G., Basic Clinical Radiobiology, Arnold, London (2002).

STERLING, T.D., PERRY, H., KATZ, L., "Automation of radiation treatment planning", Br. J. Radiol. **37** (1964) 544–550.

STERNICK, E.S. (Ed.), The Theory and Practice of Intensity Modulated Radiation Therapy, Advanced Medical Publishing, Madison, WI (1997).

in water phantoms in off-axis planes of rectangular fields of open and wedged photon beams, Phys. Med. Biol. **40** (1995) 511–527.

VAN DYK, J. (Ed.), The Modern Technology for Radiation Oncology: A Compendium for Medical Physicists and Radiation Oncologists, Medical Physics Publishing, Madison, WI (1999).

VAN DYK, J., "Radiation oncology overview", ibid., pp. 1–18.

VAN DYK, J., BARNETT, R.B., BATTISTA, J., "Computerized radiation treatment planning systems", ibid., pp. 231–286.

VAN DYK, J., BARNET, R., CYGLER, J., SHRAGGE, P., Commissioning and quality assurance of treatment planning computers, Int. J. Radiat. Oncol. Biol. Phys. **26** (1993) 261–273.

VAN DYK, J., PURDY, J., "Clinical implementation of technology and the quality assurance process", The Modern Technology for Radiation Oncology: A Compendium for Medical Physicists and Radiation Oncologists (VAN DYK, J., Ed.), Medical Physics Publishing, Madison, WI (1999) 19–52.

VEETH, J.M., "Intraoperative radiation therapy in treatment of cancer", Frontiers of Radiation Therapy and Oncology, Vol. 31, Karger, Basle (1997).

VENSELAAR, J., WELLEWEERD, H., MIJNHEER, B., Tolerances for the accuracy of photon beam dose calculation of treatment planning systems, Radiother. Oncol. **60** (2001) 203–214.

WEBB, S., The Physics of Conformal Radiotherapy, Institute of Physics Publishing, Bristol (1997).

WILLIAMS, J.R., THWAITES, D.I. (Eds), Radiotherapy Physics in Practice, Oxford Univ. Press, Oxford (2000).

WOLKOV, H.B., "Intraoperative radiation therapy", Textbook of Radiation Oncology (LEIBEL, S.A., PHILIPS, T.L., Eds), W.B. Saunders, Philadelphia, PA (1998).

WORLD HEALTH ORGANIZATION, Quality Assurance in Radiotherapy, WHO, Geneva (1988).

YAYARAMAN, S., LANZL, L.H., Clinical Radiotherapy Physics, CRC Press, Boca Raton, FL (1996).

INDEX

electrometer, 78, 308
electron
    applicators, 289
    arc therapy, 295
    backscatter factor, 294
    beams, 273
    beam therapy, 273
    beam transport, 146
    bolus, 291
    capture, 21
    charge, 1
    classical radius, 2
    Compton, 30, 39
    conversion, 19
    cut-out, 289
    energy, 281, 367
    gun, 140, 142
    interactions, 22, 274
    internal shielding, 289
    loosely bound, 28
    mass, 1
    pseudo-arc, 295
    range, 22, 277
    recoil, 30, 39
    shielding, 289
    tightly bound, 28
electronic
    attenuation coefficient, 27
    personal dosimeter, 117
    portal imaging device, 55, 261, 434, 436, 438
    transition, 14
electrostatic accelerator, 133
electron–orbital electron interaction, 22
electron–nucleus interaction, 22
electron–positron pair, 32
electron–positron annihilation, 38
Elekta, 540, 545
endocavitary rectal irradiation, 529
endocurie therapy, 451

endorectal treatment, 529
energy
    absorption coefficient, 27
    fluence, 45, 46, 162
    imparted, 49
    level diagram, 13, 14
    levels, 11
    transfer coefficient, 27
    threshold, 62
engineering technologist, 416
EPID, 55, 261, 434, 436, 438
EPID dosimetry, 443
EPD, 117
equilibrium
    secular, 18
    transient, 18
    charged particle, 56
equipment
    acceptance, 355, 358, 419, 533, 570
    commissioning, 355, 370, 384, 400
    specification, 419
equivalent
    activity, 459
    circle, 173
    dose, 7, 555
    square, 173
    TAR method, 250
error of measurement, 72, 301, 352, 400
ESTRO, 414, 446, 588
europium-152; 130
evaluation
    of treatment plan, 256
    of treatment, 260
ExacTrac system, 542
excitation of atom, 12, 23
excitation potential, 48
exit dose, 170, 172, 442
exposure, 8, 60

647

Monte Carlo technique, 64, 206, 299, 328, 391
MOSFET, 90
MRI in treatment planning, 238
MU calculation, 264
MVCT, 539
multielectron atom, 12, 14
multileaf collimator (MLC), 148, 173, 179, 373, 532
multiple coplanar beams, 253
multiple non-coplanar arcs, 510
multiple non-coplanar beams, 255
multiple scattering, 21, 25
multiplanar reconstruction (MPR), 235
mutation, 489
muon, 5

NACP, 307
Nahum, A., 63
NAP, 127, 337
narrow beam geometry, 336, 600
NCRP, 491, 600
NEMA, 400
neutrino, 20
neutron
    activation, 19
    generator, 133
    mass, 1
    production, 605
    survey meter, 105
NIST, 33
nitrogen-13; 541
nominal accelerating potential, 127, 337
Nomos, 542
non-coplanar beams, 255, 510
non-electronegative gas, 104
non-ionizing radiation, 5
non-stochastic (deterministic) effect, 491, 550

normal temperature and pressure, 313
normal tissue complication probability, 397, 410, 497, 534, 544,
normalization, 270, 402
normalized incident photon energy, 30
NTCP, 397, 497, 534, 544
nuclear
    activation, 19
    binding energy, 15
    reaction, 15, 16
    structure, 7, 14, 15
    transformation, 16
nucleon, 7, 15
nucleus of cell, 485
number of electrons per mass, 8
number of atoms per mass, 8
number of electrons per volume, 8

OAR, 285, 390
oblique beam incidence, 200
occupancy factor, 599
occupational exposure, 553, 561, 577
occupational worker, 598
ODI, 300
OER, 151, 499
off-axis ratio, 194, 285, 390
    for photon beams, 194, 390
    for electron beams, 285
on-line portal imaging, 55, 261, 434, 436, 438
one electron atom, 10
operational quantities, 101, 558
optical density (OD), 81, 360
optical distance indicator, 364, 424
optically stimulated luminescence (OSL), 85, 88, 116
optimization, 403, 477, 559, 584
organ, 486
organ dose, 555

650

This publication is aimed at students and teachers involved in programmes that train professionals for work in radiation oncology. It provides a comprehensive overview of the basic medical physics knowledge required in the form of a syllabus for modern radiation oncology. It will be particularly useful to graduate students and residents in medical physics programmes, to residents in radiation oncology, as well as to students in dosimetry and radiotherapy technology programmes. It will assist those preparing for their professional certification examinations in radiation oncology, medical physics, dosimetry or radiotherapy technology. It has been endorsed by several international and national organizations and the material presented has already been used to define the level of knowledge expected of medical physicists worldwide.